



University
of Glasgow

Gehl, Bernadette (2009) *Functional and molecular characterisation of two stomatin-like proteins from Arabidopsis thaliana*.
PhD thesis.

<http://theses.gla.ac.uk/640/>

Copyright and moral rights for this thesis are retained by the author

A copy can be downloaded for personal non-commercial research or study, without prior permission or charge

This thesis cannot be reproduced or quoted extensively from without first obtaining permission in writing from the Author

The content must not be changed in any way or sold commercially in any format or medium without the formal permission of the Author

When referring to this work, full bibliographic details including the author, title, awarding institution and date of the thesis must be given

**Functional and Molecular
Characterisation of Two Stomatin-like
Proteins from *Arabidopsis thaliana***

Bernadette Gehl

January 2009

Thesis submitted for the degree of Doctor of Philosophy

Division of Biochemistry and Cell Biology,
Faculty of Biomedical and Life Sciences,

University of Glasgow

Abstract

Stomatins belong to the band-7 (or SPFH domain) family (short for Stomatin, Prohibitin, Flotillin HfiC/K) of diverse membrane proteins. This protein family is evolutionary conserved with members found in all sequenced eukaryotes and in most prokaryotes. Band-7 family proteins have the ability to oligomerise and generally aid in the assembly and regulation of large membrane-bound protein complexes. In animals, stomatins have been demonstrated to regulate ion channels by direct protein interactions. Additionally, they localise to membrane microdomains where they actively contribute to their assembly by binding sterols, and they also associate with the actin cytoskeleton. The *Arabidopsis* genome encodes for two structurally similar stomatin-like proteins that are functionally completely unknown yet. They will be referred to as AtSlp1 (for *Arabidopsis thaliana* stomatin-like protein) and AtSlp2. The aim of this thesis was to provide a detailed characterisation of these two genes on a molecular and functional level. Both proteins are expressed ubiquitously throughout plant development, but they accumulate at particularly high levels in pollen and other metabolically active cells. Phylogenetic analysis reveals that AtSlps are homologous to stomatin-like proteins of type 2. Amongst these, the human stomatin-like protein 2 (HsSlp2) is localised to mitochondria where it participates in large membrane-bound protein complexes and is also involved in the proliferation of cancer cells. Evidence is provided here that demonstrates mitochondrial localisation of both *Arabidopsis* Slp proteins *in vitro* and *in vivo*. On a functional level, mitochondria from an *slp1* knockout mutant plant have a decreased mitochondrial membrane potential and increased oxygen consumption rates. This is interpreted as a defect in coupling efficiency and an impairment of the mitochondrial inner membrane integrity. This defect results in a variety of other growth phenotypes that are related to metabolically active tissues and cell types. Knockout plants are delayed in overall growth of shoots and roots and have decreased seed germination rates. Additionally, these plants are less resistant to conditions of high salinity and are less fertile. Overexpression of a protein acting as a putative dominant-negative Slp fragment results in plants with a dwarf phenotype and early onset of leaf senescence. This phenotype correlates with increased levels of reactive oxygen species and altered organelle ultrastructure. Guard cells from these plants in particular have enlarged chloroplasts and are impaired in transpirational control. It is concluded that also in plants, stomatins act together with other band-7 family proteins as parts of large protein complexes that have regulatory roles important for development and stress responses. Their main role is probably to provide membrane scaffolds that affect mitochondrial function and morphology during cell division and in situations of mitochondrial stress.

Table of Contents

LIST OF TABLES	8
LIST OF FIGURES	9
LIST OF ABBREVIATIONS	12
ACKNOWLEDGEMENTS	15
AUTHOR'S DECLARATION	16
1 GENERAL INTRODUCTION	17
1.1 The SPFH/Band-7 domain protein family	17
1.1.1 Stomatins.....	19
1.1.2 Prohibitins	19
1.1.3 Flotillins and Erlins.....	22
1.1.4 HflC/K proteins.....	24
1.2 Stomatin-type proteins	25
1.2.1 Stomatin protein characteristics	25
1.2.1.1 First cloning and characterisation of the stomatin gene.....	25
1.2.1.2 Subcellular localisation	28
1.2.1.3 Association of stomatin with lipid microdomains	29
1.2.1.4 Phosphorylation	32
1.2.1.5 Palmitoylation	33
1.2.1.6 Oligomerisation.....	33
1.2.1.7 Stomatin protein interactors	34
1.2.2 Ion channel regulation by stomatin homologues	36
1.2.2.1 Human and mammalian homologues.....	37
1.2.2.2 Stomatin proteins from <i>C.elegans</i>	39
1.2.3 Prokaryotic stomatins.....	43
1.3 The Band-7 protein family in plants	47
1.3.1 Stomatins in plants	47
1.3.2 Plant prohibitins	48
1.3.3 Flotillins and erlins.....	52
1.3.4 HIR proteins	53
1.4 Human Slp2, a close homologue of Arabidopsis stomatins	55
1.4.1 Characteristics of human stomatin-like protein 2	55
1.4.2 HsSlp2 functions	56
1.5 Aims and objectives of this study	60
2 MATERIALS AND METHODS	61
GENERAL MATERIALS AND METHODS	61
2.1 RNA extraction, quantification and cDNA synthesis	61

2.2	Plant genomic DNA extraction	62
2.3	PCR and agarose gel electrophoresis	63
2.4	Cloning procedures	66
2.5	<i>A.tumefaciens</i> transformation	70
2.6	Arabidopsis stable transformations	71
2.7	Plant growth conditions.....	72
2.8	Plant crude protein extraction	73
2.9	SDS-PAGE and Western blotting.....	74
METHODS FOR CHAPTER 3: PHYLOGENETIC ANALYSIS AND TISSUE EXPRESSION.....		77
2.10	Sequence alignments and phylogenetic trees.....	77
2.11	Cloning of AtSlp open reading frames.....	78
2.12	Antibody Production.....	79
2.13	AtSlp expression analysis	87
METHODS FOR CHAPTER 4: ATSLP SUBCELLULAR LOCALISATION AND ATSLP1 PROTEIN ANALYSIS		94
2.14	Subcellular targeting.....	94
2.15	Biochemical methods	94
2.16	<i>In vivo</i> localisation of AtSlps	100
2.17	Biochemical characterisation of AtSlp1	104
METHODS FOR CHAPTER 5: FUNCTIONAL CHARACTERISATION OF ATSLPS.....		107
2.18	Isolation of T-DNA insertion lines.....	107
2.19	Characterisation of <i>slp1</i> growth phenotypes	108
2.20	<i>slp1</i> mitochondrial phenotypes	112
2.21	Stable AtSlp RNAi lines.....	115
2.22	Dominant-negative (DN) Slp overexpressing lines.....	116
2.23	Characterisation of DN Slp phenotypes.....	118
RESULTS CHAPTERS		123

3 ARABIDOPSIS STOMATIN-LIKE PROTEINS- PHYLOGENY, STRUCTURE AND TISSUE EXPRESSION	123
INTRODUCTION	123
3.1 Arabidopsis stomatins and their phylogenetic context.....	125
3.1.1 The Arabidopsis band-7 family.....	129
3.1.2 The relationship of Arabidopsis stomatins with those from other species	133
3.1.3 Arabidopsis Slps and band-7 proteins from a variety of species	137
3.1.4 Comparison of Slps on the sequence level- AtSlps and HsSlp2.....	140
3.1.5 Sequence comparison of AtSlps and stomatins from other species.....	143
3.2 Structural features of Arabidopsis and human stomatin-like proteins	148
3.2.1 AtSlp1- structural features	148
3.2.2 AtSlp2- structural features	151
3.2.3 HsSlp2- structural features.....	152
3.3 Cloning of AtSlp open reading frames.....	155
3.4 Production of specific antibodies against AtSlp1 and AtSlp2.....	156
3.4.1 Design of AtSlp1 and AtSlp2 epitope expression constructs in bacteria.....	156
3.4.2 Overexpression and purification of His-tagged fusion proteins	159
3.4.2.1 Assessment of protein induction properties (denaturing)	161
3.4.2.2 Purification of epitope proteins under native conditions in a small scale batch format	164
3.4.2.3 Large scale purification of 6xHis-tagged Slp1 epitope.....	165
3.4.3 Assessment of anti-Slp1 specificity on Western blots	169
3.4.4 GST-fusion of Slp2 epitope and attempted expression in bacteria.....	171
3.4.5 Commercial antibody production based on peptide epitopes of AtSlp1 and AtSlp2	173
3.4.5.1 AtSlp1-peptide specific antiserum	173
3.4.5.2 AtSlp2 peptide specific antiserum	174
3.5 Expression analysis of AtSlp1 and AtSlp2.....	179
3.5.1 Expression levels of AtSlps from public microarray data	179
3.5.1.1 Expression levels during plant development	179
3.5.1.2 Tissue specific expression.....	182
3.5.1.3 AtSlp expression in seeds	184
3.5.1.4 Chemical and hormone treatments of seedlings.....	186
3.5.1.5 Response to abiotic stresses in shoots and roots	189
3.5.2 AtSlp transcript analysis by Northern blotting	194
3.5.3 Analysis of AtSlp gene structures and promoter activities	201
3.5.3.1 AtSlp genomic organisation.....	201
3.5.3.2 Response elements in the AtSlp promoter sequences.....	205
3.5.3.3 AtSlp tissue expression pattern- transgenic promoter-GUS fusion plants.....	209
3.5.3.4 Stress and hormone treatments of promoter-GUS fusion plants.....	219
3.5.4 Tissue distribution of AtSlps on the transcript and on the protein level.....	225
3.6 Discussion.....	229
3.6.1 Phylogenetic relationship between AtSlps and other band-7 family proteins.....	229
3.6.2 Structural features of Arabidopsis stomatins and human Slp2	231
3.6.3 Antibody production against AtSlp1 and AtSlp2	233
3.6.4 Tissue expression of AtSlp1 and AtSlp2 and changes upon stress treatments	235

4	SUBCELLULAR LOCALISATION OF ARABIDOPSIS STOMATIN-LIKE PROTEINS AND CHARACTERISATION OF THE ATSLP1 PROTEIN	241
	INTRODUCTION	241
4.1	Subcellular targeting of AtSlp proteins	241
4.1.1	Prediction of AtSlp subcellular targeting	243
4.1.2	Analysis of putative signal sequences as amphipathic alpha helices	246
4.2	Biochemical evidence for mitochondria localisation of AtSlp1	248
4.2.1	Aqueous 2-phase partitioning	248
4.2.2	Isolation of mitochondria from Arabidopsis leaves	249
4.2.3	Sub-mitochondrial localisation of AtSlp1	254
4.3	<i>In vivo</i> evidence for Slp localisation to mitochondria	259
4.3.1	Stable fluorescent protein overexpressing lines	259
4.3.1.1	AtSlp1- overexpression under the constitutive promoter	260
4.3.1.2	Co-localisation of Slp1-YFP with MitoTracker	263
4.3.1.3	AtSlp2- overexpression under its native promoter	264
4.3.1.4	Co-localisation of AtSlp2-GFP with MitoTracker	268
4.3.1.5	Phenotypes of stable AtSlp overexpressing lines	270
4.4	Biochemical characterisation of the AtSlp1 protein	271
4.4.1	Effects of formaldehyde crosslinking on AtSlp1	271
4.4.2	Membrane insertion of AtSlp1	273
4.4.2.1	Protease K assay	273
4.4.2.2	Chemical treatments of microsomal fractions	275
4.4.3	Putative S-acylation of AtSlp1	279
4.5	Discussion	284
4.5.1	Subcellular targeting of AtSlps	284
4.5.2	AtSlp1 localisation to mitochondria	287
4.5.3	<i>In vivo</i> evidence for AtSlp localisation to mitochondria	291
4.5.4	Biochemical characterisation of AtSlp1	294
5	PHENOTYPICAL AND FUNCTIONAL CHARACTERISATION OF ATSLP MUTANTS	305
	INTRODUCTION	305
5.1	Isolation of homozygous AtSlp1 T-DNA insertion lines	305
5.1.1	Genotyping PCR	306
5.1.2	RT-PCR and Western blotting	308
5.2	Associated knockout mutant phenotypes	311
5.2.1	Shoot growth and morphology	311
5.2.2	Seed germination	313
5.2.3	Root growth	315
5.2.4	Leaf osmolarity	317
5.2.5	Flowering time	317
5.2.6	Seed production/Fertility	318
5.2.7	Sensitivity to salt stress	319
5.2.8	Photosynthetic activity and transpiration rate	322

5.3	Mitochondrial phenotypes of <i>slp1</i> knockout plants	326
5.3.1	Membrane potential	326
5.3.2	Oxygen consumption rates	330
5.3.3	Reactive oxygen species	339
5.4	Dexamethasone-inducible RNAi knockdown lines	345
5.4.1	Construct design.....	345
5.4.2	Time course of RNAi knockdown effect	345
5.5	Overexpression of putative dominant-negative Slp fragments (DN Slps)	348
5.5.1	Design of constructs.....	349
5.5.2	Dexamethasone induction properties	350
5.5.3	Solubility of DN Slps	351
5.5.3.1	Assessment of DN protein solubility	351
5.5.3.2	Putative S-acylation of DN Slps	352
5.6	Associated DN growth phenotypes	355
5.6.1	Growth phenotypes and reduction of leaf surface area	355
5.6.2	Leaf osmolarity	359
5.6.3	Flowering time	359
5.6.4	Guard cell phenotypes.....	360
5.6.5	Water content and whole plant transpiration	364
5.6.6	Reactive oxygen species	372
5.6.7	Mitochondrial membrane potential	376
5.7	Cross of DN(Slp1) and <i>slp1-1</i> knockout line	378
5.8	Discussion.....	380
5.8.1	General <i>slp1</i> mutant phenotypes	380
5.8.2	<i>slp1</i> mitochondrial phenotypes	383
5.8.3	DN-Slp growth phenotypes.....	391
5.8.4	DN-Slp effects on guard cells	394
5.8.5	Effects of DN expression on ROS production	396
6	GENERAL DISCUSSION	399
6.1	Summary of main results	399
6.2	General functions of AtSlp proteins	400
6.3	General functions of band-7 family proteins.....	404
6.4	Outlook and suggestions for further experiments	407
	APPENDIX 1.....	411
	APPENDIX 2.....	419

List of Tables

Table 3-1. Overview over the domains of all band-7 family proteins.....	125
Table 3-2. Plant band-7 proteins.....	126
Table 3-3 Animal and bacterial band-7 proteins.....	127
Table 3-4 Yeast band-7 proteins.....	128
Table 3-5 Identities and similarities of the Arabidopsis band-7 family.....	132
Table 3-6 Identities and similarities between relatives of AtSlp1 and AtSlp2.....	136
Table 3-7 Samples and their numbers used to create the plot in Figure 3-22.....	181
Table 3-8 Samples used to plot the eFP data in Figure 3-23.....	183
Table 3-9 Samples plotted in Figure 3-24.....	185
Table 3-10 Chemical and hormone treatments used in Figure 3-25.....	189
Table 3-11 Abiotic stress treatments.....	193
Table 3-12 Genomic organisation of AtSlp genes.....	202
Table 3-13 Genome duplication between Arabidopsis loci on chromosomes 4 and 5.....	204
Table 3-14 Promoter response elements.....	207
Table 3-15 Summary of hormone and stress treatments with promoter-GUS plants.....	219
Table 4-1. Target sequence predictions for AtSlp1 and AtSlp2.....	244
Table 4-2. Target sequence prediction for AtSlps.....	244
Table 4-3. Target sequence predictions for HsSlp-2.....	245
Table 4-4. Detergent/protein ratios.....	258
Table 4-5. Chemical treatments of microsomal fractions.....	276
Table 5-1. Isolated knockout mutant lines.....	308
Table 5-2. Replicates of photosynthesis measurements.....	323
Table 5-3. Respiration substrates and inhibitors.....	334

List of Figures

Figure 1-1. Stomatocytotic erythrocytes.....	27
Figure 1-2. Ion channel regulation by Mec-2 in <i>C.elegans</i> mechanosensation.....	40
Figure 1-3. Crystal structure of the core domain from the prokaryotic stomatin PH1511.....	45
Figure 3-1. Phylogenetic tree of the Arabidopsis band-7 family.....	131
Figure 3-2. Phylogenetic tree of stomatin protein sequences from various species.....	135
Figure 3-3. Phylogenetic tree of all band 7 sequences from various species.....	139
Figure 3-4. Multiple sequence alignment of AtSlp1 and HsSlp2.....	142
Figure 3-5. Multiple sequence alignment of all stomatins analysed in this study.....	145
Figure 3-6. Schematic presentation of the membrane insertion model of human stomatin.....	149
Figure 3-7. Structural features of the AtSlp1 protein.....	150
Figure 3-8. Structural features of the AtSlp2 protein.....	153
Figure 3-9. Structural features of the human Slp2 protein.....	154
Figure 3-10. Overview of pQE80L constructs.....	157
Figure 3-11. Schematic presentations of AtSlp1 and AtSlp2 epitopes.....	158
Figure 3-12. Outline of protein expression and purification steps.....	160
Figure 3-13. Detection of His-tagged epitope proteins.....	163
Figure 3-14. Coomassie stained SDS PAGE gel of Slp1 epitope.....	165
Figure 3-15. Coomassie-stained SDS-PAGE gel of the first large scale purification.....	166
Figure 3-16. Coomassie stained SDS-PAGE gels of the final purification.....	168
Figure 3-17. Western blots to assess the specificity of anti-Slp1.....	170
Figure 3-18. GST fusion of Slp2 epitope and protein expression in bacteria.....	172
Figure 3-19. Western blots to determine antiserum against Slp1.....	174
Figure 3-20. Western blots of Slp2 antibody.....	176
Figure 3-21. Western blot probed with anti-Slp2 sera.....	177
Figure 3-22. AtSlp transcript levels in different organs.....	181
Figure 3-23. Tissue specific expression levels of AtSlps.....	183
Figure 3-24. Transcript levels of AtSlps in seeds.....	185
Figure 3-25. AtSlp transcript levels in response to chemical and hormone treatments.....	188
Figure 3-26. Abiotic stress treatments of 18 days old agar-grown wild type plants.....	191
Figure 3-27. UV-B treatment of wild type plants.....	192
Figure 3-28. Northern blots and quantified signals.....	197
Figure 3-29. Gene duplication between Arabidopsis chromosomes 4 (At chr4) and 5.....	201
Figure 3-30. Genomic structures of the AtSlp1 and AtSlp2 genes.....	203
Figure 3-31. Genomic surrounding of AtSlp1 and AtSlp2 genes.....	209
Figure 3-32. Schematic presentation of the AtSlp promoter-GUS fusion constructs.....	210
Figure 3-33. AtSlp1 promoter-GUS fusion stains.....	214
Figure 3-34. AtSlp1 promoter-GUS fusion stains from more mature plants.....	215
Figure 3-35. Inflorescence organs from AtSlp1 promoter GUS stained plants.....	216
Figure 3-36. GUS stained plants carrying the AtSlp2 promoter construct.....	217
Figure 3-37. Inflorescence details from AtSlp2 promoter-GUS fusion plants.....	218
Figure 3-38. Stress treatments of AtSlp promoter-GUS fusion plants.....	223
Figure 3-39. UV-B treatment of promoter-GUS transgenic plants.....	224
Figure 3-40. RT-PCR on Arabidopsis organs.....	226
Figure 3-41. Western blots of protein extracts from organs.....	228
Figure 4-1. Alpha-helical wheel projection of N-terminal presequences of AtSlps.....	247
Figure 4-2. Aqueous 2-phase partitioning from Arabidopsis leaves.....	249
Figure 4-3. Western blot of organelle pellets after differential centrifugation.....	250
Figure 4-4. Western blot of a mitochondrial purification on a linear Percoll gradient.....	251
Figure 4-5. Mitochondria purifications on three-step Percoll gradients.....	253
Figure 4-6. Western blot of of mitochondria isolated on the linear Percoll gradient.....	255

Figure 4-7. Western blot of mitochondria fractions isolated on step gradients	256
Figure 4-8. Overview of 35S::Slp::YFP constructs.	259
Figure 4-9. T-DNA of genomic GFP fusion construct of AtSlp2.....	260
Figure 4-10. Three-dimensional reconstructions of a guard cell and an epidermal cell.	261
Figure 4-11. Western blots of seedlings overexpressing Slp1-YFP.	262
Figure 4-12. Co-localisation of MitoTracker DeepRed and Slp1-YFP.	263
Figure 4-13. Three-dimensional reconstruction of MitoTracker-infiltrated root hair.....	264
Figure 4-14. AtSlp2-GFP expression in seedling organs.....	265
Figure 4-15. Three-dimensional reconstructions of AtSlp2-GFP expression in leaves.....	266
Figure 4-16. Western blot probed with anti-GFP.	267
Figure 4-17. Confocal images of AtSlp2-GFP co-localisation with MitoTracker Orange	269
Figure 4-18. Colocalisation of AtSlp2-GFP with MitoTracker Orange from an independent transgenic line.	269
Figure 4-19. Phenotypes of Slp-Y/GFP overexpressing plants.	270
Figure 4-20. Effects of FA crosslinking of isolated mitochondria on Slp1.	272
Figure 4-21. Western blot probed with anti-Slp1 of FA treatment.....	273
Figure 4-22. Membrane insertion models for peripherally attached (A) and single transmembrane spanning proteins (B).	274
Figure 4-23. Western blot of protease K treated (“+”) microsomal fractions in the presence (“+”) or absence (“-“) of 1% Triton-X100.....	275
Figure 4-24. Western blots of microsomal fractions treated with chemicals to solubilise membrane-attached proteins.	278
Figure 4-25. Amino acid sequences surrounding the putatively palmitoylated cysteine residues.....	280
Figure 4-26. Western blots of seedlings treated with the palmitoylation inhibitor BPA on MS agar plates.....	282
Figure 5-1. Scheme of the AtSlp1 gene with three isolated T-DNA insertion sites.....	305
Figure 5-2. Genotyping PCR for homozygous T-DNA insertion of <i>slp1-1</i> and <i>slp1-3</i>	306
Figure 5-3. Genotyping PCR for BASTA resistant <i>slp1-2</i> and <i>slp1-4</i> mutant lines.....	307
Figure 5-4. DNA agarose gel of RT-PCR reactions	309
Figure 5-5. Western blot probed with anti-Slp1	309
Figure 5-6. Western blots probed with anti-Slp1 of protein extracts from <i>slp1-2</i> (A) and <i>slp1-4</i> (B) lines.....	310
Figure 5-7. Photographs taken of <i>slp1</i> mutant plants.....	312
Figure 5-8. Photographs and quantified leaf surface areas of <i>slp1</i> and wild type plants...312	
Figure 5-9. Germination assay of <i>slp1</i> mutant seeds.	314
Figure 5-10. Main root length measurements of <i>slp1</i> and wild type seedlings	316
Figure 5-11. Osmolarity (in mOsM) of rosette leaf sap from <i>slp1</i> and wild type	317
Figure 5-12. Determination of flowering time of <i>slp1-1</i> , <i>slp1-3</i> and wild type plants.	318
Figure 5-13. <i>slp1-1</i> and wild type siliques	319
Figure 5-14. Root bending assay.....	321
Figure 5-15. Quantification of root bending assay.	322
Figure 5-16. Quantifications of photosynthetic parameters.....	325
Figure 5-17. TMRE fluorescence in <i>slp1-1</i> and wild type (Wt) roots.	328
Figure 5-18. Quantification of TMRE fluorescence	329
Figure 5-19. Schematic presentation of mitochondrial electron transport chain	332
Figure 5-20. Oxygen consumption rates of <i>slp1-1</i> and wild type mitochondria.....	335
Figure 5-21. Relative responses of oxygen consumption rates.....	338
Figure 5-22. DAB-stained leaves from <i>slp1</i> and wild type plants	341
Figure 5-23. Three-dimensional reconstructions of confocal images.....	342
Figure 5-24. Quantified H ₂ DCFDA fluorescence.....	343
Figure 5-25. Schematic presentation of the pOpOff2(Hyg) T-DNA.	345
Figure 5-26. Western blot of time course showing RNAi-mediated knockdown of Slp1.	347
Figure 5-27. Construct design of DN Slps.....	348

Figure 5-28. Schematic presentation of DN(Slp) encoding T-DNA.....	349
Figure 5-29. Dexamethasone induction kinetics of a DN(Slp1) transgenic line.	350
Figure 5-30. Assessment of DN Slp protein solubility	352
Figure 5-31. DN Slp seedlings grown on MS agar plates.....	354
Figure 5-32. Effect of BPA on DN(Slp1) protein solubility.....	354
Figure 5-33. Phenotypes of DN Slp plants grown on soil.	357
Figure 5-34. Quantification of leaf surface area	357
Figure 5-35. Growth phenotype of plants grown on soil	358
Figure 5-36. Growth phenotype of whole flowering plants and leaves.....	358
Figure 5-37. Osmolarity levels of DN and wild type plants	359
Figure 5-38. Effect of DN expression on the onset of flower transition.....	360
Figure 5-39. Enlarged guard cell chloroplasts	362
Figure 5-40. Confocal images of guard cell chloroplast autofluorescence.....	362
Figure 5-41. Guard cell density of DN and wild type plants grown in long day light.....	364
Figure 5-42. Leaf water content from DN Slp and wild type plants.....	366
Figure 5-43. Water loss rates from DN(Slp1) plants	368
Figure 5-44. Transpiration rate measurements of DN control and induced plants.....	371
Figure 5-45. DAB-stained leaves from control and DN plants.....	372
Figure 5-46. H ₂ DCFDA stained roots from DN Slp and wild type seedlings	374
Figure 5-47. Quantified H ₂ DCFDA fluorescence.....	374
Figure 5-48. Trypan Blue-stained DN and wild type leaves.....	375
Figure 5-49. TMRE-stained seedling roots of DN(Slp1) and wild type plants.	377
Figure 5-50. Quantified TMRE fluorescence	377
Figure 5-51. Phenotypes of crossed heterozygous DN(Slp1)x <i>slp1-1</i> lines.	379
Figure 6-1. Proposed model for AtSlp function in the mitochondrial inner membrane...	403

List of Abbreviations

2,4D	2,4-dichlorophenoxyacetic acid
ABA	abscisic acid
ADP-	adenosine diphosphate
AOX-	alternative oxidase
ASIC	acid sensing ion channel
At	<i>Arabidopsis thaliana</i>
ATP	adenosine triphosphate
AtSlp	<i>Arabidopsis thaliana</i> stomatin-like protein
BL	Brassinolide
BLAST	Basic Local Alignment Search Tool
BPA	2-bromo palmitic acid
cAMP	cyclic adenosine monophosphate
CMV35S	Cauliflower mosaic virus 35S promoter
CNGC	cyclic nucleotide gated channel
CoA	coenzyme A
DAB	diaminobenzidine
DEPC	Diethyl pyrocarbonate
DHA	dehydroxyascorbic acid
DMSO	dimethyl sulfoxide
DN Slp	Dominant-negative stomatin-like protein
DNA	deoxyribonucleic acid
DNP	2,4-dinitrophenol
DRM	detergent-resistant membrane
DTT	dithiothreitol
EDTA	ethylenediaminetetraacetic acid
eFP	electronic fluorescent pictograph
EM	endomembrane fraction
ENaC	epithelial sodium channel
ER	endoplasmic reticulum
ERAD	ER-associated degradation pathway
ESA	epidermal surface antigen
ESCC	esophageal squamous cell carcinoma
ETC	electron transport chain
FA	formaldehyde
FDA	fluorescein diacetate
FRAP	fluorescence recovery after photobleaching
FRET	fluorescence resonance energy transfer
GA	giberellic acid
GFP	green fluorescent protein
GPI	glycosyl phosphatidyl inositol anchor
GSH	reduced glutathione
GST	glutathione-S transferase
GTP	guanosine triphosphate
GUS	β -glucuronidase
H ₂ DCFDA	2',7'-dichlorodihydrofluorescein diacetate
HEPES	4-(2-hydroxyethyl)-1-piperazineethanesulfonic acid
HflC/K	high frequency of lysogenation locus C/K
HIR	hypersensitive induced reaction protein
HR	hypersensitive response
HsSlp2	human stomatin-like protein 2
IBA	indole-3-butyric acid

IL-6	interleukin-6
IMS	mitochondrial intermembrane space
IP3	Inositol 1,4,5-triphosphate
IPTG	isopropyl-b-D-thiogalactoside
IRGA	infrared gas analyser chamber
kDa	kilo Dalton
LB	Luria-Bertani medium
LC-MS/MS	liquid chromatography-tandem mass spectrometry
MDa	Mega Dalton
MDCK	Madine Darby canine kidney cells
MDM	mitochondrial distribution and morphology
Mec	mechanosensory
MIA	mitochondrial intermembrane space assembly machinery
MIM	mitochondrial inner membrane
MOM	mitochondrial outer membrane
mRNA	messenger RNA (ribonucleic acid)
MS	Murashige and Skoog basal medium
MTP	mitochondrial transition pore
NAA	1-Naphthylacetic acid
NADPH	nicotinamide adenine dinucleotide phosphate, reduced form
NADH	nicotinamide adenine dinucleotide, reduced form
Ndex	NAD(P)H dehydrogenases in the outer leaflet of the MIM
Ndin	NAD(P)H dehydrogenases in the inner leaflet of the MIM
NfeD	nodulation formation efficiency D locus
Ni-NTA	Nickel-nitrilotriacetic acid
NMR	nuclear magnetic resonance spectroscopy
NO	nitric oxide
NPA	N-1-naphthylphtalamic acid
NsLTP	non-specific lipid transfer protein
OhSt.	overhydrated hereditary stomatocytosis
ORF	open reading frame
PAT	palmitoyl-transferases
PCR	polymerase chain reaction
PGDD	plant genome duplication database
PHB	prohibitin
PID	proliferation, ion channel and death
PLAP	placental alkaline phosphatase
PM	plasma membrane
PMSF	Phenylmethanesulfonyl fluoride
PNO8	N-octyl-3-nitro-2,4,6-trihydroxybenzamide
PPFD	photosynthetic photon flux density
PRXII F	peroxiredoxin II F
PSI/II	photosystem I/II
PTE	palmitoyl thioesterase
Q	ubiquinone (oxidised form)
Rb	retinoblastoma protein
RH	relative humidity
RNA	ribonucleic acid
RNAi	small interfering RNA
RNS	reactive nitrogen species
ROS	reactive oxygen species
<i>rth 1</i>	<i>roothairless 1</i>
RT-PCR	reverse transcription-PCR
SA	salicylic acid

SAM	mitochondrial sorting and assembly machinery
SAR	systemic acquired resistance
SDS-PAGE	sodium dodecyl sulphate- polyacrylamide gel electrophoresis
SHAM	salicyl hydroxamic acid
SNARE	soluble NSF attachment protein receptor
SOD	superoxide dismutase
SPFH	stomatin, prohibitin, flotillin, HflC/K family
Syp	syntaxin of plant
TAE	Tris acetate EDTA buffer
Taq pol	Thermos aquaticus DNA polymerase
TCA cycle	tricarboxylic acid cycle (Krebs cycle)
T-DNA	transfer-DNA
TE buffer	Tris EDTA buffer
TIBA	2,3,5-triiodo benzoic acid
TIM	translocase of the mitochondrial inner membrane
TMRE	tetramethylrhodamine ethyl ester
TOM	translocase of the mitochondrial outer membrane
TRPC6	transient receptor potential C channel 6
UAC	human amniotic cell line (epithelial cells)
UBQ10	ubiquitin 10 (from <i>Arabidopsis thaliana</i>)
UCP	uncoupling protein
Unc	uncoordinated (<i>C.elegans</i> genes)
UTR	untranslated region
UV	ultraviolet light
Wt	wild type (<i>Arabidopsis thaliana</i>)
YFP	yellow fluorescent protein

Acknowledgements

I am indebted for the advice and encouragement I received during my Ph.D. from my supervisor, Mike Blatt. I would like to thank him for his scientific and moral support, and especially for the opportunity to be able to approach him at any time.

I would furthermore like to thank Annegret Honsbein for our special friendship that provided hours of laughter and support throughout my studies. I especially appreciate her willingness to help in all situations, and her warm personality.

I would also like to thank Cornelia Eisenach for her friendship and willingness to assist me where it was possible. I would also like to acknowledge Dr. Manuel Paneque-Corrales for his help in the beginning of my graduate studies and during my undergraduate project. Naomi Donald assisted me as a research technician in the final year of my graduate studies, and Dr. Prisca Campanoni always provided helpful advice. Finally, I would like to thank all members (past and present) of the Stevenson Laboratory for their assistance, companionship and advice.

On a personal note, I would like to thank my husband Mikko for all his support throughout my degree. I strongly believe that our relationship gave me the strength and will that I needed to accomplish my research.

I feel also indebted to my parents and my sister Ophelia for their support and their belief in my abilities.

Author's Declaration

I hereby declare that all the work presented as part of this thesis is my own, except where explicitly stated otherwise.

Bernadette Gehl

5th January 2009

1 General Introduction

A stomatin-like protein from *Arabidopsis thaliana* was identified as a putative protein interaction partner of an Arabidopsis syntaxin in a yeast split-ubiquitin screen (Obrdlik *et al.*, 2004) that was carried out by Dr. Rejane Pratelli (Stanford University, USA). Syntaxins belong to the class of SNARE proteins mediating membrane fusion processes. The identified syntaxin protein interaction partner was the AtSyp71 protein that belongs to a plant-specific subclass of syntaxins. Meanwhile, this protein was confirmed to localise to the plasma membrane and is also found in lipid microdomains (Mongrand *et al.*, 2004; Marmagne *et al.*, 2004; Alexandersson *et al.*, 2004). In the original screen, the stomatin-like protein was used as the bait, and the syntaxin was identified as a putatively interacting prey. Stomatins are so far entirely uncharacterised in plants and their functions are not fully understood even in animals. Based on the yeast screen result, the hypothesis was put forward that this Arabidopsis stomatin-like protein would be localised to the plasma membrane. Based on knowledge about stomatins in other eukaryotes, this protein was regarded as a putative plasma membrane ion channel regulator in Arabidopsis. During the first year of my graduate studies, experiments were carried out to confirm the putative protein-protein interaction between AtSyp71 and the stomatin-like protein *in vitro* and *in vivo*. However, it was soon clear that this interaction must have been a false positive result and the original research hypothesis was reviewed. The objective of this project was revised to study the functional importance of two homologous unknown Arabidopsis proteins with stomatin domains.

1.1 The SPFH/Band-7 domain protein family

Stomatins, together with prohibitins, flotillins and bacterial HflC/K proteins have been grouped into a protein superfamily termed SPFH (for Stomatin, prohibitin, flotillin, HflC/K) according to homologies in the central parts of the proteins (Tavernarakis *et al.*, 1999). Synonymous for SPFH, the conserved domain was also named the “band-7 domain” after the first identified member, the human stomatin protein (or erythrocyte band 7.2b protein). The SPFH protein family consists of diverse eukaryotic and prokaryotic membrane proteins that assemble and regulate super-molecular protein complexes (Browman *et al.*, 2007). Characteristic for this family is a conserved central stretch of 29 amino acids that forms the basis of a PROSITE signature sequence (Tavernarakis *et al.*, 1999). BLAST searches with stomatin sequences as queries identified a central cytoplasmic domain in stomatin that is homologous to sequences from prohibitins,

flotillins, bacterial HflC/K and some hypothetical prokaryotic proteins. According to these similarities, a novel domain was defined and named “SPFH” after the initials of its members (Pfam entry: Band_7, accession number PF01145). Copies of SPFH domain proteins are found in all sequenced eukaryotic genomes, and in most prokaryotes. The SPFH domain is now considered to have evolved independently in organisms by convergent evolution, indicating a fundamental biological role (Rivera-Milla *et al.*, 2006).

Most of these proteins are integral membrane proteins with the SPFH domain facing the cytoplasm. An exception are prohibitins that protrude from the mitochondrial inner membrane into the intermembrane space (Ikonen *et al.*, 1995) and bacterial HflC/K proteins that protrude from the plasma membrane into the periplasmic space (Kihara & Ito, 1998). Most SPFH proteins share some common structural features: they have a short N-terminal domain followed by a hydrophobic region and a mainly hydrophilic C-terminus. They are frequently post-translationally modified by phosphorylation or acylation, which is essential for their regulatory activities (Huber *et al.*, 2006b). Frequently, SPFH domain proteins lack known sorting motifs and are probably trafficked by unconventional targeting sequences (Browman *et al.*, 2007).

Some members assemble into higher oligomers and associate with lipid rafts; most of them share a characteristic secondary structure with β -sheets typically concentrated at the N-terminus, and α -helices at the C-terminus (Barnes *et al.*, 1996; Stewart *et al.*, 1992). Both eukaryotic prohibitins and bacterial HflC/K proteins function in the regulation of membrane-bound proteolytic complexes (for details see sections 1.1.2 and 1.1.4); thus, it is speculated that also other members of the SPFH domain family might have similar functions due to conserved structural features. For example, stomatins might be indirectly involved in the regulation of ion channels via association with membrane-bound proteases. Structurally very similar to the SPFH domain proteins are the caveolins that typically associate with caveolae, specialised membrane microdomains. Caveolins are however not functionally related to stomatins (Snyers *et al.*, 1999a). Mammalian caveolin-1 mediates protein-lipid microdomain assembly through its lipophilic characteristics (Bauer & Pelkmans, 2006).

It is now regarded that SPFH domain proteins in general share the ability to compartmentalise membranes by binding to lipids such as sterols. They have the ability to seed microdomain structures within membranes for the functional organisation of proteins in complexes (Browman *et al.*, 2007). These protein complexes are involved in a variety of cellular processes, including mechanosensation and endocytosis.

What follows now in this introduction is a brief description of the individual SPFH family members that have been studied in animals. Stomatins in particular will be described in more detail in section 1.2.

1.1.1 Stomatins

The first stomatin protein identified from erythrocyte membranes was the ubiquitously expressed human band 7.2b protein (Hiebldirschmied *et al.*, 1991b), the absence of which in the plasma membrane causes cation leakage and a reorganisation of lipid rafts and the actin cytoskeleton (Stewart *et al.*, 1993;Wilkinson *et al.*, 2008). The protein is inserted into membranes adopting an unusual monotopic structure and assembles into homo-oligomers that form large complexes facing the cytoplasm (Salzer *et al.*, 1993;Snyers *et al.*, 1999a). In erythrocytes, stomatin interacts with other cytoskeletal and ion channel regulating proteins (Sinard J.H., 1994;Moore & Shriver, 1997) and also binds to the glucose transporter GLUT-1 as a negative regulator of glucose transport (Zhang *et al.*, 2001). Other animal stomatin homologues have also been demonstrated to regulate different kinds of ion channels by direct protein interactions (see section 1.2.2 for detailed descriptions).

1.1.2 Prohibitins

Prohibitin-type proteins are identified by the presence of a PHB domain that is largely similar to the band-7 domain. They possess additional N-terminal hydrophobic domains mediating membrane anchorage and C-terminal coiled-coils. Prohibitins were identified as highly conserved mitochondrial integral membrane proteins localised to the inner membrane and protruding into the intermembrane space with their C-termini (Ikonen *et al.*, 1995;Steglich *et al.*, 1999). Similar to stomatins, they are encoded in the nucleus and ubiquitously expressed in eukaryotes; one of the major features of prohibitins is their antiproliferative property as a negative regulator of the cell cycle in the transition from the G₁ to the S-phase (Mcclung *et al.*, 1995). Prohibitin (=PHB1 or BAP32) homologues interact with prohibitone (=PHB2, also named BAP37) homologues from human, mouse, rat and *Xenopus laevis*, another mitochondrial protein that is similar in its central part and also highly conserved in eukaryotes. Deletion of both homologous genes in *Saccharomyces cerevisiae* results in a decrease of yeast replicative lifespan (premature ageing) and reduces the mitochondrial membrane potential by approximately 80% (Coates *et al.*, 1997). Another study found prohibitin associated with membrane-bound immunoglobulin M molecules in B lymphocytes, and suggested prohibitin to be a plasma membrane protein important for receptor-mediated signalling (Terashima *et al.*, 1994).

Annexin A2 and α -actinin have been identified as prohibitin and prohibitone interactors in a yeast-two-hybrid screen (Bacher *et al.*, 2002). Additionally, it was shown that both PHB1 and PHB2 assemble into heteromeric complexes and are contained in a multi-protein complex with a molecular weight of more than 500 kDa in a B cell line. Annexin A2 and α -actinin both bind actin in the presence of Ca^{2+} and are similarly ubiquitously expressed than prohibitins. Annexin A2 also binds to acidic phospholipids in a Ca^{2+} -dependent manner and influences membrane fusion processes associated with lipid rafts. The interactions with both prohibitins are mediated by coiled-coils at the C-termini of the proteins.

Human PHB1 was shown to interact with the tumor suppressing retinoblastoma protein (Rb) in a yeast 2-hybrid screen. Supposedly this interaction inhibited E2F-mediated transcription initiation (Wang *et al.*, 1999a). PHB2 was found to bind to the estrogen receptor leading to transcription repression. However, the growth suppressive activity of PHB1 was demonstrated to be mediated by the 3'UTR of the PHB mRNA (Jupe *et al.*, 1996). Prohibitins were also demonstrated to bind the ligand melanogenin. This molecule stimulates melanin production important to protect against damage upon irradiation with UV light (Snyder *et al.*, 2005). The reported differences concerning the subcellular localisation of prohibitins to mitochondria, the nucleus and the plasma membrane are now regarded to be cell-type and tissue specific. Generally, prohibitins are regarded as mitochondrial proteins in most cell types.

Another important function of prohibitin is the regulation of membrane protein turnover via association with the mAAA (for matrix AAA) protease in mitochondria (Steglich *et al.*, 1999; Langer *et al.*, 2001). The mAAA protease is a highly conserved ATP-dependent metalloprotease in the inner mitochondrial membrane exposed to the matrix. It forms a protein supercomplex (2 MDa) and interacts with prohibitin and prohibitone in yeast during mitochondrial biogenesis. A second AAA protease (iAAA protease, for intermembrane AAA protease) exists in the inner membrane with a reverse orientation to the mAAA protease; they complement each other functionally in the removal of non-assembled proteins from the inner membrane that would otherwise cause an imbalance in the assembly of the electron transport chain. Prohibitin and prohibitone negatively regulate protease activity of unassembled inner membrane proteins since their deletion causes an acceleration of protein turnover. The C-termini of prohibitin and prohibitone probably interact with the N-terminus of the mAAA protease in the intermembrane space and thereby putatively stabilise a conformation of the protease with low activity (Steglich *et al.*, 1999); another possibility is that the prohibitin complex affects the conformation or

accessibility of protease substrates that would otherwise be degraded prematurely, maybe at sites of the mitochondrial import machinery (Steglich *et al.*, 1999). In both cases, the regulation of protein turnover might also affect cellular senescence and proliferation.

A role for prohibitin and prohibitone as a novel membrane-bound chaperone complex was proved experimentally (Nijtmans *et al.*, 2002; Nijtmans *et al.*, 2000). Rather than influencing protein stability via a block of a membrane-bound protease, evidence for a role in the stabilisation of mitochondrially-synthesised proteins of the respiratory chain by direct binding was presented. Prohibitin and Prohibitone putatively act in a multiprotein complex as chaperones in a similar fashion to soluble chaperones.

PHB1 and PHB2 from the yeast *S.cerevisiae* have been demonstrated to exist in a high molecular, ring-shaped protein complex of 1.2 MDa as heteroligomers (Tatsuta *et al.*, 2005). The functions of PHB1 and PHB2 had previously been shown to be interdependent on the other protein's presence (Coates *et al.*, 2001). The ring complex consists of 16-20 assembled PHB subunits and has a diameter of 20-25 nm. It was purified from overexpressed yeast PHBs and imaged using single particle electron microscopy. Both yeast PHBs have been demonstrated to possess non-cleavable, bipartite mitochondrial targeting sequences at their N-termini. Upon mitochondrial import, intermediate complexes of 120 kDa were detected that consist of PHB1 and PHB2 heteroligomers. These complexes then assemble into the final ring complex attached to the inner membrane through the N-terminal hydrophobic domain and face the intermembrane space. The C-terminal coiled-coils are important for the assembly of these large complexes in the inner membrane. The structure of the dimeric heterologous building blocks composed of PHB1 and PHB2 has been modelled based on homology to the NMR structure of the band-7 domain from mouse flotillin-2 (Winter *et al.*, 2007a).

Mammalian prohibitins have been shown to affect cellular senescence and mitochondrial function (Coates *et al.*, 2001). Murine PHBs were shown to be expressed in virtually all tissues and cell types by immunolocalisation. Human PHB1 and PHB2 were demonstrated to be highly expressed in primary tumours. By comparison, their expression level was decreased in senescing fibroblasts. Both proteins were induced by metabolic stress imposed by treatment with thiamphenicol, an inhibitor of mitochondrial protein synthesis. This treatment caused an imbalance of protein synthesis between mitochondria and the nucleus and affected the stability of the electron transport chain. In contrast to this treatment, prohibitins were only slightly upregulated by the application of oxidative stress, heat shock or irradiation with UV light. Their function has been proposed to act as

mitochondrial chaperones upon changes in metabolism triggered by stress. Once mitochondrial function ceases as in the process of aging, prohibitins are lost which is accompanied by the accumulation of reactive oxygen species (ROS). ROS accumulation was directly linked to PHB1 function in bovine endothelial cells (Schleicher *et al.*, 2008). PHB1 was demonstrated to be mitochondrial in this cell type. The knockdown of PHB1 affected the functionality of complex I of the mitochondrial electron transport chain, one of the main sites for mitochondrial ROS production. This led to an increase in mitochondrial ROS production. The ability of complex I to pump protons into the intermembrane space was impaired, resulting in a decrease in membrane potential. However, these defects had no effects on the overall oxygen consumption rates or mitochondrial coupling efficiency. The increase in ROS accumulation led to a senescent phenotype that affected the cytoskeleton and ultimately also angiogenesis (the formation of blood vessels). Additionally, mitochondria had a flattened morphology with densely packed cristae. Remarkably, all observed phenotypes could be reversed when cells were pre-incubated with a ROS scavenger, PEG catalase. Thus, PHB1 is regarded as a regulator of mitochondrial integrity and ROS production at complex I. In its endogenous function PHB1 delays cellular senescence and affects cell proliferation.

Loss of PHB function in HeLa cells led to impaired mitochondrial fusion and fragmented mitochondria. In fact, one of the key processes of PHB function in animal cells is thought to be the proteolytic regulation of OPA1, a dynamin-like GTPase of the inner membrane that mediates mitochondrial fusion events. Mitochondria in animal cells are organised as tubular networks that are maintained by constant fusion and fission events. OPA1 was shown to be unstable via accelerated proteolysis by the mAAA protease in the absence of prohibitins (Merkwirth *et al.*, 2008). Thus, prohibitins are now regarded to act as organisers of the mitochondrial inner membrane. The ring assembly of PHB1 and PHB2 supposedly has a scaffolding function. Prohibitins are proposed to aid in the functional compartmentalisation of the inner membrane, thereby regulating the activity of embedded protein complexes as well as cristae morphology.

1.1.3 Flotillins and Erlins

Flotillins are conserved membrane proteins with a SPFH domain close to their N-terminus. In addition, they possess a unique flotillin domain at their C-terminal end. Mammalian flotillins are localised to the plasma membrane, but also to endosomes, phagosomes, the nucleus and lipid droplets (Browman *et al.*, 2007). Membrane attachment is mediated via N-terminal hydrophobic regions, but also by palmitoylation and myristoylation. Flotillins

typically associate with membrane microdomains such as lipid rafts and caveolae. Flotillins exist as homo- and heterotetramers in microdomains (Solis *et al.*, 2007). Caveolae are specialised membrane invaginations that are involved in vesicle traffic and signal transduction (Bickel *et al.*, 1997; Anderson, 1998). They are present in most cell types except in neurons (but in glial cells/astrocytes). They are characterised by a distinct lipid and protein composition and mainly composed of caveolin proteins, of which there are three major types in mammals (caveolin-1-3). Flotillin is homologous to epidermal surface antigen (ESA) that was originally named flotillin-2; however, it was later shown that ESA and flotillin-2 are two distinct proteins (Hazarika *et al.*, 1999). Flotillin-1 and -2 have a complementary tissue distribution (Volonte *et al.*, 1999) and are also found in brain (Kokubo *et al.*, 2003). Probably they have a scaffolding function at caveolae and other microdomains or might be involved in cell adhesion; other putative roles include neuronal regeneration and insulin signalling (Schulte *et al.*, 1997; Baumann *et al.*, 2000). Caveolins and flotillins are functionally homologous and assemble on the cytoplasmic site of caveolae into homo- and heterooligomers via coiled coils at the C-termini of flotillins (the “caveolar complex”) (Volonte *et al.*, 1999). Generally, flotillins define microdomains that are slightly larger than caveolae and lack caveolins (Lang *et al.*, 1998). Flotillin-1 overexpression is sufficient to induce formation of these domains in heterologous expression systems (Volonte *et al.*, 1999); flotillin-2 overexpression was found to induce formation of filopodia and thus might reorganise the cytoskeleton in epithelial cells (Hazarika *et al.*, 1999; Neumann-Giesen *et al.*, 2004). In macrophages, flotillins are also found in lipid rafts on phagosome membranes to which they are recruited from endosomal organelles. These microdomains are suggested to be sites of phagolysosome biogenesis and represent possible pathogen targets (Dermine *et al.*, 2001). Analysis of the phagosome proteome identified not only flotillin-1, but also trafficking proteins, prohibitins and stomatin (Garin *et al.*, 2001). Trafficking of flotillin-1 to plasma membrane microdomains occurs by a Golgi-independent pathway that depends on the presence of flotillin palmitoylation and myristoylation sites and the conserved SPFH domain (Morrow *et al.*, 2002; Liu *et al.*, 2005; Neumann-Giesen *et al.*, 2004). Additionally, flotillin-1 localisation has been shown to be cell-type specific and interactions with signalling proteins and the actin cytoskeleton have been confirmed (Lang *et al.*, 1998; Liu *et al.*, 2005). Flotillin-1 was also proposed to mediate a novel endocytosis pathway that is independent of clathrin-coated pits and caveolin-1. Flotillin-1 was shown to localise to punctuate structures in the plasma membrane that internalise with GPI anchored proteins and cholera toxin (Glebov *et al.*, 2006).

Erlins (for ER lipid raft protein) are relatively novel, ER localised SPFH domain proteins (Browman *et al.*, 2006). Erlin-1 and erlin-2 are localised to non-caveolar lipid rafts in the ER of human cells. They possess an N-terminal domain responsible for ER targeting and membrane binding as well as the SPFH domain. Erlin-2 is also known as SPFH2 localised to the ER lumen where it is an important component of the ER-associated degradation pathway (ERAD). It is involved in the recognition of substrates such as Inositol 1,4,5-triphosphate (IP3) receptors (Pearce *et al.*, 2007).

1.1.4 HflC/K proteins

The bacterial *hflA* and *hflB* loci (short for high frequency of lysogenisation) are involved in the lysis-lysogeny decision in the life cycle of the bacteriophage λ upon infection of bacteria. The *hflA* locus consists of three genes (*hflX*, *hflK* and *hflC*) and influences proteolytic stability of the phage protein *cII* (Noble *et al.*, 1993). This protein is a transcription factor and a major determinant of the λ lifecycle: depending on its level, the phage either follows a lytic or lysogenic lifestyle. The *hflX* gene encodes for a protein with GTP-binding motifs and might hydrolyse bound GTP. The other two genes, *hflC* and *hflK*, encode for integral membrane proteins that are distantly similar to human band 7.2b and also grouped in the SPFH domain family. At their C-termini, both proteins contain a putative proteolytic domain that is localised to the periplasmic space and together, they form a complex (Kihara & Ito, 1998).

Later it was shown that the *cII* protein is not degraded by the *hflC/K* complex, but by the protease FtsH, an ATP-dependent integral membrane protease that is encoded by the *hflB* locus (Shotland *et al.*, 1997). The *hflC/K* complex binds and modulates the activity of FtsH in a negative fashion (Kihara *et al.*, 1997; Kihara *et al.*, 1996; Shotland *et al.*, 1997). The FtsH protease is localised to the plasma membrane as a large holo-enzyme (1mDa) composed of homo-oligomers and forms hexamers with the *hflC/K* complex (Saikawa *et al.*, 2004). FtsH has a large cytoplasmic domain that contains a conserved motif belonging to the ATP-dependent AAA metalloproteases (Kihara *et al.*, 1997). Therefore FtsH is probably a bacterial ancestor protein of the mitochondrial m- and iAAA proteases. In addition, FtsH has a small periplasmic region that is responsible for protein-protein interactions with the *hflC/K* locus and substrates, and modulation of proteolytic function (Akiyama *et al.*, 1998). A gene termed *hflD* was identified and postulated to function in recruitment of the *cII* transcription factor to the plasma membrane where it is degraded by the FtsH protease (Kihara *et al.*, 2001).

1.2 Stomatin-type proteins

1.2.1 Stomatin protein characteristics

Stomatin, also known as band 7.2b integral membrane protein, or human erythrocyte band-7 integral membrane protein, is a 287 amino acid protein with an apparent molecular weight of 31 kDa. It is one of the major components of the human erythrocyte plasma membrane with approximately 410,000 copies per red cell (Hiebl-Dirschmied *et al.*, 1991a). This membrane shows a characteristic pattern of eight electrophoretic bands when resolved on SDS-polyacrylamide electrophoretic gels that have been numbered according to descending molecular weight (Hiebl-Dirschmied *et al.*, 1991a). Band-7 consists of 4 proteins: band 7.1, band 7.2a (both identified as tropomyosin polypeptides (Hiebl-Dirschmied *et al.*, 1991a)), band 7.2b and band 7.3 when electrophoresed on a two-dimensional SDS-PAGE gel (Lande *et al.*, 1982). The protein is not only present in erythrocytes, but has a wide tissue distribution in humans and other species.

1.2.1.1 First cloning and characterisation of the stomatin gene

The first cloning of the stomatin cDNA was reported almost simultaneously by two independent groups. Hiebl-Dirschmied *et al.* (Hiebl-Dirschmied *et al.*, 1991b; Hiebl-Dirschmied *et al.*, 1991a) isolated cDNA clones by immunoscreening of bone marrow and HeLa cell expression libraries with a monoclonal anti-stomatin antibody. The cDNA encodes an open reading frame of 287 amino acids, which was confirmed by nucleotide sequencing. Protein structure predictions revealed a highly charged N-terminus followed by a 29 amino acid hydrophobic domain and an overall hydrophilic C-terminus. Proteolytic digestion experiments revealed an entire cytoplasmic orientation for both ends of the protein, implicating a monotopic topology. In addition, several phosphorylation sites were predicted, amongst them one for a cAMP-dependent protein kinase. By immunoprecipitation of erythrocyte membrane proteins labelled with [³²P] phosphate, stomatin could be detected on gels both by autoradiography and staining with Coomassie blue. It was noted that the protein has unusual solubilisation properties being only completely soluble in buffers containing the non-ionic detergent Triton-X 100 in concentrations up to 5%.

Almost in parallel Stewart *et al.* (Stewart *et al.*, 1992) isolated a nearly identical (with one different nucleotide) cDNA coding for stomatin from human foetal liver and bone marrow

cDNA libraries following protein purification from healthy red cell membranes. By applying detergents during protein solubilisation, it was noted that the protein is both associated with the plasma membrane and the cytoskeleton, the later presumably by the hydrophilic C-terminus with its net positive charge. Stewart et al. also investigated the human tissue distribution of the protein by Northern blot analysis and found it ubiquitously expressed in a variety of different cells and tissues (e.g. reticulocytes, fibroblasts, liver cells, kidney, brain, gut and heart) except in granulocytes. It was noted that the protein as well as its mRNA were absent in samples derived from patients with overhydrated hereditary stomatocytosis. Topology predictions resulted in the classification of the protein as a type III membrane protein with no extracellular domain and it was suggested that stomatin acts as a bridge between the cytoskeleton and the lipid bilayer, regulating an ion channel.

Originally, the stomatin protein became of interest due to its assumed association with an autosomal-dominant disease called overhydrated hereditary stomatocytosis (OhSt.), a genetic disorder first described over 40 years ago (Lock *et al.*, 1961). The disease is a rare form of haemolytic anaemia in which the protein is either completely missing or its level in erythrocytes is reduced (Lande *et al.*, 1982;Fricke *et al.*, 2003b;Fricke *et al.*, 2003a). Overhydrated stomatocytosis is connected with a temperature-sensitive leak of the monovalent cations Na^+ and K^+ in the red cell membrane and an increase in intracellular H_2O (Innes *et al.*, 1999;Zhu *et al.*, 1999;Fricke *et al.*, 2003a). Affected erythrocytes of patients are shown in Figure 1-1. They have a characteristic cell morphology described as mouth-shaped and swollen, also called stomatocytic (Greek *stoma* = mouth). The name for the missing protein “stomatin” was later derived from the nomenclature of the extraordinary cell shape (Stewart *et al.*, 1992). Due to the net gain of intracellular ions, water passively follows the ions across the membrane, which contributes to the abnormal phenotype of swollen cells (see Figure below) and finally cell lysis; hence, overhydrated hereditary stomatocytosis can be described as a disorder of cell volume control (Hiebl dirschmied *et al.*, 1991b). Because of its association with an ion leakage, the idea was put forward that stomatin acts as a protein regulating an ion channel by direct interaction.

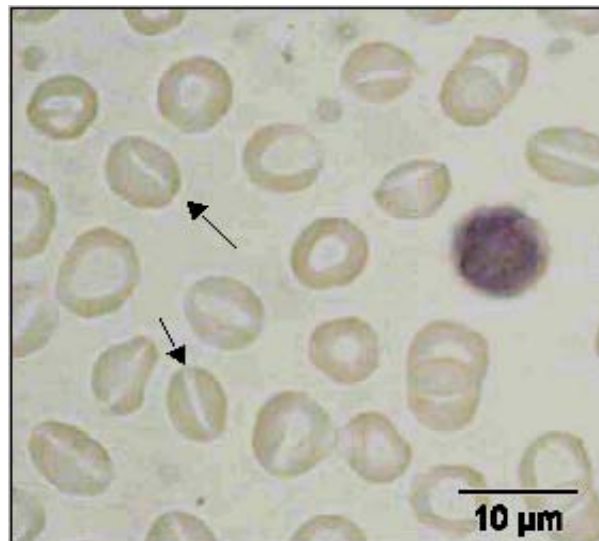


Figure 1-1. Stomatocytotic erythrocytes. A bloodsmear from a patient with overhydrated hereditary stomatocytosis. Note the characteristic stomatocytic cell morphology (arrows). Figure taken from (Green *et al.*, 2004).

Fricke *et al.* (Fricke *et al.*, 2003a) investigated stomatin levels in patients by immunocytochemistry. The protein is not completely absent from erythrocytes, but significantly reduced compared to other organs. It is assumed that stomatin is lost during maturation of red cells in the bone marrow. The authors speculate about a putative involvement of lipid rafts in a vesiculation process that leads to loss of the protein. Stomatin itself has been implicated in regulation of membrane protein expression via raft association (Tavernarakis *et al.*, 1999; Green *et al.*, 2004). More recently, stomatin deficiency in erythrocytes of stomatocytosis patients was explained by a mistrafficking event of the protein to the plasma membrane. Stomatin immunoreactivity was not present at the plasma membrane of erythroid cell cultures, but remained in multivesicular complexes of developing cells (Fricke *et al.*, 2005). Thus, stomatin is lost because of another genetic defect leading to a trafficking abnormality of this protein.

In summary, stomatin is not any longer seen as the direct cause of the disease, but its absence is rather regarded as a secondary effect due to another genetic defect (Mairhofer *et al.*, 2002). No mutation in the stomatin gene has ever been identified in patients with overhydrated hereditary stomatocytosis.

1.2.1.2 Subcellular localisation

Induced expression of stomatin by the cytokine interleukin-6 (IL-6) in combination with the glucocorticoid dexamethasone in the human amniotic cell line UAC was reported (Snyers & Content, 1994). In an attempt to identify genes that respond to treatment with IL-6, a cDNA library of treated cells was screened. Stomatin, and the metal-binding protein metallothionein, were identified as genes that change on their transcription level. Since stomatin RNA and protein levels show a striking response towards this treatment, it is speculated that these agents induce resistance to oxidative stress with metallothionein acting as a scavenger of reactive oxygen species. By applying hydrogen peroxide, pre-treatment of cells with IL-6 and dexamethasone resulted in increased cytoprotection and resistance. Metallothionein is rich in cysteine residues and known to act as an antioxidant and Zn^{2+} -storing protein (Thornalley & Vasak, 1985). Stomatin is also suggested to have a role in cytoprotection in stress situations. Speculations point towards a common stress-protective mechanism for both proteins. Induction of stomatin protein levels might assist stabilisation of membranes and protection against lipid peroxidation.

Another study in UAC cells (human amniotic cells) finally confirmed association of stomatin with the actin cytoskeleton (Snyers *et al.*, 1997). Following induction after treatment with IL-6 and dexamethasone, co-localisation of plasma membrane localised stomatin with actin microfilaments was shown by immunofluorescence and immunoelectron microscopy. This pattern even persisted disruption of the actin cytoskeleton by cytochalasin D, indicating a strong association of stomatin with the cytoskeleton. The subcellular distribution of stomatin was found in two distinct pools in UAC epithelial cells, one concentrated in plasma membrane folds and small protrusions, and the other one in juxtannuclear structures close to the nucleus. Membrane protrusions such as filopodia and microvilli are specialised structures that are enriched in actin fibres. Thus, it is not surprising to find stomatin concentrated at sites of actin clusters.

The second stomatin pool close to the nuclear region has been further investigated in another study (Snyers *et al.*, 1999a). It was shown that stomatin colocalises with the GPI-anchored protein placental alkaline phosphatase (PLAP) at the plasma membrane and the second stomatin pool. PLAP is another protein that is upregulated in UAC cells by IL-6 in conjunction with dexamethasone. By tracking down the internalisation of an anti-PLAP antibody bound to PLAP, and another GPI (glycosyl phosphatidyl inositol)-anchored protein, these stomatin containing structures were identified as endosomes. The juxtannuclear vesicles were also identified as late endosomes, a result that was further

confirmed by labelling with the late endosomal/lysosomal marker protein LAMP-2. Additionally, stomatin and PLAP were found to be co-localised in patch-like structures on the plasma membrane after crosslinking with the anti-PLAP antibody. Finally, stomatin partially associated with detergent-resistant membrane fractions, also known as lipid rafts. This observation indicates that stomatin is functionally linked to GPI-anchored proteins at lipid rafts and might therefore share the same endocytic trafficking events. Due to this observation, it is speculated that band 7.2b functions to concentrate GPI-anchored proteins at specific sites such as microvilli and acts therefore as a scaffolding protein to provide a platform for lipid rafts. In MDCK (Madin-Darby canine kidney) cells, stomatin completely changed its localisation pattern upon polarisation from intracellular vesicular structures to apical microvilli, the site of co-localisation with GPI-anchored proteins (Snyers *et al.*, 1999a).

1.2.1.3 Association of stomatin with lipid microdomains

Lipid rafts are membrane microdomains that are characterised by a specialised lipid composition (mainly cholesterol and sphingolipids) and their property of being insoluble in non-ionic detergents such as Triton-X100 at low temperatures. Classically, they have been isolated by discontinuous sucrose gradient centrifugation of Triton-X100-treated membrane preparations and are found in the low-density fraction (so called “floatation assay”) (Lucero & Robbins, 2004). The concept of liquid-ordered, sterol and sphingolipid-enriched microdomains in a “sea” of otherwise rather homogenous lipids and proteins assists the understanding of protein organisation and function in membranes. Lipid rafts have been associated with cellular processes such as cell signalling or vesicle trafficking, in which protein complexes might become locally concentrated at raft-specific sites and form clusters; in addition, the duration of protein interactions in higher complexes might be increased by association with lipid rafts (Brown & London, 2000). Therefore, a concept emerged of raft domains as regulatory mechanisms by which the function of temporarily resident proteins can be controlled (Lucero & Robbins, 2004). The application of different detergents reveals distinct raft species with specialised lipid and protein compositions. These properties in turn influence the various proteins they contain and their interaction partners. Typically, raft-associated proteins are acylated or have other additional lipid anchors such as GPI anchors. Although lipid rafts have been mainly investigated from plasma membranes, they also exist in endomembranes of organelles such as the Golgi apparatus or endosomes, and are generally involved in intracellular networks (Lucero & Robbins, 2004). It is now increasingly clear that lipid rafts are involved in membrane fusion

processes in their regulation, budding and vesiculation; additionally, they might function in cargo selection and inclusion of sorting molecules into vesicles (Salzer *et al.*, 2002; Lucero & Robbins, 2004; Salaun *et al.*, 2004).

Specific associations of stomatin and flotillins -1 and -2 with lipid rafts have been demonstrated in plasma membrane preparations from human red cells (Salzer & Prohaska, 2001b). Stomatin, flotillins and the GPI-anchored protein acetylcholine esterase were identified as the major components of detergent-insoluble membrane fractions by Western blotting. In addition, the cytoskeletal compounds actin and spectrin, and erythrocyte band 4 proteins were identified. Flotillin-1 and -2 are associated with caveolae, another type of membrane microdomains. Alkaline extraction of raft preparations allows integral membrane proteins to be distinguished from peripherally attached proteins. By applying this technique, the integral nature of stomatin and the flotillins was confirmed, in contrast to the cytoskeletal proteins that are solubilised under these conditions. It was also confirmed that both stomatin and the flotillins exist as higher oligomers in red cell lipid rafts after sucrose gradient centrifugation, although they do not interact with each other. It is assumed that both stomatin and flotillins act as scaffolding proteins in the stabilisation and localisation of protein complexes at independent types of lipid rafts, putatively associated with the cytoskeleton or signalling molecules.

Upon a rise in cytosolic Ca^{2+} -concentration, erythrocytes release specific micro- and nanovesicles by a raft-based mechanism (Salzer *et al.*, 2002). Two different vesicle species are found and characterised by their specific protein content: microvesicles enriched in stomatin, and nanovesicles mainly containing the proteins synexin and sorcin. The membranes surrounding both vesicle types contain lipid rafts with distinct protein compositions from usual plasma membrane derived rafts: they do not contain any of the classical raft proteins such as flotillin-1 or flotillin-2, but they are enriched in GPI-anchored proteins. Several other proteins are found in both vesicles, amongst them haemoglobin, carbonic anhydrase and acetylcholinesterase. Synexin, also called annexin VII is known to be involved in membrane fusion processes, probably acting in the release of vesicles from erythrocytes. Elevated Ca^{2+} levels cause synexin to be translocated from the cytosol to the plasma membrane by association with acidic membrane lipids and incorporated into vesicles, a process that does not occur when Ca^{2+} is replaced with EDTA. It is very likely that the protein itself is involved in the process of vesicle release (Gerke & Moss, 2002; Hayes *et al.*, 2004). Sorcin, the other protein that becomes enriched in nanovesicles, binds to synexin in a Ca^{2+} -dependent manner. A conformational change in the protein influences its hydrophobicity and causes association with membranes. The

protein contains several EF-hand motifs and probably acts in a Ca^{2+} -dependent signalling pathway that might have a regulatory role in exocytosis.

More recently, raft structure and functionality in erythrocytes from patients with overhydrated hereditary stomatocytosis (OhSt.) were investigated (Wilkinson *et al.*, 2008). Isolated detergent-resistant membranes from healthy erythrocytes normally associate with about 29% of the total cellular actin. By comparison, erythrocytes from stomatocytosis patients had a reduced content of DRM-associated actin (only 10%). Additionally, it was found that reduced amounts of the actin-associated protein tropomodulin were DRM-associated. Overexpression of stomatin in MDCK cells that normally express this protein only at low levels increased the amounts of actin bound to the plasma membrane. Ca^{2+} -dependent exovesiculation has been shown to involve stomatin-specific microdomains (Salzer *et al.*, 2002). The formation of these exovesicles in erythrocytes from OhSt. patients was also altered (Wilkinson *et al.*, 2008). In particular, the number of microvesicles was reduced, and they were larger in size. By comparison, nanovesicles were more abundant, but smaller in size. These vesicles contained increased amounts of flotillins-1 and -2, and the Ca^{2+} -binding proteins annexin VII, sorcin and copine1 as compared to vesicles from healthy erythrocytes. No actin was associated with exovesicles from stomatocytosis patients, as opposed to vesicles from healthy erythrocytes. Thus, association of stomatin with actin regulates Ca^{2+} -induced vesiculation by maintaining the structure and function of stomatin-associated microdomains in erythrocytes. Stomatin is considered to be a structural protein that is tethered to actin; this complex has regulatory functions in Ca^{2+} -induced vesiculation of erythrocytes.

A role for stomatin in organising lipid rafts in alpha granules (intracellular structures of platelets) to provide a platform for specific signalling complexes, or as an attachment site for the cytoskeleton in granule exocytosis was suggested (Mairhofer *et al.*, 2002). The authors found distinct types of rafts that differed in their protein composition depending on their intracellular localisation and on the detergent used in the preparation. Stomatin was shown to be specifically enriched in Triton-X100 lipid rafts from alpha granules, together with other proteins such as actin and CD36. It is also localised to the cell periphery, but to a lesser extent. Upon activation of platelets by thrombin, alpha granules with bound stomatin are specifically translocated to the plasma membrane where they fuse and release their content. Stomatin is cleaved proteolytically and specifically incorporated into released microvesicles, similar to the ones obtained from erythrocytes. Thus, the process of microvesiculation probably underlies a raft-based mechanism that distinguishes between different raft species with specific protein contents.

Overexpressed stomatin was found to be associated with lipid storage bodies in MDCK cells when treated with external oleic acid (Umlauf *et al.*, 2004). GFP-tagged stomatin and a N-terminally truncated mutant of caveolin were localised to both identical and distinct lipid raft domains on lipid bodies, and eventually co-localised. Overexpressing mutant stomatin forms lacking the hydrophobic domain abolished this association. When protein synthesis was blocked with cycloheximide, GFP-tagged stomatin redistributed to vesicles that were identified as late endosomes or lysosomes; this finding indicates trafficking routes via the endosomal pathway, consistent with previous publications that identified cytoplasmic stomatin-containing vesicles from a group of late endosomes or lysosomes (Snyers *et al.*, 1999a). A lipid body proteome analysis identified stomatin, cytoskeletal compounds, Rab GTPases and various other proteins connected to lipid metabolism, transport and signalling networks (Umlauf *et al.*, 2004). Since stomatin is a raft-associated protein, it is suggested that it acts as an oligomeric scaffold or as a signalling component in trafficking events, maybe in cargo selection or vesicle budding and fusion. Therefore, stomatin might also have an indirect role in the control of metabolic events.

1.2.1.4 Phosphorylation

The exact phosphorylation site of human band 7.2b was determined one year after the gene was cloned (Salzer *et al.*, 1993). Labelling with [³²P] phosphate in the presence of cAMP, followed by immunoaffinity purification, proteolytic digestion and sequencing of labelled peptides revealed the phosphorylation site. The only identified phosphorylation site is serine 9 close to the N-terminus, a finding that further supports the monotopic topology prediction for stomatin. The model for the membrane association of stomatin proposes insertion by a hydrophobic hairpin-like loop into the bilayer and further stabilisation by palmitoylation of the protein. In this fashion, stomatin is solely exposed at the cytoplasmic site with both termini, thereby potentially interacting with other proteins or the cytoskeleton. Very recently it was demonstrated that a single conserved proline (P47 in the hydrophobic domain) is responsible for this conformation. A small fraction of the stomatin pool exists in a single membrane-spanning conformation that is N-glycosylated at the C-terminus. This post-translational modification gives rise to a higher molecular weight upon stomatin overexpression in oocytes. This modified stomatin form was also detected in mouse erythrocytes. Upon mutation of the conserved proline, the entire stomatin pool adopted the membrane-spanning form. Currently it is not known whether this low abundance transmembrane pool has any physiological function (Kadurin *et al.*, 2008b).

1.2.1.5 Palmitoylation

Metabolic labelling with [³H]-palmitic acid of stomatin expressed in UAC cells has identified the major palmitoylation site (Snyers *et al.*, 1999b). Stomatin expression was induced and cells incubated with tritiated palmitic acid, followed by lysis with Triton-X100 and immunoprecipitation. Incorporation of [³H] is sensitive to treatment with hydroxylamine, a reagent reacting with free sulfhydryl groups from cysteine residues. Altogether, the stomatin protein sequence has three cysteines that putatively react with palmitate. The exact palmitoylation residues were determined by mutagenesis experiments. Changing cysteine 29 to serine had the most striking effect on palmitate incorporation, whereas the mutation of two other cysteines had either no effect or resulted in reduced incorporation (cysteine 86) of palmitate. Quantification of incorporated tritium by scanning densitometry further confirmed this result: 70-85% of palmitate is found attached to cysteine 29 and the rest at cysteine 86. This finding is in accordance with general assumptions concerning acylation: these two cysteine residues are likely to be located very close to the membrane on the cytoplasmic side on each site of the hairpin insertion loop, thus facilitating attachment on the intracellular site. This might also contribute to a local increase in palmitic acid at spots of stomatin oligomerisation such as in lipid rafts.

1.2.1.6 Oligomerisation

The fundamental structure of the stomatin protein has been shown to be homo-oligomeric (Snyers *et al.*, 1998). Between nine to twelve homodimers putatively assemble into a higher complex in the plasma membrane, linked via their stomatin-like C-terminal ends when overexpressed in UAC cells after induction by IL-6 and dexamethasone. This self-interaction was first indicated by crosslinking studies in UAC cells using the crosslinking agent DSS (disuccinimidyl suberate) following induction. Western Blot analysis of lysed cell extracts showed the monomeric stomatin band as well as additional bands indicating dimers, trimers and higher oligomeric species up to 300 kDa. In contrast, C-terminally truncated versions of stomatin failed to co-immunoprecipitate or localise to the plasma membrane, indicating mediation of the self-interaction by the C-terminal part. Since oligomers are found in both the plasma membrane pool and the intracellular vesicle pool, a model was suggested that favours oligomerisation of stomatin from an early stage on, probably by assembly during biosynthesis and trafficking via Golgi-derived vesicles. Stomatin oligomerises in the erythrocyte plasma membrane to even higher complexes of 200-600 kDa (Salzer & Prohaska, 2001b).

Later the exact sites responsible for oligomerisation and raft association were mapped by analysing the size and buoyancy of truncated proteins and point mutations (Umlauf *et al.*, 2006). This study actually revealed that both oligomerisation and raft association were not mediated by the SPFH/band-7 domain. The responsible residues were mapped to the C-terminus. For oligomerisation, a crucial stretch of hydrophobic residues was identified (amino acids 264-272). Within this stretch, three amino acids (266-268, IVF) were identified as responsible for the association with detergent-resistant membrane fractions. Interestingly, it was shown that oligomerisation is not a prerequisite for raft association. The N-terminal proximal hydrophobic domain supposedly aids membrane association, but is not responsible for lipid raft localisation of stomatin. When internal amino acid stretches near the hydrophobic domain were deleted, intermediate size oligomers could be observed, hinting at conformational interdependence of the C-terminus. FRAP (fluorescence recovery after photobleaching) analysis demonstrated that C-terminal truncation mutants (amino acids 1-262) were able to move laterally in the plasma membrane, whereas the native protein is relatively immobile. This further highlights the importance of membrane interaction by the C-terminal end.

1.2.1.7 Stomatin protein interactors

Stomatin interacts with the α/β heterotetramer adducin, a peripheral membrane protein modulating the erythrocyte spectrin and actin cytoskeleton (Li *et al.*, 1998; Gardner & Bennett, 1987). The interaction was found in a gel overlaying assay with the C-terminal stomatin domain (Sinard J.H., 1994) and further confirms that stomatin is linked to the cytoskeleton, putatively mediating signals related to mechanical deformation (see later). Adducin is involved in the early assembly of the cytoskeleton in the bundling of actin and spectrin, and it is phosphorylated by protein kinase C (Matsuoka *et al.*, 1998).

Another stomatin-interacting protein in red cells is calpromotin (Moore & Shriver, 1997). It is a soluble cytosolic erythrocyte protein involved in activating charybdotoxin-sensitive Ca^{2+} -dependent K^+ channels, a process in which the protein is recruited to the plasma membrane. Several erythrocyte proteins bind to a calpromotin affinity column, amongst them cytoskeletal compounds, band 6 (Glyceraldehyde-3-phosphate dehydrogenase) and band 7.2b. The interaction between calpromotin and the cytoskeletal proteins is weak, since the bound proteins were derived from extraction in low salt conditions, whereas the interaction with band 7.2b could only be proved after extraction with buffer containing Triton-X100. The stomatin interaction might be interpreted as an indication for the

involvement of both proteins in the regulation of monovalent cation channels, although this assumption is unlikely for stomatin in erythrocytes.

The glucose transporter GLUT-1 is negatively regulated by binding to stomatin in erythrocytes (Zhang *et al.*, 2001). By overexpression of human or murine band 7.2b in Clone 9 cells (a rat liver cell line expressing GLUT-1 as the only glucose transporter), glucose transport rates were significantly reduced, a relationship that correlated with the level of overexpressed protein (in some clones up to 50% reduction in glucose transport). The domain responsible for the interaction has been mapped to the cytoplasmic C-terminal end of the transporter by GST-GLUT-1 fusion protein pull-down experiments. Thus, stomatin overexpression affects glucose transport (by GLUT-1) directly via protein-protein interaction. It does not affect the expression level of GLUT-1 at the plasma membrane. This result suggests a function for stomatin in the “masking” of GLUT-1 and thus in the determination of its transport activity.

A very recent study found direct effects of stomatin in erythrocytes on the specificity of GLUT-1 transport (Montel-Hagen *et al.*, 2008). In humans, GLUT-1 is most highly expressed in erythrocytes compared to any other cell type. The authors demonstrated that GLUT-1 undergoes a switch from glucose transport to the transport of DHA (dehydroxyascorbic acid, an oxidised form of ascorbic acid). This switch is regulated by stomatin and leads to a decrease in glucose uptake during erythrocyte development under simultaneous enhancement of DHA uptake. In patients with overhydrated hereditary stomatocytosis, DHA transport was decreased by 50%, under simultaneous increase of glucose uptake. It has been previously shown that GLUT-1-association with stomatin favours localisation to detergent-resistant membrane fractions, under a simultaneous decrease of glucose uptake (Rubin & Ismail-Beigi, 2003). This is promoted during erythropoiesis (the development of erythrocytes) by an increase in stomatin mRNA. Interestingly, the change in GLUT-1 transport specificity is unique to humans and mammals unable to synthesise ascorbic acid. By comparison, mice that are capable of ascorbate synthesis express the glucose transporter GLUT-4 instead of GLUT-1 in erythrocytes. Thus, this specific co-expression of GLUT-1 and stomatin in humans is understood to be a compensatory response in mammals unable to synthesise ascorbate.

1.2.2 Ion channel regulation by stomatin homologues

Stomatin is highly conserved with homologues in all three domains of biology and must be very ancient. Its high degree of conservation is found in the stomatin-like domain that is defined by a characteristic signature sequence (29aa PROSITE pattern PDOC00977: $RX_2(L/I/V)(S/A/N)X_6(L/I/V)DX_2TX_2WG(L/I/V)(K/R/H)(L/I/V)X(K/R)(L/I/V)E(L/I/V)(K/R)$) (Tavernarakis *et al.*, 1999). All sequenced eukaryotes (except budding yeast) have at least one close homologue that is identified by the signature sequence in the central part of the proteins. Structurally, the homologues are very similar with the exception of some bipartite stomatins that have an additional functional domain. Most frequently, the N-termini and the very C-termini of stomatin homologues differ remarkably from each other. This might indicate that these residues have evolved separately to optimise protein-interactions for their different functions (Schlegel *et al.*, 1996), whereas conserved parts indicate functional importance for stomatin homologues.

Regulation of ASIC channels by stomatin

In mammals, a group of acid sensing ion channels (abbreviation ASIC) are homologous to ENaC/degenerin channels. These channels are expressed in sensory and central neurons, and are gated by protons. They assemble into homo- and heteromultimers and function by sensation of acidosis in tissue ischemia and pain reception (Price *et al.*, 2004). Stomatin is also expressed in mammalian sensory neurons as shown in mice: the protein is detected in all sensory neurons in murine dorsal root ganglia in a punctuate manner at plasma membranes of soma and axons (Mannsfeldt *et al.*, 1999). As development progresses, its expression level changes and it is particularly detectable in mature mechanical sensory neurons. Similar to stomatin homologues in *C.elegans*, vertebrate stomatin might be a part of a mechanotransduction complex. In rat, ENaC homologues and stomatin are co-expressed in trigeminal mechanosensory neurons and might play an analogous role to *C.elegans* mec genes (Fricke *et al.*, 2000). Stomatin has been shown to interact physically with various murine ASIC subunits and to decrease current amplitude when co-expressed with the ASIC-3 subunit in CHO cells, but not with the 2a or 1a subunit (Price *et al.*, 2004). The authors demonstrated that stomatin does not influence the amount of channel protein expressed, but it gates the channel by direct interaction. Thus, stomatin binding to either subunit alone is not sufficient for regulation of the channel. Stomatin might act as an accessory subunit as part of the channel, or it might gate the channel indirectly by interaction with other proteins. The whole ion channel complex might be located to lipid rafts, to which stomatin recruits other interacting proteins.

1.2.2.1 Human and mammalian homologues

Various human stomatin homologues have been identified in the past years, helping to elucidate the cellular processes in which the protein is involved.

HsSlp-1

A protein named human stomatin-like protein 1 (hSLP-1) was cloned from a human cerebral cortex cDNA library (Seidel & Prohaska, 1998). From the sequence it was deduced that this protein has a bipartite structure, consisting of an N-terminal stomatin-like domain and a C-terminal nsLTP-like (non-specific lipid transfer protein) domain. It is mainly expressed in heart, skeletal muscle and brain, especially in the basal ganglia, putatively complementing for the low expression levels of stomatin in this organ. Its closest homologue is the *C.elegans* protein UNC-24 that has the same bipartite structure (see later for details about UNC-24) indicating an evolutionary link between these two proteins. The putative lipid transfer domain might be involved in transport of lipids such as cholesterol between adjacent organelle membranes.

HsSlp-2

A second human stomatin homologue called human stomatin-like protein 2 (hSLP-2) was cloned from a human heart cDNA library and characterised (Wang & Morrow, 2000). This protein is described in detail in section 1.4, because it is the most closely related human protein to Arabidopsis stomatin-like proteins.

Stomatin-like protein-3

Murine stomatin-like protein-3 (Slp-3) has been demonstrated to be an essential subunit of a mammalian mechanotransducing protein complex (Wetzel *et al.*, 2007). It was shown that sensory neurons mediating mechanosensation in dorsal root ganglia (DRG) of mice express stomatin, and also Slp-3. The Slp-3 protein is selectively expressed in neuronal tissues. Upon overexpression of Slp-3 in HEK-293 cells, H⁺-gating of endogenous ASIC channels was measured, similar to the effect of stomatin (see above). Additionally, it was shown that Slp-3 physically interacts with and regulates mechanosensitive ASIC 2a and 2b channels. In the *slp-3* null mice, 35% of the skin mechanosensory receptors did not respond to mechanical stimuli. Thus, about one third of sensory neurons use

mechanosensory ion channels that function dependent on Slp-3. This protein is now regarded as an essential subunit of a mammalian mechanotransducing protein complex.

Podocin

A gene called NPHS2 is involved in an autosomal recessive kidney disorder and encodes a stomatin-like protein in podocytes, specialised kidney epithelial cells in the glomerulus (Roselli *et al.*, 2002). The protein was named podocin and shares the basic structural features with stomatin. *In situ* hybridisation experiments using human, murine or rat kidney revealed an expression pattern that changes according to the developmental stage of the human kidney. Podocin is mainly expressed in the mature glomerulus. Electron microscopy with a polyclonal antibody against podocin confirmed the cytoplasmic orientation of podocin in accordance with the predicted monotopic structure. The authors suggest that podocin might serve as an anchor to connect the podocyte cytoskeleton with compounds of the slit diaphragm, an intercellular junction specific for podocytes. The podocin C-terminus contains a proline-rich region that might act as an interaction site with SH3 (Src homology) domain proteins. A gene called NPHS1 encodes another protein localised to the slit diaphragm named nephrin. This protein is a membrane protein with an extracellular domain that has attachment sites for immunoglobulins and fibronectin, and a small intracellular domain. Both nephrin and podocin are involved in the permeability of the glomerulus since mutations in any of the genes cause nephrotic symptoms. Huber *et al.* demonstrated that the two proteins interact and that this interaction facilitates nephrin-mediated cell signalling (Huber *et al.*, 2001). Later the same group proved that podocin forms homo-oligomers (20-50 molecules) at the podocyte plasma membrane and associates with lipid rafts, thereby recruiting nephrin to these microdomains (Huber *et al.*, 2003). The interaction between podocin and nephrin is mediated through the podocin C-terminus with its stomatin-like domain and the C-terminal end of nephrin. Mutated podocin, as it occurs in nephrotic syndromes, fails to target nephrin to raft domains due to a failure to associate with rafts and abolishes nephrin-signalling. These findings suggest that nephrin-recruitment to lipid rafts facilitates nephrin-based signalling processes mediated through its tyrosine-phosphorylated cytoplasmic end, and might explain the basis of the pathogenesis of hereditary nephrotic syndrome.

Podocin from mouse and the *C.elegans* stomatin homologue Mec-2 were shown to bind cholesterol through their SPFH domain (Huber *et al.*, 2006a). Cholesterol binding was most efficient if a part of the adjacent N-terminal hydrophobic domain was also included. Both podocin and Mec-2 associate with ion channels and other proteins in multimeric

complexes at the plasma membrane. Podocin was shown to bind to and modulate the activity of TRPC6 (transient receptor potential C channel) and to colocalise with the channel at the slit diaphragm. TRPC6 is a relatively non-selective cation channel. Podocin is localised in a multimeric mechanosensory complex involving TRPC6, nephrin, Neph-1, Neph-2 and the cytoplasmic adaptor protein CD2AP. Mutations in any of these genes can cause nephrotic syndromes by disruption of the filtration barrier. Podocin oligomerisation does not require cholesterol binding, but cholesterol binding was proven to be crucial for modification of TRPC6 currents when expressed in oocytes. One proline residue inside the N-terminal hydrophobic domain of podocin (P120) was shown to be responsible for cholesterol binding. If mutated, the protein was no longer able to activate TRPC6 currents and did not bind cholesterol. When the two palmitoylation sites of podocin were mutated, cholesterol binding and channel activation were weaker, but still present. Thus, a specified function was shown for the SPFH domain, namely the ability to bind sterols and assemble large multimeric complexes. Cholesterol recruitment or enrichment at specific sites supposedly changes the lipid environment of embedded complexes. Generally, cholesterol leads to stiffening and widening of lipid bilayers, thus affecting locally embedded protein complexes.

1.2.2.2 Stomatin proteins from *C.elegans*

Mec-2

The best-characterised stomatin homologues are the ones from the nematode *C.elegans*. Its genome encodes thirteen Mec genes that are involved in mechanosensation and locomotion of the worm (Gu *et al.*, 1996; Tavernarakis & Driscoll, 1997) and altogether ten stomatin-like genes (Bargmann, 1998; Sedensky *et al.*, 2004). The first nematode stomatin discovered was the Mec-2 gene, that is structurally very similar to stomatin (65% identical and 85% similar to band 7.2b) (Huang *et al.*, 1995). It functions in six specified touch receptor neurons that mediate mechanosensation; *mec-2* mutants have a touch insensitive phenotype. In genetic studies, Mec-2 was found to interact with and regulate a sodium channel (Gu *et al.*, 1996) that is composed of three other Mec genes, Mec-4, Mec-6 and Mec-10 (Chelur *et al.*, 2002). This channel is most closely homologous to mammalian epithelial sodium channels (ENaC) and belongs to the degenerin family of ion channels. The ion channel regulation has been confirmed by electrophysiological measurements of overexpressed Mec-2 and degenerin subunits in *Xenopus* oocytes (Goodman *et al.*, 2002). Mec-2 interaction increases amiloride-sensitive Na⁺ currents of overexpressed Mec-4 and Mec-10 mutants about forty times and positively regulates wild type currents. This was

the first direct evidence for ion channel regulation by a stomatin-like protein. It was proposed that the stomatin-like domain of Mec-2 provides a scaffold to facilitate the interaction with the channel whereas the N-terminus of Mec-2 interacts with microtubules (Huang *et al.*, 1995). Mec-2 is expressed along touch receptor axons (Huang *et al.*, 1995); this expression pattern is disturbed when a microtubule-encoding gene, Mec-12 is mutated. Therefore, a model exists (see Figure 1-2) in which Mec-2 acts as a link between the microtubule cytoskeleton and the ion channel in touch receptor neurons. The ion channel is linked directly to the extracellular matrix (encoded by collagen genes Mec-1, Mec-5 and Mec-9) and to the underlying microtubules (Mec-7 and Mec-12 genes) via Mec-2. Other Mec genes of unknown function also contribute to this mechanosensory complex (Gu *et al.*, 1996). Deformation of the microtubules that have a particularly large diameter in the touch receptors is proposed to cause channel opening by positive regulation of the stomatin homologue (see Figure below). In addition, Mec-6 co-localises with Mec-4 in a punctuate pattern that might represent lipid rafts or other plasma membrane microdomains (Chelur *et al.*, 2002) and Mec-2 co-localises with Mec-4 in a similar fashion (Zhang *et al.*, 2004). This expression pattern requires all channel components and the stomatin-like domain of Mec-2. However, this conserved part of Mec-2 is only required for binding to Mec-4, but not for the actual regulation of the channel (Zhang *et al.*, 2004).

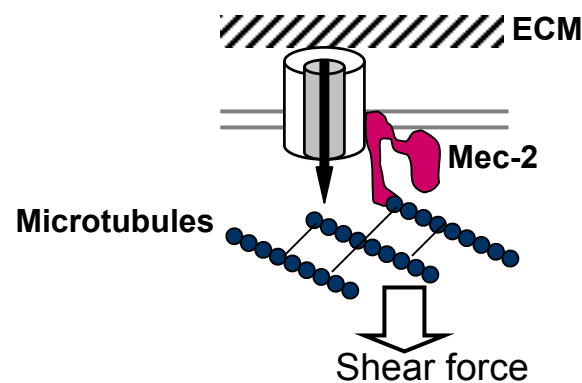


Figure 1-2. Schematic representation of ion channel regulation by Mec-2 in *C.elegans* mechanosensation. The mechanosensory ion channel is represented by the cylinder shape. Mec-2 is shown in red and functions as an adapter between the channel and the underlying microtubule cytoskeleton (shown as chain structures). Pressure put on the extracellular matrix (=ECM) is transmitted through the channel and to the microtubules resulting in the generation of shear forces. This figure is redrawn from Gu *et al.* (Gu *et al.*, 1996)

Mec-2 was also demonstrated to directly bind cholesterol through its SPFH domain in the same study as podocin was (Huber *et al.*, 2006a). Mec-2 associates with the DEG/ENaC channel at the plasma membrane of touch receptor neurons in punctuate structures. As with podocin, cholesterol binding by Mec-2 depended on the presence of the SPFH domain and

was enhanced when the protein was palmitoylated. As in podocin, a single conserved proline residue (P134) located at the same relative position was responsible for cholesterol binding. Mutation of this residue to serine abolished cholesterol binding and led to touch insensitivity of the worms. The proline mutation did not, however, affect Mec-2 localisation to the PM, oligomerisation or interaction with Mec-4. However, the punctate plasma membrane localisation of the Mec-2 protein was lost in this mutant, giving rise to a less defined plasma membrane localisation. Thus, the loss of touch sensitivity resulted from the loss of cholesterol binding by the conserved proline residue localised adjacent to the SPFH domain. Binding of cholesterol promotes the formation of higher order structures whose assembly is regulated by protein-lipid complexes constituted of Mec-2 oligomers. The formation of such higher complexes is now regarded as the conserved function of SPFH domain proteins of different types. Putatively, these complexes generate a specified lipid environment important for the regulation of the proteins' function.

This example also illustrates the possibility that stomatin-gated ion channels might be a conserved feature between invertebrates and vertebrates. However, *C.elegans* Mec-2 positively regulates the degenerin channel, whereas stomatin negatively influences acid sensing ion channel subunits. Price et al. (Price *et al.*, 2004) speculate that stomatin interaction might change the channel's specificity from a pH sensor to a mechanosensor and therefore ASICs might also be involved in vertebrate mechanosensation. Another point is that Mec-2 expression is restricted to sensory neurons, whereas stomatin has a wide tissue distribution. Probably, stomatins have evolved differently in species, and in vertebrates they might have adapted new roles depending on interacting proteins and their cellular environment.

Unc-24

Another stomatin-like protein in *C.elegans* interacts with Mec-4 and Mec-2 via its SPFH domain (Zhang *et al.*, 2004). The product of the Unc-24 gene is an unusual bipartite protein that has a stomatin-like domain at its N-terminus and a nsLTP motif (short for non-specific lipid transfer protein, also named sterol carrier protein 2) at its C-terminus (Barnes *et al.*, 1996). Functional Unc-24 is localised to lipid rafts (Sedensky *et al.*, 2004) and required for normal locomotion and sensitivity towards volatile anaesthetics (Sedensky *et al.*, 2001b) of the worm. It is also suggested to be involved in lipid transfer between closely located membranes (e.g. vesicle to target membrane) or general regulation of lipid composition. Additionally, the lipid transfer domain is implicated to have a function in

neuron outgrowth or synaptogenesis and thereby somehow influencing locomotion of the worm.(Barnes *et al.*, 1996).

Unc-1

Closely related to Unc-24 is the Unc-1 protein that also has a stomatin-like domain in its central part (Barnes *et al.*, 1996;Rajaram *et al.*, 1998). Genetically, Unc-24 is epistatic to the Unc-1 gene and physically affects Unc-1 distribution in the *C.elegans* nervous system, possibly via targeting to the plasma membrane (Sedensky *et al.*, 2001b). Unc-1 is involved in the sensitivity of the nematode to volatile anaesthetics whose putative interaction sites might be concentrated at lipid rafts. Volatile anaesthetics might interrupt protein organisation via interactions with lipids. (Sedensky *et al.*, 2001b;Sedensky *et al.*, 2004). Altogether, eight genes in *C.elegans* are involved in sensitivity to volatile anaesthetics (Sedensky & Meneely, 1987) in a functional pathway in which the Unc-1 gene is supposed to be a central player. Mutants of *unc-1* in the stomatin-like domain are affected in their normal locomotion and have an altered behaviour towards volatile anaesthetics (Rajaram *et al.*, 1999). Unc-1 is expressed widely in the nervous system of the nematode (Rajaram *et al.*, 1999) in the plasma membrane of neuronal axons (Sedensky *et al.*, 2001b). The Unc-8 gene is an ENaC subunit homologue that genetically and physically interacts with Unc-1 in motoneurons (Rajaram *et al.*, 1999) in lipid rafts (Sedensky *et al.*, 2004). Together, they form a complex with Unc-79 that controls ion flux through a sodium channel that is a possible target for interactions with volatile anaesthetics (Rajaram *et al.*, 1999), senses stretch during movement and mediates muscle contractions (Tavernarakis *et al.*, 1997).

More recently, Unc-1 was found to regulate the activity of Unc-9 gap junction channels in body wall muscle cells of *C.elegans* (Chen *et al.*, 2007a). Gap junctions are relatively non-selective channels formed by two hemichannels. Each hemichannel consists of six innexin subunits in invertebrates, or connexin or pannexin subunits in vertebrates. The *C.elegans* genome expresses altogether 25 innexins, and 10 stomatin-like proteins. Amongst these, the innexins Unc-7 and Unc-9, and the stomatin-like proteins Unc-1 and Unc-24 all display a similar mutant phenotype. Unc-24 is apparently required to stabilise the Unc-1 protein (Sedensky *et al.*, 2001a). *Unc-1* and *unc-9* knockout animals are both characterised by inhibited locomotion. Junctional currents between body wall muscle cells in *unc-1*, *unc-9* and *unc-1/unc-9* double mutants were analysed (Chen *et al.*, 2007a). Electrical coupling in all these mutants was inhibited by 70%. Unc-1 and Unc-9 co-localised at intercellular junctions and were coexpressed in neurons and body wall muscle cells. The *unc-1* mutation had no effect on Unc-9 protein expression or localisation. Curiously, overexpressed Unc-9-

GFP acted as a gain-of-function mutant that was able to form functional gap junctions in the *unc-1* mutant. Unc-1 is thus not regarded as a structural subunit of gap junction channels, but as a regulatory protein. A model was suggested in which the Unc-9 gap junction channel is closed in the absence of Unc-1. Unc-1 supposedly interacts with the gating domain of Unc-9, regulating the channel's conductance.

1.2.3 Prokaryotic stomatins

Stomatin-like proteins are not restricted to eukaryotes. Sequenced genomes of various prokaryotes contain open reading frames that encode putative stomatin-like proteins, but only few of them have been characterised yet.

A stomatin-like protein from the soil bacterium *R. etli* is involved in competition for root nodulation of the common bean (You *et al.*, 1998). Structurally, the prokaryotic version is overall quite similar to human stomatin. A stomatin mutant of the strain is defective in nodulation competition and has a decreased salt tolerance. It might be involved in ion transport coupled to nutrient uptake. However, not all nodulating rhizobium strains carry this gene. The authors suggest that it might present an advantage for nodulation competition in some rhizobia, but it is not essential for nodule formation and nitrogen fixation.

Green *et al.* have described one case of a catastrophic multisystem disease, a disorder caused by a splice variant of the stomatin mRNA (Green *et al.*, 2004). It is suggested that this mutation is causing a human knockout of stomatin and therefore affecting a wide variety of tissues rather than only red cells, as in the case of overhydrated hereditary stomatocytosis. Using BLAST searches for prokaryotic stomatins, a gene known as “nfeD” (for “nodulation formation efficiency D”) has been identified in 23 prokaryotes (Green *et al.*, 2004). In 16 of these organisms, the gene is closely connected to a prokaryotic stomatin (= pstomatin); these two genes putatively form an operon that is transcribed by a single polycistronic mRNA and are functionally linked. NfeD itself was originally assigned to be an ornithine cyclodeaminase involved in root colonisation of legumes by nitrogen fixing soil bacteria. However, the NfeD gene in the putative operon does not show any homology to the originally assigned NfeD gene product and was renamed as STOPP (for “stomatin operon partner protein”). It encodes for a hydrophobic protein with 6-8 predicted transmembrane domains and one putative ClpP-type serine protease motif. In addition, the protein has one central sterol-sensing domain that also occurs in eukaryotes; the STOPP proteolytic system might be involved in stress adaptation mechanisms of bacteria. Thus,

stomatin is proposed to act as a partner protein in a membrane-bound proteolytic process. This function for band-7 family proteins might be conserved between prokaryotes and eukaryotes.

A stomatin-containing operon has also been identified in the hyperthermophilic archaeobacterium *P.horikoshii* (Yokoyama & Matsui, 2005). Two open reading frames encode homologues to STOPP (PH1510) and stomatin (PH1511). The protease part of STOPP was purified and identified as an unusual serine protease with a catalytic dyad consisting of a conserved serine and lysine which belongs to the clan SK serine proteases. One of the protease substrates is the C-terminus of the stomatin homologue; its cleavage was suggested to cause the opening of an ion channel. Eukaryotes do not have direct homologues to the STOPP gene, but distantly related proteases such as the AAA-type proteases. The authors suggest a link between stomatin, the protease and an ion channel that is highly conserved in prokaryotes and eukaryotes: stomatin might act as an activator of the channel after it is cleaved by the protease. Finally, it is suggested that a sterol type molecule might be involved in the regulation of the protease that binds to the putative sterol-sensing domain.

The crystal structure of the N-terminus from this STOPP homologue (PH1510) was determined (Yokoyama *et al.*, 2006). It revealed that the active protease exists as a dimer with hydrophobic residues located in its active site. Previously it had been demonstrated that this NfeD homologue specifically cleaves the hydrophobic C-terminus of STOPP (PH1511) (Yokoyama & Matsui, 2005). The N-terminus of PH1510 resembles a ClpP protease from *E.coli* in its monomeric form, but not as a dimer. ClpP proteases contribute to protein unfolding and quality control in an ATP-dependent manner. The binding of the stomatin-type substrate to the catalytic site of PH1510 supposedly induces a conformational change and brings the catalytic residues lysine 138 and serine 97 in close proximity. Putatively, proteolytic cleavage of the PH1511 C-terminus prevents oligomerisation of the stomatin homologues and changes the conformation of the whole protein complex assembly. A second protease-stomatin operon was identified (PH0471 and PH0470, respectively) from *P.horikoshii*. A weak protein interaction between PH1510 and PH0470 was demonstrated by surface plasmon resonance analysis.

The first crystal structure from a stomatin-type protein was also solved from this operon. The core domain of the stomatin homologue (without the N-terminal hydrophobic region and the small C-terminal hydrophobic domain) had a novel trimeric structure and a coiled-coil fold (Yokoyama *et al.*, 2008a). The basic band-7 core domain unit occurred as a

homotrimer composed of three α/β -domains forming a triangle. Three alpha helices extend per triangle and are capable of assembly into higher structures. The α/β -domain is overall fairly rigid compared to the more flexible extending alpha helices. Each alpha helix is capable of assembling into antiparallel, 2-stranded coiled-coils containing a classic heptad repeat pattern. This leads to self-association of the core domain trimers into higher multimers. Proteolytic cleavage by PH1511 in the hydrophobic C-terminus putatively leads to dissociation of the oligomers and releases single stomatin units laterally into the membrane. The stomatin cleavage site is homologous to the identified oligomerisation domain of mammalian stomatin (Umlauf *et al.*, 2006). Overall, the basic core domain is similar to the only other solved band-7 domain protein structure available so far. The figure below (Figure 1-3) shows a stereoview of the single α/β -domain of P1511. Shown on the right side is a stereoview of a superposition of the PH1511 core domain (in cyan) on top of the mouse flotillin-2 band-7 domain (in orange). The highest similarity is found in the secondary structure beta sheets with overall 20% of identical residues between these two structures. The long extended alpha helix seems to be unique to the stomatin core domain.

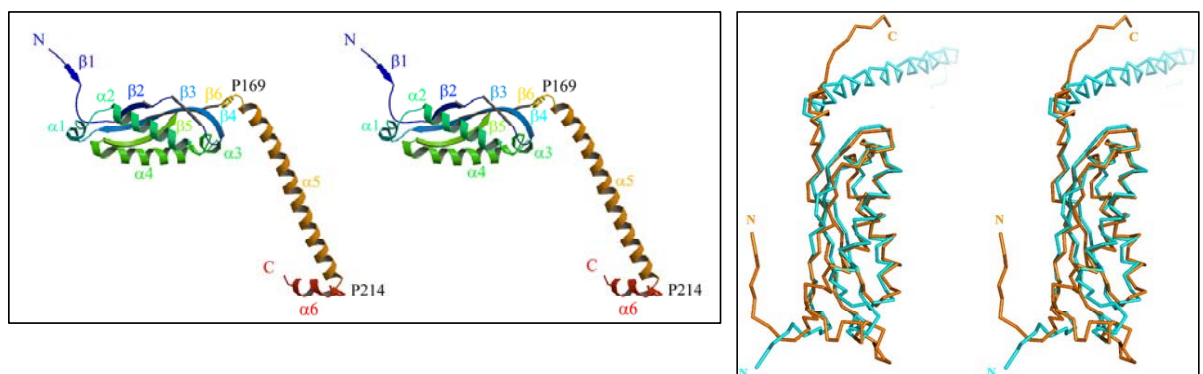


Figure 1-3. Crystal structure of the core domain from the prokaryotic stomatin PH1511. Shown on the left side is the stereoview of the single band-7 core domain with the long extended alpha helix capable of assembly into coiled-coils. Shown on the right side is a stereoview of the superposition of the prokaryotic band-7 core domain on top of the mouse flotillin-2 band-7 domain. Note that the stomatin alpha helix is unique between these two structures. This figure is redrawn from Yokoyama *et al.* (2008).

More recently, altogether 294 protease-stomatin operons were identified, each organised into neighbouring NfeD/STOPP gene pairs from 254 different prokaryotic genomes (Kuwahara *et al.*, 2008). No NfeD homologue has been identified from any eukaryotic genome. It is assumed that these operons act in the quality control of membrane proteins.

In summary, both prokaryotic and eukaryotic stomatins might be functionally linked in regulating proteolytic processes, which originally developed in prokaryotes and further evolved in eukaryotes. Therefore, it is unlikely that stomatins just fulfil housekeeping functions such as the scaffolding of lipid rafts that are eukaryote-specific; rather, it might be involved in membrane protein quality control and protein complex regulation.

1.3 The Band-7 protein family in plants

Nadimpalli et al. defined another protein superfamily called PID (short for proliferation, ion channel and death) whose members are structurally related in a wider sense as in the SPFH family (Nadimpalli *et al.*, 2000). It consists of prohibitins, stomatins, bacterial HflC/K proteins and a group of plant defense genes called HIR (for hypersensitive induced reaction). The hypersensitive induced reaction is a mechanism by which plants respond to pathogen attack. It triggers a localised necrosis that limitates pathogen spread and resembles programmed cell death in animals. BLAST searches with a HIR gene from chickpea revealed 8 putative homologues from maize, four of which are related to prohibitins, one to stomatins and three to HIR genes. A PROSITE pattern (35 amino acids) was defined that partly overlaps with the stomatin motif (29 amino acids) in the centre of these proteins, but extends beyond the stomatin-specific signature sequence. Due to the putative function of stomatin as an ion channel regulator, the authors suggested that the underlying common function of all PID members is the regulation of some kind of ion channel, a proposal that does not agree with the publication by Tavernarakis et al. (Tavernarakis *et al.*, 1999). PID proteins putatively regulate potassium channels that are involved in plant pathogen response and might also have an effect on cellular proliferation. However, the extension of ion channel regulation from stomatins to prohibitins and HflC/K proteins is not backed by explicit experimental evidence. Rather, the regulation of a potassium channel might be a secondary effect that is triggered by a primary event involving a PID protein.

The term “PID protein family” is generally not commonly used. The original nomenclature “SPFH” or “band-7” protein family are widely accepted and will be used instead throughout this thesis. The complete Arabidopsis band-7 family and their phylogenetic relationships have been investigated as part of this thesis and the results are presented as part of chapter 3.

1.3.1 Stomatins in plants

The Arabidopsis genome encodes for two structurally similar stomatin-like proteins that display common characteristic SPFH domain features. They will be referred to as AtSlp-1 (for *Arabidopsis thaliana* stomatin-like protein-1, accession no. At4g27585) and AtSlp-2 (accession no. At5g54100). So far, these genes and their products are functionally completely unknown. They have only surfaced in several organellar proteomics screens,

mainly in connection with the mitochondrial proteome. These findings will be discussed and presented in detail in the results chapters of this thesis.

An *Arabidopsis* mutant, *txr1*, is resistant to higher concentrations of thaxtomin A, an inhibitor of cellulose synthesis, than wild type plants. The increased resistance is mediated by a decreased thaxtomin uptake in the mutant plant (Scheible *et al.*, 2003). The TXR1 gene product is a conserved small protein of 116 amino acids with a coiled-coil region but no known protein motif that resides in the cytoplasm. It has a second homologue in *Arabidopsis* and homologues in other plants and eukaryotes. A mutant in the yeast homologue of *txr1* is lethal and predicted to be a mitochondrial protein. TXR1 has a broad but low expression pattern in all plant organs at various developmental stages, and the mutant plant has reduced growth compared to wild type. Microarray experiments revealed two stomatin-like genes that are expressed at two-fold higher levels in the *txr1* mutant plant. The authors suggest the TXR1 protein to be a regulator of a transport mechanism that might function together with the stomatin-like proteins in the same process.

1.3.2 Plant prohibitins

Prohibitin homologues have been investigated in plants. Two cDNAs from *Arabidopsis thaliana* and *Nicotiana tabacum* were isolated with high amino acid similarity to mammalian prohibitin (Snedden & Fromm, 1997). They are ubiquitously expressed in all plant organs in various species. Subcellular fractionation studies from tobacco leaves revealed a mitochondrial localisation for the protein. A similar function for prohibitin-like proteins in plants as in animals was suggested.

A plant homologue of the yeast mAAA protease has been identified and characterised from pea (Kolodziejczak *et al.*, 2002). Its mature form, PsFtsH, contains a chaperone-like domain that is exposed to the mitochondrial matrix. When overexpressed in yeast deletion mutants of mAAA protease subunits, the plant homologue is capable of complementing a phenotype of respiratory deficiency and protease malfunction. Finally, the authors suggest PsFtsH to influence ATP synthase subunit accumulation and assembly in the inner mitochondrial membrane. The *Arabidopsis* genome encodes for eleven isoforms of FtsH-like proteases, seven of which are predicted to be chloroplastic and two mitochondrial (FtsH3 and FtsH10), both closely homologous to the pea protein.

Using two-dimensional gel electrophoresis, differentially phosphorylated proteins from the rice lesion-mimic mutant *cdr* (short for cell death and resistance) were identified when

compared with wild type (Takahashi *et al.*, 2003). The *cdr* mutant is characterised by spontaneous cell death on leaves and an increased pathogen resistance to fungi. Two CDR genes negatively regulate phosphorylation of proteins that trigger the activation of NADPH oxidase and oxidative burst. In the *cdr* mutant plant, a prohibitin homologue showed increased phosphorylation levels compared to the wild type. A GFP fusion protein with this rice prohibitin (OsPHB1) was localised to mitochondria. The authors suggest a role for it in the hypersensitive induced reaction (HIR) in plant defense response through mitochondrial function.

A rice prohibitin protein was also found upregulated in rice cell cultures treated with the sphingolipid elicitor (SE), and in cells constantly expressing OsRac1 (Fujiwara *et al.*, 2006). OsRac1 is homologous to a human small Rac GTPase and it induces defense signalling cascades in rice plants and cell cultures.

A prohibitin protein from rice was also identified as a plasma membrane protein upregulated in the early defense against bacterial blight (Chen *et al.*, 2007b). Rice suspension cells expressing the disease resistance gene Xa21 (a rice plasma membrane receptor kinase that confers resistance to rice bacterial blight) expressed increased levels of OsPHB2 at the plasma membrane. Additionally, the protein level of the rice HIR protein OsHIR1 was also modified at the plasma membrane. These changes in protein levels were confirmed at the transcriptional level.

Two prohibitins were cloned and characterised from *Petunia* (Chen *et al.*, 2005). The two genes (designated PhPHB1 and PhPHB2) were identified from a *Petunia* inflorescence EST library. Southern blot analysis confirmed the existence of two distinct PHB families in *Petunia* that are homologous to yeast and mammalian PHB1 and PHB2. Type I prohibitins constitute a family with two members, whereas type II prohibitins contain four members. PhPHB1 is expressed in all organs, and its transcript levels decline during floral senescence. Virus-induced gene silencing of PhPHB1 caused a phenotype of dwarfed plants with distorted leaves and flowers. These plants were also later flowering, had curled leaves and misshaped anthers. Silenced flowers also had a shorter life span, earlier senescence and higher respiration rates. Analysis on flowers revealed that these contained enlarged cells as a result of reduced cell division. Additionally, the transcript levels of catalase and a small heat shock protein were specifically increased compared to controls. It was concluded that increased amounts of reactive oxygen species were responsible for the early onset of senescence. Thus, prohibitins are important for plant development and the onset of senescence.

The function of prohibitins was also investigated from *Nicotiana benthamiana* (Ahn *et al.*, 2006). Virus-mediated gene silencing of two prohibitins of both types (designated NbPHB1 and NbPHB2) also resulted in severe growth inhibition, premature leaf senescence and leaf chlorosis. NbPHB1 lead to overall milder phenotypes than NbPHB2. Both prohibitins were co-localised as C-terminal GFP fusion proteins with the mitochondrial marker dye TMRM in Arabidopsis seedling protoplasts. RT-PCR analysis revealed a wide tissue distribution in all organs. Transcript levels were decreased during senescence, and increased upon heat shock treatment. The silencing of PHB2 lead to collapsing leaves. Silencing of each gene caused a reduction in the number of mitochondria and the mitochondrial membrane potential. Additionally, mitochondria had a changed morphology. Frequently, mitochondria appeared hollow inside, and parts of the inner membrane were degraded. Chloroplast ultrastructure and fluorescence were unaffected, but oxygen evolution rates in silenced plants were also reduced. Additionally, ROS accumulated 10 to 20 times more in silenced leaf protoplasts than in the controls. Silenced leaves were also more susceptible to stress treatments with hydrogen peroxide, paraquat, antimycin A and salicylic acid as judged by ion leakage measurements. This study concluded that prohibitins are important for mitochondrial biogenesis, have a role in stress protective response mechanisms and affect senescence. It was concluded that tobacco prohibitins affect the integrity of the mitochondrial inner membrane by acting as membrane-bound chaperones that prevent the accumulation of misfolded proteins.

Arabidopsis prohibitins

Seven prohibitin genes are found in the Arabidopsis genome, and four in maize. The phylogeny of the Arabidopsis prohibitins was investigated as part of this thesis and the results are presented in chapter 3.

Arabidopsis prohibitins of type I were functionally characterised (Van Aken *et al.*, 2007). The type I prohibitins AtPHB3 and AtPHB4 were found predominantly expressed in shoot and root proliferative tissue, such as in the shoot apex, root tips, young leaves and in cell cultures. A knockout mutant of *phb4* was found to have no altered phenotype, whereas *phb3* mutants displayed several growth phenotypes. This finding was correlated with the lower expression levels of AtPHB4 compared to AtPHB3. A double mutant of both genes was not viable. The protein sequences of both prohibitins had no predicted mitochondrial targeting sequences, and were not proteolytically cleaved upon mitochondrial import. Studies on their subcellular localisation revealed however that mitochondrial targeting information must be contained within the N-terminal amino acid

sequence. A tandem affinity purification approach with PHB3 as a bait identified other prohibitins as interacting partners (PHBs 1, 2, 3, 4 and 6), as well as some enzymes and unknown proteins. Thus, prohibitins exist in multimeric protein complexes also in Arabidopsis. Quantitative RT-PCR analysis revealed high expression levels of PHBs 3 and 4 in proliferating tissues (8 to 12 days old) that decreased during the expansion phase and were almost diminished in mature organs. The *phb3* knockout mutant had retarded growth and delayed leaf development. These plants also had fewer and curled leaves. Seed germination was also delayed by one to two days. Cortex cells of the root apical meristem from *phb3* plants had reduced growth and contained less meristematic cells that expanded and divided slower than wild type cells. Root tips from *phb3* plants also contained enlarged mitochondria that appeared rounder and smoother than those from wild type. Interestingly, overexpression of PHB4 under a constitutive promoter could rescue all PHB3-associated phenotypes. PHB3 and PHB4 overexpressing plants had increased branching and irregular leaf shapes, but otherwise lacked the phenotypes described for the *phb3* knockout mutant. Microarray analysis of PHB3 overexpressing and knockout mutants revealed upregulation of stress-related response genes such as components of oxidative phosphorylation, disease resistance genes and transporters. From this study it was concluded that AtPHBs are important for increased metabolic demands related to cell division in meristems, supporting differentiation in apical tissues.

AtPHB3 was also identified as the *eer3-1* mutant (Christians & Larsen, 2007). This mutant has a single amino acid exchange in the PHB3 protein leading to an extreme constitutive ethylene response in etiolated seedlings. GFP localisation of PHB3 showed a widely distributed pattern in large patches across the cytoplasm, with no particular mitochondrial localisation. In this ethylene response pathway, PHB3 acts downstream of the ethylene response gene EIN2. It supposedly acts as a positive regulator of the expression of a subset of ethylene-response genes that maintain growth in the presence of ethylene.

An Arabidopsis prohibitin was also found accumulated in the *roothairless 1* (*rth1*) mutant (Wen *et al.*, 2005). Rth1 is a homolog to yeast Sec-3, a subunit of the exocyst complex. A prohibitin accumulated in primary roots of *rth1*, leading to delayed development and flowering.

Several Arabidopsis prohibitins have already been identified in proteomics studies. AtPHB2, AtPHB3 and AtPHB6 were identified along both AtSlps and an AAA-type protease in a study of the mitochondrial proteome of Arabidopsis suspension cells (Heazlewood *et al.*, 2004). Prohibitins 1, 2, 4, 5 and 6 were also identified in an

independent proteomics study of mitochondrial membranes isolated from suspension cells (Brugiere *et al.*, 2004). These findings all agree with a mitochondrial localisation of prohibitins.

However, some prohibitins were also identified in other subcellular localisations by proteomics approaches. The Arabidopsis prohibitins 4 and 5 were both found in plasma membrane fractions purified from cell suspension cultures (Marmagne *et al.*, 2004). A plasma membrane localisation was also confirmed for AtPHB7 from soil-grown Arabidopsis plants (Alexandersson *et al.*, 2004). Rather controversially, AtPHBs 2, 4 and 5 were additionally identified as vacuolar proteins (Carter *et al.*, 2004).

In summary, Arabidopsis prohibitins are most likely mitochondrial proteins. Interestingly, they have also been assigned to other membrane compartments such as the plasma membrane and even the vacuole. Dual localisation to mitochondria and at least one other compartment could be related to the tissue type or the developmental stage. Fluorescent fusion proteins have so far only confirmed mitochondrial localisation in protoplasts (Ahn *et al.*, 2006) and in roots (Van Aken *et al.*, 2007).

1.3.3 Flotillins and erlins

In plants, flotillins have so far not been characterised, although they surfaced in two proteomics studies. A putative flotillin-1 homologue from Arabidopsis (At5g25250) has been identified in a proteomics study as a protein found specifically enriched in detergent resistant membrane fractions isolated from mixed organellar membranes (Borner *et al.*, 2005). The same protein was also identified in a second proteomics study as a plasma membrane protein (Alexandersson *et al.*, 2004). The localisation of this flotillin homologue to lipid microdomains that are specifically enriched in sterols strongly suggests parallel functions in plants and in animals. These reported subcellular localisation have not been confirmed *in vivo*.

The Arabidopsis genome contains one gene encoding for a protein with a band-7 domain that is similar to mammalian erlins (At2g03510-in this thesis referred to as “erlin-like protein”). This protein has also been localised to the ER in a quantitative proteomics study (Dunkley *et al.*, 2006), but was not further characterised. Its phylogenetic relationship to flotillins will be further described in chapter 3 of this thesis.

1.3.4 HIR proteins

The so-called HIR genes are frequently found upregulated during the hypersensitive response (HR) following pathogen attack and in lesion mimic mutants that undergo spontaneous HR. The HR is triggered by the interaction of pathogen ligands with intra-or extracellular plant receptors leading to an incompatible reaction. This reaction is manifested by a modification of cell walls, the induction of PR proteins (pathogenesis related), the production of anti-microbial phytoalexins and the accumulation of other phenolic compounds. The HR is externally visible as browning of cells, but also includes systemic changes leading to systemic acquired resistance (SAR), an induced resistance to other pathogens. The HR response involves an accumulation of mitochondrially-produced or other ROS, elevated Ca^{2+} , the activation of nucleases (leading to DNA degradation) and proteases (e.g. the papain class of Cys proteases and vacuolar processing enzymes). In the last stages of HR, the cytoskeleton is fragmented and the tonoplast disrupted, releasing proteolytic enzymes into the cytosol. HR signalling is transmitted by a MAP kinase pathway leading to salicylic acid (SA) and ROS production, and via coiled-coil R gene products and NDR1 that act as an inductive switch (Mur *et al.*, 2008). Mitochondria play a central role in this type of programmed cell death, via ROS and nitric oxide (NO) production, the formation of the mitochondrial transition pore and Ca^{2+} release, and other cell death-inducing signals (Logan, 2006b; Logan, 2008b). The HR is regarded as a distinctive form of programmed cell death in plants that is related to apoptosis in animal cells, but involves distinct signalling pathways and proteolytic mechanisms (Rostoks *et al.*, 2003; del Pozo & Lam, 2003; Yao *et al.*, 2004).

Nadimpalli *et al.* classified HIR genes from different plant species together with other band-7 family proteins into the PID superfamily (see above). The maize HIR gene ZmHIR3 is overexpressed in the maize lesion mimic mutant *les9*. Structurally this protein resembles stomatins and it was suggested to participate in the maize HR by regulating an ion channel (Nadimpalli *et al.*, 2000). Four HIR genes were isolated from barley (HvHIR 1-4) based on homologies to maize HIR proteins (Rostoks *et al.*, 2003). These proteins also contain band-7 family domains and several conserved residues. A barley disease lesion mimic mutant has 35-fold increased level of HvHIR3 and undergoes spontaneous HR. Also in this case, the authors speculate about an ion channel regulatory activity of the HIR proteins during HR. This view is supported by the Arabidopsis lesion mimic mutants *hml1* and *dnd1* (Balague *et al.*, 2003; Clough *et al.*, 2000) that both encode cyclic nucleotide gated channels (CNGC4 and 2, respectively). Another HIR gene was cloned from wheat

(TaHIR-1) that is highly homologous to the barley HIR1 gene product. This wheat gene is also highly expressed 48 hours after leaf inoculation with rust fungus (Yu *et al.*, 2008). The rice gene OsHIR-1 was additionally found to be upregulated during cold stress in developing seedlings (los Reyes *et al.*, 2003). The protein of this gene was identified as upregulated during the early phase of defense response following bacterial infection in the plasma membrane of XA21-expressing (a receptor kinase) suspension cells (Chen *et al.*, 2007b). The rice japonica genome contains 18 PID genes, eight of which belong to the HIRs, seven are prohibitins and one is related to stomatins. A HIR protein from lotus accumulated at high levels in peribacteroid membranes from root nodules (Wienkoop & Saalbach, 2003). The lotus gene LjHIR1 was also found highly expressed in microspores during pollen development. This protein is closely related to the maize and barley HIR1 proteins and putatively function via ion channel regulation in vacuole fusion during microspore development (Hakozaki *et al.*, 2004).

Arabidopsis HIR proteins

The Arabidopsis genome contains four genes that can be classified as HIRs. All are characterised by the presence of the band-7 domain, and one member (At3g01290) contains an additional stomatin signature domain. Like flotillins, none of these genes have been functionally characterised so far. All of these HIR proteins and their phylogenetic relationships are further described in chapter 3 of this thesis.

All of these four HIR proteins were identified in a quantitative proteomics study, but their subcellular localisation was not classified (Dunkley *et al.*, 2006). A proteomics study of Arabidopsis plasma membrane fractions isolated from suspension cell cultures identified three of the HIR proteins as membrane-integral proteins (Marmagne *et al.*, 2004). Amongst them, the subcellular localisation of the protein encoded by At5g62740 was also determined by GFP fusion proteins. Transient expression of this fusion in Arabidopsis protoplasts gave a peripheral, but punctuate localisation pattern. The same three HIR proteins were also found specifically enriched in detergent-resistant membrane fractions isolated from Arabidopsis callus cultures (Borner *et al.*, 2005).

1.4 Human Slp2, a close homologue of Arabidopsis stomatins

Phylogenetic analysis of Arabidopsis stomatin-like proteins and stomatin sequences from various animals revealed close homologies between AtSlps and the human stomatin-like protein 2 (HsSlp2). These results are presented in chapter 3. Recently, the phylogenetic relationships of all stomatin-like sequences sharing a 150 amino acid domain was investigated (Green & Young, 2008). It was revealed that all Slps have their origins in an ancient duplication event that happened early in the evolution of prokaryotes. This duplication resulted in two Slp subfamilies, one of which was termed “paraslipins”. This subfamily gave rise to all eukaryotic stomatin-like proteins of type 2 and was probably acquired by mitochondrial endosymbiosis.

1.4.1 Characteristics of human stomatin-like protein 2

Originally, the gene encoding human Slp2 was cloned from a human heart cDNA library and was further characterised (Wang & Morrow, 2000). This protein presents an unusual stomatin homologue regarding several aspects: it has only 20% amino acid sequence similarity to erythrocyte stomatin, it does not have the characteristic hydrophobic stretch close to the N-terminus and it is peripherally attached to membranes (although lacking the palmitoylated Cys 29 residue present in stomatin). The authors propose that this protein provides another link for other membrane proteins to the peripheral cytoskeleton and might have similar roles as stomatin. In contrast to human Slp1, human Slp2 is also expressed in mature human erythrocytes, although at a much lower level (~ 5000 copies/red cell) than stomatin. Two distinct Slp2 pools could be identified: One was membrane associated, and the other could be extracted using high ionic strength (0.5M KCl) and was present in a high molecular weight complex. The overall tissue distribution pattern of human Slp2 is similar to that of other human stomatin homologues: mRNA was detected in heart, brain, placenta, lung, liver, skeletal muscle, kidney and pancreas. The highest expression levels were found in heart, liver and pancreas transcripts. A role for human Slp2 was suggested to link stomatin to the cytoskeleton, thereby indirectly regulating ion channels. Additionally, human Slp2 and stomatin might be functionally related in anchoring lipid rafts and providing a scaffold for other proteins. The gene encoding human Slp2 was localised to chromosome 9, just like stomatin. The exact Slp2 locus was later mapped by another group (Owczarek *et al.*, 2001) to a locus that had previously been linked to the occurrence of certain cancers.

Human Slp2 was identified as a mitochondrial protein in several proteomics studies. It was localised to the mitochondrial inner membrane of mouse liver mitochondria (Da Cruz *et al.*, 2003). Mitochondrial localisation was further demonstrated by co-localisation studies of overexpressed HA-tagged Slp2 with a mitochondrial marker protein in HeLa cells. The authors did not exclude that this protein might also have a plasma membrane localisation in other cell types such as erythrocytes. Human Slp2 was also identified as a part of the mitochondrial proteome of five rat organs (kidney, liver, heart, skeletal muscle and brain) (Reifschneider *et al.*, 2006). The proteome had been resolved by Blue-native PAGE and mild solubilisation using digitonin, with the aim of preserving protein complexes. A novel homooligomeric high molecular weight complex of 1.8 MDa containing human Slp2 was identified in liver mitochondria. From the comparison of proteomes from different organs it was concluded that the mitochondrial proteome substantially differs, dependent on the organ and cell type. Another proteomics study compared the mitochondrial proteome between an osteosarcoma cell line (143B) and a cell line lacking the mitochondrial genome (Rho0). In this study, human Slp2 protein levels were decreased by a factor of two in Rho0 mitochondria (Chevallet *et al.*, 2006). Rho0 cells grow more slowly than normal cells and rely entirely on glycolysis for their ATP production. Curiously, mitochondria from these cells still possess a proton gradient across their inner membrane, but the ATP synthase works reversely and generates the proton gradient by ATP hydrolysis. Surprisingly, Rho0 mitochondria did not have drastically decreased levels of oxidative phosphorylation complexes, although some dehydrogenases were found decreased.

1.4.2 HsSlp2 functions

Human Slp2 was identified as an interacting protein of mitofusin-2 (Mfn-2), a large GTPase located to the outer mitochondrial membrane (Hajek *et al.*, 2007). Mitofusins-1 and -2 are both localised to the outer membrane mediating mitochondrial fusion events in mammalian cells. In HeLa cells, human Slp2 was shown to participate in protein complexes composed of Slp2 and Mfn-2 heterooligomers using formaldehyde crosslinking and immunoprecipitation. Slp2 is the major constituent of these complexes, because only a small proportion of the total Mfn-2 pool localises to these complexes. Using immunocytochemistry and cell fractionation, the mitochondrial localisation of Slp2 was confirmed and the protein was localised to the inner membrane facing the intermembrane space. Its mitochondrial import was demonstrated to be dependent on the mitochondrial membrane potential and is accompanied by proteolytic processing. Knockdown of Slp2 by interference RNA caused a reduction of the mitochondrial membrane potential without

affecting the protein levels of Mfn-2, or mitochondrial morphology. It was concluded that Slp2 complexes form a scaffold in the inner membrane that interacts with and supports the mitochondrial fusion machinery localised to the outer membrane. Because the knockdown of Slp2 had generally relatively mild effects on mitochondrial function, redundancy between Slp2 and mitochondrial prohibitins was suggested.

More recently, human Slp2 was demonstrated to interact with prohibitins-1 and -2, and to support the stability of protein complexes in the mitochondrial inner membrane (Da Cruz *et al.*, 2008). The first 50 amino acids of Slp2 were identified to contain the necessary targeting information to mitochondria. Gel filtration identified Slp2 in a 250kDa protein complex that also contained prohibitins-1 and -2. Slp2 was confirmed to be localised to the inner membrane facing the intermembrane space by protease digestion of mitoplasts. Depletion of Slp2 levels by RNA interference lead to increased proteolysis of prohibitins and parts of complexes I and IV of the electron transport chain. This degradation was probably mediated by metalloproteases of the AAA type, analogous to prohibitin function. Upon application of chloramphenicol (an inhibitor of mitochondrial protein synthesis) to specifically induce mitochondrial stress, Slp2 and prohibitin-1 were found highly upregulated. This upregulation was reflected in increased proteolysis of prohibitins and the oxidative phosphorylation complexes. The plasma membrane localisation of Slp2 was interpreted as being cell specific for erythrocytes that lack mitochondria. However, a dual localisation of Slp2 to the plasma membrane and to mitochondria was not ruled out, because other human mitochondrial proteins are localised in a similar dual way.

Human Slp2 was also identified as a component of the signalosome complexes mediating signalling from activated T-cells (Kirchhof *et al.*, 2008). Slp2 was found expressed in human lymphoid tissue and was localised to internal punctuate structures and the cell periphery in the lymph node. This finding was interpreted as localisation to mitochondria and the plasma membrane. Despite the presence of the mitochondrial targeting sequence, the authors point out that the protein sequence contains six sites that could be modified by fatty acylation and give rise to anchorage at the plasma membrane. T-cell activation through the Ag receptor happens at the interface between T-cells and the so-called immunological synapse (IS). Signalosomes constitute lipid rafts, microclusters at the T-cell periphery that form a bridge between the cytoskeleton and the signalling complex. The formation of the signalosome complex involves T-cell polarisation and organelle movements and brings mitochondria in close proximity to the cell periphery. Lipid rafts were isolated from activated human T-cells and Slp2 was identified as a major component. Slp2 was highly upregulated upon T-cell activation and shown to interact with signalosome

proteins and polymerised actin fibres. Downregulation of Slp2 resulted in loss of T-cell activation and signalling and a reduction of interleukin-2 production. The role of human Slp2 in T-cells is therefore regarded as the activation and maintenance of T-cell signalling. The protein probably achieves this by providing a scaffold that links the actin cytoskeleton to plasma membrane rafts or even mitochondria. Both protein pools at the plasma membrane and inside mitochondria could even come together during the organellar rearrangements that accompany T-cell signalling. In this way, the increased energy demands of T-cells could be met.

Association of HsSlp2 with human cancers

In recent years, human Slp2 became of great interest because of its high expression levels in a variety of proliferating cancer cells. The protein was identified as being overexpressed in several types of cancers as analysed by RT-PCR, Western blotting and immunohistochemistry (Zhang *et al.*, 2006). Microarray experiments revealed a six-fold upregulation of Slp2 transcript in esophageal squamous cell carcinoma (ESCC) in cancerous epithelial cells. An antisense construct of Slp2 expressed in an ESCC cell line resulted in decreased cell growth, proliferation, tumorigenicity and cell adhesion. This effect was demonstrated to be linked to an arrest in the cell cycle in the S-phase rather than increased apoptosis. The cell adhesion molecule fibronectin was also decreased, and both fibronectin and Slp2 were co-localised at the cell periphery. Slp2 was specifically found overexpressed in premalignant lesions, whereas it is normally not expressed in healthy epithelial cells. Thus, Slp2 overexpression is an early event in esophageal cancer development. Slp2 levels further increased during cancer development. Since no mutation was found in the Slp2 gene, it was concluded that Slp2 overexpression is specifically associated with different tumour stages and could be used as an indicator for early detection of ESCC. These characteristics are probably common for other cancer types and Slp2 is now regarded as a novel type of oncogene. Most likely the protein provides a link between the extracellular matrix and the underlying cytoskeleton. Its upregulation might contribute to malignancy because cancer cells become hyperproliferative.

High levels of Slp2 were also found in 52% of primary invasive breast cancers and linked to decreased survival rates (Cao *et al.*, 2007). Additionally, human Slp2 was also overexpressed in osteosarcoma cells when compared to healthy osteoblastic cells (Guo *et al.*, 2007). High levels of Slp2 protein were also linked to superinvasive cancer cells (an *in vitro* phenotype of cancer cells used as a model for metastasis). Slp2 and other proteins such as prohibitin, cofilin, annexin, chaperonin and a voltage-gated anion channel were

specifically enriched in membranes of superinvasive cells (Dowling *et al.*, 2007). All of these proteins present candidates as potential drug targets and diagnostic markers.

The close homology on the amino acid sequence level between human Slp2 and Arabidopsis stomatin-like proteins strongly suggests a functional link. Many interesting aspects concerning human Slp2 function in different cell types and tissues could help to elucidate the function of the Arabidopsis proteins.

1.5 Aims and objectives of this study

As mentioned at the beginning of this introduction, the original aim of investigating a link between an Arabidopsis syntaxin and stomatin-like protein-1 had to be revised. Attempts to confirm this protein interaction by heterologous expression and *in vivo* approaches were abandoned. The result of the split-ubiquitin screen that used AtSlp1 as the bait is now regarded as false positive.

Because stomatin-like proteins from Arabidopsis are so far functionally completely unknown, the aim of this thesis was changed. The overall aim was to provide a detailed general characterisation of the two Arabidopsis Slp proteins. More specifically, the first aim was to investigate the phylogenetic relationship of AtSlps within the Arabidopsis band-7 protein family, and between Slp proteins from plants and animals. The second aim was to analyse the general expression pattern of AtSlp1 and AtSlp2 during plant development and under stress conditions. The results from these aims are presented in chapter 3. In addition to these general characteristics, the subcellular localisation of both proteins had to be investigated in detail. Specifically, the question of a putative dual localisation was further analysed by using biochemical and *in vivo* techniques. The results from these aims are presented in chapter 4 of the results section. The last and most important aim of this study concerned the elucidation of the physiological significance of AtSlp proteins. The idea was to analyse the effects of modified Slp expression on plant growth and development. The aim was to make use of T-DNA insertion lines and other transgenic plants modifying Slp expression levels. The results from this part of the work are presented in chapter 5 of the results section.

Mainly reverse genetic approaches were utilised to achieve these aims. A whole range of transgenic tools had to be prepared first. These tools mainly involved the creation of a set of transgenic plants that allowed modulating the expression of the endogenous Slp genes. Additionally, specific antibodies had to be raised to allow for the investigation of protein levels for expression analysis and subcellular localisation.

2 Materials and Methods

General Materials and Methods

All chemicals were purchased from Sigma Aldrich (Poole, UK), VWR International (Poole, UK) or Fisher Scientific (Southampton, UK) unless otherwise stated. Enzymes for molecular biology procedures were either from Invitrogen (Paisley, UK), New England Biolabs (NEB, Hitchin, UK) or Promega (Southampton, UK). Kits used for DNA extractions were from Qiagen (Crawley, UK), and custom primers were purchased from Invitrogen.

2.1 RNA extraction, quantification and cDNA synthesis

For the extraction of RNA, plant material was placed in a two millilitre screwcap tube (Sarstedt) together with a five millimetres (diameter) grinding ball (Qiagen) and snap frozen in liquid nitrogen. The tubes were placed in a pre-cooled rack and the samples ground while frozen using the Qiagen TissueLyser (manufactured by Retsch) for 1 minute with an oscillation frequency of 20/s.

To obtain RNase free water, one millilitre of DEPC (Diethyl pyrocarbonate, Fluka) was added to one litre of double distilled water and stirred for several hours. This water was then autoclaved and used in all following procedures involving RNA handling. One millilitre of Trizol reagent (0.8 M guanidinium thiocyanate, 0.4 M ammonium thiocyanate, 0.1 M Na acetate pH 5.0, 5 % glycerol, 38 % phenol saturated in water pH 4.5) was added to the frozen powder and the sample vortexed for one minute. This was followed by centrifugation at 12000 g for 10 minutes at 4 °C. The supernatant was removed into a new tube and allowed to equilibrate to room temperature for five minutes. 400 µL of chloroform:isoamylalcohol (24:1) were added, the samples vortexed thoroughly and incubated at room temperature for five minutes. The samples were then centrifuged at 12000 g for 15 minutes at 4 °C and the aqueous phase carefully transferred to a fresh tube. Isopropanol was added in a volume ratio of 1:1, the tubes were inverted and left to precipitate RNA at room temperature for 10 minutes. The sample was then centrifuged for 10 minutes at 12000 g at 4 °C, followed by washing with 70 % ethanol and centrifugation at 12000 g for five minutes at 4 °C. The RNA pellet was dried at air and resuspended in 50 µL of DEPC-treated water. The tube was then incubated at 65 °C for 10 minutes to ensure solubilisation of the RNA.

The amount of RNA was then quantified. A small sample was diluted 50x in DEPC-treated water and an absorbance spectrum measured ranging from 220 nm to 320 nm in a quartz cuvette in a Lambda 35 UV spectrophotometer (Perkin Elmer). RNA content was calculated as followed: $(A_{260}-A_{320}) * 40 * 50$ (dilution factor) in [ng/ μ L]. The purity of RNA was assessed as the ratio of A_{260}/A_{280} .

For use in RT-PCR, RNA was treated with RQ1 RNase free DNase (Promega) according to the instructions given by the manufacturer. One microgram of RNA was added to a final volume of 10 μ L with one μ L of 10x reaction buffer and one μ L of DNase (1U/ μ L). The reaction was incubated at 37 °C for 30 minutes and terminated by adding one μ L of the supplied stop solution followed by heat treatment at 65 °C for 10 minutes.

RNA was reverse transcribed into cDNA using SuperscriptII reverse transcriptase enzyme (200 U/ μ L, Invitrogen) as described by the manufacturer. One microgram of RNA was added to a final volume of 12 μ L together with one μ L of a 100 mM oligo dT primer stock (15 dTs) and one μ L of a 10 mM dNTP mix (Invitrogen) and DEPC-treated water. This mixture was heated to 65 °C for five minutes, and immediately placed on ice. Four μ L of the supplied 5x First-Strand buffer were added together with two μ L of 0.1 M DTT (dithiothreitol) and incubated at 42 °C for two minutes. Finally, one μ L of SuperScript enzyme was added and the reaction incubated at 42 °C for 50 minutes followed by heat inactivation at 70 °C for 15 minutes.

2.2 Plant genomic DNA extraction

Genomic DNA was extracted from leaves of soil-grown (long day light conditions) Arabidopsis plants at various stages. Up to two small leaves were placed in a 2ml screwcap tube together with a grinding ball and the tissue ground to powder using the Qiagen TissueLyser as described. 400 μ L of extraction buffer (200 mM Tris-Cl pH 7.5, 250 mM NaCl, 25 mM EDTA, 0.5 % SDS) were added to each sample followed by thorough vortexing. The sample was allowed to equilibrate to room temperature and centrifuged at maximum speed in a microcentrifuge (Eppendorf) for one minute. 300 μ L of the supernatant were transferred to a fresh tube and the same volume of isopropanol added. DNA was allowed to precipitate at room temperature for five minutes before centrifugation at maximum speed for five minutes. The pellet was dried in an Eppendorf vacufuge concentrator at 60 °C and taken up in 100 μ L of TE buffer (10 mM Tris-Cl pH 8.0, 1 mM EDTA) without additional mixing. The DNA was diluted 10 times in TE buffer to be used as a template in PCR reactions.

2.3 PCR and agarose gel electrophoresis

PCR (polymerase chain reaction) reactions were carried out either using a MJ Research PTC-2000 Peltier thermal cycler, or the Gene Amp PCR System 9700 (Applied Biosystems) using protocols that were adapted for the use of specific Taq DNA polymerase enzymes as described below.

Standard Taq polymerase

PCR reactions using standard Taq DNA polymerase (from NEB or Invitrogen) were carried out in a volume of either 50 or 20 μL . A mastermix of the following composition was prepared and aliquots added to standard thin-walled PCR reaction tubes (tube volume 0.1 ml). DNA templates were added individually to each tube. The reaction buffer from NEB contains 2 mM MgSO_4 and no extra Mg^{2+} ions were added when this enzyme was used instead of the Invitrogen enzyme.

Component	Amount added/reaction
10x Reaction Buffer	5 μL
MgCl_2 (50mM)	1.5 μL
dNTP mix (10mM)	1 μL
Taq polymerase (5U/ μl)	1 μL
Primers (10 μM stocks)	1 μL of each
Template (50ng/ μl)	1 μL of each
Water to	50 μL

These types of PCR reactions were frequently used for the detection of analytical bands like in RT-PCR reactions, but not for cloning procedures. Typically, PCR reactions were run for 30-35 cycles under the following cycling conditions:

Frequency	Step	Temperature [C]	Duration [min]
1x	Initial Denaturation	94	02:00
30-35 cycles	Denaturation	94	01:00
	Primer annealing temperature	55-60	0:30-1:00
	Extension time	72	1:00/1000bp
1x	Final extension	72	10:00
1x	Final temperature	4	∞

Knockout genotyping

PCR reactions for the genotyping of knockout mutants (Chapter 5) were performed in a volume of 20 μL using standard Taq polymerase enzymes. The following mastermix was prepared and genomic DNA (5 μL of 10x diluted DNA) added individually to each tube.

Component	Amount added/reaction
10x Reaction Buffer	2 μL
MgCl ₂ (50mM)	0.6 μL
dNTP mix (10mM)	1 μL
Taq polymerase (5U/ μL)	0.5 μL
Primers (10 μM stocks)	0.5 μL of each
Template (10x diluted gDNA)	5 μL of each
Water to	20 μL

Cycling conditions for these reaction types were as follows (these depended on the types of primers used and the length of the amplicon):

Frequency	Step	Temperature [C]	Duration [min]
1x	Initial Denaturation	95	02:00
30-35 cycles	Denaturation	95	01:00
	Primer annealing temperature	55	00:45
	Extension time	72	01:00
1x	Final extension	72	10:00
1x	Final temperature	4	∞

Alternatively to this type of enzyme, a 2x concentrated mastermix was occasionally used (2x ReddyMix PCR Master Mix, Abgene). These PCRs were performed in 25 μL final volume under the same cycling conditions as described above. Aliquots of 12.5 μL of the mastermix were pipetted into PCR reaction tubes together with a mix of the primers with enough water to make up a volume of 20 μL . The gDNA or cDNA template was then added individually to each tube in volumes of five μL .

PCR with proofreading enzymes

For the purpose of cloning PCR products into plasmids, the reactions were carried out with proofreading Taq DNA polymerase enzymes. Two different types were used, Vent_R DNA polymerase (NEB) and PhusionTM High fidelity DNA polymerase (Finnzymes; Espoo, Finland). For Vent polymerase, the following reactions were set up:

Component	Amount added/reaction
10x Reaction Buffer	5 μ L
MgSO ₄ (100mM)	1 μ L
dNTP mix (10mM)	1 μ L
Vent polymerase (2U/ μ l)	1 μ L
Primers (10 μ M stocks)	2 μ L of each
Template (50ng/ μ l)	1 μ L of each
Water to	50 μ L

The following cycling conditions were applied:

Frequency	Step	Temperature [C]	Duration [min]
1x	Initial Denaturation	94	02:00
20-25 cycles	Denaturation	94	01:00
	Primer annealing temperature	58-60	0:30-1:00
	Extension time	72	1:00/1000bp
1x	Final extension	72	10:00
1x	Final temperature	4	∞

PCR reactions using Phusion Taq polymerase were performed as follows:

Component	Amount added/reaction
5x Reaction Buffer	5 μ L
dNTP mix (10mM)	1 μ L
Phusion Taq (2U/ μ l)	0.5 μ L
Primers (10 μ M stocks)	1 μ L of each
Template (10ng/ μ l)	1 μ L of each
Water to	50 μ L

Cycling conditions were adapted specifically for this enzyme:

Frequency	Step	Temperature [C]	Duration [min]
1x	Initial Denaturation	98	00:30
20-25 cycles	Denaturation	98	00:10
	Primer annealing temperature	55-72	0:10-0:30
	Extension time	72	0:15/1000bp
1x	Final extension	72	05:00
1x	Final temperature	4	∞

Agarose gel electrophoresis and gel purification

Following PCR reactions, all products were separated on 1% agarose gels (see Table below for composition) at 100 V for 20-30 minutes in 1x TAE buffer. To each sample, 6x DNA loading buffer was added to a dilution of 1x. DNA bands were visualised under UV light on a GelDoc 2000 scanner (BioRad). A DNA lambda ladder (12 μ L) was loaded in parallel on each gel.

Buffer/Solution	Composition
DNA agarose gel	1 % agarose, 1xTAE, 40 μ l/l ethidium bromide solution
50x TAE	2 M Tris, 5.7 % acetic acid, 50 mM EDTA
6x DNA loading buffer	0.25 % Bromophenol Blue, 0.25 % Xylene Cyanol FF, 15 % Ficoll
DNA marker ladder	250 μ g 1kb+ DNA ladder, 1x DNA loading buffer in 6 ml TE buffer

Where necessary, DNA bands were excised under UV light and purified using the QiaQuick Gel Extraction Kit spin columns and buffers (Qiagen) exactly according to the manufacturer's instructions. PCR products were normally eluted from the columns in 30 μ L of the supplied elution buffer.

DNA was quantified by measuring the absorbance at 260 nm of a 200x dilution (in water) in a 1 ml quartz cuvette in the Lambda 35 UV spectrophotometer (Perkin Elmer). The DNA concentration was determined in [μ g/ μ L] by multiplying the absorbance value with 10.

2.4 Cloning procedures

Restriction digestion reactions

PCR products and plasmids were digested with restriction enzymes that were obtained from NEB or Promega. All digests were carried out in a volume of 20 μ L at 37 °C or as otherwise required by the individual enzyme for 1-2 hours. The reactions were all prepared with the reaction buffers supplied by the manufacturers and BSA added as required. Following digestion, the samples were either run on an agarose gels, or purified on QiaQuick spin columns as described as described. Usually DNA was eluted in either 30 or 50 μ L of the supplied elution buffer. If possible and necessary, digestion reactions were carried out with two separate enzymes in one tube. In this case, a reaction buffer which was compatible with both enzymes was chosen.

Setup of restriction digestions:

Component	Amount added/reaction
10x Reaction buffer	2 μ L
acetylated BSA [10 μ g/ μ l]	0.2 μ L
DNA	1 μ g
Water	to 20 μ L final volume
restriction enzyme [10U/ μ l]	0.5 μ L

DNA ligation reactions

All ligation reactions were carried out with T4 DNA ligase (Invitrogen) in a reaction volume of 20 μ L essentially as instructed by the manufacturer. Normally, an insert:vector ratio of 3:1 was used, but this was increased in certain reactions to 5:1 or even 10:1. All reactions were incubated at 23 °C for two hours in a thermostat and heat-inactivated by placing the tubes in 70 °C for 10 minutes. Aliquots of the ligation (typically 5-10 μ L) were diluted 5x and used to transform *E.coli* strain DH5 α as described below.

Component	Amount added/reaction
5x Ligase buffer	4 μ L
Vector (20fmol)	as required
Insert (60fmol)	as required
T4 Ligase (1U/ μ l)	1 μ L of 10x dilution (in 1x buffer)
Water	to 20 μ L

Preparation of chemically competent *E.coli* (strain DH5 α)

E.coli strain DH5 α cells were made chemically competent to be transformed with plasmid DNA by heat shock treatment. A culture volume of 500 millilitres LB (Luria-Bertani broth) medium (1% tryptone, 0.5 % yeast extract, 85 mM NaCl, pH 7.0-7.4) was inoculated with a glycerol stock of DH5 α bacteria. The culture was grown overnight at 25°C while shaking at 220 rpm. The next morning, the growth temperature was increased to 37 °C and the bacteria were grown for several hours until they reached an optical density (600 nm) of approximately 0.4-0.5. The cells were then harvested by centrifugation at 4000 g for 45 minutes at 4 °C. The cell pellet was very carefully resuspended on ice under sterile conditions in 125 millilitres of ice cold MgCl₂ (100 mM). This resuspension was centrifuged again at 4000 g for 10 minutes at 4 °C . The supernatant was carefully removed, and the pellet resuspended in 25 millilitres of ice cold CaCl₂ (100 mM) while kept sterile. An additional volume of 225 millilitres of cold CaCl₂ solution was added on

top, and the cell suspension kept standing on ice for 45 minutes. The cells were collected by centrifugation at 4000 g for 10 minutes at 4 °C and resuspended in 10 millilitres of storage solution (85 mM CaCl₂ in 15 % glycerol). Individual aliquots of 100 µL were prepared in 1.5 millilitres Eppendorf tubes and snap frozen in liquid nitrogen. The tubes were kept at –80 °C for long term storage until use.

Bacteria transformation

Aliquots (100 µL) of chemically competent cells were thawed on ice, and the diluted ligation reactions added directly. The cells were left on ice for 30 minutes while the tubes were carefully tapped occasionally. The tubes were then heat shocked at 37 °C by placing them in a water bath prewarmed to 37 °C for 30 seconds to one minute. They were then placed immediately back onto ice for five minutes. One millilitre of LB medium was added to each aliquot and incubated at 37 °C for one hour while shaking at 220 rpm. The cells were harvested by brief centrifugation (2 minutes at 4000 rpm in a microcentrifuge) and resuspended in 400 µL of fresh LB. 200 µL were spread on LB agar plates (1.2 % agar) under a lamellar flow hood using a Drigalski spatula sterilised by ethanol flaming. The agar plates contained the appropriate antibiotics or other supplements for selection of positive transformants as outlined in the table below. For blue/white screening with the pUC18 vector, LB plates were supplemented with 40 µL of a 20 mg/ml X-Gal (5-bromo-4-chloro-3-indolyl- beta-D-galactopyranoside solubilised in DMSO) stock and five µL of IPTG (200 mg/ml stock). All plates were incubated for at least 16 hours at 37 °C.

Antibiotic	Final concentration [µg/ml]
Ampicillin	100
Kanamycin	50
Gentamycin	25
Spectinomycin	100
Tetracycline	12.5
Chloramphenicol	34

Plasmid minipreps

Single colonies were picked with a sterile pipette tip and inoculated into liquid LB medium containing antibiotics as required. For plasmids to be used in diagnostic restriction digestions, a culture volume of two millilitres was inoculated. For plasmids that were sent away for DNA sequencing, a volume of five millilitres was inoculated. The cultures were grown overnight at 37 °C while shaking at 220 rpm. Cells were harvested by centrifugation

at maximum speed in a microcentrifuge for three minutes. Plasmids from the larger cultures were extracted with the QiaPrep Miniprep kit (Qiagen) on spin columns using the buffers supplied with the kit as instructed by the manufacturer. The resulting DNA was eluted in 50 μL of elution buffer and quantified as described. The smaller cultures were extracted with a modified protocol and the buffers listed below.

Buffer	Composition
Resuspension buffer	50 mM Tris-Cl pH 8.0, 10 mM EDTA, 100 $\mu\text{g}/\text{ml}$ RNase A
Lysis buffer	200 mM NaOH, 1% SDS
Neutralisation buffer	3 M K acetate pH 5.5

The cell pellets were resuspended in 100 μL of resuspension buffer and vortexed. 200 μL of lysis buffer were added and the tubes carefully inverted three times. 200 μL of neutralisation buffer were added and the tubes again inverted. The lysates were centrifuged at maximum speed in a microcentrifuge for 10 minutes, and the supernatants transferred to fresh tubes. One millilitre of ethanol was added to each tube, mixed and centrifuged again for 10 minutes at 4 $^{\circ}\text{C}$. The pellets were washed with one millilitre of 70% ethanol, vortexed and centrifuged for five minutes. They were then dried in the vacuum concentrator at 60 $^{\circ}\text{C}$ for 10 minutes and resuspended in 50 μL of TE buffer. For restriction digestions, five μL of miniprep DNA were normally added to the standard reaction setup.

DNA sequencing

All DNA sequencing reactions were carried out by the University of Dundee Sequencing Service (www.dnaseq.co.uk). For plasmid sequencing, 300 ng of DNA were sent in a volume of 15 μL water. Primers were supplied as 3.2 μM stock solutions. Sequencing data were analysed with the SeqMan software (part of the DNA Star package).

Bacterial glycerol stocks

Glycerol stocks for easy re-inoculation of transformed bacteria were prepared by adding 590 μL from a four millilitre overnight culture to 900 μL of 40 % glycerol under sterile conditions. The stocks were immediately frozen at -80°C for long-term storage. A sterile pipette tip was used to scrape off some frozen material for inoculation into liquid LB medium.

2.5 *A.tumefaciens* transformation

Agrobacterium tumefaciens (strain GV3101) cells were made chemically competent. A pre-culture (two millilitres of LB supplemented with gentamycin) was grown overnight at 28 °C and used to inoculate a culture volume of 400 millilitres of the same medium. This culture was grown for several hours at 28 °C while shaking until it reached an optical density (600 nm) of 0.3. The cells were harvested by centrifugation at 4000 g for 45 minutes at 4 °C in 50ml tubes. The supernatant was discarded, and the cell pellets resuspended on ice under sterile conditions in 40 millilitres of ice-cold sterile HEPES buffer (1 mM HEPES, pH 7.0). The resuspension was centrifuged again at 4000 g for 15 minutes at 4 °C. The cells were resuspended in HEPES buffer and harvested as described altogether three times. The final cell pellet was resuspended in four millilitres of ice cold, sterile glycerol solution (10 % glycerol, sterile filtered) and aliquoted in 40 µL per tube before being snap frozen in liquid nitrogen.

These cell aliquots were transformed with binary plasmids by heat shock treatment. The aliquots were thawed on ice and the plasmid DNA added (normally 10 µL of a plasmid miniprep). The mixture was left on ice for 10 minutes and snap frozen in liquid nitrogen. The tubes were then heat shocked by transferring them to a water bath prewarmed to 37 °C for five minutes. Immediately after the heat shock the tubes were transferred back to ice for five minutes, before one millilitre of LB medium was added and the cells incubated at 28°C for four hours while shaking at 220 rpm. The cells were harvested by centrifugation at 2000 g for two minutes in a microcentrifuge, and the pellets resuspended in 400 µL of fresh LB medium. This resuspension was spread under sterile conditions on LB agar plates containing gentamycin and the appropriate antibiotic for selection of the binary plasmid. Plates were incubated at 28 °C overnight and single colonies picked with a sterile pipette tip for inoculation into four millilitres of liquid LB medium supplemented with gentamycin and the appropriate antibiotic. These colonies were also streaked out with the same pipette tip on a fresh LB agar plate containing the same antibiotics for easy re-inoculation later on. Plasmids were extracted by a modified miniprep protocol. The cells were harvested as described for *E.coli*, but lysozyme at a concentration of 1 mg/ml was added to the resuspension buffer to aid cell lysis. The extracted plasmids were then retransformed into *E.coli* cells as described, selected on the appropriate antibiotic, and again extracted by miniprep. These plasmids were then analysed by diagnostic restriction digests as described to verify the transformation status of the agrobacteria clones. If the result was positive, a

small sample on the second LB plate was inoculated into a fresh LB culture of four millilitres, grown at 28 °C overnight and glycerol stocks prepared as described.

2.6 *Arabidopsis* stable transformations

Arabidopsis wild type plants (Col-0, approximately 10-12 seeds per pot) were sown on soil in round flowering pots (10 cm diameter) and grown under long day light conditions as described until several inflorescences began to appear. These plants were used for floral dipping to obtain stably transformed lines.

A culture volume of 600 millilitres of transformed agrobacteria was inoculated with an agrobacteria pre-culture of 10 millilitres in LB medium supplemented with antibiotics. The large culture was grown for 48 hours at 28 °C while shaking at 250 rpm. The cells were harvested by centrifugation at 4000 g for 45 minutes at 4 °C, and the dry cell pellets resuspended in 200 millilitres of cold infiltration buffer (0.5 xMS, 5 % sucrose, 0.02 % Silwet L-77 (Lehle Seeds, Texas)). This resuspension was kept on ice until the floral dipping was commenced. For floral dipping, the agrobacteria resuspension was poured in a small container in which the inflorescences were allowed to dip into while upside-down. This assembly was placed into a vacuum bell and vacuum applied three times for five minutes with breaks inbetween where the vacuum was slowly released. The plants were briefly washed in a bucket of water by dipping, and laid flat out on a paper towel to dry. They were then placed under a transparent plastic bag into a tray filled with water and kept at 18 °C overnight. The next morning, the trays were transferred back to the growth room and kept under long day light conditions. Two days later, holes were cut into the plastic bags, and the bags were eventually removed and replaced by Aracon tubing to protect seeds. Plants were allowed to dry out completely after the first siliques became visibly senescent. The seeds of these plants (= T1) were harvested and selected on MS agar plates (0.5 x MS, 0.5 % sucrose, 0.8 % agar with appropriate antibiotics added based on the binary plasmid these plants carried). Resistant seedlings were counted, carefully transferred to soil and left until the next generation of seeds (=T2) could be harvested. In cases where it was not necessary to obtain homozygous lines, these seeds were used to analyse transgenic plants. Where it was essential to obtain homozygotes, these seeds were selected again as described and the T3 generation of seeds harvested. Their segregation pattern was analysed based on their resistance (in % of germinated seeds) to the antibiotic. In case of 100 % resistance, these lines were assumed to be homozygous and used for analysis, and were not further selected on antibiotic.

2.7 Plant growth conditions

Arabidopsis plants were either grown on soil, or sterile on MS agar plates or in MS liquid medium. All cultures were kept either under long day (16 hours light, 8 hours darkness; light intensity 150-200 $\mu\text{moles}/\text{m}^2/\text{s}$; temperature 22 °C during day period, 18 °C during darkness; relative humidity 60 % in day period, 70 % during darkness) or short day light conditions (9 hours light, 15 hours darkness; light intensity approximately 150 $\mu\text{moles}/\text{m}^2/\text{s}$; temperature and relative humidity settings as in long day) in an environmentally controlled growth chamber (Sanyo FitoTron) with set conditions as described.

Growth on soil

Before sowing, Arabidopsis seeds were vernalised by placing seeds in a tube with one millilitre of water. The tube was then wrapped in aluminium foil and kept at 4 °C for at least 48 hours. Seeds were sown individually on moist compost (Levington F2, Fisons, Ipswich, UK) inside standard growth pots/trays with the aid of a cut pipette tip attached to a P200 Gilson pipette. The pots were placed in a tray under a propagator and transferred to either a long day or a short day photoperiod growth chamber under the conditions described above. After one week, the propagator was removed and the trays were watered every three days until visibly senescent. If seeds were to be collected from these plants, Aracon tubing was placed on top of the rosettes and watering stopped once the first siliques became discoloured. The plants were allowed to dry out completely and left thereafter drying for at least another two weeks.

Growth on agar plates

For plant culture on agar plates, autoclaved Murashige and Skoog (MS) medium (0.5x MS= 3.12g MS salts/L, 0.5 % sucrose (sometimes this was omitted), 0.8 % agar, pH 5.7 (KOH)) medium was poured sterile into either squared Petri dishes (12x12 cm dimension, Greiner) or into round (9 cm or 14 cm diameter) dishes and left to solidify and dry under a flow hood. Seeds were sterilised in 1.5 ml Eppendorf tubes by adding sterilisation solution (2.5 % Na hypochlorite, 0.1 % Tween-20), vortexing and inverting the tubes for 10 minutes to ensure thorough mixing. After this time, the solution was taken off, and the seeds washed twice with ethanol. After the last wash, the ethanol was removed and the seeds were washed at least five times with one millilitre of sterile distilled water. The seeds were then kept in water wrapped in aluminium foil for at least 48 hours until sowing.

Sterilised seeds were sown individually onto MS agar plates with the aid of a sterile cut P200 pipette tip attached to a Gilson pipette. The plates were left to dry under the flow hood before being wrapped with Nesco Film and transferred to either long day or short day light conditions.

Liquid culture

Plants grown in liquid MS medium (0.5 x MS salts, 0.5 % sucrose, pH 5.7 (KOH)) were sterilised as described above and sown directly into the medium. Typically, seeds were sown into tissue culture well plates. The plates were then wrapped with Nesco Film and placed into a special tissue culture room (16 hours photoperiod, light intensity 180 $\mu\text{moles}/\text{m}^2/\text{s}$, 21C) on a shaker set to 50 rpm or on a shelf.

2.8 Plant crude protein extraction

For analysis by SDS-PAGE and Western blotting, plant proteins were extracted under denaturing conditions. Plant material was collected and placed into a two millilitre screw cap tube with a grinding ball as described. The tissue was frozen in liquid nitrogen and ground using the Qiagen Tissue Lyser. The frozen powder was then taken up in an equal volume of plant protein extraction buffer (62.5 mM Tris-Cl pH 6.8, 30 % glycerol, 5% SDS, 1.4 M β -mercapto ethanol) and thoroughly vortexed until it was defrosted. The tubes were then boiled at 95 °C for five minutes and centrifuged for one minute at maximum speed in a microcentrifuge. The supernatant was transferred to a fresh tube and centrifuged again as described. The final supernatant represented the crude protein extract and was pipetted into a fresh tube. It was quantified by the Amidoblack protein assay.

Amidoblack protein assay

The protein content of the denatured extracts was quantified with the Amidoblack assay. Two to ten μL of protein sample were pipetted into a volume of 40 μL made up with water. 160 μL of colouring solution (10 % acetic acid, 90 % methanol, 0.05 % amidoblack dye) were added to each sample followed by incubation at room temperature for 15 minutes. The samples were then centrifuged at maximum speed in a microcentrifuge for 10 minutes and the supernatants discarded. The dyed protein pellets were washed with 200 μL of decolouring solution (10 % acetic acid, 90 % methanol) and centrifuged again. The supernatant was taken off and the pellets solubilised in 800 μL of 0.1 N NaOH (= measuring solution). The absorbance at 615 nm was measured against the measuring

solution as a blank and the protein content calculated (in [$\mu\text{g}/\mu\text{L}$] based on a standard curve. For the standard curve, BSA protein samples were prepared with the following amounts: 0, 0.25, 0.5, 1, 2, 5, 10, 15 and 20 micrograms BSA in a volume of 40 μL . These samples were treated as described and used to plot a standard curve.

2.9 SDS-PAGE and Western blotting

Protein samples were separated by SDS polyacrylamide gel electrophoresis using a mini gel format (BioRad Protean III) according to the Laemmli procedure (Laemmli, 1970). Acrylamide gels of three different strengths (10, 12 and 15 %) were routinely used to separate proteins. The compositions of these gels are given in the table below (the final volumes given are sufficient for one mini gel).

Separating gel	10 % gel	12 % gel	15 % gel
H ₂ O	1.55 ml	1.25 ml	0.9 ml
30% Acrylamide solution	1.2 ml	1.5 ml	1.85 ml
4xSeparating buffer	0.95 ml		
10% Ammonium persulfate	56 μL		
TEMED	2.5 μL		
Final volume	3.76 ml		

Stacking gel	Volume
H ₂ O	2 ml
30% Acrylamide solution	600 μL
4xStacking buffer	888 μL
10% Ammonium persulfate	28 μL
TEMED	2.5 μL
Final volume [ml]	1.78 ml

Before loading on gels, protein samples were denatured by adding 5 x SDS loading buffer (see table below) to yield a concentration of 1x and heating at 95 °C for five minutes. Plant proteins extracted under denaturing conditions were heated at 95 °C for five minutes without any further additions. A molecular weight marker (10 μL of the NEB broad range prestained protein marker or the Invitrogen BenchMark™ prestained protein ladder) was always loaded in parallel with all samples. Typically, 5-10 micrograms of proteins were separated per lane. Gels were run in 1 x SDS running buffer at 100 V for one to two hours, depending on the molecular weight range of interest. The next table contains the composition of buffers and solutions used in SDS-PAGE and Western blotting.

Buffer/Solution	Composition
5xSDS loading buffer	225 mM Tris-Cl pH 6.8, 50 % glycerol, 5 % SDS, 0.05 % Bromophenol Blue, 0.25 M DTT
10x SDS Running Buffer	250 mM Tris, 1.92 M glycine, 1 % SDS
Transfer buffer	25 mM Tris, 192 mM glycine, 20 % methanol
20x TBS	2.8 M NaCl, 54 mM KCl, 500 mM Tris pH 7.4 (HCl)
Blocking solution	5 % non-fat dried milk powder (Marvel) in 1 xTBS
TBST	1 xTBS, 0.1 % Tween-20
For SDS-PAGE gels:	
4x Separation buffer	1.5 M Tris, 0.4 % SDS pH 8.8 (HCl)
4x Stacking buffer	500 mM Tris, 0.4 % SDS pH 6.8 (HCl)

Western blotting

For Western blotting, a wet blot system (BioRad) was used. SDS-PAGE gels for Western blotting were briefly rinsed in transfer buffer before assembled into the blotting sandwich. A piece (9.5 x 6.5 cm) of nitrocellulose membrane (BioRad) and two pieces of Whatman papers (10.5cm x 8cm) were cut to fit comfortably over the gel. The membrane was first rinsed in distilled water, before left to soak in transfer buffer; the Whatman papers were also soaked in transfer buffer until assembly of the blot. Pieces of transfer buffer-soaked sponge were first put on top of the black (= negative side) part of the provided blotting clamp. One layer of Whatman paper was placed on top of that, followed by the gel. The soaked membrane was placed over the gel, followed by another layer of paper and a final piece of sponge. The clamp was closed with the white side (= positive side) facing upwards. The sandwich was then placed into the provided rack with the appropriate sides facing the negative and the positive poles and placed into a gel tank. An ice container was placed on the back and the tank filled up with transfer buffer. A small stirring bar was added before the tank was closed with the appropriate lid. The tank was placed on a magnetic stirrer and connected to a power supply (BioRad) in the cold room. The blotting was run at 100 V for one hour while stirring. Upon completion, the sandwich was disassembled and the membrane stained with Ponceau S stain solution (0.1 % Ponceau S stain in 5 % acetic acid) for 10 minutes at room temperature. Excess stain was washed off with distilled water, and the Ponceau stained membrane was scanned. The membrane was then placed into blocking solution for at least one hour or longer at room temperature while slowly rotating. Following the blocking, the membrane was incubated with primary antibody (diluted in blocking solution) overnight at 4 °C or for at least two hours at room temperature. Unbound antibody was washed off by four washes with excess volumes of blocking solution for 15 minutes at room temperature. This was followed by incubation with secondary antibody (diluted in blocking solution) for at least two hours at room

temperature. Secondary antibody was always used as an HRP (horseradish peroxidase) conjugate (Sigma). Excess antibody was washed off by four washes in TBST for 15 minutes before detection of chemiluminescence using the ECL kit (Pierce ECL Western blotting substrate) on films (Kodak Medical X-Ray Film). Films were exposed in darkness and developed using a Compact X4 Xograph (Imaging Systems, Tedbury, UK).

If membranes were reprobed with another antibody, they were placed in stripping buffer (62.5 mM Tris-Cl pH 6.7, 2 % SDS, 100 mM β -mercapto ethanol) and incubated at 65 °C for one hour while rotating inside a hybridisation oven. They were then washed twice in 1x TBST for 20 minutes before blocking and probing with another antibody as described.

Methods for Chapter 3: Phylogenetic Analysis and Tissue Expression

2.10 Sequence alignments and phylogenetic trees

The sequences of all analysed proteins listed in Tables 3-2 to 3-4 were downloaded from the UniProt Knowledgebase (web address <http://us.expasy.org/sprot/>). For the construction of phylogenetic trees, multiple sequence alignments were run using the ClustalW algorithm (Thompson *et al.*, 1994) available on the Biology WorkBench 3.2 (web address <http://workbench.sdsc.edu/>, University of California, San Diego). The specified sequences were uploaded in FASTA format and aligned using the default parameters. The alignments were downloaded as .txt files and imported to ClustalW2 (downloaded from ebi.ac.uk) for the calculation of bootstrap values (1-10000). The resulting files were then viewed with the TreeView software (version 1.6.6 available from <http://taxonomy.zoology.gla.ac.uk>) (Page, 1996) as rectangular cladograms with bootstrap values displayed at each branch node.

Identity and similarity values (in %) were calculated using the Emboss pairwise Alignment algorithms (available from ebi.ac.uk) with the Emboss Needle method for global alignments. All parameters were used in the default mode.

ClustalW multiple sequence alignments were colourcoded with the BoxShade algorithm (program version 3.3.1) available on the BiologyWorkbench. The colourcoding was set to specified colours according to the degree of conservation using the Boxshade default similarities.

The structures of AtSlp1, AtSlp2 and HsSlp2 were analysed with the Protean software (part of the DNA Star software package). The specified plots were drawn with the given algorithms (Garnier *et al.*, 1978; Parry, 1982; Eisenberg *et al.*, 1984) using the default parameters. The Kyte-Doolittle hydrophobicity profiles were calculated at ProtScale (Gasteiger *et al.*, 2005) with a window size of 7 and downloaded. These values were then imported into SigmaPlot 8.0 and the hydropathy graphs created. The positions of the band-7 and stomatin domains were obtained through the UniProt entries of AtSlps and HsSlp2 via the InterPro link. Putative transmembrane spanning regions were identified with the TMAP algorithm (Persson & Argos, 1994) available through the Biology Workbench.

2.11 Cloning of AtSlp open reading frames

As indicated in the results section, the AtSlp1 open reading frame was originally obtained by RT-PCR from Dr. Petr Obrdlik (IONgate, Frankfurt, Germany). This clone was amplified and modified by site-directed mutagenesis using the overhang method (Higuchi *et al.*, 1988; Ho *et al.*, 1989). The final frame was cloned into the pDRIVE cloning vector (Qiagen, Germany) by Annegret Honsbein (University of Glasgow) using the 3' adenine overhangs from the PCR product and the uridine overhangs inside the vector according to the manufacturer's instructions. This construct was used for all following cloning procedures as indicated.

The AtSlp2 cDNA was obtained by RT-PCR. Dr. Patrick Armengaud (University of Glasgow) provided RNA that was extracted from 14 days old Col-0 seedlings grown on agar plates. These seedlings had previously been kept under potassium-depleted conditions for 3 days. RNA was extracted by him using a home-made version of the Trizol reagent and phenol-chloroform extraction as described in the general methods. The RNA (1 µg) was reverse-transcribed as described above and the resulting cDNA used as a template for PCR using primers no 1 and 2 (see primer Table in Appendix 2). 30 cycles of amplification were performed with an annealing temperature of 55 °C and an extension time of 1 minute and 30 seconds in a volume of 50 µL. The PCR products were run on a 1 % agarose gel as described above and purified on columns provided with the Qiagen gel extraction kit. 50 ng of the purified product were in turn used as a template for another PCR. This time primers were used with PstI (forward) and EcoRI (reverse) restriction sites (numbers 3 and 4 in the primer table in Appendix 2) that amplified the complete frame by PCR. The reaction was performed with 60 °C as the annealing temperature and an elongation time of 1 minute 30 seconds and 30 cycles using Invitrogen Taq polymerase. The PCR product was again gel-purified and the eluted product restriction-digested in a single reaction with EcoRI and PstI (Promega). The cloning vector pUC 18 was digested in the same way as the PCR product. The digested reactions were purified on QiaQuick spin columns (Qiagen) and used in ligation reactions in a molar ratio of vector:insert = 1:5 with T4 ligase (Invitrogen). Ampicillin-positive clones (white in colour on X-Gal containing LB plates) were plasmid- extracted in a miniprep format and tested for the presence of the insertion by restriction digestion. Positive clones were sent for DNA sequencing at the University of Dundee Sequencing Service.

Site-directed mutagenesis by the megaprimer method

This method is based on the generation of a short fragment that includes the mutation site by PCR. In a first reaction the construct template and two primers with low melting temperatures annealing around the mutation site are utilised to create a product (25 cycles, $T_a = 43\text{ }^\circ\text{C}$, extension time 10 seconds using Vent polymerase). This first PCR product is then used in a second PCR as a “megaprimer” together with a third primer that anneals further downstream with a significantly higher melting temperature to amplify the insert without the point mutation (Kammann *et al.*, 1989) (25 cycles, $T_a = 72\text{ }^\circ\text{C}$, extension time 40 seconds, Vent polymerase). Primers 5 and 6 (see table) were used to create the megaprimer. Primer 7 was then used in PCR together with the megaprimer to amplify the full frame with PstI and EcoRI as overhangs (Ling & Robinson, 1997a). The final mutagenised PCR product was gel-purified, restriction digested with PstI and EcoRI and ligated into pUC 18 as before. Ampicillin positive clones that were white on X-Gal LB plates were selected, their plasmids extracted and sequenced as before.

2.12 Antibody Production

Design of expression constructs

For the design of suitable epitopes to be overexpressed as epitope-tagged fusion proteins in bacteria, the full length sequences of AtSlp1 and AtSlp2 were aligned using the Clustal W algorithm as described above. The sequences were further inspected for their surface exposure and antigenicity index using DNA Star Protean. The surface probability was plotted using the method of Emini (Emini *et al.*, 1985) and the antigenic index was drawn according to the algorithm by Jameson and Wolf (Jameson & Wolf, 1988).

Cloning into pQE80L vector

The areas spanning amino acids 341-411 of AtSlp1 were amplified in standard PCR reaction using Vent polymerase (NEB) as described in the General Methods section. Primers no 8 and 9 (Table) were used that contain a SphI restriction site in the forward, and PstI in the reverse primer sequence. As a template, 50 ng of the pDRIVE-AtSlp1 construct was added. For AtSlp2, primers containing BamHI (forward, no 10 in Table) and HindIII (reverse, no 11 in Table) were used in the same type of PCR using the pUC 18-AtSlp2 construct as a template for amplifying a fragment spanning amino acids 2-92. PCR

products were separated on a 1 % agarose gel, purified and restriction-digested as described above.

The pQE80L vector was restriction-digested in the same way and purified according to the General Methods section. The purified digested PCR products were ligated into the vector using T4 DNA ligase (Invitrogen) as described. Competent bacteria (strain DH5 α) that were growing on LB plates supplemented with 100 μ g/ml ampicillin were selected, plasmid- extracted and restriction digested to detect positive clones. The insertions were verified by sequencing as described.

Bacterial cultures

E.coli strain M15 [pREP4] (Qiagen) was made chemically competent and transformed with the pQE80L constructs as described. The transformants were selected on LB agar plates supplemented with 100 μ g/ml ampicillin (Sigma) and 25 μ g/ml kanamycin (Fluka). Resistant colonies were selected and glycerol stocks prepared. These were used as stocks for all following cultures.

For protein expression, glycerol stocks were inoculated in 5 ml liquid LB medium supplemented with ampicillin and kanamycin as described. An aliquot of 2ml was then used to inoculate larger volumes (50 ml-1000 ml) and grown at 37 °C until the culture had an optical density (OD at 600 nm) of approximately 0.5-0.7.

Protein expression was induced by the addition of 1 mM IPTG (isopropyl- β -D-thiogalactoside, Sigma) to the growth medium. The cultures were grown for another four hours or as described until harvesting. They were filled into 50 ml centrifugation tubes and spun for 45 minutes at 4000 g in 4 °C. The supernatants were discarded and the pellets further processed.

Cell lysis and protein purification under denaturing conditions (spin columns)

For protein purification under denaturing conditions, a volume of 50 ml bacteria was grown at 37 °C and aliquots of 10 ml taken at 2, 3, 4 and 5 hours after induction. The cultures were centrifuged at 4 °C and the pellets resuspended in 400 μ L buffer B while vortexing. The lysate was centrifuged at maximum speed in a microcentrifuge for 20 minutes at 4 °C, and the supernatant transferred to a fresh tube. Ni-NTA spin columns (Qiagen) were equilibrated with 600 μ L buffer B before loading the lysate on top. Columns

were centrifuged for 2 minutes at 2000 rpm in a microcentrifuge and the flow-through collected. The columns were washed twice by adding 600 μ L of buffer C and centrifugation at 2000 rpm. Wash fractions were collected for analysis on SDS-PAGE gels. Elution of His-tagged protein was achieved by repeatedly adding 200 μ L of buffer E and centrifugation as described above at 2000 rpm. 5x SDS loading buffer was added directly to each sample to a final concentration of 1x, the samples were boiled for 5 minutes before loading on a 12 % SDS-PAGE gel. The gels were stained with Coomassie Brilliant Blue (0.1 % Coomassie Brilliant Blue, 50 % methanol, 10 % acetic acid, 40 % water) overnight and destained for several hours (40 % methanol, 10 % acetic acid, 50 % water)

Buffers used for denaturing purification:

Buffer	Composition
Buffer B	100 mM NaH ₂ PO ₄ , 10 mM TrisCl, 8 M urea pH 8 (NaOH)
Buffer C	100 mM NaH ₂ PO ₄ , 10 mM TrisCl, 8 M urea pH 6.3 (HCl)
Buffer E	100 mM NaH ₂ PO ₄ , 10 mM TrisCl, 8 M urea pH 4.5 (HCl)

Cell lysis under native conditions- target protein solubility test

For the assessment of target protein solubility, a culture volume of 50 ml was inoculated with starter cultures (grown overnight at 37 °C) and grown until OD (600 nm) 0.6. IPTG was added and the cultures were grown for another 4 hours at 37°C. The cells were harvested as described above by centrifugation, and the cell pellets resuspended in 5 ml lysis buffer (for buffer composition see table on page 82) with added protease inhibitor (1 mM PMSF (Phenylmethanesulfonyl fluoride), 1x protease inhibitor cocktail (Roche)) on ice. Lysozyme was added to a final concentration of 1 mg/ml and incubated for 30 minutes on ice. Cell lysis was further achieved by sonication with bursts of five microns amplitude (10 seconds) and breaks in between to avoid denaturation. The lysates were centrifuged for 20 minutes at 10000g at 4 °C and the supernatant (soluble proteins) separated from the pellet (insoluble proteins). The pellet was resuspended in 5 ml lysis buffer. 20 μ L samples of the soluble and insoluble fractions were added to fresh tubes with 5 μ L 5x SDS loading buffer (see above). The samples were boiled for 5 minutes before loading on a 12 % SDS-PAGE gel. The gel was Western-blotted and probed with anti-His monoclonal antibody (Sigma) in a dilution of 1:5000 (secondary anti-mouse-HRP (horseradish peroxidase) conjugate used at 1:10000 (Sigma)) as described above.

Small scale test protein purification under native conditions (batch format)

Bacterial cultures were inoculated with glycerol stocks of the 6xHis::Slp1 epitope and the 6xHis::Slp2 epitope in a volume of 100 ml. The cultures were grown until an OD (600 nm) around 0.6. IPTG was added to 1 mM and the cultures were grown for another 4 hours (the Slp1 epitope culture at 37 °C and the Slp2 epitope culture at 30 °C) and harvested by centrifugation as described. A control culture containing the empty plasmid was processed simultaneously (growth temperature 37 °C). The cell pellets were harvested and resuspended in 4 ml lysis buffer (see Table below) supplemented with protease inhibitors, sonicated as described and lysozyme (1 mg/ml) was added. The lysates were centrifuged for 20 minutes at 20000 g (4 °C) and the cleared supernatant transferred into a fresh tube. Ni-NTA agarose (Qiagen) was equilibrated with lysis buffer by several washes and a final slurry (50 % agarose content) was produced. 250 µL of this slurry were added per ml of cleared lysate followed by incubation overnight at 4 °C while rotating. Unbound proteins were collected by centrifugation (1 minute at 4000 g) and the slurry washed five times with four millilitres of wash buffer no.1 (see table on next page). Bound protein was eluted six times with 500 µL of elution buffer no.1 (see table). Samples were quantified as described below and 10 µg of each fraction was loaded on a 12 % SDS-PAGE gel followed by Coomassie blue staining.

Buffers used for purification under native conditions:

Buffer	Composition
Lysis Buffer	50 mM NaH ₂ PO ₄ , 300 mM NaCl, 10 mM imidazole, pH 8 (NaOH)
Wash Buffer #1	50 mM NaH ₂ PO ₄ , 300 mM NaCl, 20 mM imidazole, pH 8 (NaOH)
Wash Buffer #2	50 mM NaH ₂ PO ₄ , 300 mM NaCl, 30 mM imidazole, pH 8 (NaOH)
Elution Buffer #1	50 mM NaH ₂ PO ₄ , 300 mM NaCl, 250 mM imidazole, pH 8 (NaOH)
Elution Buffer #2	50 mM NaH ₂ PO ₄ , 300 mM NaCl, 100 mM imidazole, pH 8 (NaOH)
Elution Buffer #3	50 mM NaH ₂ PO ₄ , 300 mM NaCl, 150 mM imidazole, pH 8 (NaOH)
Elution Buffer #4	50 mM NaH ₂ PO ₄ , 300 mM NaCl, 200 mM imidazole, pH 8 (NaOH)
High Stringency Buffer	50 mM NaH ₂ PO ₄ , 300 mM NaCl, 1 M imidazole, pH 8 (NaOH)

BioRad Protein Assay (Bradford method)

Protein amounts were assayed according to the microprocedure as described in the manual of the BioRad Protein Assay kit based on the Bradford method (using BioRad Protein Assay Dye Reagent Concentrate). Protein standards (0, 1, 2.5, 5, 10, 15 and 20 µg BSA/ml) were prepared in 800 µL distilled water and 200 µL of dye reagent was added as described in the manual. After an incubation time of five minutes at room temperature,

absorbances at 595 nm were recorded and a standard curve calculated. Protein samples were diluted 200x and measured as described for the standards. Concentrations were calculated in $\mu\text{g}/\mu\text{L}$ based on the standard curve.

Large scale purification of Slp1 epitope (batch format)

For the first large scale purification, a bacterial culture expressing the Slp1 epitope was inoculated with an overnight grown starter culture (5 ml) in a volume of one litre LB medium supplemented with ampicillin (100 $\mu\text{g}/\text{ml}$) and kanamycin (25 $\mu\text{g}/\text{ml}$). The culture was grown as described and protein expression induced upon addition of 1 mM IPTG for 4 hours at 37 °C. The cells were lysed as described previously (from a 50 times concentrate) and 150 μL of a 50 % slurry of Ni-NTA agarose added per millilitre of lysate and incubated overnight at 4 °C while rotating. The flow-through proteins were collected by centrifugation (1 minute, 4000 g) and the bound proteins washed five times by adding 1.4 times the volume of lysis buffer for five minutes after the following protocol (see above table for buffer compositions): four washes with wash buffer no. 1 and one wash with the same buffer containing 100 mM imidazole (= elution buffer no. 2). Bound proteins were eluted 5 times by the addition of elution buffer (1/10 the volume of lysate) and incubation for 5 minutes at 4 °C followed by centrifugation for one minute with 4000 g according to the following regime: four elutions using elution buffer no. 1 and one final elution with high stringency buffer. All collected fractions were quantified with the BioRad protein assay as described and 10 μg were loaded on a 12 % SDS-PAGE gel for analysis.

A second purification from a one litre culture volume was carried out after most of the previously purified protein sample was lost while dialysing as described below. The protocol for lysis, washing and elution buffers were modified and additional elution buffers included. All buffers now contained 1 % Triton-X100 and 20 mM β -mercaptoethanol. Small amounts of previously purified leftover protein that were not sufficiently pure were purified again under these modified conditions (separately from the fresh samples). Freshly harvested cells (grown and induced under the same conditions as above) were lysed with lysis buffer (with additional detergent and reducing agent) and incubated with Ni-NTA agarose as described. Bound samples were washed four times with wash buffer no. 2 for 5 minutes at 4 °C using 1.5 times the volume of lysate. Each addition of wash buffer was followed by centrifugation at 4000 g for one minute. Bound proteins were eluted with increasing amounts of imidazole with elution buffers nos. 1-4 (see table above) by adding 1/10 the volume of lysate: four elutions (E1-E4) with elution buffer no. 2, two elutions with buffer no. 3 (E5-E6), two elutions with buffer no. 4 (E7-E8), two elutions with buffer

no. 1 (E9-E10) and two final elutions with high stringency buffer (E11-E12). All samples were quantified as described, and 10ug of protein loaded on a 12 % SDS-PAGE gel followed by Coomassie staining.

Only fractions E1-E4 were pure enough to be processed further. Leftover sample from the previous purification (wash fraction no. 5) was pooled with E1-E4 and quantified according to the Bradford method as described. The pooled sample was dialysed overnight at 4 °C against 200 times the volume of buffer (20 mM sodium hydrogen carbonate, 0.02 % SDS) in dialysis tubing with a molecular weight cutoff of 8 kDa (Pierce SnakeSkin tubing). The dialysed sample was collected, frozen and lyophilised over several days. A sample of the powder was quantified with the Bradford assay, aliquoted and a total amount of 10mg sent for injection into rabbits at the Scottish National Blood Transfusion Service (Pentlands Science Park, Penicuik, Scotland). Two animals were repeatedly injected with the purified epitope over a time course of four months. The final unpurified serum was used subsequently for all Western blots unless otherwise indicated.

Testing of Slp1 antiserum specificity

For the assessment of antibody specificity, 10 µg of plant protein extract (prepared as described above with denaturing buffer) from wild type Col-0 and two knockout lines (*slp1-1* and *slp1-2*- see chapter 5 for description) were run on 10 % SDS-PAGE gels along with protein extract from Sf9 cell cultures, and 0.5 µg of the purified epitope (dissolved in 10 mM Tris pH 7.4) as indicated in Figure 1-17 A) and B).

The Sf9 lysates were prepared by harvesting baculovirus-infected cells overexpressing AtSlp1::myc by centrifugation at 2000 g for 10 minutes at 4 °C. The cell pellets were resuspended in buffer (50 mM Tris pH 7.4, 150 mM NaCl, 1 % Triton-X100) and incubated on ice for 30 minutes. The lysates were centrifuged at 10000 g for 15 minutes at 4 °C and the supernatant quantified with the Bradford method. Proteins were denatured by adding 5x SDS loading buffer (see above) to a final concentration of 1x, followed by heating at 95 °C for five minutes. 10 micrograms of protein were loaded on the SDS-PAGE gel.

Following Western blotting, the transferred proteins were probed with Slp1 antiserum in a dilution of 1:7500, monoclonal anti-myc antibody (1:5000, Sigma from mouse), and monoclonal anti-His antibody (1:2000, Sigma from mouse). Secondary HRP-conjugated

antibodies against rabbit or mouse were used in dilutions of 1:10000 (anti-rabbit for Slp1 and anti-mouse for Sf9 lysate) and 1:5000 (anti-mouse to detect bound anti-His).

Cloning of AtSlp2 epitope into pGEX 4T-1 vector

The Slp2 epitope was amplified by PCR using Vent Taq polymerase (NEB) from the pQE80L-Slp2 epitope construct using primers nos. 12 and 13 that include BamHI and XhoI restriction sites as indicated (see Appendix 2, primer Table no.1). The PCR product was run on a 1 % agarose gel, purified and restriction-digested as described. The pGEX4T-1 vector was processed in parallel. The digested PCR product was ligated into the vector as described and transformed into chemically competent cells of the *E.coli* strain XL1-Blue for cloning and amplification using ampicillin (100 µg/ml) and tetracycline (12.5 µg/ml) for selection. The correct plasmid was extracted by miniprep and the insertion verified by restriction digestions and DNA-sequencing.

Bacterial culture

For protein expression, cells of the *E.coli* host strain BL21(DE3)pLysS (Novagen) were made chemically competent according to the Amersham GST gene fusion system handbook. Cells were transformed with the pGEX-Slp2 epitope construct and selected on LB agar plates supplemented with ampicillin (50 µg/ml) and chloramphenicol (34 µg/ml, Sigma). Positive clones were selected and glycerol stocks prepared as described; these were then used for inoculation of bacterial cultures in the following procedures.

GST fusion protein solubility test and Western blot

To test protein expression and solubility, culture volumes of 2 ml were inoculated with two separate clones (designated “9” and “23”) and the empty pGEX vector as a control in the presence of ampicillin and chloramphenicol. The cultures were grown at 37 °C until an optical density of 0.6 was reached. Protein expression was induced by the addition of 1 mM IPTG to the medium and the cultures grown for two hours. Cells were harvested by centrifugation at 4000 g for 15 minutes, and the cell pellets were resuspended in 300 µL PBS (140 mM NaCl, 2.7 mM KCl, 10 mM NaH₂PO₄, 1.8 mM K H₂PO₄ pH 7.3) with added protease inhibitors. The suspension was sonicated five times and centrifuged for five minutes at 10000 g. The supernatant containing soluble proteins was separated from the pellet (insoluble matter), and both fractions denatured by adding SDS loading buffer to a dilution of 1x and boiling. 10 µL of each sample were loaded on a 12 % SDS PAGE gel,

separated and Western blotted as described. Monoclonal GST antibody from mouse (Novagen) was used in a dilution of 1:10000; secondary anti-mouse HRP IgG conjugate (Sigma) was used at 1:10000. The blocking and washing steps were modified according to the Novagen manual “GST tag monoclonal antibody”. Blocking solution contained 1 % alkali-soluble casein as the blocking agent in 1x TBST (10 mM Tris-Cl, 150 mM NaCl, 0.1 % Tween-20 pH 7.5). The antibodies were diluted in blocking solution containing only 0.5% casein, and membranes were washed after blocking and antibody incubation twice with TBSTT (500 mM NaCl, 20 mM Tris-Cl, 0.05 % Tween-20, 0.2 % Triton-X100) and once in TBS (10 mM Tris-Cl, 150 mM NaCl) before detection with the ECL kit (GE Healthcare).

Slp epitope design for the production of commercial antibodies (AgriSera)

Short peptide epitopes for commercial antibody production by AgriSera (Umea, Sweden) were designed based on Surface probability (Emini *et al.*, 1985) and antigenicity predictions (Jameson & Wolf, 1988) obtained from Protean (part of the DNA Star software package). As an epitope for AtSlp1, amino acids 14-27 were chosen, and for AtSlp2 amino acids 84-97. The peptides were synthesised by AgriSera, conjugated to a suitable carrier protein and injected into two host animals (rabbit A and B) per peptide. The injections were repeated over several months, and serum samples analysed by Western blotting.

Testing of antibody specificity by Western blotting

Plant protein extracts from wild type plants (Col-0) and the two *slp1* knockout lines (*slp1-1* and *slp1-2*) were extracted under denaturing conditions as described and separated on 10 % SDS-PAGE gels followed by Western blotting (Figures 1-20 and 1-22). The blots were probed with pre-immune sera and the second bleeds of rabbits immunised with the Slp1 epitope in dilutions of 1:5000 (Figure 1-20). Monoclonal anti-tubulin antibody from mouse (Sigma) was used in parallel at a dilution of 1:500. The affinity-purified antisera against the Slp2 epitope (eluted at pH 2.5 and 7.5) were used at the same concentrations to detect protein on Western blots loaded with the same samples (Figure 1-22). Secondary anti-rabbit IgG HRP conjugate (from mouse, Sigma) was used at 1:10000 for detection of bands by chemiluminescence.

For further testing of the Slp2 antiserum, plant protein extracts (extracted under denaturing conditions as described) from Slp2 RNAi and promoter CMV35S overexpressing YFP fusion lines (see Methods for Chapter 4) were separated on identical gels, Western blotted

and probed with samples of the second bleeds from two animals immunised with the Slp2 epitope (rabbits A and B) with a dilution of 1:5000. Secondary anti-rabbit IgG-HRP conjugate from mouse was used for detection at a dilution of 1:10000. Monoclonal anti-GFP antibody from rabbit (Abcam) was used at 1:1000 dilution (secondary anti-rabbit-HRP from mouse used at 1:2000) as a positive control to detect YFP fusion protein.

2.13 AtSlp expression analysis

Public Microarray expression data

Expression data (absolute values) and standard deviation values were downloaded from the eFP browser database (<http://www.bar.utoronto.ca/efp>) (Winter *et al.*, 2007b). These results are based on data obtained as part of the AtGenExpress Project. The data were plotted as bar charts in Excel with the standard deviation values as error bars given in the database. The following publications include detailed information about the actual experimental setups:

- Gene expression in different stages of plant development and organs (Schmid *et al.*, 2005);
- Tissue specific data: roots (Birnbaum *et al.*, 2003), pollen development (Honys & Twell, 2004), xylem and cork (laboratory of Dr. Malcolm Campbell, University of Oxford), stem epidermis cells (Suh *et al.*, 2005), Stigma and ovary data (Swanson *et al.*, 2005), guard cells (Yang *et al.*, 2008);
- Expression in seeds: imbibition data (Nakabayashi *et al.*, 2005; Yamauchi *et al.*, 2004), chemical treatments (Dr. Sean R. Cutler/Pauline Fung, University of Toronto);
- Treatments with hormones and chemical treatments (Goda *et al.*, 2008);
- Abiotic stress treatments (Kilian *et al.*, 2007);

Transcript analysis by Northern blotting

Plant culture and stress treatments

Wild type (Col-0) plants were sown into one ml of liquid medium (0.5x MS, 0.5 % sucrose, pH 5.8) inside a sealed 24 well tissue culture dish. Each well contained exactly 20 seeds. The plants were grown for 10 days while the plates were slowly shaken (50 rpm) under long day light conditions (16 h photoperiod). On day 11, control samples were taken (t =0) before treatments were started by individually adding chemicals into each well to the appropriate concentration as outlined in the table below.

Treatment	Stock concentration	Final concentration	Solvent
t-zeatin	20 mM	10 μ M	EtOH
kinetin	5 mM	5 μ M	0.1N NaOH
NAA	5 mM	6 μ M	EtOH
NPA	10 mM	10 μ M	DMSO
TIBA	10 mM	10 μ M	DMSO
ACC	50 mM	200 μ M	H ₂ O
Brassinolide	5 mM	5 μ M	EtOH
NaCl	5 M	150 μ M	H ₂ O

Samples were collected, dried between two layers of tissue and frozen in liquid nitrogen before grinding. Samples were taken in duplicates after 2 hours, 4 hours, 8 hours, 24 hours and 48 hours after the addition of the chemicals. RNA was extracted and quantified as described in the General Methods section.

Denaturing agarose gel electrophoresis and Northern blotting

Buffers and solutions used during this procedure:

Buffer/Solution	Composition
10x MOPS	0.2 M MOPS pH 7.0 (2 N NaOH), 50 mM Na acetate, 10 mM EDTA pH 8.0
Sample denaturing buffer	50 % formamide (deionised), 19 % formaldehyde (38 %), 1x MOPS
Loading buffer	0.25 M Na phosphate buffer pH 6.8, 15 % Ficoll, 0.02 % bromophenol blue
Agarose gel	1.2 % agarose, 1x MOPS, 20 % formaldehyde (38 %)
20x SSC	3 M NaCl, 0.3 M Na citrate pH 7.0
Methylene blue stain	0.5 M Na acetate pH 5.2, 0.02 % methylene blue
Hybridisation buffer	0.25 M Na phosphate buffer pH 7.0, 7 % SDS, 1 mM EDTA, 1 % BSA
Wash buffer no.1	2x SSC, 0.1 % SDS
Wash buffer no.2	1x SSC, 0.1 % SDS
Wash buffer no.3	0.5x SSC, 0.1 % SDS
Wash buffer no.4	0.1 xSSC, 0.1 % SDS
Probe stripping buffer	2 mM Tris pH 8.0, 2 mM EDTA, 0.1 % SDS

A total amount of 10 micrograms of RNA from one replicate per experiment were loaded per well on a 1.2 % denaturing agarose gel. Samples were prepared by adding 10 micrograms of RNA in a volume of 20 μ L DEPC-treated water. Each 20 μ L sample was then vacuum-concentrated to a 2 μ L volume. 12 μ L of sample denaturing buffer were added to each sample followed by heating at 65 °C for 15 minutes. The samples were immediately placed on ice, and 2 μ L of loading buffer added. The samples were briefly spun down, loaded on the agarose gel (see table for composition) and run at 35 V in 1x MOPS (3-(N-Morpholino)propanesulfonic acid) buffer for three hours.

The Northern blot was assembled as follows: three layers of Whatman paper and one piece of membrane (Hybond N+, Amersham) were cut exactly to the dimensions of the gel. The gel and membrane were briefly washed in DEPC treated water, and the Whatman papers and membrane soaked in 20x SSC. The gel was placed upside-down on a support tray filled with 20x SSC on top of a Whatman paper dipping into the SSC solution. The membrane was placed on top, followed by 3 layers of Whatman paper. Several additional layers of tissue were placed on top, finished by putting a small weight on top. The transfer was left to proceed overnight by upward capillary transfer at room temperature. The sandwich was disassembled, the membranes rinsed in 2x SSC solution, and UV-crosslinked at 254 nm for 1 minute. The membrane was then washed in 5 % acetic acid for 15 minutes before staining with methylene blue. Excess dye was rinsed away with DEPC treated water, and photographs taken in a BioRad transilluminator using white light. These images were later used for quantification of the transcript responses normalised to the band intensity of the methylene blue stained rRNA bands. The membrane was then destained in 0.2x SSC and 1 % SDS.

Membranes were prehybridised by incubation with hybridisation buffer inside a hybridisation tube at 65 °C for 3 hours while rotating.

Probes were synthesised as PCR products. For AtSlp1, a standard PCR reaction using NEB Taq polymerase was set up with primers nos. 14 and 15 and 5 μ L of 10x diluted cDNA (synthesised from wild type extracted RNA as described in General Methods) with 35 cycles. The probe for AtSlp2 was synthesised under identical PCR conditions with primers nos. 16 and 17. The PCR products were run on a 1% agarose gel as described and gel extracted. Two μ L of each product were run again on an agarose gel, and the DNA concentrations estimated.

Probe labelling was carried out according to the instructions given in the Rediprime II random prime labelling system kit (GE Healthcare). Briefly, 20 ng of PCR product were added with TE buffer to a volume of 45 μ L. This was followed by denaturation for five minutes at 95 $^{\circ}$ C. The tubes were immediately transferred to ice for five minutes and the contents collected by brief centrifugation. The probe was then added to a reaction tube provided by the Rediprime II kit. To this reaction, 5 μ L of 32 P-labelled dCTP (RedivueTM 32 P deoxynucleotides, GE Healthcare) were added and incubated at 37 $^{\circ}$ C for 10 minutes. The labelling reaction was stopped by addition of 20mM EDTA followed by denaturation at 95 $^{\circ}$ C for five minutes and snap-cooling on ice. The radiolabelled probe was added to a hybridisation tube containing the membrane and incubated overnight at 65 $^{\circ}$ C while rotating. Excess labelled probe was washed off by four washes for 20 minutes using wash buffers 1-4. Labelled bands were imaged on a phosphorimager (Fujifilm FLA-5000) after three days of exposure inside a developing cassette.

Membranes were stripped from bound probes by incubation with stripping buffer for one hour at 70 $^{\circ}$ C. This procedure was followed by washing in 2x SSC at room temperature. The stripped membranes were prehybridised followed by hybridisation with a new probe as described above.

Gene duplication database

The Plant Genome Duplication Database (PGDD at <http://chibba.agtec.uga.edu/duplication>) (Tang *et al.*, 2008) was queried with the At4g27585 (AtSlp1) locus. The output window was set to display 100 kbp of sequence around this locus. The results of a BLAST search of the PGDD with AtSlp1 are given in a table in Appendix 1.

Promoter response elements

The Athena database at Washington State University (O'Connor *et al.*, 2005) was queried with both AtSlp loci (<http://www.bioinformatics2.wsu.edu/cgi-bin/Athena>). The output was set to cartoon display and 2000bp of upstream sequence. The image structure was set to “separate images” and 1x magnification. Information about response elements derived from this database is linked to the AtCisDB (*Arabidopsis thaliana* Cis-element database, Agris at Ohio State Universtiy; (Palaniswamy *et al.*, 2006) database from which further details about response elements and binding transcription factors were derived. Additionally, the PLACE database (Plant cis-acting regulatory DNA elements database,

(Higo *et al.*, 1999) was also queried. All information from these three databases was pooled and summarised in Tables 3-13.

Cloning of AtSlp promoters

Genomic DNA was extracted from leaves of wild type Col-0 plants that were grown on soil for four weeks under long day light conditions as described. The promoter regions (2898 bp upstream of the start codon of AtSlp1, and 1898 bp upstream of AtSlp2) were amplified by PCR with Phusion Taq polymerase (25 cycles) using primers nos. 18 and 19 for the AtSlp1 promoter, and primers 20 and 21 for the Slp2 promoter. The PCR products were 3' adenylated by addition of 0.5 µL standard Taq DNA polymerase (Invitrogen) and dATP (1 µL of a 10 mM stock, Invitrogen) to the PCR reactions upon completion of amplification with Phusion Taq, and additional extension at 72 °C for 10 minutes. The products were gel-purified and ligated into pDRIVE using the Qiagen PCR cloning kit according to the manufacturer's instructions. Chemically competent DH5α cells were transformed as described and positive clones selected on LB agar plates containing 100 µg/ml ampicillin. The plasmids were extracted by minipreps, and the insertions verified by sequencing as described.

These constructs were used as templates (50 ng) in PCR reactions using Phusion enzyme and primers nos. 22 and 23 for the AtSlp1 promoter, and nos. 24 and 25 for the Slp2 promoter to amplify the promoters with PstI and NcoI restriction sites as overhangs. The PCR products were gel-purified and restriction digested with PstI and NcoI enzymes as described. The binary vector pCAMBIA 1301 (www.cambia.org) was digested in parallel and purified on QiaQuick PCR purification spin columns (Qiagen). A ligation reaction was set up with an insert:vector ratio of 5:1. This was transformed into *E.coli* strain DH5α, and positive clones selected on LB medium containing 50 µg/ml kanamycin. Plasmids were extracted by miniprep and sequenced.

Verified plasmids were transformed into *Agrobacterium tumefaciens* (GV3101) as described. Positive transformants were selected on LB plates containing 50µg/ml kanamycin and 25 µg/ml gentamycin. Resistant clones were further verified by extracting plasmids by miniprep, re-transformation of DH5α and restriction digests of *E.coli*-extracted plasmid DNA.

Transformed *Agrobacteria* were used to floral-dip wild type plants as described. Successfully transformed plants were selected on MS agar (0.5x MS, 0.5 % sucrose, pH

5.7) supplemented with 50 µg/ml hygromycin (Invitrogen). Positive plants were propagated until the T2 generation and these seeds used to assay for GUS activity in different growth stadiums as indicated in Figures 1-33 to 1-37.

GUS assays

GUS activity was assayed by submerging plant material in assay buffer (50 mM Na phosphate buffer pH 7.2, 0.5 mM K ferrocyanide, 0.5 mM K ferricyanide, 1 mM X-Gluc (5-bromo-4-chloro-3-inolyl-beta-D-glucuronic acid, cyclohexylammonium salt from Xgluc Direct)) and vacuum infiltrated three times for five minutes at room temperature. Samples were incubated overnight at 37 °C in the dark. The leaves were destained in 70% ethanol and stored in 100 % ethanol until imaging. Some stains were destained and fixed in a mixture of ethanol:acetic acid (3:1). A series of transgenic plants for both constructs were grown under long day light conditions (16 hours light, 8 hours dark) either in liquid 0.5x MS medium supplemented with 0.5 % sucrose, on MS agar plates (0.5x MS, 0.5 % sucrose, 0.8 % agar, pH 5.7) or on soil and harvested as a whole for GUS staining reactions. Plants were assayed at different developmental stages from each growth condition. They were then imaged either in ethanol or mounted in glycerol under a binocular microscope with a Zeiss AxioVision camera attached

Hormone and stress treatments

T2 transgenic promoter-GUS plants were grown for 10 days in liquid medium as described. Plants were treated by direct addition of chemicals and hormones as described in section 3.5.3.4. For treatment with UV-B light, plates were placed on a BioRad transilluminator imager (BioRad Chemi Doc) and irradiated with UV light for 15 minutes. Eight hours after the treatments, the seedlings were assayed for GUS activity as described. For the separate treatment with UV-B light, plants were grown for 14 days in a 12 well tissue culture plate under the same conditions. In parallel, the same plants were grown on MS agar plates (with and without 0.5 % sucrose added) as described for the same period. The plants were treated identically with UV-B light, but assayed already six hours after the irradiation period. Part of the seedlings were frozen in liquid nitrogen, ground to powder and their proteins extracted under denaturing conditions as described. 10 micrograms of protein were loaded on a 10 % SDS-PAGE gel, Western blotted and probed with anti-Slp1 antibody in a dilution of 1:5000 (secondary anti-rabbit HRP conjugate from mouse was used at 1:10000).

RT-PCR and Western blot of Arabidopsis organs

Arabidopsis wild type plants (ecotype Col-0) were grown for 8 weeks under short day light conditions (9 hours light, 15 hours dark at 21 °C) on soil and hydroponically, and organs were collected: samples from roots, rosette leaves, cauline leaves, stem tissue, buds and open flowers. The samples were frozen in liquid nitrogen and ground using the Qiagen Tissue Lyser as described. RNA was extracted, quantified and 1 µg in total used for reverse transcription reactions. The resulting cDNA was diluted 10 times, and 5 µL used as a template in PCR reactions (Invitrogen Taq DNA polymerase) with primers nos. 14 and 26 for the Slp1 transcript (30 cycles), and primers nos. 27 and 28 for the Slp2 transcript (32 cycles). Primers for the ubiquitin 10 transcript (nos. 29 and 30) were used in parallel as a control.

From the same ground samples, crude protein extracts were prepared under denaturing conditions as described. The extracts were quantified with the Amidoblack protein assay, and 10 micrograms protein loaded on a 10 % SDS-PAGE gel followed by Western blotting. AtSlp1 was detected by incubation with anti-Slp1 at 1:5000 (secondary antibody 1:10000) and chemiluminescence detection. The probed membrane was stripped and reprobed using anti-Slp2 at 1:5000 (secondary anti-rabbit-HRP conjugate used at 1:8000) followed by the same detection.

Methods for Chapter 4: AtSlp subcellular localisation and AtSlp1 protein analysis

2.14 Subcellular targeting

Prediction softwares

The complete amino acid sequences of AtSlps were entered into the search windows of the following databases: MitoProtII (<http://ihg2.helmholtz-muenchen.de/ihg/mitoprot.html>), TargetP (<http://www.cbs.dtu.dk/services/TargetP/>), Predotar (<http://urgi.versailles.inra.fr/predotar/predotar.html>), PSORT and PSORT II (<http://psort.ims.u-tokyo.ac.jp/>). The protein sequence of HsSlp2 was entered into PSORT II. Whenever possible, a window specifying plant sequences was ticked. Otherwise all settings were left as default. For the Cell eFP browser (http://bar.utoronto.ca/cell_efp/cgi-bin/cell_efp.cgi), the accession numbers of AtSlps were entered into the search window.

Alpha helical wheel plots

The Protean software (DNA Star) was used to draw alpha helical wheel plots of the predicted mitochondrial targeting sequences as indicated.

2.15 Biochemical methods

Aqueous 2-phase partitioning

The original method by Larsson et al. (Larsson *et al.*, 1987; Larsson *et al.*, 1994) was modified, downscaled and further adapted for the use of Arabidopsis shoot tissue. All buffers and stock solutions are listed in the two tables below. Approximately 10 grams of fresh weight tissue from mature short-day grown Arabidopsis Col-0 plants were harvested and put on ice immediately. All following procedures were carried out at 4 °C. 50 millilitres of homogenisation buffer (with freshly added protease inhibitors: 1 mM PMSF, 1x Protease inhibitor cocktail) were added to the tissue inside a Waring blender. The tissue was thoroughly homogenised by several strokes of 10 seconds with breaks in between. The homogenate was filtered through two layers of MiraCloth (Calbiochem) and centrifuged for 15 minutes at 10000 g and 4 °C. The supernatant was filtered through a nylon net (pore size 50 µm) and centrifuged again for 30 minutes at 100000 g and 4 °C in a Sorvall

ultracentrifuge. The supernatant was discarded and the pellet resuspended in one millilitre of microsomal buffer followed by homogenisation in a Dounce homogeniser (at least 20 strokes). A volume of 500 μ l of the homogenised microsomal pellet was layered on top of a 1.5 gram separated 2-phase system (see table). The tube was shaken vigorously for at least two minutes before centrifugation in a microcentrifuge at 2000 g for 5 minutes at 4 °C to separate the phases. Meanwhile, the separated 20 grams wash system was separated into upper (PEG) and lower (Dextran) phases by careful pipetting. The clear upper phase from the centrifuged tube was transferred into a fresh 2 ml Eppendorf tube and 900 μ L of fresh lower phase (from the 20 g wash system) were added, followed by vigorous shaking as described. To the green-coloured remaining lower phase after the spin, 900 μ L of fresh upper phase (from the 20 g wash system) were added, shaken and centrifuged as before. After each separation a new round of extraction was done as described to further purify the upper and lower phases from cross-contaminations. A total of three extractions for each phase was performed. After all extractions, the purified upper and lower phase fractions were each pooled together. The upper phase fraction was diluted 3-5 times with wash buffer, and the lower phase at least 10-20 times. Each dilution was then centrifuged for one hour at 170000 g at 4 °C in an ultracentrifuge. The supernatants were discarded and the pellets resuspended in 5xSDS buffer as described. Proteins were denatured by incubation at 37 °C for 30 minutes to avoid precipitation of the plasma membrane marker protein used. The protein content was quantified by the Amidoblack protein assay as described and equal amounts of both phases separated on a 10 % SDS-PAGE gel. Western blots were probed with anti-Slp1 (1:5000), anti H⁺-ATPase (1:1000) and anti-PRX II (1:1000) and secondary anti-rabbit HRP conjugate.

Buffer	Composition
Homogenisation buffer	150 mM Tris-Cl pH 7.5, 10 mM KCl, 2 mM EDTA, 12% sucrose (350 mM), 1 mM DTT
Microsomal resuspension buffer	330 mM sucrose, 5 mM K-phosphate buffer pH 7.8, 1 mM DTT
Wash buffer	330 mM sorbitol, 50 mM HEPES-KOH pH 7.0, 40 mM KCl, 1 mM EDTA, 1 mM DTT
PEG 3550 stock	40 % w/w
Dextran-T 500 stock	20 % w/w

Buffers and solutions used for 2-phase partitioning.

	Initial separation	Phase extraction
2-phase system	1.5 g (2 ml tube)	20 g (50 ml tube)
PEG stock	320 mg (6.4 %)	3.2 g (6.4 %)
Dextran stock	640 mg (6.4 %)	6.4 g (6.4 %)
Sucrose (2M)	247.5 μ L (330 mM)	3.3 ml (330 mM)
K-Phosphate (500mM) pH 7.8	15 μ L (5 mM)	200 μ L (5 mM)
KCl (100mM)	60 μ L (3 mM)	600 μ L (3 mM)
H ₂ O to	1.5 g	20 g

2-phase systems prepared.

Mitochondria isolation by differential centrifugation

Mitochondria-enriched pellets were isolated by differential centrifugation. 50 grams of fresh weight shoot tissue (Col-0 plants, short day grown) was harvested and homogenised in a Waring blender in 200 millilitres of buffer A (see table below for composition). Homogenisation was achieved by 2 second strokes with 5 second breaks in between. The homogenate was filtered through 2 layers of MiraCloth and centrifuged at 3000g for five minutes at 4 °C. The supernatant was centrifuged at 12000 g for 20 minutes at 4 °C. The pellet of this spin was resuspended in 4 millilitres of buffer B and further homogenised by pottering. This resuspension was then centrifuged at 1500 g for 10 minutes at 4 °C. The supernatant was centrifuged at 11000 g for 15 minutes at 4 °C and the resulting pellet resuspended in 1 millilitre of buffer B. 5x SDS buffer was added to 1x, the samples were boiled and the protein content quantified by the Amidoblack assay. 10 micrograms of protein of each fraction were loaded on a 10 % SDS-PAGE gel and Western blotted. Anti-Slp1 (1:5000) and anti-PRX II (1:1000) were used to probe the blots.

Mitochondria purification on a linear Percoll gradient

All buffers used in this experiment are listed in the table below. Approximately 50 grams of fresh weight shoot issue (short day grown, mature Col-0 plants) was harvested and placed on ice immediately. It was then homogenised in 200 millilitres of buffer A with freshly added protease inhibitors (see table below) by 5-10 two seconds strokes. The homogenised material was then filtered through MiraCloth and centrifuged at 3000 g for five minutes at 4 °C. The supernatant was centrifuged for 20 minutes at 12000 g at 4 °C. The resulting pellet was resuspended in 5 millilitres buffer B (with protease inhibitors) and centrifuged at 1500 g for 10 minutes at 4 °C. The supernatant of this spin was centrifuged at 11000 g for 15 minutes at 4 °C. The pellet was carefully resuspended in 500 μ L of 32 % (v/v) Percoll in buffer B*. This resuspension was then layered on top of a 32 % (v/v) self-

forming Percoll gradient in B* (final volume 24 millilitres) and centrifuged at 40000 g for 45 minutes at 4 °C without braking in a fixed angle rotor (Sorvall T-865). The lower 1/3 of the resulting gradient was removed with a Pasteur pipette and transferred into a fresh tube. Care was taken to remove all green material above the fraction enriched in mitochondria by careful aspiration with a vacuum pump. This mitochondrial fraction was then diluted six times in buffer B and centrifuged at 11000 g for 15 minutes at 4 °C. The resulting mitochondrial pellet was resuspended in 500 µL of buffer MB.

For analysis of the mitochondrial pellet by Western blotting, an aliquot of 100 µL was taken off and 25 µL of 5x SDS loading buffer were added. This volume was further divided into two aliquots and each was denatured either by boiling for five minutes or at 37 °C for 30 minutes. The protein content of each sample was determined by the Amidoblack protein assay and 5 micrograms were loaded on a 10 % SDS-PAGE gel followed by Western blotting and incubation with anti-Slp1 (1:5000), anti-Slp2 (1:1000) and anti-PRX II (1:1000).

Buffer	Compostion
Buffer A	20 mM MOPS pH 7.4, 300 mM sucrose, 5 mM glycine, 4 mM cysteine, 2 mM EDTA, 0.5 % PVP 40 (w/v), 0.2% BSA (w/v)
Buffer B	10 mM K phosphate buffer pH 7.2, 300 mM sucrose, 5 mM glycine, 1 mM EDTA, 0.5 % PVP-40, 0.1 % BSA
Buffer B*	15.2 mM K phosphate buffer pH 7.2, 456 mM sucrose, 7.6 mM glycine, 1.52 mM EDTA, 0.76 % PVP-40, 0.152 % BSA
Buffer MB	10 mM TES-KOH pH 7.2, 300 mM sucrose
Protease K	50x= 5 mg/ml in buffer K
Buffer K	50 mM Tris-Cl pH 8.0, 10 mM CaCl ₂
Buffer KMB	Buffer MB+ 50 mM CaCl ₂
Digitonin	50x= 25 µg/ml in Buffer KMB

Buffers and solutions used for mitochondrial isolation on the linear gradient.

Submitochondrial targeting experiment

An aliquot of 300 µL was separated and divided into 7 aliquots, each consisting of 42 µL mitochondrial resuspension. To each aliquot protease K (or buffer K in the control sample no. 1) and digitonin (or buffer KMB in the control samples) were added according to the table below. The mixtures were incubated in the cold for 30 minutes. The reactions were stopped by the addition of 10 mM PMSF (in ethanol) and 12.5 µL of 5x SDS loading buffer. The samples were denatured by boiling for five minutes and quantified by the Amidoblack protein assay. Five micrograms of protein were loaded on a 10 % SDS-PAGE gel and Western-blotted. Antibodies were used in the same dilutions as described above.

Aliquot no.	Sample	Protease K	Buffer KMB	Digitonin [μL]	Conc. Digitonin [$\mu\text{g/ml}$]
1	Control	1 μL buffer K	7 μL	0	0
2	K- Digitonin	1 μL Prot.	7 μL	0	0
3	K+ Digitonin	1 μL Prot.	6 μL	1	0.5
4	K+ Digitonin	1 μL Prot.	5 μL	2	1
5	K+ Digitonin	1 μL Prot.	4 μL	3	1.5
6	K+ Digitonin	1 μL Prot.	3 μL	4	2
7	K+ Digitonin	1 μL Prot.	1 μL	6	3

Protease K/Digitonin treatment of isolated mitochondria from the linear gradient. "Prot." stands for protease K; In sample no. 1, buffer K was added instead of protease.

Mitochondrial purification on Percoll step gradients

All buffers and solutions used for this extraction are listed in the table below. Fresh leaf tissue (50 g) from mature short-day grown *Arabidopsis* plants (Col-0) was harvested and immediately chilled. The tissue was homogenised in a Waring blender in 200 millilitres buffer A with added protease inhibitors as described. The homogenate was filtered and centrifuged three times in a row: 1100 g for 5 minutes, 3000 g for 10 minutes and 12000 g for 20 minutes at 4 °C. The final pellet was resuspended in 800 μL buffer B with the help of a fine paintbrush. This resuspension was carefully layered on top of a preformed discontinuous Percoll gradient consisting of three steps as outlined below:

Percoll density	Proportion	Setup in tube [ml]
18 %	2	6.6
29 %	4	13.2
45 %	1	3.3
	Final volume/tube	23.1

Setup of Percoll step gradients. For buffer composition, see tables below.

The gradient was prepared by carefully overlaying the different Percoll density solutions using a wide needle attached to a syringe, starting with the densest one. The loaded gradient was then centrifuged at 70000 g for 45 minutes at 4 °C with brakes off in a fixed angle rotor. The mitochondrial fraction was visible below the thylakoid-containing fractions in the bottom third of the tube. The fractions above mitochondria were carefully removed with a pipette tip attached to a vacuum pump. The mitochondrial fraction was transferred to a fresh tube, diluted six times in buffer MB and centrifuged at 17000 g for 15 minutes at 4 °C. The mitochondrial pellet was then resuspended in 500 μL of buffer MB with the help of the paintbrush and divided into aliquots.

For Western blot analysis, the samples were processed as described above for the linear gradient fractions.

Buffer	Compostion
Buffer A	20 mM MOPS pH 7.4, 300 mM sucrose, 5 mM glycine, 4 mM cysteine, 2 mM EDTA, 0.5 % PVP 40 (w/v), 0.2 % BSA (w/v)
Buffer B	10 mM K phosphate buffer pH 7.2, 300 mM sucrose, 5 mM glycine, 1 mM EDTA, 0.5 % PVP-40, 0.1 % BSA
Buffer MB	10 mM MOPS pH 7.2, 300 mM mannitol
10x FA	10 % FA in MB (w/v)
2x Glycine	250 mM glycine in MB
Protease K	50x= 5 mg/ml in buffer K
Buffer K	50 mM Tris-Cl pH 8.0, 10 mM CaCl ₂
Buffer KMB	Buffer MB+ 50 mM CaCl ₂
Digitonin	50x = 25 µg/ml in Buffer KMB

Buffer compositions for mitochondrial isolation on Percoll step gradients and submitochondrial fractionation.

Percoll density (v/v)	Percoll [ml]	1M sucrose [ml]	0.5M K-Phos. pH 7.2 [ml]	H ₂ O [ml]
18 %	9	15	1	25
29 %	14.5	15	1	19.5
45 %	22.5	15	1	11.5

Preparation of Percoll density fractions. The final volume of each fraction stock was 50ml.

Submitochondrial localisation experiment

For the assessment of the localisation of AtSlp1 to the mitochondrial inner membrane, isolated mitochondria from the step gradient were aliquoted. Altogether 7 aliquots, each containing 40 µL volume were transferred to single tubes. To each tube buffer K, protease K and KMB or digitonin were added as outlined in the table below. The reactions were treated as described above for the experiment with mitochondria from the linear gradient. Western blots were probed under the same conditions as described above.

Aliquot no.	Sample	Protease K	Buffer KMB	Digitonin [µL]	Conc. Digitonin [µg/ml]
1	Control	1 µL buffer K	9 µl	0	0
2	K- Digitonin	1 µL Prot.	9 µl	0	0
3	K+ Digitonin	1 µL Prot.	8 µl	1	0.5
4	K+ Digitonin	1 µL Prot.	7 µl	2	1
5	K+ Digitonin	1 µL Prot.	5 µl	4	2
6	K+ Digitonin	1 µL Prot.	0	10	5
7	K+ Digitonin	1 µL Prot.	0	20	8.33

Setup of mitochondrial sublocalisation experiment from discontinuous Percoll gradients.

2.16 *In vivo* localisation of AtSlps

Cloning of fluorescent fusion protein constructs- 35S::Slp::YFP

The open reading frames of Slp1 and Slp2 were amplified by PCR with primers nos. 31-34 that have additional NcoI restriction sites in their overhangs. PCR was carried out using Phusion Taq polymerase as described in the general methods. The amplified products were purified, restriction digested and ligated into pTEY opened with NcoI. This vector was constructed by Dr. Manuel Paneque (University of Glasgow) and contained a 35S promoter, a YFP flanked by an NcoI and EcoRI site, a stop codon and the NosA terminator in an expression cassette flanked by NotI sites (not published). Both NcoI and EcoRI sites were unique in the pTEY sequence. Ampicillin-positive clones were plasmid-extracted, restriction digested and sequenced to verify the insertion of either AtSlp at the N-terminus of the YFP. Simultaneously, N-terminal YFP fusions of both AtSlps were cloned by amplifying the open reading frames with primers nos. 35-38. to create EcoRI sites, and ligating these PCR products into pTEY opened with EcoRI. Once all insertions were verified by DNA sequencing, the complete expression cassettes containing either AtSlp and YFP were excised by digestion with NotI. The binary vector pTKAN⁺ was opened with PspOMI (NEB Biolabs) and the cassettes ligated with the compatible NotI ends. All obtained constructs were verified by restriction digestions and DNA sequencing.

Cloning of genomic sequence GFP fusion constructs- Promoter(Slp2)::gSlp2::GFP6

The genomic sequences of AtSlp1 and AtSlp2 were amplified from Arabidopsis genomic DNA with Phusion Taq polymerase. DNA was extracted as described from wild type plants. AtSlps were amplified with primers nos. 39 and 40 for AtSlp1 (4551 bp), and nos. 41 and 42 for AtSlp2 (4427 bp). Both amplicons were ligated into the pGEM T-Easy vector kit (Promega) using 3' adenine overhangs that were attached after the original amplification by adding 1mM dATP and standard Taq polymerase at 72 °C for 10 minutes. Positive clones were selected on ampicillin LB agar plates as described and the insertions were verified by DNA sequencing.

To fuse GFP to the C-terminus of either Slp gene, an additional restriction site had to be created. The cloning of a C-terminal GFP fusion inside the genomic sequence of AtSlp1 failed at this step and will not be described further. GFP fusion to the C-terminus of AtSlp2 was accomplished by inserting a KpnI site in front of the stop codon inside the last exon of this gene. This was done by making use of the overlap method and primers nos. 43-46

(Higuchi *et al.*, 1988). This insertion was again verified by DNA sequencing. GFP6 was amplified from a suitable template by primers nos. 47 and 48 with Phusion Taq polymerase, restriction digested with KpnI and ligated into pGEM-gSlp2(KpnI) that had been digested with KpnI prior to ligation. This insertion was in turn verified by DNA sequencing. The complete expression cassette (P(AtSlp2)::gAtSlp2::GFP6) was excised out of pGEM-T easy by digestion with ApaI and PstI. The binary vector pTKAN⁺ was digested with the same enzymes and used for ligation of the genomic GFP fusion cassette. Positive clones were selected on 100 µg/ml spectinomycin and verified by restriction digestions and DNA-sequencing.

Stable transformation and plant culture

All constructs were used to transform *Agrobacterium tumefaciens*. Positive transformants were selected on LB agar plates containing 100 µg/ml spectinomycin and 25 µg/ml gentamycin. Confirmed positive clones were used in the stable transformation of flowering Arabidopsis wild type plants (Col-0) as described. Positively transformed plants were selected on MS agar plates containing 50 µg/ml kanamycin, and propagated until the T2 generation. For imaging of whole seedlings, either kanamycin resistant T1 seedlings were directly used from kanamycin plates, or T2 seedlings that had been further selected. For imaging, whole seedlings or tissue samples were carefully removed and mounted in water on a standard microscope objective slide. Silicone-based glue was used to attach coverslips. Care was taken that the samples did not dehydrate while being imaged.

For the images in Figure 2-10, kanamycin-resistant T1 seedlings expressing Slp1-YFP were transplanted from agar plates to soil and leaf tissue was collected. The presented images were derived from plants approximately 30 days old.

For root imaging of Slp-YFP with MitoTracker, T2 seedlings were grown in hydroponic culture in a 6-well plate format in 0.5x MS pH 5.7 (KOH) supplemented with 0.5% sucrose under long day light conditions for 5 days. Seedlings were transferred into fresh medium containing 100 nM MitoTracker DeepRed (Molecular Probes; stock solution 1 mM in DMSO). MitoTracker was allowed to be taken up by the plants for 45-60 minutes. The seedlings were briefly rinsed in fresh MS medium, before being mounted on microscopy slides.

Slp2-GFP in Figure 2-14 was imaged on 14 days old T1 seedlings selected on kanamycin supplemented MS plates. Images of Slp2-GFP from Figures 2-15, -17 and -18 were taken

from 30 days old kanamycin-resistant T1 seedlings grown on agar plates. Whole seedlings were incubated for 45 minutes with 100 nM MitoTracker Orange in MS medium (Molecular Probes; stock solution 1mM in DMSO). Before imaging, excess dye was briefly washed off in fresh MS medium, and pieces of leaves were mounted in water on microscope slides.

The phenotypes photographed and presented in Figure 2-19 were from T2 plants that were grown unselected on soil (long day light, 27 days old). Photography was done in a dark room using a Nikon D1x camera.

Confocal imaging and settings

Slp1-YFP and MitoTracker DeepRed

Confocal imaging was done on a Carl Zeiss CLSM510 inverted confocal microscope. Leaf material in Figure 2-10 was imaged using a 63x apochromat water immersion objective. YFP was excited with an Argon laser run at 6.1 A using the 514 nm line and transmission set to 12 % output. The laser light was reflected using a first dichroic mirror (458/514). Transmitted light was collected in the brightfield channel. Emitted fluorescence was subsequently passed through a secondary dichroic mirror (635 VIS) and chlorophyll autofluorescence was collected using a Meta detector between 606 and 723 nm. Reflected fluorescence was passed through a third dichroic mirror (515nm cutoff) and long pass 530 nm filter to detect YFP signal. Three-dimensional images from z-stacks were reconstructed using the supplied Zeiss LSM imaging software.

Root hairs of Slp1-YFP plants were imaged using a 40x Plan Neofluar oil immersion objective. For co-localisation of YFP and MitoTracker DeepRed, YFP was excited with the Argon laser as above using the 514nm line and transmission at 21 % output. MitoTracker was excited using a Helium Neon laser with laser line at 633nm and 30 % laser power. A primary 514/633 dichroic mirror was used for excitation and to collect emitted fluorescence. Transmitted light was collected in the brightfield channel. Emitted fluorescence was passed through a secondary dichroic mirror (635VIS). MitoTracker DeepRed fluorescence above 635 nm was collected using the Meta detector between 659 and 756 nm. Shorter wavelengths were passed through a third dichroic mirror (515nm) and YFP fluorescence was collected through a long pass 530 nm cutoff filter.

Slp2-GFP and MitoTracker Orange

Slp2-GFP whole seedlings (Figures 2-14) were imaged using a 20x Plan Apochromat objective. GFP was excited using an Argon laser as above with the 488nm line and transmission set to 10 % power. Laser excitation and emission made use of a primary dichroic mirror reflecting 488 nm light and transmitted light was collected in the bright field image. Emitted fluorescence was reflected by a mirror and passed through a third dichroic mirror (545 nm). GFP fluorescence was collected after filtering through a band pass 505-530 nm filter. Chlorophyll fluorescence was collected through a long pass 560 nm filter.

All other images of Slp2-GFP and MitoTracker Orange were imaged using a 63x water immersion objective. GFP was excited with the Argon laser 488nm laser line and transmission at 15 % power. MitoTracker Orange was excited with a Helium-Neon laser at 543 nm using 100 % laser power. Laser light was passed through a first dichroic mirror (488/543 nm) and transmitted light collected in the brightfield channel. Emitted fluorescence was passed through a secondary dichroic mirror (635 VIS) and chlorophyll autofluorescence detected with the Meta between 574 and 713nm. Reflected fluorescence was passed through a third dichroic mirror (545 nm cutoff). Reflected light was collected through a long pass 505 nm filter as GFP fluorescence. Light that passed through the 545 nm dichroic mirror was filtered through a band pass 560-615 nm and detected as MitoTracker Orange fluorescence.

Western blot analysis of stable lines

Proteins were extracted from seedlings in denaturing buffer as described. Seedlings were grown on MS plates for 14 days (supplemented with 0.5 % sucrose as indicated in Figure 2-11 A) or in hydroponic culture in long day light for 40 days (kanamycin included as indicated in Figure 2-11 B) and proteins were extracted. UV-B treatment was applied to 14 days old seedlings grown on agar plates as described in the methods of chapter 3. Protein samples from Slp2-YFP/GFP expressing plants were extracted from leaf material of kanamycin-resistant T1 seedlings that had been transplanted to soil. The protein content was quantified by the Amidoblack assay and 5 (Slp1-YFP samples) or 10 micrograms (Slp2-GFP samples) were separated on a 10 % SDS-PAGE gel and Western-blotted. Anti-GFP (monoclonal from rabbit, Abcam) was used at 1:1000 and anti-Slp1 at 1:5000.

2.17 Biochemical characterisation of AtSlp1

FA crosslinking experiment

Mitochondria that were isolated on discontinuous Percoll gradients were crosslinked by FA treatment (solutions listed above in the Table under “Mitochondrial purification on Percoll step gradients”). Two aliquots of 45 μL were transferred to fresh tubes. To one aliquot, 5 μL of buffer MB were added (= control), and to the other one 5 μL of 10x FA in buffer MB (= crosslinked sample). The reactions were then incubated for 15 minutes at room temperature, before 50 μL of 250 mM glycine in MB buffer were added to quench FA crosslinking. This reaction was also incubated for 15 minutes at room temperature. 25 μL of 5x SDS buffer were added to each tube (final volume now 125 μL), before each volume was again splitted in two aliquots of 62.5 μL each. One set of 62.5 μL aliquots were then denatured by boiling at 98 $^{\circ}\text{C}$ for at least 15 minutes, whereas the other was denatured by incubation at room temperature. The protein contents of all samples was analysed before Western blotting. The blots were probed with anti-Slp1 (1:5000).

Protease K assay- isolation of microsomes

10-20 grams of fresh shoot tissue (from mature short-day grown Col-0 plants) was harvested and chilled immediately. All solutions used for this experiment are listed in the table below. The tissue was thoroughly homogenised in 50 millilitres homogenisation buffer in a Waring blender by repeated strokes at 4 $^{\circ}\text{C}$. The homogenate was filtered through two layers of MiraCloth and centrifuged at 10000g for 15 minutes at 4 $^{\circ}\text{C}$. The supernatant was filtered through a 50 μm pore nylon net and centrifuged at 100000 g for 30 minutes at 4 $^{\circ}\text{C}$. The resulting microsomal pellet was resuspended in 1 millilitre of microsomal resuspension buffer and divided in four aliquots of 250 μL (samples 1-4). Protease K or buffer K, and Triton-X 100 or microsomal resuspension buffer were added as outlined below to each aliquot:

Sample no.	BK [ml]	Protease K [25mg/ml]	micr. RB [ml]	T-X100
1	1	0	12.5	0
2	0	1	12.5	0
3	1	0	0	12.5
4	0	1	0	12.5

BK (= buffer K), micr. RB (= microsomal resuspension buffer. Final volume of each aliquot was 263.5 μL .

The reactions were incubated for one hour at 4 °C while fixed to a rotating wheel before digestions were stopped by the addition of 10 mM PMSF. 70 µL of 5x SDS sample buffer were added to each tube and the samples were denatured by boiling for two minutes. The protein content was analysed by the AmidoBlack assay, and five micrograms of each sample were loaded on a 10 % SDS-PAGE gel and Western-blotted. Anti-Slp1 was used at 1:5000 and anti-Syp121 at 1:10000.

Buffer	Composition
Homogenisation buffer	50 mM Tris-Cl pH 8.2, 330 mM sucrose, 1mM DTT
Microsomal resusp. Buffer	25 mM Tris-Cl pH 7.5, 330 mM sucrose, 10 mM CaCl ₂ , 1 mM DTT
Buffer K	50 mM Tris-Cl pH 8.0, 10 mM CaCl ₂
Protease K	250x = 25 mg/ml in buffer K- final 100ug/ml
Triton-X100 stock	20 % Triton-X100 in micr. resusp.buffer

Buffers and solutions used for protease K digestion of microsomal fractions.

Chemical treatments of microsomes

Microsomal pellets were extracted from wild type Arabidopsis plants (Col-0) exactly as described above for the protease K experiment. The only exception was that protease inhibitors were added in this experiment; they were omitted in the other experiment to avoid inhibition of protease K digestion. The resulting microsomal pellet was resuspended in 1 millilitre of microsomal resuspension buffer (containing no CaCl₂) as above. This resuspension was aliquoted into 8 tubes of 125 µL each. To each tube, 125 µL of a reagent (2x concentrated in microsomal resuspension buffer) were added as outlined in the following table:

Sample no.	Reagent/stock	Final concentration
1	micr. RB	Control
2	0.2 M NaOH	0.1 M NaOH
3	0.2 M Na ₂ CO ₃	0.1 M Na ₂ CO ₃
4	2 M NaCl	1 M NaCl
5	5 M urea	2.5 M urea
6	2 % T-X100	1 % T-X100
7	0.2 % SDS	0.1 % SDS

Chemical treatments of microsomal fractions.

All samples were incubated for one hour at 4 °C while rotating. The content of each tube was collected by brief centrifugation, and was then transferred to fresh ultracentrifugation tubes specifically designed for small volumes. The samples were centrifuged for 30

minutes at 100000 g at 4 °C, and the resulting supernatants were transferred to fresh tubes. Each pellet was resuspended in 250 µL of microsomal resuspension buffer and 60 µL of 5xSDS buffer were added. All samples were denatured at 37°C for one hour before their protein content was quantified using the Amidoblack assay. Western blots were loaded with 10 micrograms of protein. Antibodies were applied as described in the protease K experiment above.

BPA assay

Seeds of wild type and transgenic plants were sterilised and sown on MS agar plates (0.5 x MS, 0.5 % sucrose supplemented with 10 µM dexamethasone and/or 1 mM BPA (stock solution 1 M in DMSO)). Plants were grown for 20 days under long day light conditions on vertical Petri dishes. They were harvested (approximately 20 seedlings/treatment) and snap frozen in liquid nitrogen, followed by grinding in the Qiagen Tissue Lyser as described. The frozen powder was homogenised in 500 µL of homogenisation buffer with added protease inhibitors (see table for protease K experiment for composition) and microsomal fractions extracted as described above. The microsomal pellets were resuspended in 200 µL of microsomal resuspension buffer (no CaCl₂ added) and 5x SDS buffer added. Samples were boiled for 5 minutes and the protein content quantified by the Amidoblack protein assay. Five micrograms of soluble and microsomal proteins were separated on SDS-PAGE gels followed by Western blotting. Anti-Slp1 was used at a 1:5000 dilution.

Methods for Chapter 5: Functional characterisation of AtSlps

2.18 Isolation of T-DNA insertion lines

AtSlp1 T-DNA insertion lines

The following T-DNA insertion lines were ordered from NASC (European Arabidopsis stock centre, Nottingham, UK). Insertions in the AtSlp1 gene: *slp1-1* (SAIL_210_D11), *slp1-2* (SAIL_65_C05), *slp1-3* (SAIL_128_H07), *slp1-4* (SAIL_114_D09). Insertions in the AtSlp2 gene (no homozygotes were isolated from these): SALK_090074 which has supposedly an insertion in the 5'UTR, SM_3_810 which has a promoter insertion and SALK_017306 (promoter insertion).

Initially, seeds were sown out directly on soil, and genomic DNA was extracted from single leaves as described in the general methods section. Genotyping PCR was performed in a volume of 20 µL and standard Taq polymerase as described in general methods. Primers nos. 49-58 were used for genotyping of *slp1* mutants as indicated in the primer table in Appendix 2. The T-DNA insertion products for *slp1* mutants were obtained using the following primer combinations: *slp1-1* (210_D11_RP/LB3), *slp1-2* (65_C05-RP/LB3), *slp1-3* (J-RP/LB3), *slp1-4* (114_D09-LP/LB3). Primers nos. 59-65 were used for genotyping of *slp2* mutants.

Seeds from plants with identified insertions were harvested and selected on MS agar plates supplemented with 50 µM BASTA (SAIL lines) or 50 µg/ml kanamycin (SALK lines) as appropriate. Before any PCR was performed with *slp1-2* and *slp1-4* lines, these were directly selected on MS agar plates containing 50 µM BASTA (glufosinate ammonium, or PESTANAL, Fluka) as described. If no homozygotes were identified from the first seed generation, the offspring was further analysed by genotyping PCR, until homozygous T-DNA insertions were identified. The T-DNA insertion sites were verified by DNA sequencing of PCR products at the University of Dundee Sequencing Service as instructed on their website.

RT-PCR and Western blotting

For some *slp1* mutants, transcript levels were analysed as indicated by RT-PCR. RNA was extracted as described in section 2.1 from leaves detached from soil-grown plants. RT-PCR was performed as described in section 2.3 with primers nos. 66-69 for *slp1-1* and *slp1-3* lines and the number of cycles indicated in Figure 3-4.

Proteins were extracted under denaturing conditions from detached leaves of BASTA-resistant *slp1* plants as described in section 2.8. Protein extracts were quantified with the Amidoblack assay and separated on 10 % SDS-PAGE gels as described. Western blots were prepared and probed with anti-Slp1 at 1:5000 dilution as described before.

2.19 Characterisation of *slp1* growth phenotypes

Quantification of leaf surface area

Knockout and wild type plants were grown on soil under long day light as described. Photographs were taken at the indicated age with the Nikon D1x camera. Leaf surface areas of plants were determined using the Image J software (Rasband, W.S., ImageJ, U. S. National Institutes of Health, Bethesda, Maryland, USA, <http://rsb.info.nih.gov/ij/>, 1997-2008). Briefly, images were uploaded in the jpg format and converted to binary images in black and white. The surface areas were subsequently determined according to a scale entered into the software that converted pixels into cm². Statistical significance was determined using the t-test functions in Microsoft Excel (normally as two-tailed t-tests). Alternatively, p-values were calculated using the Vassarstats website (<http://faculty.vassar.edu/lowry/VassarStats.html>). T-tests were run using the independent samples and two-tailed options, and p-values were obtained.

Germination assay

Seeds of mutant and wild type plants harvested at the same day were sterilised as described and sown individually on MS agar medium (0.5x MS, pH 5.7 (KOH)) on square Petri dishes. Each dish was subdivided into two halves, each containing six lines of at least 10 seeds. Care was taken to leave space between the seeds. Three plates per medium were sown out, each containing at least 60 seeds per genotype. In addition to MS plates, seeds were also sown on plates supplemented with 1 µM ABA or 2 µM GA. Plates were

wrapped with NescoFilm and placed into a tissue culture chamber under a long day light regime. Seed germination was counted each day after sowing. Seeds were regarded as germinated when the radicle was clearly protruding from the seeds.

Root growth analysis

Seeds of wild type and mutant plants were sown directly on squared Petri dishes containing MS agar medium, or MS agar supplemented with 0.5 % sucrose. They were placed vertically under long day light as described. After 10 and 13 days, plates were scanned and images were analysed using the EZ Rhizo software according to the instructions given on the web site (www.psr.org.uk). Only the main root lengths were compared between mutants and wild type seedlings as indicated.

Osmolarity measurements

Rosette leaves of 37 days old long day grown mutant and wild type plants were harvested and ground in a 1.5ml Eppendorf tube using a plastic pestle. The tubes were closed immediately and centrifuged for one minute at maximum speed in a Benchtop centrifuge. The supernatant was transferred to a fresh tube and centrifuged again. The final supernatant was directly measured in a Vapro vapour pressure osmometer (Wescor, ChemLab Scientific Products, Laindon, UK) by pipetting 10 μ L of leaf sap onto a suitable filter pad that was then placed into the chamber. The instrument was calibrated before using three osmotic standard solutions supplied by the manufacturer.

Flowering time

The flowering time was determined as the number of rosette leaves of mutant and wild type plants grown under long day light for 23 days. A plant was considered flowering once the shoot apex was located at least one centimetre above the soil.

Seed production

Mature siliques that were still green were harvested from flowering long day grown mutant and wild type plants. Siliques were always harvested from the main branch approximately at the same relative position between individual plants. Harvested siliques were cleared in ethanol under gentle agitation and seeds were counted from 10 individual siliques from six individual plants.

Sensitivity to salt

Mutant and wild type seeds were sown directly on MS agar plates (0.5x MS, pH 5.7 (KOH)) in square Petri dishes and grown vertically for four days under long day light. On day four, seedlings were transferred under sterile conditions to identical plates containing either no salt (= control), 100 mM NaCl or 200 mM NaCl. The plates were turned upside down by 180 degrees and grown vertically for another four days. Plates were then unwrapped and photographed as described. The distance of root growth after the transfer was measured using the ImageJ software by drawing lines along the roots from the point of bending (pink arrowhead) to the root tip (yellow arrowhead).

IRGA measurements

Photosynthetic assimilation rates, transpiration rates and stomatal conductivities of mutant and wild type plants were measured simultaneously in an LCpro+ infrared gas analyser chamber (IRGA, ADC BioScientific). The smallest available chamber suitable for large *Arabidopsis* rosette leaves was used for all measurements. Plants were grown in short day light for 12 weeks. One individual rosette leaf (taken from the same relative position in the rosettes) was attached to the chamber and carefully sealed. The pots were placed into small trays filled with water to ensure maximum transpiration. For each measurement, one mutant (either *slp1-1* or *slp1-2*) and one wild type plant were always measured in parallel using two identically programmed analysers. External light sources were placed directly above the clamped leaves. A light response curve was set up that started with 0 PPFD and ended with 1600 PPFD (in $\mu\text{mol}/\text{m}^2/\text{s}$) under ambient CO_2 concentrations and 25C temperature. Leaves were left in darkness for 10 minutes, before light intensities were increased stepwise by approximately 80 PPFD for 10 minutes over a time course lasting approximately 90 minutes. The analysers were first calibrated to zero CO_2 for at least one hour before the settings were changed as described. All photosynthetic parameters were calculated according to an Excel template provided by Dr. Peter Dominy (University of Glasgow, UK). For the quantitative comparison between mutant and wild type plants, all photosynthetic parameters were taken at 500 PPFD. No additional comparisons at different light intensity values were made.

Water content and whole plant transpiration

Rosette leaves from 32 days old long day-grown mutant and wild type leaves were carefully excised and their fresh weight determined immediately. They were then wrapped

in pre-weighed aluminium foil pieces and put into a drying incubator set to 70 °C for two days. After this period the tin foil parcels were weighed again and the leaves' dry weight determined. From the difference between fresh and dry weights, the absolute water contents were determined. The relative water content was then calculated as the percentage of initial fresh weight.

Whole plant transpiration was measured in a customised environmentally-controlled chamber (provided by a University of Glasgow workshop). The setup was such that the chamber was connected to an external heating and cooling system, as well as a fogging device. An attached fan allowed water vapour to enter the chamber set to a specified relative humidity level (% RH). This allowed for the simultaneous control of relative humidity and temperature. Inside the chamber two micro-balances were placed connected to a computer that recorded the weight on each balance every two minutes. Additionally, a temperature/RH sensor was also placed inside, hanging above the balances. Software provided by Adrian Hills (University of Glasgow) allowed for the control of temperature and RH conditions and simultaneously recorded the weights, temperature and RH inside the chamber. Light banks were placed above the whole chamber and set to a light intensity approximately corresponding to the level inside the growth chamber.

Two well-watered mature mutant and two wild type short day grown plants were placed on each balance. The plants were grown in squared pots of five cm length/width and the pots were completely sealed before placing them inside the chamber to avoid any water evaporation from the soil. This was achieved by covering the soil around the rosette with clear plastic sheets and sealing off any remaining holes with elastic tape. The small hole in the middle of the sheet where the rosette emerged was additionally sealed with Vaseline. The software was programmed to change RH levels every six hours from high (80%) to low (40%) levels. The light was kept on constantly for the first three days (4800 minutes). After this point, RH levels were set to 60% constantly, and the light period was changed to short day light for the remaining time of the experiment.

Transpiration rates were calculated from the plants' weights recorded every two minutes. The difference in weight between each time step was divided by the time step (two minutes) and expressed in mg/min. After each experiment was finished, the complete rosettes were detached from the pots and all leaves removed. These were flattened out on sticky tape and scanned. From the obtained images, the complete leaf surface area of each plant was determined using the ImageJ software as described. The transpiration values were then divided by the area in cm² to account for differences in the size of plants and

plotted using SigmaPlot software (version 8.0). The raw transpiration data were filtered using the lowpass (80) function in the software.

2.20 *slp1* mitochondrial phenotypes

TMRE imaging

Mutant and wild type seedlings were grown in hydroponic culture for five days as described in section 2.7. A stock solution of TMRE was prepared at 1mM in DMSO, aliquoted and kept frozen at -20°C . TMRE was diluted to 50 nM in MS medium identical to the plant growth medium and seedlings were placed inside dye solution for five minutes. They were then carefully transferred twice to fresh MS medium for one minute each to rinse off excess dye. The whole seedlings were subsequently placed on microscope slides mounted in water for imaging on the confocal microscope.

Seedling roots were imaged using a 20x Plan Apochromat objective. TMRE was excited with a 543 nm Helium-Neon laser set to 15 % output. Laser light was passed through a primary 488/543 nm dichroic mirror and transmitted light was collected in the brightfield channel. Emitted fluorescence was reflected by a mirror and passed through a third dichroic mirror (545 nm cutoff). Light passed through this mirror was filtered with a long pass 560 nm filter and collected as TMRE fluorescence. Z-stacks were taken through the entire root diameter and reconstructed into three-dimensional images using the Zeiss LSM software.

TMRE fluorescence was quantified using the ImageJ software and three-dimensional reconstructions of scanned roots. Black and white masks were created and superimposed onto the original images (converted to 8 bit format). Fluorescence intensities were measured from the combined images of each root area.

Oxygen consumption measurements

Mitochondrial pellets were extracted from mature *slp1-1* and wild type plants grown under short day light for 13 weeks. 25 grams of fresh weight tissue were harvested and chilled immediately. The tissue was homogenised in 100 millilitres of buffer A (section 2.15 “Mitochondrial purification”) in a Waring blender using five strokes each lasting two seconds at the lowest speed. The homogenate was filtered through two layers of MiraCloth and centrifuged at 1100 g for five minutes at 4°C . The supernatant was carefully poured

into a fresh centrifugation tube and spun at 3000 g for 10 minutes at 4 °C. The supernatant was again removed and centrifuged at 12000 g for 20 minutes at 4 °C. The pellet after this spin was the organellar pellet containing mitochondria. It was resuspended in 500 µL of buffer MB (see below) using the fine paintbrush. The resuspension was kept on ice until use in the oxygen electrode. The protein content of the organellar pellet was determined with the Amidoblack protein assay.

A Clark-type oxygen electrode was set up as instructed by the manufacturer (Rank Brothers, Cambridge, UK). A 3 M solution of potassium chloride was prepared as the electrolyte. An oxygen-permeable Teflon membrane was cut to size (approximately 1 cm²) and put into place above a drop of KCl on the electrode. The membrane was secured with the help of a silicone O-ring and screwed into place. It was submerged into a water-filled thermostat bath set to 25 °C. The electrode was connected as instructed to the controller and to a chart recorder. A voltage of -0.6 V was applied to the Pt electrode. The electrode chamber was filled with three millilitres of mitochondrial assay buffer (see table below for buffer compositions) and a magnetic stir bar was put into place. The buffer had previously been fully oxygenated by vigorous stirring on a magnetic stirrer while being exposed to air. Under this condition the oxygen content of the assay buffer was assumed to be 250 µM O₂ at 25 °C. The electrode was calibrated by adding a few crystals of sodium dithionite to the buffer under stirring, which caused the complete deoxygenation of the assay medium. The full deflection of the chart recorder thus represented the oxygen content of the medium.

Component	Concentration
Mitochondrial assay buffer	
MOPS pH 7.4	10 mM
Mannitol	300 mM
KH ₂ PO ₄	5 mM
NaCl	10 mM
MgSO ₄	2 mM
BSA	0.1%
Buffer MB	
MOPS pH 7.4	20 mM
Mannitol	300 mM
BSA	0.1 %

Buffer composition for the isolation of mitochondrial pellets.

200 µL of mitochondrial resuspension were added to 2.8 millilitres of assay medium previously pipetted into the chamber. The magnetic stirrer was switched on to a low speed and the chart recorder was started (1cm/min). Once the pen reached a steady rate, the first substrate was added to the chamber via injection with a Hamilton syringe. The table below

lists all substrates used and their concentrations. The injection protocol always consisted of the substrate (succinate, NADH, pyruvate, malate/glutamate), followed by the addition of ADP and inhibitors, the last one always being NaCN. Sufficient time was always given until the next substrate/inhibitor was added. In some cases, oxygen consumption rates clearly slowed down after a while, in other cases it was so slow that the next substance was injected earlier. Once a run was complete, the chamber was rinsed thoroughly with distilled water and filled for the next run.

Substrate/Inhibitor	Concentration [mM]	Stock solution [mM]	Solvent	Injected [μ L]
Succinate	10	610	H ₂ O	50
NADH	1	61	H ₂ O	50
Pyruvate	10	610	H ₂ O	50
Malate/Glutamate	10	610	H ₂ O	100
ADP	0.1	30.6	H ₂ O	10
SHAM	0.2	30.6	EtOH	20
DNP	2 μ M	0.3	H ₂ O	20
Oligomycin	2 μ g/ml	1mg/ml	EtOH	6
NaCN	1	100	H ₂ O	30

Substrates used for injection into the oxygen electrode.

The quantification of oxygen consumption rates was done manually. A line was drawn with a ruler corresponding to the most steady slope visible on the chart recorder paper. From the slopes, the amount of consumed oxygen (vertical direction) according to the full chart recorder deflection was determined over time (horizontal direction). This value was then normalised to the amount of protein present in the mitochondrial resuspension. Values from three independent experiments were then averaged and presented in Figures 3-20 and 3-21.

DAB staining

Rosette leaves from 30 days old mutant and wild type plants grown under long day light were detached and immediately immersed into 2.5 mM EDTA pH5.5 to limit the Ca²⁺-mediated wounding response resulting in excessive ROS formation. The leaves were cut again close to the submerged petiole and placed into two millilitre Eppendorf tubes filled with 0.5 millilitres of DAB (Sigma) staining solution (1 mg/ml in 0.1 N HCl pH 3.8) with the petioles dipping into the stain. The lids were kept open and the tubes were covered slightly to avoid direct exposure to light. They were left standing in the solution for at least 6-8 hours to take up DAB stain through their transpiration stream. Leaves were then

cleared in 80 % ethanol overnight, with two exchanges. Afterwards they were placed into 60 % glycerol until imaging by scanning.

H₂DCFDA imaging

Mutant and wild type seedlings were grown in liquid MS medium for seven days under long day light. A 100mM stock of H₂DCFDA dye was prepared in DMSO (AnaSpec, San Jose, USA). The final working concentration was 2 μ M in MS medium. Seedlings were placed for five minutes into H₂DCFDA-containing MS medium. Afterwards they were placed once for five minutes into fresh MS medium to wash out excessive dye. They were then mounted in water on microscope slides and roots were imaged on the confocal microscope. The roots of three seedlings per genotype were imaged by scanning through the entire root at four independent areas.

Confocal images were taken with a 20x Plan Apochromat objective. H₂DCFDA was excited with an Argon laser using the 488 nm laser line set to a 1 % transmission output. Laser light was passed through a primary HFT488 dichroic mirror and transmitted light was collected in the brightfield channel. Emitted fluorescence was passed on to a mirror where it was reflected and passed to a third mirror. The reflected fluorescence was filtered through a long pass 505 nm filter and collected as H₂DCFDA fluorescence.

H₂DCFDA fluorescence intensity was quantified using the Zeiss LSM imaging software. Briefly, three-dimensional images were reconstructed from z-stacks of roots. The outlines of the root stacks were traced using the software, and the average fluorescence intensity values inside the traced outline used for quantitative analysis.

2.21 Stable AtSlp RNAi lines

The RNAi fragments of AtSlps were ordered from the NASC (provided by AGRIKOLA-www.agrikola.org). For AtSlp1, the catalogue number was N264068 and for AtSlp2 N255522. These sequences were specific for the 3' regions of both genes and were obtained as Gateway-based entry clones in the vector pDONR207. The clones were delivered as bacterial stabs (*E.coli*) that were selected with 15mg/l gentamycin. The plasmids were extracted by miniprep and the insertions verified by DNA-sequencing. The RNAi fragments were subsequently cloned into the binary Gateway-based pOpOFF2(hyg) vector using the standard recombination protocol given by Invitrogen. Positive clones were selected on spectinomycin and transformed into *Agrobacterium tumefaciens* as described.

Flowering Arabidopsis Col-0 plants grown under long day light were transformed using the floral dip method as described and positive transformants selected on MS agar plates supplemented with 50 µg/ml hygromycin. Positive transformants were propagated until homozygous plants were obtained (based on their segregation pattern on hygromycin selection).

RNAi-mediated gene knockdown was assessed in a time course. Seedlings were grown in liquid culture as described for 10 days under long day light. Dexamethasone (water soluble version from Sigma) was added to a concentration of 10 µM and samples were taken over a time course of 48 hours as indicated. Samples were snap-frozen in liquid nitrogen and ground to powder using the Qiagen Tissue Lyser as described. Proteins were extracted under denaturing conditions and quantified with the AmidoBlack protein assay. Two micrograms of total protein per sample were loaded on a 10 % SDS-PAGE gel and Western blotted. Slp1 protein was detected using anti-Slp1 at 1:5000 dilution. For quantification of the knockdown level, band intensities from the Western blots were quantified using the BioRad Chemi Doc transilluminator software as described for the Northern blot quantification. The band intensities were normalised to the intensities of the Rubisco bands seen on the Ponceau S stains.

Slp RNAi plants grown on soil were sprayed continuously with dexamethasone solution (30 µM dexamethasone (ethanol soluble), 0.01 % Tween-20) using a mister every other day. In parallel, identical plants were sprayed with control solution (0.15 % ethanol, 0.01 % Tween-20). Rosette leaves of plants that had been sprayed regularly for over two weeks were harvested, frozen and their proteins were extracted. The protein content was quantified using the AmidoBlack assay and 10 micrograms of total protein were separated on a 10 % SDS-PAGE gel followed by Western blotting as described.

2.22 Dominant-negative (DN) Slp overexpressing lines

Cloning of DN constructs

The dominant-negative fragments of both Slp open reading frames were amplified by PCR using primers nos. 70-77. First, the DNA fragments were amplified using Phusion Taq polymerase as described and primers nos. 70 and 71 for DN(Slp1), and primers nos. 72 and 73 for DN(Slp2). The PCR products were purified and used as templates in a second set of PCR reactions in which the N-terminal myc tag was added and the restriction sites (XhoI at the 5' end and SpeI at the 3' end of each fragment). These PCRs were performed with

Phusion Taq enzyme and primers nos. 74 and 75 for DN(Slp1) and nos. 76 and 77 for DN(Slp2). The resulting PCR amplicons contained the XhoI site followed by a myc tag and the DN fragment with a SpeI site at the 3' end. The PCR products were purified as described and ligated into pTA7002 that had previously been opened with XhoI and SpeI. Positive bacteria colonies were selected on kanamycin as described in section 2.4. Clones were verified by DNA sequencing and transformed into *Agrobacterium tumefaciens* as described. Flowering Col-0 plants grown under long day light were floral dipped with both constructs as well as the empty pTA7002 vector. Positive transformants were selected on MS agar plates supplemented with 50 µg/ml hygromycin as described. Resistant plants were propagated until homozygous lines were obtained. At least three independent lines were selected as homozygotes for each DN construct.

Dexamethasone induction properties

Dexamethasone induction was assessed in a time course as described for the Slp RNAi lines. Plants were grown for 10 days in liquid medium under long day light. Dexamethasone was added to 10µM and samples taken over a time course of 48 hours as indicated in Figure 3-29. For the dexamethasone gradient, dexamethasone was added to the indicated concentrations and samples harvested after 12 hours. Proteins were extracted as described with denaturing buffer and quantified using the AmidoBlack protein assay. Five micrograms of total protein were loaded on a 12 % SDS-PAGE gel and Western blotted. Proteins were detected using monoclonal anti-myc antibody from mouse (Sigma) at 1:1000 dilution.

Solubility of DN proteins

For the DN protein solubility test, DN Slp and wild type seedlings were grown sterile on vertical MS agar plates under long day light for 14 days. Seedlings were harvested and soluble and microsomal extracts prepared as described in section 2.15. One millilitre of homogenisation buffer with added protease inhibitors (see table for protease K experiment) was added to the ground seedling material. The samples were then centrifuged for 15 minutes at 10000 g at 4 °C. The supernatant was transferred to a small ultracentrifuge tube and spun at 100000 g for 30 minutes at 4 °C. The resulting microsomal pellets were resuspended in 200 µL of microsomal resuspension buffer (no CaCl₂ added) and 5x SDS buffer added. Samples were denatured and quantified with the AmidoBlack protein assay. Five micrograms of total protein were separated on a 12 % SDS-PAGE gel and Western blotted. Proteins were detected with anti-myc used at 1:1000 dilution.

BPA treatment of seedlings

Seedlings of both DN Slp constructs and wild type were grown on vertical MS agar plates under long day light for 20 days. Medium contained either plain MS (with 0.5% sucrose), MS supplemented with 10 μ M dexamethasone, MS supplemented with 1 mM BPA, or MS with added dexamethasone and BPA. BPA was dissolved as a 1 M stock in DMSO and diluted appropriately. Before harvesting seedlings, the plates were unwrapped and photographed as described.

Microsomal pellets were extracted as described in section 2.13. Seedlings were harvested (approximately 20 seedlings/treatment) and snap frozen in liquid nitrogen, followed by grinding in the Qiagen Tissue Lyser as described. The frozen powder was homogenised in 500 μ L of homogenisation buffer with added protease inhibitors (see table for protease K experiment for composition) and microsomal fractions extracted as described above. The final pellets were resuspended in 200 μ L of microsomal resuspension buffer (without added CaCl_2), and denatured by boiling with 5x SDS buffer. Proteins were quantified and separated on 10 % SDS-PAGE gels followed by Western blotting. Anti-myc was used at 1:1000 and anti-Slp1 at 1:5000 dilutions.

2.23 Characterisation of DN Slp phenotypes

Growth and dexamethasone treatment of plants on soil

Homozygous plants were sown out directly on soil and grown under long day or short day light. Dexamethasone was applied in a spray solution as described for the Slp RNAi plants in section 2.21. Spraying was normally begun approximately one week after seed germination. In some cases, dexamethasone induction was only started once plants were flowering. For some short day grown plants, spraying with dexamethasone was only started when the rosettes were larger, but still growing. The same DN Slp and wild type plants were always grown in parallel in a separate tray and were treated with control solution. Spray solution was applied with the aid of a mister until all plants were equally covered with droplets of solution. Normally, plants were sprayed every other day until senescent.

Plants grown in long day light for 29 days were photographed. The leaf surface areas were quantified using the ImageJ software as described in section 2.19.

Determination of leaf osmolarity and flowering time

For the measurements of leaf sap osmolarity, leaves were detached from treated plants grown for 47 days under short day light. For one measurement, approximately 2-3 leaves were harvested and placed into Eppendorf tubes. Measurements were carried out as described in section 2.19 for knockout mutants.

The timing of flowering was determined as described in section 2.19 for knockout mutants. For the counting of DN plants, 32 days old DN Slp and wild type plants grown under long day light in the growth chamber were used. These plants had been treated with dexamethasone from an early stage on to ensure continuous protein induction.

Guard cell imaging

Epidermal strips from long day grown DN(Slp) and wild type leaves were prepared by peeling off pieces of the lower epidermis of rosette leaves using sharp forceps. The strips were mounted on silicone-based glue stuck on cover slips and covered with depolarisation buffer (10 mM MES-NaOH pH 6.1, 60 mM KCl). For imaging, the cover slips were attached to a microscope perfusion chamber and images were taken on a Zeiss AxioVert S100TV light microscope .

For confocal microscopy, mature rosette leaves were harvested from treated plants. A stock solution of 30 mM propidium iodide (Sigma) was prepared in water. Leaf pieces were infiltrated with 30 μ M propidium iodide (Sigma) in water. This was achieved by placing cut pieces of leaf into a 20 millilitre plastic syringe and de-aerating the tissue by applying a vacuum. The tissue was then mounted in water on microscope slides and imaged on the confocal microscope using a 63x water immersion objective. The infiltrated tissue was simultaneously excited with a 458 nm Argon laser set to 52 % and a 543 nm Helium-Neon laser set to 100 % output. Laser light was passed through a first dichroic mirror (458/543) and transmitted light collected in the brightfield channel. Emitted fluorescence was passed through a second dichroic mirror (635 VIS). Passed light was collected using the Metahead detector between 574 and 713nm as chlorophyll fluorescence. Reflected light was passed through a third dichroic mirror (545). Light that was passed through was filtered using a band pass 560-615 and collected as propidium iodide fluorescence.

Guard cell density

DN Slp and wild type plants were grown for 38 days under long day light and treated with dexamethasone from an early stage on. Three plants were chosen per line and per treatment to determine stomatal densities. Per plant, two leaves were harvested, one mature and one expanding leaf. All stomata inside 12 randomly chosen areas were counted per leaf, each area spanning 230x230 μm^2 . Stomata were counted using the confocal microscope and a HeNe laser with 11 % transmission at 543nm. Brightfield images were collected and divided into the counted areas. Stomata were counted per area by focussing up and down while running fast xy scans.

Leaf water content

Rosette leaves were harvested from the same relative positions from treated DN Slp and wild type plants. For Figure 3-42 (A), leaves were harvested from short day grown plants that were 53 days old and had been sprayed with dexamethasone from a later stage on. For Figure 3-42 (B), leaves were taken from long day grown plants (23 days old). The water contents were determined as described in section 2.19 for knockout plants.

Whole plant transpiration

To follow water loss over time from excised shoots, rosettes were harvested by cutting just above the soil. The shoots were taken from 42 days old short day grown treated plants. The cuts were sealed with Vaseline and plants were placed onto pre-weighed trays. Their fresh weight was recorded immediately ($t = 0$). Weight loss was then recorded every 15 minutes for the first hour after cutting, and then every 30 minutes up to eight hours post-harvesting. After eight hours, the shoots were wrapped in aluminium foil (pre-weighed) and let to dry out in an incubator set at 70 °C for two days. At each measured time point, the water content was calculated as the % of the initial fresh weight. Water loss over time was expressed as the deficit of the initially calculated water content in percent.

Whole plant transpiration measurements were carried out in the fogging chamber as described in section 2.19 for knockout mutants. For Figure 3-44 (A), DN(Slp1) plants were grown under short day light for 52 days and treated with dexamethasone. During the first 4000 minutes of the experiment, the light was kept on constantly, and the humidity levels changed every six hours from 80 % to 40 %. Afterwards the light was still kept constant, but the humidity level was set to 60 % to follow internal stomatal rhythms. For the result

shown in Figure 3-44 (B), wild type plants were grown under long day light for 29 days and treated with dexamethasone or control solution. For the transpiration measurements, the long day light regime was kept according to the conditions set in the growth chamber. The humidity levels were changed as described before every six hours. Transpiration rates were calculated as described before and plotted using the SigmaPlot software.

DAB staining

Leaves were harvested as described from DN and wild type plants grown under long day light for 21 days. DAB staining was carried out exactly as described before in section 2.20 for knockout mutant plants.

H₂DCFDA imaging and quantification

DN Slp and wild type seedlings were grown for five days under long day light in liquid culture as described in section 2.7. The plants were then stained with the ROS probe as described in section 2.20 for the knockout mutants. Confocal imaging was carried out exactly as described in the same section using identical microscope settings. Four seedlings per treatment and genotype were imaged at three areas across the root length. Fluorescence was quantified using ImageJ software as described for the TMRE staining of knockout mutants in section 2.20.

Trypan Blue staining

Rosette leaves from 33 days old long day grown DN Slp and wild type plants were harvested. Trypan Blue (Sigma) staining solution was prepared (0.025 % Trypan Blue, 25 % lactic acid, 25 % phenol, 25 % glycerol). The harvested leaves were placed into tubes filled with 10 millilitres of staining solution and gently shaken for two weeks at room temperature. Leaves were subsequently destained in 2.5 g/ml chloral hydrate (VWR International) for one week and washed with several exchanges of distilled water. The leaves were then placed between plastic sheets and scanned.

TMRE imaging and quantification

DN Slp and wild type seedlings were grown in hydroponic culture for three days under long day light with 10 μ M dexamethasone as appropriate. The seedlings were stained with TMRE exactly as described for knockout mutants in section 2.20. Three seedlings per

genotype and treatment were scanned on the confocal microscope at three to four areas along the entire root length. The microscope settings were identical as described in section 2.20. TMRE fluorescence was quantified using the ImageJ software as described.

Cross of DN(Slp1) and *slp1-1* plants

For crossing, closed buds of *slp1-1* plants grown in long day light were carefully opened under a dissecting microscope using a pair of sharp forceps. The anthers (which were still completely green) were all removed, together with the sepals and petals. The unfertilised pistil was left over and pollinated. Pollen from untreated flowering DN(Slp1) plants were used for fertilisation by gently dipping opened flowers onto the pistils. The seeds of developed siliques were harvested and sown out directly on soil. All plants were supposed to be heterozygous for *slp1-1* and the DN(Slp1) insertion. In parallel, *slp1-1* mutants and wild type plants were also sown out. Plants were grown in long day light for 45 days until photographing. Dexamethasone treatment was started at an early stage before flowering.

Results Chapters

3 Arabidopsis Stomatin-like Proteins- Phylogeny, Structure and Tissue Expression

Introduction

So far, the study of band-7 family proteins and stomatins in particular has mainly focussed on proteins from animals and human (see general introduction). This chapter provides detailed phylogenetic and structural information as well as expression data about the Arabidopsis stomatins, and more generally the Arabidopsis band-7 family. The first part investigates the phylogenetic context of stomatin-like proteins and the remaining Arabidopsis band-7 family members, and investigates the phylogenetic relationships of the Arabidopsis proteins with the band-7 family as a whole. This type of analysis has been published before for animal stomatins and prohibitins from plants and animals (Tavernarakis *et al.*, 1999; Browman *et al.*, 2007; Van Aken *et al.*, 2007; Green & Young, 2008), but not in detail for Arabidopsis stomatins and the Arabidopsis band-7 family. With the availability of more genome sequences from plants such as grape, rice, maize and moss, this study extends the previous analyses by including sequences from more species and detailed information about differences on the sequence level.

Following up the phylogenetic analysis is a study investigating the structural features occurring in Arabidopsis stomatin-like proteins and human stomatin-like protein-2, the closest related and best-studied human homolog. The information gained from this analysis was used to design suitable epitopes for the production of specific antibodies against AtSlp1 and AtSlp2. Two different approaches are described, the first one involving overexpression of epitope-tagged fusion proteins in bacteria, and the second one the design of short peptide epitopes. Both approaches have been used in the past to produce specific antibodies obtained by immunisation of host animals. The last part of this chapter presents a comparison of results obtained by different approaches about the tissue-specific expression of Arabidopsis stomatins and the implications of these data for their putative functions. Public microarray data from the eFP browser (Winter *et al.*, 2007b) provide vast knowledge about changes in transcript levels during development and upon treatments with chemicals or stresses. To supplement and verify these data, alternative approaches were taken involving transcript analysis by Northern blotting, RT-PCR, Western blotting

and assaying the promoter activities. The advantages and disadvantages of these approaches are further discussed at the end of this chapter. A picture of the tissue distribution of AtSlps and their responses to internal and external stimuli emerges from overlapping information of all these approaches. None of these aspects have so far been studied before and give novel insight about plant stomatin-like proteins and the relations to their animal and human homologs.

3.1 Arabidopsis stomatins and their phylogenetic context

To give an overview of Arabidopsis stomatin-like proteins and their evolutionary and functional context, phylogenetic trees and sequence alignments are presented. First, the position of the Arabidopsis Slps amongst the other band-7 proteins in Arabidopsis and other stomatin type proteins in the plant kingdom was investigated. Secondly, phylogenetic data are presented that deal with the relationship of Arabidopsis stomatin-like proteins and animal, yeast and bacterial band-7 proteins, with a particular focus on the stomatin subfamily. Tables 3-2, 3-3 and 3-4 give an overview of the proteins used in this survey together with their UniProt identifiers, amino acid lengths and proposed or confirmed subcellular localisations. A more detailed version of these tables is included in Appendix 1 that also contains information about other conserved domains and their position in the protein sequence. These compiled lists are by no means complete, but aim to give information about a representative section of the band-7 family from a wide variety of species. An overview over all conserved domains of the band-7 family members investigated here is given in Table 3-1.

Class	Identifier	Name
PROSITE	PS01270	Stomatin
InterPro	IPR001107	Band7
InterPro	IPR001972	Stomatin
InterPro	IPR003033	SCP2 sterol carrier protein domain
InterPro	IPR000163	Prohibitin
InterPro	IPR004851	Flotillin
InterPro	IPR010200	HflC
InterPro	IPR010201	HflK
PANTHER	PTHR13806	Flotillin-related*

Table 3-1. Overview over the domains of all band-7 family proteins investigated in this study. Abbreviations are according to InterPro, PROSITE and TAIR databases. The asterisk indicates that this domain is not fully annotated by either of these databases.

UniProt ID	Species	Name	Abbreviation used	Length (aa)	Subcellular Localisation
Q93VP9	<i>Arabidopsis thaliana</i>	Stomatin-like protein-1	AtSlp1	411	Mitochondrion, Plastid
Q9LVW0	<i>Arabidopsis thaliana</i>	Stomatin-like protein-2	AtSlp2	401	Mitochondrion, Plastid
Q9SRH6	<i>Arabidopsis thaliana</i>	HR induced (HIR)	At3g01290	285	Membrane, PM
Q9FHM7	<i>Arabidopsis thaliana</i>	Band7/HIR-like protein	At5g51570	292	Membrane
Q9FM19	<i>Arabidopsis thaliana</i>	HR induced (HIR)	At5g62740	286	PM
Q9CAR7	<i>Arabidopsis thaliana</i>	HIR-like	At1g69840	286	PM
Q9ZQ87	<i>Arabidopsis thaliana</i>	ER protein (Erlin-like)	At2g03510	356	ER
Q501E6	<i>Arabidopsis thaliana</i>	Flotillin/nodulin-like	At5g25250	470	unknown
Q4V3D6	<i>Arabidopsis thaliana</i>	Flotillin/nodulin-like	At5g25260	463	unknown
Q9LV90	<i>Arabidopsis thaliana</i>	Flotillin/nodulin-like	At5g64870	479	unknown
O49460	<i>Arabidopsis thaliana</i>	Prohibitin-1	At4g28510	288	Mitochondrion
Q9ZNT7	<i>Arabidopsis thaliana</i>	Prohibitin-2	At1g03860.1	286	Mitochondrion, Plastid
Q3EDJ1	<i>Arabidopsis thaliana</i>	Prohibitin-2	At1g03860.2	221	Membrane
O04331	<i>Arabidopsis thaliana</i>	Prohibitin-3	At5g40770	277	Mitochondrion
Q9LK25	<i>Arabidopsis thaliana</i>	Prohibitin-4	At3g27280	279	Mitochondrion, Cell wall?
Q9LY99	<i>Arabidopsis thaliana</i>	Prohibitin-5	At5g14300	249	Mitochondrion
Q9SIL6	<i>Arabidopsis thaliana</i>	Prohibitin-6	At2g20530	286	Mitochondrion
Q9FFH5	<i>Arabidopsis thaliana</i>	Prohibitin-7	At5g44140	278	Membrane/Mitochondrion
A7P6L9	<i>Vitis vinifera</i>	Band7 protein	A7P6L9	420	Membrane
A9T1F8	<i>Physcomitrella patens</i>	pred. protein (fragment)	A9T1F8	292	Membrane
Q7EZD2	<i>Oryza sativa subsp. japonica</i>	Band7 protein	Q7EZD2	377	Membrane
A2YRF1	<i>Oryza sativa subsp. indica</i>	Band7 protein	A2YRF1	377	Membrane
A3BPU1	<i>Oryza sativa subsp. japonica</i>	Band7 protein	A3BPU1	405	Membrane
Q9M585	<i>Zea mays</i>	Stomatin-like protein	Q9M585	394	Membrane
A8JI52	<i>Chlamydomonas reinhardtii</i>	pred.protein (fragment)	A8JI52	372	Membrane

Table 3-2. Plant band-7 proteins (as identified by IPR001107) that were used for the phylogenetic analysis. Sequences and other related information were downloaded from the UniProt and TAIR database using the identifiers given. The column entitled “Abbreviations used” refers to the abbreviations that are given in the following phylogenetic trees. Highlighted in blue are proteins that have an additional stomatin domain (IPR001972). Length (aa) refers to amino acids. All information given in this table was retrieved from the UniProt database or TAIR.

UniProt ID	Species	Name	Abbreviation used	Length (aa)	Subcellular Localisation
P27105	<i>Homo sapiens</i>	Stomatin	HsStomatin	288	PM, Endosomes
Q9NP85	<i>Homo sapiens</i>	Podocin	HsPodocin	383	PM
Q9UBI4	<i>Homo sapiens</i>	Stomatin-like protein-1	HsSlp-1/STORP	398	Membrane
Q9UJZ1	<i>Homo sapiens</i>	Stomatin-like protein-2	HsSlp-2	356	Mitochondrion
Q8TAV4	<i>Homo sapiens</i>	Stomatin-like protein-3	HsSlp-3	291	Membrane
P35232	<i>Homo sapiens</i>	Prohibitin	HsPHB	272	Mitochondrion
Q99623	<i>Homo sapiens</i>	Prohibitin-2	HsPHB-2	299	Mitochondrion
O75955	<i>Homo sapiens</i>	Flotillin-1	HsFlotillin-1	427	PM
Q14254	<i>Homo sapiens</i>	Flotillin-2	HsFlotillin-2	379	PM
O75477	<i>Homo sapiens</i>	Erlin-1	HsErlin-1	346	ER
O94905	<i>Homo sapiens</i>	Erlin-2	HsErlin-2	339	ER
P54116	<i>Mus musculus</i>	Stomatin	MmStomatin	284	PM
Q8CI66	<i>Mus musculus</i>	Stomatin-like protein-1	MmSlp-1	399	Membrane
Q99JB2	<i>Mus musculus</i>	Stomatin-like protein-2	MmSlp-2	353	Membrane
Q6PE84	<i>Mus musculus</i>	Stomatin-like protein-3	MmSlp-3	287	PM
P67778	<i>Mus musculus</i>	Prohibitin	MmPHB	272	Mitochondrion, Cytoplasm, Nucleus
O35129	<i>Mus musculus</i>	Prohibitin-2	MmPHB-2	299	Mitochondrion, Cytoplasm, Nucleus
Q27433	<i>Caenorhabditis elegans</i>	Mec-2	CeMec-2	481	Membrane
Q19200	<i>Caenorhabditis elegans</i>	Stomatin-1	CeSto-1	330	Membrane
Q19958	<i>Caenorhabditis elegans</i>	Stomatin-2	CeSto-2	314	Membrane
Q20657	<i>Caenorhabditis elegans</i>	Stomatin-3	CeSto-3	267	Membrane
Q22165	<i>Caenorhabditis elegans</i>	Stomatin-4	CeSto-4	281	Membrane
Q21190	<i>Caenorhabditis elegans</i>	UNC-1	CeUNC-1	285	Membrane
Q17372	<i>Caenorhabditis elegans</i>	UNC-24	CeUNC-24	415	Membrane
P0ABC3	<i>Escherichia coli</i>	HflC	EcHflC	334	Membrane
P0ABC7	<i>Escherichia coli</i>	HflK	EcHflK	419	Membrane

Table 3-3. Animal and bacterial band-7 proteins (identified by IPR001107). These sequences were downloaded from UniProt and used in phylogenetic analysis. Highlighted in blue are again proteins with a stomatin signature domain (IPR001972). Abbreviations are as before.

UniProt ID	Species	Name	Abbreviation used	Length (aa)	Subcellular Localisation
P40961	<i>Saccharomyces cerevisiae</i>	Prohibitin-1	ScPHB-1	287	Mitochondrion
P50085	<i>Saccharomyces cerevisiae</i>	Prohibitin-2	ScPHB-2	310	Mitochondrion
Q9P7H3	<i>Schizosaccharomyces pombe</i>	Prohibitin-1	SpPHB-1	282	Mitochondrion
O94550	<i>Schizosaccharomyces pombe</i>	Prohibitin-2	SpPHB-2	279	Mitochondrion
O60121	<i>Schizosaccharomyces pombe</i>	N/A	O60121	354	Mitochondrion
Q59X52	<i>Candida albicans</i>	Stomatin-like protein-2	Q59X52	263	N/A
Q59XK2	<i>Candida albicans</i>	Stomatin-like protein-2	Q59XK2	263	N/A
Q5A411	<i>Candida albicans</i>	Stomatin-like protein-99	Q5A411	350	N/A
Q59SS4	<i>Candida albicans</i>	Prohibitin-1	Q59SS4	283	N/A
Q5AEB1	<i>Candida albicans</i>	Prohibitin-12	Q5AEB1	321	N/A
Q5AND0	<i>Candida albicans</i>	Prohibitin-2	Q5AND0	303	N/A
A3LYB1	<i>Pichia stipitis</i>	Stomatin-like protein-3	A3LYB1	340	N/A
A3LTY5	<i>Pichia stipitis</i>	Stomatin family protein	A3LTY5	367	N/A

Table 3-4. Yeast band-7 proteins (as identified by IPR001107). The sequences of these proteins were retrieved from UniProt after a search for yeast band 7 proteins. Only those are shown and were used in the analysis, which were already annotated as stomatins or prohibitins. Highlighted in blue are proteins with a stomatin domain.

3.1.1 The *Arabidopsis* band-7 family

The genome of *Arabidopsis thaliana* contains altogether 17 different genes that encode for proteins with a band-7 domain (as identified by InterPro IPR001107). These genes give rise to 18 proteins, amongst these three with an additional stomatin domain (InterPro IPR001972), 8 with a prohibitin domain (InterPro IPR000163)) and 3 proteins that have domains similar to those found in animal flotillins (PTHR13806). The remaining *Arabidopsis* band-7 members are made up of 4 HIR (for hypersensitive induced reaction) proteins and one ER-localised protein. The genes of the HIR proteins are commonly upregulated during the hypersensitive response. One of these, encoded by the gene At3g01290, also has a stomatin signature domain (recognised by InterPro IPR00192), although the structural similarity to AtSlp1 and AtSlp2 is low (see section 3.1.5).

To investigate the relationships between the *Arabidopsis* band-7 proteins, a series of phylogenetic trees were constructed based on ClustalW multiple sequence alignments. Figure 3-1 shows a tree (presented as a rectangular cladogram using TreeView with bootstrap values from 1-10000) that includes all members of the *Arabidopsis* band-7 family. The tree reveals one large cluster that contains most of the band-7 family members, including AtSlp1 and AtSlp2 (marked in red). AtPHB1 and AtPHB6 fall out of this group and represent the most distantly related proteins to these ones. Amongst the proteins of the largest cluster, the two splice variants of AtPHB2 separate and represent an own group with AtPHB7 as its next close relative. The remaining proteins clearly divide into three separate groups, which can be assigned as prohibitins 3-5, flotillin-like proteins and AtSlps together with the HIR proteins. The tree reveals that the stomatin-like proteins probably share a common ancestor with the HIR proteins, as these represent the closest neighbours. Amongst the HIRs, At5g51570 is the next closely related protein to AtSlp1 and 2. The tree also shows a closer relationship of the stomatins and HIR proteins with the group containing the flotillin-like proteins rather than with the prohibitins. The group containing the flotillin-like proteins also contains a so far uncharacterised ER protein that resembles mammalian Erlin proteins but has otherwise only little similarity to any of the other band-7 proteins. Previously, *Arabidopsis* prohibitins have been demonstrated to fall into two subtypes: AtPHB1, 6, 2 and 7 form type II prohibitins and AtPHB3, 4 and 5 type I prohibitins (Van Aken *et al.*, 2007). In accordance with this, prohibitins 3, 4 and 5 fall into a cluster representing type I prohibitins that has separated earlier from the group containing the stomatins, HIRs and flotillins.

In addition to the tree, the actual identity and similarity values in percent were calculated between each Arabidopsis band-7 family member. These values are based on pairwise sequence alignments that were performed using the Emboss-needle method for global alignments (available on www.ebi.ac.uk) and are shown in Table 3-5. From this table it becomes obvious that apart from a significant percentage of identity between AtSlp1 and AtSlp2 (61.8 % identity and 66.3 % similarity) there is actually very little sequence identity between these two proteins and all other Arabidopsis band-7 family members. Even the identity between stomatins and their closest neighbour, the HIR protein At5g51570, is surprisingly low at only 17.5 % (31.1 % for similarity to AtSlp1). Amongst the HIR proteins, the level of identity is generally high, for example up to 85.7 % between At5g62740 and At1g69840. This can also be seen from the tree in which these two proteins represent the closest neighbours. Sequence identity inside the flotillin group is also high, particularly between the three proteins that contain the flotillin-like domain (for example >90 % identity between At5g25250 and At5g25260). The ER protein At2g03510 falls into the same cluster with the flotillin-like proteins, but the actual identity to the flotillins is very low at only 14 to 16 %. As expected from the tree, the level of identity amongst the prohibitins also reflects their division into the prohibitin subtypes. PHB3, 4 and 5 (type I) share between 60 and almost 90 % sequence identity, whereas these levels drop to around 40 % when they are compared to the prohibitins belonging to subtype II. These prohibitins (PHB1, 6, 2 and 7) also share much higher levels of identity amongst themselves (ranging from 60 to > 80 %). According to these results, the Arabidopsis band-7 family clearly divides into distinct subgroups, similar to those previously identified from animals (Tavernarakis *et al.*, 1999). However, the Arabidopsis genome also contains novel members in the shape of the HIR proteins that appear to be unique to plants. The total number of stomatin-domain containing proteins is low in Arabidopsis (only 3) compared to animals and humans. On the contrary, Arabidopsis contains 7 prohibitin genes that give rise to 8 proteins compared to only 2 proteins in humans and yeast.

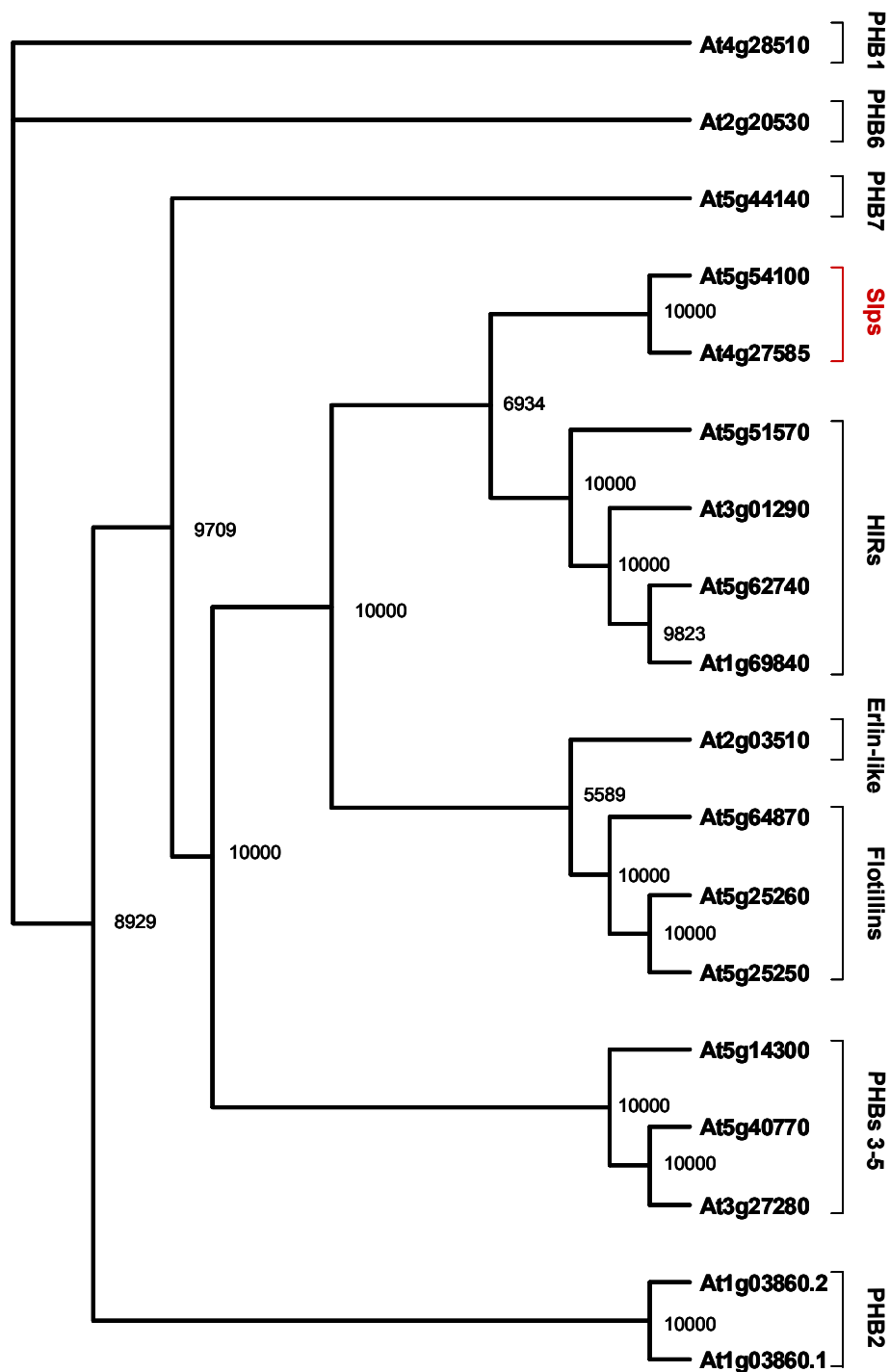


Figure 3-1. A phylogenetic tree of the Arabidopsis band-7 family. The tree is based on a ClustalW multiple sequence alignment and was constructed using the TreeView software. Bootstrap values of 1-10000 are given at each branch point. AtSlp1 and AtSlp2 fall into an own clade that is marked in red. Other functional group names are given on the right. Abbreviations are PHB (prohibitin), HIRs (hypersensitive induced reaction). Names given are according to Table 3-2.

% Identity

ER
protein

Slps

HIRs

Flotillin-like

Prohibitins

	AtSlp-1	AtSlp-2	At5g51570	At3g01290	At5g62740	At1g69840	At2g03510	At5g64870	At5g25260	At5g25250	At5g14300	At5g40770	At3g27280	At5g44140	At1g03860.1	At1g03860.2	At2g20530	At4g28510
AtSlp-1		61.8	17.5	18.5	17.1	16.3	18	10.6	10.8	10.4	18.5	16.3	16.4	13.9	15.6	12.6	15.9	14.2
AtSlp-2	66.3		18.8	18.7	18.1	16.7	13.2	11.5	9.6	9.7	14.9	15.5	15.9	15.2	16.4	12.5	13.2	16.6
At5g51570	31.1	32.1		55.8	55.8	55.4	18.2	10.4	12.6	11.6	20.9	16.3	17	17.7	15.9	14.3	17.9	16.6
At3g01290	32.4	31.1	76		79.7	73.8	18.7	10.1	14	11.8	17.6	17	15.5	16.5	16.5	15.3	14.9	15.4
At5g62740	30.8	31.5	77.1	91.6		85.7	18.5	12	14.2	14.1	15.9	15.1	16.3	17.4	16.6	15.4	16	14.6
At1g69840	28.9	30.4	74.5	87.8	92		17.4	10.5	11.1	10.8	17.7	15.5	14.9	17.2	14.2	13.8	16.4	15.9
At2g03510	31.3	26	33.8	32.7	32.5	33.7		14.1	16.6	16.1	16.1	16.5	17.8	19.2	13.9	12	17.1	18.1
At5g64870	23.5	23.4	19.5	19.9	22.8	22.4	23.9		82.5	84.6	10.9	10.2	10.3	10.1	15.2	8.3	11.8	14.7
At5g25260	23.7	20.8	23.5	25.9	26	23	29.7	90		93.2	11.2	12.3	12.7	11	9.2	8.7	10.4	13
At5g25250	23.3	19.9	22.3	22.9	25.2	22.7	27.7	92.1	95.3		10.8	7.7	12	9.7	9.4	9.4	9.2	14.5
At5g14300	29.6	26.7	32.7	33.2	27.9	33.3	30.7	19.4	19.2	18.3		60.8	60.8	40.4	42.8	36.7	45	41.7
At5g40770	30	30.8	31.7	28.8	26.5	28.5	30.3	19.8	20.3	16.1	72.8		88.9	46.9	48.5	40.8	45.8	45.3
At3g27280	31.9	33.7	28.4	29.7	30	27.8	31.9	19.3	22.7	22.1	73.1	93.9		46.9	48.3	41	45.6	48.3
At5g44140	27.7	28.3	33.3	32.1	31.5	31.5	35.2	18.5	19.1	17.8	59.6	65.7	65.6		78.7	62.2	73.1	77.4
At1g03860.1	25.1	26.1	32.6	31	29.6	30.9	25.1	26.5	20.6	20	61	65	66	89.5		77.3	81.7	85.4
At1g03860.2	24.2	20.4	31.5	30.6	29.4	30.5	23.4	19.2	19.8	20.2	52.2	55.3	55.8	68.9	77.3		68.9	69.4
At2g20530	28.2	26	31.5	30	29.4	31.5	32.6	21.5	20.7	19.4	61.9	64.1	63.9	83.1	90.7	74.5		87.2
At4g28510	27.3	30.2	32.9	31.7	29.4	30.3	34.9	26.4	21.8	27.9	61.4	63.3	66	85.4	92.7	74	93.4	

% Similarity

Table 3-5. Identities and similarities between protein sequences of the Arabidopsis band-7 family. Identities and similarities (in %) were calculated using the Emboss pairwise alignment algorithm. Identity numbers are given in the top half of the table and similarity values in the bottom half.

3.1.2 The relationship of *Arabidopsis stomatins* with those from other species

On the next level of phylogenetic analysis, the relationships amongst stomatins from various kingdoms were investigated. Stomatin domain (IPR001972) containing protein sequences were downloaded from the UniProt database from various animals, humans, yeast, bacteria and plants. Altogether 33 different sequences were used to construct a phylogenetic tree that is presented in Figure 3-2. It is apparent that there seems to be a clear division between animal, nematode and mouse stomatins, *C.elegans*-specific proteins and other types of stomatin-like proteins from plants, animals and yeast. The tree shows that 2 clusters containing animal stomatins and stomatin-like proteins 3 separated early on from the remaining large group that contains all other sequences. The first cluster closest to the bottom contains four proteins from the nematode *C.elegans*. The second cluster that separated includes 2 subgroups: one that contains the human and mouse stomatin proteins and a second one that contains human and murine stomatin-like proteins 3 as well as the *C.elegans* protein stomatin 2. The remaining large cluster that contains all other sequences can be further divided: *C.elegans* stomatin 3 represents a sole branch that seems to have separated early from the remaining proteins. Human podocin, a kidney specific stomatin isoform also clearly separated from these proteins and forms an own branch. Next in the tree, a cluster is formed by orthologues of the stomatin-like 1 proteins. These human, murine and nematode bipartite proteins all contain a sterol-carrier protein domain (IPR003033, Table 3-1) additionally to their stomatin domain. Two uncharacterised stomatin-like proteins from 2 yeast species form the next group, followed by a cluster that contains the *E.coli* HflK protein together with the Arabidopsis HIR protein At3g01290. This result is surprising, especially considering the species divergence between a bacterium and a higher plant. The HflK protein is involved in the life style decision of the lambda phage upon infection of its host (Noble *et al.*, 1993), whereas the Arabidopsis protein is implicated to function in plant defence during the hypersensitive response. The remaining large cluster is made up of plant and yeast stomatins and stomatin-like 2 proteins. It can be divided into two subgroups, one containing the plant proteins and the other consisting of mammalian stomatin-like proteins 2 (Slp2) and yeast stomatin-like proteins. Amongst the plant proteins, a protein with a stomatin domain from the unicellular alga *Chlamydomonas* represents an early descendant. The remaining proteins can be divided into clusters according to monocotyledons and dicotyledons/moss. To the monocotyledon proteins belong stomatin domain proteins from rice and maize, with the rice proteins clearly

grouping together. The dicotyledon/moss cluster contains sequences from the moss *Physcomitrella patens*, grape (*Vitis vinifera*) and *Arabidopsis thaliana*.

Taken together, plant stomatin-like proteins fall into one clade with stomatin-like proteins 2 from mammals and stomatin-like proteins from yeast. Thus it appears that a common ancestor of these proteins separated from the bipartite proteins and other stomatins from yeast and animals. Yeast stomatin proteins also seem to have split into two different subgroups, of which the larger one is closely related to mammalian stomatin-like proteins 2. Notably, the budding yeast *Saccharomyces cerevisiae* does not contain a stomatin domain protein in its genome, but two prohibitins. Fission yeast (*Schizosaccharomyces pombe*) does encode two prohibitins and one protein with a stomatin domain (O60121), a close relative of human stomatin-like protein 2. Complementing this tree of stomatin proteins is Table 3-5, which shows the actual values of calculated identity and similarity (in %) between *Arabidopsis* stomatin-like proteins and their neighbours from the same clade. This table reveals that the closest match to AtSlp1 in terms of sequence identity is the stomatin domain protein from grape with 67 % identity and 75% similarity, higher than the identity level even between AtSlp1 and AtSlp2. The degree of identity amongst the plant stomatins is around 50 %, but much higher between the monocotyledons (>90 %). The identity between AtSlps and the moss protein is higher (57 %) or as high as with the monocot sequences (52-57 %). This is surprising, since the *Physcomitrella* protein is only a predicted fragment rather than a complete sequence, but also considering the divergence between mosses and dicots. The protein that has been studied most in mammals out of this clade is the human stomatin-like protein 2 (HsSlp2), which shares 41.7 % and 39.8 % identity with AtSlp1 and AtSlp2 respectively, and a similar identity value with the other plant proteins. Yeast stomatin proteins share approximately 40-50 % identity with human and mouse Slp2. The sequences from the multicellular yeast *Candida albicans* share the lowest % identity with all other sequences, even with those ones from other yeasts.

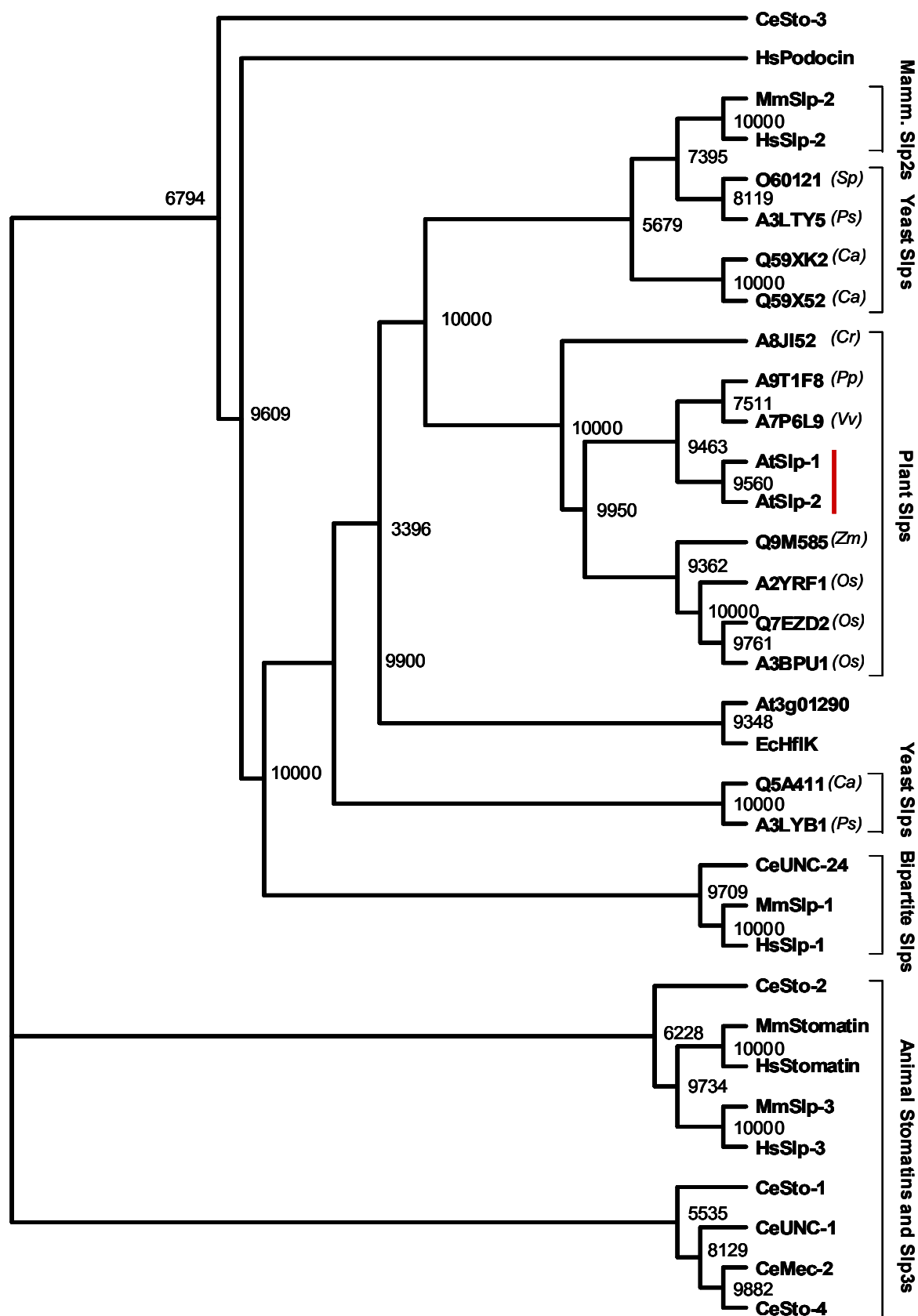


Figure 3-2. A phylogenetic tree of stomatin protein sequences from various species. Abbreviations are as indicated in tables 3-3 and 3-4. Where only the UniProt ID is given as a sequence name, the species is indicated in brackets right next to the abbreviated name. A red bar indicates the position of AtSlp1 and 2. Species are as follows from top to bottom: *Sp* (*Schizosaccharomyces pombe*), *Ps* (*Pichia stipitis*), *Ca* (*Candida albicans*), *Cr* (*Chlamydomonas reinhardtii*), *Pp* (*Physcomitrella patens*), *Vv* (*Vitis vinifera*), *Zm* (*Zea mays*), *Os* (*Oryza sativa*). Bootstrap values from 1-10000 are given at each branch point. Abbreviated names are given according to tables 3-2 to 3-4.

% Identity

	Dicotyledons			Monocotyledons					Mammals		Yeast Slps				
	Moss														
	AtSlp-1	AtSlp-2	A9T1F8	A7P6L9	Q9M585	A2YRF1	Q7EZD2	A3BPU1	A8JI52	MmSlp-2	HsSlp-2	A3LTY5	O60121	Q59XK2	Q59X52
AtSlp-1		61.8	56.9	67	52.8	53	57.2	53.5	44	43	41.7	41.7	39.3	19.3	18.9
AtSlp-2	66.3		57.1	56.4	47.7	46.2	46.2	45.9	51.6	40.1	39.8	42.6	40.5	20.5	22.1
A9T1F8	64.2	65.6		56.4	51	53.1	53.1	49.6	48.2	47	46.1	42.5	42.4	18.3	18.3
A7P6L9	75.1	62.2	64		56.3	56.2	57.8	54.5	44.9	40.7	43.2	38.4	37.6	18.1	18.3
Q9M585	65.4	59.6	63.7	67.4		63.5	62.7	58.9	42.9	43.3	45.7	39.3	38.1	17.4	18.4
A2YRF1	63.9	56.3	62.9	65.1	77.7		99.2	92.3	40.8	41	41.3	36.8	37.6	19.4	19
Q7EZD2	68.5	56.1	62.9	66.6	76.4	99.2		93.1	40.8	40.7	41.5	36.6	37.9	19.4	19
A3BPU1	64	56.4	58.8	62.5	71.3	92.3	93.1		40.7	36.8	37.9	35.2	36.4	18.4	18.3
A8JI52	56.4	65.7	62.4	58	54.6	53.7	54	52.7		41.4	40.9	40.7	38.7	23.3	23.6
MmSlp-2	60.6	54.3	63.7	57.1	58.9	58	57.8	52.4	56.9		93.8	44.6	48.6	20.1	22.2
HsSlp-2	59.5	55.1	62.9	60.6	61.9	57	56.8	52.6	56.9	96.1		44.4	48.3	21.1	21.1
A3LTY5	58.1	60.3	59.9	55.5	56.6	53.9	53.7	50.7	60.9	61.4	60.7		49.7	27.6	27.6
O60121	57.1	55.4	60.7	55.1	54.8	54.4	54.9	53	55.4	65.1	64	65.4		26	25.7
Q59XK2	33	34.9	31.7	31	29.3	33.2	33.2	31.3	37.7	31.5	33.1	40.2	37.1		99.2
Q59X52	31.9	37.1	31.7	31.2	29.6	33	33	31.2	38.1	33.8	33.1	40.7	37.4	99.2	

% Similarity

Table 3-6. Identities and similarities between the closest relatives of AtSlp1 and AtSlp2. Identities and similarities (in %) were calculated using the Emboss global pairwise alignment algorithm. Identity numbers are given in the top half of the table and similarity values in the bottom half. Values were calculated as described before with the Emboss pairwise global alignment algorithm.

3.1.3 *Arabidopsis* Slps and band-7 proteins from a variety of species

Finally, the relationship of AtSlps with band-7 proteins from *Arabidopsis*, animals, bacteria and yeast was investigated. A bootstrap tree (rectangular cladogram) was constructed based on a ClustalW multiple sequence alignment of altogether 57 sequences that is presented in Figure 3-3. From this tree, a clear division between stomatins, stomatin-like proteins 2, prohibitins, flotillins, erlins and the bacterial HflC/K proteins becomes visible. The stomatin-like proteins 2 form an own clade at the bottom of the tree that includes AtSlp1 and 2 (highlighted by a red bar). As before, they cluster together with mammalian Slp2s and yeast Slps. The *Arabidopsis* HIR proteins are not a part of this group and form a separate clade. On this level of evolutionary conservation, AtSlp1 and 2 are clearly more related to yeast and mammalian Slps and Slp2s rather than with the HIRs. The clade above the Slp2 cluster is comprised of the other stomatins and Slps from *C.elegans*, mouse and human. Again the bipartite stomatin-like proteins 1 form another cluster that is separated from the other stomatins and stomatin-like proteins 3. All remaining proteins fall into one clade that contains the flotillins, erlins, prohibitins and bacterial proteins. These bacterial band-7 members are clearly the most distantly related ones from the other subgroups. *E.coli* HflK has separated earliest from these; *E.coli* HflC also represents an early divergent that has not much similarity with the eukaryotic members of the clade. The remaining proteins form two distinct clusters containing prohibitins and flotillins together with erlins. The flotillins and erlins fall again into the same cluster in which they divide accordingly. The *Arabidopsis* ER protein At2g03510 is clearly related to mammalian erlins and is therefore referred from this point as an erlin-like protein. The *Arabidopsis* flotillin-like proteins fall into one group with the human flotillin proteins. However, they are not recognised by the flotillin specific domain IPR004851 like the human proteins are. So far they have only been classified as flotillin-like by the domain PTHR which has not been fully annotated yet. They also do not contain the band-7 domain as recognised by the domain IPR001107, but are otherwise related to human flotillins. Most likely, these plant proteins have evolved further from their mammalian orthologs. The prohibitin group can be divided into 2 large subgroups in accordance with the results published by van Aken et al. (2007). *Arabidopsis* PHBs fall into the same two subtypes as seen before in Figure 3-1. Type I prohibitins include mammalian and *S.cerevisiae* PHB1 proteins as well as *Arabidopsis* PHBs 3, 4 and 5 and the *S.pombe* ortholog Q9H7P3. *Arabidopsis* PHBs 1, 6, 2 and 7 form a cluster in the type II prohibitin clade, separated from the other subgroup containing mammalian and yeast prohibitins 2. Taken together, this tree clearly

demonstrates that both AtSlps belong to the subgroup of the stomatin-like proteins 2 that contains members from mammals, yeast and plants.

3.1.4 Comparison of Slps on the sequence level- AtSlp1 and HsSlp2

The phylogenetic analysis presented so far has dealt with the overall protein similarities. To look in more detail at the level of the actual protein sequences, multiple sequence alignments using the ClustalW algorithm were prepared and colour-coded with the Boxshade software. An alignment of AtSlp1, AtSlp2 and HsSlp2 is presented in Figure 3-4. As mentioned above, the overall similarity between these proteins is almost 60%. From the BoxShade plot it can be seen that most of those residues lie inside the conserved band-7 domain. Inside this domain, several stretches of amino acids are highly conserved amongst all three proteins, lots of which contain alanine residues and an abundance of charged amino acids. Most of these conserved amino acids lie in the centre and around the band-7 domain. Amongst these, a short stretch containing a conserved cysteine residue (marked with a black arrowhead) is apparent. This cysteine might be putatively post-translationally modified by S-acylation and therefore an important feature of the stomatin-like proteins. Palmitoylation might have an important function in the proteins' ability to attach to membranes analogous to the palmitoylated cysteine residue in the human stomatin protein (Cys29) (Snyers *et al.*, 1999b). There are two more cysteine residues highlighted by an asterisk, one each in the AtSlp2 and the HsSlp2 sequences. Both lie inside the band-7 domain and might also be modified to aid membrane attachment of these proteins. Alternatively, they could be oxidised to form disulfide bridges. That seems a possible scenario especially for HsSlp2, since the two cysteines lie so close to each other. Furthermore, an alanine residue just outside the band-7 domain is indicated by a pink arrowhead. This residue is completely conserved amongst all members of the Arabidopsis band-7 family, and also in the human stomatin-like 2 protein. The overall similarity between the two Arabidopsis proteins becomes clearly visible in this alignment. It appears that only the very N- and C-termini of the proteins are unique, whereas the central parts are highly conserved, especially inside and proximal to the band-7 domain. The N-termini of both Arabidopsis proteins contain an unusual high number of proline residues that are putatively contributing to their peculiar way of membrane attachment (described later in this chapter in section 3.2.1). The unique elongated N-terminus of the AtSlp2 protein probably arises from the presence of an additional exon in the gene structure (section 3.5.3.1). AtSlp1 on the contrary has a unique C-terminus of about 80 amino acids that partly aligns with the human protein, but stretches another 30 residues beyond that. Overall, the human protein aligns better and seems more closely related to AtSlp1 than AtSlp2. However, both Arabidopsis proteins are longer in their sequences than any of the

human stomatin-like proteins. Also marked in Figure 3-4 are the positions of areas that were chosen as epitopes for the production of antibodies against the Arabidopsis proteins. These will be further explained in the next section of this chapter. Overall, this alignment highlights the high level of conservation in the band-7 domain that might hold important information for the function of these proteins. It also shows that only few residues are conserved on the N-termini of the proteins, those ones probably being important for correct subcellular targeting (e.g. arginine). The C-terminus of AtSlp1 appears to bear unique features that are putatively related to its individual function.

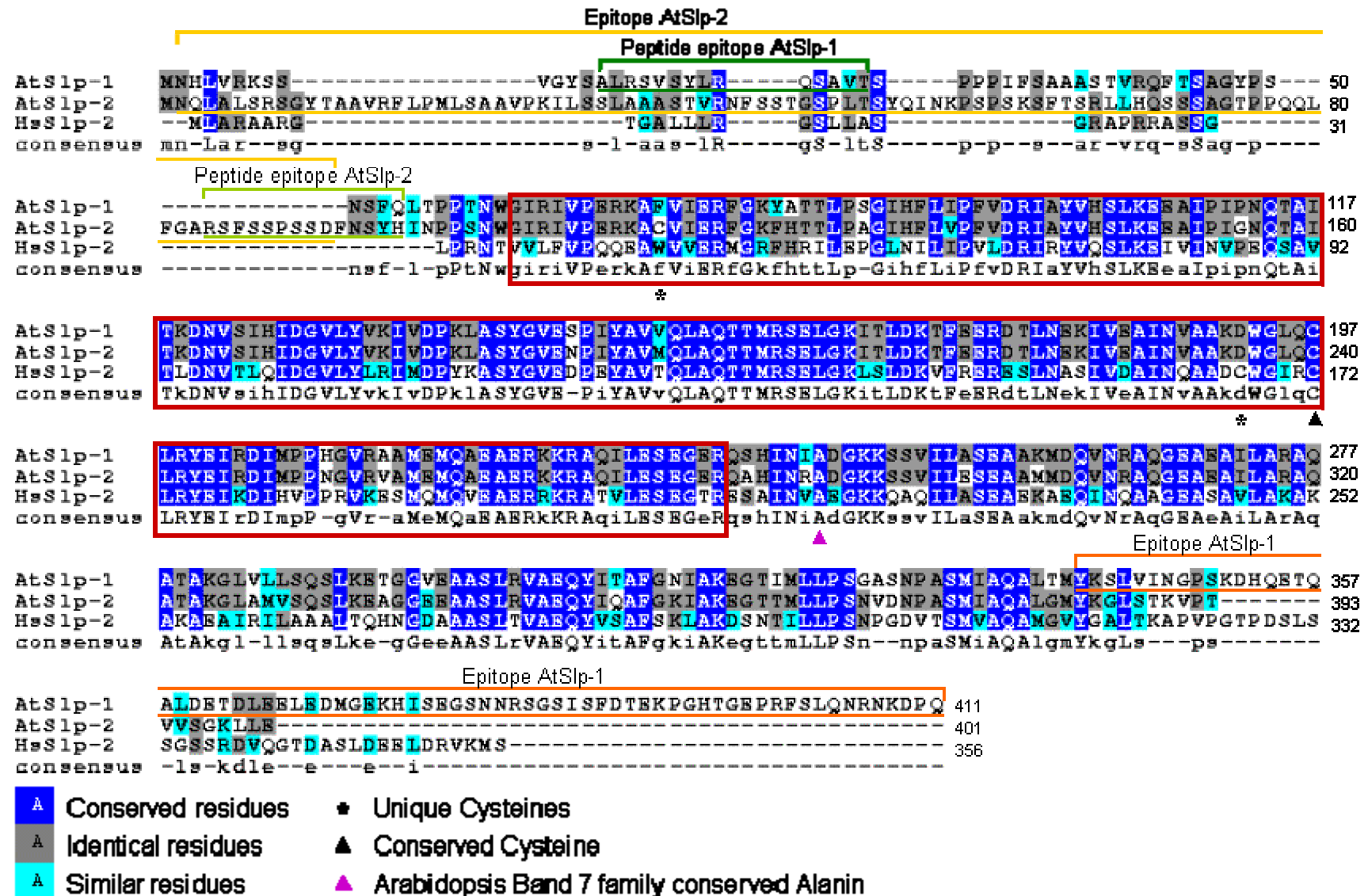
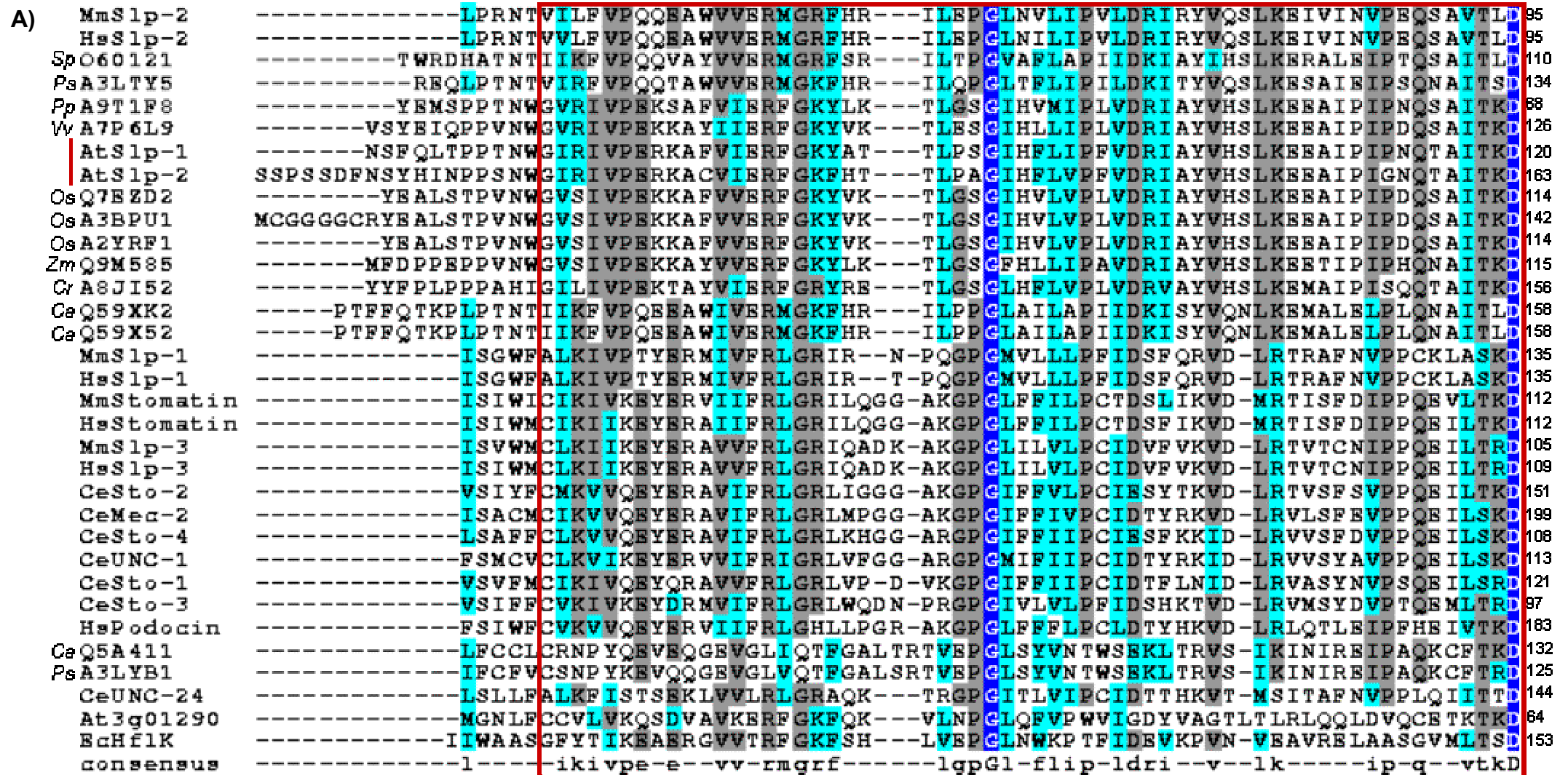


Figure 3-4. A multiple sequence alignment of AtSlps and HsSlp2 with BoxShade colour coding. Colours correspond to the degree of conservation between residues as indicated at the bottom left. Areas that were chosen as epitopes to raise antibodies are colour coded as follows: Orange line (Epitope AtSlp1 used for protein expression in bacteria); Yellow line (Epitope AtSlp2 used for attempted protein expression in bacteria); Dark green line (Peptide epitope used for commercial antibody production by AgriSera); Light green line (Peptide epitope chosen for commercial antibody production by AgriSera); the red box indicates the position of the band 7 domain.

3.1.5 Sequence comparison of AtSlps and stomatins from other species

To gain more information about the sequence similarities amongst other stomatin domain proteins, a BoxShade coloured ClustalW multiple sequence alignment of 33 stomatin sequences (the same ones used to construct the tree in Figure 3-2) is shown in Figures 3-5 (A-C). For simplicity, only the sequences around the band-7 domain are shown. Outside the band-7 domain there is very little sequence conservation amongst these proteins. In total, only three residues inside the band-7 domain are completely conserved. Two of those are glycine residues and one is an aspartate residue. Several other short stretches of amino acids bear high similarities in the conserved domain from this diverse set of proteins. The residue just in front of the second conserved glycine (glycine 194 in AtSlp1) is almost completely conserved as a tryptophane in all sequences apart from the *C.elegans* UNC24 protein, the *E.coli* HflK protein and the Arabidopsis HIR protein At3g01290. It appears that this Arabidopsis protein and the bacterial HflK have the least similarity to all other stomatins used in this study. This is in agreement with the results from the phylogenetic tree in Figure 3-2 that shows a separation of these proteins from the other plant, yeast and mammalian Slp-2 type proteins. It also becomes now clear that the cysteine residue in the AtSlp2 sequence marked by an asterisk in Figure 3-5 (A) is exclusively at this place in this protein and unrelated to the other stomatins. Thus, it probably has no crucial role related to general stomatin function; however, it might still serve as an additional membrane anchor in this particular protein. The second cysteine marked by the black arrowhead in Figure 3-5 (C) is only conserved in the mammalian Slp2 proteins and the yeast and plant Slps, but not in the other stomatin type proteins. These proteins have a hydrophobic residue such as isoleucine, leucine or valine at this position. This property mirrors the division of the cysteine-containing proteins into one phylogenetic clade as previously seen in the tree of Figure 3-2. Other chunks of sequences are identical throughout the stomatin proteins, for example stretches containing an abundance of alanines and glutamates towards the end of the band-7 domain. The alanine residue that is conserved amongst all Arabidopsis band-7 proteins is present only in the mammalian Slp2 type proteins, the bacterial HflK protein, the Chlamydomonas protein and the dicot and moss sequences. It is absent from the monocot proteins or replaced by a serine residue as in the case of the maize protein. It is also not present in the yeast proteins apart from the *S.pombe* and *Pichia* sequences. In short, this residue is present in most members of the Slp2 type clade as identified in Figure 3-2. Overall, the sequence conservation between stomatins and Slps is unsurprisingly highest in the conserved band-7 domain. A total of only three residues are conserved

amongst all sequences, these being putatively important for specialised functions unique to stomatin proteins amongst the band-7 family.



A Conserved residues
A Identical residues
A Similar residues

* Unique Cysteine AtSlp-2

Figure 3-5 (A). A multiple sequence alignment of all stomatins analysed in this study. The alignment was colour coded by the BoxShade algorithm according to the degree of conservation as indicated. Where only the UniProt ID is given as the name, the species is given abbreviated next to it as before as explained in Figure 3-2. The red box indicates the position of the band-7 domain and numbers on the right indicate the position in each sequence. The asterisk marks the unconserved cysteine of AtSlp2. The red bar on the left marks the two AtSlps. This figure is continued on the following two pages.

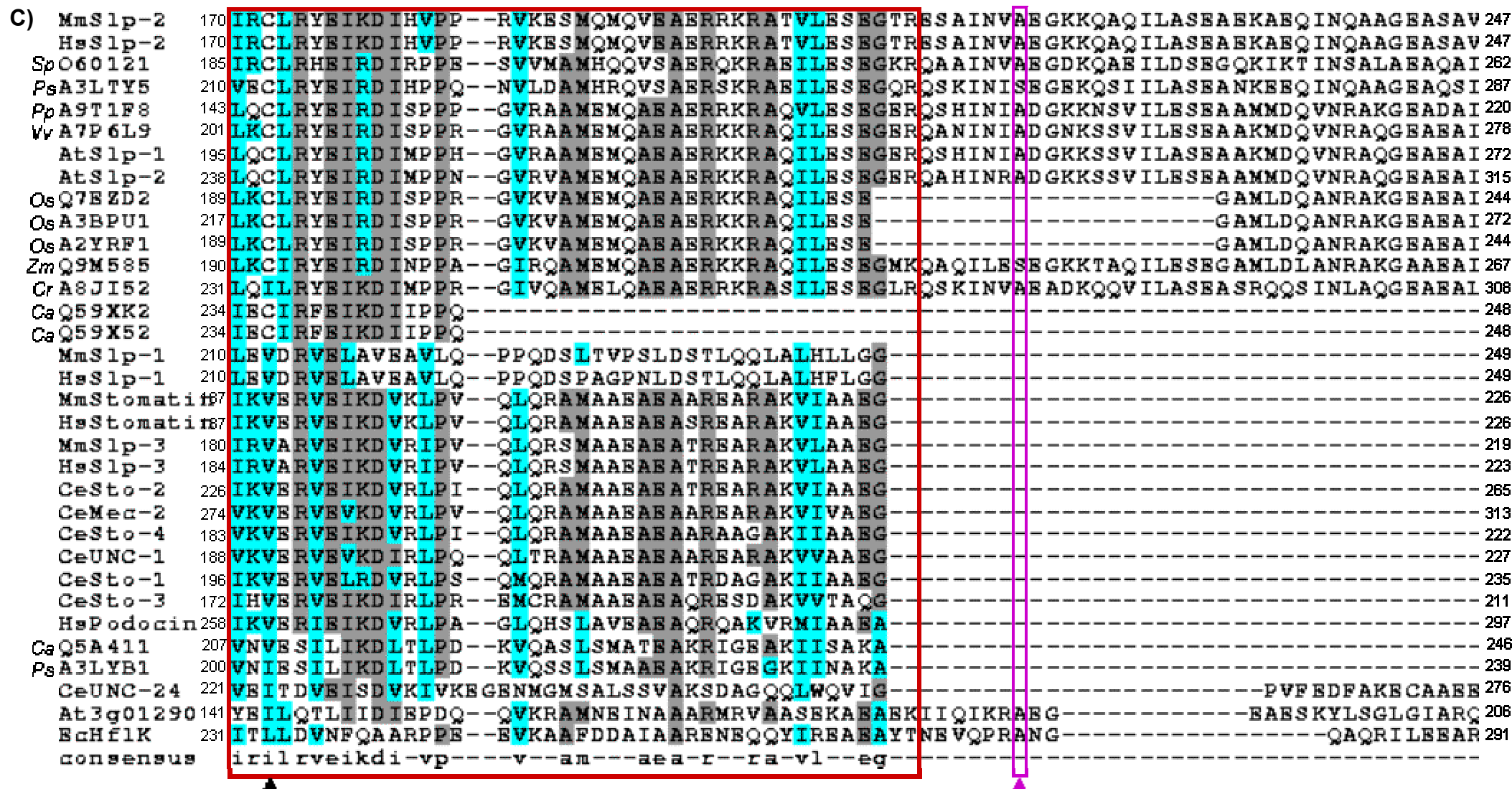
B)

MmSlp-2	96	NVTLQIDGVLYLRIMDPYK--ASYGVEDPEYAVTQLAQTTRMSELGKLSLDKVFRR--ERESLNANIVDAINQAADC--W	169
HsSlp-2	96	NVTLQIDGVLYLRIMDPYK--ASYGVEDPEYAVTQLAQTTRMSELGKLSLDKVFRR--ERESLNASIVDAINQAADC--W	169
SpO60121	111	NVSLGLDGVLYIQVYDPYK--ASYGVEDADYAISQLAQTTRMSEIGRLTLDHVLR--ERQSLNIHITDAINKAABS--W	184
PsA3LTY5	135	NVSLLELDGILYIKVIDPYK--ASYGVEDFKFAISQLAQTTRMSEIGSMTLDAVLK--ERQLLNNNINHVINDAARDN--W	209
PpA9T1F8	69	NVSI SIDGVLYLKIIVDPYR--ASYGVENPIYAVIQLAQTTRMSELGKITLDKTFE--ERDTLNEKIVKAINEAASD--W	142
VvA7P6L9	127	NVSI LIDGVLYVKIIVDPKL--ASYGVENPIYAVIQLAQTTRMSELGKITLDKTFE--ERDTLNEKIVLAINEAAKD--W	200
AtSlp-1	121	NVSI HIDGVLYVKIIVDPKL--ASYGVESPIYAVVQLAQTTRMSELGKITLDKTFE--ERDTLNEKIVBAINVAAKD--W	194
AtSlp-2	164	NVSI HIDGVLYVKIIVDPKL--ASYGVENPIYAVMQLAQTTRMSELGKITLDKTFE--ERDTLNEKIVBAINVAAKD--W	237
OsQ7BZD2	115	NVSI QIDGVLYVKIIVDPYL--ASYGVENPIFAVIQLAQTTRMSELGKITLDKTFE--ERDTLNEQIVRSINSAATD--W	188
OsA3BPU1	143	NVSI QIDGVLYVKIIVDPYL--ASYGVENPIFAVIQLAQTTRMSELGKITLDKTFE--ERDTLNEQIVRSINSAATD--W	216
OsA2YRF1	115	NVSI QIDGVLYVKIIVDPYL--ASYGVENPIFAVIQLAQTTRMSELGKITLDKTFE--ERDTLNEQIVRSINSAATD--W	188
ZmQ9M585	116	NVTI QIDSVIYVKIMDPYL--ASYGVENPIYAVLQLAQTTRMSELGKITLDKTFE--ERDALNEKIVSAINSAATD--W	189
CrA8J152	157	NVTI TIDGVLYVKVMDAFK--ASYGVDNALYAVGQLAQTTRMSELGKITLDKTFE--ERREALNHNIVRTINEAABA--W	230
CaQ59XK2	159	NVKIKLNGI IYIKI IIDPYK--ASYGIDDYKYSILKLIESRLNLQIGKLELSKILK--NRELLNDLIVKI INEAAMEN--W	233
CaQ59X52	159	NVKIKLNGI IYIKI IIDPYK--ASYGIDDYKYSILKLIESRLNLQIGKLELSKILK--NRELLNDLIVKI INEAAMEN--W	233
MmSlp-1	136	GAVLSVGADVQFRIWDPVL--SVMVVKDLNTATRMTAHNAMTKALLRRPLQEIQM--EKLKIGDQLLLEINDVTRA--W	209
HsSlp-1	136	GAVLSVGADVQFRIWDPVL--SVMVVKDLNTATRMTAQNAMTKALLKRPLREIQM--EKLKISDQLLLEINDVTRA--W	209
MmStomati#13	113	SVTI SVDGVVYYRVQNATL--AVANI TNADSATRLLAQTTLRNALG TKNLSQ ILS--DREBIAHHMQSTLDDATDD--W	186
HsStomati#13	113	SVTI SVDGVVYYRVQNATL--AVANI TNADSATRLLAQTTLRNVLG TKNLSQ ILS--DREBIAHNMQSTLDDATDA--W	186
MmSlp-3	106	SVTTQVDGVVYYRIYSAVS--AVANVNDVHQATFLLAQTTLRNVLG TQTLSQ ILS--GREBIAHSIQTL LDDATEL--W	179
HsSlp-3	110	SVTTQVDGVVYYRIYSAVS--AVANVNDVHQATFLLAQTTLRNVLG TQTLSQ ILA--GREBIAHSIQTL LDDATEL--W	183
CeSto-2	152	SVTTSVDAVIYYRISNATV--SVANVENAHHSTRLLAQTTLRNMLG TRSLSE ILS--DRETLAASMQTI LDEATES--W	225
CeMec-2	200	SVTVAVDAVVYFRI SNATI--SVTNVEDAARSTKLLAQTTLRNILG TKTLAEMLS--DREAI SHQMOTT LDEATEP--W	273
CeSto-4	109	SVTVSVDAVIYFRI SNATV--SVINVEDAARSTKLLAQTTLRNFLG TRTLAEMLS--SRDAISMQMQAALDEATDP--W	182
CeUNC-1	114	SVTVSVDAVVYFRTSDPIA--SVNNVDDAIYSTKLLAQTTLRNALG MKTLTEMLT--EREAI AQLCETI LDEGTEH--W	187
CeSto-1	122	SVTVSVDAVVYFQVDFPIT--SVVGVGNATDSTKLLAQTTLRTILG THTLSE ILS--DREKISADMKIS LDEATEP--W	195
CeSto-3	98	SVTI GVDAAVYRTSDPIA--SLARVNDAHMSTRQLAQSSLRNVLG TRSLAE LMT--DRHGIAVQVKYI LDSATLF--W	171
HsPodocin	184	MFIMEIDAICYRMENASL--LLSSLAHVSKAVQFLVQTTMKRLLAHRSLTE ILL--ERKSIAQDAKVALDSVTCI--W	257
CaQ5A411	133	NVSI TITSVVYYNIIDPMK--AIFDIDNIHQAI IERTQTTLRDVI GGRILQDVVE--KREEVAESIELI ISKTAAD--W	206
PsA3LYB1	126	NVSVI IITSVVYYNIIDPQK--AIYSIANIHDAI IVERTQTTLRDVI GGRITLQEVVE--KREEIAESIEHV IAKTAFD--W	199
CeUNC-24	145	RGLVELGATVFLKIRDEIA--AVCGVQDRNASVRTLANTMLYRYISKKRICDVTSSQDRRI ISANLKDELGSFTCQ--F	220
At3g01290	65	NVFTVVASIQYRVLADKASDAFYRLSNPTTQIKAYVFDVIRACVPKLNLDVVE--QKNEIAKSVEEBE LDKAMTA--Y	140
EcHflK	154	ENVVRVEMNVQYRVTNPEK--YLYSVTSPDDSLRQATDSALRGVIGKYTMDRILT--EGRTVIRSDTQRE LEE TIRPYDM	230
consensus		nvtl-idgvlyfrindp----avygve----av--laqttr--lgk-tl--vl---ere-l---i---indaa----wG	

A Conserved residues Figure 3-5 (B). Continued from the previous page. Labelling is as described above. The alignment continues on the following page.

A Identical residues

A Similar residues



A Conserved residues
A Identical residues
A Similar residues

▲ Conserved Cysteine
▲ Conserved Alanin

Figure 3-5 (C). The last part of the alignment. Labelling is as described above. The black arrowhead indicates the position of the conserved cysteine of the stomatin-like proteins 2. The pink arrowhead marks the position of an alanine residue that is conserved amongst all members of the Arabidopsis band-7 family.

3.2 Structural features of Arabidopsis and human stomatin-like proteins

The aim of this section is to give an overview over secondary structural features of selected stomatin-like proteins and to investigate whether sequence similarities translate into similar structural features. The following proteins were chosen: the Arabidopsis proteins Slp1 and Slp2 and their human ortholog Slp2. Only very basic features are presented as part of this section.

3.2.1 *AtSlp1- structural features*

Figure 3-7 summarises a schematic presentation of the AtSlp1 protein. Part (A) represents a Kyte-Doolittle hydrophathy profile in which positive values indicate the degree of hydrophobic properties and negative values correspond to hydrophilic residues. This plot shows that the overall degree of hydrophilicity increases towards the C-terminus of the protein, with the last 50 amino acids being entirely in the negative range of the plot. The N-terminus of the protein has several hydrophobic stretches. One of these (marked with a red box in part B of Figure 3-7) is 26 amino acids long (position 78-103) and predicted to be a membrane spanning region according to the TMAP algorithm (SDSC Biology Workbench). However, the prediction has only a very low probability score and therefore this region presents most likely no true transmembrane domain. Despite this it does probably contribute to membrane attachment of the protein as discussed in chapter 4.

In part B a schematic presentation of the protein is given with an indication of the positions of the band-7 domain in blue and the stomatin domain in violet underneath (according to InterPro database). AtSlp1 consists of 411 amino acids with the band-7 domain spanning from position 62-236 (174 amino acids). The band-7 domain contains the hydrophobic region important for membrane attachment as indicated in red. The stomatin domain (InterPro IPR001972) actually consists of 5 individual sequence blocks but is drawn as a continuum for clarity. It is slightly shorter than the band-7 domain and does not stretch as far into the N-terminal region. The conserved cysteine residue (position 197) lies towards the end of the band-7 domain and is indicated by a black arrowhead.

Part C shows some basic structural features obtained with the DNA Star Protean software. Shown in blue are alpha helical regions and below in black regions with a higher likelihood to form beta sheets (as predicted by the Garnier-Robson algorithm). Overall

more alpha helices are located towards the C-terminus and more sheets towards the N-terminus. A prediction indicating the presence of a coiled-coil is shown in green. However, this prediction has again a very low confidence score and represents most likely no real secondary structure. Underneath the Kyte-Doolittle profile a charge distribution plot is drawn that supports the hydrophilic nature of the very C-terminus that includes many negatively charged residues. In the centre of the protein around position 240 is another area with many positively charged residues. This area also corresponds to a negative peak in the hydrophobicity profile. Some positive residues are located at the very N-terminus. These are most likely important for correct subcellular targeting and will be further investigated in chapter 4. A plot indicating the likelihood of alpha (blue shaded) and beta (black shaded) amphipathic regions is shown below. From this plot it can be seen that three blocks of predicted amphipathic alpha helices are located at the very N-terminal end that correspond to the positively charged areas as indicated in the charge distribution plot. This supports the possibility of the formation of an amphipathic alpha helix in this part of the protein.

Figure 3-6 gives an impression of the proposed membrane topology of the human stomatin protein. The hydrophobic region (shown in red) does not span through the membrane, but gives rise to a hairpin loop insertion. As a consequence of this, both the N- and the C-terminus face the same side of the membrane. This model has also been suggested for other members of the band-7 family and related coat proteins (eg caveolin) (Bauer & Pelkmans, 2006). All the results presented in Figure 3-7 strongly suggest that a similar topology is also adapted by the Arabidopsis and human stomatin-like proteins.

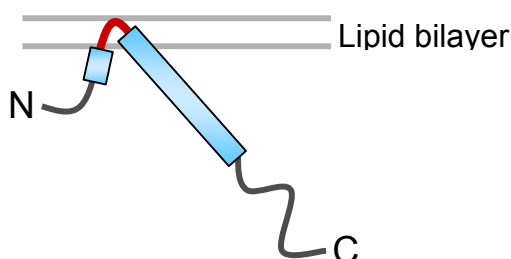


Figure 3-6. A schematic presentation of the membrane insertion model of human stomatin. Most likely this model also applies to AtSlp1. Colour coding is identical to Figure 3-7. Shown in blue is the band 7 domain with the hydrophobic region in red penetrating the lipid bilayer. Both termini are located on the same side of the membrane.

A) AtSlp-1

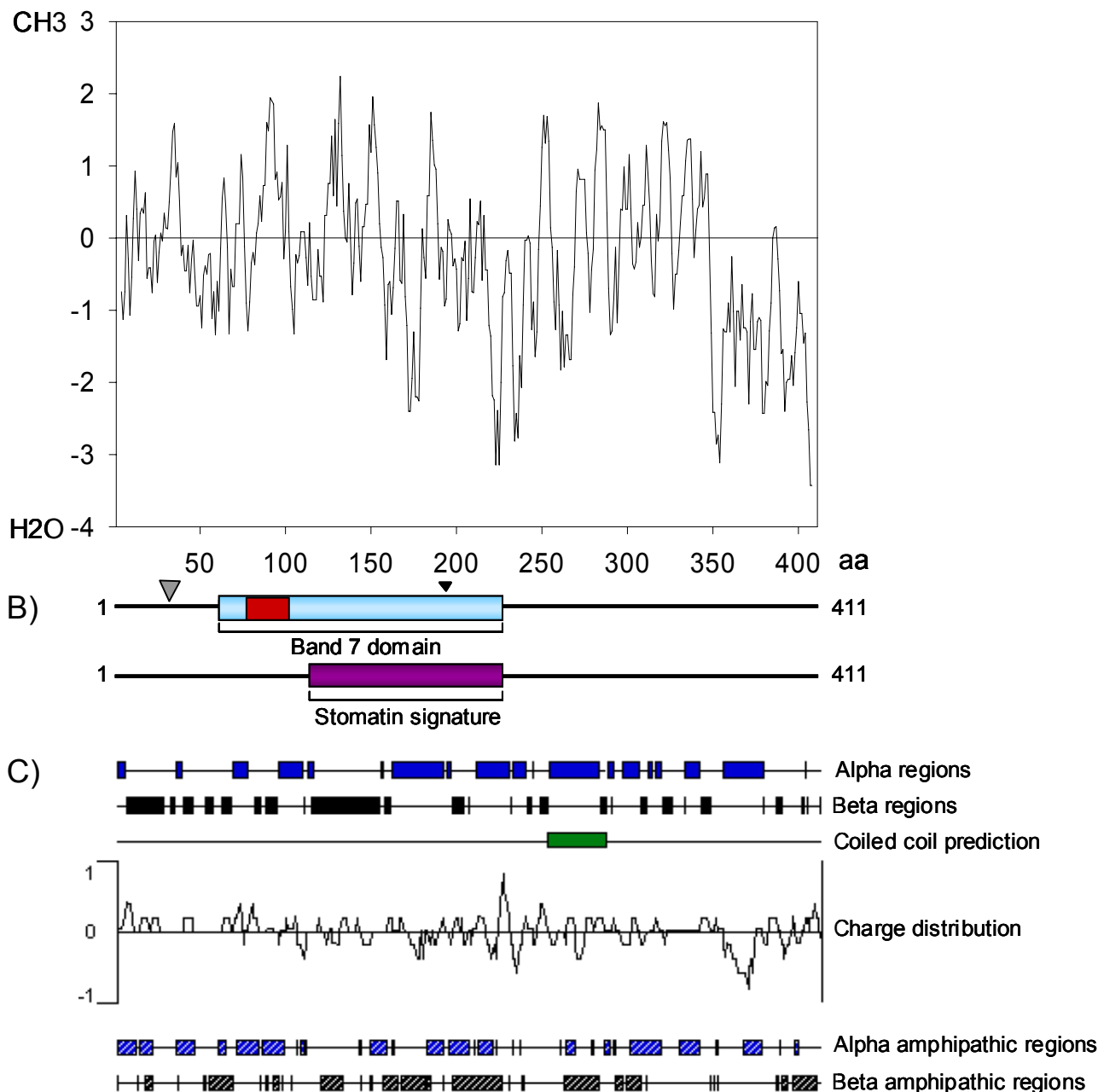


Figure 3-7. Structural features of the AtSlp1 protein.

A) Hydrophobicity profile after Kyte-Doolittle. Positive values correspond to hydrophobic residues (CH₃), negative ones to hydrophilic amino acids (H₂O). The plot was constructed with a window size of 7 amino acids. Numbers at the bottom scale correspond to amino acids (aa).

B) A schematic presentation of AtSlp1 and the position of the band 7 (light blue) and stomatin domains (violet). Indicated in red is the hydrophobic domain that is predicted to mediate membrane spanning (after the TMAP algorithm). Indicated as a black arrowhead is the conserved cysteine residue. The grey arrowhead indicates the cleavage site of the mitochondrial targeting sequence according to TargetP (see Chapter 4).

C) Secondary structural features obtained from Protean. Alpha (blue) and beta (black) regions correspond to predicted stretches of alpha-helices and beta-sheets according to the Garnier-Robson algorithm. Regions with a prediction for coiled coil conformations are shown in green. A charge distribution plot indicates areas of positive and negative charges as indicated on the left. Alpha (blue diagonal stripes) and beta (black diagonal stripes) amphipathic regions indicate the likelihood of the formation of amphipathic helices according to the Eisenberg method.

The whole figure is drawn to scale.

3.2.2 *AtSlp2- structural features*

A structural presentation of AtSlp2 is shown in Figure 3-8. This protein is 401 amino acids long and has a different hydrophathy profile from AtSlp1. Part A) shows the Kyte-Doolittle hydrophobicity plot of this protein. Similar to AtSlp1, it has a stretch of hydrophilic residues towards its C-terminus (position 260-290), but the overall profile changes towards the hydrophobic area of the plot at the end of the sequence. Compared to AtSlp1 it has an even more hydrophobic N-terminus that includes two predicted membrane-spanning domains (shown as red boxes underneath the plot in part B) according to the TMAP prediction. The profile as a whole only resembles that of AtSlp1 in the area of the band-7 domain that is indicated in B) as a blue box.

Part (B) presents the position of the band-7 and the stomatin domains in the AtSlp2 sequence. The first membrane-spanning domain is 29 amino acids long and located at position 12-40 in the protein. The second TMAP predicted hydrophobic domain is 26 amino acids long (position 121-146) and corresponds to the one seen in AtSlp1 with the same relative position inside the band-7 domain. The conserved cysteine residue (position 240) is also located in the same relative position towards the end of the band-7 domain as in AtSlp1. The second cysteine that is unique to AtSlp2 (position 115) is located at the beginning of the band-7 domain, close to the hydrophobic domain. Overall the position of the band-7 domain (105-279) is shifted towards the C-terminus by 43 amino acids compared to the location in its paralog. The stomatin signature domain is shifted accordingly and ends at the same position as the band-7 domain.

In Part (C) of this figure the same secondary structural profile is given as in Figure 3-7. The overall distribution of alpha helices and beta sheets in AtSlp2 looks similar to AtSlp1, with most helices located towards the C-terminal end. Looking in more detail, the two profiles are in fact different. The alpha helix stretches are much longer in AtSlp2, and there are more frequent but shorter stretches of beta sheets predicted near the N-terminal end. The coiled coil prediction is also shifted towards the C-terminus with a slightly higher prediction probability. The charge distribution plot shows several positively charged areas towards the C-terminus and in a part of the protein that has the highest predictions for hydrophilicity; this corresponds again to an area in AtSlp1, but is shifted further towards the C-terminus. The characteristic highly negatively charged stretch of amino acids at the AtSlp1 C-terminus is missing in AtSlp2. The distribution of alpha and beta amphipathic regions is also slightly different between these two proteins. The AtSlp2 profile also shows alpha amphipathic stretches close to the N-terminus, but these are slightly longer than in its

paralog. Potentially these stretches will also form structures important for correct subcellular localisation of this protein (see chapter 4).

Also on a structural level there are clear differences between the two Arabidopsis stomatin-like proteins. Despite the high sequence similarity in the centre of the proteins, their unique termini result in different structural properties that will have impact on their subcellular environments and functions.

3.2.3 HsSlp2- structural features

The human Slp2 protein is shorter than the Arabidopsis orthologs with only 356 amino acids. The hydrophobicity profile of the human protein looks overall very similar to that of AtSlp1 (Figure 3-9 A). The area of the band-7 domain has the same characteristic shape as in the Arabidopsis proteins and is followed by an almost identical hydrophilic region at the very C-terminal end when compared to AtSlp1. The position of the band-7 domain is shifted towards the N-terminus compared to the Arabidopsis proteins (Figure 3-9B). No region of human Slp2 is hydrophobic enough to be predicted as being membrane spanning when the TMAP algorithm is applied. The conserved cysteine residue is located at the same relative position than in the Arabidopsis proteins (Figure 3-9 B). The general distribution of alpha helices and beta sheets resembles that of AtSlps in the sense that helices are more abundant towards the C-terminus and sheets at the N-terminal end (Figure 3-9 C). However, the C-terminal end does contain a stretch with more beta sheets followed by helices at the very end. This protein has two predicted coiled coil regions. The first one is similar in length to the ones seen in the Arabidopsis proteins, and the second one is longer, but in the same relative position compared to AtSlp1. The charge distribution plot also resembles that of AtSlp1. There is an area of highly positively charged residues towards the end of the band-7 domain and a stretch of negative charges at the C-terminus. The N-terminus also contains a series of positive charges that are putatively involved in subcellular targeting. This area corresponds to predicted alpha amphipathic helices shown in the plot beneath, strongly suggesting the presence of a mitochondrial signal sequence. It appears that the human Slp2 protein has an overall highly similar profile to AtSlp1, with the only difference lying in the truncated N-terminus.

The overall structure of these three proteins resembles that of most other investigated band-7 proteins. Most of these have a hydrophobic domain close to their N-terminus and a comparably rather hydrophilic C-terminus (Browman *et al.*, 2007).

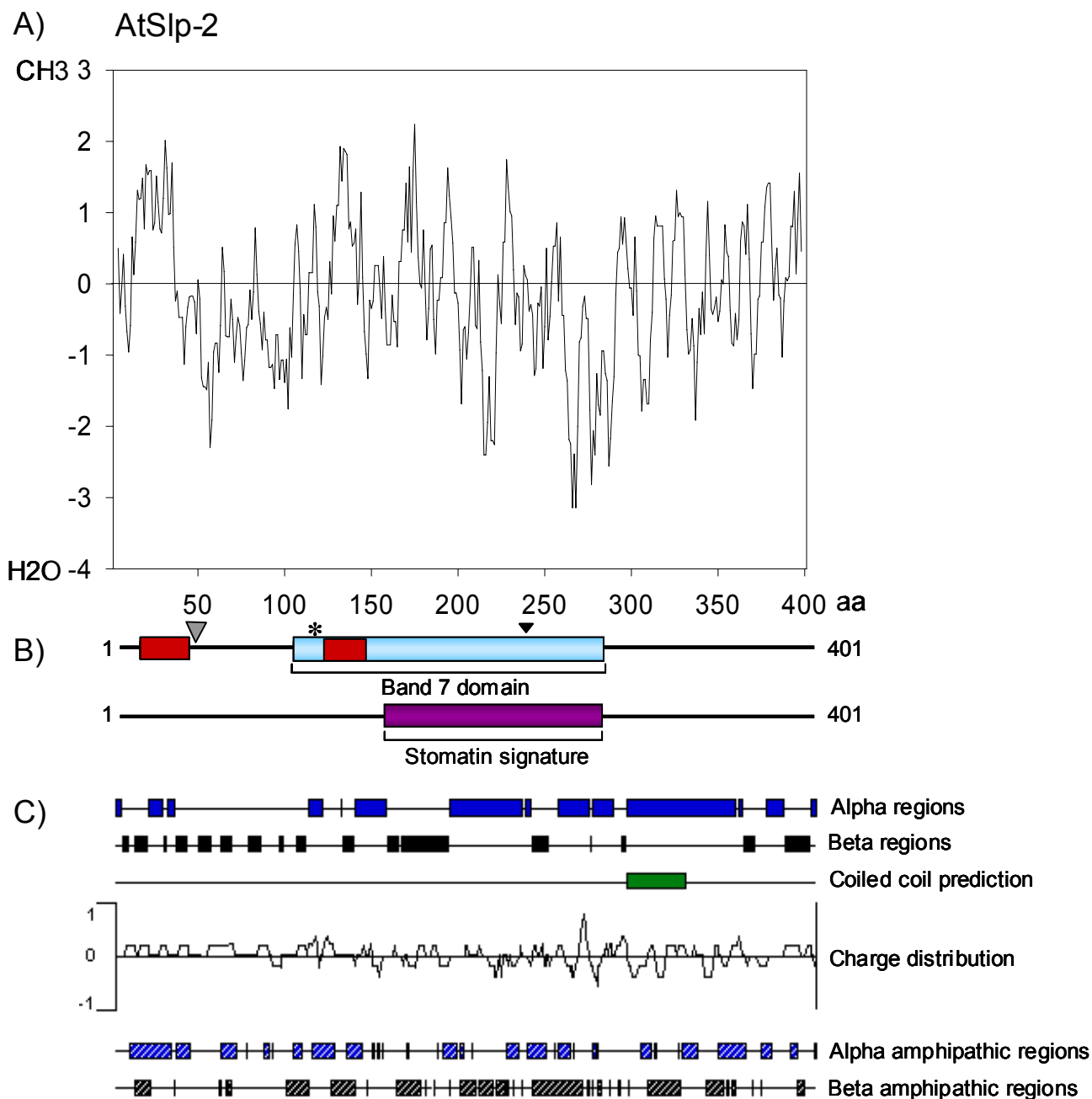


Figure 3-8. Structural features of the AtSlp2 protein.

A) Hydrophobicity profile after Kyte-Doolittle (window size 7). Labelling is identical to Figure 3-7. CH3 indicates hydrophobicity, H₂O stands for hydrophilicity.

B) A schematic presentation of AtSlp2 and the position of the band 7 (light blue) and stomatin domains (violet). Indicated in red are the two hydrophobic domains predicted to be membrane spanning (after the TMAP algorithm). Indicated as a black arrowhead is the conserved cysteine residue and with an asterisk the unique cysteine. The grey arrowhead indicates the cleavage site of the mitochondrial target sequence according to TargetP (see Chapter 4).

C) Secondary structural features obtained from Protean. Predicted stretches of alpha-helices (blue) and beta-sheets (black) according to the Garnier-Robson algorithm. A coiled coil prediction is shown in green. The charge distribution plot beneath indicates charge distribution as explained before. Alpha (blue diagonal stripes) and beta (black diagonal stripes) amphipathic regions are drawn underneath according to Eisenberg.

The whole figure is drawn to scale.

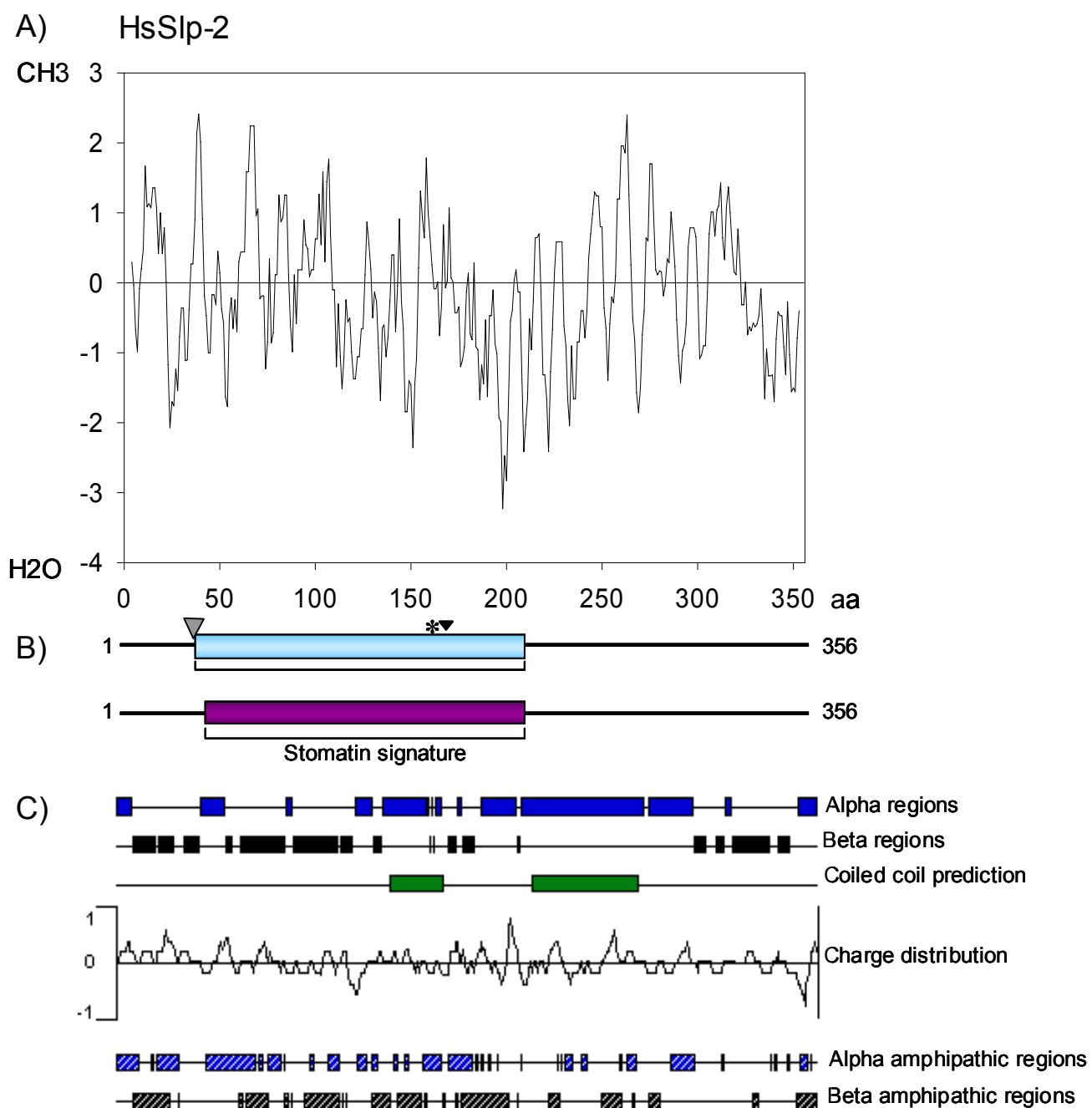


Figure 3-9. Structural features of the human Slp2 protein.

A) Kyte-Doolittle hydrophobicity profile with window size 7. Labelling is as before.

B) Schematic presentation of HsSlp2 with the band- 7 (light blue) and stomatin domains (violet). No membrane-spanning domains are predicted using TMAP. Indicated as a black arrowhead is the conserved cysteine residue and with an asterisk the unique cysteine. The grey arrowhead indicates the mitochondrial target sequence cleavage site according to MitoProt II (see Chapter 4).

C) Secondary structural features obtained from Protean. Alpha (blue) and beta (black) regions according to Garnier-Robson. Two regions with a prediction for coiled coil conformations are shown in green. Charge distribution is indicated in the plot below. Alpha (blue diagonal stripes) and beta (black diagonal stripes) amphipathic regions according to the Eisenberg method.

The whole figure is drawn to the amino acid scale given in A).

3.3 Cloning of AtSlp open reading frames

The open reading frame of AtSlp1 (At4g27585) was originally amplified by Petr Obrdlik for the preparation of the split ubiquitin screen conducted by Dr. Rejane Pratelli. A clone made by Rejane Pratelli designed for protein expression in *Pichia pastoris* was used as a template for further cloning in this project. However, a point mutation had to be removed by site-directed mutagenesis to yield the correct frame as published by TAIR. This procedure was carried out during this project but will not be described here any further. Finally, a correct full-length open reading frame was obtained by myself and further subcloned into the pDRIVE cloning vector (Qiagen) by Annegret Honsbein (University of Glasgow). This was the final template used in all following cloning procedures for constructs of AtSlp1.

The open reading frame of At5g4100 (AtSlp2) had to be newly cloned from cDNA. This was done in a series of steps as outlined below and yielded a clone in the pUC18 cloning vector using the PstI and EcoRI sites of the multiple cloning site. In the first step, cDNA was synthesised from 1 µg of total RNA according to the manufacturer's protocol. The RNA was previously extracted by Dr. Patrick Armengaud from 14 days old Arabidopsis seedlings (ecotype Col-0) that were potassium starved for 3 days. The obtained cDNA was used as a template for PCR with primers spanning the complete open reading frame of AtSlp2. 30 cycles of PCR were necessary to amplify weakly visible bands of the correct size that were purified and used as a template for a second round of PCR. This time, primers were used with PstI and EcoRI restriction sites as overhangs that amplified the complete reading frame. The resulting products were restriction digested and cloned into the pUC 18 vector as described above. Several clones were obtained and the insertion verified by sequencing. All of the isolated clones had a point mutation at the same position, which resulted in an exchange of alanine to valine at amino acid 380. This mutation was removed in another cloning step using the megaprimer method (Kammann *et al.*, 1989; Ling & Robinson, 1997b) and yielded one final clone with the complete open reading frame of At5g54100 inside pUC18. This clone was subsequently used in all of the following cloning procedures involving AtSlp2 as a template for PCR. As mentioned, a rather high number of cycles were necessary to amplify the open reading frame of this gene; even after 30 cycles of PCR the amplified product was barely visible. This already indicates that AtSlp2 is not expressed at high levels in Arabidopsis seedlings.

3.4 Production of specific antibodies against AtSlp1 and AtSlp2

Specific antibodies present a powerful tool for the study of protein localisation, molecular aspects, and for the verification of mutants. For this reason, areas with good epitope properties were chosen within the AtSlp sequences to raise polyclonal antiserum in rabbits. Two strategies were designed: in the first one, longer stretches of amino acids were chosen for inducible overexpression in bacteria as 6x His- or GST-fusion proteins. In the second strategy, short peptide epitopes were selected. These were synthesised artificially and injected into rabbits as carrier protein conjugates by a company (Agrisera, Sweden). This section begins with the description of the epitope design for both strategies. The epitope design is followed by a description of the bacteria overexpression, protein purification and the testing of the received antiserum. In the second part of this section (3.4.5), the results from the commercial antibody production are presented and discussed.

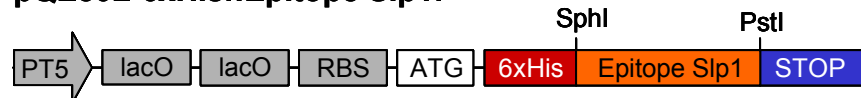
3.4.1 Design of AtSlp1 and AtSlp2 epitope expression constructs in bacteria

As seen in the multiple sequence alignment in Figure 3-4, both Arabidopsis Slps share a high degree of sequence identity in their central parts. There are several requirements for successful overexpression of a plant protein epitope in bacteria: the epitope must be unique and large enough to be stably expressed and purified; it is preferable that the epitope is soluble to avoid formation of inclusion bodies; finally it should be surface exposed in the endogenous protein and have good antigenic properties when injected into a host animal. Both protein sequences were scanned for unique areas that bear all these features and lie outside the conserved band-7 domain. For AtSlp1, the last 71 amino acids (341-411) were chosen and for Slp2 an N-terminal stretch of 91 amino acids (position 2-92). Both areas are indicated in Figure 3-4, 3-10 and 3-11 by orange and yellow bars, respectively. Figure 3-11 also shows plots (obtained with the Protean software) indicating the probability of surface exposure (after (Emini *et al.*, 1985)) and antigenicity (after (Jameson & Wolf, 1988)) for both proteins. The surface probability plot of AtSlp1 shows that the highly hydrophilic C-terminal end is also predicted to be surface exposed. The antigenic index also indicates high probability scores in this region to cause immunogenic reactions in animals. It gives a measure of how potentially antigenic a particular area is likely to be based on structural properties according to (Jameson & Wolf, 1988). For AtSlp2, the N-terminal part was mainly chosen to keep the epitope as unique as possible. The surface probability plot gives

an indication that at least part of this area is surface exposed. The antigenic index also predicts this part of the epitope to have good immunogenic properties. The two areas were amplified by PCR and fused in frame to an N-terminal tag consisting of 6 histidine residues in the pQE80L vector (Qiagen). These fusion constructs allow for easy one step affinity purification on Ni-NTA agarose (Qiagen) to obtain a purified epitope ready for injection into rabbits.

Figure 3-10 gives an overview over the two pQE80L constructs cloned, together with the resulting fusion protein sequences. The AtSlp1 epitope was cloned in frame by using the SphI and PstI sites in the multiple cloning site of the vector. The resulting 6x His tagged epitope is 91 amino acids long and has a predicted molecular weight of 10 kDa. The AtSlp2 epitope was cloned using the BamHI and HindIII restriction sites and results in a protein that is 106 amino acids long and is approximately 11.3 kDa in size.

pQE80L-6xHis::Epitope Slp1:



Fusion protein Slp1:

MRGSHHHHHHGSACYKSLVINGPSKDHQETQALDETDLEELEDMGKEH
ISEGSNNRSGSISFDTEKPGHTGEPFSLQNRNKDPQAAAKLN.

pQE80L-6xHis::Epitope Slp2:



Fusion protein Slp2:

MRGSHHHHHHGSNQLALSRSGYTA AVRFLPMLSA AVPKILSSLAAASTVR
NFSSTGSPLTSYQINKPSPSKSFTS RLLHQSSAGT P PQQFLGARSFSSPS
SDKLN.

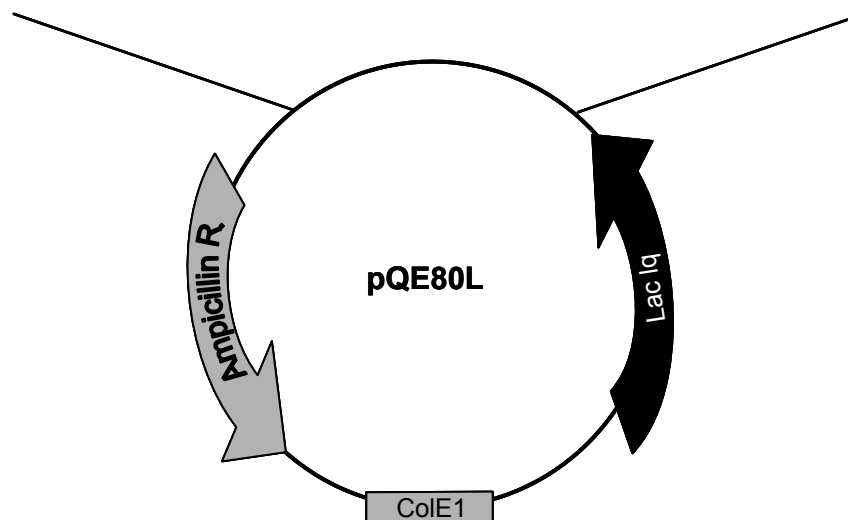
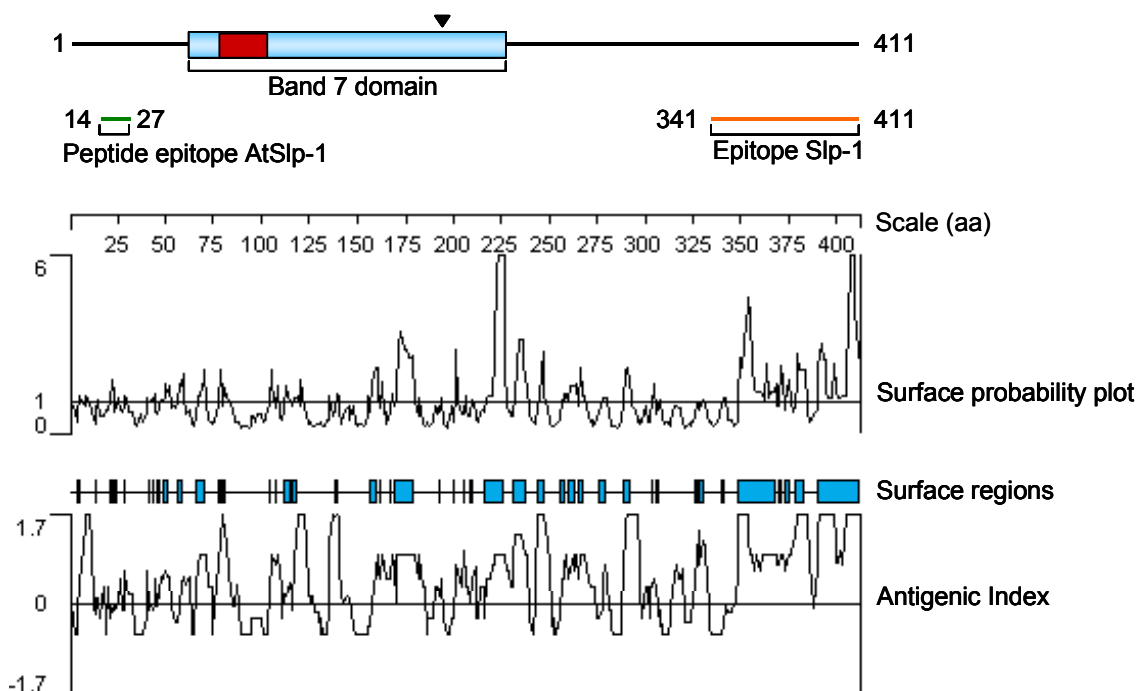


Figure 3-10. Overview of pQE80L constructs. The His tag is highlighted in red and the epitopes in orange and yellow respectively. Shown on top is the expression cassette under the IPTG inducible operon system and below a schematic presentation of the vector. The vector also contains an ampicillin resistance gene, a ColE1 origin of replication and the lacIq repressor gene for additional control of protein expression. Abbreviations are: PT5 (T5 promoter), lacO (lac operator), RBS (ribosome binding site), ATG (start codon).

A) AtSlp-1



B) AtSlp-2

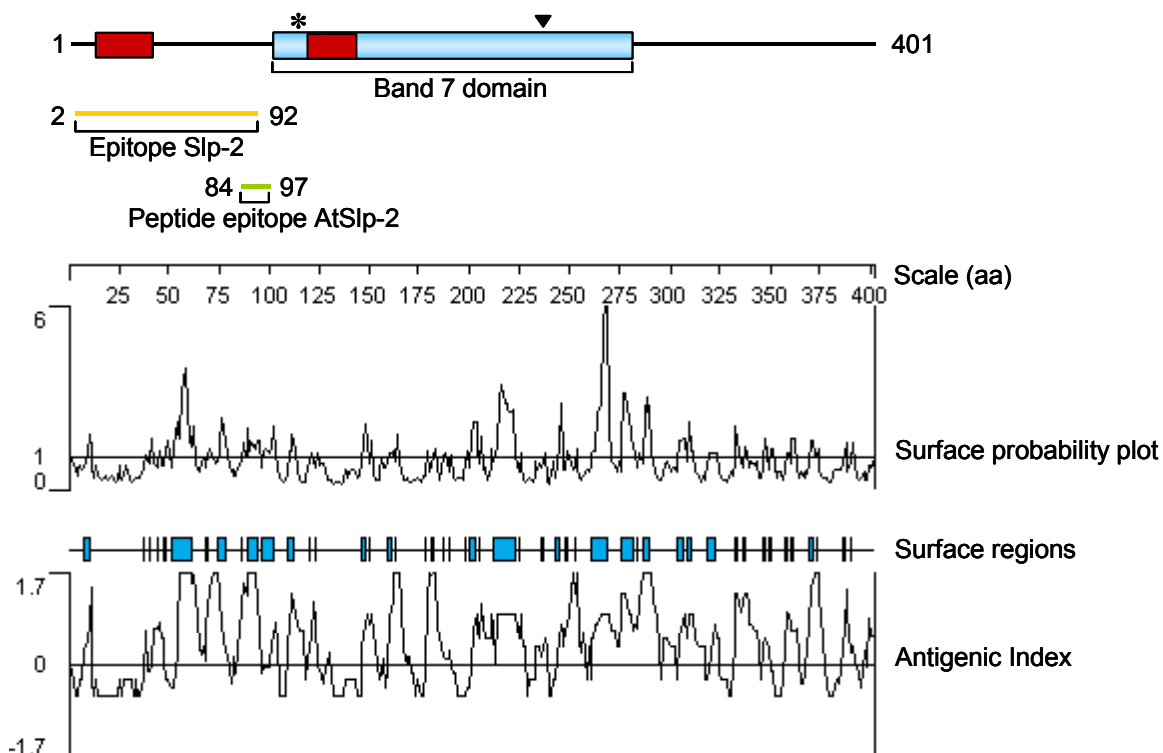


Figure 3-11. Schematic presentations of AtSlp1 and AtSlp2 and the areas chosen as unique epitopes.

A) The band-7 domain is indicated in blue and the hydrophobic domain in red as before. The black arrowhead indicates the conserved cysteine residue. The area chosen as an epitope for bacterial overexpression is indicated by an orange bar and the peptide epitope in dark green. Numbers indicate amino acid positions. Shown below is a surface probability plot indicating surface exposed regions as displayed below by blue bars. The antigenic index gives an indication for the likelihood of areas causing an immunogenic response in animals.

B) The same parameters as described above are drawn for AtSlp2. The area chosen as an epitope for bacterial overexpression is indicated by a yellow bar, and the peptide epitope by a light green one. Labelling is as described in A).

3.4.2 Overexpression and purification of His-tagged fusion proteins

The resulting plasmids were transformed into the *E.coli* strain M15 (Qiagen) that is particularly suitable for this type of protein expression. Figure 3-12 gives a detailed overview of the protein expression and purification strategy including the steps taken that follow these. Briefly, a bacterial pre-culture of small volume is set up and used to inoculate a larger volume. This is grown to a density of ca. 0.6 (measured at 600nm) and IPTG (isopropyl- β -D-thiogalactoside) added to a final concentration of 1 mM. The culture is grown for another four hours and bacteria are harvested. In the following steps these are lysed with the aid of lysozyme and sonication, and the soluble proteins are separated from the insoluble matter by centrifugation. The resulting lysate is then incubated with Ni-NTA agarose overnight at four degree Celsius. Unbound proteins are washed off and bound proteins eluted with an increasing amount of imidazole. The imidazole ring is part of the histidine structure and replaces bound His-tagged proteins from the agarose support into the surrounding solution. The eluates are pooled and dialysed against a low ionic strength buffer that does not interfere with rabbit immunisation. The dialysed proteins are then lyophilised and the final protein content analysed by the Bradford method. A suitable host animal is selected based on the ability of its preimmune serum not to bind to plant protein extracts. Finally the animal is immunised by a series of injections, the antiserum is collected and tested for its specificity using Western blotting.

Before any large-scale protein purification was attempted, several small-scale test experiments were carried out to assess the solubility and induction properties of the proteins.

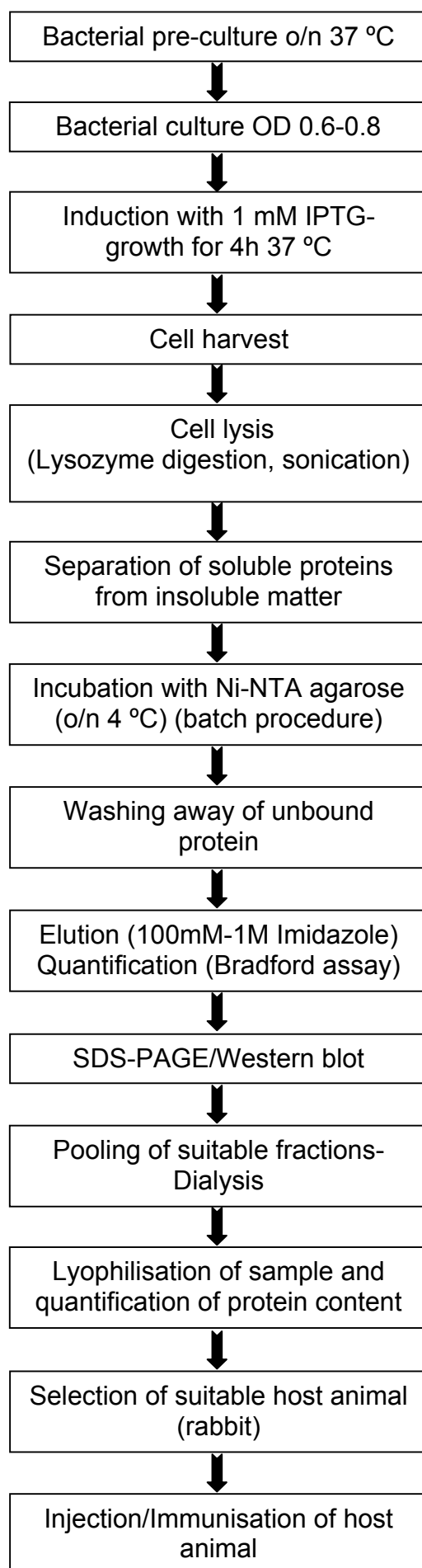


Figure 3-12. Outline of protein expression and purification steps with follow-up procedures.

3.4.2.1 Assessment of protein induction properties (denaturing)

To get an idea of whether the transformed M15 bacteria were actually capable of expressing the His-tagged fusion proteins, small volumes of bacteria (50 ml) were inoculated with starter cultures for both constructs and grown to a suitable density. IPTG was added and samples of 10 ml taken after 2, 3, 4 and 5 hours to assess the development of induction in a time course. The cells were lysed under denaturing conditions in the presence of 8 M urea, and purified on Ni-NTA spin columns (Qiagen-see Materials and Methods). These conditions were chosen as a quick measure for protein expression because they allow for detection of any His-tagged proteins independent of their solubility in bacteria. The spin columns contain a macroporous silica support with Ni-NTA that binds the tagged proteins. They allow for rapid purification of small protein amounts using a micro-centrifuge. As a control sample, a culture containing the empty pQE80L vector was treated in the same way. Following washing and elution steps using an acidic pH gradient, samples were run on a 12 % SDS-PAGE gel and Coomassie stained to detect eluted fusion protein. Fusion protein of the Slp1 epitope was detectable in this way already 2 hours after initial induction (not shown) and peaked at 4 hours post-induction. Unfortunately, no fusion protein of the Slp2 epitope was detectable in this time course. As an example for the denaturing purification, Figure 3-13 A) shows a Coomassie-stained gel showing 3 elution fractions (E1-E3) 4 hours after induction of the 6xHis::Slp1 and 6xHis::Slp2 cultures. Only the Slp1 epitope can be clearly seen as a single band migrating at around 15 kDa. The control and the Slp2 samples are empty.

To assess whether the Slp epitopes were soluble in bacteria, 50 ml cultures (control, Slp1 and Slp2 epitopes) were inoculated and induced for four hours at 37 °C. The cells were harvested and lysed under native conditions (no urea present) in the presence of a low amount of imidazole (10 mM) in the lysis buffer. Cell lysis was achieved by the addition of 1mg/ml lysozyme and incubation for 30 min on ice; this was followed by sonication with breaks in between to avoid denaturation. Following cell lysis, the soluble proteins were separated by centrifugation from the insoluble matter. The supernatant containing soluble proteins was taken off and SDS loading buffer added directly. The pellet was resuspended in the same amount of lysis buffer and SDS loading buffer added to the same volume. The samples were loaded on a 12 % SDS-PAGE gel and Western-blotted. Bands were detected using monoclonal Histidine antibody. The Western blot in Figure 3-13 B) shows two prominent bands in the soluble fractions of Slp1 epitope lysate, but no bands in the control or in the Slp2 epitope lysates. The majority of the Slp1 epitope is clearly present in the

soluble fraction. Upon prolonged exposure of the blots, faint bands could also be detected in the insoluble matter, but to a much lesser extent. Thus, the Slp1 epitope had good solubility properties and was suitable for large scale batch purification on Ni-NTA agarose under native conditions.

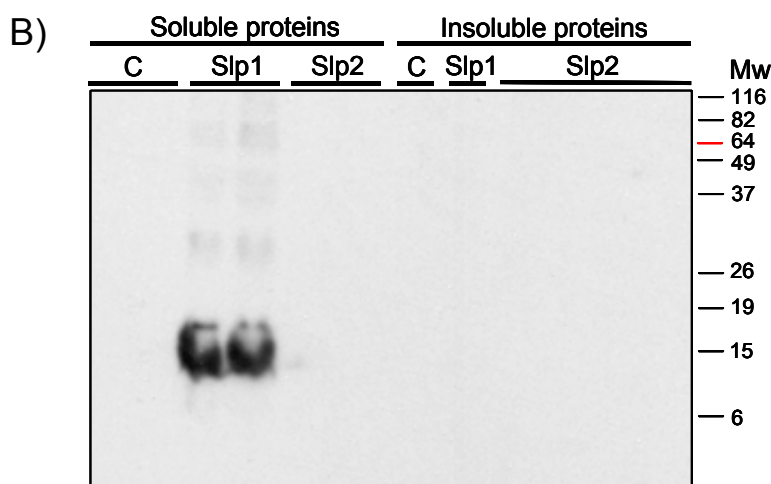
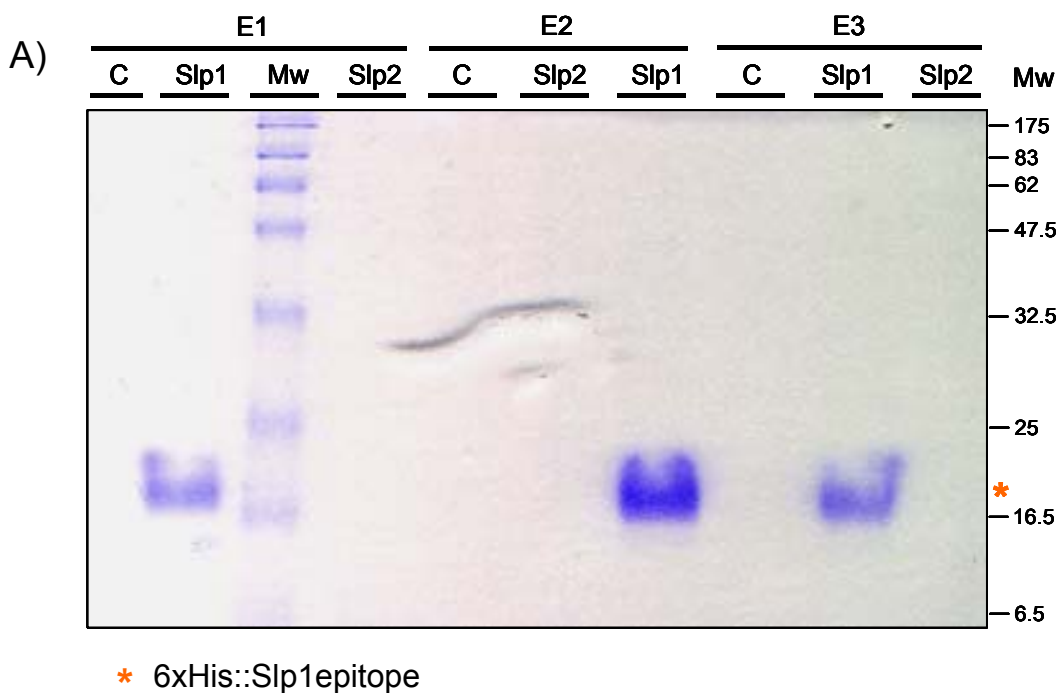


Figure 3-13. Detection of His-tagged epitope proteins.

A) Coomassie stained SDS-PAGE gel with elution fractions (E1-E3) of Slp1 and Slp2 epitopes following denaturing protein purification on spin columns 4 hours after induction at 37 °C . The control sample (C) represents the empty induced pQE80L vector. The Slp1 epitope is visible (marked with an orange asterisk) in all three elution fractions. The Slp2 epitope is not expressed. Mw indicates molecular weight markers (NEB) and the numbers correspond to kDa units.

B) Western blot to assess protein solubility of Slp1 and Slp2 epitopes 4 hours post-induction at 37 °C. The samples were probed with anti-His antibody from mouse at 1:5000. Slp1 protein is almost exclusively in the soluble fraction. The control does not express any His-tagged protein as expected. Mw indicates the protein marker used (Invitrogen) with numbers corresponding to kDa.

3.4.2.2 Purification of epitope proteins under native conditions in a small scale batch format

In the next step of assessing purification properties, larger volumes of bacteria (100ml) were inoculated and induced for 4 hours, followed by purification under native conditions. For the Slp1 epitope, the growth temperature was kept at 37°C, and for the Slp2 epitope it was set down to 30 °C, in the hope this reduction might lead to improved protein stability. The cells were harvested by centrifugation and lysed in the presence of 10 mM imidazole using lysozyme (1mg/ml) and sonication as described. The soluble supernatant was separated and incubated with a small volume of Ni-NTA agarose (Qiagen) overnight at 4 °C. The flow-through fractions (unbound proteins) were collected by centrifugation and the bound proteins washed in the presence of 20 mM imidazole altogether 5 times. Elution was achieved by addition of buffer containing 250 mM imidazole at physiological pH 8 altogether 6 times. The protein content of the samples collected throughout the purification procedure was quantified using the Bradford method (BioRad protein assay). It revealed that approximately 800 µg of purified Slp1 epitope could be extracted from a culture of 100 ml volume. SDS loading buffer was added to the various fractions and loaded on a 12 % SDS PAGE gel that was stained with Coomassie Blue to detect proteins. Figure 3-14 shows a Coomassie Blue stained gel with wash (W) and elution (E) fractions of the Slp1 epitope. This protein is clearly visible in the first two elution fractions around 15 kDa and to a lesser extent in the third elution fraction. The control samples by comparison do not show this band. The wash fractions 1-4 do not contain the band either, but multiple contaminants of higher molecular weight. The elution fractions are not completely pure, as contaminating bands of higher molecular weight are visible in the lanes of the control and Slp1. The Slp2 epitope was again not detectable (gel not shown). Changing the growth temperature of the bacteria did not result in an increased stability as it was anticipated.

For the Slp2 epitope, no further experiments using the Ni-NTA system were performed. Most likely, the fusion protein was not stable in *E.coli* because it might have had toxic effects for the bacteria, or it was readily degraded upon translation. The chosen epitope site for Slp2 lies partly inside a putative signal sequence and might have lead to toxic side effects. As an alternative to the His fusion system, the same epitope was cloned into the pGEX4T-1 vector (Novagen) that results in an N-terminal GST (glutathione-S-transferase) fusion protein (see section 3.4.4). The rationale behind this type of fusion is that the larger GST tag might lead to increased stability in bacteria upon induction and can be purified on glutathione sepharose.

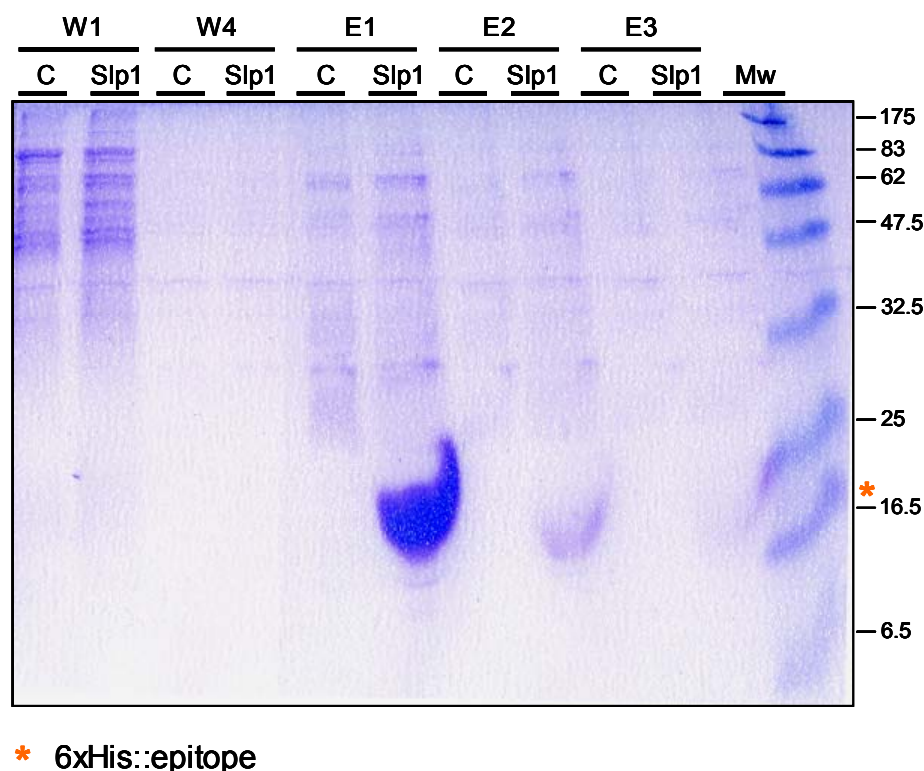


Figure 3-14. Coomassie stained SDS PAGE gel of wash (W) and elution (E) fractions from Ni-NTA purification of Slp1 epitope. W1 and W4 stand for wash fractions 1 and 4 respectively. E1-E3 indicate elution fractions 1 to 3. Mw indicates molecular weight marker with numbers corresponding to kDa. The orange asterisk indicates the position of the 6xHis::Slp1 epitope.

3.4.2.3 Large scale purification of 6xHis-tagged Slp1 epitope

To cause an immune reaction in a host animal like a rabbit, the epitope must be of high purity and present in a quantity of at least 2 mg per injection. It was estimated that under the tested conditions, a bacteria culture of 1-2 litres in volume would provide sufficient amounts of purified epitope for the immunisation procedure. In a first attempt, a culture volume of 1 litre was induced for 4 hours at 37 °C. To increase purity of the epitope, two separate wash buffers were prepared containing 20 mM and 100 mM imidazole respectively. The cells were lysed in the presence of 10mM imidazole and washed 4 times with 20mM imidazole wash buffer and one time (W5) with 100mM imidazole. Altogether 5 elution fractions were collected, the first four with a buffer containing 250mM imidazole and the last one with a high stringency buffer with an imidazole content of 1M. All fractions were quantified using the Bradford protein assay and loaded on a SDS-PAGE gel followed by Coomassie staining. From this purification, a total amount of 3 mg protein in the combined elution fractions was purified. Figure 3-15 shows the stained gel with the

flow-through, wash and elution fractions. It can be seen that the first 2 washes (W1 and W2) eluted little epitope protein, but the last wash (W5) in the presence of 100 mM imidazole caused a significant release of the protein. The following elution fractions 1-4 °C contained the majority of protein, but also high levels of contaminating proteins of higher molecular weight (ca. 26 kDa) that were not present as much in the W5 fraction. From this gel it seems that increasing amounts of imidazole also release more contaminants. These contaminating proteins seem to bind with even higher affinity to the Ni-NTA than the actual epitope. Because of this high contamination level, it was decided to re-purify these elution fractions and to modify the washing and elution steps. In order to bind again to Ni-NTA agarose, the eluted fractions had to be dialysed against lysis buffer to overcome the high imidazole content of the elution buffer. However, while dialysing in a tubing with a molecular weight cutoff of 8 kDa against an excess volume of lysis buffer, most of the sample was lost due to a hole and only a small amount could be rescued. Thus, a new bacteria culture of 1 litre was set up and a new purification protocol established.

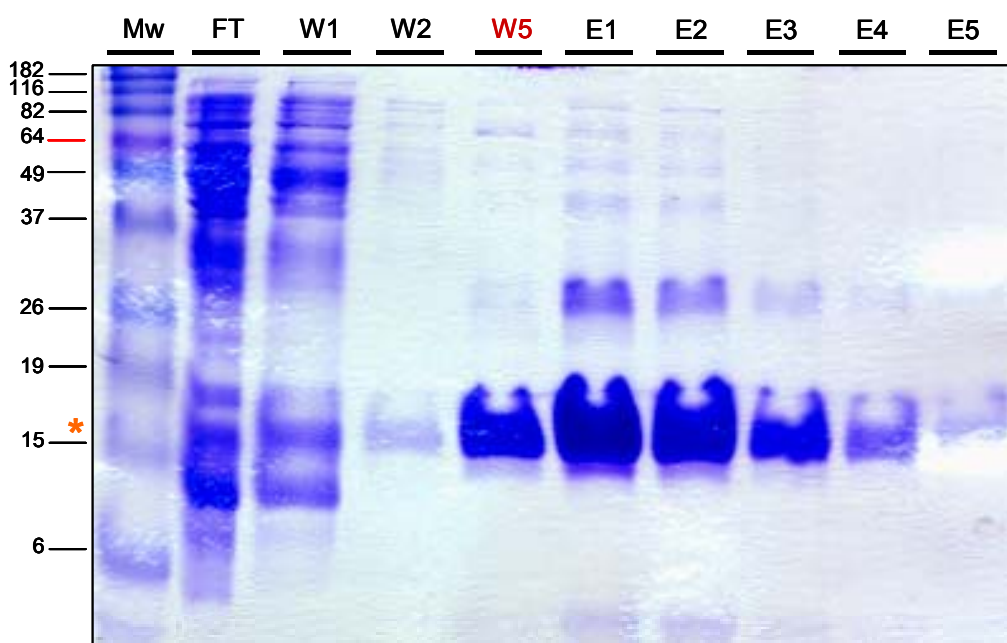
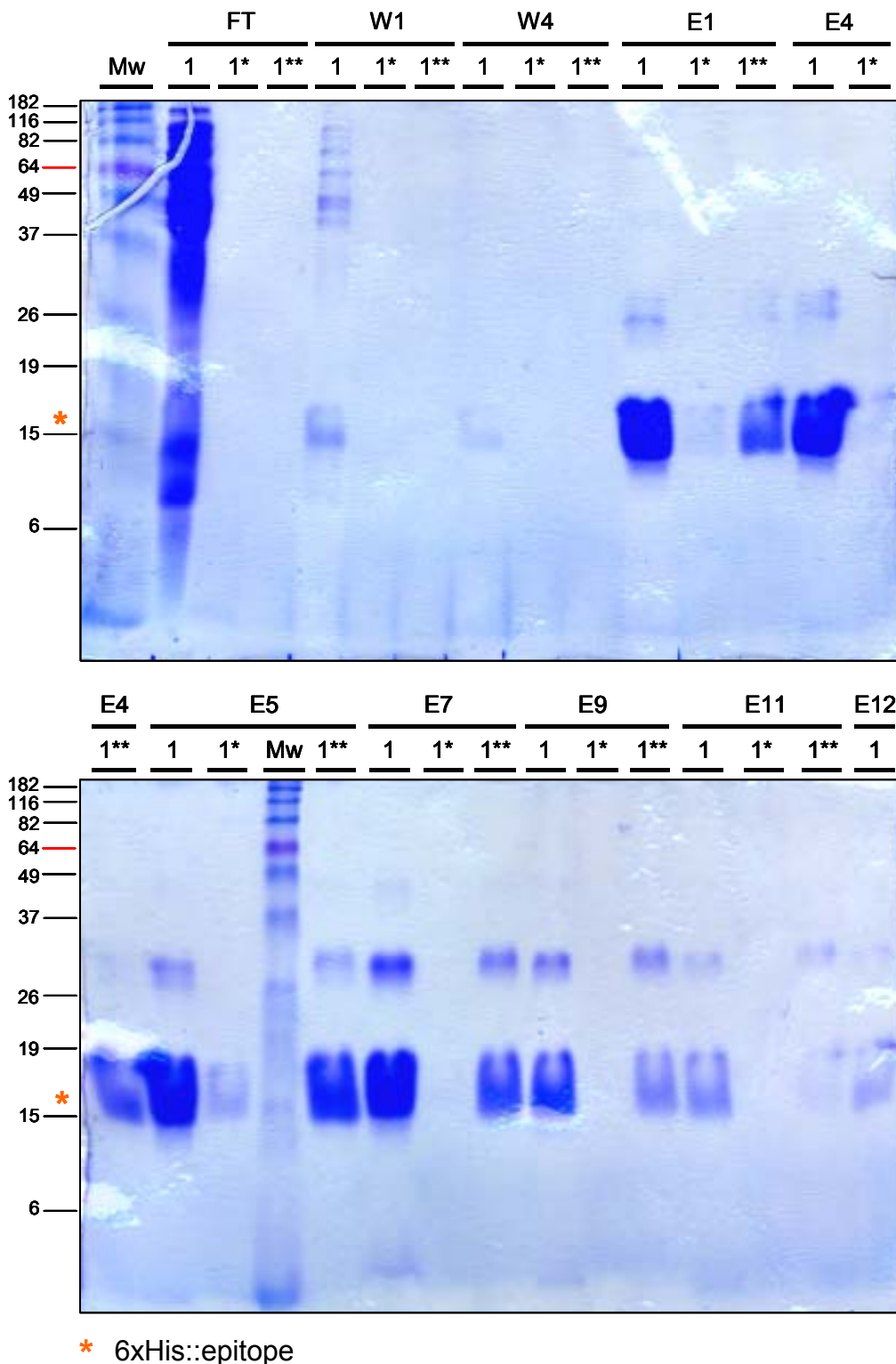


Figure 3-15. Coomassie-stained SDS-PAGE gel of the first large scale purification. The pellet of 1 litre of bacteria culture was lysed and bound to Ni-NTA agarose. Wash 1 and 2 (W1 and W2) were done in the presence of 20 mM imidazole and wash 5 (W5 marked in red) with 100mM imidazole. Elutions 1-4 (E1-E4) were done with 250 mM imidazole present and E5 with a high stringency buffer containing 1M imidazole. FT indicates the flow-through fraction (unbound proteins) and Mw stands for molecular weight markers. Numbers represent kDa molecular weight. The orange asterisk marks the position of the eluted Slp1 epitope.

Major changes were introduced to the washing and elution steps. To reduce contamination, 1% Triton-X100 and 20 mM β -mercaptoethanol were included in the lysis, wash and elution buffers. Additionally, the imidazole content of the wash buffer was raised to 30 mM and elution was done with an imidazole gradient ranging from 100 mM up to 250 mM in steps of 50 mM. A final elution with the high stringency buffer (1 M imidazole) was included to achieve complete removal of any His-tagged proteins. Figure 3-16 shows two Coomassie stained SDS-PAGE gels with representative samples from the final large scale purification. Samples from the purification included new samples from a fresh 1 litre culture (marked as “1” in Figure 3-16), the rescued combined eluates from the dialysis tubing (designated “1**” in Figure 3-16) and some leftover eluates from the previous purification that were not used in the dialysis (marked “1*”). All samples were purified in the same way: following cell lysis as described, the lysates were incubated with Ni-NTA agarose overnight at 4 °C. Unbound proteins were washed off with buffer containing 30 mM imidazole. Elutions were performed as follows: Eluates 1-4 (E1-E4) in the presence of 100mM imidazole, eluates 5-6 (E5-E6) with 150mM imidazole, eluates 7-8 (E7-E8) with 200mM imidazole and eluates 9-10 (E9-10) with 250mM imidazole. The final two elutions (E11-E12) were done with high stringency buffer in 1 M imidazole. The Coomassie stained gel shows the same result as seen in Figure 3-15. Imidazole concentrations of 150mM or higher release more contaminating proteins but not more His-tagged protein than concentrations of 100 mM. The wash fractions with 30 mM also released some His-tagged protein (seen in lanes marked with “1”), but not to a significant extent. Eluates 1-4 on the other hand gave the purest results with good amounts of protein released. Thus, all elution fractions 1-4 (from all three samples 1, 1* and 1**) were pooled and combined with leftover fractions of W5 from the previous purification. The pooled fractions had a total protein content of 15.5 mg and were dialysed against excess amount of low stringency buffer (20 mM sodium hydrogen carbonate and 0.02 % SDS). Following dialysis, the sample was lyophilised and its final protein content determined using the Bradford protein assay.



* 6xHis::epitope

Figure 3-16. Coomassie stained SDS-PAGE gels of the final purification. Flow-through (FT), wash (W1-W4) and elution (E1-E12) fractions of all three purified samples (1, 1* and 1) were loaded. Elutions 1-4 were done in the presence of 100mM imidazole and have the least amount of contaminating proteins. Elutions 5-12 were performed with 150 mM imidazole or higher concentrations and have more contaminants. The prominent contaminating band of about 30 kDa could be a dimeric form of the epitope that binds with higher affinity to the Ni-NTA resin. Numbers on the left indicate molecular weight markers in kDa and the orange asterisk marks the position of the His-tagged epitope. Labelling of the three purified samples is as follows: 1- newly purified culture; 1*- leftover previously impure elution sample from the first large scale purification; 1**- rescued sample from the first dialysis attempt.**

3.4.3 Assessment of anti-Slp1 specificity on Western blots

A total amount of 10 mg purified epitope was sent away for injection into rabbits at the Scottish National Blood Transfusion Service (SNBTS). The injections were repeated 3 times over a period of 4 months and samples taken and tested for their binding specificity on Western blots. SDS-PAGE gels were loaded with protein extracts from wild type seedlings (Col-0), Sf9 insect cell lysate overexpressing Slp1::myc, and the purified His-tagged epitope. Figure 3-17 (A) shows a Western blot probed with the first bleed of the Slp1 polyclonal antiserum. In the wild type extract, 2 bands are recognised: the lower one corresponds to the endogenous molecular weight of the Slp1 protein (around 45 kDa) and the upper one (around 60 kDa) is probably a crossreacting contaminant. The antibody also recognises a pattern of higher weight bands in the Sf9 lysate that is overexpressing a tagged version of Slp1. The His-tagged epitope used for immunisation is clearly recognised by the antibody, as well as a band of approximately double the epitope weight, which might be a dimer. As a control, the same blot was probed with anti-myc that recognises the same band pattern as anti Slp1 in the Sf9 lysate, and anti-His that recognises the epitope only. Thus, the polyclonal anti-Slp1 serum binds to a protein from Arabidopsis of the right molecular weight, but is crossreacting with at least one other species.

Figure 3-17 B) shows a Western blot with crude protein extracts from two *slp1* knockout lines (described in chapter 5) and wild type Arabidopsis. The blot was probed with the preimmune serum of anti-Slp1 and the polyclonal antiserum. No bands are detectable with the preimmune serum. The antiserum does recognise the band corresponding to the endogenous wild type Slp1 protein, but nothing of the same weight in the knockout extracts despite similar protein levels on the blot (see the Rubisco loading control). The same contaminating bands at 60 kDa than in (A) are equally visible in the knockout and wild type extracts when compared with the Rubisco loading control (bottom). The difference seen between the knockout and wild type protein extracts confirms the specificity of the antibody towards AtSlp1. As a control, the same lanes were probed with monoclonal tubulin antibody (Sigma) that recognises the same band pattern in all three lanes (see blot in the middle).

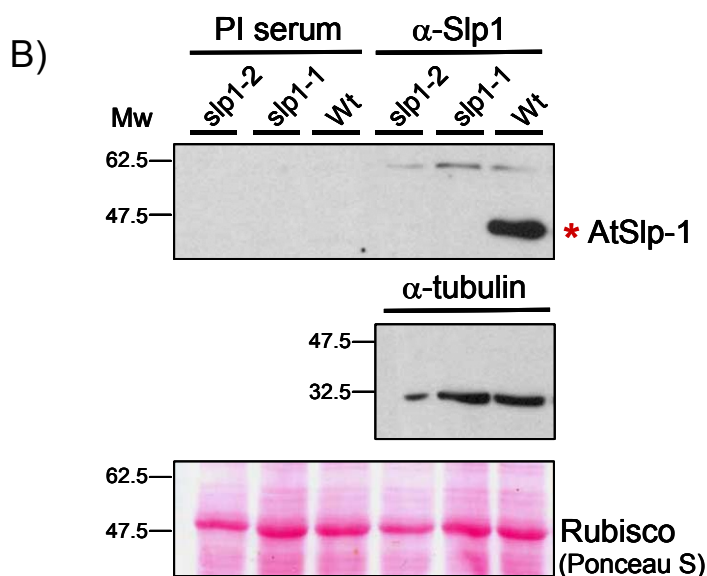
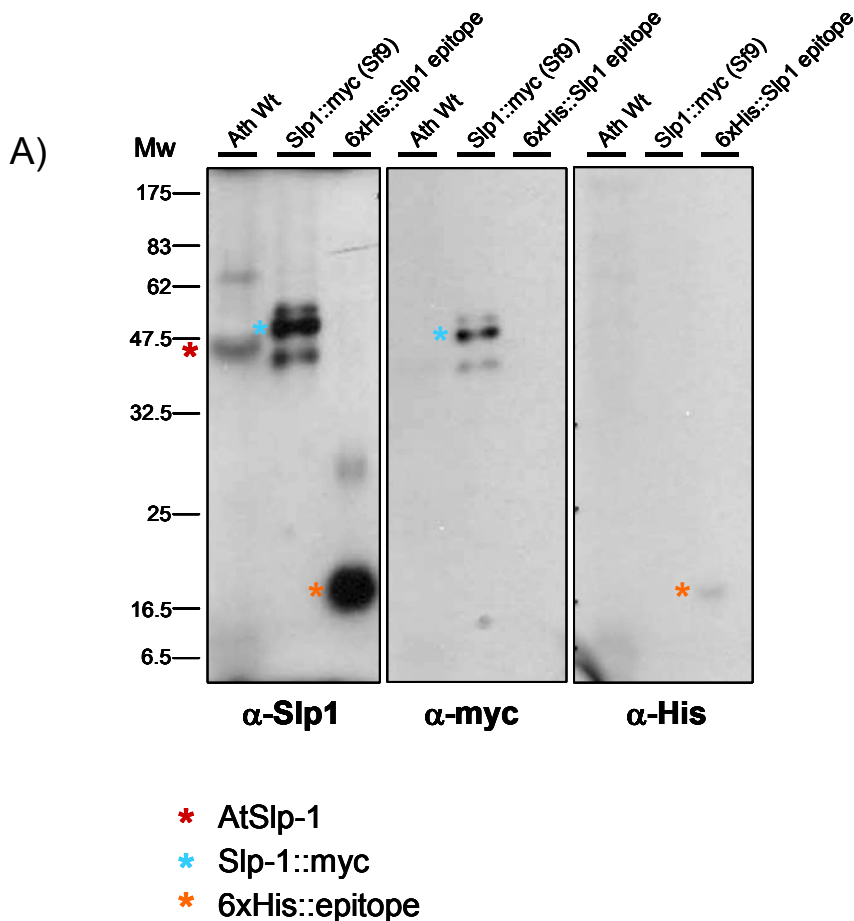


Figure 3-17. Western blots to assess the specificity of anti-Slp1 on different protein extracts.

A) Western blot probed with anti-Slp1 (blot on the left), anti-myc (middle blot) and anti-His (right blot) as controls. Arabidopsis wild type extract (Ath Wt) is always loaded on the left lane, Sf9 lysate (Slp1::myc Sf9) in the middle and the epitope control (6xHis::Slp1 epitope) on the right lane. The red asterisk indicates the presence of the endogenous AtSlp1 protein in the wild type extract, the blue asterisk the myc fusion protein in the Sf9 lysate and the orange asterisk marks the epitope originally used to raise the antibody. Numbers indicate molecular weight markers (Mw) in kDa.

B) Western blot of total protein extracts from two slp1 knockout lines and wild type probed with preimmune serum (left side) and anti-Slp1 (on the right). The red asterisk indicates the presence of the Slp1 protein. The blot in the middle shows the same lanes probed with anti-tubulin as a control. Shown on the bottom is the Rubisco loading control (Ponceau stain).

3.4.4 GST-fusion of Slp2 epitope and attempted expression in bacteria

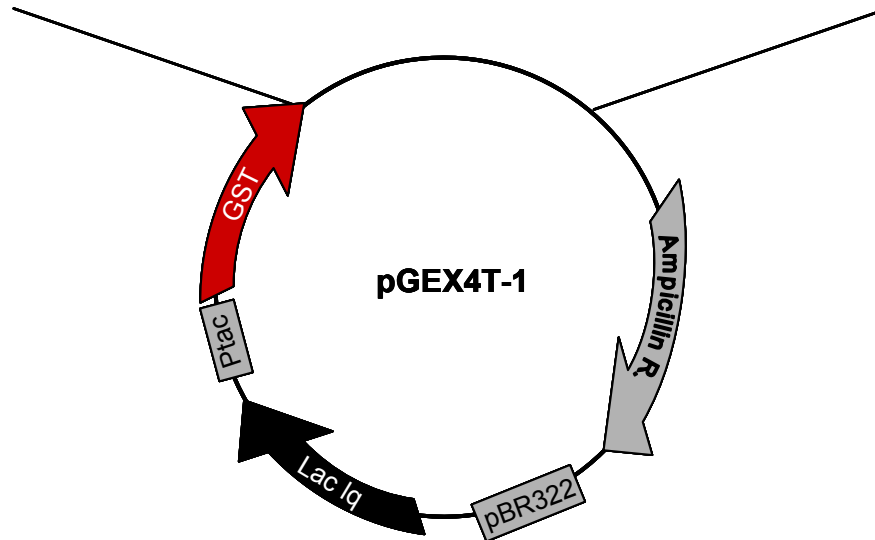
As an alternative to the His-tagged fusion protein for the Slp2 epitope, the same frame was cloned into the pGEX4T-1 GST (glutathione-S-transferase)-fusion vector (Amersham/GE Healthcare) and used to transform *E.coli* strain BL21 (Novagen) for protein expression. Figure 3-18 (A) gives an overview over the designed construct and the restriction sites used. The GST fusion protein expression is driven by an IPTG-inducible promoter that is regulated by the product of the lac repressor gene. The resulting fusion protein is 324 amino acids long and has a predicted mass of 36.7 kDa. The GST protein alone contributes 29kDa in weight to the final mass. To test the protein expression level, a small culture volume (2ml) of two identical constructs (nos. 9 and 23) was inoculated, grown to a suitable density and induced with 1 mM IPTG for 2 hours at 37 °C. The cells were harvested and lysed by sonication in PBS buffer supplemented with protease inhibitors. The solubilised proteins were separated by centrifugation from the insoluble matter and SDS loading buffer added to both fractions. An SDS-PAGE gel was loaded, Western blotted and probed with a GST specific antibody (Novagen) to detect GST fusion protein. Figure 3-18 (B) shows the Western blot of the two constructs used (no. 9 and no. 23) and the soluble and insoluble protein fractions. Bands of approximately the predicted weight (yellow arrowhead) are visible in both fraction types, but more prominently in the soluble proteins. All lanes show additional bands of lower molecular weight, particularly in the soluble protein fractions, which are most likely degradation products.

This initially positive result indicated that it might be possible to purify the GST::Slp2 epitope fusion using glutathione sepharose 4B (Novagen) and elution via thrombin cleavage. A thrombin cleavage site is located adjacent to the BamHI site used for cloning and allows for elution under mild conditions, while the GST moiety remains bound to the sepharose support. A total of three separate protein purifications from bacteria cultures of 50-100 ml volume were attempted. However, none of these purifications resulted in any specific band in the final eluate on Coomassie Blue stained SDS-PAGE gels (not shown). These purification trials will not be described in more detail and were not continued after it was clear that no Slp2 epitope protein was detectable after the thrombin cleavage, despite it was expressed in the bacteria. In a last attempt to obtain a specific Slp2 antibody, peptide epitopes were designed and used for commercial antibody production as described in the next section (3.4.5).

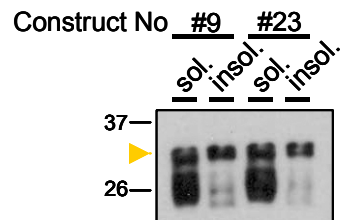
A) **pGEX4T-1-GST::Epitope Slp2:**

Fusion protein:

M[...]LVPRGSNQLALSRSGYTA AVRFLPMLSAAVPKILSSLAAASTVRNFSS
 TGSPLTSYQINKPSPSKSFTSRLLHQSSSAGTPPQQLFGARSFSSPSSDLE
 RPHRD.



B)



▶ GST::epitope AtSlp2

Figure 3-18. GST fusion of Slp2 epitope and protein expression in bacteria.

A) Overview over the GST fusion construct. The Slp2 epitope was cloned into pGEX4T-1 vector using BamHI and XhoI creating the sequence shown. Red letters indicate the GST sequence and yellow letters the Slp2 epitope; black letters are derived from the vector open reading frame. Abbreviations are: Ptac (tac promoter), ATG (start codon), STOP (stop codon), Lac Iq (Lac repressor gene), pBR322 (origin of replication), Ampicillin R. (Ampicillin resistance gene).

B) Western blot using a GST specific antibody of two induced bacteria cultures (constructs 9 and 23). The cells were lysed and soluble proteins separated from insoluble ones by centrifugation and loaded on a SDS-PAGE gel. The yellow arrowhead indicates the position of the GST::Slp2 fusion protein in all fractions loaded.

3.4.5 Commercial antibody production based on peptide epitopes of AtSlp1 and AtSlp2

In addition to the epitopes expressed as fusion proteins in bacteria, short specific peptide epitopes of ca. 15 amino acids were designed for each protein. The chosen epitope areas are marked in Figure 3-4 and Figure 3-11 by a dark green line for AtSlp1, and a light green line for AtSlp2. Both epitopes are located in the N-terminal part of the proteins. For Slp1, the aim was to have an epitope at the opposite end of the protein to the one previously used in His-tagged protein purification. For Slp2, the N-terminus had to be chosen again to keep the sequence as specific as possible. The Slp2 peptide epitope lies in the unique region of the Slp2 N-terminus and has good antigenic properties as judged by the antigenic index (Figure 3-11). The Slp1 peptide epitope on the other hand lies in a region that is still fairly specific for the Slp1 protein, but does not give good values for surface exposure or antigenicity. However, no other region could be identified without compromising on epitope specificity. The two chosen epitopes were synthesised, conjugated to a carrier protein and injected over a period of several months into two rabbits per protein. Samples of preimmune sera and bleeds were tested for their specificity on Western blots of *slp1* knockout and wild type extracts.

3.4.5.1 AtSlp1-peptide specific antiserum

For Slp1, Figure 3-19 shows Western blots probed with preimmune sera and sample bleeds of two different animals. As a control, the same protein samples were also probed with tubulin antibody to control for loading differences. The Rubisco band of the Ponceau S stains is also included for reference. The two animals gave similar results in the lanes probed with antiserum, but looked very different when the preimmune sera are compared. The preimmune serum (PI) of rabbit A gave only weak signals in the higher molecular weight ranges, but PI of rabbit B resulted in a prominent band (ca. 30kDa) in the *slp1-1* knockout extract. Some higher weight crossreacting bands were also detected. The antiserum of rabbit A showed bands of similar weight than AtSlp1 (marked with a purple asterisk in Figure 3-19), but there was no visible difference between knockout and wild type extracts. Thus, it was concluded that these bands were unspecific. The bands of higher weight (around 80 kDa) were also discounted as crosscontaminants. The antiserum of rabbit B shows the same band pattern of similar size as AtSlp1, but again there were no differences between mutant and wild type extracts. The 80 kDa bands are also present, and additional lower weight bands at around 20 kDa. None of these bands was regarded as a

specific signal. The tubulin and Rubisco control showed approximately even loading of all samples blotted. Because of these negative results, the rabbit immunisation protocol was terminated early. Most likely the chosen Slp1 epitope was not leading to the expected result because it is likely to be located in an area that is processed by proteolytic cleavage upon correct subcellular localisation (see chapter 4). Thus, the native Slp1 protein probably lacks the full length N-terminal end that is encoded in the open reading frame (see chapter 4).

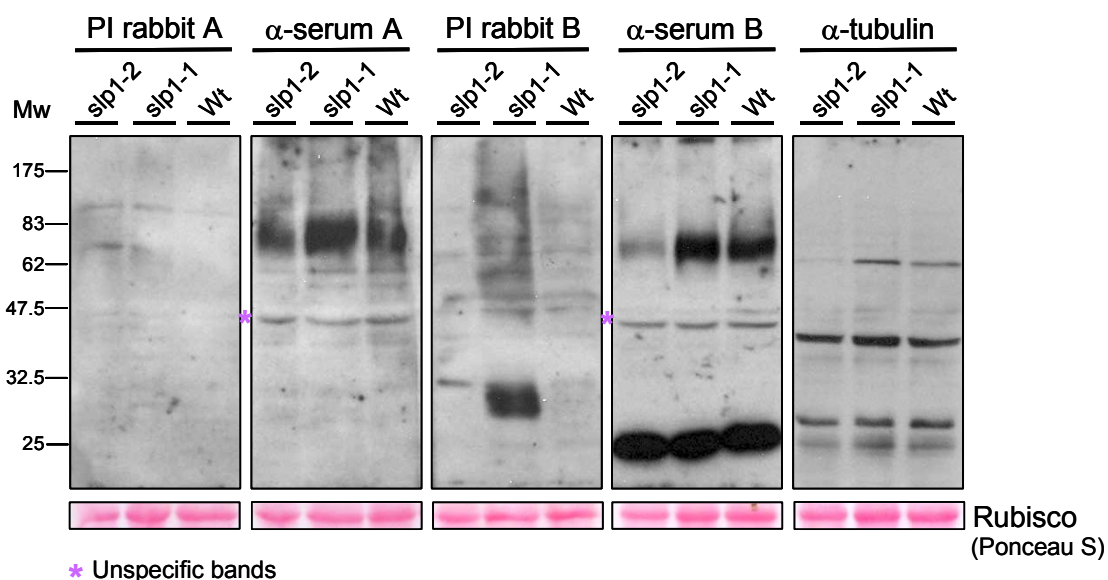


Figure 3-19. Western blots to determine peptide epitope-specific antiserum against Slp1. All blots are loaded with the same samples. On the left lane, protein extract of *slp1-2* knockout seedlings is loaded and in the middle an extract from *slp1-1* plants. The right lane always contains the wild type protein extract. The blots are probed with preimmune sera (PI) and antisera (α-serum) of each rabbit A and B. Tubulin antibody was used on the blot on the right side as an internal control. The Rubisco bands from the Ponceau S stains are included at the bottom. Molecular weight markers are included and labelled as in the figures before. A purple asterisk indicates the position of unspecific bands that have a similar molecular weight as the native Slp1 protein (45 kDa).

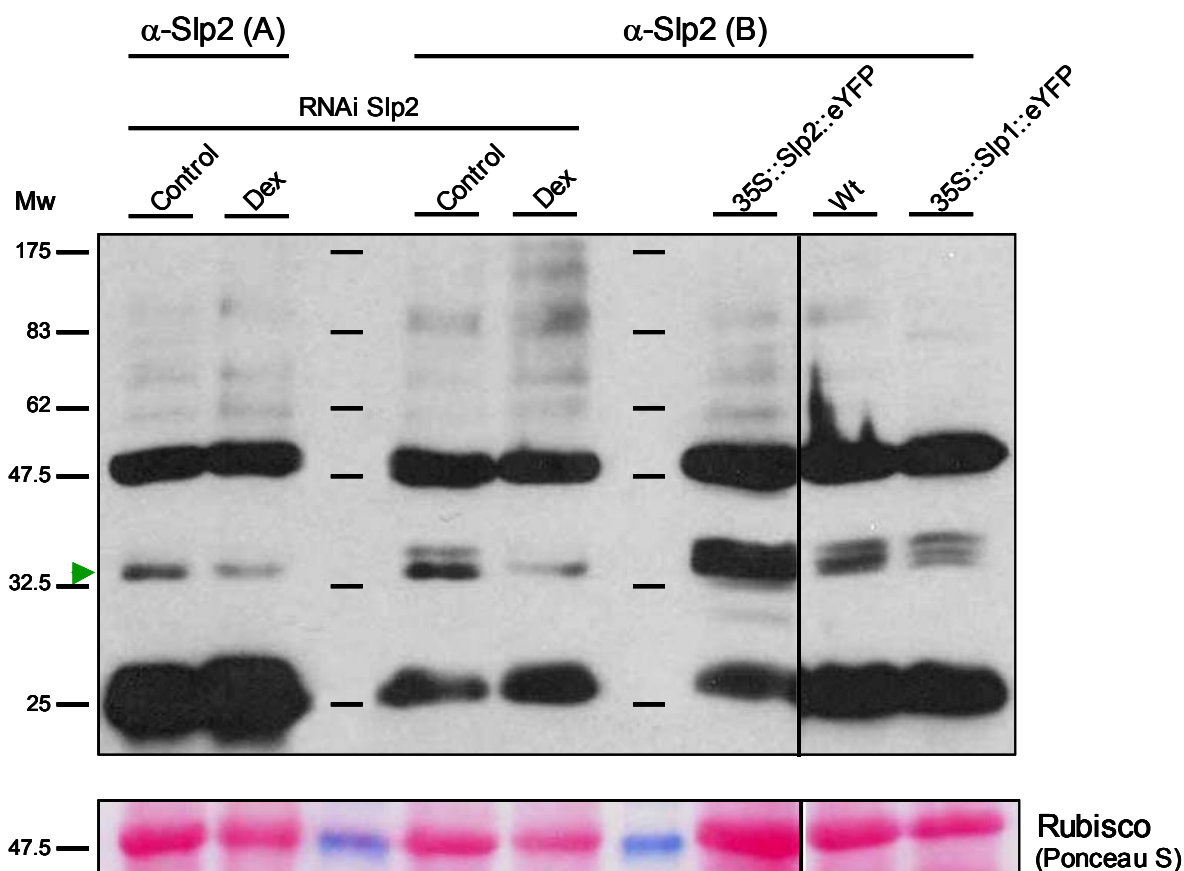
3.4.5.2 AtSlp2 peptide specific antiserum

Antiserum production against the N-terminus of the Slp2 protein did not result in a clean antibody either. Figure 3-20 shows a Western blot of protein samples from various transgenic Arabidopsis plants that will be described further in the following chapters. The first four panels from the left side are loaded with extracts (control and Dex) from a dexamethasone-inducible Slp2-RNAi transgenic plant (marked RNAi Slp2) and were probed with the antisera (2. bleeds) of two different rabbits (A and B). The antisera of both animals show an array of bands. The predicted molecular weight of AtSlp2 is

approximately 43 kDa if the protein is not further processed. The bands seen with anti-Slp2 in this image do not match this expected size. The strongest visible bands of highest (approximately 50 kDa) and lowest (25 kDa) molecular weight are most likely contaminants; the lowest 25 kDa bands resemble the bands seen in Figure 3-19 probed with anti-Slp1 from rabbit B. The double bands of Figure 3-20 in the middle (around 35kDa) might stem from a proteolytic product of AtSlp2. The lower band of this doublet shows a reduction in density in the dexamethasone-treated extract compared to the control. Therefore it is assumed that only this lower band (marked with a green arrowhead) is related to AtSlp2.

The three lanes on the right side are loaded with wild type extract and extracts from Slp2-YFP and Slp1-YFP overexpressing transgenic plants. The antiserum from rabbit B however does not recognise the overexpressed Slp-2YFP fusion protein that has a molecular weight of approximately 60 kDa. This band could be easily detected using a GFP specific monoclonal antibody (Figure 4-16). On the other hand, there is a visible increase in band density around 35 kDa in this sample that could be related to more protein loaded on the blot (see Ponceau S stain), or higher levels of Slp2 protein (without the YFP tag). Otherwise no obvious difference between the Slp2 overexpressor, the wild type and a 35S overexpressing Slp1-YFP transgenic plant extract could be detected. It could well be that the native molecular weight of the final gene product of AtSlp2 is indeed smaller (by ca. 8 kDa) than the one predicted from the genome. This might be caused by proteolytic processing upon subcellular targeting. The peptide epitope chosen for AtSlp2 lies downstream of a predicted signal sequence (see Chapter 4) and is therefore not lost after processing as it is in the case of the peptide epitope of AtSlp1. The fact that there is a clear difference between the control and the dexamethasone treated samples from the inducible RNAi plants strengthens the assumption of a smaller processed protein. It is however not easy to explain why the antiserum does not recognise the YFP fusion protein that is readily detectable with an antibody against its fluorescent tag. It is possible that this fusion protein is not stable in Arabidopsis and therefore partly cleaved between the Slp2 protein and the YFP part. The excess level of Slp2 protein could be detected by the antibody and explain the increased band density. However, no second band corresponding to any free YFP could be detected with the GFP specific antibody on this extract (not shown). Another possibility to explain the failure of detection by the Slp2 antibody could be coverage of the epitope by the YFP moiety. Because the Slp2 protein also most likely adapts the same loop insertion as Slp1, the large YFP tag might obscure access to the N-terminal epitope, even under denaturing conditions in the presence of SDS. The Slp2 antibody also does not

crossreact with any proteins derived from AtSlp1, since there is no band recognising the Slp1-YFP fusion protein.



► Putative AtSlp2

Figure 3-20. Western blots of Slp2 antibody raised against the peptide epitope from two different animals (A and B). The four panels on the left side are loaded with extracts from dexamethasone-inducible RNAi plants (control and Dex). Antisera from both rabbits recognise the same pattern of bands. The band that putatively corresponds to AtSlp2 is marked by a green arrowhead. The 50kDa and 25kDa bands are supposedly crossreacting contaminants. The three lanes on the right side are loaded with Slp2-YFP, wild type and Slp1-YFP extracts from Arabidopsis leaves. The band pattern looks identical to the RNAi samples. The 35kDa band in the Slp2-YFP overexpressor extract is stronger than in the other samples. No band corresponding to the full length YFP fusion protein is detected with the antiserum from rabbit B. The corresponding Rubisco bands from the Ponceau S stain are shown underneath as a loading control. Numbers correspond to kDa molecular weight (Mw).

Because the antiserum from rabbit B gave better results on the Western blot (less prominent contaminating bands and a stronger 35 kDa band), it was decided to affinity-purify the antiserum only from this animal. The serum was purified on the peptide epitope and eluted under acidic conditions (pH 2.5) or physiological pH (7.4). These purified sera were tested together with the preimmune serum from rabbit B on *slp1* knockout plant and wild type extracts (Figure 3-21). The *slp1* knockout plant extracts were used to determine

the crossreactivity of the antibody against Slp1 and to check for differential Slp2 protein levels between the mutants and the wild type. The preimmune serum of this animal shows some bands that are also visible with the purified sera. Notably, the upper band of the 35 kDa band doublet is also recognised together with the 50 kDa band. This further suggests that only the lower band in the doublet might arise from Slp2. Compared to the band pattern recognised before the purification, there are additional bands reacting with the purified antiserum between 40 and 50 kDa in size. Against the expectations of a cleaner antibody that recognises less contaminating bands, the opposite seems to be the case. There is also no obvious difference between the two affinity-purified sera (pH 2.5 and pH 7.4). Finally, no differences could be seen in the density of the bands between the knockout plants and the wild type.

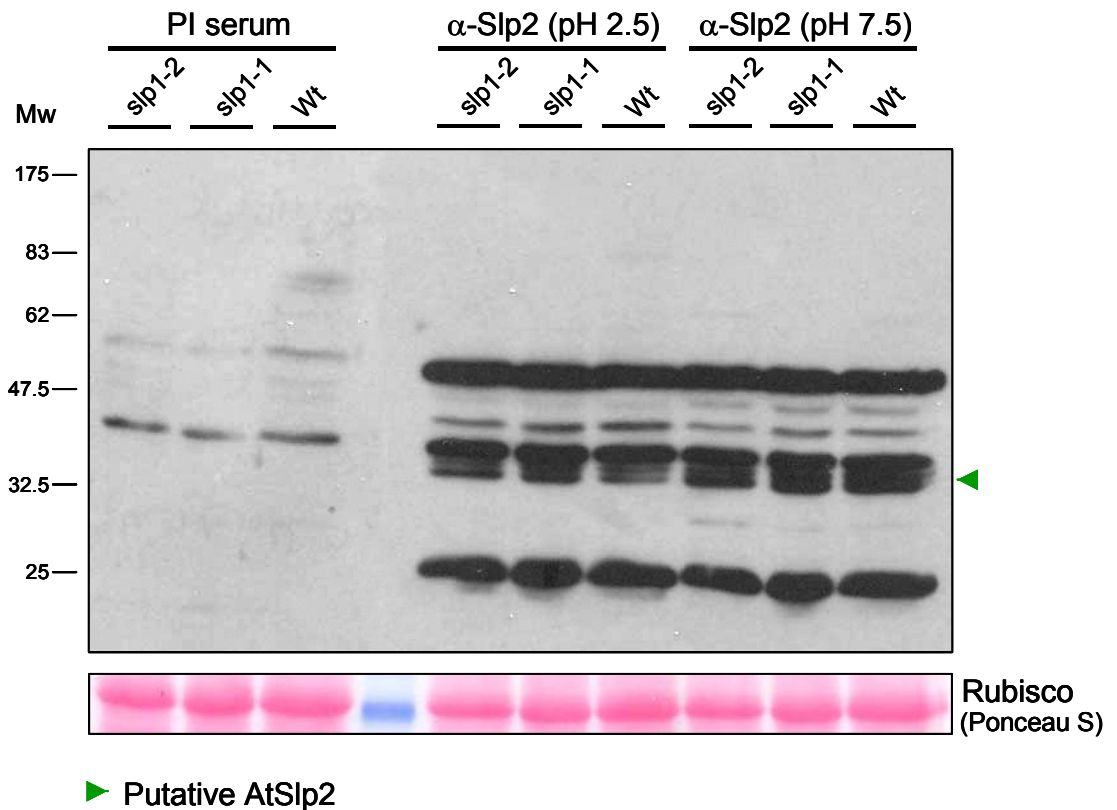


Figure 3-21. Western blot probed with preimmune serum and affinity-purified anti-Slp2 sera from rabbit B. The protein samples are from *slp1* knockout plants and wild type plants as before to assess the antibody's cross-reactivity towards AtSlp1. Lanes probed with the preimmune serum (PI) show that some bands remain. These arise from the endogenous rabbit serum. The 50kDa band and the upper band of the 35 kDa doublet are also present when the PI serum is used. Two different affinity-purified fractions (eluted under pH 2.5 and pH 7.5) still give the same contaminating bands as seen before at 25 kDa and 50 kDa. Additional bands are visible in between. The position of the putative Slp2 protein is marked with a green arrowhead. The Rubisco bands from the Ponceau S stain are shown underneath; the blue band stems from the molecular weight marker. Numbers on the left indicate molecular weight (Mw) in kDa.

In summary, the peptide-specific antibody production did not result in specific antiserum against the N-terminus of AtSlp1. This however, is down to a bad choice of epitope since this part of the protein is most likely cleaved upon intracellular targeting. For AtSlp2, the final antiserum does seem to recognise bands specific for this protein, but it also recognises even more contaminating proteins. With this amount of background bands on a plant extract it is difficult to use this antibody for any localisation or molecular studies. In conclusion, the purified Slp1 epitope from bacteria gave the best results. This is not surprising since the epitope was much larger and probably more suited to recognise the endogenous AtSlp1 protein.

3.5 Expression analysis of AtSlp1 and AtSlp2

The aim of this section of chapter 3 is to give an overview over what is already known about the expression of the two Arabidopsis stomatin-like proteins, combined with newly researched data contributed by this work. The focus is first on the gene expression in tissues and throughout development on the transcript level, and how these basic levels can be modified if plants are treated with chemicals and phytohormones. This is based both on public data derived from microarray experiments, but the transcript levels of AtSlps in response to hormones and stress treatments were also directly investigated. Second, the gene structures of AtSlp1 and AtSlp2 were analysed together with their promoter sequences. As part of this section, results from promoter-GUS transgenic plants are presented that aim to examine the promoter activity in different tissues and under stress conditions. In the last part, the expression levels in different organs are analysed both on the transcript and on the protein level.

3.5.1 Expression levels of AtSlps from public microarray data

A wealth of publicly available expression data based on microarray experiments is available online through TAIR. Amongst these tools, the so-called eFP browser (Winter *et al.*, 2007b), <http://www.bar.utoronto.ca/efp>) provides comprehensive transcript level analysis of Arabidopsis gene levels during plant development and under stress conditions. Colour-coded maps are available that indicate changes in transcript levels. The data of these maps (as absolute values) were downloaded and plotted with the standard deviations given on the web site. According to this database, both genes give the same responses under all conditions. It is however possible that the probes used in these microarrays are not 100% gene specific and thus reflect the transcript levels of both AtSlp1 and AtSlp2 combined.

3.5.1.1 Expression levels during plant development

Expression data from transcript levels during plant development are plotted in Figure 3-22. The corresponding data descriptions are given in Table 3-7 underneath; these data were obtained by (Schmid *et al.*, 2005). From this plot several organs have clearly increased transcript levels: the transcript is overall highest after 24 hours of seed imbibition (sample 2). In very young seedlings (2 days old), the highest expression level is reached in the root (no. 5), followed by the hypocotyls (no 3) and the cotyledons (no 4). Once the rosette is

established, the expression is highest in the first two leaves (sample 6) and decreases over the next stages. The expression in cauline leaves (no. 11) is generally lower than in rosette leaves (no. 10). Senescing leaves (no. 12) have approximately the same transcript levels as cauline leaves. Comparing the overall vegetative rosette (before flowering, no 12) to the root (no. 13), the expression is clearly higher in leaves. After the flower transition, the expression decreases by almost 50% in the rosette leaves (no. 14) and is very high in the vegetative shoot apex (no. 15) and the inflorescence apex (no. 16). Flowers at stage 9 (no. 17) also give very high Slp levels, but these decrease upon flower maturation. Stage 12 flowers that are not opened (nos. 18-22) have high Slp levels in the sepals (no. 19) compared to the petals (no. 20) and extremely low levels in the stamens (no. 21). Stage 15 flowers (no. 23) have overall slightly less transcript than stage 12 flowers. The sepals (no. 24) remain the flower parts with the highest levels and the stamens have the lowest levels (no. 26). Mature pollen grains have the lowest overall levels (no. 29), indicating that the transcription is repressed at this stage of pollen development. Expression levels in developing and mature siliques and seeds are low (nos. 30-32) compared to leaves and young flowers. In summary, this profile generally suggests that AtSlps are higher expressed in young plants mainly in the leaves. Flowering plants have high Slp levels in developing flowers and in the shoot apices.

Expression levels of AtSlps- Plant Development

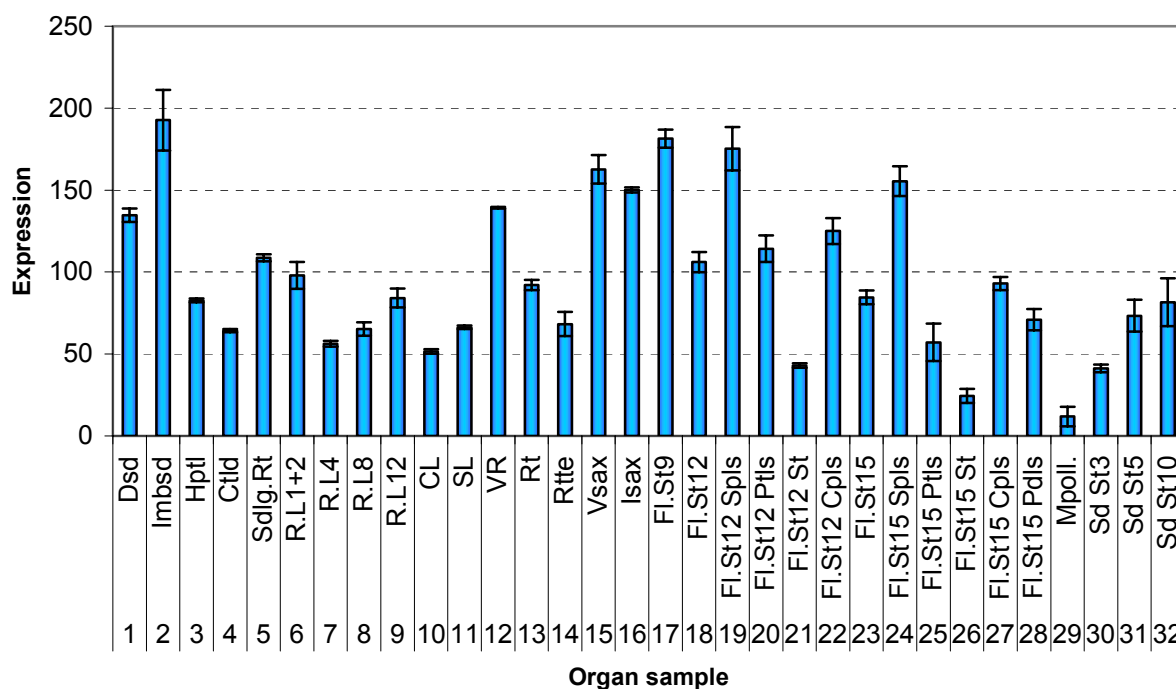


Figure 3-22. AtSlp transcript levels in different organs. The numbers beneath the labelling indicate the position in Table 3-7. Abbreviations are according to this table too. Error bars represent standard deviations that were downloaded from the eFP website with At4g27585 as a query.

Developmental stage	Number in graph	Abbreviation	Developmental stage	Number in graph	Abbreviation
Dry seed	1	Dsd	Flower Stage 9	17	Fl.St9
Imbibed seed (24 h)	2	Imbsd	Flower Stage 12	18	Fl.St12
Hypocotyl	3	Hptl	Flower Stage 12, Sepals	19	Fl.St12 Spls
Cotyledon	4	Ctld	Flower Stage 12, Petals	20	Fl.St12 Ptlis
Root	5	Sdlg.Rt	Flower Stage 12, Stamens	21	Fl.St12 St
Leaf 1+2	6	R.L1+2	Flower Stage 12, Carpels	22	Fl.St12 Cpls
Rosette Leaf 4	7	R.L4	Flower Stage 15	23	Fl.St15
Rosette Leaf 8	8	R.L8	Flower Stage 15, Sepals	24	Fl.St15 Spls
Rosette Leaf 12	9	R.L12	Flower Stage 15, Petals	25	Fl.St15 Ptlis
Cauline Leaf	10	CL	Flower Stage 15, Stamen	26	Fl.St15 St
Senescing Leaf	11	SL	Flower Stage 15, Carpels	27	Fl.St15 Cpls
Vegetative Rosette	12	VR	Flowers Stage 15, Pedicels	28	Fl.St15 Pdls
Root	13	Rt	Mature Pollen	29	Mpoll.
Entire Rosette after flower transition	14	Rtte	Seeds Stage 3 Siliques	30	Sd St3
Vegetative Shoot Apex	15	Vsax	Seeds Stage 5 Siliques	31	Sd St5
Inflorescence Shoot Apex	16	Isax	Seeds Stage 10 Siliques	32	Sd St10

Table 3-7. Samples and their numbers used to create the plot in Figure 3-22. The descriptions have been downloaded together with the actual data from the eFP website. "Abbreviation" refers to the name given for a specific sample in the bar chart of Figure 3-22. More detailed descriptions are available from the website and some are given in the text.

3.5.1.2 Tissue specific expression

A second dataset was downloaded that quantifies expression levels more detailed in specific tissues. Figure 3-23 summarises these data in a bar chart with the corresponding details given in Table 3-8. Samples from Columbia 0 (6 days old seedlings grown on MS agar plates supplemented with 4.5% sucrose) mature stage III roots analyse Slp expression in various types of root cells (samples 1-5). Root endodermis (no. 2) and the stele (no. 1) both express AtSlps, but at a slightly lower level compared to the cortex and epidermal atrichoblasts (nos. 3 and 4). Different stages of pollen development (Landsberg erecta plants, soil-grown) confirm that the expression level is initially high in the uninucleate microphore (no. 6) and the bicellular stage (no. 7). There is a dramatic drop in expression by a factor of 10, once the pollen enter the tricellular stage (no. 8) and become mature (no. 9). At this stage the transcription of AtSlps is repressed- this shift from very high level expression to a silenced transcription must mark an important developmental progress and it appears likely that the transcription must be tightly regulated at this stage. Other tissues such as xylem (no. 10) and cork (no. 11) from Columbia-0 (soil-grown) do not maintain high levels of Slps. Also stem epidermal cells taken from the bottom (no. 13) and the top (no. 12) of the shoot of Col-0 plants do not show any major differences and are low compared to other tissues. On the other hand, expression in the stigma (no. 16, from Ler ecotype) is significantly higher than in the stem as a whole (nos. 14, 15 from Col-0). The ovaries (no. 17, from Ler) have expression levels that are almost as high as in the early pollen development. Thus, it appears that Slp expression might be essential for gamete development and might have an impact on flower fertilisation.

Slp transcript levels were also analysed from different types of leaf cells by microarrays. Mesophyll and guard cell protoplasts of 5 weeks old Col-0 plants were prepared and their transcription profile analysed. Untreated mesophyll cells have very low Slp expression (data not shown). These transcript levels do not change when the cells are treated with 100 μ M ABA (abscisic acid). On the contrary, untreated guard cell protoplasts have approximately 10 times higher transcript levels, and there is a further increase by a factor of 1.5 when protoplasts of these cells are treated with the same amount of ABA. However, these measurements were only taken in duplicates and have very large standard deviations. The difference between the basal level in guard cells and mesophyll control cells is still significant, but the stimulation by ABA in guard cells is not. Therefore, these data are not regarded as reliable and are not included here.

Expression Levels of AtSlps- Tissues

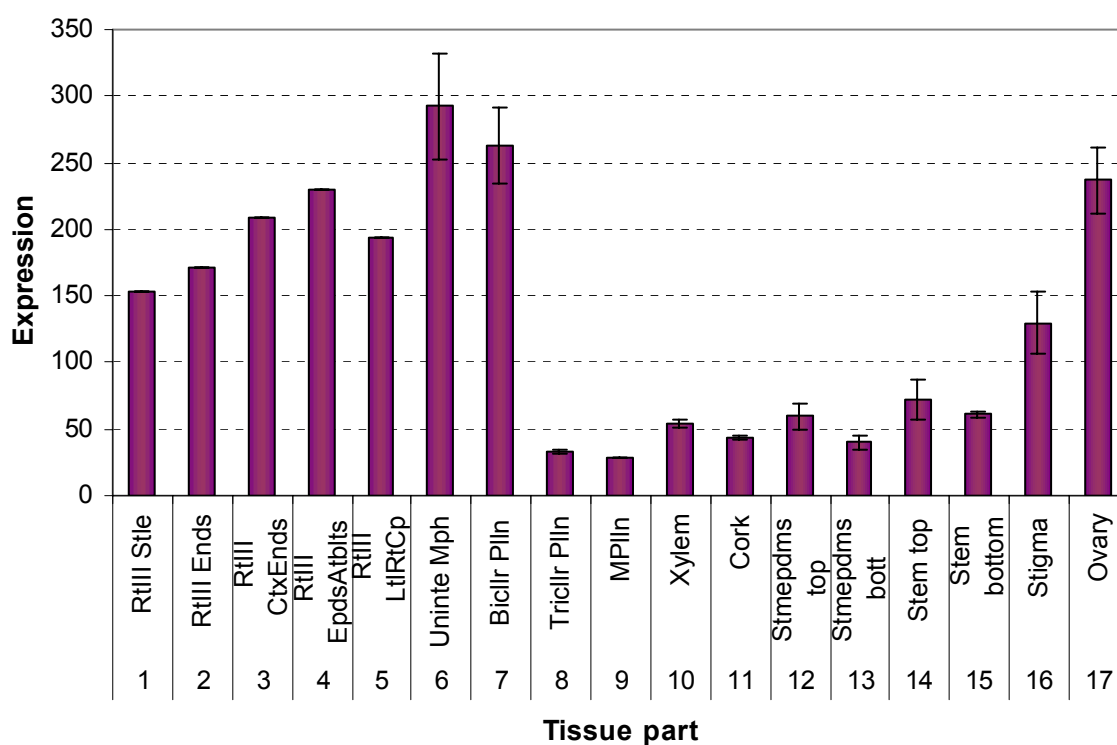


Figure 3-23. Tissue specific expression levels of AtSlps. The sample abbreviations are given in the table below. Expression values and standard deviations were obtained from the eFP database with At4g27585 as a query.

Organ/Cell type	Developmental stage/Treatment	Number in graph	Abbreviation
Root	Root Stage III Stele	1	RtIII Stle
Root	Root Stage III Endodermis	2	RtIII Ends
Root	Root Stage III Cortex + Endodermis	3	RtIII CtxEnds
Root	Root Stage III Epidermal Artrichoblasts	4	RtIII EpdsAtblts
Root	Root Stage III Lateral Root Cap	5	RtIII LtIRtCp
Pollen	Uninucleate Microphore	6	Uninte Mph
Pollen	Bicellular Pollen	7	Biclr PlIn
Pollen	Tricellular Pollen	8	Triclr PlIn
Pollen	Mature Pollen Grain	9	MPlIn
Stem	Xylem Col-0	10	Xylem
Stem	Cork Col-0	11	Cork
Stem	Stem epidermis, top of stem	12	Stmepdms top
Stem	Stem epidermis, bottom of stem	13	Stmepdms bott
Stem	Whole stem, top of stem	14	Stem top
Stem	Whole stem, bottom of stem	15	Stem bottom
Flower	Stigma tissue	16	Stigma
Flower	Ovary tissue	17	Ovary

Table 3-8. Samples used to plot the eFP data from Figure 3-23. Numbers correspond to the order given in the graph. More detailed descriptions of the developmental stages and the cell types can be found on the eFP website.

3.5.1.3 AtSlp expression in seeds

An additional analysed microarray dataset quantifies AtSlp transcript levels in dry (dormant) and water-imbibed Col-0 seeds. Figure 3-24 represents a bar chart of these data; Table 3-9 contains more information about the labelling of the data points. A time course of transcript accumulation (taken in triplicates) during seed imbibition is shown (samples 1-6). Dried seeds (no. 1) have the lowest transcript levels. These rise after 3 hours by a factor of 3 where they peak (data point 3) and then slowly decrease to approximately twice the level of the dry seeds (no. 6). In a different experiment, transcript levels were compared between wild type seeds that were imbibed for 1 hour in the dark. The seeds were then irradiated with a FR light pulse to inhibit germination and incubated in the dark for another 96 hours at 4 °C and at 22 °C (Yamauchi *et al.*, 2004). Clear differences can be seen in AtSlp transcript levels between the two temperature conditions. The incubation at 4 °C caused almost three times more transcript to accumulate when compared to the incubation at room temperature.

In the last set of treatments, wild type seeds were stratified for 4 days at 4 °C in the dark on agar plates containing MS medium supplemented with either 1 % DMSO (control treatment), 1 % cycloheximide or 1 % DNP (2,4-dinitrophenol). The seeds were then transferred to room temperature but were kept in the dark for 24 hours before RNA was extracted (data from Sean R. Cutler, University of Toronto). Compared to the DMSO control seeds, treatment with cycloheximide causes a threefold increase in AtSlp transcript levels. Cycloheximide is a bacterial inhibitor of protein biosynthesis that interferes with translational elongation. The uncoupling agent DNP on the other hand only caused a slight decrease in transcript levels compared to the DMSO control treatment.

In summary, seed imbibition and treatment with cycloheximide cause significant accumulations of AtSlp transcripts. It is therefore likely that both proteins are important for seed germination. Cycloheximide causes disruption of protein biosynthesis and will therefore cause stress on a cellular level. Whether AtSlp1 and AtSlp2 might have a direct impact on protein biosynthesis or whether their upregulation in response to the disruption of it is connected to general cellular stress responses remains open at this stage.

Expression levels of AtSlps- Seeds

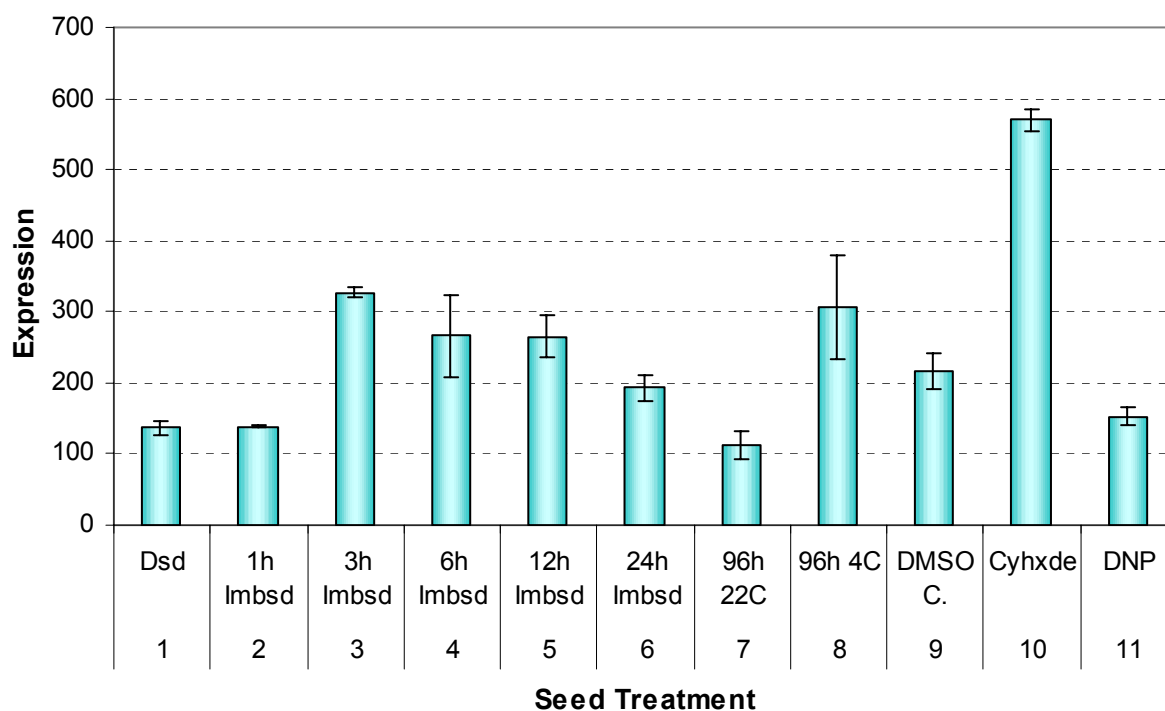


Figure 3-24. Transcript levels of AtSlps in seeds. Seed imbibition was followed in a time course over 24 hours (1-6). Samples 7 and 8 represent a different experiment in which responses of imbibed seeds to cold were investigated. Samples 9-11 are taken from chemical treatments of imbibed seeds. Labelling is as outlined in Table 3-9.

Seed Treatment	No in graph	Abbreviation
Dry Seeds	1	Dsd
1 h Imbibed Seeds	2	1h Imbsd
1 3 h Imbibed Seeds	3	3h Imbsd
6 h Imbibed Seeds	4	6h Imbsd
12 h Imbibed Seeds	5	12h Imbsd
24 h Imbibed Seeds	6	24h Imbsd
96 h at 22 °C, germination inhibited	7	96h 22 °C
96 h at 4 °C, germination inhibited	8	96h 4 °C
DMSO	9	DMSO C.
Cycloheximide	10	Cyxhde
2,4-DNP	11	DNP

Table 3-9. Samples plotted in Figure 3-24. Seeds were treated as described in the text. No in graph and the column “Abbreviation” refer to the labelling in the bar chart.

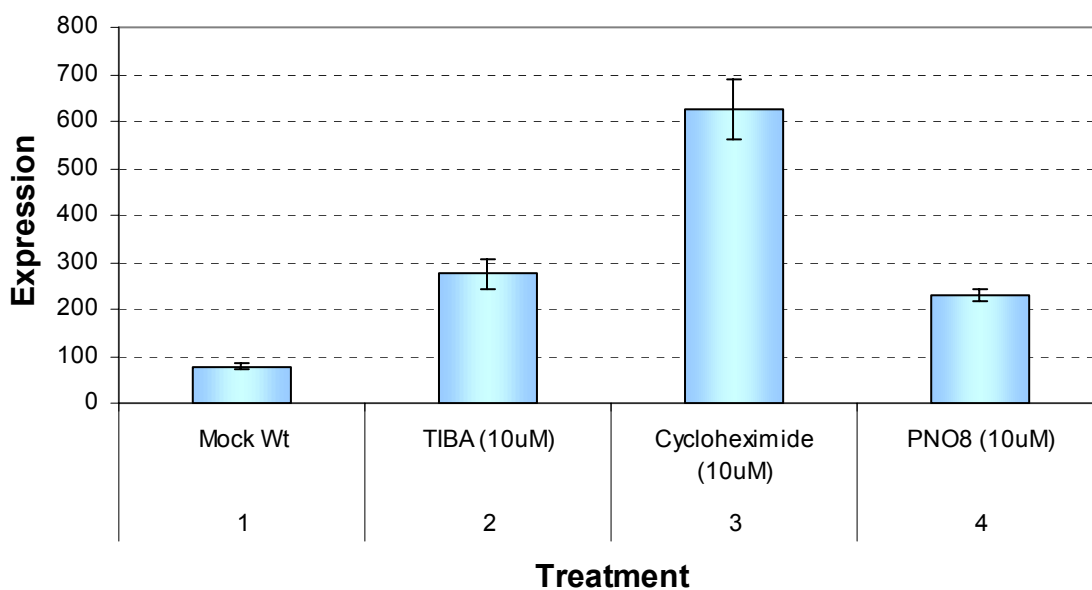
3.5.1.4 Chemical and hormone treatments of seedlings

Figure 3-25 shows a bar chart of downloaded data (eFP browser) from experiments in which wild type (Col-0) seedlings were treated with various chemicals and phytohormones. 7 days old seedlings were grown in liquid MS medium under continuous light and treated for 3 hours with either a mock solution or with the relevant chemical. Treatment for this time period with either 10 μ M of the auxin transport inhibitor TIBA (2,3,5-triiodo benzoic acid), the protein biosynthesis inhibitor cycloheximide, or the photosystem II inhibitor PNO8 (N-octyl-3-nitro-2,4,6-trihydroxybenzamide) resulted in a significant increase of AtSlp transcript levels. Amongst these, cycloheximide had the largest effect with an increase in transcript nearly 6 times above the control level. TIBA treatment caused a threefold increase, whereas PNO8 approximately doubled the transcript levels. Amongst the phytohormones, the cytokinin t-zeatin had the strongest effect. For this experiment, 21 day-old wild type (Col-0) plants grown on agar were treated (in triplicates) for 3 hours either with a mock solution or with 20 μ M t-zeatin (samples 1 and 2 in Figure 3-25). Following the cytokinin treatment, the transcript levels doubled. On the contrary, treatment of 7 day-old wild type seedlings with 10 μ M ABA for 3 hours caused a drop to one half of the control level (samples 3 and 4). Treatments of the same age seedlings for 30 minutes with 1 μ M zeatin (no. 6), 10 μ M ABA (no. 7) or 1 μ M GA (no. 8) had hardly any effects when compared to the 30 minutes control treated sample (no. 5). Seedlings of the GA biosynthesis mutant *gal-5* were also treated for 30 minutes with either a mock solution (no. 9) or with 1 μ M of GA (no. 10). Compared to the Col-0 seedlings, the *gal-5* mutant seedlings have a significant increase of Slp levels already in the control treated plants. No further increase was observed when these seedlings were treated with GA. Brassinosteroid treatment of wild type seedlings (7 day-old as described above) with 10nM brassinolide for 30 minutes also caused a small but significant increase of transcript levels (samples 11 and 12). In the last set of experiments, seeds from Col-0 plants were analysed in duplicates under constant light 24 h after imbibition in water (14) or in the presence of 3 μ M ABA (no. 15). In untreated seeds (no. 13) the transcript levels were approximately 50% less than in imbibed seeds. There was no obvious difference between the water imbibition and imbibition in the presence of ABA.

In summary, this set of treatments confirms the previous observation of increased transcript levels upon cycloheximide treatment. The same effect is also observed in mature seedlings to an even larger extent. Amongst the hormone treatments, the cytokinin t-zeatin has the biggest effects on Slp transcript levels. Interestingly, AtSlp transcription seems to

be suppressed in seedlings treated with ABA for 3 hours. Thirty minutes after ABA addition this effect is not yet visible. Other types of hormones such as GA, brassinolide or the cytokinin zeatin do not show any significant effects after 30 minutes of treatment either. Remarkably, AtSlp levels are strongly upregulated in the *gal-5* mutant seedlings, independent of the addition of ABA. Imbibition of seeds in water or water supplemented with ABA does not give different effects either. It is obvious that imbibition in itself causes upregulation of AtSlp mRNA.

Expression Level of AtSlps- Chemical treatments



Expression level of AtSlps- Hormone treatments

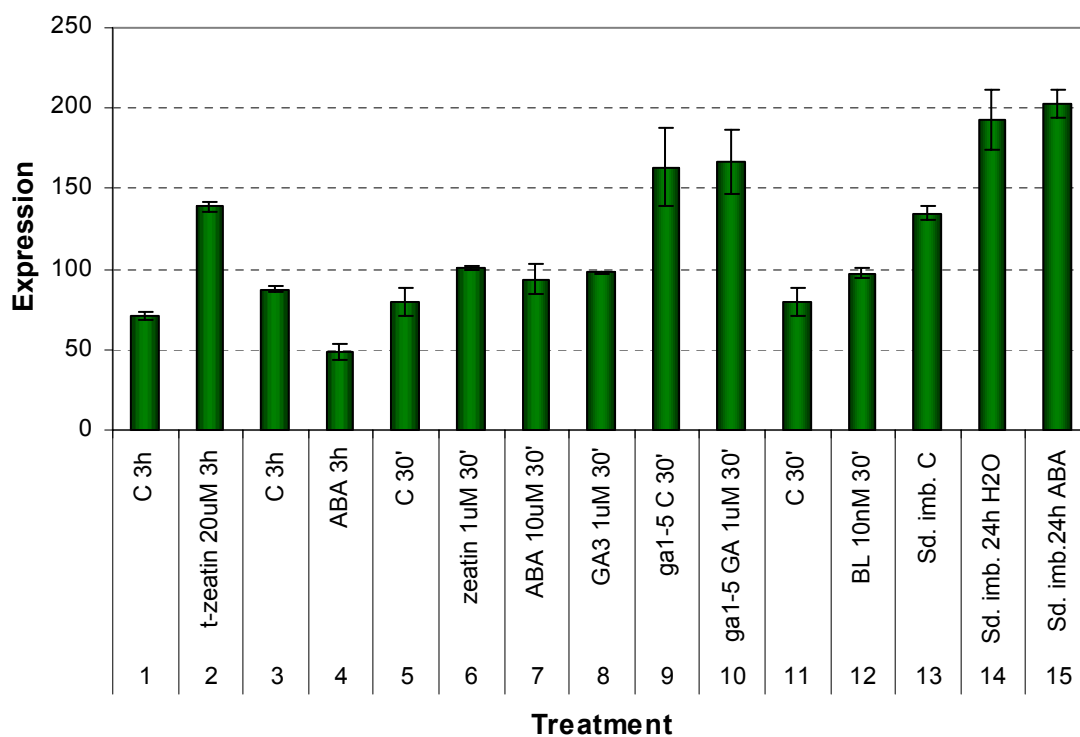


Figure 3-25. AtSlp transcript levels in response to chemical (top) and hormone (bottom) treatments. All treatments were carried out in duplicates on seven days old liquid grown seedlings or as otherwise stated in the text. Numbers correspond to the order given in Table 3-10 below.

Chemical treatment	No in Graph	Abbreviation
Mock Wt	1	Mock Wt
TIBA (10uM)	2	TIBA (10 μ M)
Cycloheximide (10 μ M)	3	Cycloheximide (10 μ M)
PNO8 (10 μ M)	4	PNO8 (10 μ M)
Hormone treatment	No in Graph	Abbreviation
Control Wt 3h	1	C 3h
t-zeatin (Wt 20 μ M 3h)	2	t-zeatin 20 μ M 3h
Control Wt 3h	3	C 3h
ABA (Wt 10 μ M 3h)	4	ABA 3h
control Wt 30 min	5	C 30'
zeatin (Wt 1 μ M 30min)	6	zeatin 1 μ M 30'
ABA (Wt 10 μ M 30min)	7	ABA 10 μ M 30'
GA3 (Wt 1 μ M 30 min)	8	GA3 1 μ M 30'
ga1-5 mutant mock 30min	9	ga1-5 C 30'
ga1-5 mutant+ GA (1 μ M 30min)	10	ga1-5 GA 1 μ M 30'
WT mock 30min	11	C 30'
WT BL (10 nM 30min)	12	BL 10nM 30'
Seed imbibition control Wt	13	Sd. imb. C
Seed imbibition Wt 24h water	14	Sd. imb. 24h H2O
Seed imbibition Wt 24h 3uM ABA	15	Sd. imb.24h ABA

Table 3-10. Chemical and hormone treatments used in Figure 3-25. Numbers correspond to individual bars as before. Details of treatments were taken from the eFP website with At4g27585 as a query.

3.5.1.5 Response to abiotic stresses in shoots and roots

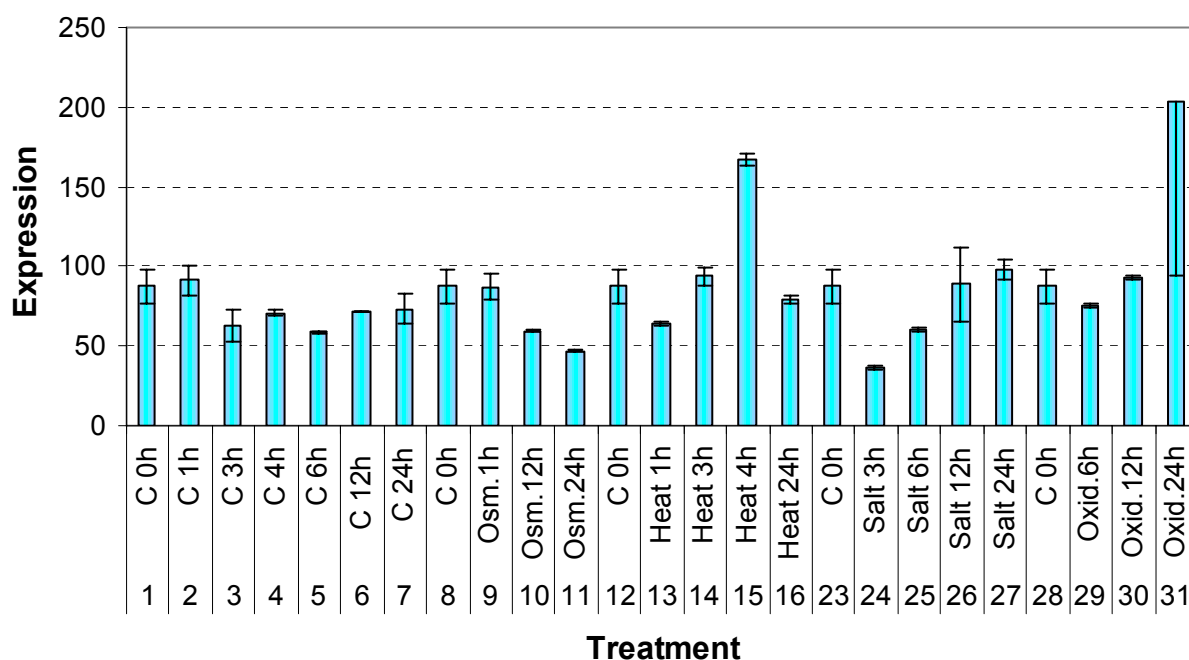
The transcript responses (in duplicates) of 18 day-old wild type plants (Col-0) grown on MS agar were analysed by microarrays after treatments with various abiotic stresses in a time course over 24 hours (Figure 3-26 and Table 3-11). Shoot material was separated from root tissue and only the treatments that gave visible responses or otherwise valuable information are presented here. In the shoot tissue, osmotic stress brought upon the plants by treatment with 300mM mannitol caused only a slight reduction in the transcript level after 24 hours (sample 11). The response was similar in roots (11), but not significantly different from its control (8). Heat treatment in the shoot tissues on the other hand caused doubling of the transcript level at the 4 hours time point (15). For this treatment, plants were transferred to 38 °C for 3 hours and then allowed to recover. However, this increase is only of transient nature and the levels return to normal 24 hours (16) after the recovery period was started. The standard deviation value of the 4 hours time point (15) is small, indicating that this event is reproducible. In the roots this rise in transcript abundance was surprisingly not observed at any time point (13-16). This could be down to the lower

expression level in this part of the plant, but is more likely to stem from specific heat damaging effects that occur only in leaves. Transfer of plants grown under control conditions into a growth medium containing 150 mM sodium chloride resulted in visible differences, but this time only in the root tissues (24-27). The response in the root tissue is marked by a dramatic 3-fold increase in gene transcription 6 (25), 12 (26) and 24 (27) hours after transfer to high salt medium. The standard deviation value is very high in the 12 hours sample making this not a significant change, but it looks significant in the 6 and 24 hours bars. Thus it is assumed that the response as a whole occurs in reality and is not down to an artefact in the microarray. In the shoot, there is only a slight increase in transcript level 24 hours (27) after the transfer. Finally, treatment with paraquat (10 μ M), a toxic herbicide that causes oxidative bursts, results in a transcript increase in the shoots after 24 hours (31), but not in the roots (samples 29-31). However, the standard deviation of this single averaged value is so high that it is probably not a reliable indicator of a true response.

The only other treatment that caused significant changes was irradiation with UV-B light for a period of 15 minutes (Figure 3-27 and Table 3-11). Time points were taken ranging from 1 hour up to 24 hours following the end of the irradiation period. This treatment resulted in a 6-7 fold upregulation of transcript in the shoot that peaked at 3-6 hours (samples 3 and 4 in Figure 3-27) and then gradually returned to control levels after 24 hours (sample 6 in the same figure). This built-up of transcript levels was also monitored in the roots (2-6 in bottom Figure), but the peak level lasted shorter and fell already after 6 hours (sample 4) back to control values.

In summary, only few treatments caused significant changes in AtSlp transcript levels. Amongst the abiotic stress treatments, heat treatment followed by a 4 hours recovery period increased the transcript levels in shoots but not in roots. Salt treatment on the other hand had a remarkable upregulating effect in roots starting from 3 hours after the transfer. Finally, irradiation with UV-B light causes strong upregulation in both tissue types, but the effect is longer lasting in shoots.

Expression Levels AtSlps- Abiotic Stresses in Shoots



Expression Levels AtSlps- Abiotic Stresses in Roots

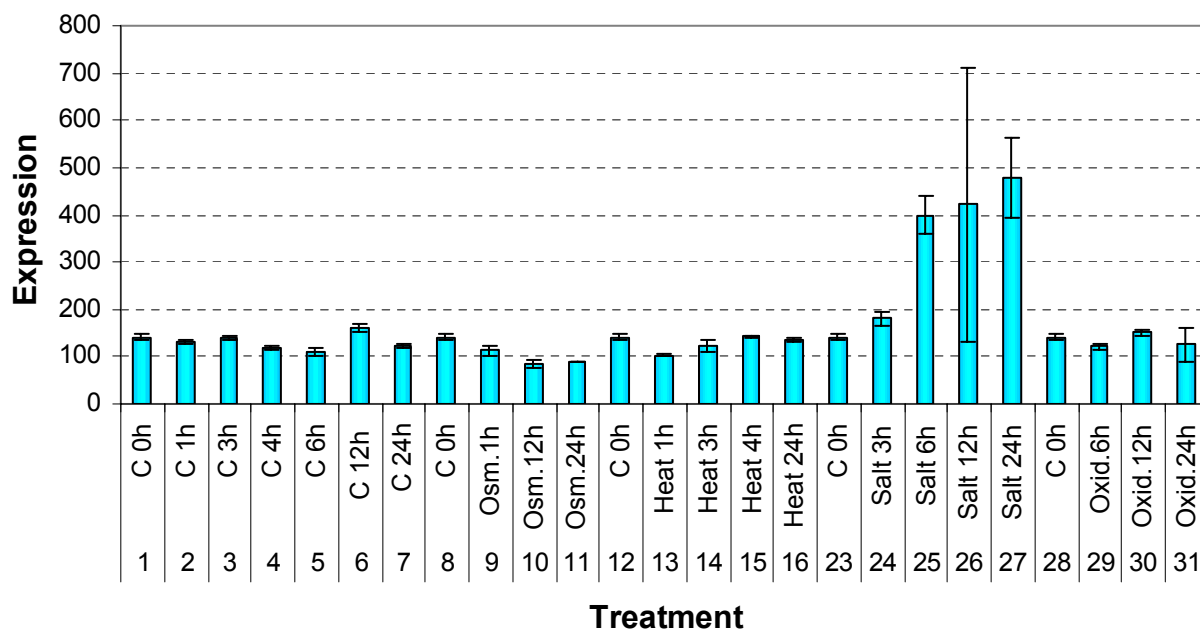
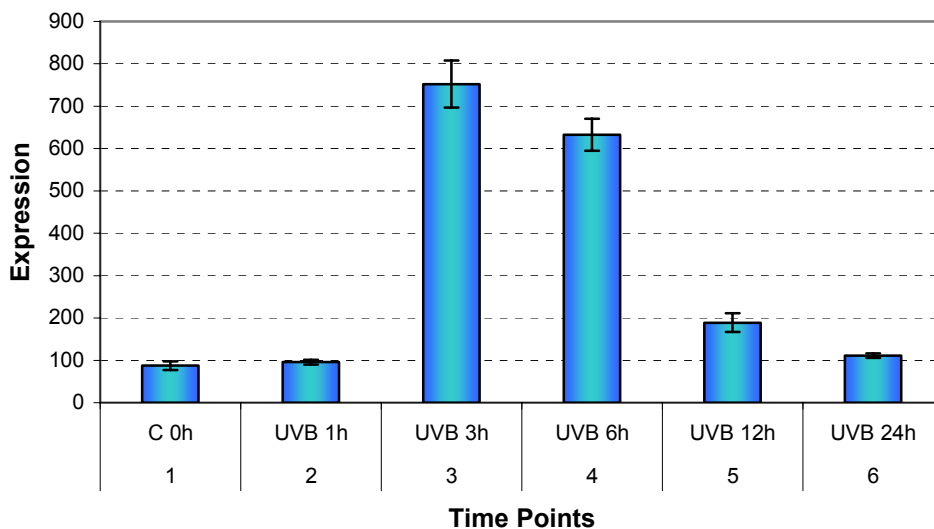


Figure 3-26. Abiotic stress treatments of 18 days old agar-grown wild type plants. The bars corresponding to numbers 1-7 represent control samples (untreated) taken at the same time points than the treated samples. The upper plot represents the responses in shoot tissue and the plot beneath from root tissue with identical treatments. Table 3-11 contains information about the individual treatments. All data were downloaded from the eFP browser website using *At4g27585* as a query. Numbers mentioned in the text above in brackets refer to the sample numbers in these two plots.

Expression Levels AtSlps in Shoots- UV-B Treatment



Expression Levels AtSlps in Roots- UV-B Treatment

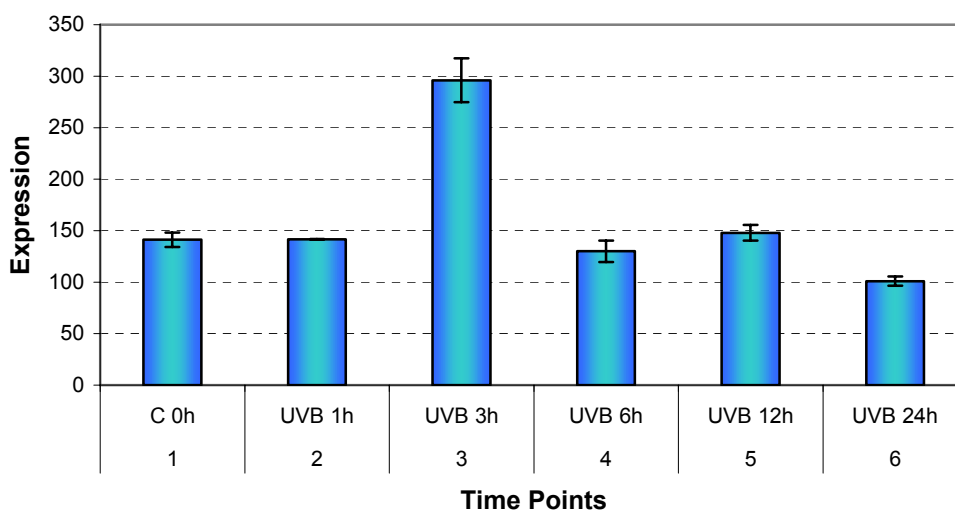


Figure 3-27. UV-B treatment of wild type plants (15 minutes) and transcript responses in the recovery period. The upper plot contains data taken from shoot tissue and the lower plot the response in roots. Sample labelling is as described in Table 3-10 below.

Treatment Shoot/Root	No in graph	Abbreviation
Control 0 Hours	1	C 0h
Control 1 Hour	2	C 1h
Control 3 Hours	3	C 3h
Control 4 Hours	4	C 4h
Control 6 Hours	5	C 6h
Control 12 Hours	6	C 12h
Control 24 Hours	7	C 24h
Control 0 Hours	8	C 0h
Osmotic stress 1 Hour (300 mM Mannitol)	9	Osm.1h
Osmotic stress 12 Hour (300 mM Mannitol)	10	Osm.12h
Osmotic stress 24 Hour (300 mM Mannitol)	11	Osm.24h
Control 0 Hours	12	C 0h
Heat 1 Hour (back to 25 °C)	13	Heat 1h
Heat 3 Hours (back to 25 °C)	14	Heat 3h
Heat 4 Hours (back to 25 °C)	15	Heat 4h
Heat 24 Hours (back to 25 °C)	16	Heat 24h
Control 0 Hours	23	C 0h
Salt 3 Hours (150 mM NaCl)	24	Salt 3h
Salt 6 Hours (150 mM NaCl)	25	Salt 6h
Salt 12 Hours (150 mM NaCl)	26	Salt 12h
Salt 24 Hours (150 mM NaCl)	27	Salt 24h
Control 0 Hours	28	C 0h
Oxidative stress 6 Hours (10 μ M Paraquat)	29	Oxid.6h
Oxidative stress 12 Hours (10 μ M Paraquat)	30	Oxid.12h
Oxidative stress 24 Hours (10 μ M Paraquat)	31	Oxid.24h

Treatment Shoot/Root	No in graph	Abbreviation
Control 0 Hours	1	C 0h
UV-B 1 Hour	2	UVB 1h
UV-B 3 Hours	3	UVB 3h
UV-B 6 Hours	4	UVB 6h
UV-B 12 Hours	5	UVB 12h
UV-B 24 Hours	6	UVB 24h

Table 3-11. Abiotic stress treatments as described in the text and plotted in Figure 3-26 and 3-27. Numbers refer to the position in the graphs and “Abbreviation” to the corresponding label. Treatments were identical for shoot and root tissues. All information was obtained through the eFP browser website with AtSlp1 as a query.

3.5.2 *AtSlp* transcript analysis by Northern blotting

To gain better understanding of actual changes in transcript levels upon hormone and stress treatments, a different experimental approach to microarray analysis was taken. Wild type *Arabidopsis* plants (ecotype Col-0) were grown for 10 days in a liquid MS medium supplemented with sucrose in a 24 well plate format. At day 11, control samples were taken before a variety of treatments were started and further samples were taken in a time course over 48 hours. All chemicals were added from 1000x concentrated stock solutions (apart from NaCl or as otherwise indicated) directly to each well individually. RNA was extracted from each sample, quantified and 10µg of total RNA was run on a denaturing agarose gel. The gel was then subjected to Northern blotting and the membranes probed with ³²P radiolabelled DNA probes synthesised specifically by PCR for each gene. The blots were washed and the radiolabel visualised on a phosphorimaging system. Band intensities were quantified and normalised to the intensity of total RNA visible (Methylene blue stain) on each blot. The overall changes in response were calculated based on band intensities (normalised to the amount of RNA) and the responses normalised to the control level at time zero. Treatments included the addition of 20 µM t-zeatin, 5 µM kinetin, 5 µM of the auxin analog NAA (1-Naphthylacetic acid), 10 µM of the auxin transport inhibitor NPA (N-1-naphthylphthalamic acid), 10 µM of the auxin transport inhibitor TIBA (2,3,5-triiodobenzoic acid), 200 µM of the ethylene precursor ACC (1-aminocyclopropane-1-carboxylic acid), 5 µM of brassinolide and treatment with 150 mM sodium chloride in the growth medium. Figure 3-28 (A-D) summarises only the most relevant changes in transcript levels of *AtSlp1* and *AtSlp2* that were only observed with certain treatments. The treatments that are not included here did not result in clear reproducible response patterns and are therefore not presented. Overall, most of the experiments were done in triplicates, but only two out of the three Northern blots were finally used for the quantification in this figure. On the third set of data, the hybridised signal was either too weak or gave smears on the phosphorimager screen. It was not possible to quantify these signals properly. The NAA treatment was only done in duplicates, of which the second set could not be quantified for the given reason. The actual phosphorimager signals shown in figure 3-28 were always taken from one of the two replicates and might not necessarily always reflect accurately the changes as seen in the bar charts. These plots represent the results from a combination of two different blots.

The transcript levels of AtSlp1 were upregulated in response to treatment with 20 μ M t-zeatin (Figure 3-28A). The levels started to rise 2 hours after the hormone was added to the medium and peaked at the 8 hours time point (9-fold upregulation), however the standard deviation for the 4 and 8 hour time points are high. 48 hours after the addition, the levels had returned to their normal control levels. This response was observed with a similar temporary behaviour in all three blots and confirms the results from the eFP browser (see section 3.5.1.4), in which a 2-fold upregulation was found 3 hours after treatment. AtSlp2 gives a virtually identical transcript response to t-zeatin treatment, however the relative differences compared to the control are smaller (only 3-fold upregulation after 8 hours), and the standard deviation values are also very high for this sample. Thus the overall response is the same for both genes, but AtSlp1 is upregulated to a much larger extent.

Figure 3-28 (A) and (B) show the response to treatment with the auxin analog NAA. AtSlp1 (3-28 (A)) responds with a threefold increase in transcript levels 8 hours after the initial treatment and gradually returns to its starting values after 48 hours. This treatment was only performed in duplicates of which only one sample is shown and quantified. No estimate of standard deviation can be given and the extent of change seen in this particular experiment is probably not reproducible to the same level. AtSlp2 (3-28 (B)) gives a similar behaviour, but increases only by a factor of nearly 2 after 8 hours.

Treatment with the auxin transport inhibitor NPA (Figure 3-28 (B)) leads to a slight increase in AtSlp1 transcript (2-fold after 2 and 4 hours), but these samples have again high standard deviation values. AtSlp2 does hardly change in response to this chemical, considering the similarly high standard deviations. Overall there is a small early upregulation of AtSlp1 in response to NPA, but probably not of AtSlp2.

Figure 3-28 (C) shows the results obtained after treatment with 10 μ M TIBA. There is a clear pattern of upregulation of AtSlp1 at 4 and 8 hours after the start of this treatment, despite the high standard deviation at the 8 hours time point. The 4 hours sample shows that there is a 3-fold upregulation of the AtSlp1 gene, and there might be a 2-fold upregulation of AtSlp2. However, the high standard deviations throughout this sample indicate that the response is probably much smaller in this gene. Compared to the NPA response, the signal from the TIBA treatment rises 2 hours later and becomes only obvious at the 4 hours time point. Thus it seems that NPA evokes earlier transcript upregulation than TIBA.

Finally, the response to treatment with 150 mM NaCl was quantified and is presented in Figure 3-28 (D). In both genes there are only very subtle changes in transcript level. AtSlp1 increases slightly 8 hours after the plants were given salt, and AtSlp2 does not change at all to a significant extent as judged by the standard deviation values. Compared to the results published by the eFP browser from roots (Figure 3-26), the changes seen here are not as dramatic. However, the RNA used in these experiments originates from whole seedlings and does not accurately reflect differences that occur between roots and shoots. The response to salt stress seen in the microarray results was root specific and therefore probably not picked up in this Northern blot.

Overall these experiments reflect the main changes seen with the eFP browser data, despite the fact that only 2 replicates were used for these quantifications. The cytokinin t-zeatin indeed induces transcription of both Slps after 4 and 8 hours, but of AtSlp1 to a much larger extent. This behaviour represents definitely not an immediate response to this phytohormone and is more likely down to secondary effects that follow the cytokinin signal transduction cascade. The same is true for the response to auxin, where the peak of upregulation only occurs 8 hours after the initial signal uptake. NPA on the other hand seems to cause AtSlp1 upregulation already at the 2 hours time point, whereas TIBA also has later effects on transcription. These differences are probably down to the different modes of action of these two auxin transport inhibitors, or related to unspecific side effects. Both TIBA and NPA are known inhibitors of mechanisms affecting auxin efflux, but they also affect more generally trafficking processes (Geldner *et al.*, 2001). For the salt treatment it is hard to estimate when the actual upregulation occurs since the changes are only of minor nature and seem restricted mainly to AtSlp1.

Taking all these observations together, it appears that both Slp genes respond in a virtual identical pattern. The changes in AtSlp2 however are always smaller than in AtSlp1, which might also be explained by the lower overall expression level throughout seedlings. This identical response pattern is very likely connected to similarities on the genome level that are investigated in the next section.

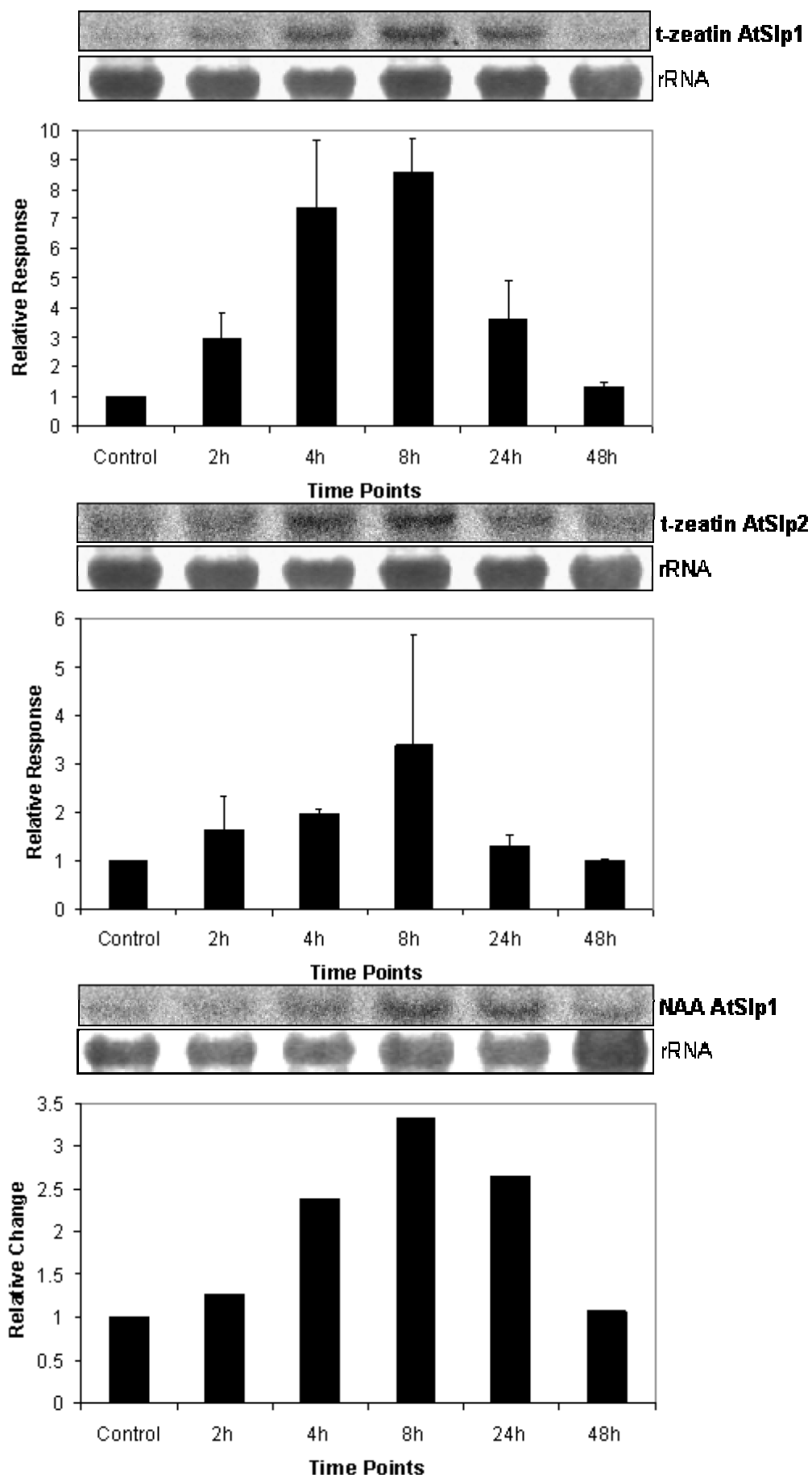


Figure 3-28 (A). Northern blots and quantified signals. The top lane (=phosphorimager signal) is labelled with the treatment and the gene-specific probe used for the hybridisation. The lane underneath shows the total RNA level loaded (=methylene blue stain) that was used for the quantification. The bar charts show the fold change in signal upon start of each treatment (normalised to the control at time zero). Error bars are standard deviations (n=2).

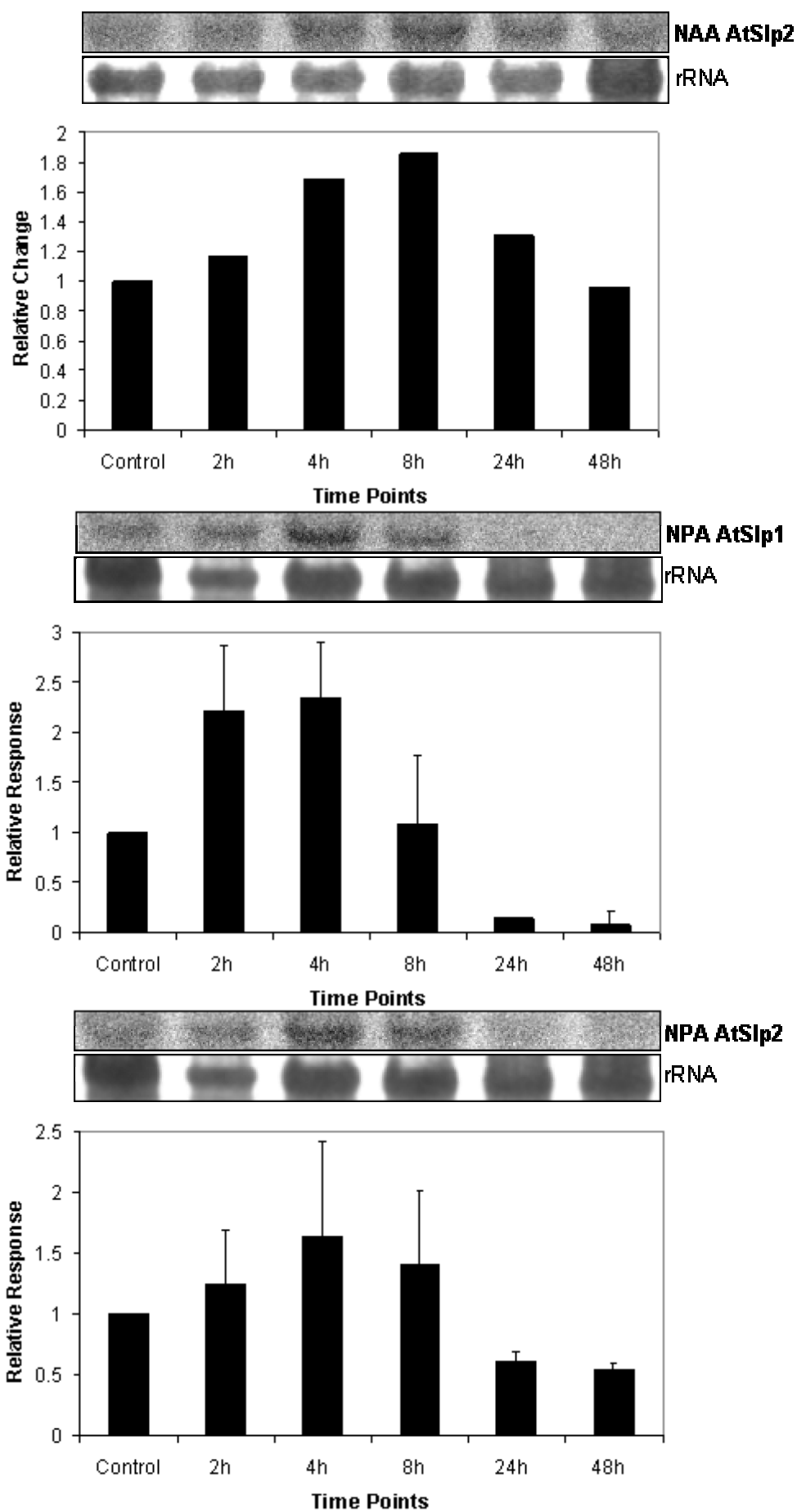


Figure 3-28 (B). 1-28 (A) Continued. Labelling is identical to (A). Where no error bars are plotted in the graph, the blot was only quantified once. The figure is continued on the next page.

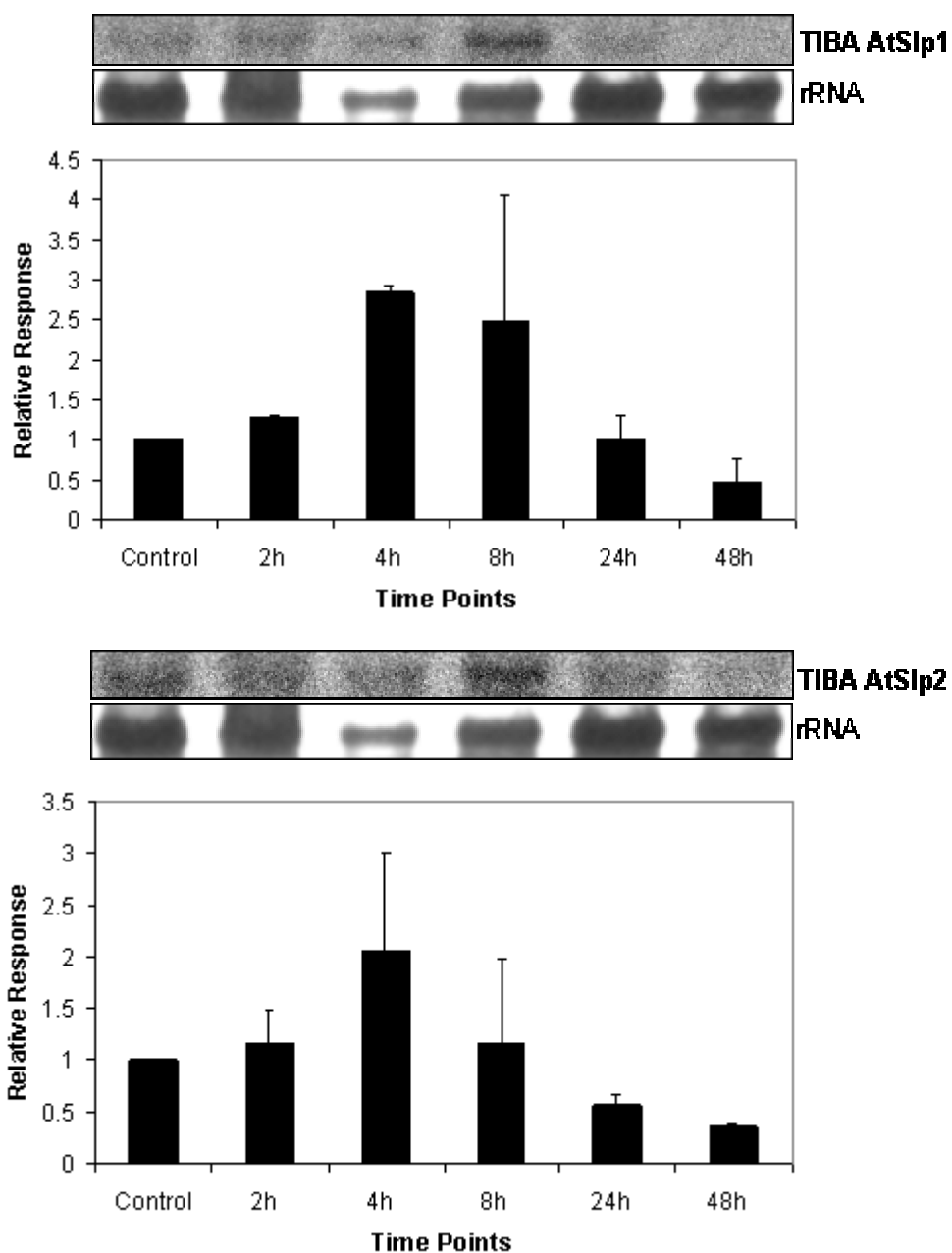


Figure 3-28 (C). 1-28 (B) continued. Treatment with 10 μ M TIBA. The actual signals from the phosphorimager screen are taken from one dataset only that was representative for the two sets used in the quantification. Labelling is as described before. The figure continues on the next page.

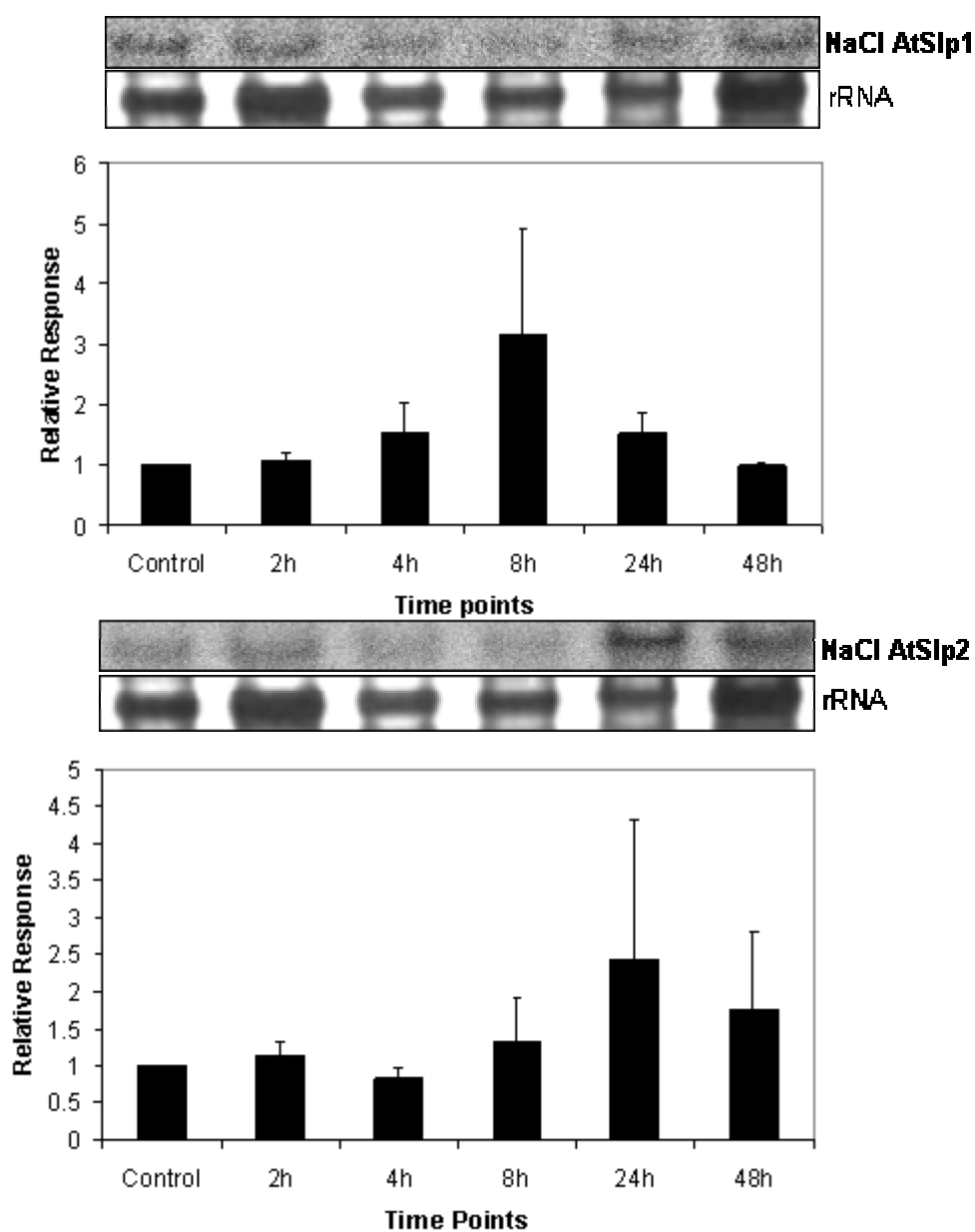


Figure 3-28 (D). Treatment with salt stress. This treatment was quantified from 2 replicates and only one phosphorimager signal is shown with the corresponding RNA blot picture underneath. The quantified bar chart does reflect the combined behaviour of the two different datasets and is therefore not necessarily showing the same behaviour as seen in the phosphorimager signal.

3.5.3 Analysis of AtSlp gene structures and promoter activities

In this section, the genome organisation around the AtSlp genes was investigated on Arabidopsis chromosomes 4 and 5. The actual gene structures of the two Slps were compared and their promoter sequences analysed for response elements. This comparison is followed by the determination of tissue-and development specific activation of AtSlp promoters using transgenic Arabidopsis plants that carry promoter-GUS fusion constructs. In the last part, the impact on promoter activation by various stress treatments was determined.

3.5.3.1 AtSlp genomic organisation

AtSlp1 (At4g27585) is localised on Arabidopsis chromosome 4 and AtSlp2 (At5g54100) on chromosome 5. Both genes are found on the antisense strands. To determine whether the two genes might have evolved through a gene duplication event, the AtSlp1 locus was queried against the Plant Genome Duplication Database (PGDD, (Tang *et al.*, 2008)). According to this database, the whole genomic surrounding of AtSlp1 on chromosome 4 was indeed duplicated and can be located on chromosome 5. AtSlp1 lies in a block of altogether 11 gene pairs on chromosomes 4 and 5 that arose from this gene duplication event. Figure 3-29 shows a subset of 7 gene pairs (labelled from 2-8) out of this block and their relative positions to each other on the chromosomes.

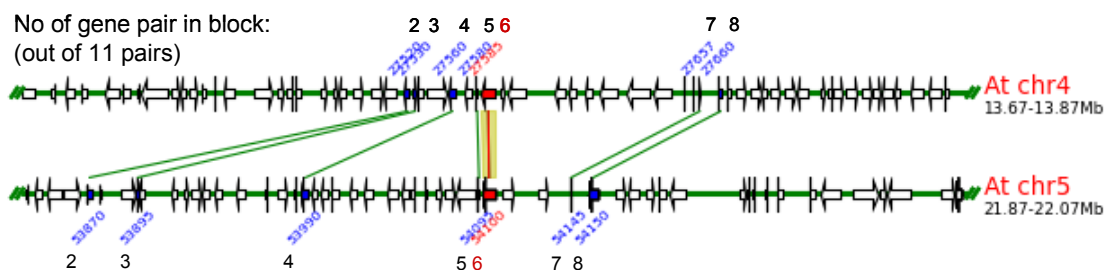


Figure 3-29. Gene duplication between Arabidopsis chromosomes 4 (At chr4) and 5 (At chr5). Shown are 7 gene pairs taken out of a block of 11 pairs. The numbers indicate the relative positions inside the block. AtSlp1 and AtSlp2 are in 6th position and are highlighted in red. This figure was downloaded from the Plant Genome Duplication Database (see text) result page when At4g27585 was used as a query. The relative positions within chromosomes 4 and 5 are indicated on the right side. The window for display was set to 100kbp.

Complementing this figure is Table 3-13 that gives detailed information about the 7 duplicated gene pairs from Arabidopsis (upper table). Querying the database with AtSlp1 for duplications amongst different plant species reveals that this area of Arabidopsis chromosome 4 is also found in the chromosomes of papaya (*Carica papaya*) and in 2 loci of poplar (*Populus trichocarpa*) (Table 3-13 lower part). In papaya, the duplicated region contains an even larger block of altogether 40 duplicated gene pairs in which a stomatin-like protein is in the 15th position. Two such areas are also found in the poplar genome, where At4g27585 matches 2 loci on chromosomes 12 and 15. The first locus contains a block with 15 gene pairs and the second one a block with 18 gene pairs. The gene pair containing AtSlp1 is the first one of each block. Remarkably, the database gives only hits for duplication from other dicotyledon species but not from monocots. This could indicate that this duplication event only happened after the evolutionary separation of monocotyledons and dicotyledons. Due to this duplication event in the Arabidopsis genome, AtSlp1 and AtSlp2 can be described as true paralogous genes within one species. Often, gene duplication is followed by further genomic shuffling that leads to increased variety between sequences. It would still be expected that the duplication event left many identical features within the genomic sequences of AtSlp1 and AtSlp2.

The gene duplication is also clearly reflected in the genomic structure of the AtSlp genes. Table 3-12 lists the total number of exons and introns of both genes, the length of the mRNAs and the open reading frames (ORF). The overall gene and mRNA sequence of AtSlp1 is longer than in AtSlp2, despite an additional exon present in the AtSlp2 sequence close to the 5'end. This extra exon gives rise to the unique elongated N-terminus of the AtSlp2 protein.

Name	AGI	mRNA length [bp]	No. exons	No. introns	Exons+Introns [bp]	ORF [bp]
AtSlp1	At4g27585	3199	9	8	2849	1236
AtSlp2	At5g54100	2756	10	9	2466	1206

Table 3-12. Genomic organisation of AtSlp genes. The table contains the length of the mRNA (=cDNA) transcribed from the gene, the total numbers of exons and introns, the length of the genes from the start to the stop codon (exons+introns) and the length of the open reading frame (ORF) in base pairs (bp). Source: TAIR.

Figure 3-30 gives a visual overview over the genes' organisation. The gene duplication is clearly visible between the exons and introns and indicated by dotted lines. All exons have been duplicated apart from exon 2 of AtSlp2. This exon must have evolved from a separate event. Exon 9 from AtSlp1 on the other hand is much longer than exon 10 from AtSlp2. This explains the elongated unique AtSlp1 C-terminus. The lengths of the 5'UTRs

(untranslated regions) are also different between the two genes. AtSlp2 has a much shorter 5' region than AtSlp1, whereas the 3'UTRs are almost identical in their lengths. Thus, the high level of similarity between AtSlp1 and AtSlp2 on the DNA and protein level is based on this duplication event. The individual protein parts originate from the genes' structures.

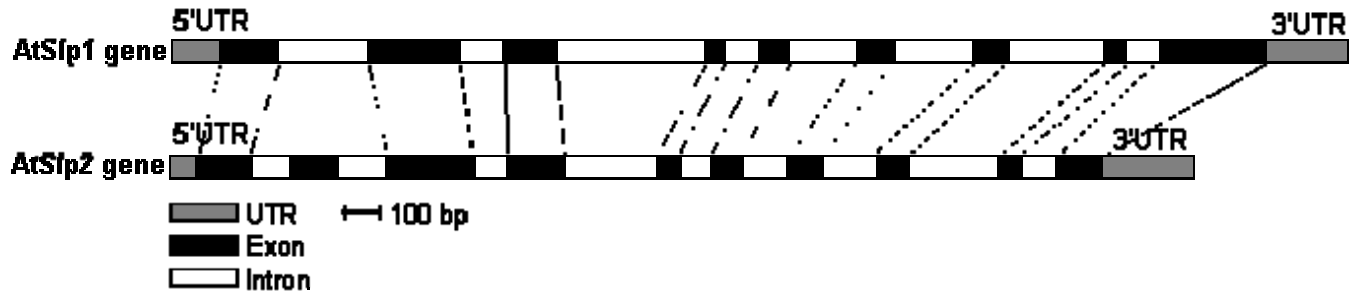


Figure 3-30. Genomic structures of the *AtSlp1* and *AtSlp2* genes. Exons are represented by black bars, introns by white bars and the untranslated regions (UTRs) at each end by grey bars. The whole figure is drawn to the same scale as indicated by the 100bp scale bar. Informatin source: TAIR.

Position in block	No. Genes in block	Locus 1	Annotation 1	Locus 2	Annotation 2	Ka	Ks
2	11	At4g27520	plastocyanin-like domain-containing protein	At5g53870	plastocyanin-like domain-containing protein	0.47	1.51
3	11	At4g27530	similar to unknown protein [Arabidopsis thaliana] (TAIR:AT5G53895.1)	At5g53895	similar to unknown protein [Arabidopsis thaliana] (TAIR:AT4G27530.1)	0.31	1.09
4	11	At4g27560	glycosyltransferase family protein	At5g53990	glycosyltransferase family protein	0.23	1.08
5	11	At4g27580	similar to unknown protein [Arabidopsis thaliana] (TAIR:AT5G54095.1)	At5g54095	similar to unknown protein [Arabidopsis thaliana] (TAIR:AT4G27580.1); similar to ribonuclease E [marine gamma proteobacterium HTCC2207] (GB:ZP_01223791.1)	0.27	0.68
6	11	At4g27585	Band-7 family protein	At5g54100	Band-7 family protein	0.15	0.6
7	11	At4g27657	similar to unknown protein [Arabidopsis thaliana] (TAIR:AT4G27652.1)	At5g54145	similar to unknown protein [Arabidopsis thaliana] (TAIR:AT4G27657.1)	0.15	1.63
8	11	At4g27660	similar to unknown protein [Arabidopsis thaliana] (TAIR:AT5G54150.1); similar to hypothetical protein MtrDRAFT_AC119415g5v1 [Medicago truncatula] (GB:ABE85158.1)	At5g54150	similar to unknown protein [Arabidopsis thaliana] (TAIR:AT4G27660.1); similar to hypothetical protein MtrDRAFT_AC119415g7v1 [Medicago truncatula] (GB:ABE85160.1)	0.49	2.66

15	40	At4g27585	Band-7 family protein	Cp0003g0176	NULL	0.21	1.38
1	15	At4g27585	Band-7 family protein	Pt12g0366	NULL	0.27	1.21
1	18	At4g27585	Band-7 family protein	Pt15g0018	NULL	0.31	1.03

Table 3-13. Genome duplication between Arabidopsis loci on chromosomes 4 and 5 (upper table) and between areas of Arabidopsis chromosome 4 and papaya (Cp) and poplar (Pt) loci (lower table). The areas that are duplicated in Arabidopsis chromosomes 4 and 5 contain 11 gene pairs and their relative position in the block is indicated in the left column. Locus 1 and locus 2 represent the duplicated genes. AtSlps are highlighted in red letters. Ka and Ks are computed parameters by the database. The lower table contains information about the duplication of even larger areas of Arabidopsis chromosome 4 within papaya and poplar. A block of 40 genes is duplicated between Arabidopsis and papaya, and 2 sets of blocks are found in poplar, one containing 15 gene pairs and the other 18 gene pairs. All information was obtained from the PGDD database (see text).

3.5.3.2 Response elements in the AtSlp promoter sequences

The upstream sequences of At4g27585 and At5g54100 were analysed with the Athena software (O'Connor *et al.*, 2005) for promoter response elements (Tables 3-14). Each hit was further analysed with the AtCisDB (*Arabidopsis thaliana* Cis-element database, (Palaniswamy *et al.*, 2006) or with the PLACE (Plant Cis-acting regulatory DNA elements, (Higo *et al.*, 1999) database to obtain more detailed information about specific transcription factors or response elements. An area of 1225 bp of the 5' upstream sequence (away from the start codon) was analysed for AtSlp1, and 1814 bp of upstream sequence for AtSlp2. The AtSlp1 promoter sequence contains a total of 12 different known motifs and the AtSlp2 promoter 26 different elements on both strands. Out of this number, 9 elements are found in both promoters (highlighted in grey in Table 3-14) and 3 of these (red lettering) have the same relative position away from the start codons. Remarkably, the AtSlp2 promoter sequence is longer but also contains a bigger variety and density of elements than the Slp1 sequence. Out of these elements, most are binding sites for transcription factors that are involved in a variety of stress responses and in development. For example, the Myb1AT and the Myc binding sites have been linked to drought stress response, whereas other sites are putatively involved in light signalling (eg the I-box promoter motif and the Myc2 binding sites). Interestingly and with respect to the known AtSlp tissue expression (see section 3.5.1.1), the CARGCW8GAT motif, which binds transcription factors of the MADS type, is involved in development of flowers. It is not yet known which transcription factor binds to the T-box promoter motif that is also located in the same relative position in both sequences, but this motif was previously linked to light-mediated transcription initiation (Chan *et al.*, 2001). Other common motifs between the two promoters bind the Myb4 transcription factor (Chen *et al.*, 2002). This binding motif has been associated with a variety of effects such as cell cycle control, development and secondary metabolism. In lots of cases, the transcription factors that actually bind to the motifs have not been determined yet and clues towards their function are mainly derived from few very specified examples in which a known gene contains one of these motifs. The AtSlp1 promoter sequence does contain two motifs that are not found in the Slp2 promoter. One of these motifs (GAREAT) is a putative GA responsive element and has been linked to a role in seed germination. This gives further support for the strong upregulation of this gene seen in imbibed seeds (section 3.5.1.3). One of the other two unique elements found in this sequence might simply act as an enhancer element (SV40 core motif). The Rav1B motif is known to bind transcription factors of the ABI3VP type (Kagaya *et al.*, 1999), but an exact function for these proteins has not been established so

far. The AtSlp2 promoter has some interesting unique binding elements that are not shared between the two sequences. Amongst these are several sites important for hormone signalling transduction. An Arf1 binding site (Ulmasov *et al.*, 1999) that interacts with an auxin response factor is located ca. 1700 bp upstream of the start codon. The Bellringer binding site motif (Bao *et al.*, 2004) interacts with a transcriptional repressor that has important roles in inflorescence development. Notably, many other of the unique AtSlp2 promoter elements are linked to both plant defense reactions or flower development. For example, the G-box elements, the W-box motifs, the Myb1 response elements and the DPBF 1 and 2 binding sites are all involved in pathogen defense responses. The leafy binding site (Lamb *et al.*, 2002) and the DREB1A motif that binds transcription factors of the AP2- EREBP family (Riechmann & Meyerowitz, 1998) are both regulating inflorescence development amongst other roles (see Table 3-14 second part).

Overall, both promoters have common elements that mediate stress responses or are activated by light signals, control flower development and are involved in pathogen defense responses. The AtSlp2 promoter has a larger variety of these response elements and its activation or repression might therefore be more tightly controlled. The distribution and the kinds of elements found in these promoters suggest that AtSlp gene expression is important for reproductive development and responses to environmental stimuli.

Promoter	Element and Position	Strand	TF Family	Function	Database
AtSlp1	SV40 Core promoter motif (-39->-32)	antisense	N/A	Enhancer	AtCisDB
	Myb4 binding site (-45->-39, -136->130)	sense	Myb	Cell cycle control, secondary metabolism, development	AtCisDB
	lbox promoter motif (-70->-65)	sense	N/A	Light response	AtCisDB
	Myb1AT (-221->-216)	antisense	Myb	Drought response	PLACE
	Myb1AT (-452->-447)	sense	Myb	Drought response	PLACE
	Rav1B binding site (-320->-315)	sense	ABI3VP1		AtCisDB
	TATA box motif (-434->-429)	antisense	N/A		AtCisDB
	TATA box motif (-508->-503)	sense	N/A		AtCisDB
	TATA box motif (-1200->-1195)	antisense	N/A		AtCisDB
	AtMyc2 binding site (-731->-726)	antisense	bHLH	Photoreceptor signalling?	AtCisDB
	MYCATERD1 (-731->-726)	sense	Myc	Water stress	PLACE
	Dre core motif (-791->-786)	antisense	N/A		Literature
	CARGCW8GAT (-821->-812)	sense	MADS	Flower development	PLACE
	CARGCW8GAT (-821->-812)	antisense	MADS	Flower development	PLACE
	T-box promoter motif (-992->-987)	sense	N/A	Light-induced transcription	AtCisDB
	GAREAT (-1030->-1024)	antisense	N/A	GA responsive (germination)	PLACE

Table 3-14. Promoter response elements found in the 1225 bp upstream sequence of the AtSlp1 gene. The table continues overleaf for the AtSlp2 gene (1814 bp of upstream sequence analysed). The response elements were located with the Athena software that is linked to the AtCis (Agris) and to the PLACE databases. Further information about the transcription factor families was obtained from the AtTF database or through links from Athena to PLACE. The positions given refer to numbers (in bp) upstream of the start codons. Highlighted in grey are response elements that are shared between the AtSlp1 and AtSlp2 promoter sequences. Elements written in red are shared elements found in the same relative positions to the start codons. The elements found on the antisense strands are located in the same orientation as the genes. Several elements occur more than once in each sequence on both strands and are therefore listed multiple times. For the initial search with the Athena software the output window was set to the cartoon display and 2000 bp of upstream sequence.

Promoter	Element and Position	Strand	TF Family	Function	Database
AtSlp2	W-box promoter motif (-62->-57, -931->-926)	antisense	WRKY	Pathogen defense, senescence, trichome formation	AtCisDB
	W-box promoter motif (-124->-119)	sense	WRKY	Pathogen defense, senescence, trichome formation	AtCisDB
	lbox promoter motif (-152->-147, -1264->-1259)	sense	N/A	Light response	AtCisDB
	lbox promoter motif (-253->-248)	antisense	N/A	Light response	AtCisDB
	TELObox promoter motif (-183->-175)	antisense	N/A		AtCisDB
	AtMyc2 binding site (-237->-232, -266->-261)	sense			AtCisDB
	AtMyc2 binding site (-264->-259, -1168->-1163)	antisense	bHLH	Photoreceptor signalling?	AtCisDB
	MYCADERD1 (-237->-232, -266->-261)	antisense	Myc	Water stress	PLACE
	MYCADERD1 (-264->-259, -1168->-1163)	sense	Myc	Water stress	PLACE
	TATA box motif (-342->-337, -600->-595, -780->-775, -1510->-1505, -1591->-1586, -1608->-1603)	antisense	N/A		AtCisDB
	TATA box motif (-1606->-1601, -1308->-1303)	sense	N/A		AtCisDB
	CCA1 binding site motif (-405->-398)	antisense	Myb related		AtCisDB
	Myb4 binding site (-480->-474, -484->-478)	sense	Myb	Cell cycle control, secondary metabolism, development	AtCisDB
	Myb4 binding site (-1418->-1412, -1464->-1458, -1468->-1462, -1476->-1470)	antisense	Myb	Cell cycle control, secondary metabolism, development	AtCisDB
	Myb3 binding site (-481->-474, -485->-4478)	sense	Myb	Cell cycle control, secondary metabolism, development	AtCisDB
	Myb1LEPR (-480->-474, -484->-478)	antisense	N/A	Plant defense	PLACE
	Myb1LEPR (-1476->-1470)	sense	N/A	Plant defense	PLACE
	Myb2AT (-500->-495, -660->-655)	sense	Myb	Water stress	PLACE
	CARGCW8GAT (-858->-849, -990->-981, -1276->-1267, -1549->-1540)	sense	MADS	Flower development	PLACE
	CARGCW8GAT (-858->-849, -990->-981, -1276->-1267, -1549->-1540)	antisense	MADS	Flower development	PLACE
	T-box promoter motif (-998->-993)	antisense	N/A	Light-induced transcription	AtCisDB
	BoxII promoter motif (-1176->-1171)	sense	N/A		AtCisDB
	Dre core motif (-1223->-1218)	antisense	N/A		Literature
	Dre core motif (-1203->-1198)	sense	N/A		Literature
	DREB1A/CBF3 motif (-1223->-1216)	sense	AP2-EREBP	Flower development, leaf epidermis, stress response	AtCisDB
	Myb binding site promoter (-1468->-1461)	antisense	Myb	Cell cycle control, secondary metabolism, development	AtCisDB
	Myb1AT (-1470->-1465, -1478->-1473)	antisense	Myb	dehydration responsive	PLACE
	AtMyb2 binding site (-1478->-1472)	antisense	Myb	Cell cycle control, secondary metabolism, development	AtCisDB
	G-box binding site (CACGTGmotif) (-1642->-1637)	sense	N/A	Defense related gene expression	PLACE
	G-box binding site (CACGTGmotif) (-1642->-1637)	antisense	N/A	Defense related gene expression	PLACE
	Bellringer/replumless/pennywise BS1 IN AG (-1057->-1050)	sense	Homeobox	Inflorescence development, ABA response	AtCisDB
	ATB2/AtbZIP53/AtbZIP44/GBF5 binding site in ProDH (-398->-393)	sense	bZIP	Pathogen defense, light signalling, stress response, seed maturation, flower development	AtCisDB
	ARF1 binding site motif (-1742->-1737)	antisense	ARF	Auxin response factor	AtCisDB
	DPBF1&2 binding site motif (-208->-202, -241->-235, -270->-264, -1172->-1166, -1391->-1385)	sense	bZIP	Pathogen defense, light signalling, stress response, seed maturation, flower development	AtCisDB
DPBF1&2 binding site motif (-1646->-1640)	antisense	bZIP	Pathogen defense, light signalling, stress response, seed maturation, flower development	AtCisDB	
LFY consensus binding site motif (-320->-315, -1541->-1536)	sense	LFY	Flower meristem identity	AtCisDB	

3.5.3.3 AtSlp tissue expression pattern- transgenic promoter-GUS fusion plants

To determine in which parts of the plant the Slp promoters are activated and therefore the proteins probably expressed, different promoter sequences were cloned from genomic DNA and fused to a GUS (β -glucuronidase) reporter gene (Jefferson, 1989) inside the pCAMBIA 1301 (www.cambia.org) vector. Figure 3-31 gives an overview over the genomic surroundings of both Slp genes and the sequences chosen as promoters displayed in red. For the AtSlp1 promoter, 2989 base pairs upstream of the start codon were amplified from genomic DNA by PCR and cloned into the pDRIVE cloning vector (Qiagen). This sequence covers the complete distance between At4g27585 and the next upstream gene on the same strand, At4g27595. It also includes a complete gene on the opposite strand (At4g27590). For the AtSlp2 promoter, 1989 base pairs were amplified and ligated into the same vector using the 3' adenine overhangs created by the Taq polymerase. This sequence covers the longest possible upstream sequence that does not contain an NcoI restriction site for easy cloning into the pCAMBIA vector. It also includes the 5'UTR and a part of the last exon of a gene on the complementary strand (At5g54110). Both cloned sequences contain all the promoter elements described in Tables 3-14.

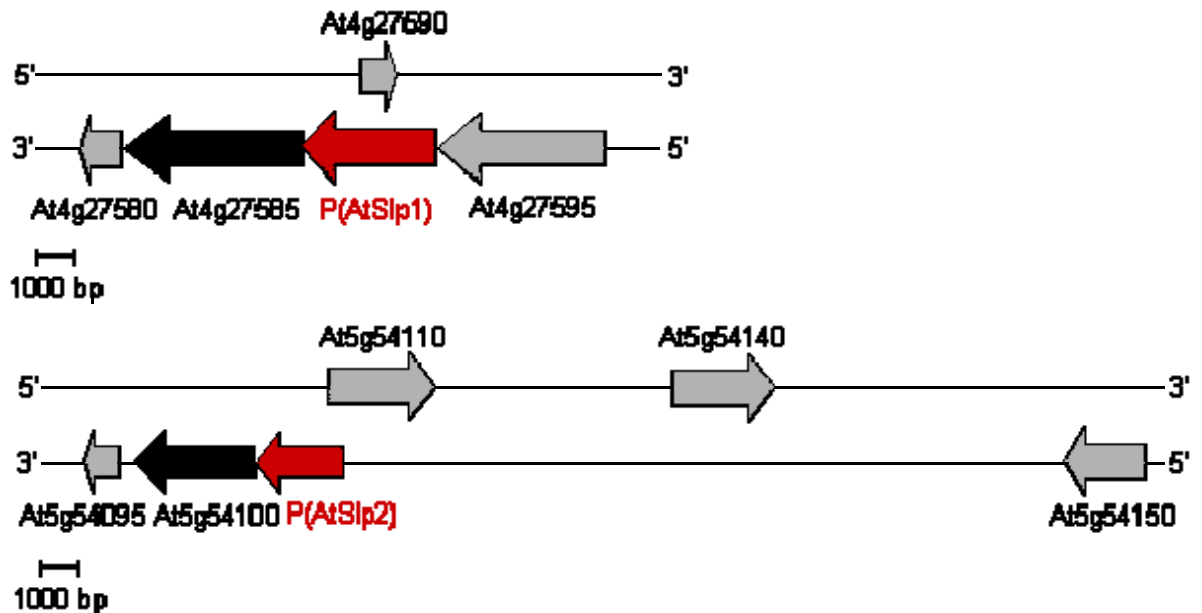


Figure 3-31. Genomic surrounding of AtSlp1 and AtSlp2 genes (black arrows) with the cloned promoters shown as red arrows. Surrounding genes are shown as grey arrows. The AtSlp1 promoter spans a region of 2989 bp upstream of the start codon and includes a complete gene on the opposite strand (At4g27590). This promoter sequence covers the complete genomic sequence that lies between AtSlp1 and the gene in front, At4g27595. The AtSlp2 promoter sequence is 1989bp long and includes the 5'UTR and stretches into the last exon of At5g54110. This length was chosen because it is the longest part that does not include an NcoI site and was therefore easily fused to the GUS gene in pCAMBIA 1301. The distance between At5g54100 and the next upstream gene on the same strand is ca. 20kbp. The figure reflects the true distances and gene lengths as obtained from TAIR. The scale bar represents 1000bp length. The whole figure is drawn to this scale.

The promoter insertions were verified by sequencing and further amplified with primers that contained additional restriction sites (*Pst*I and *Nco*I). These sites were used for ligation into pCAMBIA 1301 to create the GUS fusions. The start codon for the GUS expression is localised within the *Nco*I restriction site. Figure 3-32 shows a schematic presentation of the final T-DNA created by this fusion. The GUS gene inside this vector consists of two exons that are separated by a catalase intron to avoid expression in bacteria during the cloning procedures.

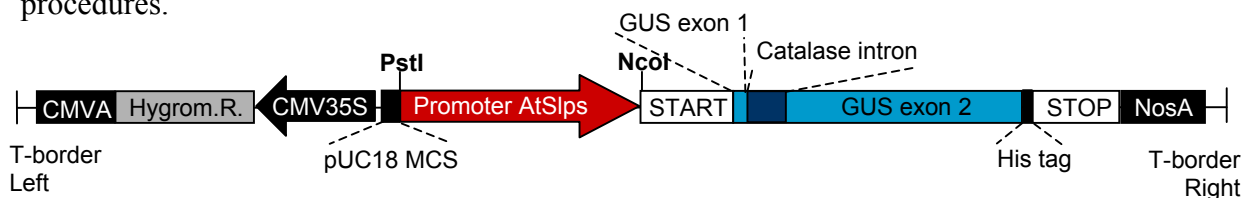


Figure 3-32. Schematic presentation of the AtSlp promoter-GUS fusion constructs inside pCAMBIA 1301. The AtSlp promoter sequences (red arrow) were cloned using the *Pst*I site of the pUC18 multiple cloning site (MCS) and *Nco*I that contains the ATG codon of the GUS reporter gene. The GUS gene in this vector lies in frame with a 6xHis tag before the stop codon. The T-DNA also contains a hygromycin resistance (Hygrom.R.) gene for plant selection. Abbreviations are: CMVA (Cauliflower mosaic virus poly A), CMV35S (Cauliflower mosaic virus 35S promoter), START (start codon), STOP (stop codon), NosA (Nopaline synthase poly A).

These constructs were transformed into *Agrobacterium tumefaciens* (strain GV3101) and used for stable transformation of Arabidopsis wild type plants (Col-0). Hygromycin resistant plants were selected and further propagated until the second generation (T2). A series of transgenic plants for both constructs was grown under long day light conditions (16 hours light, 8 hours dark) either in liquid MS medium supplemented with 0.5% sucrose, on MS agar plates or on soil and harvested as a whole for GUS staining reactions. Plants were assayed at different developmental stages from each growth condition. Figures 3-33 to 3-35 are a selection of images from transgenic plants carrying the AtSlp1 promoter-GUS fusion construct and Figures 3-36 to 3-37 are images taken from AtSlp2 promoter GUS fusion plants. Details about age and growth condition of each image are given in the figure legends. Overall, the tissue distribution pattern between the AtSlp1 and the AtSlp2 promoter activities are virtually identical. Both promoters are active at high levels just after germination and in very young seedlings (2 and 3 days old, Figure 3-33 A and B, Figure 3-36 A). The GUS stain is mainly localised to the cotyledon tissues and in the hypocotyls. Once the radicle has elongated, GUS stain is also visible inside the seedling roots (1-33 B). No stain localised to the root tip was observed with either construct. When the seedlings are older (10 days, Figure 3-33 C), the stain is mainly localised to vascular tissue in the stem, leaves and roots. The stain is strongest in the stem. At this stage (13 days old) and when grown in liquid medium, leaves also have intense GUS stain in stipules at the base of the growing rosette (1-33 D) and in hydathodes (1-33 E

and 1-36 D). The very prominent stain in stipules was also observed in plants grown on soil and on plates and is a feature that occurs with both constructs (1-36 B and C). The AtSlp1 promoter was also active in guard cells (Figure 3-33 F-G, 21 days old), but only when the plants were grown submerged in liquid medium. This staining type was never observed on plants that were grown in air on soil. An example of a GUS-stained leaf from a soil-grown plant (34 days old) is shown in Figure 3-33 H. In mature plants grown under this condition, the stain is still mainly localised to the vasculature tissue throughout the plant in leaves, the stem and in roots. A 20 days old plant is pictured in Figure 3-34 A for the AtSlp1 promoter and in Figure 3-36 B and E for the AtSlp2 promoter. The overall stain is rather weak for both constructs in these plants and specifically localised to only few tissues. Both constructs give stronger staining intensity inside the emerging inflorescence stem (1-34 B and 1-36 E), which is probably localised inside or around the shoot vasculature. Leaves from mature GUS-stained plants from the AtSlp1 promoter fusion construct were sectioned in a cryomicrotome. They were mounted in embedding resin, frozen and 20-40 μ m thick sections prepared. These were collected and mounted in a water-based reagent (Aquatex) prior to imaging on a light microscope. However, all the sections prepared were of low quality because of smearing effects caused during the cutting. An example of a 40 μ m leaf cross section is presented in Figure 3-34 C. It is difficult to localise specific staining from this image, but most of the GUS stain is probably associated within the vascular tissue, but also in the surrounding cells. Further attempts to obtain clean sections were not made.

Examples of two very mature whole rosettes (36 days old) from each construct are shown in Figure 3-34 D (AtSlp1) and 1-36 H (AtSlp2). The staining pattern looks identical and is mainly associated with vascular tissue in the leaves. Weak staining in roots was observed for AtSlp1 (Figure 3-34 F). More prominent root stain was observed in younger plants of the AtSlp1 construct grown on soil (23 days old) in the root vasculature. In the shoot tissue after flower transition, AtSlp1 promoter driven GUS stain was observed mainly in emerging inflorescence buds and around them in the stem at the point of branching (Figure 3-34 G, 36 days old plant grown on soil). Emerging buds were also stained with the AtSlp2 promoter construct (Figures 3-36 F and G, 23 and 38 days old respectively), especially inside the developing flowers. Curiously the AtSlp2 promoter GUS fusion plants also showed defined spots of high GUS stain intensity at the branch points along the stem (see Figure 3-36 I red arrowhead). The strongest staining patterns were observed for both promoter constructs inside flowers. The stain was clearly localised to pollen grains from various flower stages.

Figure 3-35 A-D gives several examples for inflorescence stain patterns obtained with the AtSlp1 promoter construct. Images A and B are from 23 days old soil-grown plants, and images C and D from 34 days old plants. Image A shows flowers at a fairly young stage with very prominent stain inside the anthers. Picture B shows a fertilised opened flower with an emerging silique where GUS stain is localised at the bottom, and also at the bottom of the stigma. Image C is a magnified part of image D of a fertilised flower with attached pollen grains. The pollen grains still attached to the anthers are heavily GUS stained. Very similar pictures can be seen with the AtSlp2 promoter GUS construct. Figures 3-37 A-D are all taken from flowers of 34 days old soil-grown plants. Image A shows a fertilised flower with heavily stained pollen grains and some stain located on the stigma tissue. Image B is a magnification of a similar flower that clearly shows stained pollen grains but hardly stain on the papillae. Instead, it is probably the underlying pistil/stigma tissue that has some blue stain. Picture C is a magnification of anthers with pollen grains. It is clearly visible that the anthers itself are not stained in contrast to the pollen grains. Image D shows a growing silique with the same staining pattern as seen in Figure 3-35 B. The growing tip and the bottom are GUS stained, whereas the middle part containing the ovaries is unstained.

In summary, both AtSlp promoters drive GUS expression in the same tissue types throughout development. The promoters are more active in young seedlings than in leaves of mature plants. Flowering plants have high promoter activity in pollen grains but not in other parts of the inflorescence. There are only minor differences between the two promoters. In particular, the guard cell stain seen with the AtSlp1 promoter construct in liquid-grown plants has not been observed (or was too weak to be visible) in the AtSlp2 promoter plants. In plants grown on soil this guard cell stain was never observed, even when the plants were kept under a propagator to keep the humidity conditions high. It was also notable that general staining in liquid MS medium supplemented with 0.5% sucrose was much stronger compared to growth conditions in air. This might be down to the extreme humidity conditions or linked to the transpiration state under these growth conditions. Whatever the exact reason is, both AtSlp promoters are induced under these conditions. The AtSlp1 promoter gives overall higher GUS expression than the AtSlp2 promoter. This is probably not linked to the different length but due to the individual response elements located in these sequences. It is therefore likely that AtSlp1 is the higher expressed Arabidopsis stomatin-like protein.

These observations agree in some, but not all aspects with the microarray data from the eFP browser. The strong stain in pollen is also seen in the microarray experiments (Figure

3-23), but these predict only expression in the developing pollen grains, and no expression in mature pollen. What is stained in these GUS stains are probably pollen grains from all stages. The eFP browser also predicts high expression in the ovaries and other flower parts, which are not seen in the promoter-GUS fusion plants. For seedlings, the eFP browser indicates the strongest expression in the radicle, followed by the hypocotyls and the cotyledons (Figure 3-22). The opposite picture is seen in these stains. The strongest stained parts of the seedling are the cotyledons followed by the hypocotyls and only weak or no stain in the radicle (Figure 3-33 and 1-36). The eFP browser also suggests strong stain in the shoot apex, but this was not observed in these experiments. The majority of stain seen in leaves and roots was clearly associated with vascular tissue. Neither in the stem nor in the roots did the eFP browser data show high transcript levels (Figure 3-23) that originate from the xylem/cork or root stele tissues. Instead the highest expression levels are predicted in the epidermis and atrichoblasts, which cannot be confirmed by the promoter-GUS stains. The eFP expression levels in leaves of a growing rosette agree with the observed stains. More stain is seen in early leaves than in later ones. Between the root and the leaves, the GUS stains indicate higher overall expression in the leaves in agreement with the eFP browser (Figure 3-22). The staining pattern of these promoter-GUS fusion plants does correspond roughly with the microarray data, but seems different in some details. These are two very different approaches with very different sensitivities for the investigation of the tissue expression pattern and can only be compared on a crude level. Additionally, both approaches do not reflect the true situation on the protein level. This aspect is the topic in section 3.5.4.

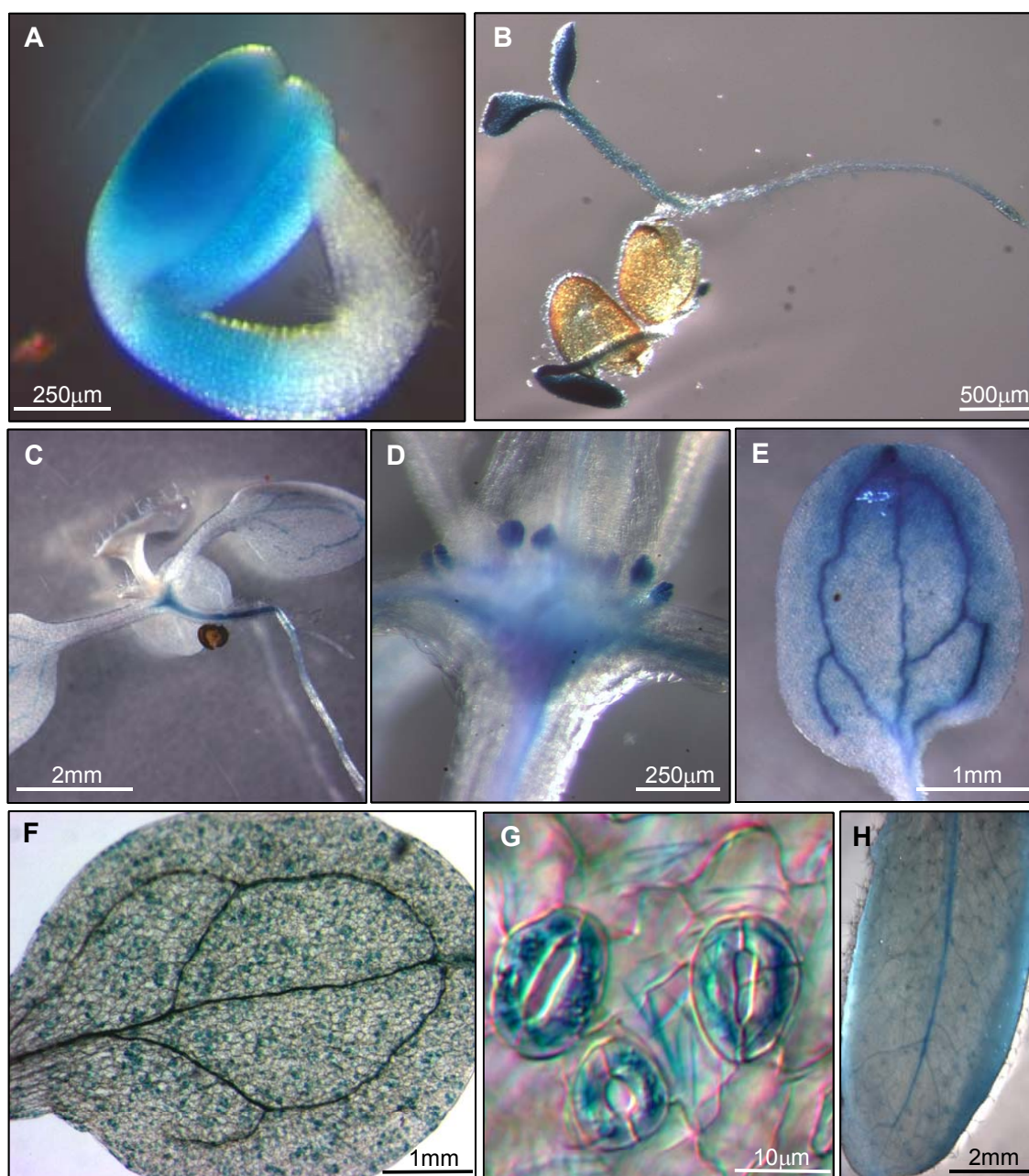


Figure 3-33. AtSlp1 promoter-GUS fusion stains. Plants were grown either in liquid 0.5x MS medium with 0.5 % sucrose, on agar plates containing 0.5x MS and 0.5 % sucrose, or on soil under long day light (16 h light, 8 h dark).

A) 2 days old seedling grown in liquid medium.

B) 3 days old seedling grown in liquid medium.

C) 10 days old seedling grown on an agar plate.

D) and E) Details from 13 days old seedling from liquid medium.

F) and G) leaves from 21 days old plants grown in liquid medium.

H) Leaf from 34 days old plant grown on soil. All scale bars represent the distance written in each picture.

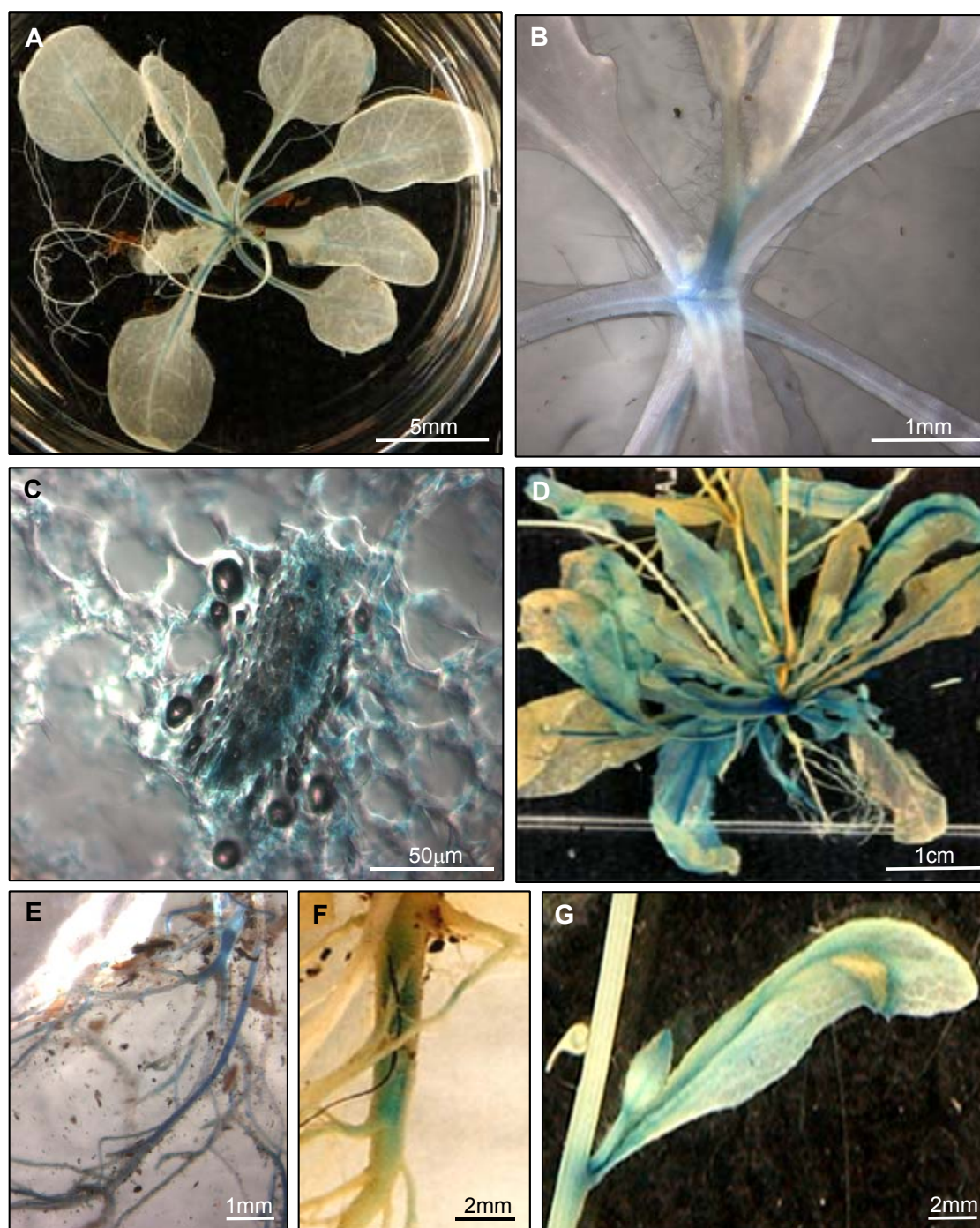


Figure 3-34. AtSlp1 promoter-GUS fusion stains from more mature plants. Growth conditions were as described in Figure 3-34.

A) 20 days old plant from soil

B) and C) 23 days old soil-grown plant and 40µm thick cross section from a leaf

D) Rosette from a 36 days old plant grown on soil

E) Roots from a 23 days old soil-grown plant.

F) and G) Root and branch from a 36 days old plant grown on soil.

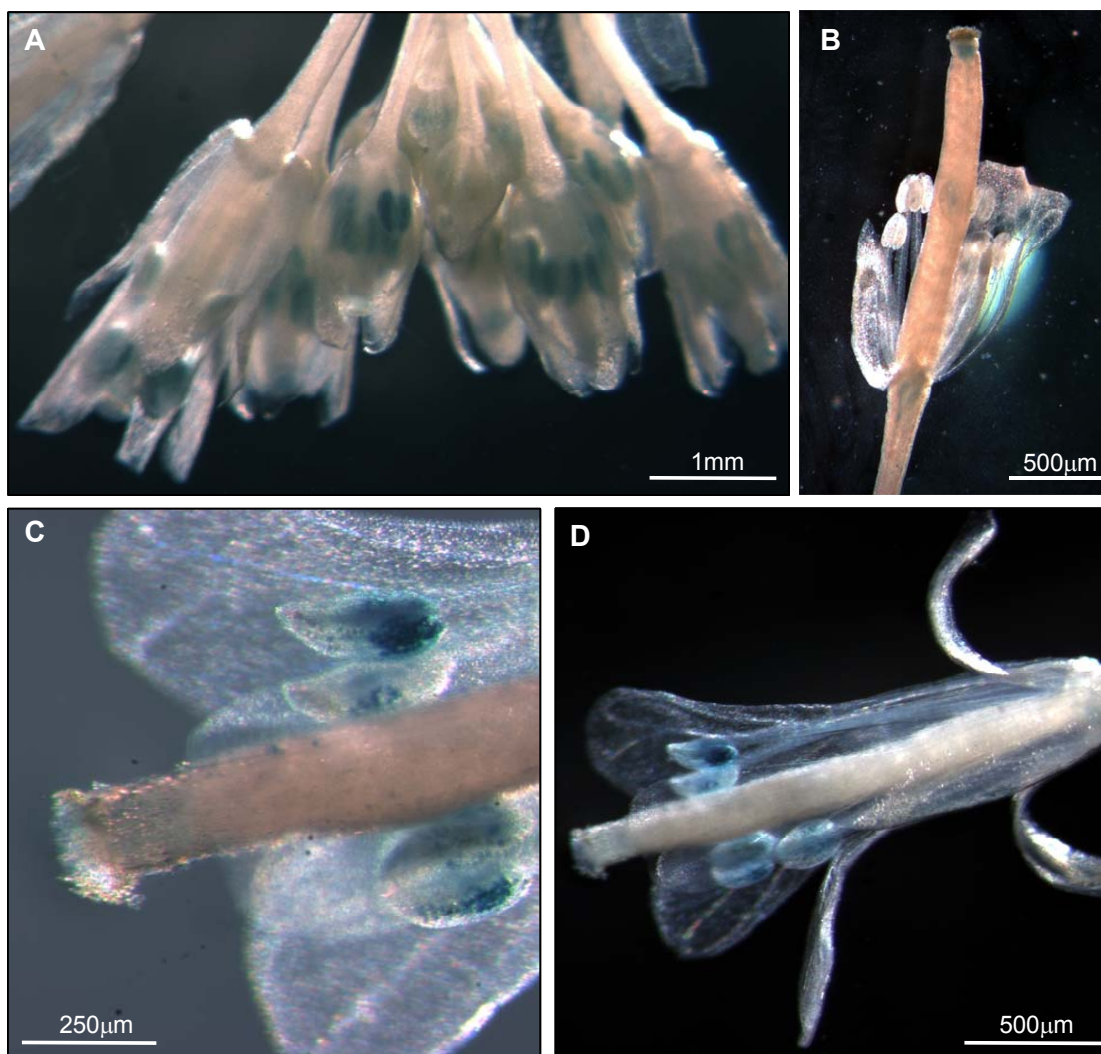


Figure 3-35. Inflorescence organs from *AtSlp1* promoter GUS stained plants. Growth conditions are as described above.

A) and B) Whole flowers from 23 days old soil-grown plants.

C) and D) Flower details from 34 days old soil-grown plants.

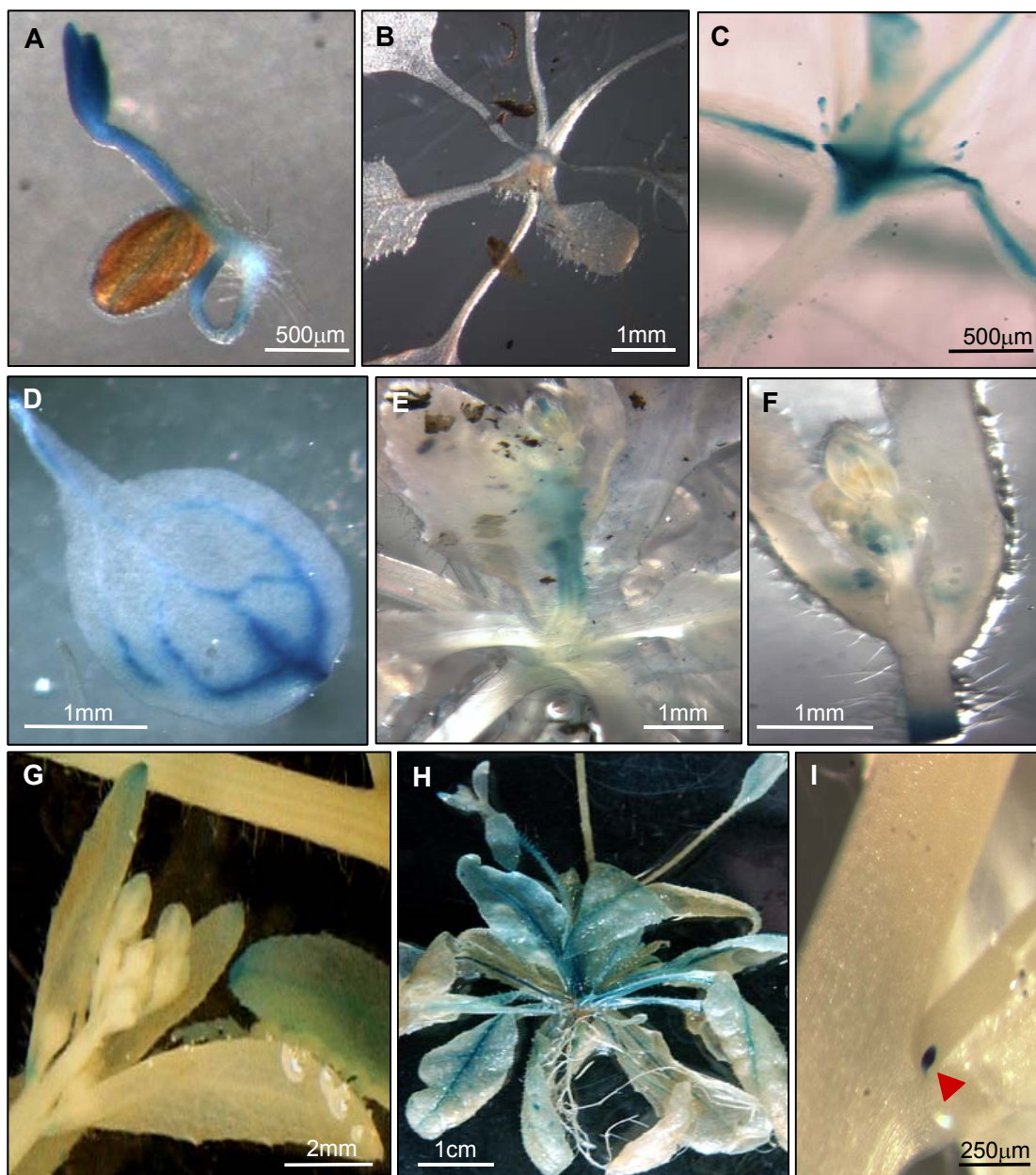


Figure 3-36. GUS stained plants carrying the AtSlp2 promoter construct. Growth conditions are as described before.

A) 3 days old seedling grown in liquid MS medium.

B) Rosette from 13 days old plant grown on soil.

C) and D) Details from a 13 days old seedling grown in liquid MS medium.

E) and F) Inflorescence stem and rosette details from 23 days old soil-grown plants.

G) and H) Inflorescence and rosette from a 38 days old plant grown on soil.

I) Stem and branch from a 34 days old soil-grown plant. The red arrowhead marks the GUS-stained blue spot at the branching point.

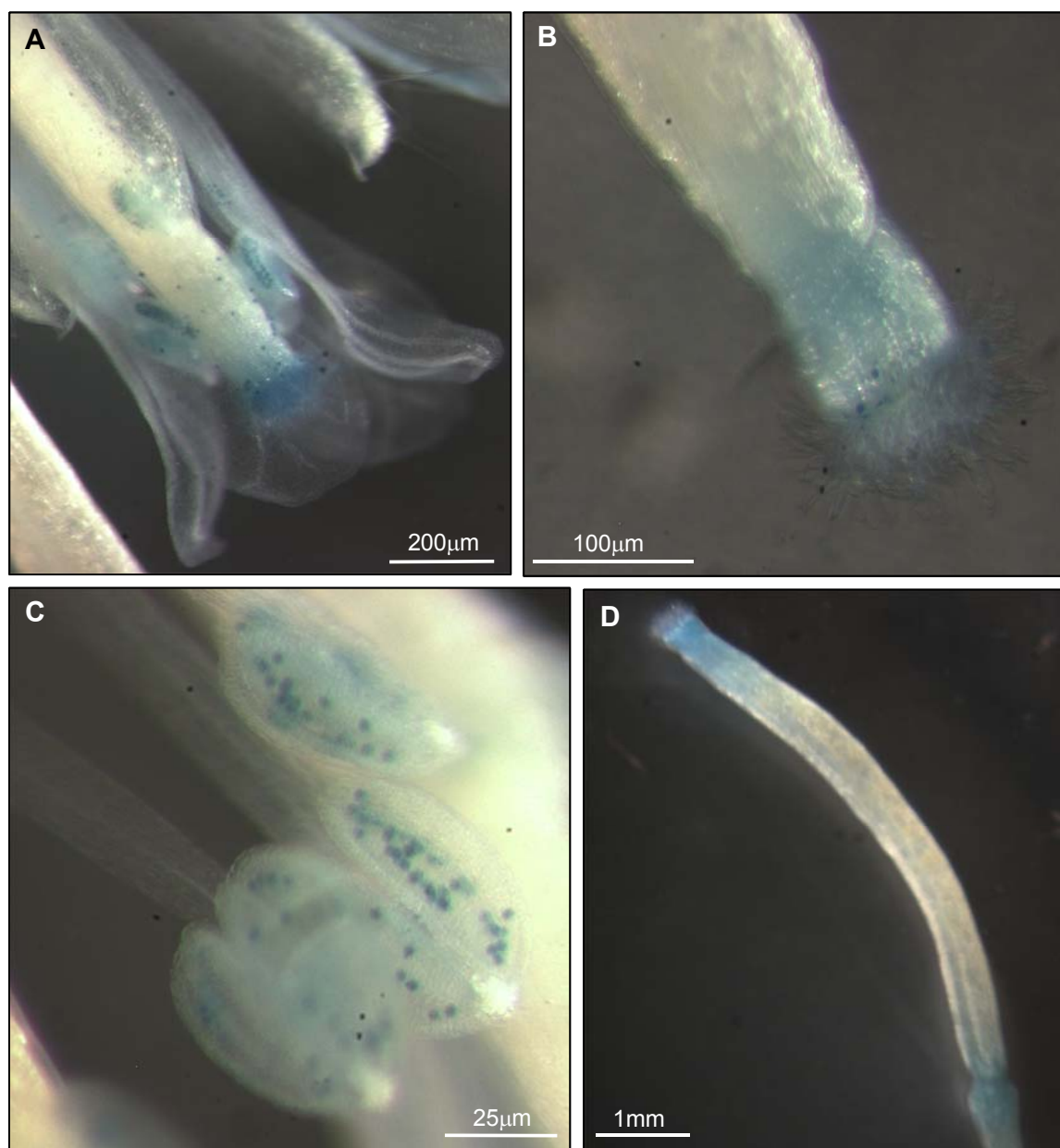


Figure 3-37. Inflorescence details from *AtSlp2* promoter-GUS fusion plants. All images are taken from 34 days old plants grown on soil.

A) Fertilised flower with stained pollen and stigma.

B) Magnification of the stigma tissue.

C) Anthers with stained pollen grains.

D) Growing silique with stigma and ovaries.

3.5.3.4 Stress and hormone treatments of promoter-GUS fusion plants

To complement the data from section 3.5.2 on transcription changes seen after stress treatments, the transgenic promoter-GUS fusion plants were grown in the same fashion and treated with the same reagents or stresses. Five seeds of each line were sown into 24 well tissue culture plates each containing 1ml volume of half strength MS medium supplemented with 0.5% sucrose. The plants were grown for 10 days while rotating at 50 rpm under long day light conditions. On day 11, treatments were commenced by adding hormones straight into the medium of an individual well or by transferring seedlings into fresh medium on a new plate for treatments with cold or irradiation with UV-B light. After 8 hours, the seedlings were harvested and assayed for GUS-activity as described before. For each promoter-GUS line, two controls were harvested: the first one before the treatments were started (time= zero), and the second one after 8 hours without treatment in the same plate as the treated plants. Table 3-15 contains a summary of all the treatments and the solvents that were used.

Well no.	Reagent	Final concentration	Solvent
1	Control t=0	N/A	N/A
2	NaCl	150 mM	H ₂ O
3	H ₂ O ₂	10 μ M	H ₂ O
4	NAA	5 μ M	EtOH
5	IBA	5 μ M	H ₂ O
6	2,4D	5 μ M	EtOH
7	Mannitol	500 mM	H ₂ O
8	ABA	50 μ M	MetOH
9	NAA	5 μ M	EtOH
10	IBA	5 μ M	H ₂ O
11	2,4D	5 μ M	EtOH
12	Kinetin	5 μ M	0.1N NaOH
13	Kinetin	5 μ M	0.1N NaOH
14	Brassinolide	1 μ M	EtOH
15	GA	10 μ M	EtOH
16	SA	50 μ M	EtOH
17	UV-B	15 minutes	N/A
18	Cold	8 hours	N/A
19	Control t=8h	N/A	N/A
20	Brassinolide	1 μ M	EtOH
21	GA	10 μ M	EtOH
22	JA	50 μ M	EtOH
23	UV-B	15 minutes	N/A
24	Cold	8 hours	N/A

Table 3-15. Summary of hormone and stress treatments of promoter-GUS plants in a 24 well plate format. Each number corresponds to the well treated. The final concentration in each well is given together with the solvent used to prepare the 1000x stock solutions for the hormones. Stocks for NaCl and Mannitol were 5 M and 1 M respectively.

Some of the treatments were done in duplicates: NAA, the auxin IBA (indole-3-butyric acid), the synthetic auxin 2,4D (2,4-dichlorophenoxyacetic acid), the cytokinin kinetin, the brassinosteroid brassinolide, GA (gibberillic acid), UV-B (15 minutes irradiation on a UV transilluminator), and cold treatment (8 hours at 4 °C). Figure 3-38 shows photographs of the two treated plates after the tissue was cleared and fixed in an ethanol:acetic acid mixture (3:1). Compared to the control wells 1 (time zero) and 19 (8 hours), only few treatments caused major differences in the overall stain intensity. For the *AtSlp1* promoter, treatment with 150mM sodium chloride (well 2) increased the GUS intensity slightly compared to the untreated control stained at 8 hours. A slight increase was also observed with the *AtSlp2* promoter construct (lower panel in Figure 3-38). This mild upregulation in the presence of salt agrees with the microarray data from the eFP browser (Figure 3-26) and the Northern blots (Figure 3-28 D). However, only root tissue showed upregulation of *AtSlp1* in the microarray experiments. The image in Figure 3-38 gives the impression that mainly leaves are more intensely stained by GUS activity. A more obvious change in promoter *AtSlp1*-GUS plants could be seen in wells 5 (IBA), 11 (2,4D) and 12 (kinetin) which all caused upregulation of the GUS stain intensity. An increase caused by auxins was also observed with the promoter *AtSlp2* construct in wells 11 (2,4D) and 4 (NAA). However, with both constructs only 1 of the 2 treated wells showed this increase (compare wells 5 and 10 (IBA), 11 and 6 (2,4D), 12 and 13 (kinetin) for *AtSlp1* and wells 11 and 6 (2,4D), 4 and 9 (NAA) for *AtSlp2*). Treatment with auxins caused no or only very minor changes according to the eFP browser data (not shown), but changes were observed when NAA was applied as seen in Figure 3-28 A and B at the same time point for both genes. Kinetin treatment only provoked an obvious change in the *AtSlp1* promoter-GUS plants, but hardly anything could be seen with the *AtSlp2* promoter-GUS plants. However, these plants showed little GUS stain intensity in the corresponding controls, which makes it difficult to assess small changes as judged by the visual difference only. It seems that treatment with cytokinins generally elevates *AtSlp1* gene transcription, but much more pronounced when t-zeatin is used (see response from Northern blot Figure 3-28 A).

Treatment with gibberellic acid (GA) also caused activation of the *AtSlp* promoters compared to the 8h control (well 19), as seen particularly in wells 15 and 21 of the promoter *AtSlp1* plate, and in well 15 (although weaker) of the promoter *AtSlp2* plate. This finding also agrees with the results seen in the eFP browser data (Figure 3-25). Within 30 minutes of adding GA, the *AtSlp* transcripts showed mild upregulation. In the eFP experiment, only 1 μ M GA was used and the response measured after 30 minutes, whereas for the promoter-GUS plants treatment 10 μ M were used and a period of 8 hours. Curiously

the AtSlp transcripts are strongly upregulated in the *gal-5* mutant according to eFP, which has impaired GA biosynthesis (Huttly & Phillips, 1995; Phillips *et al.*, 1995). The finding from this promoter-GUS plant treatment experiment might suggest that there are indeed GA-specific effects on AtSlp expression and there might be some compensatory upregulation in this GA deficient mutant.

Treatment with cold (8 hours at 4 °C) also caused high activation of both promoter-GUS transgenic plant lines (wells 18 and 24) grown in liquid culture to a similar extent. This type of treatment however was not reflected by the microarray data obtained from the eFP browser (data not shown). Virtually no change was observed in these experiments (2 replicates) over a time course of 24 hours. Treatment with 50 μ M ABA resulted in no visible change for the AtSlp1 promoter-GUS plants, but a slight increase in GUS activity was observed for the AtSlp2 promoter-GUS plants (well 8) compared to the two control wells (1 and 19).

The strongest upregulatory effects however were observed 8 hours after a 15 minutes irradiation period with UV light (wells 17 and 23) with both promoter-driven constructs. These results completely agree with the data from the microarrays (Figure 3-27) that show high transcription induction 3 and 6 hours after a 15 minutes irradiation period. The response is equally strong with both promoter-GUS constructs as can be easily seen when wells 17 and 23 are compared with the two controls in wells 1 and 19. This experiment was repeated again under similar conditions. Seedlings carrying the same constructs were grown for 14 days in a 12 well tissue culture plate submerged in the same liquid medium as described above. Half of the seedlings were left untreated, and the other half were irradiated with UV-B light for 15 minutes before being transferred back into the growth room. After 6 hours the plants were harvested and assayed for GUS expression. The result of this experiment is shown in Figure 3-39 (A). A clear upregulation with both constructs can be seen 6 hours following the UV irradiation.

To clarify whether this promoter and transcript induction can also be seen on the protein level, wild type plants were grown on MS agar plates or in liquid culture and treated in the same way. 6 hours after the UV irradiation, plants were harvested, a crude protein extract prepared and run on a SDS-PAGE gel followed by Western blotting. Figure 3-39 (B) shows the blot probed with anti-AtSlp1. Treatment with UV light of plants grown in liquid culture did not have a major effect on the protein amount detected by the antibody. However, plants grown on agar plates did show a visible difference between the control and the UV-treatment. This accumulation of Slp1 protein is present independent of sucrose

in the medium. Growth of seedlings in liquid culture clearly induced AtSlp1 protein expression when both controls from liquid medium and agar plates are compared. It is likely that the high amount of AtSlp1 present in the liquid-grown seedlings overshadows the induction by UV irradiation. Combined with the previous results, treatment with UV light does cause changes in AtSlps that are reflected on the level of the promoter induction, transcript accumulation and also protein amount.

These experiments are a crude attempt to study promoter activation and therefore transcription, but they do add evidence to some of the published microarray data and the transcript analysis by Northern blotting. Treatments that caused the same changes in all three experimental setups (eFP data, Northern blots and promoter-GUS stains) include salt stress, application of GA and cytokinins, and irradiation with UV-light. Other treatments such as the application of auxins and auxin transport inhibitors did not change transcript levels according to the microarray data, but did induce transcript levels as seen by Northern blotting and promoter activation. An upregulating response to cold treatment was only observed with the promoter-GUS plants, but not confirmed by the microarray data. In summary, conditions that caused changes seen in all three setups are the ones that most likely reflect real changes in transcript levels. These changes apply equally for AtSlp1 and AtSlp2.

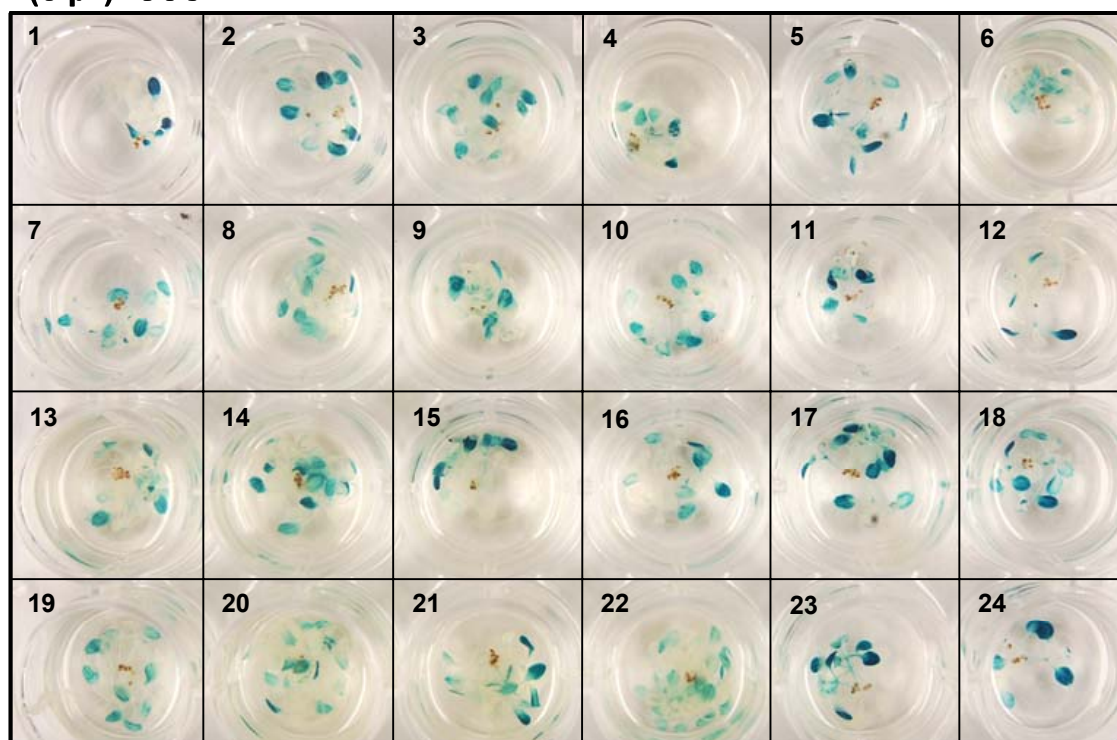
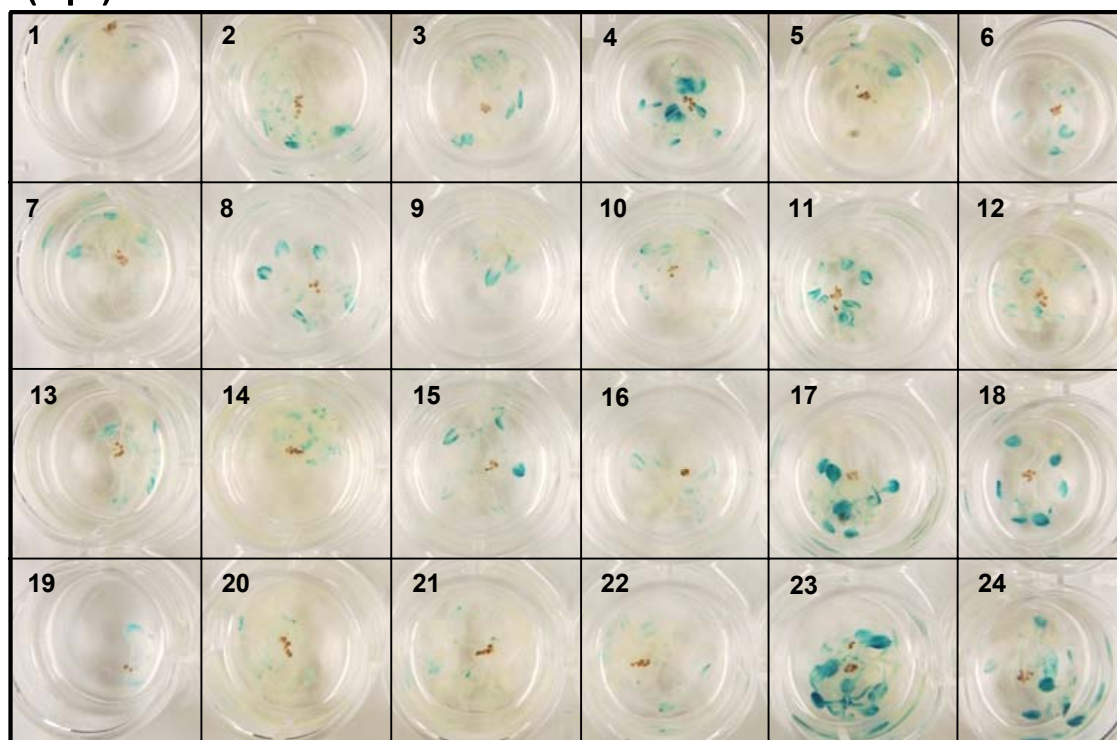
P(Slp1)::GUS**P(Slp2)::GUS**

Figure 3-38. Stress treatments of AtSlp promoter-GUS fusion plants in 24-well tissue culture plates. Both plates were treated with identical chemicals as outlined in Table 3-15. The numbers correspond to each treated well. Plants that had to be transferred to a fresh plate for treatment with UV-B light and cold were put back after the treatment was finished to assay GUS activity.

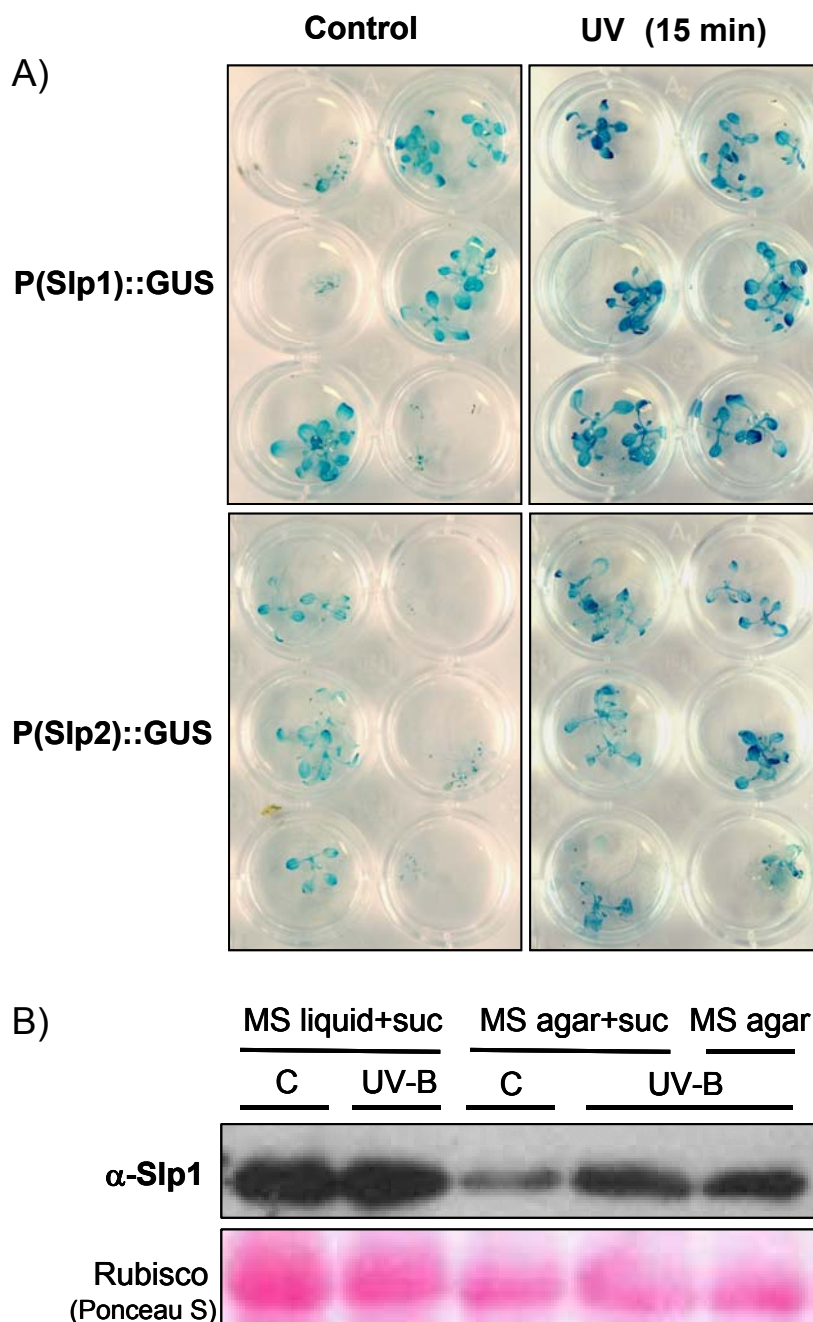


Figure 3-39. UV-B treatment of promoter-GUS transgenic plants.

A) Plants were grown in a 12 well plate format for 14 days and then irradiated with UV light for 15 minutes. The plates were transferred back to the growth room and plants were assayed for GUS activity after 6 hours. The upper panel are seedlings carrying the promoter AtSlp1 construct, and the lower panel shows images taken from the promoter AtSlp2 constructs. Untreated seedlings are shown on the left side, and irradiated plants on the right side.

B) Western blot of UV- treated wild type plants grown either in liquid MS medium with 0.5 % sucrose (MS liquid+suc), or on MS agar plates with sucrose (+suc) or without (MS agar). The blot (upper panel) was probed with anti-Slp1. The Rubisco band seen on the Ponceau S stain is shown in the lower panel as a loading control. Abbreviations are: C (control untreated), UV (irradiated for 15 minutes).

3.5.4 Tissue distribution of AtSlps on the transcript and on the protein level

In the final part of this section the tissue distribution patterns of AtSlp1 and AtSlp2 were directly assessed by RT-PCR and Western blotting.

For the RT-PCR, organs (roots, rosette leaves, cauline leaves, stem tissue, buds and open flowers) from 8 week old flowering Arabidopsis wild type (Col-0) plants grown in short day light conditions (9 hours light, 15 hours dark) were harvested and RNA extracted. cDNA was synthesised and used as a template in PCR reactions with transcript-specific primers for each gene. As a control, primers specific for the ubiquitin 10 gene from Arabidopsis were used in parallel to distinguish for differences between the template amount in each reaction. Figure 3-40 shows the results from the RT-PCR reactions. A relatively high number of cycles was necessary to amplify AtSlp1 and AtSlp2. For Slp1, 30 cycles were sufficient to amplify transcripts that were just at the limit of detection for samples from cauline leaves and roots. By contrast, transcript levels from buds and fertilised flowers were saturated with this cycle number. Overall, AtSlp1 transcripts in the flowering plant are highest in the inflorescence organs, followed by much lower levels in the stem and the rosette leaves. The lowest levels are present in the roots and the cauline leaves. Amongst the flowering organs, expression was slightly higher in closed buds compared to fertilised flowers. For rosette leaves, two different samples were taken: one from a plant that had not reached flower transition and the other from a plant that had already started flowering. The AtSlp1 transcript is present at slightly elevated levels in rosette leaves from the non-flowering plant compared to leaves from the flowering plant. This pattern occurs identically in the data from the eFP browser (Figure 3-22).

AtSlp2 is expressed at even lower levels in the same organs as AtSlp1. For this gene, 32 cycles of PCR were not enough to amplify the transcripts in organs such as roots and cauline leaves. As seen with the AtSlp1 transcript, mRNA levels in flower organs were highest throughout the plant. The transcript was also detectable in stem tissue and rosette leaves, but hardly in root samples and cauline leaves. After these numbers of cycles, the samples from buds and fertilised flowers, and the bands obtained with the ubiquitin 10 primers were all saturated. Flowering plants also have reduced AtSlp2 levels in their rosette leaves compared to non-flowering plants. Overall, the tissue expression pattern on the transcript level between both genes looks identical. As seen in the promoter-GUS assayed plants, strikingly high levels of transcription are detected in flowers. This

observation also agrees with the microarray data (Figures 3-22 and 3-23). Taken all these results together, developing pollen grains contain the high transcript levels in *Arabidopsis* inflorescences. Considering the overall expression pattern as seen with the GUS stained plants, the RT-PCR confirms most of the observations made with some exceptions. Stem tissue for example did not appear to be heavily stained in the GUS plants (Figures 3-34 and 3-36), but it shows transcript levels in the RT-PCR that are as high as those in rosette leaves. In summary, data obtained by RT-PCR, microarrays and promoter-GUS stains all point towards an identical expression pattern between AtSlp1 and AtSlp2. It seems that they are regulated by the same or similar stimuli and are therefore most likely expressed in the same tissues and cells also on the protein level.

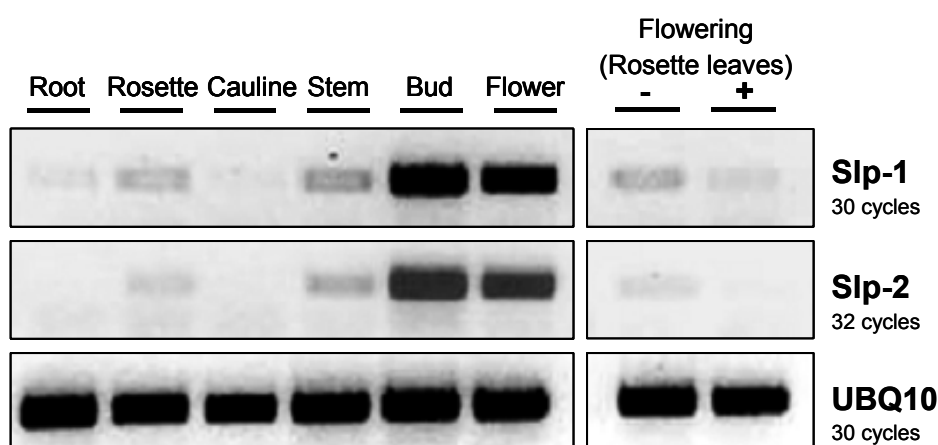


Figure 3-40. RT-PCR on *Arabidopsis* organs. For all genes, the same amount of template was used in each reaction. For AtSlp1, 30 cycles of PCR were performed, and 32 cycles for AtSlp2. The ubiquitin 10 transcript (UBQ10) is saturated with this amount of cycles, as are the inflorescence samples. “+” and “-“ in the right panel indicate whether the samples were taken from plants that flowered (“+”) or not (“-“).

To investigate the tissue expression pattern on the protein level, the same organs as described above plus siliques were harvested and proteins extracted. Figure 3-41 shows two Western blots, the upper one probed with anti-Slp1 (part A) and the lower one with anti-Slp2 (part B). Surprisingly, the distribution of AtSlp1 protein does not completely resemble the tissue expression as seen with the RT-PCR above. In contrast to its transcript levels, the AtSlp1 protein was present in higher amounts in the root tissue, and in lower amounts in the rosette leaves. In agreement with the RT-PCR and the promoter-GUS fusion results, the protein expression pattern looks otherwise identical. The highest amounts of protein were found in the flowers, particularly in the buds, followed by opened flowers. The protein level in the stem was approximately the same as in the roots. Siliques

also expressed AtSlp1, but at a lower level. Protein expression in the rosette and cauline leaves was identically low according to this blot. For AtSlp2, the band that is assumed to represent the protein was not present in roots at all, but strangely enough at high levels in the cauline leaves. Upon longer exposure time, bands of various molecular weights also appeared in the stem, flower and silique samples. With respect to the observations made with the promoter-GUS plants and the eFP data, the protein expression pattern as seen on this Western blot was most likely not representative of the real situation. It is assumed that the antibody raised against the peptide epitope located in the AtSlp2 N-terminus was not specifically recognising this protein. Probably AtSlp2 is also present at very low levels as a protein (see RT-PCR) and might not be visible on a Western blot with this quantity of background bands.

The differences seen between the expression of AtSlp1 in RNA and protein extracts from roots and rosette leaves are surprising. The finding that the protein is present in higher amounts in the roots compared to the leaves might point towards some kind of post-translational modification that ensures high protein content in the roots but not in the leaves.

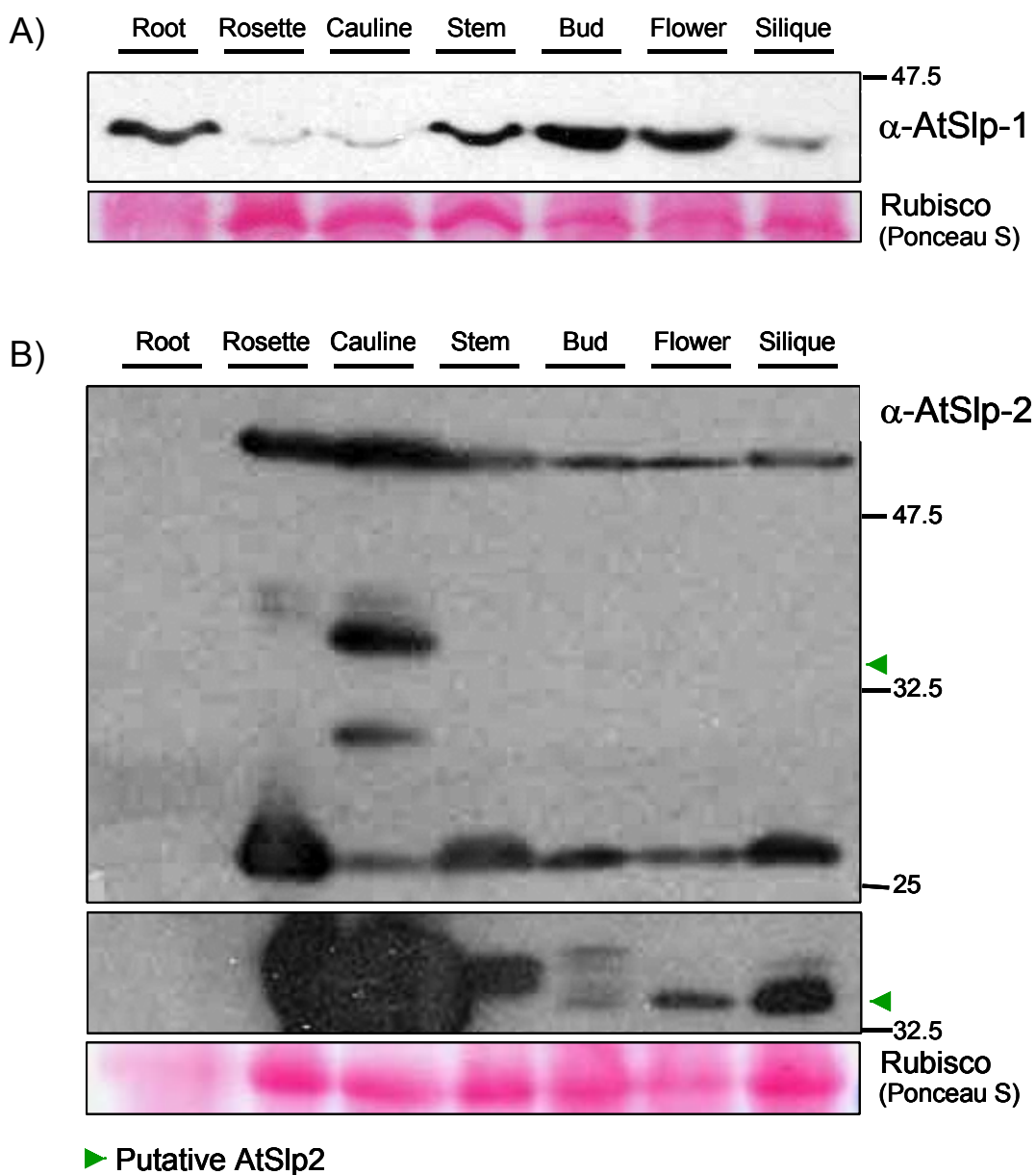


Figure 3-41. Western blots of protein extracts from organs.

A) Western blot probed with anti-Slp1. Approximately 10 μ g of protein was loaded in each lane according to the Amidoblack protein assay. The Rubisco band from the Ponceau S stain is shown underneath. The number indicates the molecular weight marker.

B) Western blot probed with anti-Slp2. The panel in the middle represents a section from the blot above but with a longer exposure time. Numbers indicate molecular weight markers. The green arrowhead marks the presumed position of the Slp2 protein. Additional bands appear upon longer exposure time in the region of the 32 kDa marker band (mid panel). The rubisco band from the Ponceau S stain is shown underneath as a loading control.

3.6 Discussion

3.6.1 Phylogenetic relationship between *AtSlps* and other band-7 family proteins

Out of the Arabidopsis band-7 family, there are only 3 proteins that can be classified as stomatins based on their additional signature sequence as described in section 3.1.2 and listed in Table 3-1. These proteins include the two stomatin-like proteins (*AtSlp-1* and *AtSlp-2*) and one member of the HIR proteins (Nadimpalli *et al.*, 2000), *At3g01290*. Despite the presence of this additional domain in the HIR protein, these proteins actually share only very little sequence and structural identity. The phylogenetic tree in Figure 3-1 groups *Slps* and HIR proteins together, but the *At3g01290* protein is not even the closest related HIR protein. Instead, *At5g51570*, a protein with no stomatin signature, is the next neighbour in this tree. The protein product of *At5g51570* has no clearly predicted target sequence, and it has not been identified in proteomics studies so far. The four HIR proteins resemble proteins from other plant species that are upregulated during the hypersensitive response and in lesion mimic mutants (Nadimpalli *et al.*, 2000). None of these HIR proteins has so far been investigated in further detail, nor is it clear what the functional implications of the band-7 domain and the stomatin signature sequence are. All of the HIR proteins are associated with membranes (TAIR). With the exception of *At5g51570*, the remaining three proteins are supposedly localised to the plasma membrane (Chen *et al.*, 2007b), (Marmagne *et al.*, 2004). The proteins encoded by *At3g01290*, *At5g51570* and *At5g62740* are additionally post-translationally modified by N-myristoylation to facilitate membrane attachment.

Surprisingly, the overall identity between *Slps* and all other major groups of the Arabidopsis band-7 family (prohibitins, HIRs and flotillin-like) is very low (10-18 %) and probably restricted to the region of the band-7 domain. Apart from the HIR proteins, the next related group of proteins includes the erlin-like protein that has an overall similar level of identity to the *Slps* as the HIRs have. The flotillin-like proteins from the same subgroup have the least identity, on average only 10 %. Thus, stomatin-like proteins take a unique place in the phylogeny of the Arabidopsis band-7 family.

Amongst stomatins from animals, yeast and plants, AtSlps are clearly grouped together with stomatin-like proteins of type 2 from mammals and yeast (Figure 3-2). This subfamily has already been suggested to have evolved by a duplication event in a prokaryotic ancestor and was classified as “paraslipins” (Green & Young, 2008). The studied members of this group are all localised to mitochondria, which is linked to their evolution from prokaryotes in the course of the mitochondrial endosymbiosis. Amongst the plant stomatin sequences, a protein from grape (A7P6L9) shares the highest level of identity with AtSlp1, followed by a protein fragment from the moss *Physcomitrella*. Plant stomatins from monocotyledons are the next related proteins, followed by a protein from *Chlamydomonas*. The close relationship between Arabidopsis stomatin-like proteins and a protein from a moss comes as a surprise, since AtSlps would have rather been expected to be closer related to stomatins from monocotyledon species. However, one has to keep in mind that the *Physcomitrella* protein is only a fragment (292 amino acids) obtained by shotgun sequencing and might align differently if the complete protein sequence would be used. The HIR protein At3g01290 does not align in one clade with the remaining plant proteins and curiously groups with the bacterial HflK protein. Apart from the position taken by the moss protein in the tree, the overall sequence distribution reflects the evolution of higher plant species from unicellular algae. It is also obvious that the HIR proteins do not have the typical hallmarks of stomatin-like proteins of the type 2 and are therefore likely to have different functional implications. This special position amongst the stomatins is also reflected by the tree in Figure 3-3, that contains all band-7 family members. All HIR proteins group together and form a separate clade. A second independent clade is formed by the “paraslipins” (or stomatin-like proteins of type 2) clearly highlighting the uniqueness of this subgroup from the remaining stomatins and other band-7 family proteins. Amongst the representatives from yeast, two proteins from *C.albicans* (Q5A411) and *P.stiptilis* (A3LYB1) are separated from the other yeast proteins as also seen in Figure 3-2. As mentioned before, not all yeast species possess stomatin proteins. *Saccharomyces cerevisiae* for example only expresses two prohibitin proteins, but no stomatin. This example suggests that stomatins might not be vital proteins and that their roles might be taken over by other band-7 proteins such as prohibitins. Such an assumption implicates a certain level of redundancy amongst the members of the band-7 family. Interestingly it has been shown that human Slp2 can physically interact with human prohibitin-1 and -2, and that reducing the amount of Slp2 has effects on the stability of the prohibitins (Da Cruz *et al.*, 2008). This provides evidence for a certain level of inter-dependence between different band-7 family proteins at least in one example. Thus it seems that during the course of

evolution, certain organisms have probably evolved alternative mechanisms encoded by similar proteins.

The role of the stomatin signature sequence is not at all clear, especially in relation to the band-7 domain. These two domains span almost identical regions in proteins with the only difference being that the stomatin domain is actually composed of several short stretches of amino acids, whereas the band-7 domain is defined as a continuum (see Uniprot and InterPro databases).

The sequence alignments provided in Figures 3-4 and 3-5 (A-C) mainly highlight the high degree of conservation inside the band-7 domain sequences between very diverse species. The similarity between Arabidopsis and human Slps is high beyond the band-7 domain, but not at the N- and C-termini. Remarkably, a cysteine residue lying inside the band-7 domain is conserved. This turns out to be a hallmark for stomatin-like proteins of type 2. The sequence alignment between stomatins from a wide range of species reveals that this particular amino acid is only conserved between members of the paraslipins with the exception of the protein from *Chlamydomonas* (A8JI52). This residue could be acylated and aids in membrane anchorage of these proteins. A palmitoylated cysteine site has been identified in the human stomatin protein (Snyers *et al.*, 1999b) and the prospect of this post-translational modification in AtSlp1 is further investigated in chapter 4. The cysteine is replaced by hydrophobic residues (valine or isoleucine) in some of the other stomatin sequences. Overall, only three residues are completely conserved between the stomatin sequences in Figure 3-5. It is not immediately obvious what kind of implications these residues might have for the protein structures. Aspartate carries a negative charge and could have several important structural functions. An alanine that is conserved amongst all Arabidopsis band-7 proteins is also present in some of the Slp2 proteins, notably in the mammalian members and in the yeast proteins, but rather intriguingly not in proteins from monocotyledons. As for the other conserved residues, it is impossible to imply whether this residue is of any specific importance.

3.6.2 Structural features of Arabidopsis stomatins and human Slp2

Overall, it appears that AtSlp1 is structurally more similar to HsSlp2 than is AtSlp2. AtSlp1 and the human protein have a hydrophilic C-terminus and a similar hydrophathy profile. Between the two Arabidopsis proteins, the hydrophobicity profile is only similar in the central part. The AtSlp2 protein has a unique N-terminus with distinct hydrophobic

stretches that do not occur in AtSlp1 and HsSlp2. The predictions for the transmembrane regions in the band-7 domain of the Arabidopsis proteins are based on very low probability scores and are therefore not truly membrane-spanning. Instead, it is proposed that these hydrophobic areas serve in membrane anchorage via a hydrophobic loop insertion, as is the case for the human stomatin protein, human Slp2 and other SPFH proteins (Browman *et al.*, 2007; Bauer & Pelkmans, 2006; Hajek *et al.*, 2007). Thus, despite their sequence diversities outside of the band-7 domain, the overall conformations of all stomatin-like proteins are actually fairly similar. Membrane association is further facilitated by additional lipid anchors towards the end of the band-7 domain as outlined above. Remarkably, all three proteins have positively charged, alpha amphipathic stretches in their N-termini that act as putative targeting sequences (see chapter 4 for further investigation). As mentioned before, the evolution of the stomatin-like proteins of this type (“paraslipins”) (Green & Young, 2008) is thought to have occurred from a prokaryotic ancestor, and it is likely that all of these proteins are localised to mitochondria.

All stomatin proteins are characterised by the presence of two conserved domains: the band-7 domain and the stomatin signature sequence that is made up of several short sequence blocks (Table 3-1 and Appendix 1). The stomatin signature domain as a whole is shorter than the band-7 domain, but contains essentially the same elements (InterPro database). The exact function of the band-7 domain (and thus, also the stomatin signature domain) has been under debate for a long time. Since the proteins carrying this domain are otherwise rather diverse, it has not been clear what their underlying common function might be. Remarkably however, most of the band-7 proteins that have been characterised so far are localised to membrane microdomains. In fact it is now assumed that this trait is a hallmark of the whole protein family. It was only in the past four years, that new fundamental concepts about the presence of the band-7 domain surfaced. It is now assumed that the band-7 domain itself actively contributes to the formation of microdomains and thus has the ability to cluster and assemble proteins. The first evidence for this concept came from the *C.elegans* Mec-2 protein, a homolog of stomatin. The first investigation of the Mec-2 band-7 domain reported a protein-interaction function that is necessary for the regulation of the degenerin-like sodium channel Mec-4, and recruitment to the channel in puncta along the plasma membrane of touch receptor neurons (Zhang *et al.*, 2004). A second study demonstrated the ability of the Mec-2 and podocin band-7 domains to bind cholesterol. This function was dependent on the presence of a proline residue and lead to the assembly and regulation of higher protein complexes important for touch sensation (Huber *et al.*, 2006a). A palmitoylated cysteine residue also contributes to this function of the band-7 domain. Thus, it seems likely that the conserved cysteine in the AtSlps and the

human Slp2 protein plays a similar important role. Cholesterol-binding of the band-7 domain is not restricted to stomatins, but was also demonstrated to be essential for correct PM trafficking of human flotillin-2 (Langhorst *et al.*, 2008).

The first solved protein structure of a band-7 family protein was the band-7 domain of the mouse flotillin-2 protein (PDB entry 1win), (Miyamoto *et al.*, 2004) Recently, the crystal structure of the core domain of the prokaryotic stomatin PH1511 from the hyperthermophilic archaeon *Pyrococcus horikoshii* was also solved (Yokoyama *et al.*, 2008b). Both structures resemble each other in an α/β domain. The prokaryotic protein exists as a homotrimeric unit capable of interacting with other stomatin units via coiled coils formed by one extended alpha helix per unit. Stomatin oligomerisation is known to be mediated by a small set of hydrophobic residues close to the C-terminus. Three of those residues- Isoleucine (I), valine (V) and phenylalanine (F)- are crucial for the protein's ability to be located in membrane microdomains (detergent-resistant membrane fractions) (Umlauf *et al.*, 2006). These residues are not completely conserved in HsSlp2 and in the Arabidopsis Slps. The human Slp2 protein instead has the residues I-L-L and the Arabidopsis proteins M-L-L. This tri-peptide is however followed by a completely conserved proline residue that is part of the sequence crucial for oligomerisation, but not required for microdomain association (Umlauf *et al.*, 2006). The authors concluded that stomatin oligomerisation is therefore not a prerequisite for microdomain association of the protein. In summary, it is now accepted that the presence of a band-7 domain generally enables assembly and putatively also regulation of higher protein-lipid structures in membranes. Certain band-7 proteins such as stomatins are thought to regulate protein complexes, whereas other functions might be to provide scaffolds and aid in the formation of coats. For the Slps of type 2, it seems that most of the characteristics identified in human stomatin are conserved and that the underlying principle of the band-7 domain is shared amongst the whole family. Outside of the band-7 domain the Slp2 proteins might have evolved additional features to adapt to unique functions.

3.6.3 Antibody production against AtSlp1 and AtSlp2

Two different approaches were chosen to obtain specific polyclonal antisera against both Arabidopsis stomatin-like proteins. The choice of the type and position of the epitopes proved crucial for the final result. Overexpression of a small part of AtSlp1 as an epitope-tagged fusion protein in bacteria resulted in a specific antibody that is capable of recognising the AtSlp1 protein on Western blots from plant extracts. However, it was recognised together with another, but weaker contaminating band of higher molecular

weight (Figure 3-17). This epitope resulted in a good antibody because the area chosen was predicted to be purely hydrophilic, surface exposed and most importantly non-toxic for the bacterial host. The protein epitope for AtSlp2 on the other hand had to be taken from the protein's N-terminal end and could not be detected as a His-fusion protein on Coomassie stained gels. Most likely the reason for this failure goes back to the design of the epitope. The N-terminus of AtSlp2 contains a putative signal sequence for targeting to mitochondria that probably had toxic effects for bacteria; however, no slowed bacterial growth was detected when compared to bacteria carrying the construct with the AtSlp1 epitope. The protein was probably unstable in the host strain due to mistargeting or rapid degradation upon translation. The epitope itself contained several hydrophobic elements that might have also led to the formation of insoluble inclusion bodies. Additionally, its small size might have rendered it unstable. To stabilise the protein, a larger GST tag was fused to the N-terminus of the same epitope and attempted to be overexpressed and purified in a different host strain. The GST fusion system supposedly generally gives higher protein yields for otherwise unstable proteins in bacteria. Indeed, protein overexpression was at last detectable on Western blots probed with a GST-specific antibody. However, this approach also failed at the elution step from the GSH affinity column. In this case, the elution can only be achieved by proteolytic cleavage with thrombin. According to the Western blot in Figure 3-18, the overexpressed fusion protein was detectable with a GST-specific antibody and present in both soluble and insoluble fractions. After the cleavage however it could not be specifically detected any more on Coomassie-stained gels. In the following steps it was not possible to purify sufficient amounts for the immunisation of rabbits.

The alternative approach to obtain antibodies involved the design of short peptide epitope sequences that were synthesised *in vitro*. They were injected directly into host animals as conjugates to a carrier protein. In this case, two N-terminal epitopes for AtSlp1 and AtSlp2 were chosen to keep the antisera as specific as possible. For Slp1, the epitope did not result in a good antibody. Most likely, this epitope lies within the mitochondrial targeting sequence and is lost upon organellar import. Otherwise the absence of any specific bands is not easily explainable with respect to the strong bands always observed with the other Slp1 antibody. The observation does hint towards the synthesis of this protein as a larger precursor that is specifically cleaved following organellar import (for a more detailed investigation into this topic see chapter 4). The peptide epitope from the N-terminus of the AtSlp2 protein gave rise to antiserum. This resulted in bands on Western blots from plant crude extracts, but it also resulted in a lot of background bands that appear much stronger compared to what the assumed signal is. The peptide chosen to function as the antigenic

epitope lies behind the predicted mitochondrial targeting signal (see chapter 4), and was therefore not lost upon import. If the identified bands are indeed specific for AtSlp2, the protein does appear smaller than it is predicted from the database (approximately 35kDa compared to 43kDa), presumably because it is cleaved upon organellar import. It could even be that AtSlp2 gives rise to a ladder of bands (as seen with the purified antiserum in Figure 3-21) once it has been processed. However, this antibody failed to recognise the 35S overexpressed YFP fusion protein. One explanation for the lack of a fusion protein band could be related to different folding in the presence of the C-terminal YFP tag. The epitope might be buried even in the presence of SDS and therefore not recognised. Alternatively, this fusion protein might not be stable and the N-terminal part is lost because it might be cleaved proteolytically. This interpretation seems unlikely, since the complete fusion protein was easily recognised by a monoclonal anti-GFP serum as a whole unit. It is therefore difficult to assess the specificity of this antibody. With respect to the organ distribution of AtSlp2 as judged by promoter-GUS staining and RT-PCR, it is hard to see any clear correlation with the pattern seen on the Western blot in Figure 3-41. Both the GUS stains and the RT-PCR gave identical results for AtSlp1 and AtSlp2, and this is also expected on the protein level between the two proteins.

Taken together, epitopes overexpressed as fusion proteins in bacteria gave better results than short and artificially synthesised peptides. This result is both linked to the choice of N-terminal epitopes in this case, but also to the number of regions recognised as epitopes by the immune system of the host animal. Peptide epitopes function as highly specific antigens if they are recognised by the immune system. The resulting antiserum can be used to address specific aspects of a particular protein if its epitope is not buried underneath the surface. The correct folding of proteins overexpressed in bacteria is often an issue of concern. However, the resulting protein epitopes give rise to more diverse and therefore stronger immune responses than a single short peptide epitope. Proper folding is important for the production of antibodies to be used for *in silico* studies such as immunohistochemistry. In this case, the resulting antiserum is mainly used for the pure purpose of recognising Slp1 in a denatured state and can be employed for further studies.

3.6.4 Tissue expression of AtSlp1 and AtSlp2 and changes upon stress treatments

Three different methods were applied and compared to investigate the tissue expression pattern of the Arabidopsis stomatin-like proteins. Public microarray data, promoter-GUS

fusion plants, RT-PCR and Western blotting all gave overlapping but also some divergent results. Overall, the transcripts of these genes are mainly active in very young seedlings, in imbibed seeds and the inflorescence, particularly in developing pollen. These tissues or developmental stages have two things in common: the requirement for active growth accompanied by changes in metabolism. This pattern between the two genes was completely identical as judged by all three approaches. Thus, the fundamental question arises how redundant both genes and their encoded proteins are. On the tissue level they clearly appeared to be expressed together and thus might well act in one pathway. The eFP browser does not allow us to distinguish between AtSlp1 and AtSlp2 transcripts. On the promoter level, some differences exist that are reflected by subtle variations in the GUS stains. Generally the AtSlp1 promoter showed stronger activity and the gene transcript and protein were present at higher levels than AtSlp2. The guard cell stain was only observed for the AtSlp1 promoter, but this finding does not exclude the possibility that AtSlp2 is also expressed in these cells at a low level. The promoter-GUS stain is often not particularly sensitive or absolutely specific. Between the results from these different methods, major differences arise with respect to expression in flowers, roots and vascular tissue. The promoter-GUS fusion plants showed the highest activity associated with the vascular system throughout the leaves and the roots. By contrast, the prediction from the eFP browser points towards strong expression in the epidermis and cortex, particularly in roots. High levels of GUS activity were localised specifically to stipules. These are leaf formations located between petioles in the rosette and contain highly metabolically active cells that also display high auxin response activity (Ulmasov *et al.*, 1997). Consistent with the observations from other parts of the plant, the high stipule expression fits together with the idea of phytohormone-regulated processes that involve metabolic changes.

The pattern of expression observed and predicted from the eFP browser in flowers was in agreement on pollen grains, but according to the microarray data the transcripts are only high in the first two stages of pollen development. By contrast, GUS staining was apparent also in more mature flowers. With respect to the flowers otherwise, the eFP browser predicts high level expression in sepals and carpels, both not observed by the GUS-staining patterns. Additionally, the eFP browser data suggest strong expression in the shoot apices, another observation that was not made with the promoter-GUS fusion plants. Between the data from the organ protein extracts and RT-PCR, there is considerable disagreement between samples from root tissue. According to Western blot analysis, the roots expressed more Slp1 protein than the rosette and cauline leaves. This is also predicted by the eFP browser in young seedlings and in plants that have been sampled after flower transition.

Regardless of these details, the overall pattern in flowers and seedlings is confirmed by all three methods. The high-level expression in the inflorescence is also indicated by some of the promoter-response elements found in the AtSlp1 and AtSlp2 genes. Several elements bind specifically to transcription factors known to be important for flower development (Table 3-14). The AtSlp2 promoter is considerably richer in these elements. It appears that the expression of this gene is more tightly regulated than AtSlp1.

Certain treatments with phytohormones, chemicals and abiotic stresses were predicted to cause upregulation of AtSlps by the eFP browser data. Two additional approaches were used to confirm these observations. Treatments of seedlings grown in liquid medium followed by transcript analysis using Northern blotting confirmed some of the microarray data. Additionally, promoter-GUS fusion plants were treated and assayed for changes in GUS activity. Amongst these treatments, application of t-zeatin (and kinetin), auxins (NAA, IBA and 2,4D) and to a certain extent gibberellic acid (GA) all had upregulatory effects on AtSlp transcripts. The eFP browser does not show upregulation upon treatment with auxins, but upregulation following treatment with the auxin efflux inhibitor TIBA. These effects were confirmed by the Northern blot in Figure 3-28 C. The addition of TIBA to seedlings resulted in a threefold enhancement of AtSlp1 transcript levels after 4 hours, and to a lesser extent an upregulation of AtSlp2 transcript. The Northern blots reveal a similar effect upon treatment with NPA with a similar temporary response. This effect was not reported in the microarray results (not shown). Both TIBA and NPA inhibit auxin efflux by affecting the cycling of PIN efflux carrier protein. However, both agents are known to act not specifically just on these proteins, but are thought to have broader effects on protein trafficking mechanisms (Geldner *et al.*, 2001).

No such effect is reported following treatment with inhibitors of gibberellic acid biosynthesis (eFP). Amongst the other types of treatments, strong upregulation was observed after the application of cycloheximide and after irradiation with UV light. The response to UV light was confirmed by the accumulation of AtSlp1 protein and by enhanced activity of the GUS reporter gene driven by both Slp promoters. The microarray data also indicate upregulation in response to salt stress in roots, and to a lesser extent also in shoots starting 6 hours after transfer to high salt containing medium (150mM NaCl). The transcript levels of both genes indicate such an upregulation as seen in Figure 3-28 D at the 6h and 24h time points, but with extremely high standard deviation values. The promoter-GUS stain for both genes also indicates increased dye intensity 8h after addition of 150mM NaCl, as compared to the untreated control taken at the same time point. In the

GUS stain it is not possible to see increased staining specifically in the roots. Instead, the stain seems most prominent in the leaves.

Generally, the observed changes in transcript levels can be divided into two classes. The first one includes effects of several classes of phytohormones and chemicals affecting hormone distribution. These substances all have crucial influences on plant growth and development. Auxin and cytokinins are known to act in a complementary fashion to drive cell division and proliferation (Swarup *et al.*, 2002). GA has multiple effects, notably in seed germination and flower development (Holdsworth *et al.*, 2008;Blazquez & Weigel, 2000). The AtSlp transcripts are also strongly upregulated during the breaking of dormancy while seeds are imbibed (eFP browser data), and a putative GA responsive element is found in the AtSlp1 promoter. The AtSlp2 promoter has an auxin response element that might explain the upregulation in response to NAA, IBA and indirectly also auxin transport inhibitors. Additional response elements in both promoters indicate the importance of these genes in flower development, a process that is also regulated by these phytohormones. These facts all point towards a requirement for AtSlp proteins in processes involving metabolic changes, cell division and growth. Because the changes in transcript levels are not immediate, it is assumed that AtSlps are not directly involved in acute hormone-mediated signalling responses, but are instead required further downstream. With regard to cell division, AtSlps might be factors involved in the redistribution and maintenance of mitochondria during that process.

The second class of upregulatory factors involves strong cytotoxic agents like UV-B light and cycloheximide. UV-B light is known to have multiple effects on genomes: it induces DNA damage and therefore interferes with transcription, and it also inhibits DNA replication (Sinha & Hader, 2002). Cycloheximide blocks protein biosynthesis at the translocation step at the ribosome and imposes general strain on cellular function leading to cell death (Kominek, 1975;AbouElela & Nazar, 1997). With regard to mitochondria, UV-B light or block of general protein biosynthesis could induce stress responses that are similar to those observed after chloramphenicol treatment (Da Cruz *et al.*, 2008). Chloramphenicol represses mitochondrial protein synthesis and imposes stress specifically on mitochondria (Li *et al.*, 2005). Protein levels of the human Slp2 protein and prohibitin-1 were significantly increased upon this treatment (Da Cruz *et al.*, 2008). Notably, protein levels of human Slp2 were virtually unaffected upon addition of cycloheximide to HeLa cells. HsSlp2 is assumed to be upregulated to stimulate proteolysis and regulate protein turnover in the mitochondrial inner membrane (Da Cruz *et al.*, 2008). In the case of Arabidopsis Slps, it seems that the effects on protein levels by cycloheximide are caused

by more general cytotoxic stress conditions that in turn put strain on mitochondrial function through secondary effects. On the contrary, UV-B irradiation might have direct effects on mitochondria by damaging their genomes and thereby influencing mitochondrial replication mechanisms. Alternatively, UV-B effects on mitochondria could also be of a secondary nature and triggered by reduced translation of important mitochondria-targeted proteins. Interestingly and as mentioned before, both AtSlp promoters contain multiple response elements in their promoters involved in light- and environmental stress signalling (Table 3-13). A more specific role of AtSlps in light-mediated response pathways cannot be excluded. As with the other treatments, the responses to UV-B irradiation and cycloheximide are not immediate, but occur within 3-6 hours after the initial signal was given. Therefore they are probably part of downstream events that follow initial signalling events.

All the methods used for this expression study are of a very different nature and therefore the observed variations are not surprising. In fact they assess completely different aspects of gene expression. The microarray data, Northern blots and RT-PCR data reflect changes on the transcript level, whereas the promoter-GUS fusion plants only reflect the activities of an isolated promoter sequence that regulates transcription of an unrelated reporter gene. The data obtained by the promoter-reporter gene approach do not necessarily even relate directly to the transcript levels, as mRNA is often unstable and degraded before any protein is made. Any regulatory mechanisms taking place on the epigenetic levels are also likely to be missed out by this approach. Additionally, both approaches do not reflect directly on the levels of actual protein accumulating in the plant. For example, no information is obtained about any post-translational changes that might lead to differences in the actual expression levels. Thus, all these methods can only give hints towards an understanding of the real situation. In the following paragraph, more specific disadvantages of each method are discussed.

The eFP browser data often rely on only very few replicates (normally 2-3) and might not always reflect real changes in transcription. These data should therefore always be confirmed by an independent method.

The Northern blot results were also obtained from only two independent experiments, because the probe-hybridisation of the third replicate did not give signals that could be quantified. The hybridisation and detection of radiolabelled probes does not always result in clean bands and often results in high background signals. There is also considerable difference between the two replicates that were quantified. An overall trend towards

upregulation is recognisable in several samples, but the absolute values of relative changes are often not reproducible between two or even three replicates.

The data presented that were obtained by RT-PCR do not allow us to identify small differences in the amount of template loaded between each sample. The transcript levels of the UBQ10 control gene are completely saturated with the number of cycles used. Such a high number was necessary to amplify transcripts from leaves and roots of both genes. To act as a better control, the UBQ10 reactions should have been amplified with less cycles (20-25) to make accurate assumptions about loading differences.

There are several limitations associated with the promoter-GUS fusion plants, some of them were mentioned above already. The issues discussed below refer more to problems associated with the actual method. As mentioned, the GUS staining reaction is not always very sensitive and depends on the age and storage condition of the GUS substrate, X-Gluc. The intensity of the reaction also depends on the incubation time and on how accessible a tissue is. Weak or no stain does not necessarily mean a protein is not present in a specific tissue. The insertion site of the T-DNA can also influence the intensity of the stain, as the promoter activity can be enhanced or repressed by other genomic elements. Several independent transgenic lines for each promoter were analysed in this study and no major differences were observed. Once the substrate is converted to the blue end product by the enzyme, diffusion of the dye can also be a problem. For these experiments, the stained tissue was fixed using a mixture of acetic acid and ethanol. Another problem might arise from the lack of additional sequence elements that are missing in the final plasmid construct. In this particular case, only the promoter region including the 5'UTR sequence was fused to GUS, but regulatory elements located in the introns or the 3'UTR are missing. As a final point, some approaches like the promoter-GUS stains or some of the eFP data only refer to a single time point (6 or 8 hours) after the commencement of a treatment and might miss out very early occurring responses.

4 Subcellular localisation of Arabidopsis stomatin-like proteins and characterisation of the AtSlp1 protein

Introduction

The first part of this chapter presents data investigating the subcellular localisation of the two Arabidopsis stomatin-like proteins. Reports in the literature already provide evidence for localisation to mitochondria and putatively also to chloroplasts. These reports are based on screens in attempts to characterise the mitochondrial or other organellar proteomes. However, these data have so far never been confirmed by any other means. This chapter contains the first *in vivo* evidence and additional biochemical data for the presence of these proteins in mitochondria. Furthermore, experimental data are presented that aim to elucidate the membrane localisation of these proteins inside mitochondria and the mechanism of membrane attachment. These findings lead to speculations about how these proteins might fulfil their biological roles inside mitochondria.

4.1 Subcellular targeting of AtSlp proteins

A proteomics study of Arabidopsis mitochondria identified a prohibitin and a peptide of 10 amino acids matching both AtSlp-1 and AtSlp-2 (Kruft *et al.*, 2001). A second study identified five *Arabidopsis* prohibitins and At4g27580, a gene that has been split into AtSlp-1 and a smaller protein of 104 amino acids. At4g27580 was identified from a two-dimensional gel spot after tryptic digestion and mass spectrometry analysis (Millar *et al.*, 2001). A third investigation identified both AtSlp-1 and AtSlp-2 independently in mitochondrial preparations using liquid chromatography-tandem mass spectrometry (LC-MS/MS) (Heazlewood *et al.*, 2004). AtSlp-2 was identified directly from gel-based separations, whereas AtSlp-1 was identified from LC-MS/MS data of whole mitochondrial digests. A database, AMPDB (Arabidopsis Mitochondrial Protein Database), was created with all identified mitochondrial proteins from this particular study (Heazlewood & Millar, 2005).

AtSlp1 was also identified in a proteomics approach that studied the protein content of detergent-resistant membrane fractions from mixed organelle membrane preparations from Arabidopsis root callus cultures (Borner *et al.*, 2005). The AtSlp1 protein was specifically

enriched in Triton-X100 insoluble membrane fractions that were derived from plasma membrane and endomembrane vesicles as identified on 2D-PAGE gels. Other band-7 family members from Arabidopsis were also found enriched in these detergent-resistant membranes: a flotillin protein (At5g25250- designated AtFlot-1) and three members of the HIR proteins (At1g6984, At3g01290 and At5g62740). The authors generally assumed that the majority of detergent-resistant membrane associated proteins were derived from the plasma membrane.

A quantitative proteomics study of the organellar protein content from Arabidopsis identified both AtSlp1 and AtSlp2 as localised to mitochondria and/or chloroplasts (Dunkley *et al.*, 2006). These findings were based on a different approach. Rather than isolating separate organelles, the authors made use of the LOPIT (Localisation of Organelle Proteins by Isotope Tagging) method. This approach relies on measuring the relative abundance of proteins from a specific density gradient fraction by tagging proteins with isotope labels.

The AtSlp1 protein was also identified by LC-MS/MS data derived from detergent extracted microsomal fractions from liquid-grown seedlings (Mitra *et al.*, 2007). Two different approaches were utilised to solubilise membrane-bound proteins: extraction with 2% of the non-ionic detergent Brij-58, and extraction with 60% methanol. Interestingly, AtSlp1 was only retrieved from the Brij-58 extracted fractions, but not from the methanol-treated membranes. Methanol-extracted proteins were reported to be of a more diverse nature than detergent-solubilised proteins, which generally tend to be more hydrophobic. This could be explained by the different solubilisation properties of a detergent extract versus an extract with organic solvents.

Treatment of Arabidopsis suspension cell cultures with the bacterial elicitor harpin from *Pseudomonas syringae* resulted in a two-fold reduction of AtSlp1 protein as determined by 2D-PAGE and MALDI-TOF MS analysis of purified mitochondria (Livaja *et al.*, 2008). Overall 28 mitochondrial proteins were identified that changed in spot intensity at least two-fold over control treated samples. AtSlp1 decreased two-fold in protein content eight hours after the treatment, but recovered after 24 hours.

Based on this proteomic evidence, AtSlp proteins are most likely only localised to mitochondria, and not to other organelles. Further support for this localisation is given in the following sections that analyse in detail putative targeting sequences.

4.1.1 Prediction of AtSlp subcellular targeting

The protein sequences of AtSlp1 and AtSlp2 were analysed with various subcellular targeting prediction softwares that screen the sequences for the presence of conserved signal peptide motifs. Analysis of both proteins revealed in all cases strong predictions for targeting to mitochondria. The MitoProt II software (Claros & Vincens, 1996) gave high probability scores for both proteins as summarised in Table 4-1. TargetP (Emanuelsson *et al.*, 2000) assigned both proteins to mitochondria over a localisation to chloroplasts (Table 4-1), with a lower probability score (0.7 versus 0.99 predicted by MitoProt). The Predotar database (Small *et al.*, 2004) also assigned mitochondrial localisation for both Slps over a localisation to chloroplasts, but with a lower probability score of only 0.36 for AtSlp1. This algorithm predicted the possibility of another subcellular localisation with higher scores than for mitochondria (0.61 for AtSlp1), which was not further specified. The fourth database to be queried with AtSlp sequences was PSORT, for which the plant specific version was chosen (Nakai & Kanehisa, 1991). This database indicated mitochondrial localisation and further predicted targeting to submitochondrial compartments. For both Arabidopsis Slps the highest scores were given for localisation to the mitochondrial matrix, followed by localisation to the inner membrane or the intermembrane space (Table 4-2). This database does not assign any membrane-spanning domain for both proteins and thus assumes the proteins are soluble. However, taking other predictions into account and with respect to a clear membrane association of AtSlp1, the more likely prediction is certainly for localisation to the inner membrane either facing the matrix or the intermembrane space.

Finally, the Cell eFP browser that is based on the SUBA database (the Arabidopsis subcellular database, (Heazlewood *et al.*, 2007)) predicted mitochondrial localisation for both AtSlps. For AtSlp1, this database also predicted localisation to chloroplasts, but with a weaker confidence score than for mitochondria. AtSlp2 was only predicted to be targeted to mitochondria.

Mitochondrial import commonly involves proteolytic cleavage by a mitochondrial processing peptidase after the signal peptide in the precursor protein. Such processing is called the general protein import pathway (Bolender *et al.*, 2008). The positions of the indicated cleavage sites in AtSlps vary remarkably between the databases queried. For AtSlp1, the cleavage sites were all predicted to lie between amino acid 50 (TargetP) and 66 (MitoProt, PSORT). Cleavage after these sites results in mature proteins of 40 and 38 kDa in molecular weight, respectively. A grey arrowhead in Figure 3-7 of Chapter 3 indicates

the cleavage site as predicted by TargetP. It lies before the band-7 domain; if the protein was cleaved after position 66, this cleavage site would lie within this domain. Cleavage within the band-7 domain seems unlikely given the high conservation of this domain amongst stomatin-type proteins, and therefore the prediction by TargetP seems more plausible. This conclusion is also consistent with the observed molecular weight which appears very close to the full length precursor on Western blots (see Figure 3-17).

The precursor of AtSlp2 is cleaved only after the first 109 amino acids according to the MitoProt database. This prediction implies a mature protein of only 32 kDa. On the other hand, TargetP and PSORT both predict cleavage around amino acid residue 48, which would give rise to a protein of 39 kDa. Like AtSlp1, the cleavage further into the protein sequence would give rise to a mature protein lacking part of the conserved band-7 domain. A grey arrowhead in Figure 3-8 of Chapter 3 indicates the shorter signal sequence predicted by the TargetP software. On the basis of this model, the molecular weights of both mature stomatin-like proteins differ by only one kilo-Dalton.

Database	Protein	Mitochondria	Chloroplast	Secreted	Other	Cleavage site
MitoProt II	AtSlp1	0.9926	N/A	N/A	N/A	66
	AtSlp2	0.9543	N/A	N/A	N/A	109
TargetP	AtSlp1	0.704	0.298	0.027	0.011	50
	AtSlp2	0.672	0.046	0.006	0.013	48
PREDOTAR	AtSlp1	0.36	0.03	0.02	0.61	N/A
	AtSlp2	0.17	0.06	0.1	0.7	N/A

Table 4-1. Target sequence predictions for AtSlp1 and AtSlp2. Databases (MitoProt II, Target P and PREDOTAR) were queried with the amino acid sequences of AtSlps. The predicted likelihoods for targeting to a certain organelle are indicated. Red numbers indicate strongest prediction for mitochondrial targeting. See text for references.

Database	Protein	Mitochondria			Other organelles			Cleavage site
		Matrix space	MIM	IMS	Chloroplast	Nucleus	Peroxisome	
PSORT	AtSlp1	0.497	0.214	0.214	N/A	0.3	N/A	66
	AtSlp2	0.541	0.264	0.264	N/A	N/A	0.3	49

Table 4-2. Target sequence prediction for AtSlps as indicated by the PSORT algorithm. Abbreviations are: MIM (mitochondrial inner membrane), IMS (intermembrane space); red numbers highlight the highest prediction scores.

By comparison, the human Slp2 protein is also predicted to be mitochondrial by the same databases. Both MitoProt II and TargetP annotate this sequence with high scores to mitochondria (Table 4-3) when the parameters are changed for protein sequences derived from animals. The other databases (as listed in Table 4-3) also agree on targeting to mitochondria. PSORT II (Horton & Nakai, 1997) is a database specifically created for sequences from animals; PSORT was queried as before but with parameters set for sequences derived from animals. As for Arabidopsis Slps, this database indicated localisation to the matrix space was favoured over association with the inner or outer mitochondrial membrane, and also predicted the presence of the protein in the intermembrane space. Like the Arabidopsis proteins, human Slp2 does not contain a predicted transmembrane spanning domain. Thus, the database identified it as a soluble protein that is imported and translocated to the matrix space. Since it is known that this protein is actually localised to the inner membrane facing the intermembrane space (Hajek *et al.*, 2007), it appears likely that the same could be true for the Arabidopsis orthologs.

Human Slp2 has been shown to be imported into mitochondria and to be processed proteolytically (Hajek *et al.*, 2007). The databases employed here indicated the presence of a cleavage site after amino acid 36, which would give rise to a mature protein of 35 kDa. When expressed in HeLa cells, human Slp2 migrated only as a single band with the molecular weight of the precursor protein (Da Cruz *et al.*, 2008). However, the same study proved the presence of a signal sequence responsible for targeting to mitochondria, and immunoprecipitated Slp2 protein was identified to contain the precursor and the mature protein (Da Cruz *et al.*, 2008). Based on this evidence, it seems likely that Arabidopsis Slps might share the same proteolytic processing and submitochondrial localisation.

Database	Protein	Mitoch.	Mitochondria				Other organelles					Cleavage site
			Matrix	MIM	IMS	MOM	ER	Secr.	Cytoplasm	Nucleus	Other	
MitoProt II	HsSlp-2	0.9904	N/A	N/A	N/A	N/A	N/A	N/A	N/A	N/A	N/A	36
TargetP	HsSlp-2	0.958	N/A	N/A	N/A	N/A	N/A	0.03	N/A	N/A	0.032	N/A
PREDOTAR	HsSlp-2	0.8	N/A	N/A	N/A	N/A	0.25	N/A	N/A	N/A	0.15	N/A
PSORT	HsSlp-2		0.742	0.422	0.422	0.422	N/A	N/A	N/A	N/A	N/A	36
PSORT II	HsSlp-2	0.739	N/A	N/A	N/A	N/A	N/A	N/A	0.174	0.087	N/A	N/A

Table 4-3. Target sequence predictions for HsSlp-2. The same databases were queried with this protein sequence. Values indicate likelihood for targeting to a particular organelle. Values highlighted in red indicate the strongest prediction made. Where possible, cleavage sites are indicated. Abbreviations are: Mitoch. (mitochondria), MOM (mitochondrial outer membrane), ER (endoplasmic reticulum), Secr. (secreted).

4.1.2 Analysis of putative signal sequences as amphipathic alpha helices

Commonly mitochondrial N-terminal signal sequences are characterised by the formation of an alpha amphipathic helix that aids the import process via interaction with the receptor and translocase of the mitochondrial outer membrane (= TOM) (Pfanner, 2008). Alternative import pathways exist, that rely on co-translational import on ribosomes attached to the mitochondrial surface (Mackenzie, 2005). However, most nuclear-encoded proteins destined for the mitochondrial inner membrane (except carrier proteins) or the matrix are synthesised in the cytosol and imported by the TOM -and TIM (translocase of the inner membrane) complexes in a membrane potential- and ATP-dependent manner (Bolender *et al.*, 2008). Following import, the N-terminal leader sequence is cleaved by a peptidase in the matrix or the inner membrane, and the mature protein is released. Frequently, proteins of the outer chloroplast envelope and the mitochondrial outer membrane (MOM) are synthesised in the cytosol without a cleavable targeting sequence (Bolender *et al.*, 2008; Soll & Schleiff, 2004). Most commonly, plant mitochondrial import sequences are longer than those from animals or fungi (between 18 and 107 amino acids), and they are frequently rich in alanine, serine and positively charged residues such as arginine or lysine (Mackenzie, 2005). The hallmark of the mitochondrial alpha amphipathic import sequence of an inner membrane protein is the presence of several positively charged residues, which are frequently followed by hydrophobic amino acids that can act as a sorting signal to the inner membrane.

The N-terminal protein sequences of the Arabidopsis Slps were investigated for the presence of a putative mitochondrial targeting sequence. According to the structural predictions given in Figure 3-7 of Chapter 3 for AtSlp1, a stretch starting at amino acid 1 and ending at position 20 containing a number of positive charges, was predicted to form an amphipathic alpha helix. This sequence was projected into an alpha helical wheel and is shown in Figure 4-1 with the amino acid sequence shown underneath. The plot highlights the amphipathic nature of the formed helix, with positively charged residues located on one side, and hydrophobic amino acids on the opposite. For AtSlp2, a similar helix can be projected (Figure 4-1) using a stretch of amino acids from position 8 to 31. This sequence was also predicted to be alpha amphipathic (Figure 3-8) and positively charged. It is worth noting that the human Slp2 protein also contains N-terminal amino acids that adopt this conformation, further highlighting the structural similarity to the Arabidopsis proteins. Of course, these plots are merely examples illustrating the possibility of a specific sequence

stretch adopting the conformation of an alpha amphipathic helix. The true signal sequences after which the targeting sequences are cleaved off stretch most likely beyond these analysed regions.

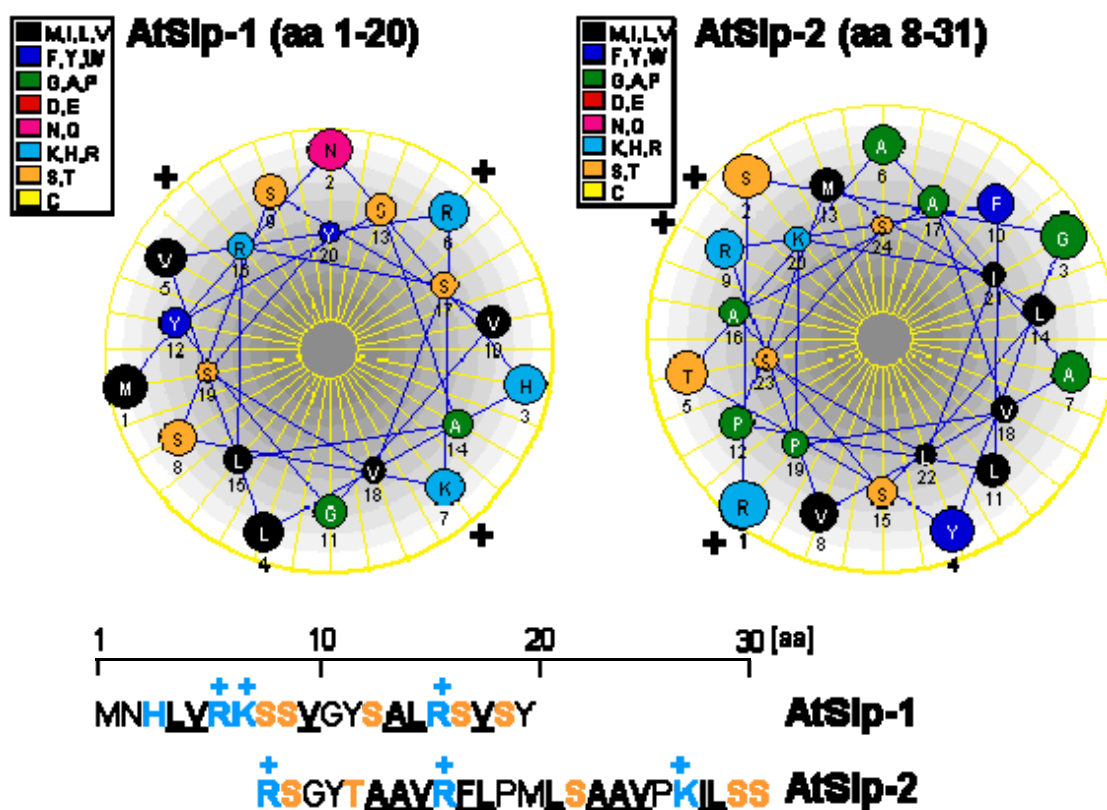


Figure 4-1. Alpha-helical wheel projection of N-terminal presequences of AtSlps. Two N-terminal sequences of each protein with predicted alpha-amphipathic stretches and positive charges were projected as helical wheel plots using the Protean software. Shown below are the chosen amino acids with positively charged residues highlighted in blue and hydrophobic residues underlined; hydroxylated residues are indicated by orange letters. [aa] stands for amino acids.

4.2 Biochemical evidence for mitochondria localisation of AtSlp1

Following the investigation of predicted target sequences of AtSlps, the following sections provide experimental evidence for the mitochondrial localisation of AtSlp1. The same experimental approaches were attempted to prove mitochondrial localisation of AtSlp2, but were ultimately not entirely satisfactory because of the poor quality of the antibody against this protein.

4.2.1 Aqueous 2-phase partitioning

As discussed earlier, several stomatin-type proteins from animals and humans are known to reside in the plasma membrane of various cell types. Amongst them, even human stomatin-like protein 2 was localised to the plasma membrane in T-helper cells and erythrocytes (Kirchhof *et al.*, 2008), but also to mitochondria in HeLa cells (Da Cruz *et al.*, 2008).

To exclude the possibility of dual targeting of AtSlp1 to mitochondria and to the plasma membrane, an aqueous 2-phase partitioning approach was applied. This method is based on the separation of vesicles according to their surface properties. Vesicles derived from the plasma membrane frequently contain glycosylated proteins and thus differ in their surface properties from vesicles derived from the endomembrane system or from organelles. The vesicles are separated between two aqueous solutions of high molecular weight polymers, in this case polyethyleneglycol (PEG 3350) and dextran (fraction T-500). Several extractions between these two phases yield a highly purified plasma membrane fraction (PM), and a separate endomembrane fraction (EM).

For the experiments described here, the original protocol of Larsson *et al.* (Larsson *et al.*, 1994; Larsson *et al.*, 1987) was modified and adapted for the use with Arabidopsis shoots grown on soil. Microsomal fractions from leaves were extracted and separated on the pre-formed 2-phase system. It has been previously shown that membrane fractions isolated in this manner contain plasma membrane and endomembrane fractions (eg from the ER or the Golgi apparatus), but they also contain membranes derived from organelles such as mitochondria (Mitra *et al.*, 2007; Borner *et al.*, 2005). The protein content of each fraction was determined, and samples separated on a 10% SDS-PAGE gel followed by Western blotting and detection of proteins. Figure 4-2 shows the Western blots of various samples

taken during the procedure. AtSlp1 clearly localised to the microsomal fraction, and was absent from the soluble protein supernatant. Between the two phases, the protein was strongly enriched in the lower phase containing the endomembrane vesicles. No clear band was detectable in the PM fraction. However, several weak bands were visible after prolonged exposure of the same molecular weight as AtSlp1, but also of higher molecular weights. To control the purity of the vesicle separation, an antibody against the PM – localised proton ATPase was used (Palmgren *et al.*, 1991). This antibody only recognised protein in the microsomal fraction and in the PM fraction. To control the purity of the endomembrane fraction, the mitochondrial marker protein peroxiredoxin II F (Finkemeier *et al.*, 2005) was probed with a specific antiserum. This antibody only recognised a band in the endomembrane fraction, as it was expected. These controls indicate that the separation was of high purity. The weak Slp1 bands observed after prolonged exposure of the Western blot probably indicate small levels of contamination of the PM fraction with material from the EM fraction. Based on this result, it was concluded that AtSlp1 does not reside at the plasma membrane, but is endomembrane associated.

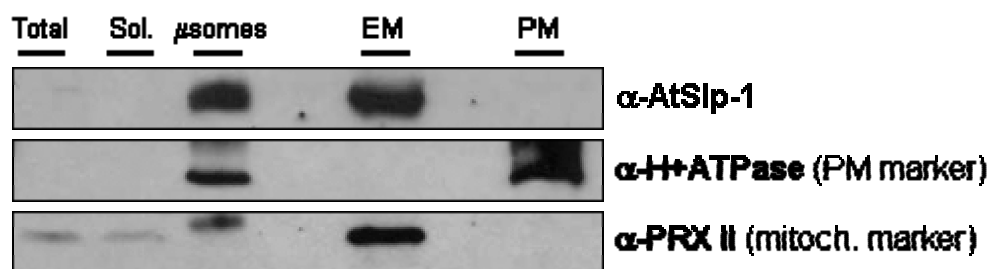


Figure 4-2. Aqueous 2-phase partitioning from Arabidopsis leaves. Shown is a Western blot that was probed with three different antibodies. Upper row: anti-Slp1, middle panel: anti-H⁺ATPase (a marker for the plasma membrane), bottom panel: anti-peroxiredoxin II (mitochondrial protein). The fractions shown are the total protein extract (Total), soluble proteins (sol.), microsomal fraction (μ somes), endomembrane fraction (EM) and the plasma membrane fraction (PM). The observed molecular weights were: ca. 45 kDa for Slp1, 100kDa for H⁺ATPase, 40kDa for PRXII.

4.2.2 Isolation of mitochondria from Arabidopsis leaves

To further clarify the subcellular targeting of AtSlp1 to mitochondria, organelles were isolated from Arabidopsis shoots using differential centrifugation followed by separation on linear and discontinuous Percoll gradients.

In a first attempt, mitochondria were pelleted by differential centrifugation only. About 50 grams of fresh weight tissue from mature short-day grown Col-0 rosettes were homogenised and processed by two series of low speed (<3000 g) and medium speed (12000 g) spins. This process resulted in a final pellet that was green in colour and also contained various other organelles, or fragments of organelles. Proteins were denatured and solubilised, followed by separation on a SDS-PAGE gel and Western blotting. Figure 4-3 shows a Western blot probed with anti-Slp1 and anti-peroxiredoxin II as a marker for the presence of mitochondria. The Slp1 protein was clearly present in all pellets, but absent from the supernatants after each spin that contains the soluble proteins. The mitochondrial marker PRX II was present in the same fractions as AtSlp1. Since the final pellet contained thylakoids amongst other organelle material such as peroxisomes, one can only conclude from this experiment that AtSlp1 is associated with a heavy organelle that was pelleted out by a medium speed spin at 12000 g.

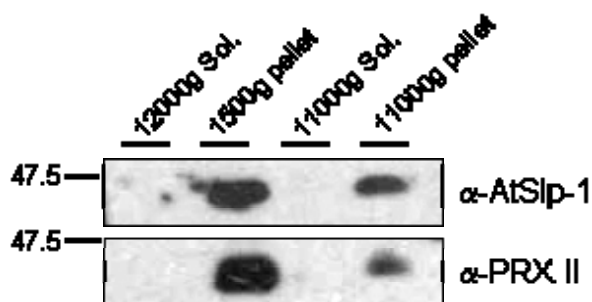


Figure 4-3. Western blot of organelle pellets after differential centrifugation. The first soluble fraction (Sol.) represents the supernatant after a 12000g spin. This spin was followed by a short spin at 1500g, after which both proteins are present in the pellet. The next soluble fraction (Sol.) is the supernatant after the final spin at 11000g; this pellet is designated as the final pellet and also contains both proteins.

Mitochondria were specifically purified from leaf material by differential centrifugation and separation of organellar material on a linear Percoll gradient. A series of differential centrifugation steps was used which ended with a spin at 11000 g before the resulting pellet was loaded on the gradient and was centrifuged. Figure 4-4 shows a Western blot of mitochondrial pellets probed with antibodies against Slp1, Slp2 and PRX II as a mitochondrial marker protein. Slp1 was present in the pellet after centrifugation at 11000g, but was barely resolved in the supernatant, indicating that it is associated with a pelletable organelle. The Slp1 protein was also present in the final mitochondrial fraction after loading the resuspended 11000 g-pellet material on the gradient. The antibody raised against the Slp2 protein only recognised a low molecular weight band at 25 kDa in the

mitochondrial fraction which probably represents unspecific binding (as seen in Figure 3-20 and 3-21 of Chapter 3). Since this band was also the most abundant band present in crude extracts (Figure 3-21), it cannot be ruled out that the true Slp2 protein was present at a higher molecular weight (as indicated in Figure 3-20), but was not detected by this antibody because of its low expression level or instability. Peroxiredoxin II was also present in the mitochondrial fraction at its monomeric molecular weight, but the dimeric form was also visible as a band running at approximately 40 kDa. This observation indicates that the isolated fraction contains mitochondria.

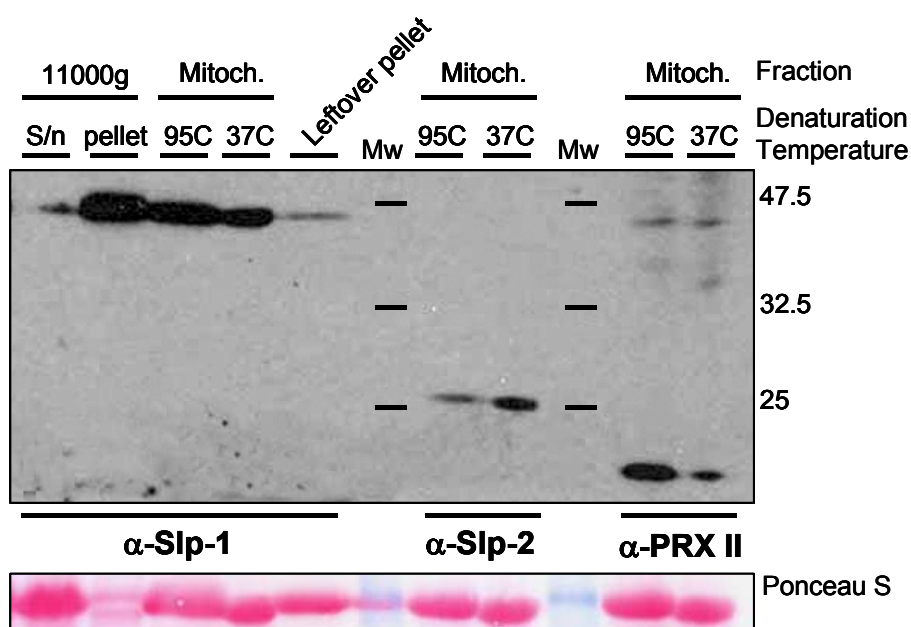


Figure 4-4. Western blot of a mitochondrial purification on a linear Percoll gradient. Shoot tissue was homogenised and separated by differential centrifugation before loading on a linear Percoll gradient. The final mitochondrial fraction (Mitoch.) and the supernatant (S/n) and pellet after an 11000g spin are shown. The sample named “Leftover pellet” refers to a translucent pellet visible at the bottom of the tube after the gradient spin. It was solubilised and loaded to check whether any remaining Slp protein might be present. The blot was probed with three different antibodies against Slp1, Slp2 (not purified) and peroxiredoxin II (PRX II). The Slp1 protein is present after the final spin (11000 g pellet) before loading the sample on the gradient, but hardly in the supernatant (S/n). Slp1 is present in the mitochondrial fraction following separation of the 11000 g pellet material on the gradient. Two samples of the final mitochondrial fraction are loaded that were denatured by boiling (95 °C) or at 37 °C. The Ponceau S stained membrane (proteins in red; molecular weight marker band (62.5 kDa) in blue) is included underneath the blot. Mw stands for molecular weight markers; the numbers on the right refer to the molecular weight of the marker bands (in kDa) as indicated by black horizontal bars.

To obtain mitochondrial preparations of enhanced purity, the isolation protocol was modified. A discontinuous Percoll gradient consisting of three steps was applied to improve separation of mitochondria from chloroplasts and chloroplast fragments. Mitochondria purified in this way were tested for the presence of AtSlp1 by solubilising the pellet in SDS loading buffer and separation on an SDS-PAGE gel followed by Western blotting. Figure 4-5 A) and B) show two Western blots of two separate purifications probed with antibodies against Slp1 and Slp2. Figure 4-5 A) shows a Western blot with samples from a mitochondrial purification on a first step gradient. The Slp1 protein was clearly present in the isolated mitochondria fraction. The antibody raised against Slp2 recognised a band at 25 kDa as seen before in Figure 4-4, but also a high molecular weight band at 83 kDa and two bands between 32 and 47 kDa that could stem from the full length Slp2 protein (green arrowhead). In a second purification, AtSlp1 was present as a strong band at 45 kDa in the 12000 g pellet following differential centrifugation, before this pellet was resuspended and loaded on the step gradient. The protein was also present in the mitochondrial fraction isolated from the gradient after centrifugation, although the signal was noticeably weaker than in the 12000 g pellet (Figure 4-5 B). This loss in band strength is probably a consequence of loss of mitochondrial material during the isolation of the mitochondria-enriched fraction, which was achieved by aspirating fractions above the mitochondria. Additionally, some material was probably lost by fragmentation of intact mitochondria during homogenisation or resuspension of pellet material. To control for the presence of mitochondria, the antibody against PRX II was used on aliquots from this separation as shown in Figure 4-7. In both mitochondrial separations from step gradients, no contamination with thylakoids could be detected as judged by Ponceau S stained Western blot membranes (no Rubisco bands visible).

These separations clearly demonstrate localisation of AtSlp1 and probably also AtSlp2 to mitochondria-enriched fractions. These results further support the idea that both Arabidopsis Slps are targeted to mitochondria and imported through their signal sequences.

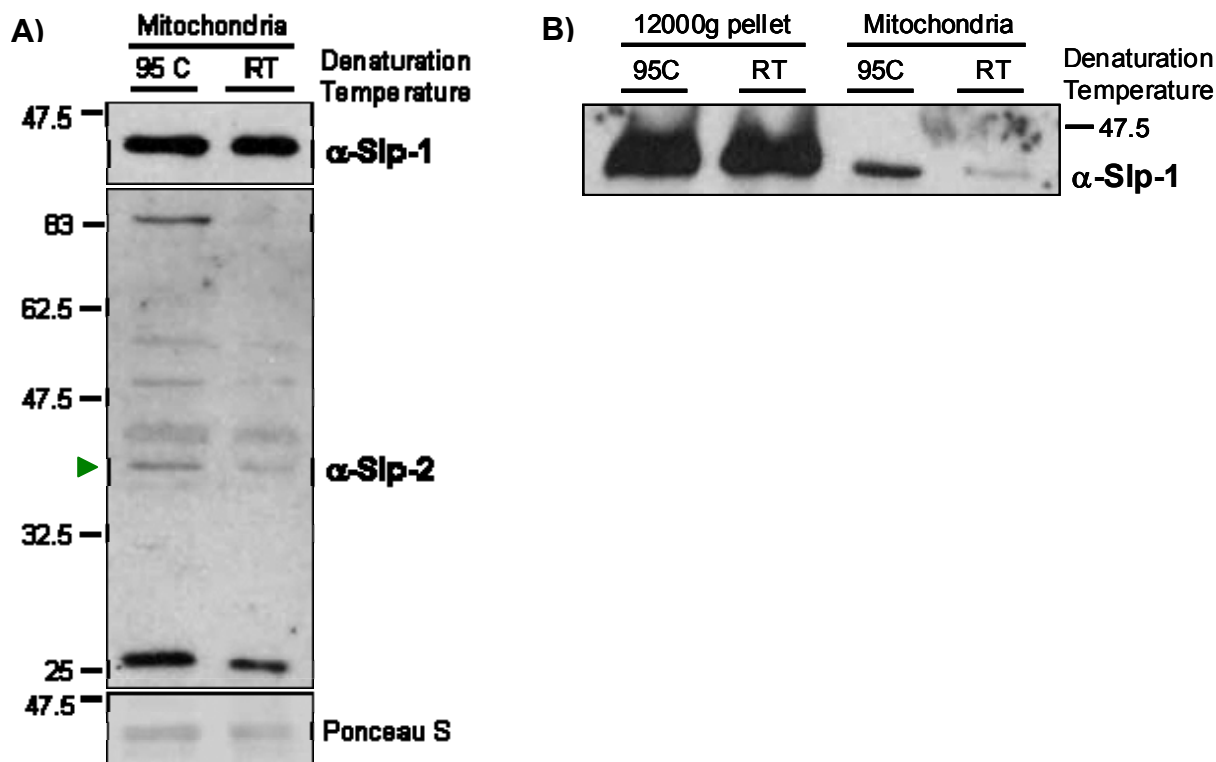


Figure 4-5. Mitochondria purifications on three-step Percoll gradients.

A) Western blot of a mitochondrial purification prepared on a step gradient. The mitochondria pellet was solubilised and denatured by boiling (95 C) or at room temperature (RT). The upper panel is probed with anti-Slp1 antibody; the blot in the middle was probed with the unpurified anti-Slp2 antibody. The bands visible with this antibody at 25 kDa are probably unspecific; the bands between 32 and 47 kDa molecular weight might stem from the full length protein (indicated by the green arrowhead). Shown at the bottom is a section of the Ponceau S stained nitrocellulose membrane for reference of loading levels. Numbers on the left side indicate molecular weight markers in kDa. More bands are visible after heat treatment at 95 °C than at room temperature because a higher degree of denaturation is achieved by boiling the samples.

B) Western blot of a second mitochondrial purification prepared as in A). Pellets obtained after differential centrifugation (12000 g pellet) and discontinuous Percoll gradient centrifugation (Mitochondria) were probed with anti-Slp1. All fractions were denatured by boiling (95 °C) and at room temperature (RT). The number on the right side indicates the molecular weight marker band in kDa. Note the loss of material after retrieving mitochondria from the gradient.

4.2.3 Sub-mitochondrial localisation of AtSlp1

To investigate the localisation of AtSlp1 inside mitochondria, isolated organelles were treated with protease in the absence and presence of increasing amounts of digitonin. Digitonin, when applied in low amounts, is reported to specifically dissolve the mitochondrial outer membrane, but leaves the inner membrane intact (Hoppel & Cooper, 1968; Morton *et al.*, 1968; Newman *et al.*, 1968). This property is down to the digitonin structure that enables it to replace sterols in membranes, thereby rupturing lipid bilayers (Akiyama *et al.*, 1980). The structure of the mitochondrial outer membrane differs from that of the inner membrane in terms of lipid composition and protein content (Malisan & Testi, 2003), notably in having a higher sterol content. This difference accounts for the selective action of digitonin on the outer membrane. Treatment of mitochondria with protease K in combination with digitonin has been previously reported in studies addressing protein localisation within the mitochondrial membranes (Hajek *et al.*, 2007; Da Cruz *et al.*, 2008).

Mitochondria isolated on a linear Percoll gradient (see Figure 4-4) were aliquoted and treated without (= control) and with protease K and a gradient of digitonin ranging from 0-3 $\mu\text{g/ml}$ concentration. Figure 4-6 shows a Western blot from this experiment probed with anti-Slp1 and anti-Slp2. The Slp1 protein is clearly present in the control sample without protease or detergent added (lane no. 1). When protease K is present in the absence of digitonin, the protein is not degraded indicating that it is most likely not localised on the outer membrane facing the cytoplasm if the isolated mitochondria were intact. Addition of digitonin at low concentrations up to 2 $\mu\text{g/ml}$ does not have any effect on the Slp1 protein, indicating that it is probably protected from degradation by the presence of the outer mitochondrial membrane. Increasing the amount of digitonin to 3 $\mu\text{g/ml}$ in the presence of protease K caused partial degradation of Slp1 (lane no. 7; compare loading level between lanes on Ponceau S stain). This result indicates that the protein is not facing the cytoplasmic site of the outer membrane, but it is more likely that it is attached to the mitochondrial inner membrane orientated towards the intermembrane space. The concentration of digitonin used here (2.4 μM) is sufficiently low not to penetrate and disrupt the mitochondrial inner membrane (Hajek *et al.*, 2007) and therefore does not give the protease access to proteins present in the matrix. A confirmation of this idea by using a mitochondrial marker protein of known localisation is not included in this blot. The proposed localisation of AtSlp1 to the inner membrane with an orientation towards the intermembrane space is thus purely an assumption based on reports of digitonin treatment

in the literature. The antibody raised against AtSlp2 was also used to probe the same Western blot. It recognised the band at 25 kDa as seen before in Figure 4-4 and 4-5 as well as a band of approximately 45 kDa in the untreated control sample (lane no. 1). Upon addition of protease, this higher band was degraded, hinting that this protein is associated with the outside of the organelles; it is most likely unrelated to Slp2. The band at 25 kDa molecular weight behaved like the Slp1 protein, indicating that this protein is protected from degradation by the outer membrane up to a certain amount of digitonin added. This 25 kDa protein is either unspecific, or it might be a degradation product of Slp2. Several faint bands around 35 kDa might stem from the full length Slp2 protein as indicated by the green arrowhead.

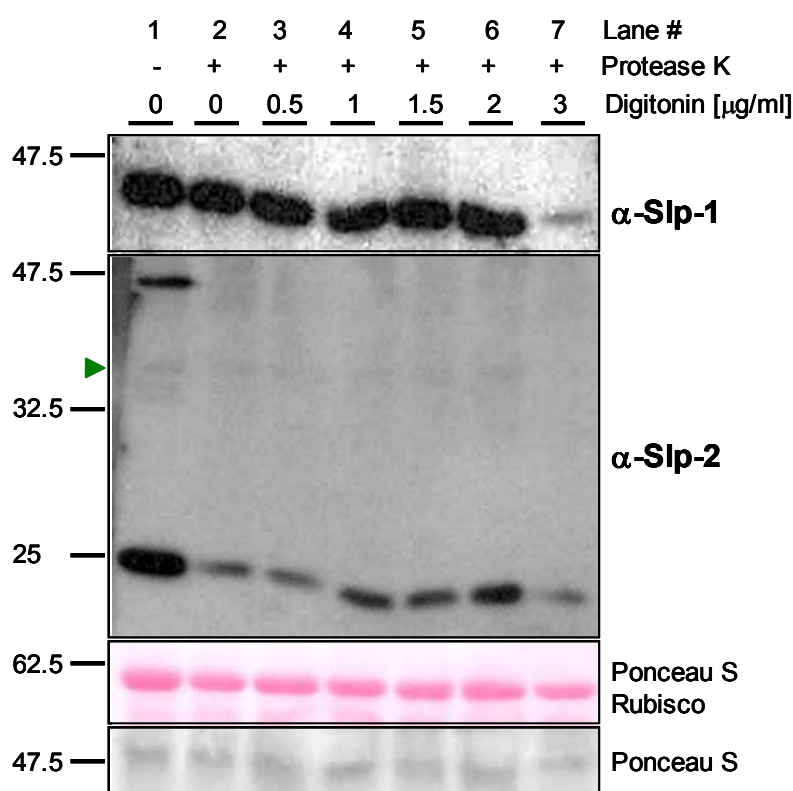


Figure 4-6. Western blot of mitochondria isolated on the linear Percoll gradient and treated with protease K and digitonin. The upper blot was probed with anti-Slp1 and the blot in the middle with anti-Slp2. Each lane is numbered (1-7), and the addition of protease K is indicated by “+”; the amounts of added digitonin are given in [$\mu\text{g/ml}$]. Two sections of the Ponceau S stain are included on the bottom to indicate the presence of Rubisco (ie thylakoid contamination) and to give an independent loading reference. Numbers on the left side refer to molecular weight markers in kDa. 5 micrograms of protein were loaded per lane.

This experiment was repeated twice with mitochondria isolated on step gradients (see Figure 4-5). The first experiment was performed with identical amounts of protease K and digitonin. Figure 4-7 (A) shows a Western blot of treated mitochondrial fractions probed with anti-Slp1. In contrast to the previous experiment, the protein was not degraded in the

presence of 3 $\mu\text{g/ml}$ digitonin (= 2.4 μM). In the second experiment (Figure 4-7 B), mitochondria were isolated identically (see Figure 4-5 B), but treated with higher amounts of digitonin (up to 8 $\mu\text{g/ml}$). Digitonin concentrations of up to 5 $\mu\text{g/ml}$ (= 4 μM) did not affect the stability of Slp1 in this case. However, when the concentration was raised to 8 $\mu\text{g/ml}$ (= 6.5 μM), the protein was completely degraded. As a control, fractions treated with 1 and 8 $\mu\text{g/ml}$ digitonin were run on a separate gel and Western blots probed with the antibody against PRXII. This protein must reside in the mitochondrial matrix as it was not affected by protease degradation under these conditions. This result indicates that the inner membrane structure was preserved during the experiment and further provides evidence that Slp1 is localised to the mitochondrial inner membrane facing the intermembrane space. A very similar behaviour was also reported for the human Slp2 protein, further supporting the idea that these proteins are orthologs. The human Slp2 protein was also only degraded when higher amounts of digitonin (up to 3 $\mu\text{g/ml}$) were applied to isolated mitochondria (Hajek *et al.*, 2007).

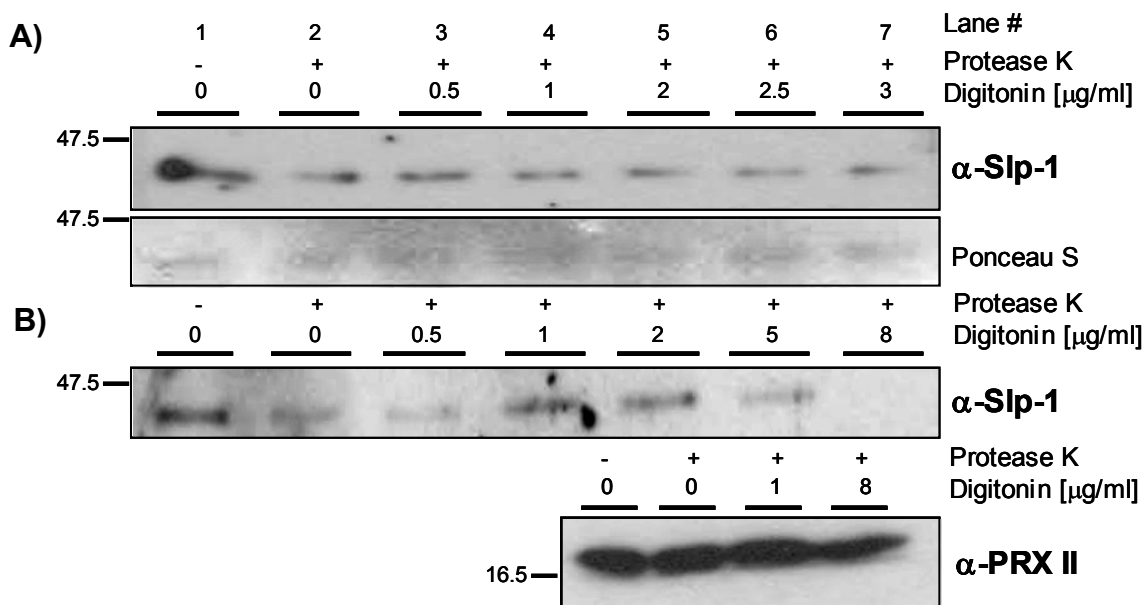


Figure 4-7. Western blot of mitochondria fractions isolated on step gradients that were treated with protease K and increasing amounts of digitonin.

A) Western blot probed with anti-Slp1 from the first mitochondrial isolation on a step gradient (corresponding to Figure 4-5 A). The Ponceau S stain indicates equal amounts of protein loaded on each lane. Two micrograms of protein were loaded on each lane.

B) Western blot probed with anti-Slp1 of a second experiment with mitochondria purified on another step gradient (Figure 4-5B) and treated with higher amounts of digitonin. Five micrograms of protein were loaded on each lane. Shown underneath is a Western blot of some of the fractions probed with anti-PRXII as a matrix marker protein. A total amount of 7 micrograms of protein were loaded on this blot. Labelling of lanes is as described in Figure 4-6 and numbers on the left side of each blot indicate molecular weight markers in kDa.

The differences in Slp1 degradation between Figures 4-6 and Figures 4-7 A and B in the presence of different amounts of digitonin first seem surprising. However, the solubilisation of membranes by digitonin is known to be dependent on the ratio of detergent to the amount of protein present (Boyer *et al.*, 1994). If the protein concentration is below 20 mg/ml, the authors report that increased amounts of digitonin are necessary to achieve solubilisation of the mitochondrial outer membrane compared to situations when the protein concentration is 50 mg/ml. No such effect was reported on the disruption of the inner membrane by digitonin. For a better comparison of the three individual experiments, the ratios of digitonin to the actual protein content of each sample (in μg digitonin/mg mitochondrial protein) were calculated and are presented in Table 4-4. The first mitochondrial preparation contained most protein (64 micrograms per aliquot), but it was also less pure than the following two purifications from step gradients. Only four micrograms of digitonin per milligram protein were necessary to affect the stability of Slp1. The same concentration of digitonin (3 $\mu\text{g}/\text{ml}$) did not cause degradation in the second experiment (step gradient no. 1) that had a much lower concentration of mitochondrial protein (only 7 micrograms per treated aliquot). This sample was also purer and thus reflects a more realistic situation in terms of the actual amount of mitochondrial protein present. The digitonin/protein ratio was 22. Taking into account the amounts of protein in these two samples, the sample from the step gradient should have also been visibly degraded compared to the sample from the linear gradient, although this was clearly not the case. Alternatively, the linear gradient sample should have required a higher digitonin/protein ratio had it been of higher purity. It is possible, therefore, that the mitochondria from this preparation were not entirely intact and therefore required less detergent to rupture the outer membrane sufficiently.

The Slp1 protein was completely degraded in the last experiment in the presence of 8 $\mu\text{g}/\text{ml}$ digitonin (sample 7, step gradient no. 2). This sample had a digitonin to protein ratio of approximately 11, and a protein content that was five times higher compared to the purification on the first step gradient. Thus, higher protein amounts do seem to require relatively less digitonin to dissolve the outer membrane to an extent that the protease has access to the Slp1 protein. When these two purifications are compared, the sample from the first step gradient would have required a detergent/protein ratio of almost 60 to ensure solubilisation of the outer membrane. Boyer *et al.* (Boyer *et al.*, 1994) report that for protein concentrations of 20 mg/ml or lower, digitonin/protein ratios of 0-400 $\mu\text{g}/\text{mg}$ are required to ensure complete rupture of the outer membrane. By comparison, HsSlp2 was degraded by protease K with a detergent/protein ratio of 1.5 $\mu\text{g}/\text{mg}$ (Hajek *et al.*, 2007).

However, in this study the overall protein concentration was 2 mg/ml, about twice as high as in these preparations (1mg/ml in step gradient no. 2).

Despite the discrepancies in terms of digitonin concentrations required for solubilisation amongst the three experiments, it can be concluded that the Slp1 protein is indeed associated with the mitochondrial inner membrane. Based on the behaviour of the matrix protein PRXII (Figure 4-7), Slp1 probably faces the intermembrane space, analogous to HsSlp2. How stable Slp1 is in this compartment probably depends on its protein-lipid environment. Most likely it is embedded in a larger protein complex and might be partially protected from degradation by protease K in these experiments. To fully confirm the successful rupture of the outer membrane, an unrelated intermembrane space protein should have been included here. Additionally, another protein residing in the outer membrane should have been tested to finally confirm the behaviour of Slp1.

For AtSlp2, it remains difficult to determine its localisation in a specific mitochondrial membrane compartment due to the questionable specificity of the antibody. If the 25kDa band is related to this protein (i.e. if it is a mature form of a longer precursor), one could conclude from Figure 4-6 that this protein behaves similar to Slp1. The Slp2 antibody was used to probe the Western blots seen in Figure 4-7, but no clear protein bands were detected. With respect to the targeting predictions for this protein, it is most likely also associated with the mitochondrial inner membrane, either facing the intermembrane space or the matrix side.

Sample #	Linear gradient (64 µg mitoch. protein/aliquot)		Step gradient # 1 (7 µg mitoch. protein/aliquot)		Step gradient # 2 (37 µg mitoch. protein/aliquot)	
	Digitonin [µg/ml]	Digitonin/protein [µg/mg]	Digitonin [µg/ml]	Digitonin/protein [µg/mg]	Digitonin [µg/ml]	Digitonin/protein [µg/mg]
1	0	0	0	0	0	0
2	0	0	0	0	0	0
3	0.5	0.69	0.5	3.6	0.5	0.67
4	1	0.7	1	7.2	1	1.34
5	1.5	1.06	1.5	10.8	2	2.68
6	2	1.4	2	14.3	5	6.7
7	3	4.11*	3	22	8	10.7

Table 4-4. Detergent/protein ratios for each of the three experiments in µg digitonin/mg mitochondrial protein present in each sample. The left table contains the ratios calculated for the preparation from the linear gradient. The middle and right tables show ratios calculated from the two step gradient preparations. The first row always indicates the total amount of protein (in micrograms) present in each aliquot. The asterisk in the left table indicates that sample no. 7 from this experiment had a protein content that was only half (approximately 35 µg) of that from samples nos. 1-6; thus the detergent/protein ratio is higher than one would expect with respect to the other values. Red numbers indicate ratios that caused degradation of Slp1.

4.3 *In vivo* evidence for Slp localisation to mitochondria

To investigate the subcellular localisation of AtSlps in the living plant, fluorescent fusion constructs were prepared. In a first attempt, N- and C-terminal fusions with YFP were cloned for each of the two Arabidopsis Slps. The expression of these constructs was driven by the constitutive Cauliflower Mosaic Virus 35S promoter (CMV 35S). To compare the expression observed under this condition, a C-terminal GFP fusion was created inside the genomic sequence of AtSlp2, driven by its native promoter. A similar construct was attempted for the genomic sequence of AtSlp1, but proved technically too time consuming and was not continued.

4.3.1 *Stable fluorescent protein overexpressing lines*

The open reading frames of AtSlp1 and AtSlp2 were amplified and fused to YFP. Constructs were made in both N- and C-terminal orientations inside a bacterial cloning vector. The expression cassette of this vector (named pTEY) also contained the 35S promoter sequence upstream, and the NosA terminator sequence after a stop codon behind the YFP. The complete expression cassette containing one of the Arabidopsis Slp sequences was then excised out of pTEY and inserted into the binary vector pTKAN⁺ (Schaaf *et al.*, 2006) for expression in plants. This was accomplished by digestion of pTEY with NotI and ligation with pTKAN⁺ that was opened with PspOMI. Figure 4-8 gives an overview over the T-DNAs of the cloned fusion protein constructs in the C-terminal fusion orientation.

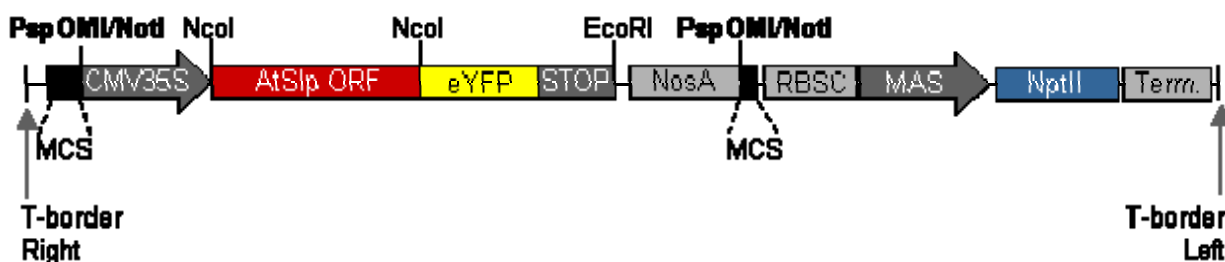


Figure 4-8. Overview of 35S::Slp::YFP constructs. Only the T-DNA is shown. The same clones were also produced with YFP fused to the N-terminus of AtSlps for comparison. The AtSlp open reading frames (ORF) are shown in red. Abbreviations are: MCS (multiple cloning site), CMV35S (Cauliflower Mosaic Virus 35S promoter), eYFP (enhanced yellow fluorescent protein), STOP (indicates stop codon), RBSC (Rubisco terminator sequence), MAS (promoter), NptII (neomycin phosphotransferase II- kanamycin resistance gene), Term. (terminator sequence).

A second type of construct was created by fusing GFP to the C-terminus of AtSlp2 inside its entire genomic sequence. This sequence was 4427 bp long and included 1713bp of upstream promoter sequence, followed by all exons and introns and the 3'UTR. This cassette was excised from a bacterial cloning vector and ligated into pTKAN⁺ for plant transformation. Figure 4-9 shows the T-DNA for this expression construct.

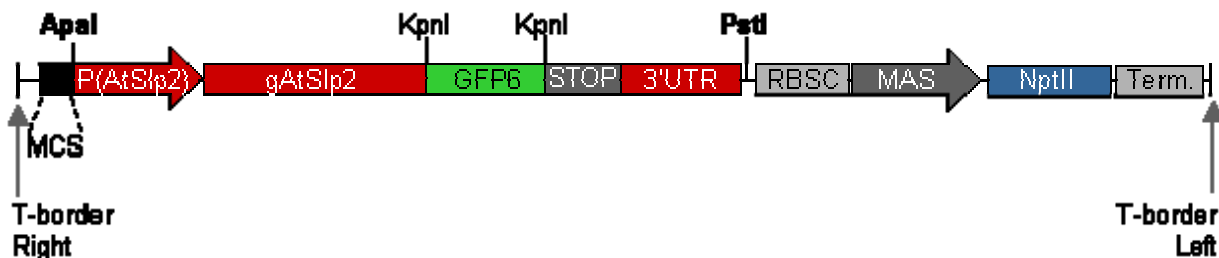


Figure 4-9. T-DNA of genomic GFP fusion construct of AtSlp2. The genomic sequence was cloned from genomic DNA into a bacterial cloning vector. A KpnI restriction site was inserted just before the stop codon (STOP) and used to insert GFP. This fusion cassette was exerted by restriction digestions with Apal and PstI and inserted into pPTKAN⁺. Abbreviations are: P(AtSlp2) (promoter region of AtSlp2), gAtSlp2 (genomic sequence of AtSlp2), GFP6 (green fluorescent protein 6), 3'UTR (3' untranslated region), RBSC (Rubisco terminator sequence), MAS (promoter), NptII (neomycin phosphotransferase II), Term. (terminator sequence).

All constructs were transformed into *Agrobacterium tumefaciens* and used for stable transformation of Arabidopsis wild type plants (ecotype Col-0) by the floral dip method. Positive transformants were selected based on resistance to kanamycin on agar plates. The segregation patterns were counted and positive plants propagated. For fluorescent protein analysis by confocal microscopy, only T1 and T2 generation transformants were used.

4.3.1.1 AtSlp1- overexpression under the constitutive promoter

Positive transformants (T1) expressing Slps fused to YFP at their C-terminal end were selected on kanamycin, transplanted to soil and leaves were collected for imaging. Figure 4-10 shows confocal images of a guard cell and an epidermal cell expressing Slp1::YFP. The yellow fluorescent stain is clearly visible in punctae distributed throughout the cells. It is present in both guard cells and epidermal cells as expected from the activity of the 35S promoter. The yellow labelled structures were highly mobile when they were followed by images taken in time series (not shown). Fluorescence was not present in chloroplasts or at the plasma membrane. An identical expression pattern was also observed with the 35S::Slp2::YFP fusion construct (not shown).

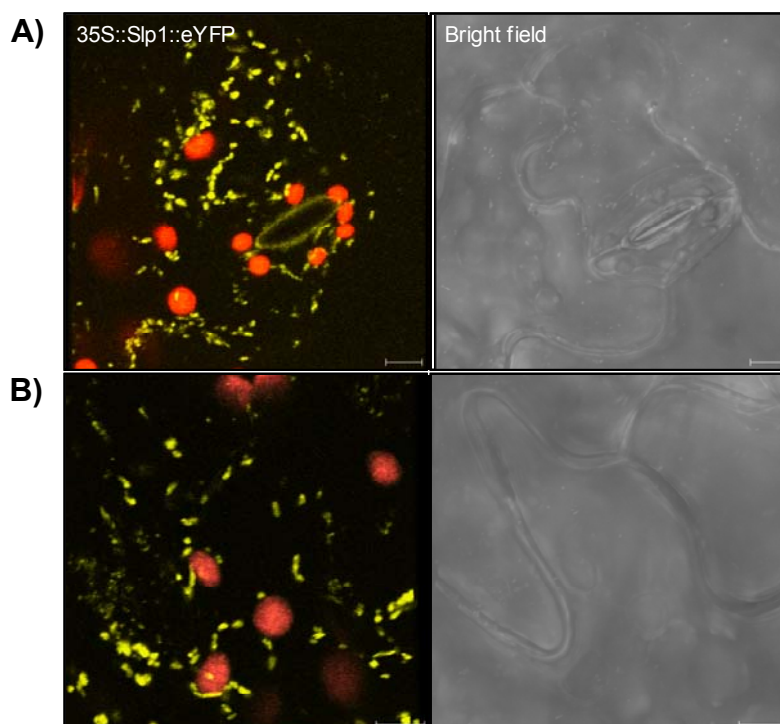


Figure 4-10. Three-dimensional reconstructions of a guard cell (A) and an epidermal cell (B) from a stably transformed line expressing Slp1-YFP. The scale bars represent 5 μ m distance. Slp1-YFP is shown in yellow, and chloroplast autofluorescence in red in the left panel. Bright field images are included on the right side for reference.

To confirm the presence of Slp1 fusion protein, proteins were extracted from seedlings and separated on a SDS-PAGE gel followed by Western blotting. The fusion protein could be detected with antibodies against GFP and Slp1 at the correct molecular weight of 65 kDa (Figure 4-11). Part (A) shows a Western blot of seedlings treated with UV-B light for 15 minutes as described in chapter 3 section 3.5.3.4. The Slp1-YFP seedlings were treated with UV light, after which the protein level of the fusion protein increased (sample grown on MS, third from left). For comparison, wild type protein extracts from untreated seedlings (separated into microsomal and soluble fraction) are also included to demonstrate specificity of the antibody. When probed with antibody raised against GFP, the same pattern of bands was seen in the Slp1-YFP samples. Thus, the observed pattern of fluorescence stems indeed from the stable expression of Slp1-YFP. Curiously, antibody against Slp1 only recognised the YFP fusion protein (at 65 kDa) in the samples of the overexpressor plants, but not the endogenous Slp1 protein. This protein can be seen in the wild type microsomal fraction at the normal molecular weight (45 kDa). Part (B) shows a second Western blot from a separate experiment probed with anti-Slp1. Seedlings were grown in hydroponic culture and proteins extracted. Slp1-YFP was again seen only in the overexpressor samples at the expected molecular weight (65 kDa). The antibody

recognised Slp1 in the wild type sample (red arrowhead), but this band was again much reduced in the samples of the overexpressing seedlings. This observation could lead to the conclusion that the expression of Slp1 in the overexpressing plants is suppressed by the presence of the Slp1-YFP fusion protein. Alternatively, Slp1 in its monomeric form might participate in SDS-resistant high molecular weight complexes with Slp1-YFP.

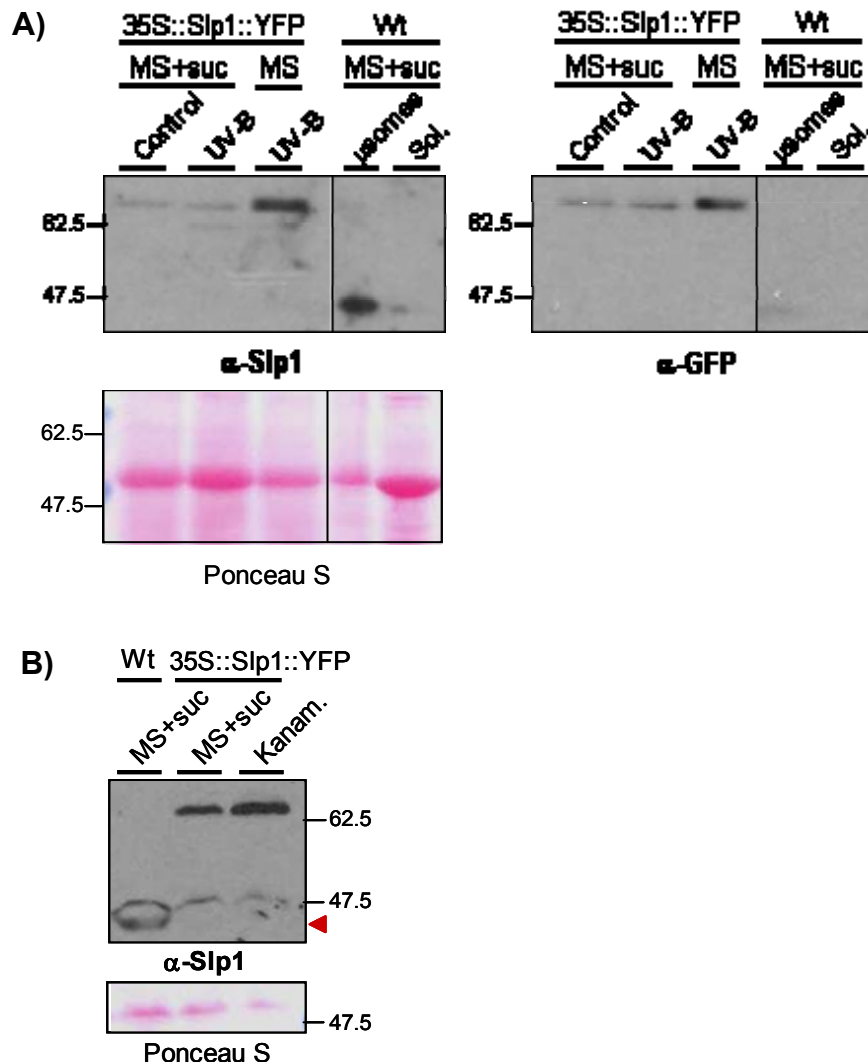


Figure 4-11. Western blots of seedlings overexpressing Slp1-YFP.

A) Western blot probed with anti-Slp1 and anti-GFP of seedling extracts from Slp1-YFP overexpressing plants and wild type plants. The Slp1-YFP overexpressors were grown on agar plates in the presence of added sucrose (MS+suc) and without (MS). Seedlings were treated with UV-B light (UV-B), after which the protein level of Slp1-YFP is increased in the sample grown on MS agar plates (MS). The samples from wild type plants (Wt) are protein extracts from seedlings separated into the microsomal fraction (μ somes) and soluble proteins (Sol.). These plants were set up for an unrelated experiment but are included here as a comparison between wild type extract and Slp1-YFP overexpressor extract. The Ponceau S stain is shown below for comparison of loading levels. Numbers indicate molecular weight markers in kDa.

B) Western blot probed with anti-Slp1 showing an unrelated example of wild type and Slp1-YFP seedling protein extracts. All plants from this setup were grown hydroponically in parallel. One sample of Slp1-YFP plants was grown in the presence of kanamycin to select for positive transformants. The red arrowhead indicates the endogenous Slp1 protein. As in A), this protein is strongly reduced in the overexpressor samples. Labelling is as above.

4.3.1.2 Co-localisation of Slp1-YFP with MitoTracker

To confirm that the observed organelle pattern of Slp1-YFP corresponds indeed to mitochondria, root hairs of overexpressing lines were incubated with MitoTracker DeepRed (Molecular Probes), a marker dye that specifically accumulates in active mitochondria. This imaging was done on root hairs rather than leaf epidermal cells because of their high autofluorescence background associated with chloroplasts in the leaves. MitoTracker DeepRed gave strong fluorescence in the range of chlorophyll and thus blurred mitochondria when applied to leaf pieces. Slp1-YFP plants were grown hydroponically, and young seedlings were incubated with MitoTracker prior to imaging by confocal microscopy. Figures 4-12 and 4-13 show confocal microscopy images of root hairs that clearly show co-localisation of the marker with Slp1-YFP in the merged images. As observed in leaves, mitochondria were highly mobile in healthy root hairs and were seen to fuse frequently with each other in time series (not shown). The clear co-localisation pattern of Slp1-YFP with the mitochondrial marker dye MitoTracker provides the first *in vivo* evidence for mitochondria localisation of this protein. It also confirms the Western blots where Slp1 was detected in mitochondrial pellets (Figures 4-4 and 4-5).

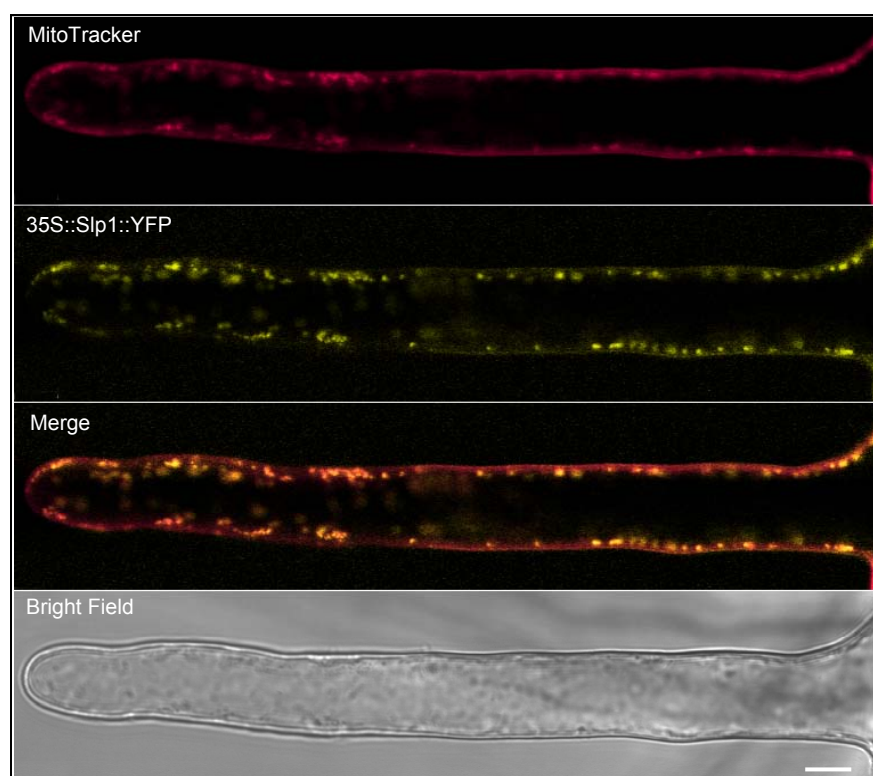


Figure 4-12. Co-localisation of MitoTracker DeepRed and Slp1-YFP. Slp1 overexpressing seedlings were incubated with MitoTracker before confocal microscopy. Co-localised organelles are shown as orange spots. These images were taken from a time series where movements of mitochondria along actin filaments were tracked during cytoplasmic streaming. Scale bar indicates 10 μ m.

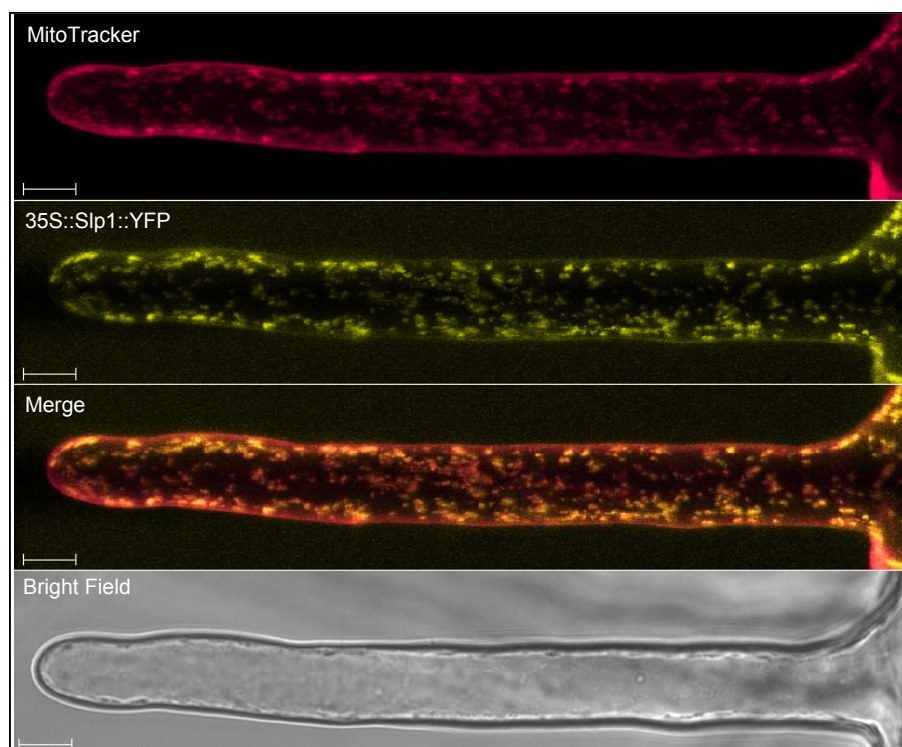


Figure 4-13. Three-dimensional reconstruction of MitoTracker-infiltrated root hair from Slp1-YFP overexpressing plant. The same root hair is shown as in Figure 4-12. Labelling is as before. Scale bar = 10 μ m.

4.3.1.3 AtSlp2- overexpression under its native promoter

Seedlings of plants transformed with the genomic GFP fusion of AtSlp2 (T1) were grown on agar plates in the presence of kanamycin and used for confocal imaging. Figure 4-14 shows a series of images showing expression in different plant parts. Expression of AtSlp2-GFP was strong as distinct moving punctae throughout the seedlings when epidermal cells were imaged. Around the rosette, GFP fluorescence was readily detectable in stipules (Figure 4-13 top panel red arrowheads), but also all over the leaf and stem epidermis. GFP fluorescence was also visible in root epidermal cells and in the root tip, where it was excluded from the meristematic centre. AtSlp2 expression was present evenly along the root epidermis, and also in root hairs (red arrowhead). Along the stem epidermis, GFP fluorescence was evenly spread over epidermal cells and guard cells in discrete and mobile organellar structures. No GFP fluorescence was detected in chloroplasts or at the plasma membrane.

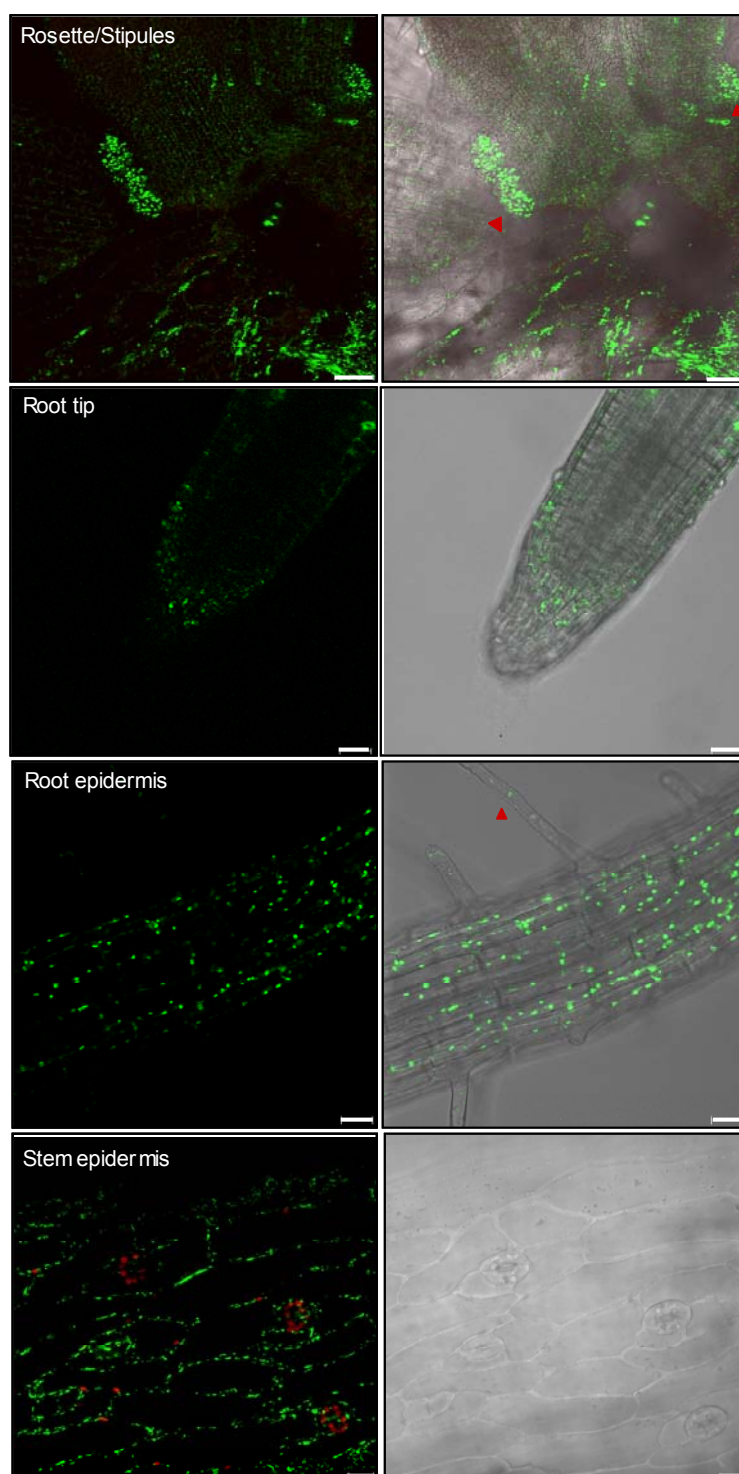


Figure 4-14. AtSlp2-GFP expression in seedling organs. The top images show the interior of a rosette with stipules highlighted by red arrowheads (Scale bar = 50 μ m). The mid panels show images of a root tip and root epidermal cells (Scale bars = 20 μ m). The red arrowhead points out GFP expression in a root hair. The bottom images show stem epidermal cells (Scale bar = 10 μ m). Red fluorescence indicates chlorophyll autofluorescence of guard cell chloroplasts.

In leaves, AtSlp2-GFP from the same seedlings was highly expressed in epidermal pavement cells and in guard cells (Figure 4-15). As seen before, the GFP fluorescence was detected in distinct moving organellar structures. No GFP label was detected at the cell periphery or in chloroplasts.

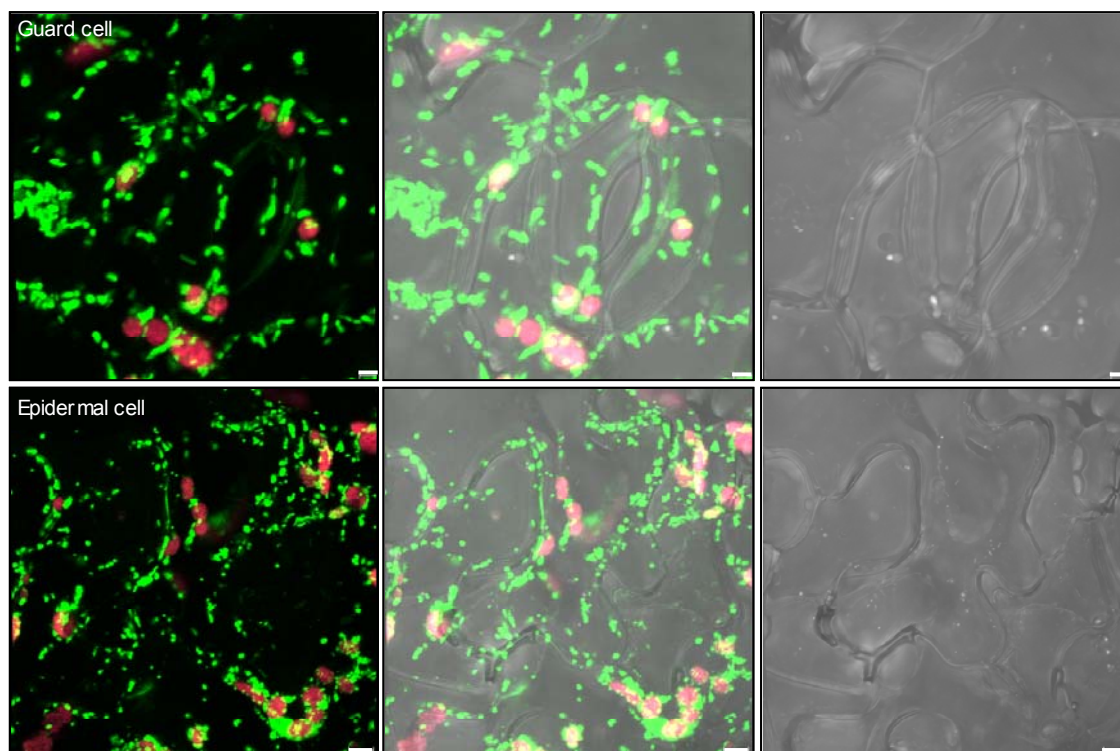


Figure 4-15. Three-dimensional reconstructions of AtSlp2-GFP expression in leaves. The top images show a guard cell. Slp2-GFP is seen in distinct organellar structures evenly between the guard cell pair and the surrounding epidermal cells. Red spots are chloroplast autofluorescence. The images underneath show epidermal cells with Slp2-GFP highly expressed within all cells. All images are three-dimensional reconstructions. Scale bars =5 μ m.

The high expression level of AtSlp2-GFP under its own promoter was surprising. Based on what was observed from the promoter-GUS stains of this gene and the high number of cycles necessary to amplify it from cDNA, much lower GFP fluorescence levels were expected. In particular, the high expression level in epidermal cells was unexpected. From the promoter-GUS stains seen in Figure 3-36 it was assumed that no, or very little expression would be observed in leaf epidermal cells. However, the GUS approach is much less sensitive than detection of GFP fluorescence by confocal microscopy. Additionally, the actual Slp2 protein is expressed under its own promoter in this experiment, compared to β -glucuronidase in the GUS fusions. It is also possible that the AtSlp2-GFP protein was more stable than β -glucuronidase expressed under the Slp2 promoter. To further confirm that AtSlp2-GFP was expressed in these plants, proteins were

extracted and Western blots probed with monoclonal GFP antibody. Figure 4-16 shows the Western blot from crude protein extracts from plants expressing either Slp2-GFP under its own promoter, or the Slp2 open reading frame fused to YFP under the 35S promoter. This construct is described in Figure 4-8. As a comparison, wild type extract was also included. From this Western blot it can be seen that the Slp2 fusion proteins are expressed at the expected molecular weight in all cases. When controlled by the 35S promoter, the expression level is much higher than when expression is controlled by the native promoter, further indicating that this gene is expressed at relatively low levels. The presence of the Slp2-GFP band at the expected molecular weight (60 kDa) also indicates that the gene fused to GFP after its last exon is spliced correctly when expressed in Arabidopsis. No band is detected in the wild type extract, indicating that the fusion proteins are specifically expressed in transformed seedlings. Thus, the observed GFP fluorescence pattern in organelles must originate from overexpressed, stable AtSlp2 fusion protein.

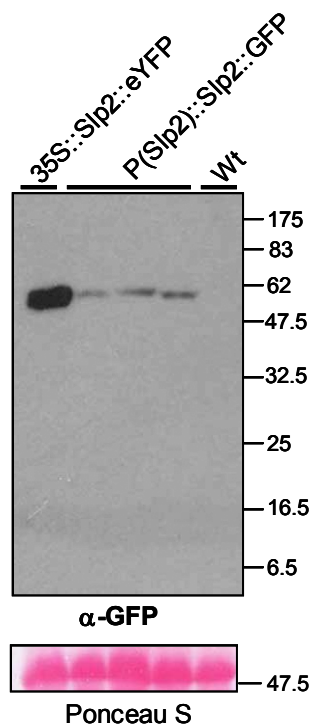


Figure 4-16. Western blot probed with anti-GFP of proteins extracted from leaves of plants expressing Slp2-YFP under the 35S promoter (35S::Slp2::eYFP) or Slp2-GFP under its own promoter (P(Slp2)::Slp2::GFP). Wild type extract (Wt) is included as a comparison. For reference of loading levels, the Ponceau S stain showing Rubisco bands is shown at the bottom. Numbers indicate molecular weight markers in kDa.

4.3.1.4 Co-localisation of AtSlp2-GFP with MitoTracker

To confirm that the observed organellar structures seen as AtSlp2-GFP were indeed mitochondria, co-localisation experiments with MitoTracker Orange were carried out. To observe co-localisation, leaf pieces from stable transformed lines (T1) were infiltrated with the marker dye, followed by incubation (45 minutes) and confocal imaging. The MitoTracker used to study co-localisation with GFP did not give background fluorescence that coincided with chlorophyll autofluorescence. Therefore, leaves were chosen for imaging, also because the expression level of AtSlp2 was assumed to be higher in leaves, and most phenotypes described in chapter 5 were related to leaf growth. Figure 4-17 shows a series of images taken from Slp2-GFP expressing leaf epidermal cells infiltrated with MitoTracker Orange. As expected, the GFP fluorescent organelles co-localised well with MitoTracker-labelled structures, confirming this assumption. A second example showing epidermal cells and a guard cell from an independent line is shown in Figure 4-18. As seen before, most green fluorescent organelles colocalise with MitoTracker-labelled mitochondria. In this image, some spots are not labelled with MitoTracker, especially those inside the guard cell. However, overall the MitoTracker dye was weaker in this image compared to the image in Figure 4-17. When time series were taken of both examples, co-localisation of the two fluorescent labels could be easily traced. This parallel movement further confirmed their identity as mitochondria.

These results confirm that also AtSlp2 is a mitochondrial protein *in vivo*, and with its expression under its own promoter and genomic sequence, indicate that the protein is expressed widely throughout the plant tissues. This demonstration also supports the view that both Arabidopsis Slps are expressed together in the same subcellular compartment and thus might form one unit. For AtSlp2, this is also the first confirmation of mitochondrial localisation *in planta*.

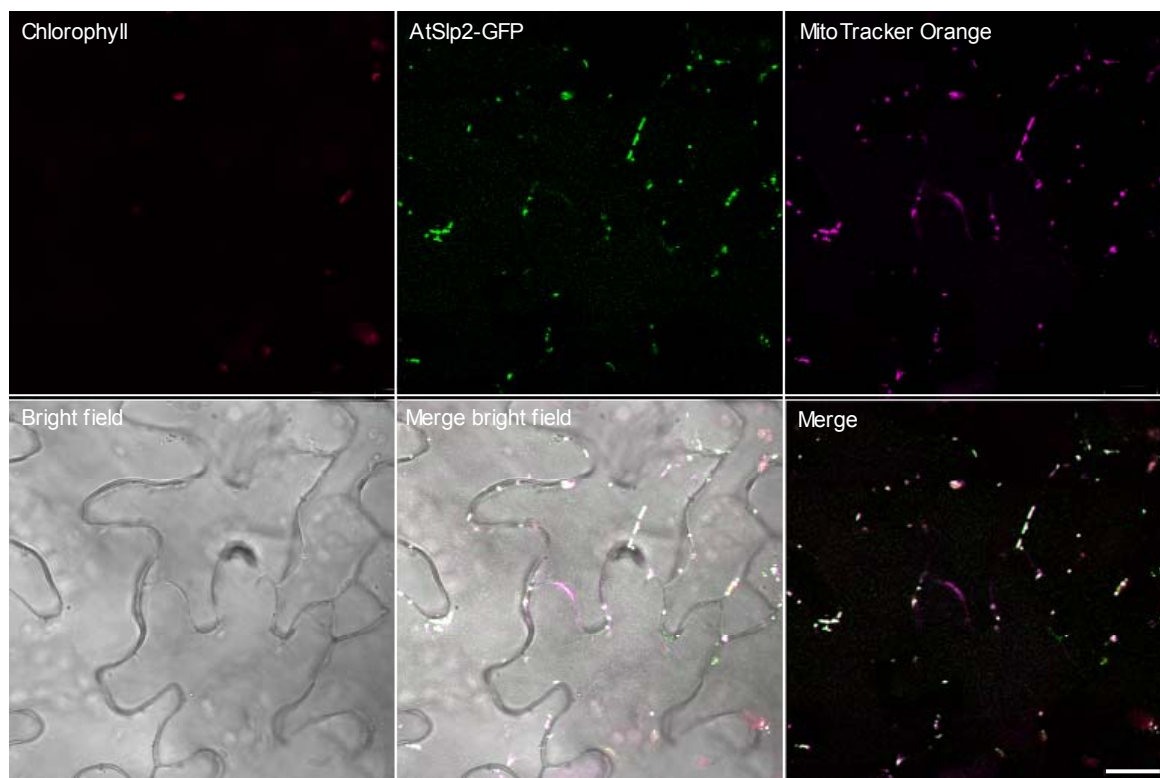


Figure 4-17. Confocal images of AtSlp2-GFP co-localisation with MitoTracker Orange. The image on the top left shows chlorophyll autofluorescence. Shown in green is the Slp2-GFP fluorescence, and in purple the MitoTracker signal. The merged images on the bottom show co-localised organelles as white punctae. Scale bar = 20 μ m.

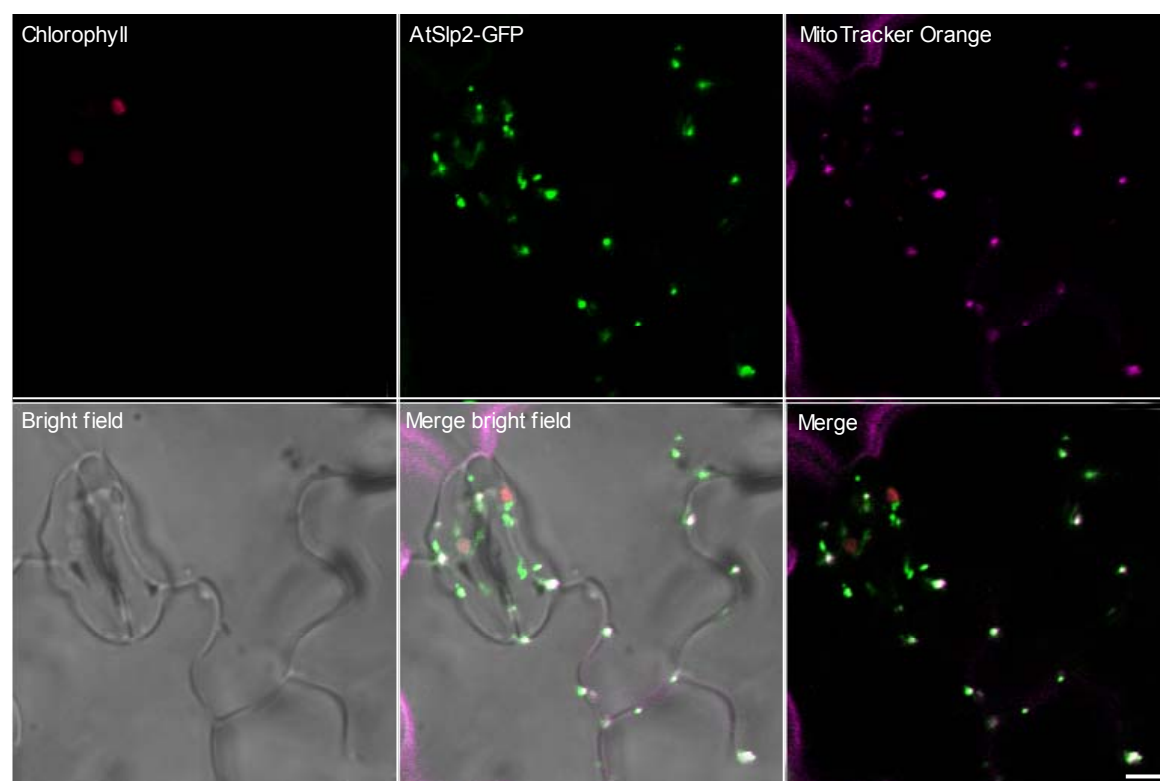


Figure 4-18. Colocalisation of AtSlp2-GFP with MitoTracker Orange from an independent transgenic line. Labelling is as above. Scale bar = 5 μ m.

4.3.1.5 Phenotypes of stable AtSlp overexpressing lines

Transgenic plants grown on soil were examined for morphological phenotypes. Overexpression of Slp1-YFP under the 35S promoter did not result in any obvious growth phenotype when plants were grown on agar plates or on soil. These plants were indistinguishable from wild type plants in either growth condition (Figure 4-19 left side). However, overexpression of Slp2-YFP under the 35S promoter resulted in plants that were reduced in size. Additionally, these plants frequently displayed lesions and premature senescence (Figure 4-19 third picture from left side). The expression of Slp2-YFP was checked by confocal microscopy, and Western blotting confirmed high overexpression levels (Figure 4-16). Unfortunately, only one transgenic line could be propagated out of four lines that were initially selected from the T1 seeds. Therefore, this growth phenotype lacked confirmation by an independent line and could also be caused by the T-DNA insertion site. By comparison, expression of Slp2-GFP under its own promoter (picture on right side) also caused a reduction in growth, but the plants did not look as chlorotic and did not have as many lesions as under the 35S promoter. From these lines, a total number of 12 could be isolated and propagated to the T2 generation. Subsequently, three homozygous lines were isolated and maintained. Plants of all three independent lines frequently showed this growth reduction. Thus, it appears that enhanced expression of Slp2-GFP causes the phenotype rather than the insertion site of the T-DNA. This finding is somehow surprising, given that Slp2-GFP is expressed at levels that should correspond to the endogenous expression of AtSlp2. One explanation is that the growth reduction is related to inclusion of the GFP moiety at the C-terminus of Slp2. For example, fusion with GFP could result in misfolding or could prevent other proteins to interact with Slp2 *in vivo*.

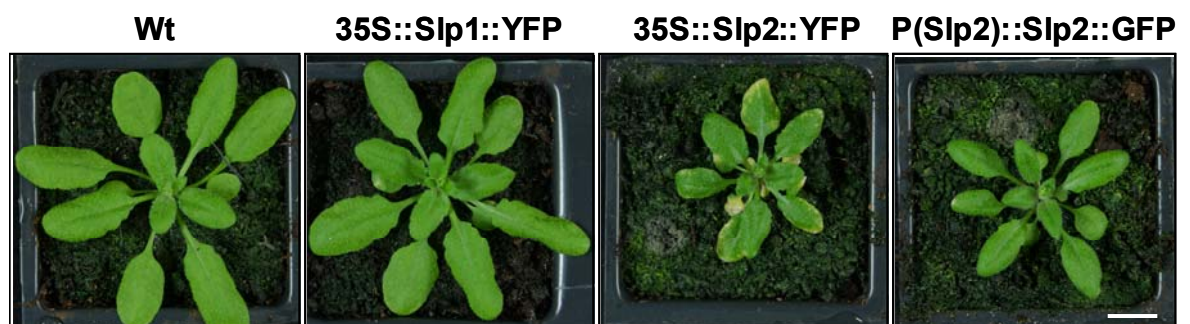


Figure 4-19. Phenotypes of Slp-Y/GFP overexpressing plants. A wild type plant is shown on the left side for comparison. T2 and wild type plants were grown soil. Scale bar = 1cm.

4.4 Biochemical characterisation of the AtSlp1 protein

Experiments addressing structural similarities between AtSlp1 and HsSlp2 are presented in this section that further support their close homology. Evidence is presented for the existence of Slp1 in a protein complex inside mitochondria. Additionally, the membrane insertion model that has been suggested for other stomatin-type proteins is confirmed for AtSlp1. The final part of this section deals with the putative post-translational modification of Slp1 by palmitoylation and the possible consequences for Slp1 function.

4.4.1 Effects of formaldehyde crosslinking on AtSlp1

HsSlp2 has been shown to be part of high molecular weight protein complexes containing oligomers of HsSlp2 and mitofusin-2 through crosslinking experiments with formaldehyde (Hajek *et al.*, 2007). Formaldehyde (FA) quickly penetrates membranes and crosslinks proteins and nucleic acids within a range of 2 Å by the formation of methylene bonds (Kiernan, 2000). To test whether AtSlp1 also exists in a similar protein complex than HsSlp2, mitochondria isolated on a step gradient were incubated with 1% formaldehyde, lysed and separated on an SDS-PAGE gel. Crosslinking effects by formaldehyde are reversible by heat treatment (boiling for 10 minutes), and can thus be easily controlled. Figure 4-20 shows a Western blot probed with anti-Slp1 of untreated and FA crosslinked mitochondria that were lysed at room temperature (lanes nos. 5 and 6) or by boiling sufficiently long to ensure reversal of FA crosslinking (lanes nos. 3 and 4). Slp1 is visible as a single band of approximately 45 kDa molecular weight in the control samples (lanes 3 and 5). Treatment with FA causes a band shift (lane no. 6), yielding a protein band visible at approximately double the molecular weight at around 90 kDa. This band shift did not occur when the FA treated sample was boiled (lane no. 4). This result indicates that Slp1 exists in a protein complex together with other proteins. It is possible that Slp1 might form homodimers and/or higher oligomers *in organello*, although FA crosslinked proteins of higher molecular weight than 90 kDa were not detected. The Slp1 bands from the FA treated samples (lanes nos. 4 and 6) are visibly weaker in appearance than the bands from the control samples. This phenomenon is probably linked to protein precipitation caused by application of FA.

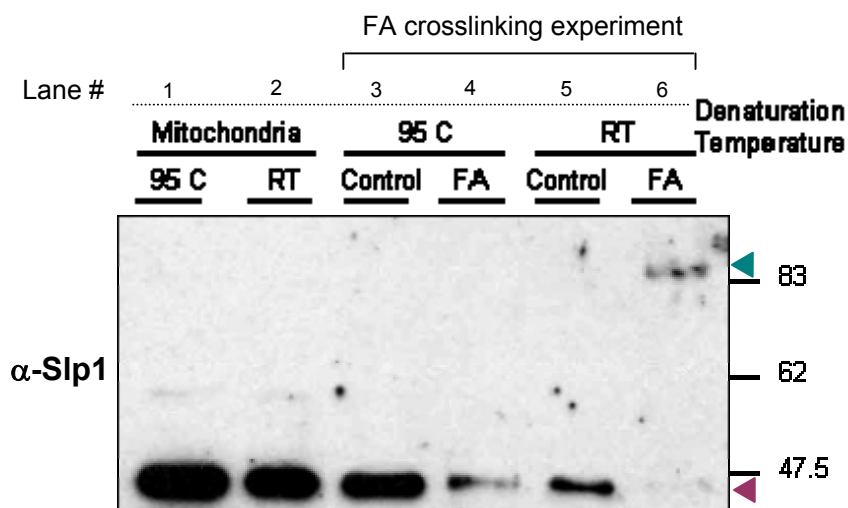


Figure 4-20. Effects of FA crosslinking of isolated mitochondria on Slp1. Mitochondria were isolated on a step gradient (no. 1, see Figure 4-5A) and incubated with 1% FA for 15 minutes before lysis in SDS sample buffer and boiling. Shown is a Western blot of mitochondrial extracts probed with anti-Slp1. The first two lanes (nos. 1 and 2) are mitochondrial extracts denatured by boiling (95 °C) or at room temperature (RT). The other lanes (nos. 3-6) present fractions of mitochondria that were treated without (control) or FA and denatured either by boiling (95 °C) to reverse crosslinking or at room temperature (RT). The monomeric form of Slp1 is indicated by the purple arrowhead; the crosslinked form is marked by a blue arrowhead. Numbers on the right side indicate molecular weight markers in kDa.

FA treatment of mitochondria was repeated with a separate mitochondrial purification on a step gradient (see Figure 4-5 B). The Western blot of lysed mitochondria probed with anti-Slp1 is shown in Figure 4-21. As in the previous experiment, Slp1 was only present as a monomer in the control samples (lanes nos. 2 and 4), and in the FA treated sample after boiling (lane no. 1). This time, however, the protein was present as two bands (lane no. 3) after FA treatment. The upper band (marked by the blue arrowhead) corresponds to the band seen in Figure 4-20 (lane no. 6). Interestingly, the lower band (marked by a red arrowhead) was slightly higher in molecular weight than the bands seen in the other lanes. This might reflect incomplete crosslinking, or it could also indicate that Slp1 was bound to a smaller protein or was captured here as a precursor of higher molecular weight. On the other hand, this band might present an artefact created by FA crosslinking. The appearance of two bands might also indicate that Slp1 does not purely exist in a higher complex, but also (and maybe transiently) as a monomer or an immature precursor.

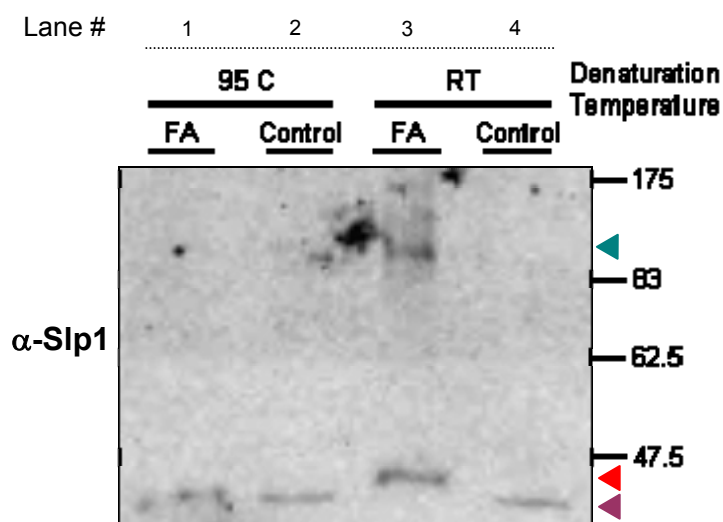


Figure 4-21. Western blot probed with anti-Slp1 of FA treatment of mitochondria under identical conditions as in Figure 4-20. Lanes nos. 2 and 4 are control treated samples denatured either by boiling (95 °C) or at room temperature (RT). Lanes nos. 1 and 3 are samples treated with FA and denatured as described. Numbers on the right side correspond to molecular weight markers in kDa. The red arrowhead indicates the higher molecular weight band of AtSlp1 seen in lane no. 3, and the blue arrowhead indicates the crosslinked Slp1 band. The purple arrowhead indicates the original single band as observed before.

4.4.2 Membrane insertion of AtSlp1

A series of experiments were carried out to test whether the membrane insertion model suggested for other stomatin-type proteins (see Figure 3-6) is also correct for AtSlp1. Secondly, the nature of Slp1 membrane attachment was further investigated, and additional ways of anchorage by a post-translational modification were explored.

4.4.2.1 Protease K assay

The orientation of AtSlp1 in membranes was investigated by isolating microsomal fractions from rosette leaves of short-day grown plants and treatment with protease K in the presence and absence of Triton-X100. This experimental approach is commonly used to study the orientations of transmembrane proteins localised to different compartments (Leimer *et al.*, 1996; Hiebl dirschmied *et al.*, 1991a). The theory behind this kind of experiment is that the protease will have limited access to degrade proteins if they are buried inside formed vesicles or organelles, but it will fully degrade proteins once the vesicle membranes are lysed by the application of a detergent. The degradation products formed under the different conditions are then detected on Western blots probed with antibodies against specific parts of the proteins. In this case, the proteolytic products of

AtSlp1 were compared to those of the Arabidopsis plasma membrane localised syntaxin AtSyp121. Figure 4-22 illustrates the theory behind this experiment and the expected outcome.

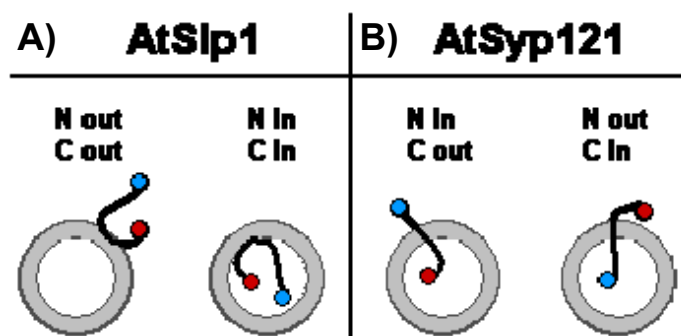


Figure 4-22. Membrane insertion models for peripherally attached (A) and single transmembrane spanning proteins (B). Schematic presentation of vesicles formed upon tissue homogenisation from membranes (grey) with two types of membrane-associated proteins. The N-termini (= N) are presented by a red dot and the C-termini (= C) by a blue dot.

A) Upon vesicle formation, a protein that is not spanning the membrane becomes trapped inside a vesicle (N in, C in), or it is located entirely on the outside (N out, C out) depending on the orientation of the vesicles. This is the model suggested for AtSlp1.

B) The Arabidopsis syntaxin 121 on the other side is a membrane spanning protein. Its N-terminus is either located inside the vesicle or on the outside, with the C-terminus lying on the opposite site (N in, C out) or (N out, C in). Two degradation products are expected that can be detected with antibodies recognising an epitope at the N-or the C-terminus.

Figure 4-23 shows a Western blot probed with anti-Slp1 that was later reprobed with anti-Syp121. The control sample (lane no. 1) shows both proteins present as a single band at their expected molecular weight. In lane no. 2, protease K was added, but no detergent. AtSlp1 was detected in this case as a band of weaker intensity, but at the same molecular weight. No other degradation product was visible under these conditions. Thus, the protein was partly accessible to the protease as a whole, since no smaller degradation product was detected. This observation strongly suggests that this protein is entirely located on one side of the vesicles and confirms that it is not membrane-spanning; in effect the simple explanation for these findings is that a subpopulation of vesicles exist in an inside-out orientation, thus leaving a fraction of the AtSlp1 protein fully exposed and the remainder fully protected from degradation. Of course, the epitope that was recognised by the antibody lies in the C-terminus of this protein. When this part is degraded, no protein can be detected by this antibody. By comparison, the Arabidopsis plasma membrane syntaxin 121 is known to be membrane-spanning and has a transmembrane domain close to its C-terminus. This intrinsic property leads to the appearance of a smaller degradation product

of this protein in lane no. 2 because a part of Syp121 was exposed to the outside of the vesicles and thus degraded by the externally added protease. The reduction in molecular weight of this product compared to the full-length protein corresponds to the C-terminal tail that is located after the transmembrane domain. The antibody raised against Syp121 recognises a part of the N-terminal domain localised on the opposite side to the C-terminus in the vesicles. The smaller degradation product expected if the N-terminus were degraded, could not be detected because no antibody against the Syp121 C-terminus was available. The appearance of the degradation product in lane no. 2 confirms the theory behind this experiment and proves the nature of membrane orientation of both AtSlp1 and AtSyp121. Lane no. 3 shows samples that were treated with detergent only. This treatment has no effect on stability of the proteins which are detected as full length proteins just as in lane no. 1. Upon addition of protease and detergent however (lane no. 4), both proteins are fully degraded as expected under these conditions. It can be concluded from this experiment that AtSlp1 conforms with the model that has been suggested (Salzer *et al.*, 1993;Umlauf *et al.*, 2006;Kadurin *et al.*, 2008a) for other stomatins and band-7 family proteins with both the N- and C-terminal regions of the protein exposed on the same side of the membrane; these proteins are not membrane-spanning.

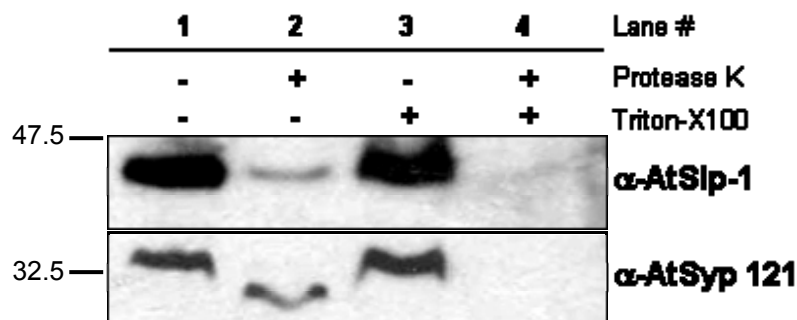


Figure 4-23. Western blot of protease K treated (“+”) microsomal fractions in the presence (“+”) or absence (“-“) of 1% Triton-X100. The upper blot was probed with anti-Slp1 and the blot on the bottom was probed with anti-Syp121. Numbers on the left side indicate molecular weight markers in kDa.

4.4.2.2 Chemical treatments of microsomal fractions

The membrane insertion of AtSlp1 was further examined by chemical treatments of microsomal fractions isolated from Arabidopsis rosette leaves. These types of experiments have been frequently used to address membrane attachment of proteins (Lu & Hrabak, 2002;Ikeda *et al.*, 2004). Microsomal fractions were resuspended, aliquoted and various

chemicals added, as summarised in Table 4-5. After an incubation time of one hour, the preparations were separated again by centrifugation into soluble proteins and insoluble matter before denaturation and separation on SDS-PAGE gels and Western blotting.

Treatment	Concentration
H ₂ O	Control
NaOH	0.1 M
Na ₂ CO ₃	0.1 M
NaCl	1 M
Urea	2.5 M
Triton-X100	1%
SDS	0.1%

Table 4-5. Chemical treatments of microsomal fractions isolated from Arabidopsis leaves. List of individual treatments and the concentrations which were applied. Microsomal pellets were resuspended in buffer, and the individual treatments started by adding a two-fold concentrated stock solution in the same buffer.

Figure 4-24 shows Western blots probed with anti-Slp1 and anti-Syp121 of the treated membrane fractions. The Slp1 and the Syp121 proteins were present in the membrane-associated pellet after the control treatment with water (sample labelled H₂O) as previously seen (Figure 4-2). Remarkably, addition of 0.1 M sodium hydroxide to microsomal fractions caused complete solubilisation of Slp1 (Figure 4-24 A), but did not affect the membrane association of the integral protein Syp121 (Figure 4-24 B). By contrast, treatment with sodium carbonate only partially solubilised Slp1, with the majority of the protein still associated with the membrane pellet. The Arabidopsis syntaxin was completely unaffected by this treatment, as expected from a membrane spanning protein. Carbonate treatment of microsomal fractions is commonly used to detach peripheral membrane proteins. The addition of 0.1 M carbonate has been shown to cause formation of membrane sheets out of vesicles derived from the ER, while membrane lipids and integral proteins are retained. Soluble and peripheral proteins also become detached following the rise in pH (around 11) and an increase in ionic strength (Fujiki *et al.*, 1982). Another publication reports the partial release of lipids after extraction of *Drosophila* microsomal fractions with carbonate (Mastrogiacomo *et al.*, 1998). The different behaviour of Slp1 after sodium hydroxide extraction can be explained by the harsher nature of this treatment compared to carbonate extraction. Sodium hydroxide is known to denature protein structures, thereby affecting membrane binding of proteins (Steck, 1974).

The relative sensitivity of Slp1 to these various solubilising agents thus supports the idea that this protein probably penetrates the lipid bilayer by means of its hydrophobic domain without actually crossing the bilayer, and that this is an endogenous property of its structure. Additionally, its membrane attachment might be supported by palmitoylation at the conserved cysteine residue (Figure 3-7).

Treatment with 1M sodium chloride did not affect the solubility of either protein, both AtSlp1 and Syp121 remained firmly attached to the membrane fraction. This result indicates that electrostatic interactions are not important for keeping these proteins membrane associated. Addition of a medium concentration (2.5 M) of the chaotropic reagent urea caused partial dissociation of both Slp1 and Syp121 from membranes. Urea is known to reduce hydrophobic interactions by disrupting hydrogen bonding in proteins, and therefore promotes unfolding (Bennion & Daggett, 2003). It also affects protein-lipid interactions, but does not disrupt membranes per se (Bowie, 2004). Partial membrane dissociation of both proteins by urea indicates that hydrophobic effects important for the proteins' conformations probably also partially mediate membrane anchorage. Additionally, membrane attachment might be further assisted by a specific protein environment. Putatively, protein-protein interactions might support membrane anchorage of both proteins, further supporting the idea that they exist in a complex.

Application of the non-ionic detergent Triton-X100 solubilised the majority of Slp1, with only a small fraction remaining membrane-bound. By comparison, a much higher proportion of Syp121 remained Triton insoluble following this treatment. Protein solubility caused by non-ionic detergents such as Triton-X100 is a consequence of disruption of the proteins' membrane anchorage via hydrophobic interactions with lipids. Nonionic detergents like Triton-X100 are generally not denaturing and solubilise membrane proteins as protein-detergent complexes. Partial Triton-insolubility indicates that both proteins are partly associated with detergent-resistant membrane fractions and confirms the findings of the proteomics studies (Borner *et al.*, 2005). Interestingly, treatment with the ionic detergent SDS completely solubilised Slp1, but only partially detached Syp121 from membrane fractions. SDS generally leads to the denaturation of proteins and disrupts membranes. SNAREs are known to form SDS-resistant complexes (Pellegrini *et al.*, 1995; Scales *et al.*, 2001; Hayashi *et al.*, 1994). It has to be noted however, that this experiment was carried out at 4 degrees Celsius, a temperature where SDS precipitates. Thus, SDS solubilisation of Syp121 may not have been complete because the detergent was not present in its soluble form to sufficiently disrupt membranes and release this protein.

The behaviour of Slp1 and Syp121 after detergent extraction further illustrates the different nature of their membrane association. Complete solubilisation of the integral membrane protein Syp121 required a stronger detergent than was necessary to release Slp1.

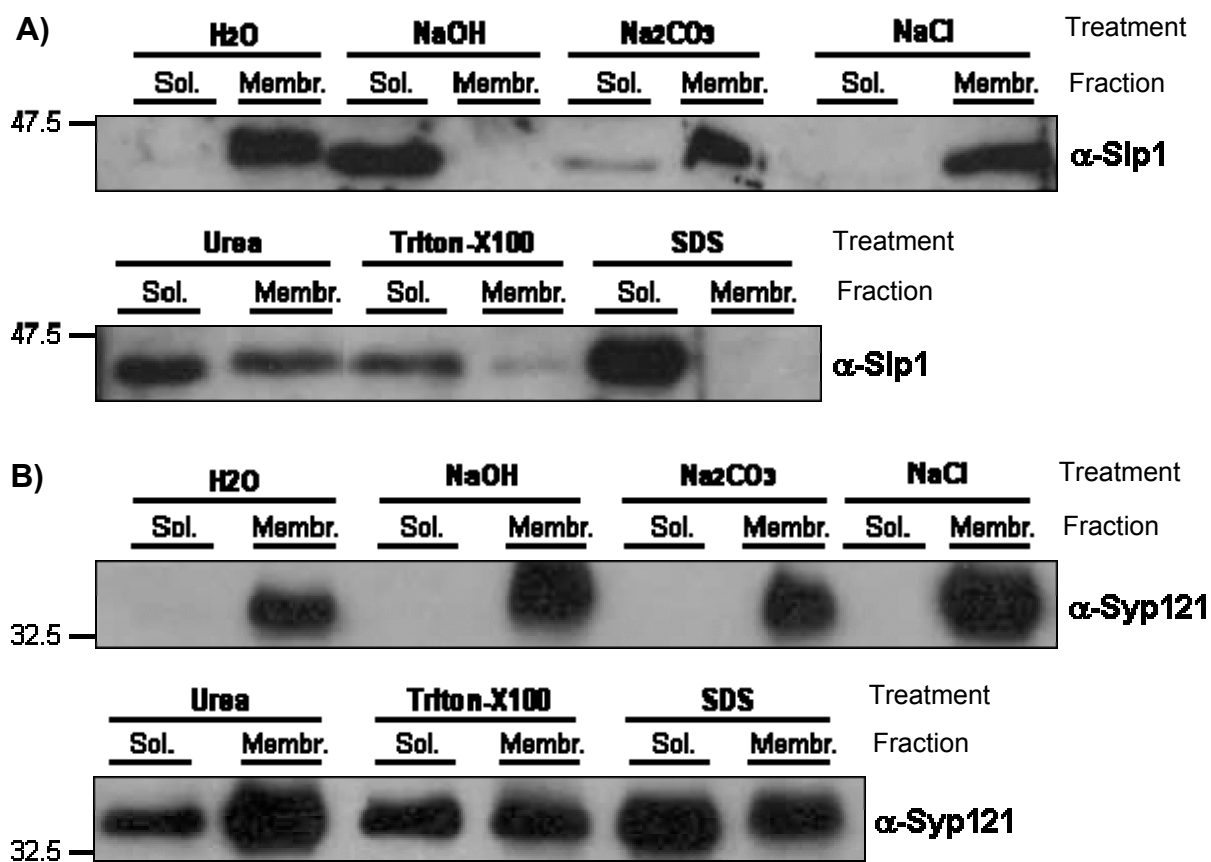


Figure 4-24. Western blots of microsomal fractions treated with chemicals to solubilise membrane-attached proteins.

A) Western blot probed with anti-Slp1. Following each treatment, the microsomes were spun down again and the supernatant collected as the soluble fraction ("Sol."). The pellet ("Membr." for membrane) was resuspended, denatured and separated on the gel with the soluble fraction. Numbers on the left side indicate molecular weight markers in kDa.

B) Western blot of identical fractions probed with anti-Syp121. Labelling is as described above.

4.4.3 Putative S-acylation of AtSlp1

Although the above results suggest protein lipid interactions are important for positioning AtSlp1 in the membrane, the data do not rule out other anchoring mechanisms. As both AtSlp1 and AtSlp2 exhibit a conserved cysteine residue, the possibility of palmitoylation or another form of S-acylation of the cysteine residue in AtSlp1 (Figures 3-4 and 3-7) was investigated. The protein sequences of AtSlp1 and AtSlp2 were scanned for other putative lipidation motifs such as myristoylation, prenylation and for sites that would permit the addition of a glycosylphosphatidyl inositol (GPI) anchor. Each of these possibilities was excluded based on the lack of suitable acceptor residues in the Slp sequences, or a conserved prenylation motif. Palmitoylation emerged as the most likely way of protein modification of AtSlps by the addition of a fatty acid chain to the side chain of a cysteine.

S-acylation of cysteines is a post-translational modification of thiol groups by the formation of a thioester bond with a fatty acid residue such as palmitate. The fatty acid chain is transferred to proteins via acyl-CoA in a reaction that can occur spontaneously in some proteins *in vitro*, but is thought to be promoted by palmitoyl-transferases (PATs) in cells (Linder & Deschenes, 2003; Dietrich & Ungermann, 2004). Non-enzymatic palmitoylation is often slow and inefficient, and it crucially depends on the surrounding amino acids of the target cysteine and the free concentration of palmitoyl-CoA. Quite often, basic and hydrophobic, or aromatic residues surround the modified cysteines and aid the attachment to membranes through negatively charged phospholipids. Palmitoylation normally always occurs close to hydrophobic surfaces on, or proximal to membranes or in proteins (Dietrich & Ungermann, 2004), and often in concert with other lipid modifications such as N-myristoylation or prenylation (Yalovsky *et al.*, 1999). Since no consensus motif exists to predict palmitoylation, it is thought to be target sequence specific. The surrounding amino acids also have an important function in lowering the pKa value of the cysteine. The free thiol has to be deprotonated to form a thiolate anion, which is needed for ester bond formation with palmitate. Figure 4-25 highlights the neighbouring amino acids of the putatively modified cysteine residues of AtSlp1, AtSlp2, and for comparison also of HsSlp2. In all three cases, the highlighted cysteines are surrounded by several positively charged residues. Additionally, several hydrophobic and aromatic amino acids are also present, amongst them a remarkably conserved tryptophane. The close homology of these residues further supports the possibility that the cysteine can be modified by S-acylation. HsSlp2 has an additional cysteine just few amino acids away from the conserved one that could also be palmitoylated, or oxidised to form a disulfide bond with the other cysteine.



Figure 4-25. Amino acid sequences surrounding the putatively palmitoylated cysteine residues in AtSlp1, AtSlp2 and HsSlp2. The cysteines to be modified are shown in red surrounded by a box. Positively charged residues are indicated by blue letters, negatively charged amino acids are shown in orange. Hydrophobic and aromatic residues are underlined. Numbers on the left and right side of the sequences indicate the positions of the chosen amino acid sequences within the proteins.

The function of PATs is controversial in the sense that no direct enzymatic activity has been demonstrated (Dietrich & Ungermann, 2004). It is therefore thought that these proteins merely assist spontaneous acylation to occur more efficiently by binding acyl-CoA and assisting the transfer reaction (Dietrich & Ungermann, 2004). In yeast, proteins with a DHHC motif and cysteine-rich domains are known to act as PATs in the ER and Golgi (Linder & Deschenes, 2003). Arabidopsis contains 23 PATs that are thought to act in an organelle and tissue specific manner (Hemsley & Grierson, 2008). Palmitoylated proteins have been identified from animals, yeast and plants from a variety of organelles and compartments, amongst them mitochondria (Berthiaume *et al.*, 1994; Corvi *et al.*, 2001). In this case, palmitoylation is thought to occur spontaneously, aided by protein-protein interactions that provide a suitable amino acid environment. In fact, palmitoylation of mitochondrial proteins is more common than previously assumed, especially amongst matrix proteins and enzymes, and it provides additional levels of metabolic control (Kostiuk *et al.*, 2008).

Palmitoylation is enzymatically reversible by the action of palmitoyl thioesterases (PTEs). As such, it is a dynamic modification of proteins that can occur in integral, peripheral and soluble proteins. S-acylation has several consequences on protein mobility and increases their affinity to membranes. It allows proteins to shuttle between organelles and the cytosol, and the addition of a fatty acid chain can also promote association with specific lipid environments such as microdomains. Frequently, palmitoylated proteins are assembled into complexes in microdomains that have important functions for signalling. As such, palmitoylation can promote the formation of specific protein-protein interactions

and provide an additional level of assembly control. Protein palmitoylation can also have other functions, for example it can determine the trafficking route of a protein. This has been reported to be the case for stathmins, a family of neuron microtubule-regulatory phosphoproteins attached to organelles in the cytosol. Depending on the availability of palmitoylated cysteine residues in one domain, the proteins are targeted to the Golgi or to mitochondria (Chauvin *et al.*, 2008).

In the studies described below, a palmitoylation inhibitor was utilised to test for possible effects of palmitoylation on the solubility of Slp1. 2-Bromo palmitic acid (BPA) is a competitive palmitate analogue that is poorly metabolised by cells and blocks incorporation of palmitate into proteins (Resh, 2006). Wild type *Arabidopsis* seedlings (ecotype Col-0) were grown under sterile conditions on MS agar plates or on plates supplemented with 1mM 2-bromopalmitic acid (BPA) for 20 days. Seedlings were harvested and their microsomal proteins separated from the soluble protein fraction. The proteins were separated on SDS-PAGE gels followed by Western blotting. The blots were probed to detect Slp1 in the soluble and in the microsomal fractions (Figure 4-26). The rationale behind this experiment was to test whether a larger fraction of Slp1 would become soluble upon BPA treatment. In parallel, seedlings of stable transgenic *Arabidopsis* lines (described in chapter 5 section 5.5) were treated in the same way to provide an independent comparison. These plants overexpress a dominant-negative version (DN) of Slp1 under the control of an inducible promoter and are further described in chapter 5. The Western blot shown in Figure 4-26 for this experiments is from proteins extracted from seedlings that were not induced and should thus behave phenotypically like wild type plants. They were included in this figure to present an independent example of BPA effect on Slp1 localisation. In the wild type seedlings grown on MS, Slp1 is almost completely associated with the microsomal fraction as seen before in Figures 4-24 (A) and 4-2. In seedlings treated with BPA, the protein seems to be even stronger associated with membranes when compared to the MS control that has approximately equal loading levels (Figure 4-26 A). In the microsomes extracted in parallel from DN seedlings, Slp1 was present to a small extent in the soluble fraction, but was mainly associated with membranes. This observation was made previously and was not regarded as unusual. Surprisingly, BPA treatment in this example caused the complete disappearance of Slp1 from the soluble fraction. The protein was completely membrane-bound, even to a slightly greater extent than in the MS control. Thus, BPA treatment seemed to have no effect on Slp1 solubility, or even an opposite effect on membrane association than anticipated. If the inhibitor was indeed active in blocking palmitoylation during growth of the seedlings, no membrane association aided by palmitoylation should have occurred. On the other hand,

AtSlp1 is most likely membrane-associated through its hydrophobic domain and does not rely solely on palmitoylation to accomplish this. BPA might therefore have no effect on membrane association of this protein. Palmitoylation of Slp1 might only occur temporarily to increase the protein's affinity to associate with certain lipid microdomains, but probably does not affect its membrane localisation in general. This type of experiment makes use of an inhibitor of palmitoylation and is a rather indirect approach to probe for protein S-acylation. It cannot deliver a final proof for S-acylation of a particular protein.

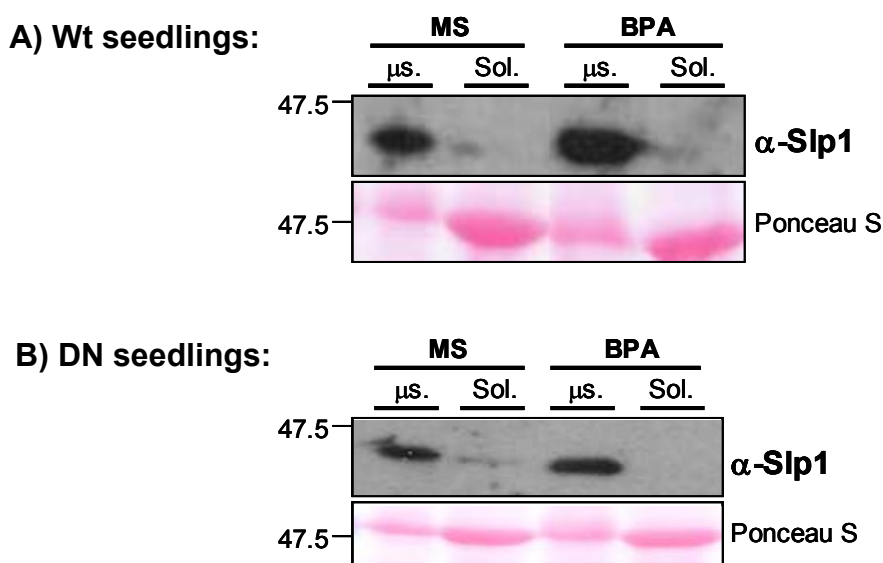


Figure 4-26. Western blots of seedlings treated with the palmitoylation inhibitor BPA on MS agar plates.

A) Wild type *Arabidopsis* seedlings were grown on MS plates (MS) or on MS plates supplemented with 1mM BPA (BPA). Microsomal extracts (μ s.) were prepared and separated on SDS PAGE gels together with the soluble protein fraction (Sol.). The blot is probed with Slp1 antibody. The Rubisco band from the Ponceau S stain is shown underneath for reference of loading levels. Numbers on the left indicate molecular weight markers in kDa.

B) Microsomal and soluble protein extracts of transgenic seedlings (DN) grown on MS agar plates or on MS plates supplemented with BPA. Labelling is as described above.

S-acylation of AtSlp1 was further investigated by utilising the newly established biotin switch method to directly detect cysteine-modified proteins from plant microsomal extracts. This method was established as a direct approach to test for S-acylated proteins without the need to incubate plants with radiolabelled palmitate. The method relies on the detection of chemically modified palmitoylated cysteines from microsomal fractions. These modified proteins are then specifically tagged with biotin and affinity purified using neutravidin beads. The S-acylated proteins are then detected by Western blotting with a specific antibody to confirm palmitoylation (Hemsley *et al.*, 2008).

This assay was performed on wild type microsomal extracts by Dr. Piers Hemsley at the University of Bristol (Bristol, UK). He made use of the anti-Slp1 antibody to detect S-acylated Slp1. Preliminary results indeed suggest that Slp1 can be detected on Western blots by this method after cysteine modification, biotin conjugation and affinity purification (result not shown). If confirmed, this provides the first direct evidence for S-acylation of AtSlp1, and also the first report of a palmitoylated protein in plant mitochondria. It provides further evidence that S-acylation of Slp1 and putatively also of Slp2 are important modifications that can add an additional level of control for the function of these proteins.

4.5 Discussion

4.5.1 Subcellular targeting of AtSlps

The proteomics studies of Arabidopsis organelles so far only identified AtSlps in mitochondria, with the exception of one quantitative study (Dunkley *et al.*, 2006) that also assigned chloroplasts as a possible localisation. However, the method applied in this study to assign proteins to subcellular compartments relies on their quantitative distribution in a certain gradient fraction. Since chloroplast membranes are the most likely contaminants of mitochondrial purifications even after density centrifugation, it is possible that the dual prediction in this study originates in a chloroplast membrane contamination. The quantitative method applied in this study is highly sensitive, and therefore even minor chloroplast protein contaminations of fractions containing otherwise mitochondrial proteins are likely to be picked up.

Putative AtSlp1 chloroplast localisation is also supported by the Cell eFP browser that assigns AtSlp1, but not AtSlp2, to mitochondria and possibly also to chloroplasts. This database summarises results from different prediction programs and proteomics data, but does not give any other evidence for chloroplast localisation of AtSlp1. Out of all prediction softwares listed in the database, only one predicts chloroplast localisation for Slp1 over mitochondria (LOCtree), (Nair & Rost, 2005). This assignment is probably dependent on similarities between mitochondria and chloroplast import presequences. The target sequences of proteins destined to chloroplasts (transit peptides) are generally longer, but also contain positively charged and hydrophobic residues important for import. In contrast to mitochondrial targeting sequences, transit peptides generally do not adapt the conformation of an amphipathic alpha helix *per se*, and they lack clear common structural motives (Inaba & Schnell, 2008; Bruce, 2000). In some imported proteins, hydroxylated amino acids are phosphorylated and form complexes with cytosolic proteins to form a so-called guidance complex that aids transport through the cytosol (Mackenzie, 2005; Martin *et al.*, 2006; Soll & Schleiff, 2004). Certain proteins, such as parts of the transcription and translation machinery, or proteins involved in redox detoxifying pathways, are even targeted to both mitochondria and chloroplasts. These proteins have either two targeting sequences arranged in a tandem, or a target sequence that is recognised by the mitochondrial and the chloroplast import receptors (Mackenzie, 2005).

The targeting sequences of both AtSlp proteins are overall more often recognised as typical cleavable mitochondrial import signals by the databases queried. This suggests a typical proteolytic processing of nuclear encoded proteins destined for the mitochondrial inner membrane or the matrix. Additionally, all major Arabidopsis chloroplast proteome studies so far failed to identify either of the two Arabidopsis Slps from highly purified organelles (Friso *et al.*, 2004;Peltier *et al.*, 2004). Based on these predictions and proteomic evidence, Arabidopsis Slps are most likely not targeted to both organelles but are only localised to mitochondria.

With regard to dual localisation, the targeting of the putative human ortholog HsSlp2 is also controversial. This protein has been originally identified as putatively plasma membrane localised in human erythrocytes with a wide tissue expression pattern (Wang & Morrow, 2000). However, several other reports subsequently found it localised in mitochondria using proteomics screens from a variety of mammalian tissues (Da Cruz *et al.*, 2003;Reifschneider *et al.*, 2006;Chevallet *et al.*, 2006;Hajek *et al.*, 2007). In a recent study, HsSlp2 was identified as a protein expressed in T-cells. Its expression is strongly induced by T-cell activation which in turn induces signalling events (Kirchhof *et al.*, 2008). In these cells, the protein is distributed between two pools, one found at the plasma membrane, and one in mitochondria. The protein was also found to be enriched in lipid rafts, and it associated with polymerised actin in a specialised protein signalling complex at the immunological synapse. The authors concluded that HsSlp2 is important for T-cell activation and signalling, and it accomplishes these actions by providing a specialised protein-lipid environment to maintain signalling complexes. The interesting idea was put forward that the dual localisation of this protein reflects a localised concentration of mitochondria and plasma membrane signalling complexes through polymerised actin at the peripheral area of the immunological synapse. It is thought that HsSlp2 modulates mitochondrial function by providing a scaffold for components of the respiratory chain, and thereby ensuring that energy requirements for sustained T-cell signalling are met. Based on the proposed homology between HsSlp2 and the Arabidopsis stomatin-like proteins, a dual localisation to mitochondria and the plasma membrane certainly cannot be ruled out completely. In humans at least, this dual localisation seems to be tissue specific and probably also specific for certain developmental stages and cell-types. T-cells are highly specialised human cells- a finding proven for these cells cannot be easily projected on plants.

However, the concept of two separate protein pools that might merge in certain situations that require specialised signalling involving mitochondria could also exist in plants. A

plasma membrane localisation of AtSlp1 seems highly unlikely, given that no signal sequence directing the protein to the secretory pathway could be detected by any of the prediction softwares used. Dual localisation of band-7 family proteins was also reported for human prohibitins. In this case, localisation to the plasma membrane, mitochondria and even to nuclei were reported (Snyder *et al.*, 2005;Tatsuta *et al.*, 2005;Schleicher *et al.*, 2008;Wang *et al.*, 1999b). In Arabidopsis however, all prohibitins have so far been assigned to mitochondria (Van Aken *et al.*, 2007;Chen *et al.*, 2005;Ahn *et al.*, 2006), indicating that promiscuous localisation might be a feature of animal proteins. Generally however, the concept of dual localisation could be extended to several classes of animal band-7 family proteins.

The identification of AtSlp1 as a resident of detergent resistant membrane fractions from mixed organellar membranes is surprising for a mitochondrial protein (Borner *et al.*, 2005). In this study, the protein was clearly found enriched in the Triton-X100 insoluble membrane fraction compared to control extracted membranes. The originally isolated membrane fractions were derived from the plasma membrane, but also contained most endomembrane organelles as well as mitochondrial and plastid membranes. After detergent extraction, the authors concluded that the isolated detergent-resistant membrane fractions were largely derived from the plasma membrane. However, given the presence of AtSlp1 in these fractions, microdomains must have also been isolated from mitochondrial membranes. Based on the targeting information obtained from AtSlp protein sequences, it is assumed that these proteins are purely mitochondrial.

With regard to the high solubility of AtSlp1 after Triton extraction in this study (Figure 4-24), this enrichment in microdomains is surprising and leads to the conclusion that it is only a subfraction of AtSlp1 that is anchored to microdomains. The proteomics study by Borner *et al.* applied approximately equal amounts of Triton than were used to test the membrane association of AtSlp1 in Figure 4-24 A. The putative palmitoylated cysteine residue of the protein could explain this phenomenon. As mentioned in section 4.4.3, palmitoylation is regarded to provide a mechanism to specifically enrich and target proteins to certain microdomains in membranes. In AtSlp1, this cysteine might not be constantly modified, or only a small proportion of the Slp1 pool might be acylated at any given time and therefore associated with microdomains.

The original concept of lipid rafts presumed that they only exist at the plasma membrane. However, this idea has since been revised and extended to the endomembrane system (Lucero & Robbins, 2004). Considering the structural organisation and the variety of

metabolic activities that are accommodated at the mitochondrial inner membrane, the concept of microdomains indeed makes sense. So far, microdomains from mitochondria have only been described in studies with animal cells (Malorni *et al.*, 2008; Martinez-Abundis *et al.*, 2007), but not in plants. Proteins with a band-7 domain have been previously associated with the compartmentalisation of membranes (Browman *et al.*, 2007), and this concept can probably be extended to all types of biological membranes. As such, AtSlp1 could be actively involved in the formation of microdomains inside mitochondrial membranes.

So far, only AtSlp1 has been identified from detergent-resistant membrane fractions, but not AtSlp2. This does not exclude the possibility that this protein co-localises to the same membrane compartments as AtSlp1. It is more likely that AtSlp2 has not been identified in this proteomics study because of its lower expression level.

4.5.2 AtSlp1 localisation to mitochondria

The result of the two-phase partitioning in Figure 4-2 clearly indicates that AtSlp1 is not present at the plasma membrane. This provides further evidence that this protein does not have a dual localisation, at least not in shoot tissue. The protein is clearly enriched in endomembranes that must be derived from mitochondria. This means that mitochondria must have been broken during tissue homogenisation and mitochondrial membrane vesicles were released. When whole mitochondria were isolated, more care was taken during tissue homogenisation to prevent rupture of organelles.

Mitochondria isolation after differential centrifugation alone resulted in a strong Slp1 band on Western blots. However, the preparation was highly impure, mainly because of contamination by chloroplast material and peroxisomes. Mitochondria purification on a linear density gradient partly improved this result, but still contained thylakoids as seen on the Ponceau S stain in Figure 4-4. AtSlp1 was clearly visible in the final pellet, but at this stage it was not possible to confirm a single organelle localisation to mitochondria for this protein. The protocol was modified, and a discontinuous density gradient applied to improve purity of the mitochondrial preparation. Step gradients have the advantage that cellular material separates in a manner that is more clearly visible at the interfaces between fractions with abruptly changing densities. The separation of the mitochondria band in this case was readily distinguishable from thylakoids, and the final mitochondrial pellet contained no Rubisco band as seen on the Ponceau-S stained Western blot membrane. During the isolation procedures, a lot of membrane material must have been lost. There is a

clear difference in band intensity between the fraction containing the pellet after the last centrifugation step at 12000g, and the final pure mitochondrial pellet (Figure 4-5 B). This decrease in band intensity of AtSlp1, but also PRXII must be down to loss of mitochondrial material caused by rupture of organelles during tissue homogenisation and resuspension. The purity and also quantity of these preparations could probably still be improved by upscaling the procedure. For these preparations, a maximum of 50 grams of fresh weight tissue was used on average. The mitochondrial band in the density gradient was not well visible, especially after fractionation on the linear gradient.

A rather curious observation concerns the molecular weight of AtSlp1. Since this protein possesses a mitochondrial targeting sequence that is presumably removed proteolytically upon mitochondrial import, one would expect a reduced molecular mass in isolated mitochondria. As mentioned in section 4.1.1, the mature form of AtSlp1 should have a molecular weight of 40 kDa or even smaller. However, in all Western blots probed with anti-Slp1, the observed molecular weight always corresponded to the expected mass as deduced from the uncleaved protein sequence. No double band was ever detected that would correspond to the presence of a precursor and a mature protein. The fact that the commercially produced antibody against this protein failed to recognise the chosen N-terminal epitope peptide (chapter 3, Figure 3-19) would further support the idea that a part of the protein's N-terminus is lost upon maturation in mitochondria.

Slp1 probably possesses a bipartite targeting sequence. The protein is synthesised in the cytosol and targeted to mitochondria by its N-terminal target sequence. It is transported across the outer membrane by the TOM complex and passed to a translocating complex of the inner membrane. This complex (TIM 23 in yeast) then redirects the protein to the inner membrane in a membrane potential-dependent manner. Once in the inner membrane, it is cleaved by an inner membrane peptidase (Nunnari *et al.*, 1993) and emerges protruding into the intermembrane space. In principle, its hydrophobic domain should act as a stop-transfer signal and Slp1 should be inserted as a single protein or assembled into oligomers inside the MIM. This type of mitochondrial targeting has been shown to apply to the inner membrane protein cytochrome c_1 and also for cytochrome b_2 (Vanloon *et al.*, 1987; Glick *et al.*, 1993; Glick *et al.*, 1992).

Generally, intermembrane space-localised proteins are imported through the TOM complex and then fully folded by proteins in the intermembrane space. In fact, the intermembrane space is an oxidising environment. Frequently, imported proteins are temporarily linked to soluble assembly complexes via disulfide bridges. Cysteine oxidation

promoted by soluble intermembrane space factors (MIA-mitochondrial intermembrane space assembly machinery) can also promote the assembly of oligomeric complexes that might be inserted subsequently into the inner membrane (Bolender *et al.*, 2008). In this light, the conserved cysteine residue in AtSlp1 could have an additional function. When oxidised in the intermembrane space, it would link several Slp1 subunits via disulfide bridges to assemble into higher oligomeric complexes. This assumption is currently purely speculative and not supported by any experimental evidence.

Other mitochondrial inner membrane proteins, mainly carrier proteins with multiple transmembrane spanning domains, lack an N-terminally cleavable target sequence. Instead, these proteins possess internally encoded targeting signals at various places. This type of targeting has been studied extensively for the inner membrane ADP/ATP carrier from yeast. The N-terminal sequence of this protein is bound by soluble intermembrane space factors and directed to the inner membrane, where it is bound by the TIM22 complex and inserted in a membrane potential-dependent manner (Leuenberger *et al.*, 1999; Rehling *et al.*, 2003). Since both AtSlps are synthesised with detectable N-terminal targeting sequences, these proteins probably do not follow this insertion pathway. The most likely scenario appears to be the one suggested above that has been proven for cytochrome c1. However, this pathway always seems to involve proteolytic cleavage by a processing peptidase located in the inner membrane or in the matrix. Thus, the failure to detect a smaller Slp1 protein can only be explained by insufficient resolution on the SDS-PAGE gels (mini format) used to separate the fractions. Alternatively, Slp1 is post-translationally modified by another mechanism or simply imported as described, but not cleaved. Localisation of Slp1 to the outer mitochondrial membrane facing the intermembrane space seems unlikely, given the presence of the N-terminal targeting sequence. Outer membrane proteins of the beta barrel type are normally imported by the TOM complex in an ATP-dependent manner and possess no cleavable target sequence. Following transport across the outer membrane, they are guided to a second complex (SAM- sorting and assembly machinery) and eventually a third (MDM- mitochondrial distribution and morphology) after which maturation and assembly is completed (Bolender *et al.*, 2008; Becker *et al.*, 2008).

Discrepancies also exist concerning the molecular weight of HsSlp2. When this protein was originally characterised, it was detected as three distinct bands from different tissues and cell types (Wang & Morrow, 2000). The expected full-length protein has a molecular weight of 38.5 kDa as predicted from its open reading frame. Two bands of 45 and 34 kDa were detectable in most tissues and cell types. The lower band of 34 kDa was only detected

in erythrocytes, COS cells and A431 cells. The major band was always the highest at 45 kDa. When the protein was expressed with an *in vitro* translation system, an additional smaller band of 26 kDa was also detected. The authors concluded that the protein is tissue-specifically modified by alternative splicing, or initiated at additional downstream start codons. Triton-X100 extraction of Slp2 overexpressing COS cells only left the two largest bands associated with the insoluble, cytoskeleton associated fraction. In erythrocytes, only the band detected at 44 kDa became soluble after the same treatment, all other bands remained associated with insoluble matter.

The study that characterised HsSlp2 in mitochondria (Hajek *et al.*, 2007) detected the protein with a molecular weight of 42 kDa when co-immunoprecipitated from crosslinked HeLa cell lysates. However, a band with higher molecular weight was detected after *in vitro* translation of Slp2. When this protein was incubated with import-competent mitochondria from HeLa cells, a smaller band was detected, dependent on whether the membrane potential was intact. Thus, this protein was demonstrated to be proteolytically processed upon mitochondrial import. The authors did not comment further on the larger size of the detected Slp2 protein (42kDa in whole cell lysates compared to 38 kDa expected molecular weight). In a second study, HsSlp2 was detected with its expected molecular weight of 38 kDa from whole HeLa cell lysates (Da Cruz *et al.*, 2008).

These observations demonstrate that many factors could influence the processing and final form of a stomatin-like protein of the HsSlp2 type. With this knowledge as a background, it is interesting to speculate that AtSlp1, like HsSlp2, may be proteolytically cleaved, but the mature version not readily detected. It is possible that the cleavage is dependent on some kind of secondary event, or that the mature protein has a high turnover rate.

To demonstrate localisation of AtSlp1 to the inner mitochondrial membrane facing the intermembrane space, the experiment using protease K and digitonin treatment should be repeated. Specific marker proteins for each mitochondrial subcompartment should be used to test more specifically for the effective digestion of proteins in each compartment. As an alternative to the method used here, purified mitochondria could directly be separated into their compartments. Mitoplasts (mitochondria of which the outer membrane has been removed by freeze-thawing or hypotonic shock) can be separated from outer membrane fractions and the intermembrane space compartment (Da Cruz *et al.*, 2008; Da Cruz *et al.*, 2003). This way, AtSlp1 could be localised with higher confidence to either the inner or the outer mitochondrial membrane.

It is worth noting that these types of experiments require higher protein concentrations than achieved here, and would need to be scaled up by using at least double the amount of tissue. Alternatively, seedlings rather than mature rosettes could be used, or Arabidopsis suspension cell cultures. These types of mitochondria sources are more frequently mentioned in the literature because of the higher yield of mitochondria. When using suspension cells, one could make use out of dark-adapted cell cultures that lack chloroplasts and therefore yield mitochondrial pellets that are free of thylakoid membranes.

4.5.3 *In vivo* evidence for AtSlp localisation to mitochondria

Before stable transformations with the 35S driven Slp-YFP expression constructs were imaged, transient expression was attempted as a quick measure to test the expression levels of these constructs. Both *Agrobacterium* infiltration and transfection of *Nicotiana tabacum* leaves, and particle bombardment of onion epidermal cells resulted in very high expression levels of the 35S driven constructs. However, the expression pattern with both transient methods did not resemble the distribution expected for mitochondria. Under these conditions, Slp1 and also Slp2 expressed with C-terminal YFP resembled large, mobile vesicular structures (not shown). Onion epidermal cells even showed sheet-like internal structures that resembled ER distributions. Fusion of YFP to the N-terminus of either Slp resulted in expression patterns that were similar to those observed with the C-terminal fusions in these systems. Again, large vesicular structures were fluorescently labelled that were mobile and frequently fused. However, the observed distribution and size of these structures did not correspond to mitochondria and looked very different from the pattern observed upon stable expression in Arabidopsis. It is plausible that fusion of YFP to the N-terminus of either Slp could cause mistrafficking of the proteins since the N-terminal targeting sequence would be buried. The C-terminal fusions should not have affected targeting of these proteins, as it was seen in Arabidopsis. Therefore, the heterologous expression systems, despite being plant cells, must have caused mistrafficking. The expression of the genomic construct of AtSlp2 required correct splicing, which was clearly accomplished in Arabidopsis stable lines. This construct was also transiently expressed in onion epidermal cells and tobacco leaf epidermis cells as described before. The expression pattern with this construct showed smaller and mobile organelles similar to the mitochondrial pattern seen in Arabidopsis. In tobacco cells, these organelles appeared larger than in Arabidopsis, whereas in onion cells they were smaller, but much more abundant. It was not confirmed whether these structures were indeed mitochondria. These results clearly demonstrate the advantages of stable expression in a native system,

compared to heterologous and transient overexpression which caused mistrafficking of Slp-YFP under the 35S promoter.

MitoTracker labels active mitochondria after it has been taken up in a membrane potential dependent manner. However, the use of these dyes is not free from controversy. Care must be taken not to overload cells, and in the case of plant cells, additional worries concern the accumulation of MitoTracker dyes in chloroplasts. In the examples presented here, both MitoTracker dyes did not seem to yield chloroplast labelling. The confocal settings (laser power, detector gain) were kept low deliberately to avoid artefacts. In some cases, co-localisation between fluorescently labelled Slp proteins and MitoTracker was not complete. However, this could be related to the state of the imaged mitochondria. As mentioned, MitoTracker is only taken up by actively respiring mitochondria. Mitochondria that did not take up MitoTracker, or did so only weakly might still have been labelled with fluorescent Slp protein. Overall, the observed organelle patterns corresponded well to what has been published previously for Arabidopsis mitochondria (Logan & Leaver, 2000). Plant mitochondria are highly amorphous in shape, ranging from tubules and networks to distinct spots. This plasticity depends on the cell cycle and also the stress levels of cells. Additionally, the number of mitochondria per cell varies greatly between specific cell types. Guard cells and other cells found in actively metabolising tissues have frequently higher numbers than epidermal cells for example (Taiz & Zeiger, 2002), page 232).

Concerning the proposed dual localisation of HsSlp2 protein in specific cells, epidermal cells and root hairs imaged here definitely did not show evidence of such a phenomenon. Neither Slp protein was detected at the cell periphery nor was visible in chloroplasts. This observation concurs with the results obtained from the 2-phase partitioning experiment and to what has been observed elsewhere. In some cases, chloroplasts displayed weak fluorescence in the YFP or GFP channel during confocal imaging. However, this signal was not quantitatively different from that observed in control tissues and was therefore regarded as artefacts down to the confocal settings and bleedthrough of the chlorophyll autofluorescence. Arabidopsis Slps are not regarded as dually localised to mitochondria and chloroplasts based on these observations.

Rather curiously, 35S-driven Slp1-YFP expression reduced the protein level of the endogenous Slp1 as seen on Western blots in Figure 4-11. Phenotypically, these plants looked like wild types and seemed to grow normally on plates, hydroponic culture, or on soil. The clear reduction in Slp1 protein levels could be down to transcriptional or

translational repression of the Slp1 gene. Such an effect might arise if the Slp1-YFP fusion was functional inside mitochondria, and therefore did not cause a growth phenotype.

Co-localisation of Slp1-YFP with MitoTracker was confirmed by confocal analysis in root hairs because of the ease of imaging in this system. Several attempts were made in leaf epidermal cells, but were not successful because of high background autofluorescence in the MitoTracker channel. The co-localised pattern in root hairs assumes that the protein is expressed naturally in this cell type. Currently this assumption cannot be firmly confirmed based on the microarray data and the promoter-GUS fusion lines. However, given that Slp2 is expressed in the root epidermis and in hairs, it seems likely that Slp1 would share the same pattern when expressed under its own promoter. The protein extracts from roots clearly showed high levels of Slp1 protein on a Western blot (Figure 3-41 A).

Overexpression of Slp2-YFP under the 35S promoter resulted in a strong growth phenotype. Assuming that this phenotype was not related to the T-DNA insertion site, it must have been caused by large amounts of Slp2-YFP protein inside mitochondria. These plants were small, had necrotic lesions and became prematurely senescent. This phenotype was only observed in this severe form when the fusion protein was expressed under the 35S promoter. One explanation for this observation is that Slp2-YFP was not functional because of the YFP fusion. For example, although the fusion protein was targeted to mitochondria, once imported it might be mislocalised or might prevent other proteins from interacting with Slp2. Alternatively, the highly increased expression levels under the 35S promoter could have caused malfunctioning of this protein simply through saturation of its interaction(s) with other (unknown) partner proteins. As concluded in chapter 3, AtSlp2 normally is not as highly expressed as AtSlp1. It might be that high Slp2 levels are toxic to the plants and its expression must be tightly regulated. Since it is assumed that both AtSlps act in a complex together, AtSlp2 could have an important regulatory function.

Compared to the expression of Slp2-YFP under the 35S promoter, the expression of Slp2-GFP from its genomic sequence caused a milder growth phenotype. This finding in itself was unexpected, given that the expression of this fusion protein was controlled entirely by its own genomic sequence. Under these circumstances, the presence of GFP at the protein's C-terminus could have caused this change in growth for the same reasons as mentioned above for Slp2-YFP. The GFP fusion protein was expressed at overall higher levels than it was expected originally. GFP fluorescence could be detected in T1 seedlings in all organs examined. The high expression of the protein in stipules agrees with what has been observed in the promoter-GUS fusion lines (Figure 3-36 C). If Slp2-GFP was

expressed at slightly elevated levels than in wild type plants, the growth phenotype of these plants could also be related to increased protein levels. As a third possibility, this growth phenotype could indicate that the native Slp2 protein is indeed processed by proteolysis for example. When the protein is expressed as a C-terminal GFP fusion, this processing might be impaired. This in turn could result in the accumulation of unprocessed fusion protein that hinders mitochondrial function and plant growth.

4.5.4 Biochemical characterisation of AtSlp1

FA crosslinking

The detection of a higher molecular weight band with anti-Slp1 after crosslinking of mitochondria with FA does not come as a surprise. Based on what is known about HsSlp2, the Arabidopsis protein was expected to exist in a protein complex. The human Slp2 protein was detected in crosslinked complexes with mitofusin-2, a GTPase of the outer membrane that mediates mitochondrial fusion (Hajek *et al.*, 2007). An HsSlp2 dimer, and a ladder of additional higher complexes with mitofusin were detected from FA-treated mitochondria and cells. HsSlp2 was also identified in a 250 kDa protein complex, where it binds prohibitins (Da Cruz *et al.*, 2008). The low resolution of the gel format used here (minigel) does not allow detection of very large complexes of the kind reported by Hajek *et al.* However, it would be interesting to repeat the crosslinking experiment and isolate the crosslinked band from a SDS-PAGE gel followed by mass spectrometry analysis. This way, it would be possible to confirm whether this band contains only AtSlp1 or an additional mitochondrial protein. Additionally, this experiment should be repeated, and the proteins separated on a maxi gel format to improve resolution of separation. To avoid loss of protein material by precipitation effects by FA, an alternative crosslinker could be applied. A good example would be DSP (Dithiobis[succinimidyl propionate]) that has been successfully applied to isolated mitochondria by da Cruz *et al.* (Da Cruz *et al.*, 2008). Crosslinking by DSP can also be reversed by applying strong reducing agents and heating of samples during denaturation.

Interestingly, Arabidopsis does not encode a direct mitochondrial homolog to mitofusin-2. GTPases that are similar belong to the FZO type proteins and have been identified from the chloroplast outer membrane (Gao *et al.*, 2006). However, given the conserved features between HsSlp2 and AtSlps, interacting Arabidopsis proteins that could be involved in mitochondrial fusion would also be expected in this case. Additionally, the conservation of

prohibitins between humans and plants would strongly suggest that AtSlps can also interact with *Arabidopsis* prohibitins.

The question remains whether Slp1 continuously exists as a dimer (or even higher oligomer) or bound to other proteins, or whether it is associated with other proteins only temporarily. The rather different results seen in Figures 4-20 and 4-21 with respect to the monomeric band in the FA treated sample would argue that the latter is probably the case. In the first experiment in Figure 4-20, no monomeric band could be detected after FA treatment. In Figure 4-21, a monomer with an increased mass was detected in addition to the 90 kDa band. As mentioned in section 4.4.1, the increased weight could represent a precursor that was crosslinked while processed, a post-translational modification, or the binding to a small protein. The result seen in Figure 4-21 would also argue that only a part of the Slp1 pool is available for dimerisation/complex formation, whereas the other part exists at least temporarily in a monomeric form. Slp1 oligomerisation would support the concept of a scaffolding protein in the mitochondrial membranes. As such, oligomeric Slp complexes could associate with microdomains and regulate interacting or surrounding protein complexes, as has been suggested for HsSlp2 and stomatin (Hajek *et al.*, 2007; Snyers *et al.*, 1999b; Salzer & Prohaska, 2001a).

AtSlp1 membrane association properties

Microsomal extraction and protease K digestion

During the extraction procedure to obtain microsomal fractions from leaf tissue, mitochondria must have been broken during homogenisation in a blender, and their membrane fractions released. Mitochondrial membranes were detected in microsomal fractions that were isolated by similar protocols before (Borner *et al.*, 2005; Mitra *et al.*, 2007). The extraction involved a first spin at 10000 g to remove cellular debris, but also unbroken organelles such as mitochondria, chloroplasts and nuclei. Since the majority of Slp1 is always associated with microsomes, a significant proportion of mitochondrial membrane material must have been released before this spin. A second spin at 100000g was applied to pellet microsomes. The isolated membrane fraction must have contained at least in parts vesicles of two orientations, right-side out and inside-out. This can be concluded by the result of the protease K treatment in the absence of detergent. Both degradation products of Slp1 and Syp121 were weaker in band intensity than the untreated or the detergent-treated samples (Figure 4-23 lane no. 2). Particularly the Slp1 band lost intensity; a good proportion of the protein must have been exposed to the outside of the

vesicles. To homogenise tissue for this experiment, blending in homogenisation buffer was applied with repeated strokes. The isolated microsomal pellet was resuspended by careful pipetting. These procedures supposedly produce mainly vesicles that are not inverted, but right-side out. With this concept in mind, membrane material derived from the mitochondrial inner membrane was probably also of this orientation. Thus, the loss in Slp1 band intensity seems a plausible consequence of the formation of right-side out vesicles. AtSyp121 on the other side is localised to the inside of the plasma membrane, with the N-terminus protruding into the cytosol. The N-terminal part of the protein is also recognised by the antibody used to detect this protein. If the plasma membrane also generated mainly right-side out vesicles, the largest fraction of the N-terminal part must have been located inside the vesicles and was thus protected from protease degradation with no detergent present. Indeed, this appears to be the case as observed in the Western blot in Figure 4-23. This theory would further support that Slp1 is facing the intermembrane space on the inner membrane.

The orientation of Slp1 to just one membrane side is in agreement with what has been demonstrated for the human stomatin protein (Salzer *et al.*, 1993; Umlauf *et al.*, 2006). This concept of membrane association through a loop and the consequential orientation of both termini to the same compartment has been suggested to be a conserved feature of many band-7 family proteins, with the exception of the prohibitins and bacterial HflC/K proteins (Browman *et al.*, 2007; Kihara & Ito, 1998). For human Slp2, this model has been experimentally tested using protease K digestion in the presence of digitonin (Hajek *et al.*, 2007). The N-terminus of AtSlp1 is unusually rich in proline, an amino acid that commonly occurs at sites where the protein structure bends. Four proline residues are also found within and around the putative hydrophobic domain of Slp1, further supporting the idea that the structure probably bends to accommodate the proposed hydrophobic loop insertion. The possibility of Slp1 membrane attachment by this hydrophobic area is further explored in chapter 5.

AtSlp1 membrane association

The most interesting finding about membrane association properties of AtSlp1 is the complete extraction by sodium hydroxide, compared to only partial solubilisation after sodium carbonate extraction. Treatment with sodium hydroxide causes hydrolysis of thioester and ester bonds, and denaturation of proteins. As a consequence, protein-lipid interactions are disrupted under these conditions. Carbonate on the other side and mild alkali treatment affect ionic bonds, but generally do not hydrolyse thioester bonds. Proteins

that have no membrane anchor (ie peripheral proteins) are normally detached from membranes under this condition. Slp1 was also resistant to carbonate extraction as reported by some of the proteomics papers (Borner *et al.*, 2005; Mitra *et al.*, 2007; Dunkley *et al.*, 2006). In these studies, membranes were isolated and carbonate-washed to remove peripheral proteins before their proteome was analysed.

Alternatively, treatment of S-acylated proteins with hydroxylamine at neutral pH also cleaves thioester bonds and releases the fatty acid moiety. This procedure is commonly used to test specifically for membrane anchorage of proteins by thioester bonds (Magee *et al.*, 1984). To distinguish whether Slp1 is mainly attached by a hydrophobic loop rather than post-translational modification, an S-acylated control protein in combination with hydroxylamine treatment should have been used in the experiment of Figure 4-24. The S-acylated protein would be expected to be completely solubilised by hydroxylamine and sodium hydroxide, but not by carbonate. AtSlp1 on the other side is expected to be partially solubilised by hydroxylamine and completely extracted by hydroxide.

Slp1 solubilisation after sodium hydroxide extraction only confirms that Slp1 is not an integral membrane protein like Syp121. From the outcome of this experiment, it is not possible to exclude the possibility that Slp1 is exclusively membrane anchored by S-acylation. Since Slp1 contains only a single cysteine in its sequence this possibility seems unlikely, regarding the strong association with microsomal fractions. S-acylation normally occurs in concert with other types of membrane anchorage (Hemsley & Grierson, 2008; Yalovsky *et al.*, 1999). Acylation of proteins can also occur by other amino acid modifications. Attachment of palmitate or another type of fatty acid by an ester bond to a serine residue offers another possibility to anchor proteins. Modification of proteins by acylation via an amide bond presents a third possibility. Amide bonds however are resistant to alkali hydrolysis (Towler *et al.*, 1988) and are therefore not considered for Slp1 membrane attachment. Furthermore, the stretch of hydrophobic amino acids close to the N-terminus of Slp1 does not necessarily have to penetrate the lipid bilayer, but might aid membrane attachment by providing a hydrophobic surface if the protein is otherwise post-translationally modified. Currently, Slp1 membrane attachment via a hydrophobic loop insertion is just a model based on what has been proposed for other stomatin proteins. Modification by S-acylation is supported by the association of Slp1 with microdomains (Borner *et al.*, 2005), and by the result of the biotin-switch assay.

The differences seen regarding membrane solubility between Slp1 and Syp121 after carbonate and sodium hydroxide extraction might also relate to the nature of the

membranes where these proteins localise. AtSyp121 is localised to the plasma membrane facing the cytoplasm with its N-terminus. The lipid and protein composition of the plasma membrane is remarkably different to that of the mitochondrial inner membrane, a membrane that is highly specialised to provide a tight barrier for ions, solutes and proteins. Therefore, carbonate and sodium hydroxide might be differentially effective in solubilising membranes of different lipid compositions. This fact might also contribute to the different solubility properties of these two proteins after extraction with detergents. Regardless of this possibility, the characteristics of membrane attachment of Syp121 as seen in Figure 4-24 clearly correspond to the expected behaviour of an integral protein. Such a protein can only be solubilised by the application of detergents.

Overall, the solubilisation characteristics of AtSlp1 are strikingly similar to those observed for HsSlp2. The human protein was also fully extractable from erythrocyte ghost membranes after sodium hydroxide application, but it was not extracted by 0.5M potassium chloride (Wang & Morrow, 2000). As a control for an integral protein, the human stomatin protein was used. This protein was not detached from membranes under either of these two conditions. Stomatin was assumed to insert itself into the plasma membrane by a hydrophobic loop as suggested for AtSlp1. Curiously, human Slp2 from erythrocytes remained almost insoluble after extraction with Triton-X100, only a small proportion became solubilised. The authors concluded from this result that HsSlp2 is associated with the insoluble cytoskeletal matrix and therefore localised to the plasma membrane where it is a peripheral, but well attached membrane protein (Wang & Morrow, 2000). In a second study the membrane association of HsSlp2 was investigated from mitoplasts (Hajek *et al.*, 2007). The membrane localisation was completely unaffected by treatment with 1.5M sodium chloride and 0.1 M carbonate. However, in this study HsSlp2 was almost completely extracted by the application of 1% Triton-X100, as it was observed for AtSlp1 in Figure 4-24. From the study of mitochondrial inner membranes, the authors concluded that HsSlp2 is membrane-attached by acylation or the addition of a GPI anchor. The different behaviour of HsSlp2 upon Triton extraction between these two studies could again reflect the nature of the membranes used. In the study by Wang *et al.*, erythrocyte plasma membranes were examined, whereas Hajek *et al.* used purified mitochondria extracted from HeLa cells. The two membrane types probably possess different properties upon Triton extraction because of their varying lipid and protein compositions.

The identical membrane association properties of AtSlp1 and HsSlp2 (as observed by Hajek *et al.* in mitochondria (Hajek *et al.*, 2007)) lead to the conclusion that membrane association of these proteins is generally mediated by the same mechanisms. The

hydrophobic domain in AtSlp1 could penetrate the lipid bilayer, or it could also only facilitate membrane attachment without actually protruding into the membrane. In this case, acylated amino acids would mediate membrane attachment, as it has been suggested for HsSlp2 by Hajek et al. (Hajek *et al.*, 2007) and Wang and Morrow (Wang & Morrow, 2000). This protein does not possess a hydrophobic domain as predicted for the Arabidopsis Slps, but the amino acid sequence is nevertheless highly similar in this region, with a high number of conserved hydrophobic residues (Figure 3-4). AtSlp2 contains the same prediction for a hydrophobic domain as AtSlp1, and it probably has membrane association properties identical to AtSlp1. AtSlp2 contains a second cysteine further upstream very close to the hydrophobic domain that is not conserved, but could nevertheless be acylated.

S-acylation of AtSlps in mitochondria

Based on homologies and the experimental evidence by the biotin switch assay, the conserved cysteine residue of AtSlp1 is most likely modified. As mentioned, the nature of the modification is most likely by a thioester bond and attachment of a palmitate residue. Alternatively, this cysteine might also be modified by other means, for example by the attachment of another long chain fatty acid. Attachment of a fatty acid residue by an ester bond on a hydroxylated amino acid might be another type of post-translational modification occurring in Slp1. A third way of modification would be the possibility that this cysteine could be S-nitrosylated. S-nitrosylation also happens non-enzymatically and is dependent on the target sequence. This type of modification provides an additional level of regulatory control in proteins and complexes implicated in stress-mediated signalling (Moller *et al.*, 2007; Wang *et al.*, 2006). Whatever the exact type of modification is, the conserved cysteine probably has an important role in the regulation of the function of Slps of type 2. Palmitoylation of this residue would imply consequences on the protein's hydrophobicity, or on its ability to interact with other proteins. As other palmitoylated proteins frequently partition into detergent-resistant membrane fractions, this type of modification provides means to specifically target and shuttle proteins within membranes. It cannot be excluded however, that palmitoylation of Slp1 provides the main way of attaching itself to membranes. In this case, its hydrophobic domain would in fact not penetrate the bilayer or only aid membrane attachment on the surface. An intriguing possibility could also be that this cysteine could be modified by multiple post-translational mechanisms at any given time, especially considering that these types of modifications are reversible.

The reversal of palmitoylation always happens enzymatically, thus it is presumed that some kind of thioesterase would exist in mitochondria. As mentioned, palmitoylation of mitochondrial proteins is thought to occur spontaneously depending on the protein environment and the target sequence. One of the first reports about acylated proteins in mitochondria came from the discovery that radiolabelled myristate and palmitate was found incorporated in proteins from rat liver mitochondria *in vitro* (Stucki *et al.*, 1989). Most of the radiolabel was localised to the matrix and the inside of the inner membrane. The authors demonstrated that fatty acid incorporation was reversible and that acylation and deacylation were rapid processes. Examples of mitochondrial acylated proteins include bovine methylmalonyl semialdehyde dehydrogenase (MMSDH) (Berthiaume *et al.*, 1994) and rat liver carbamoyl-phosphate synthetase I (CPSI) (Corvi *et al.*, 2001). In these cases, acylation occurs spontaneously at cysteines in the active sites and inhibits the metabolic activity of these enzymes. The majority of mitochondrial fatty acylated proteins were found localised in the matrix, but also in the inner membrane. No radiolabel was detected in the outer membrane or the intermembrane space (Corvi *et al.*, 2001). The inhibition by palmitoyl-CoA of CPSI was found to be dependent on the palmitoyl-CoA concentration and was time-dependent. As such, it resulted in irreversible enzyme inactivation. S-acylated proteins were not only detected in rat liver mitochondria, but also in other tissues, although most acylated mitochondrial proteins were found in the liver. Thus, the degree of protein S-acylation in mitochondria depends on the metabolic state of a particular tissue, but it is also regulated by the level of tissue specific expression of a particular protein. In the case of CPSI, the function of this inhibition is thought to have impact on the degradation of amino acids under starvation conditions. Enzyme inhibition by fatty acyl CoA has been previously demonstrated on other enzymes and is thus a general mechanism of metabolic control. Examples include the glycolytic enzyme glyceraldehyde-3 phosphate dehydrogenase (Yang *et al.*, 2005), rat adipocyte pyruvate dehydrogenase (Moore *et al.*, 1992), rat liver ADP/ATP translocase (Morel *et al.*, 1974) and bovine liver glutamate dehydrogenase (Kawaguchi & Bloch, 1976). A recent publication identified as many as 21 S-acylated mitochondrial proteins from rat liver by applying a similar detection mechanism to the biotin-switch assay (Kostiuk *et al.*, 2008). The majority of these proteins were matrix-localised enzymes involved in β -oxidation and dehydrogenases. In this case, it was concluded that the main function of fatty acylation is probably not the direct inhibition of all identified enzymes, but the promotion and stabilisation of protein-protein interactions. Matrix proteins for example could be anchored to the inner membrane by this mechanism. Thus, palmitoylation can have direct regulatory roles on enzymes and provides additional levels of metabolic control (Linder & Deschenes, 2003).

In the case of Slp1, palmitoylation probably happens spontaneously inside mitochondria once the protein has reached the inner membrane. Palmitoylation however is dependent on the availability of palmitoyl-CoA that has to be transported into mitochondria. Fatty acyl-CoA is the substrate for the breakdown of fatty acids by β -oxidation in animal, fungal and plant cells and for the synthesis of glycerolipids. Fatty acyl CoA is generally synthesised by fatty acyl CoA synthetase, an enzyme that is localised to the ER and the outer mitochondrial membrane in animal cells. In plant cells, these enzymes are found on various organelles: in the lumen of peroxisomes (and glyoxysomes) (Goepfert & Poirier, 2007), the outer envelope of chloroplasts (Schnurr *et al.*, 2002; Schnurr *et al.*, 2004), the ER and mitochondria (Thomas *et al.*, 1988). Beta-oxidation of fatty acids in animals happens in mitochondria and peroxisomes. For β -oxidation in animal mitochondria to occur, fatty acyl CoA must be transported across the inner membrane. In animals, this happens via the acyl carnitine carrier operating across the mitochondrial inner membrane. There is evidence that similar carriers exist also in plants, and carnitine has also been identified in plant cells (Wood *et al.*, 1992). A putative acylcarnitine carrier-like protein has been identified in mitochondria named BOU. It was demonstrated that this protein is necessary for lipid breakdown and seedling growth in the light (Lawand *et al.*, 2002).

In plants, beta-oxidation is active in peroxisomes of vegetative tissue and glyoxysomes of storage tissue. It is generally considered that peroxisomes are the only organelles in which β -oxidation occurs. Generally, β -oxidation is important for seed development and germination, but also for vegetative and reproductive growth, and in stress responses (Goepfert & Poirier, 2007). There is evidence however for β -oxidation in mitochondria. In this case, acyl-CoA is shuttled across the inner membrane by an carnitine shuttle analogous to that of animals. It is proposed that a fatty acyl CoA synthetase exists in the outer membrane (facing the intermembrane space) where it activates fatty acids by conjugation to CoA. Acyl CoA is then converted to acylcarnitine and translocated across the inner membrane by a carnitine/acylcarnitine translocase. Once in the matrix, it is converted back to carnitine and acyl CoA by a carnitine acyl transferase. Acyl CoA is then used as the substrate for β -oxidation as in peroxisomes (Masterson & Wood, 2000). Assuming that Slp1 faces the intermembrane space, palmitoyl CoA would be directly available for palmitoylation without the need to be transported across the inner membrane by a carnitine carrier-like system.

Use of the palmitoylation inhibitor BPA

The application of BPA to *Arabidopsis* wild type liquid cultures did not result in an increased pool of soluble Slp1 as anticipated (not shown). This negative result could either mean that BPA application over a prolonged time was not effective in blocking palmitoylation, or that palmitoylation of AtSlp1 is indeed not important for its membrane association.

BPA was supplied in excess in the experiments presented in Figure 4-26 on agar plates at a concentration of 1mM. BPA itself is highly insoluble in aqueous solutions and had to be applied from a stock solution dissolved in DMSO. The agar plates had visible fatty acid precipitates, thus not all of the BPA applied was actually taken up by seedlings. At this point it is also not known whether BPA was chemically stable for the period of plant growth (20 days). Plants grown on these plates displayed a strong phenotype. Root and shoot growth was dramatically restricted, and green tissue became very rapidly chlorotic. Images of treated seedlings are presented in chapter 5 (Figure 5-31). Reduction of growth was also reported for the *tip1* mutant that encodes a putative PAT protein with an ankyrin repeat domain. These plants are defective in polar tip growth of root hairs and their phenotype can be mimicked by the application of BPA on wild type plants (Hemsley *et al.*, 2005).

On the base of the observed phenotype, it is assumed that BPA must have had effects on lipid metabolism and protein acylation in this treatment. An issue that remains open concerns the specificity of the anticipated effect on protein palmitoylation. BPA competes with palmitate for transfer on CoA and therefore reduces available palmitoyl-CoA pools (Resh, 2006). However, given that the inhibitor was applied in excess amounts and was taken up sufficiently, it is likely to have depleted a large proportion of the acyl-CoA pool from cells. When incorporated, Br-palmitoyl-CoA is not transferred to protein thiol groups and could potentially form an inhibitory complex with a PAT enzyme. If incorporated into proteins as bromo-palmitate by spontaneous acylation, it might diminish membrane association because the bromine group increases hydrophilicity and bulkiness of the acyl chain. Additionally, BPA could prevent uptake of palmitate into cells and mitochondria. It is poorly metabolised and cannot undergo β -oxidation itself, and it could even prevent oxidation of other long chain fatty acids. Thus, BPA has the potential to cause changes in lipid metabolism and could have other pleiotropic effects on metabolism (Resh, 2006; Webb *et al.*, 2000). With regard to the spontaneous palmitoylation expected to occur

on Slp1, BPA could have effects either by diminishing the available acyl-CoA pool, or by being incorporated, but not mediating membrane association.

Given these circumstances and issues with the use of such an inhibitor, the experimental protocol should be modified in a repeat of this experiment. Incubation with BPA for shorter periods (eg for one day only) would probably constitute a better experimental setup. In addition, effects on the mitochondrial distribution of Slp1 could be followed directly if plants overexpressing Slp1 with a C-terminal fluorescent protein are to be used in combination with a mitochondrial marker such as MitoTracker (as described in chapter 4). This way, it could be established whether Slp1 palmitoylation is important to keep the protein anchored inside mitochondria, or whether it might then be degraded or lost if it becomes soluble. To control for the efficiency of BPA treatment, the solubility of a known palmitoylated protein should have been tested in parallel.

The palmitoylation of band-7 family proteins is not a new concept. Several classes of band-7 proteins are post-translationally modified by acylation, including stomatins and flotillins (Browman *et al.*, 2007). In Arabidopsis, some of the HIR proteins mentioned in chapter 3 are N-myristoylated at N-terminal acceptor glycines. The first report of such a modification came from the human stomatin protein. This protein was demonstrated to be palmitoylated at cysteine 29, and at a second site further downstream (Snyers *et al.*, 1999b). Other palmitoylated band-7 proteins include podocin and Mec-2 (Huber *et al.*, 2006a). These two proteins are palmitoylated at two cysteine residues that both lie inside the conserved band-7 domain. The ability of the band-7 domain to bind cholesterol depends in these proteins on the acylation status of the cysteine residues. Mutations of these residues dramatically reduced cholesterol binding and rendered *C.elegans* touch insensitive. Thus, the availability of palmitoylated cysteines is crucial for these proteins to accomplish their function in mechanosensation of the nematode. Whether increased hydrophobicity by palmitoylation targets these proteins to microdomains and therefore a cholesterol rich environment, or whether palmitoylation has other effects on cholesterol binding of these proteins is currently not known. Given the high degree of conservation of the band-7 domain, palmitoylated cysteines are probably a part of this conservation and have a common underlying function. Thus, mutation of this residue in AtSlps and putatively also in HsSlp2 might be expected to yield similar strong phenotypes as demonstrated for the *C.elegans* protein Mec-2. Human Slp2 is not known to be modified by S-acylation, but this would an expected feature at the same conserved residue (see Figures 3-4 and 4-25), given the degree of homology to the Arabidopsis proteins. Additionally, surrounding residues as highlighted in Figure 4-25 could also be mutated

since they are putatively important to provide a suitable protein environment for palmitoylation to occur spontaneously. In particular, the conserved arginine two residues downstream of the cysteine would be a good candidate for site-directed mutagenesis, as well as the nearby leucine and tryptophane residues, all conserved residues between AtSlps and HsSlp2. Cholesterol binding of the band-7 domain of podocin was also shown to be crucially dependent on the presence of a conserved proline residue located directly in upstream of the band-7 domain (Huber *et al.*, 2006a; Kadurin *et al.*, 2008b). Such a proline is also present in the AtSlp and HsSlp2 sequences at the same relative position as in podocin and Mec-2 (four amino acids upstream of the start of the band-7 domain). This residue would be another prime candidate for mutagenesis in an attempt to prove the importance of cholesterol binding for the function of these proteins.

In conclusion, the results presented in this chapter provide new details about the structure, mitochondrial localisation and membrane association properties of Arabidopsis stomatin-like proteins. They suggest these proteins reside at the inner membrane surface, and they underline close similarities between these plant proteins and their human ortholog, consistent with the idea of functional homology. These results provide now the basis to investigate how these proteins function in the plant.

5 Phenotypical and functional characterisation of AtSlp mutants

Introduction

This chapter describes the phenotypical analysis of different mutants associated with AtSlp genes. First, T-DNA insertion lines will be described that were isolated for the AtSlp1 gene. Various associated growth phenotypes are presented and discussed. In particular, phenotypes associated with mitochondrial function were further investigated. In addition to the characterisation of T-DNA insertion lines, the creation of inducible RNAi lines for both genes is briefly described and prospects of a double knockout plant. Finally, effects on plant growth and morphology by the overexpression of truncated versions of AtSlps, so called dominant negative proteins, are presented and discussed. These results are summarised at the end and put into context with a proposed model for Slp function in Arabidopsis.

5.1 Isolation of homozygous AtSlp1 T-DNA insertion lines

Altogether four different homozygous T-DNA insertion lines were isolated in and around the AtSlp1 gene named *slp1-1* to *slp1-4*. All of these lines stem from the SAIL collection (Sessions *et al.*, 2002) and were selected based on their putative position in the AtSlp1 gene as given by the database. All lines were resistant to BASTA (glufosinate ammonium), and isolated based on the homozygous presence of the T-DNA and their ability to suppress AtSlp1 transcript and protein levels. Figure 5-1 gives an overview over the Slp1 gene and three of the four isolated insertions.

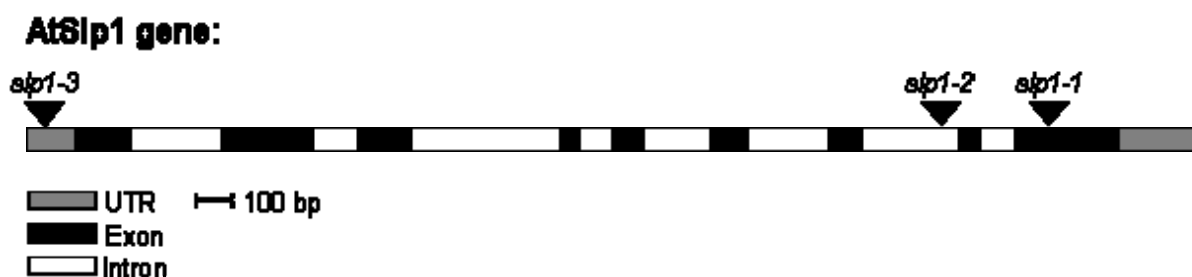


Figure 5-1. Scheme of the AtSlp1 gene with three isolated T-DNA insertion sites (*slp1-1* to *slp1-3*) marked by black triangles. The *slp1-4* insertion site lies upstream of *slp1-3* and is not included in this figure.

The same results were also obtained for the two other isolated mutant lines, *slp1-2* and *slp1-4*. These two lines were isolated after the first two lines and supposedly had insertion sites in exons towards the 3' end (*slp1-2*) and the 5' end (*slp1-4*) of the gene. Figure 5-3 shows agarose gels with the relevant PCR products for the genotyping of these lines. This time, plants were selected straight for resistance to BASTA on MS agar plates, and only resistant individuals were subsequently analysed for their genotype. A total number of 10 plants for each line were analysed and the results are presented below (Figure 5-3). All individual plants had T-DNA insertions as can be seen from the presence of the T-DNA products. For *slp1-2*, only a single homozygous line could be detected (no. 2 in part (A) of Figure 5-3). For *slp1-4*, altogether four different homozygotes were identified (nos. 2, 4, 5 and 6 in part (B) of Figure 5-3).

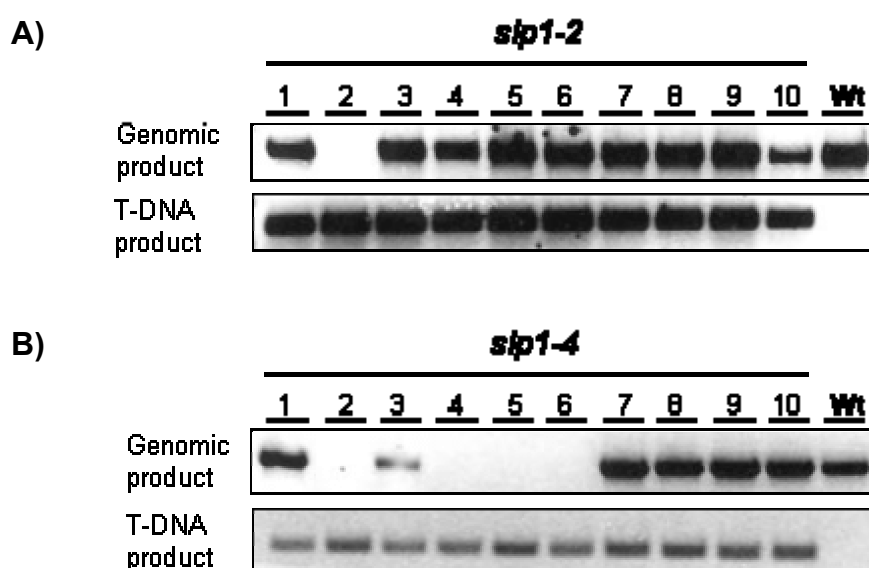


Figure 5-3. Genotyping PCR for BASTA resistant *slp1-2* and *slp1-4* mutant lines.

A) 10 individual plants (nos. 1-10) were probed for an insertion site (Genomic product) and the presence of the T-DNA (T-DNA product) in *slp1-2* mutant lines. The wild type control (Wt) only has the genomic product, but no T-DNA insertion product. Individuals nos. 1, 3 to 10 are all heterozygous for the T-DNA insertion. Only no. 2 is a homozygous plant that cannot form the genomic product.

B) 10 individuals (nos. 1-10) for the *slp1-4* line were probed for T-DNA insertions. Nos. 1, 3 and 7-10 are all heterozygous for the insertion, whereas nos. 2 and 4 to 6 are homozygotes. All 10 plants have the T-DNA insertion present.

All homozygous insertion lines were also verified by DNA-sequencing of the formed PCR products. This resulted in the confirmation of the exact T-DNA insertion sites. Table 5-1 summarises the positions of the T-DNA insertions of each line. The mutants *slp1-1* and *slp1-2* had indeed insertion sites in the last exon (*slp1-1*) and in the second last intron (*slp1-2*) of the AtSlp1 gene, respectively. However, *slp1-3* was revealed to have an

insertion outside of the open reading frame in the 5'UTR. The mutant line *slp1-4* had an insertion site in the promoter region upstream of the 5'UTR.

Mutant line	Insertion site	Location
<i>slp1-1</i>	110 bp upstream of TAG	9. Exon
<i>slp1-2</i>	480 bp upstream of TAG	7. Intron
<i>slp1-3</i>	79 bp upstream of ATG	5'UTR
<i>slp1-4</i>	150 bp upstream of ATG	Promoter

Table 5-1. Isolated knockout mutant lines and their respective T-DNA insertion sites as determined by DNA-sequencing of genotyping PCR products. TAG (stop codon), ATG (start codon).

For AtSlp2, several attempts were also made to isolate homozygous knockout lines. However, identified lines had T-DNA insertions, but it could not be confirmed that they were indeed homozygous. In other cases, it was already clear from the genotyping PCR that several insertion sites must have been present. None of the analysed lines from the Salk collection was resistant to the antibiotic marker present on the T-DNA. No further attempts were made to isolate additional mutant lines for this gene.

5.1.2 RT-PCR and Western blotting

The homozygous mutant lines *slp1-1* and *slp1-3* were further analysed for AtSlp1 transcript production by RT-PCR. Figure 5-4 shows the result of one individual plant of the *slp1-3* line (5'UTR insertion) and three individuals of the *slp1-1* line. The T-DNA insertion into the 5'UTR of the Slp1 gene did not result in any transcript interruption as judged by this RT-PCR. It had RNA levels just like wild type plants. The *slp1-1* insertion however caused a sharp reduction in transcript accumulation. When primers were used to probe for transcript in the area around the last exon (where the insertion site is), no transcript at all could be detected. By contrast, *slp1-3* had RNA levels like wild type plants in this region. However, when primers were used for RT-PCR to probe transcript accumulation around the first exon in *slp1-1*, small amounts of transcript could be detected after 35 cycles. This leads to the conclusion that the T-DNA insertion interrupts transcription downstream in the gene, but small amounts can still be produced further upstream of the insertion site. However, these transcripts are most likely incomplete and therefore unstable. It is unlikely that they would lead to the production of any protein.

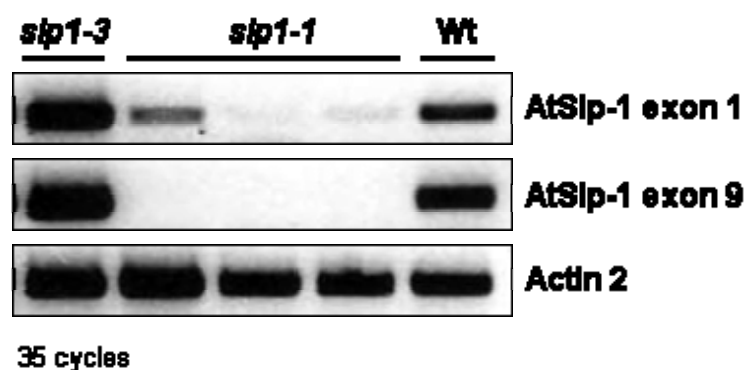


Figure 5-4. DNA agarose gel of RT-PCR reactions to probe for transcript levels in *slp1-1* and *slp1-3* mutants. Only one individual plant of *slp1-3* was probed, and three plants of *slp1-1*. Wild type (Wt) is included for comparison. Actin 2 was used as a control for total transcript amounts present. 35 cycles of PCR were applied.

The interruption of the AtSlp1 gene and thus also protein was further analysed by Western blotting of crude protein extracts obtained from the four individual lines. Figure 5-5 shows a Western blot of protein extracts from *slp1-1* and *slp1-3* plants. Corresponding to the results obtained from the RT-PCR experiments, the *slp1-1* mutation abolishes any protein produced that can be detected by the Slp1 antibody. More specifically, the C-terminus of the Slp1 protein that is recognised by this antibody is not expressed any more in these plants. Whether some protein nearer to the N-terminus is still made cannot be excluded based on this blot. This is however assumed to be unlikely. The *slp1-3* insertion does not cause reduction of the Slp1 protein compared to wild type plants. This finding is also in agreement with the RT-PCR of this line, where transcript was clearly detectable despite the T-DNA insertion in the gene's 5'UTR.

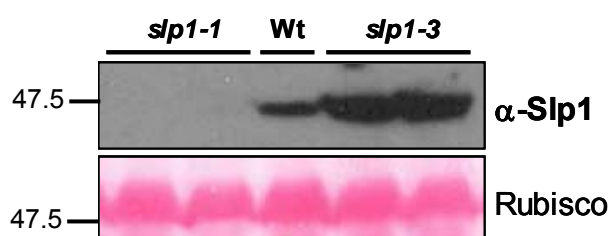


Figure 5-5. Western blot probed with anti-Slp1 to test for the presence of Slp1 protein in the T-DNA insertion lines *slp1-1* and *slp1-3*. Two individual plants were tested from *slp1-1* and *slp1-3*. Wild type (Wt) protein extract is included in the middle for comparison. The Ponceau S stain (Rubisco band) is included at the bottom for comparison of loading levels. Numbers on the left side indicate molecular weight markers in kDa.

Figure 5-6 shows Western blots of the 10 individual lines of *slp1-2* and *slp1-4* insertions (see Figure 5-3 A and B) that were all BASTA resistant. The single homozygous individual (no. 2) of *slp1-2* was confirmed to lack detectable Slp1 protein. All other heterozygotes had protein levels like wild type. In *slp1-4*, no difference could be seen between homozygous plants (nos. 2, 4, 5 and 6) and heterozygous ones (nos. 1, 3, 7-10). As expected from the insertion site in the promoter of the gene, this T-DNA insertion, even when homozygous, does not affect Slp1 protein levels compared to wild type plants. Based on this evidence, the mutant lines *slp1-3* and *slp1-4* were not further used for phenotypic analysis. Only *slp1-1* and *slp1-2* (individual no. 2) were propagated and their phenotypes experimentally analysed.

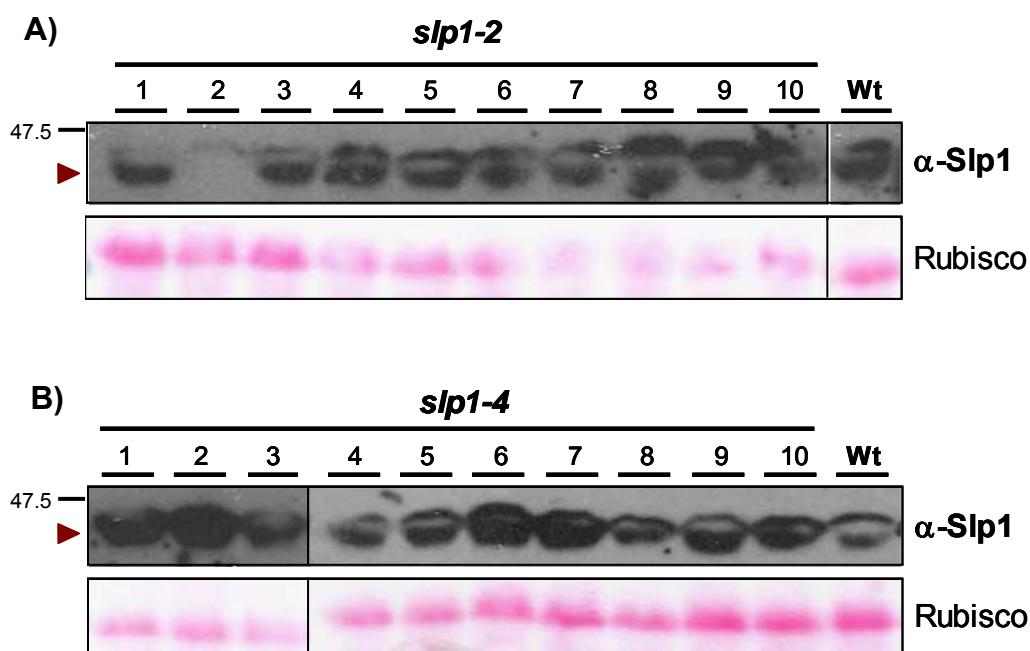


Figure 5-6. Western blots probed with anti-Slp1 of protein extracts from *slp1-2* (A) and *slp1-4* (B) lines.

A) The homozygous individual no. 2 was already identified from the genotyping PCR (Figure 5-3 A) and is confirmed to lack the Slp1 protein (indicated as red arrowhead). All other heterozygous plants of this line have protein levels like wild type (Wt). The Rubisco bands from the Ponceau S stained membranes are included for loading control. The number indicates the molecular weight marker in kDa.

B) Protein extracts from the 10 individual *slp1-4* lines that were genotyped in Figure 5-3 (B). All plants have protein levels like wild type plants with no difference between homozygotes (nos. 2, 4, 5 and 6) and heterozygotes (1, 3, 7-10). Labelling is as above.

5.2 Associated knockout mutant phenotypes

The following sections contain results about the phenotypic analysis of the isolated *slp1* mutants. Most phenotypes were observed in the *slp1-1* mutant, but were absent in the *slp1-3* mutant. Some experiments also contain results comparing defects in *slp1-1* with *slp1-2*. Since this mutant was isolated later than *slp1-1*, it is not included in all analyses. Where it is present however, *slp1-2* did not always show the same phenotype as *slp1-1*. These results and the prospective implications for the study of Slp function in Arabidopsis are discussed at the end of this chapter.

5.2.1 Shoot growth and morphology

The growth of *slp1-1*, *slp1-3* and wild type plants on soil was compared. Figure 5-7 shows photographs taken from these plants grown in long day light conditions for 23 days. Compared to the wild type and *slp1-3*, *slp1-1* had smaller leaves and a different leaf morphology. When the whole surface area of these plants was quantified (see bar chart below photographs), *slp1-1* had reduced growth by approximately 40% compared to wild type plants. Leaves from *slp1-1* plants were rounder in shape, and had shorter petioles. Additionally, the leaves were observed to be flatter than in control plants and did not curl as much once they were mature. Frequently, small lesions were noticed at the leaf margins that did not appear in wild type plants. The *slp1-3* mutant plants looked phenotypically like the wild type, and their surface area and leaf shape were indistinguishable from these plants. Since the Slp1 protein is present at levels comparable to wild type plants in *slp1-3* plants, the lack of a phenotype is not surprising.

Figure 5-8 shows photographs of *slp1-1*, *slp1-2* and wild type plants that had been grown on soil under the same conditions as above for 28 days. As seen before, *slp1-1* plants were smaller and had rounder leaves than wild type plants. Leaves from *slp1-2* plants however did not show this phenotype, despite the lack of Slp1 protein in these plants. *slp1-2* plants were indistinguishable from wild type rosettes in terms of leaf surface area. Interestingly, the difference in measured leaf surface area between *slp1-1*, *slp1-2* and wild type disappeared once the plants were mature and flowering at a late stage (see second bar chart on the right side). This result would indicate that *slp1-1* plants have a delay in growth, but do eventually catch up with wild type plants in terms of leaf surface area. However, it was noted that even at the mature stage, the leaves from *slp1-1* plants still differed in shape from wild type leaves as described above.

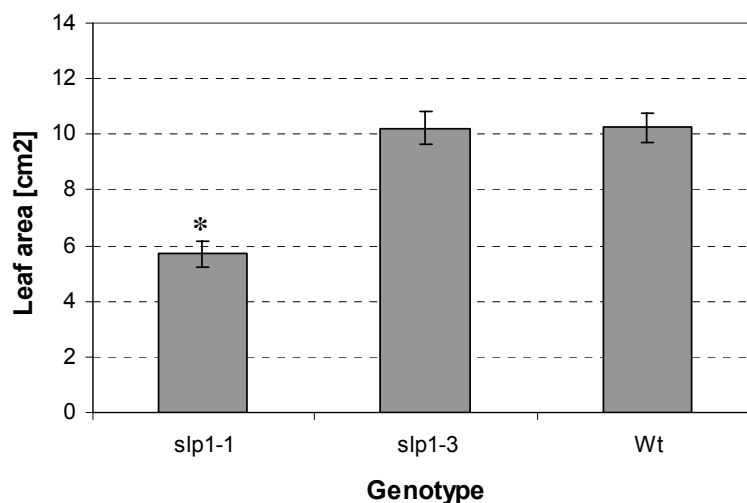


Figure 5-7. Photographs taken of *slp1* mutant plants grown in long day light conditions on soil for 23 days. Scale bar = 1cm. Shown below is a bar chart of the quantified leaf surface area with standard errors. The asterisk indicates a significant difference (paired t test, $p < 0.05$; $n=12$ (*slp1-1*), $n=6$ (*slp1-3*, Wt)).

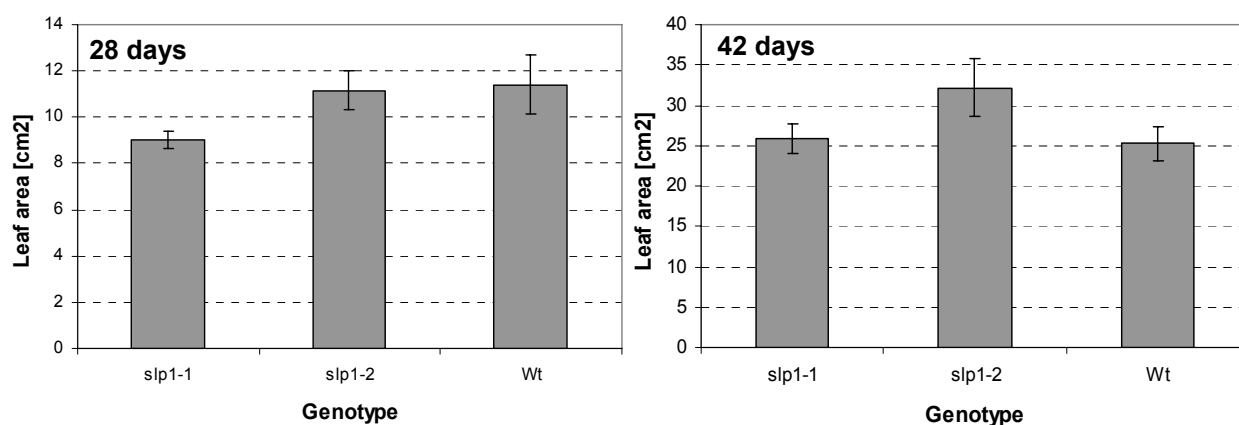


Figure 5-8. Photographs and quantified leaf surface areas of *slp1-1*, *slp1-2* and wild type plants grown on soil for 28 and 42 days in long day light conditions. Scale bar = 1cm. Error bars represent standard error values ($n=9$ (*slp1-1*), $n=10$ (*slp1-2*), $n=8$ (Wt)).

5.2.2 Seed germination

Because of the high upregulation of AtSlps during seed imbibition as proven by microarray data (see Figures 3-22 and 3-24), the germination rates of *slp1* mutant seeds were tested. Seeds of the *slp1-1* and *slp1-2* mutants were sown with wild type seeds sterile on MS agar plates (no sucrose present in the medium). In parallel, the same seeds were also sown on the same plates supplemented with either 1 μ M ABA or 2 μ M GA (gibberillic acid). The experimental setup was always such that half of a squared Petri dish was used for *slp1* seeds, and the opposite half for wild type seeds. Approximately 60 seeds per line were sown on a single plate and their germination checked every day after sowing. Figure 5-9 shows the quantified germination rate of *slp1-2* and wild type seeds over time on MS (A), ABA (B) and GA (C) agar plates. On MS medium alone, *slp1-2* seeds showed a delay in germination rate compared to wild type seeds at days one and two. Over the time course of eight days, the germination rate of *slp1-2* seeds caught up with wild types, but stayed slightly lower overall. On MS medium supplemented with ABA, the delay in germination remained at days one and two, but germination quickly resembled wild type levels at day three. This effect of germination delay was surprisingly even more pronounced on plates containing GA, but only at day one. The germination rate of wild type seeds on GA medium resembled that on MS medium. Identical experiments were also set up for *slp1-1* seeds with similar results (not shown). In this case, the delay on GA containing medium was not quite as pronounced as shown for *slp1-2* seeds in Figure 5-9 (C), but there was nevertheless a reduction in germination rate.

This result confirms that the Slp1 protein (and putatively also the Slp2 protein) has an important function in the germination of seeds after the breaking of seed dormancy. Putatively, these proteins are involved in metabolic changes during seed germination, some of which take place in mitochondria (e.g. the conversion of succinate to malate during the glyoxylate cycle).

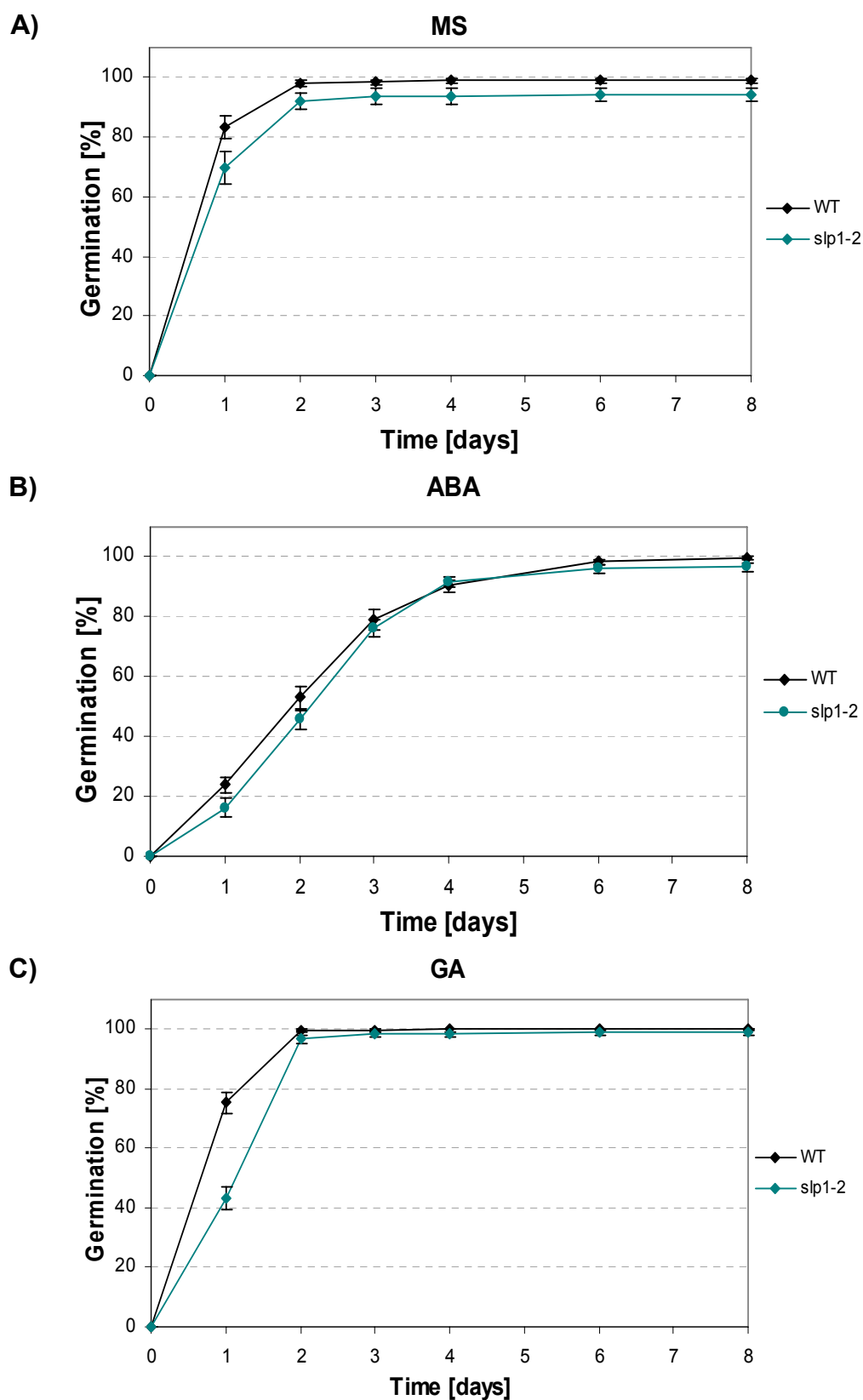


Figure 5-9. Germination assay of *slp1* mutant seeds. Seeds were germinated on three different media, and the proportion of germination counted on each day after seed imbibition.

A) Germination on 0.5x MS medium on agar plates.

B) Germination on 0.5x MS agar plates supplemented with 1 μ M ABA.

C) Germination on 0.5x MS agar plates supplemented with 2 μ M gibberillic acid (GA).

5.2.3 Root growth

To investigate whether *slp1* mutant plants would be affected in root growth, *slp1* and wild type seedlings were grown on vertical plates. To control for any influence of sucrose in the medium, plain MS plates and MS plates supplemented with 0.5 % sucrose were used. The lengths of the main roots were measured after 10 (A) and 13 (B) days and are plotted in Figure 5-10. After 10 days of growth, *slp1-2* seedling main roots were visibly shorter in length than the corresponding wild type plants (Wt *slp1-2*). *Slp1-1* roots were also shorter, but this was not statistically different from the wild type seedlings (Wt *slp1-1*). On medium supplemented with sucrose however, the opposite was measured. *Slp1-1* root lengths from mutant plants were shorter than those of wild types. *Slp1-1* roots however, had the same lengths as *slp1-2* and the corresponding wild type plants. Considering the overall lengths of roots, the addition of sucrose did not cause differences in the absolute lengths of *slp1-1* and *slp1-2* seedlings at this stage.

After 13 days of growth, differences between *slp1* mutants and their corresponding wild types were more pronounced. When grown on MS medium alone, both *slp1* mutants were visibly shorter than their corresponding wild type roots (Figure 5-10 B). When this was compared to growth on MS medium with sucrose, this difference was persistent for *slp1-1* seedlings, but not so obvious for *slp1-2* seedlings. However, as seen in Figure 5-10 (A), growth on sucrose containing medium did not change the overall total length of the main root after 13 days significantly when compared to MS medium alone. Overall, *slp1* mutants generally seem to grow at a slower rate than wild type seedlings. This has previously been demonstrated for shoots, and it also appears to apply to root growth. However, the data presented here only represent one experiment and therefore have to be validated independently before any final conclusion can be made.

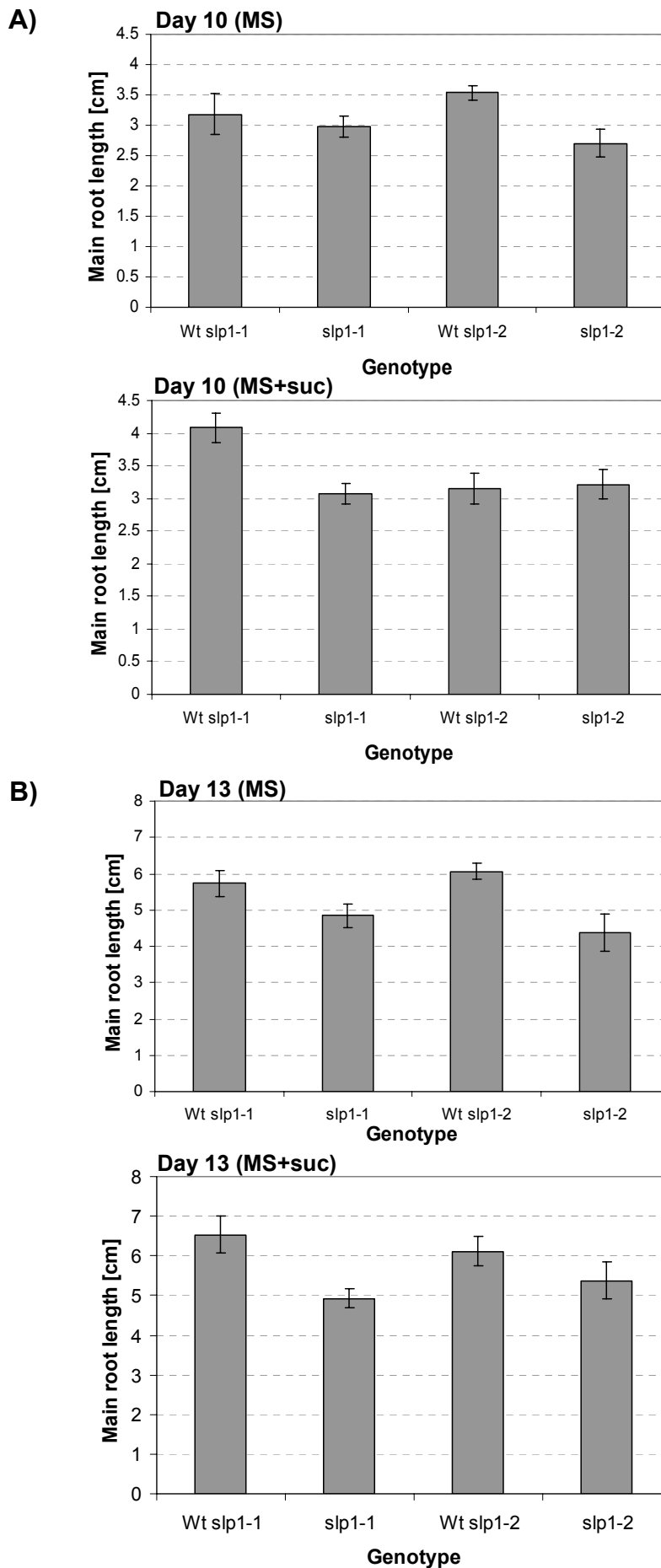


Figure 5-10. Main root length measurements of *slp1-1*, *slp1-2* and wild type seedlings grown for 10 (A) or 13 (B) days on MS agar plates (MS) or MS supplemented with sucrose (MS+suc). The path length of the main root was measured from seedlings grown vertically on squared Petri dishes. “Wt *slp1-1*” indicates that wild type seeds were used to compare root growth that had been harvested together with each mutant seeds. Error bars indicate standard error values.

5.2.4 Leaf osmolarity

Since stomatin-type proteins are known to interact with various ion channels in animals and humans, *slp1* mutants were analysed for differences in overall osmolarity levels in leaves. Rosette leaves of mature, long day grown plants on soil were harvested and ground using a pestle. Squeezed-out leaf sap was collected by centrifugation, and directly measured in a vapour-pressure osmometer. Figure 5-11 shows the quantified result from these measurements. The *slp1-1* mutant has significantly higher osmolarity levels (350 mOsM) in leaves than the *slp1-3* mutant and wild type plants (320 mOsM). These differences are however small and still fall into an expected range for plant cell osmolite levels. Therefore, this elevated osmolarity is unlikely to cause large differences in cell function and is not expected to affect leaf growth. This experiment was not carried out on *slp1-2* leaves, therefore no assumption can be made about leaf osmolarity levels in this allele.

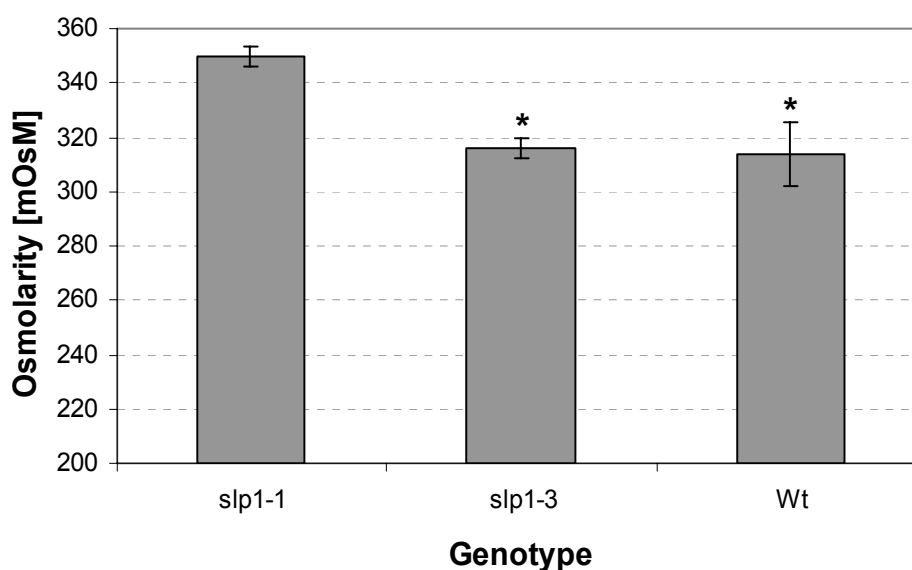


Figure 5-11. Osmolarity (in mOsM) of rosette leaf sap from *slp1-1*, *slp1-2* and wild type plants. Leaves were ground and the sap collected by centrifugation. Osmolarity was measured in a vapour-pressure osmometer in a volume of 10 μ L. Asterisks indicate significant differences from *slp1-1* osmolarity (n= 6, t test, p< 0.05).

5.2.5 Flowering time

AtSlp promoter sequences were shown to contain response elements involved in the timing and development of flowers (Tables 3-14) and AtSlps are highly expressed in developing

pollen (Figures 3-35 and 3-37). To determine whether *slp1* mutants would have delays in the timing of flower transition, vegetative leaves were counted as a measure of flowering timing. Figure 5-12 shows the result from these counts. No significant difference in the number of rosette leaves was observed between *slp1-1*, *slp1-3* and wild type plants grown in long day light conditions. Leaves were counted from plants that visibly bolted as judged by the appearance of the shoot apex at least 1 cm from the soil. *slp1-1* plants had on average slightly less rosette leaves than wild types, but the difference was not statistically significant. Therefore, no effect on the timing of flower transition in *Slp1* lacking plants could be observed.

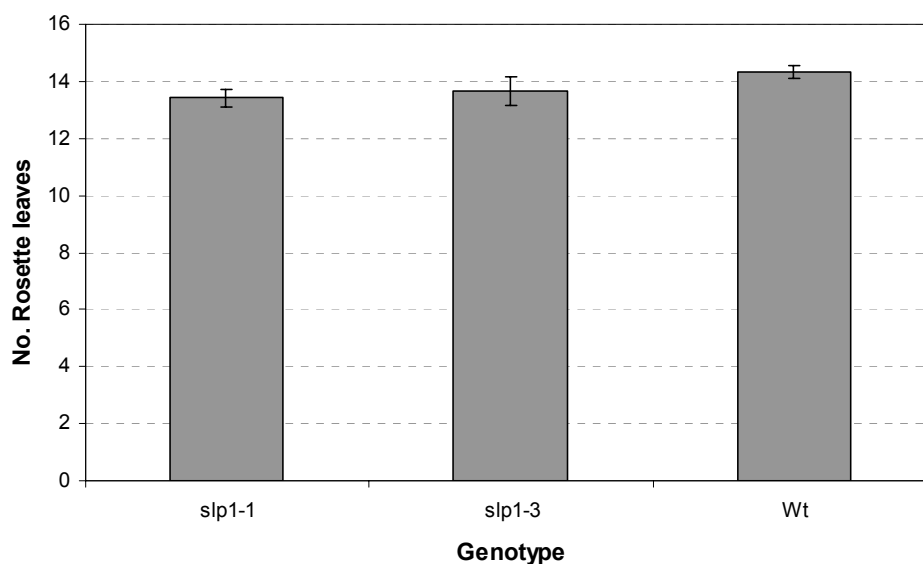


Figure 5-12. Determination of flowering time of *slp1-1*, *slp1-3* and wild type plants as measured by the number of vegetative leaves upon bolting. Rosette leaves were counted of bolting plants grown under long day light. No statistically significant difference between mutants and wild type was observed. Error bars represent standard error values (n=12).

5.2.6 Seed production/Fertility

Because both *Slp* proteins are highly expressed in pollen, effects on plant fertility or flower development would be expected in mutant plants. To assess for differences in fertility, the total number of seeds per silique from *slp1-1*, *slp1-2* and wild type plants were counted. Figure 5-13 (A) shows the result of an example count. Siliques from *slp1-1* plants contained frequently less seeds (approximately 20 %) than those from *slp1-2* and wild type plants. This was statistically significant as judged by a t-test. By comparison, siliques from *slp1-2* plants also had on average less seeds, but this was not significantly different from

wild type plants. Additionally, siliques from both *slp1-1* and *slp1-2* plants were noticed to differ in shape from wild type siliques. Frequently, mutant siliques were shorter, had gaps where seeds would be normally expected, and were also thicker in appearance. These observations were not further quantified. Figure 5-13 (B) shows example photographs of counted siliques.

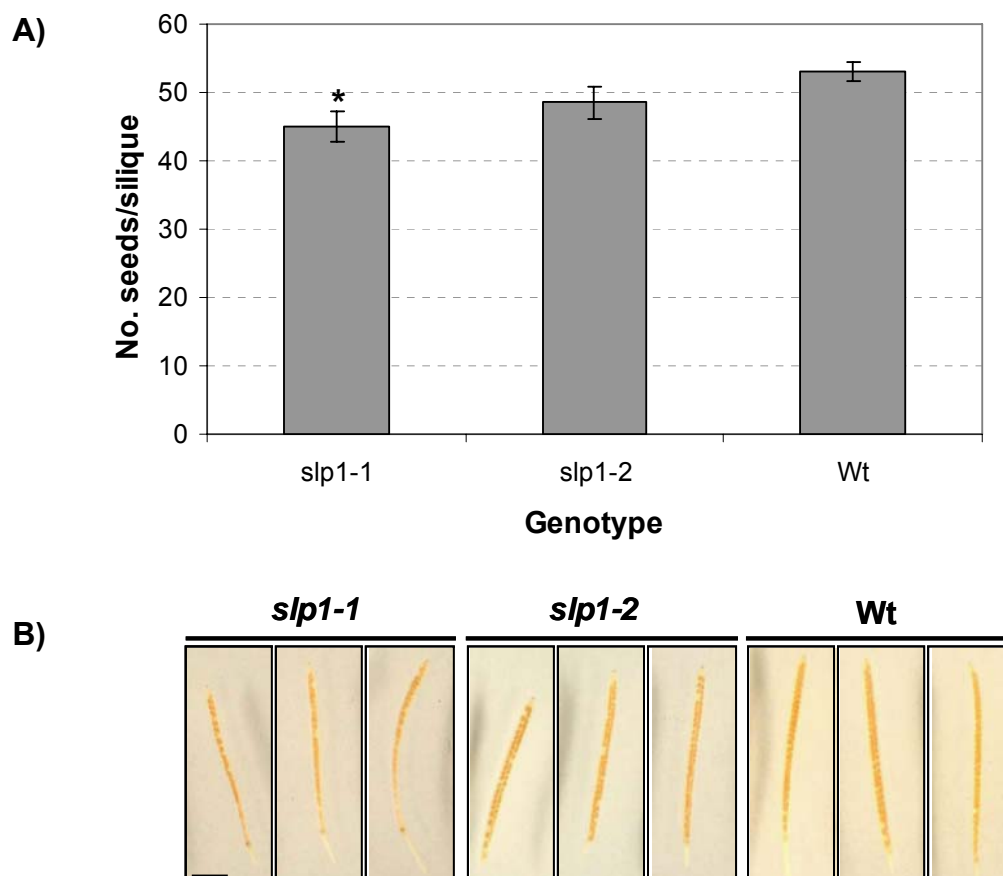


Figure 5-13. *slp1-1* plants produce siliques with significantly less seeds than *slp1-2* and wild type plants.

A) Seeds per mature silique were counted from a total of 10 plants per genotype. Error bars indicate standard error values. The asterisk indicates a significantly reduced value compared to the wild type (t test, $p < 0.05$, $n = 10$).

B) Images of cleared siliques from mutants and wild type plants. Scale bar = 0.5 cm.

5.2.7 Sensitivity to salt stress

AtSlp transcripts were specifically upregulated in roots by salt stress as described in section 3.5.1.5. To test for any differences related to salt tolerance in roots, a root bending assay (Wu *et al.*, 1996) was conducted. Wild type and mutant seedlings were grown for

four days on MS medium before being transferred to medium containing either MS, MS supplemented with 100mM sodium chloride, or MS supplemented with 200mM sodium chloride. At the point of transfer, vertical plates were turned by 180°, and the seedlings were grown for another four days until imaging. The distance of root growth after the transfer was then measured and compared between wild type, *slp1-1* and *slp1-2* plants. Figure 5-14 shows a series of images taken from seedlings of each genotype and medium. From these photographs it can be seen that wild type seedlings were larger in size, and had also greener leaves than mutant seedlings, even on MS medium. Both leaves and roots were overall larger in wild type plants. Additionally, wild type seedlings developed visibly more lateral roots than *slp1-1* mutants, but not *slp1-2* mutants on MS medium (not further quantified). Overall the root gravitropic response was not impaired in mutant plants. These seedlings had root tips that bended and reoriented themselves like wild type root tips. Upon shift to medium containing 100mM sodium chloride, these differences between wild type and *slp1* mutants were even more pronounced. Whereas the wild type roots were visibly impaired in the size of leaves and the lengths of root growth after the transfer, they still developed lateral roots. *Slp1* mutants by comparison hardly had any lateral roots, and their rosettes were visibly smaller than those of wild type seedlings. Transferring seedlings to 200mM sodium chloride impaired all genotypes heavily in overall growth. However, differences could be seen again between wild type and *slp1* seedlings. Wild type plants still had green tissue and shorter lateral roots. Root bending still occurred, but further root growth was almost completely restricted. By comparison, *slp1-1* seedlings were visibly chlorotic in appearance and had no lateral roots at all. Root bending was impaired equally as in wild type seedlings, but *slp1-1* roots grew less than wild type roots. *slp1-2* seedlings resembled *slp1-1* plants growth characteristics on medium containing 200mM sodium chloride.

Root growth of all genotypes after the transfer was quantified and is presented in Figure 5-15. *slp1-1* seedlings showed significantly decreased growth (by approximately 20 %) compared to wild type plants after the transfer on all media tested. The roots of *slp1-2* seedlings were also impaired on MS and 100 mM sodium chloride, but not significantly different from wild type roots as tested with a t-test. On 200 mM sodium chloride, *slp1-2* roots grew as much as wild type, whereas *slp1-1* was significantly decreased compared to *slp1-2* and the wild type.

These results demonstrate that *Slp1* is indeed required for responses to salt stress in roots and also in shoots. They confirm the results from microarrays that indicate upregulation of the *AtSlp* genes upon salinity stress in roots.

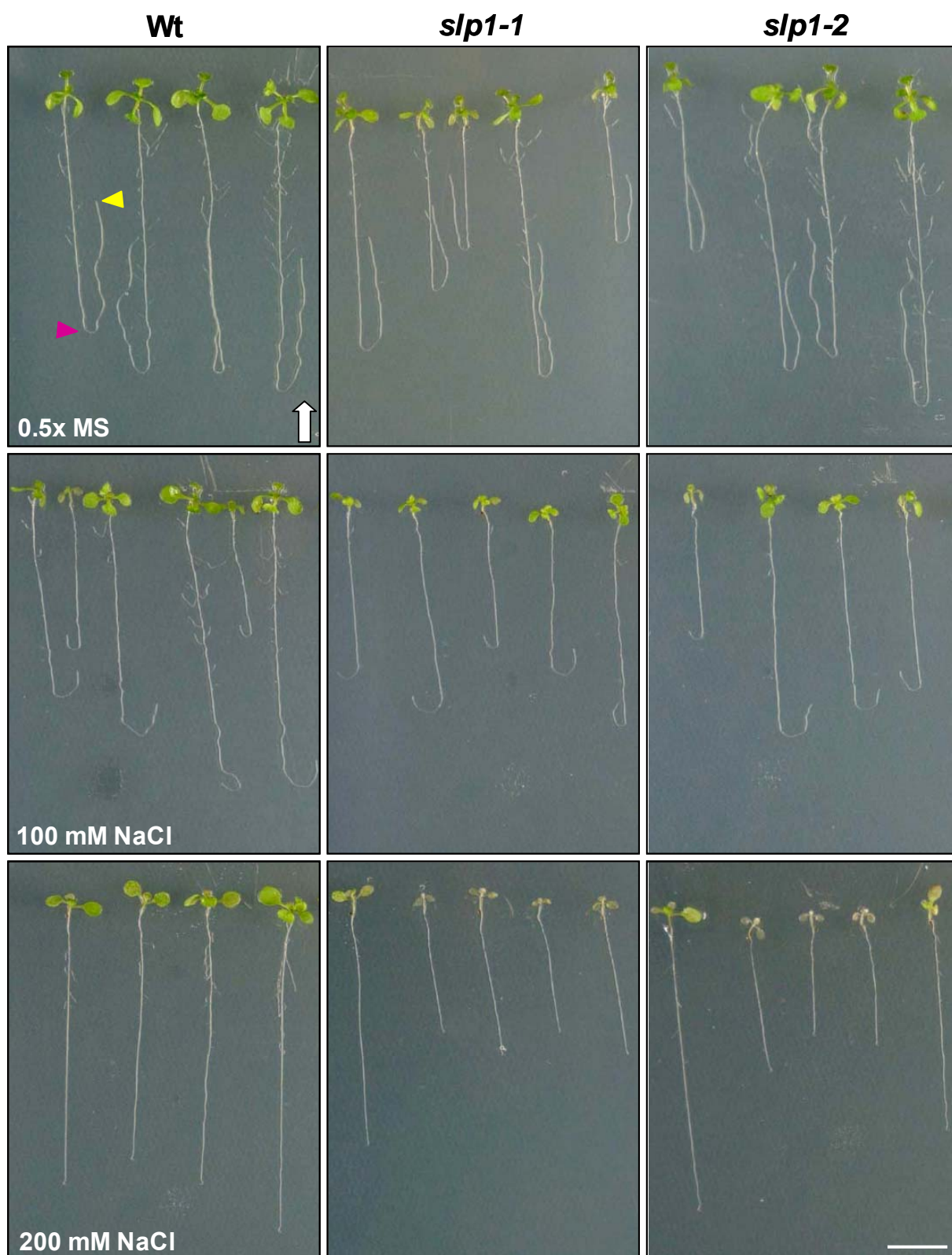


Figure 5-14. Root bending assay. Images were taken four days after the transfer to either control medium (0.5 x MS), or medium containing 100 or 200 mM NaCl. Images are shown from wild type plants (*Wt*), *slp1-1* and *slp1-2* mutants. The pink arrowhead indicates the point of turning, and the yellow arrowhead the end point after four days of growth. The distance between those two points was quantified in Figure 5-15 shown below. Scale bar = 1 cm. The images are shown upside down for clarity; the white arrow indicates the direction of gravity after turning the plates.

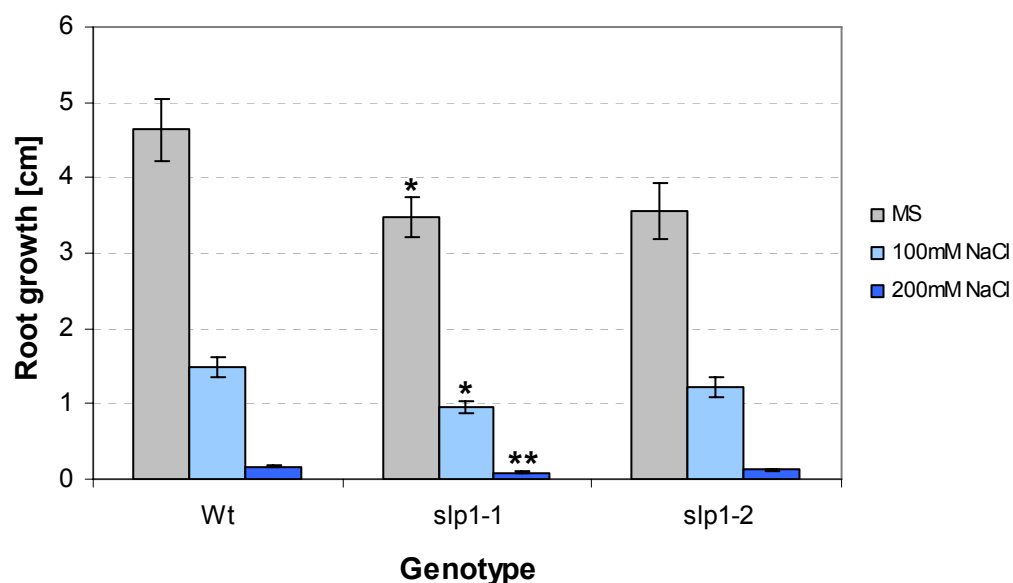


Figure 5-15. Quantification of root bending assay. Root growth after the transfer to either control medium (MS), or medium containing 100 or 200 mM sodium chloride was quantified. *Slp1-1* root growth after the transfer is significantly decreased on all three media tested compared to wild type (indicated by a single asterisk). Root growth of *slp1-1* is also significantly less on 200 mM salt compared to *slp1-2* (indicated by a double asterisk). These differences were tested with a two-tailed t-test ($n = 20-30$, $p < 0.05$). Error bars indicate standard error values.

5.2.8 Photosynthetic activity and transpiration rate

The *AtSlp1* promoter was demonstrated to be active in guard cells upon growth in liquid medium. Additionally, *AtSlp* transcripts were found present in guard cells in microarray studies (chapter 3 section 3.5.1.2.). These results lead to a question whether *slp1* mutant plants would be impaired in photosynthesis and transpiration.

The photosynthetic activity and transpiration rates of *slp1* mutants and wild type plants were measured in an infrared gas analyser chamber (IRGA) as a function of light intensity. A light response curve was set up to follow photosynthetic parameters over increasing photon flux densities. Mature rosette leaves of short-day grown plants were sealed in a round leaf chamber attached to the analyser. The CO_2 assimilation rates, stomatal conductances and transpiration rates of the plants were analysed and compared. Each run was always performed in parallel with one wild type and one mutant plant. Altogether four runs were set up for each mutant and one wild type plant. Table 5-2 lists the number of replicates used for the quantitative analysis. Because of technical problems, not all runs yielded all parameters anticipated and could thus be quantified. All values were compared

at 500 $\mu\text{mol}/\text{m}^2/\text{s}$ photosynthetic photon flux density (PPFD) because neither parameter should have been saturated under this condition.

Genotype	No. replicates		
	Assimilation rate	Stomatal conductance	Transpiration rate
Wt	5	8	8
<i>slp1-1</i>	3	4	4
<i>slp1-2</i>	2	3	3

Table 5-2. Replicates of photosynthesis measurements in the IRGA chambers for wild type (Wt), *slp1-1* and *slp1-2* plants.

Figure 5-16 shows graphs of the analysed datasets. No significant differences could be detected between any of the mutants and wild type plants in any of the analysed parameters. The CO_2 assimilation rate of *slp1-2* plants was reduced compared to wild type and *slp1-1* plants, but only two replicates could be analysed from the recorded data. The stomatal conductance and transpiration rate in *slp1-2* plants were also reduced, but not to a significant extent as judged by paired t- tests at $p < 0.05$.

In addition to these parameters, the light efficiency or quantum yield of photosynthesis (superimposed as a linear regression on top of the assimilation rate at low range light values), and the dark respiration rate were also determined. Neither of these values was statistically significantly different in *slp1* mutants compared to wild type plants (not shown). An independent experiment to investigate leaf water content was set up as described later in this chapter in section 5.6.5. The water content of detached leaves was determined by comparing fresh weight and dry weight as the percentage of initial fresh weight. *Slp1-1* mutant leaves had marginally reduced (by 1 %) water content compared to wild type and *slp1-3* leaves. This difference has probably no effect on the water status of these plants. Whole plant transpiration rates were measured as it will be described in section 5.5.6. An example of such a measurement is shown in Figure 5-15B. In these experiments, *slp1-1* mutants had slightly decreased transpiration rates and responded less well to light changes than wild type plants. However, also these differences have probably no effect on the overall water homeostasis of these plants.

From these data it can be concluded that the single *slp1* knockout has no effect on the photosynthetic capacities of these mutant plants. Thus, the delayed/reduced growth of *slp1-1* plants is not the result of impaired capacities of carbon fixation or transpiration.

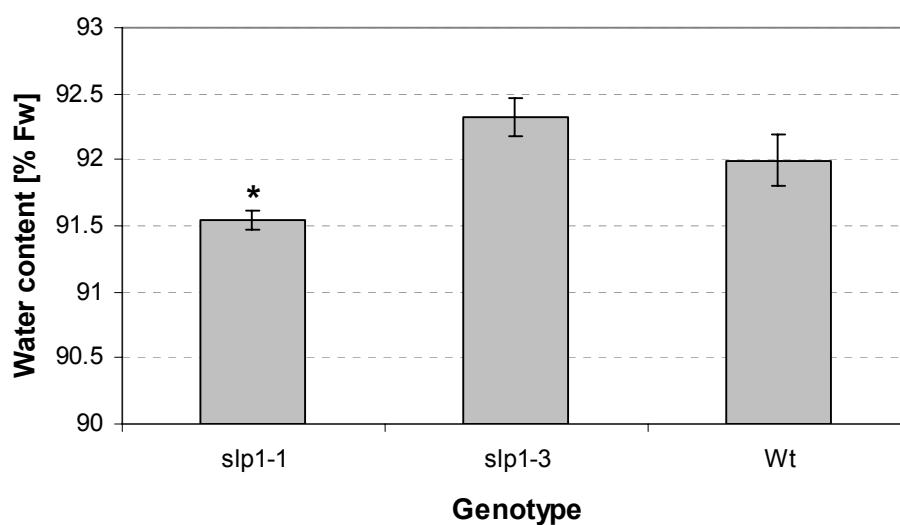


Figure 5-15A. Water content of *slp1* mutants and wild type plants. Water content was quantified as the percentage of weight after drying of the initial fresh weight. *Slp1-1* leaves had significantly reduced water contents (by 1 %) than *slp1-3* and wild type leaves (paired t-test, $p < 0.05$, $n = 12$).

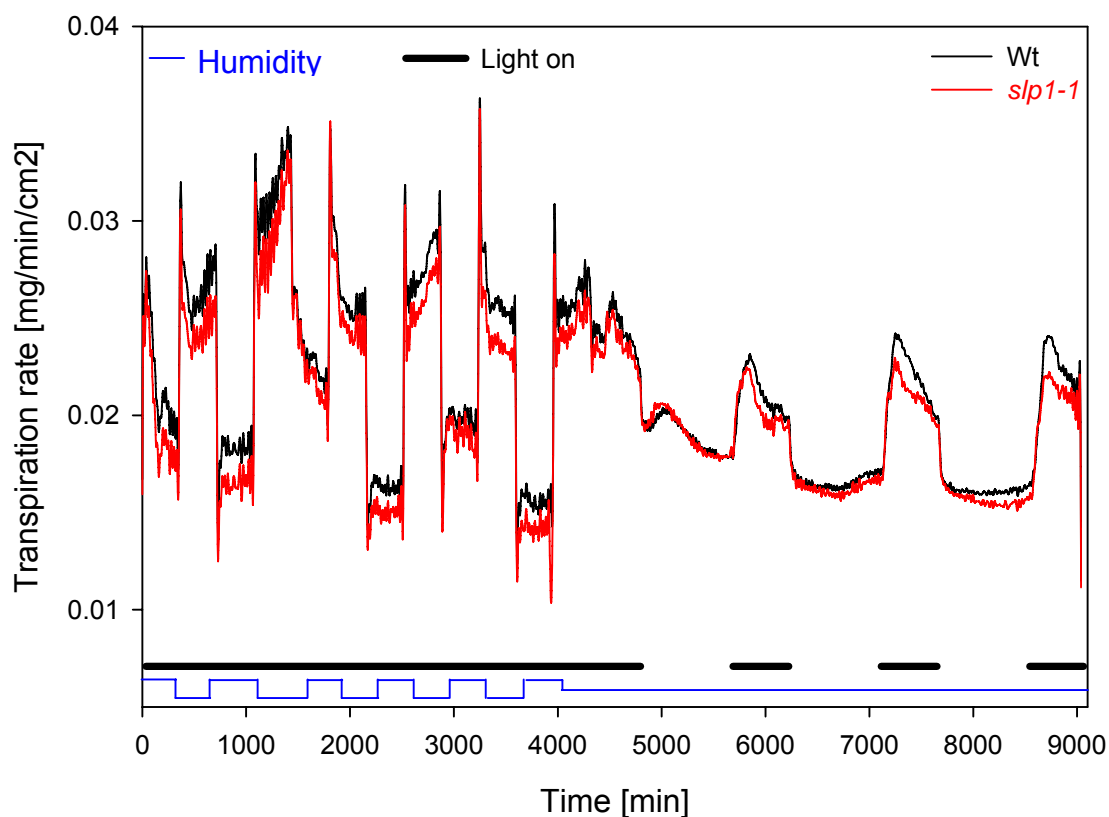


Figure 5-15B. Whole plant transpiration rates between *slp1-1* (red line) and wild type plants (black line) over time. A humidity response experiment (from 0-4700 minutes) was followed by a light response experiment. Humidity levels were set high (80 %) or low (40 %) as indicated by the elevation of the blue line. The presence of light is indicated by the thick black line. Further explanations to the experimental setup are given in section 5.5.6 and Figure 5-44.

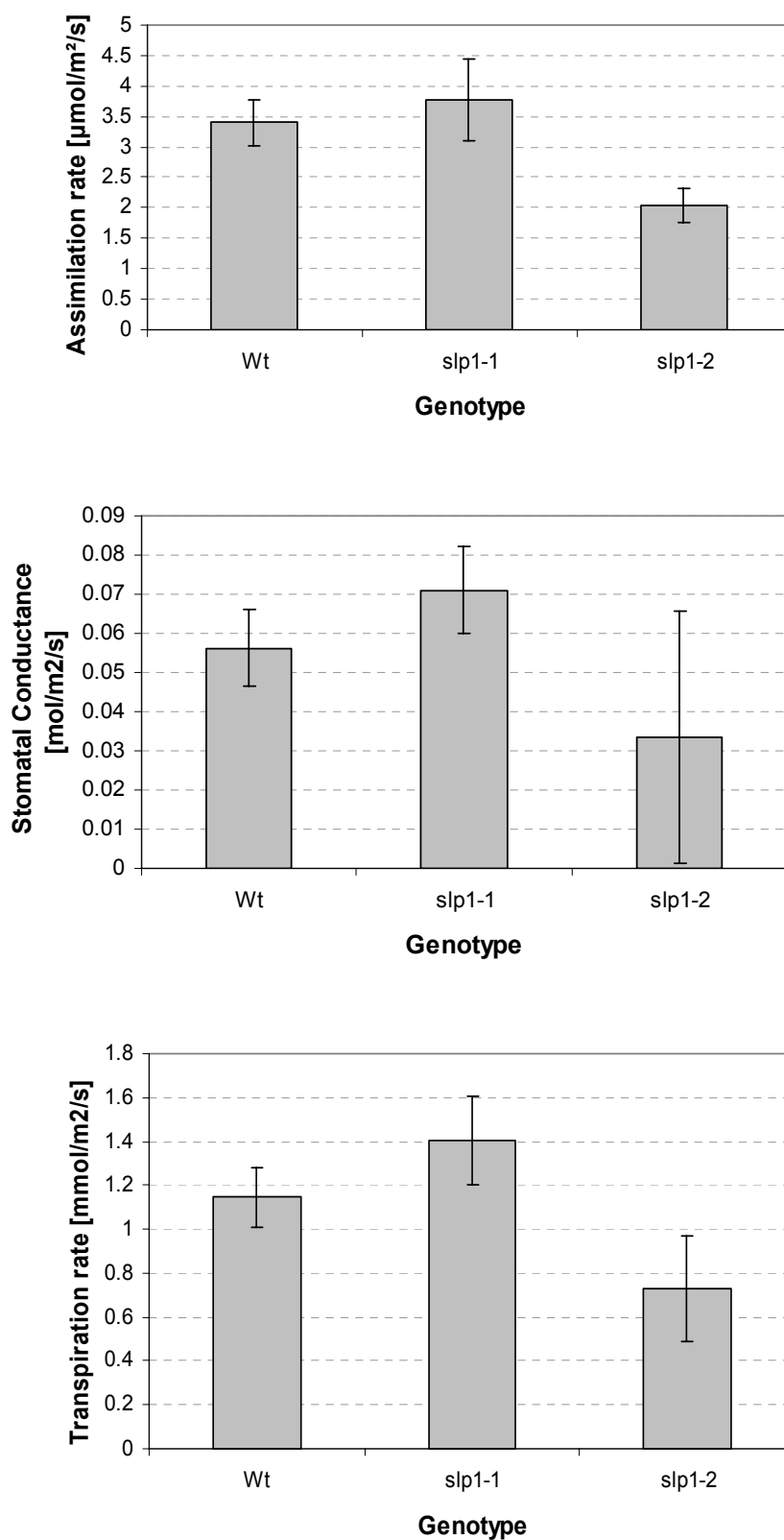


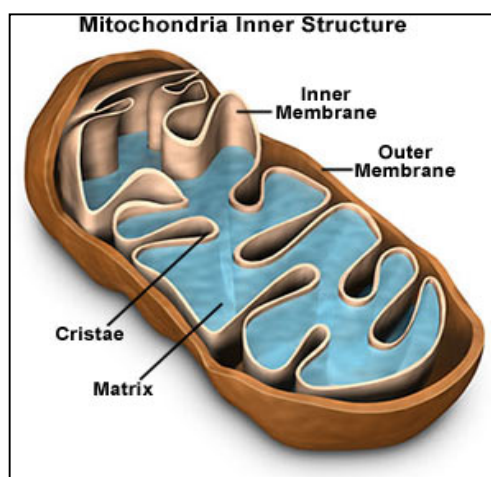
Figure 5-16. Quantifications of assimilation rates, stomatal conductances and transpiration rates between wild type and *slp1* mutants at 500 $\mu\text{mol}/\text{m}^2/\text{s}$ photon flux density. None of these results were statistically different from each other. Error bars indicate standard error values.

5.3 Mitochondrial phenotypes of *slp1* knockout plants

Because of the specific subcellular localisation of AtSlps, *slp1* mutant plants were analysed for phenotypes related to mitochondrial function. The first objective was to compare whether there would be any notable differences in the mitochondrial membrane potential between *slp1* plants and wild type. Secondly, oxygen consumption rates from mitochondrial preparations were measured and compared between *slp1-1* and wild type plants. Finally, two attempts were utilised to monitor differences in the accumulation of reactive oxygen species in these plants.

5.3.1 Membrane potential

The diagram shown below gives an overview over the different mitochondrial compartments for orientation purposes. The inner membrane has multiple invaginations (cristae) that increase the overall membrane surface area. The matrix (shown in blue) is the space surrounded by the inner membrane. The outer membrane surrounds the whole organelle and gives rise to the intermembrane space inbetween the inner membrane and the outer membrane.



Scheme of the mitochondrial ultrastructure. This image was taken from the web (<http://www.cartage.org.lb/en/themes/sciences/zoology/AnimalPhysiology/Anatomy/AnimalCellStructure/Mitochondria/Mitochondria.htm>)

Mitochondria are characterised by the presence of a membrane potential across the inner mitochondrial membrane. The membrane potential (negative on the matrix side) consists of an electrical potential across the membrane and a proton gradient generated by proton-pumping protein complexes of the electron transport chain. This proton gradient is

maintained by the integrity of the inner membrane and is utilised to synthesise ATP, but also for the transport of metabolites, ions and proteins across the inner membrane.

TMRE (tetramethylrhodamine ethyl ester) is a potentiometric fluorescent probe that is taken up by cells and mitochondria, dependent on their membrane potential. It is a rhodamine derivative and can be described as a lipophilic cationic, or redistribution probe that is membrane permeable (Ehrenberg *et al.*, 1988). The uptake of this class of fluorescent dye into the mitochondrial matrix happens relatively fast (the half time of equilibrium distribution at 100nM TMRE is six minutes at 22C for animal cells (Farkas *et al.*, 1989)) and is dependent on the positive charge and lipophilic nature of the molecules (Scaduto & Grotyohann, 1999). Rhodamine derivatives are characterised by low toxicity to cells, low self-aggregation and low membrane binding (Ehrenberg *et al.*, 1988; Farkas *et al.*, 1989). Estimates for the mitochondrial membrane potential of animal cells such as fibroblasts by using rhodamine derivatives range from -105 to -150 mV, compared with a plasma membrane potential of approximately -50 mV (Farkas *et al.*, 1989).

Rhodamine derivatives can serve as qualitative indicators of the mitochondrial membrane potential of individual cells. Their uptake by cells and mitochondria is largely governed by the Nernst equation that allows for quantitative estimates of the mitochondrial membrane potential. Upon uptake of these dyes by cells, they distribute at equilibrium between the extracellular space, the cytoplasm and organelles such as mitochondria (Farkas *et al.*, 1989). The final concentration of TMRE inside mitochondria is dependent on both the plasma membrane and the mitochondrial membrane potentials. Dissipation of the mitochondrial membrane potential by ionophores such as dinitrophenol (DNP) results in a sharp decrease of TMRE fluorescence that leaks into the cytosol (Johnson *et al.*, 1981). Thus, differences in mitochondria-associated fluorescence reflects changes in the functional state of the organelles and the magnitude of the mitochondrial membrane potential (Johnson *et al.*, 1981).

TMRE was utilised here to check for any differences in fluorescence between *slp1* mutants and wild type plants. *Slp1* and wild type seedlings were grown for five days in hydroponic culture. They were incubated with 50 nM TMRE for a few minutes, rinsed and mounted on microscope slides for imaging on the confocal microscope. Only roots were imaged because of high background fluorescence observed in green tissue. Whole roots were scanned completely across the entire root diameter, and three-dimensional images were reconstructed. Figure 5-17 shows an example of the observed fluorescence pattern of *slp1-1*, *slp1-2* and wild type roots. Scanned *slp1-1* roots frequently had visibly weaker TMRE

fluorescence than wild type roots or *slp1-2* roots as seen in the image on the left side. This was observed across three independent experiments. TMRE-stained mitochondria were clearly visible as bright punctate structures in *slp1-2* and wild type roots. In *slp1-1* roots, individual mitochondria were barely visible besides the cytosolic and other background fluorescence.

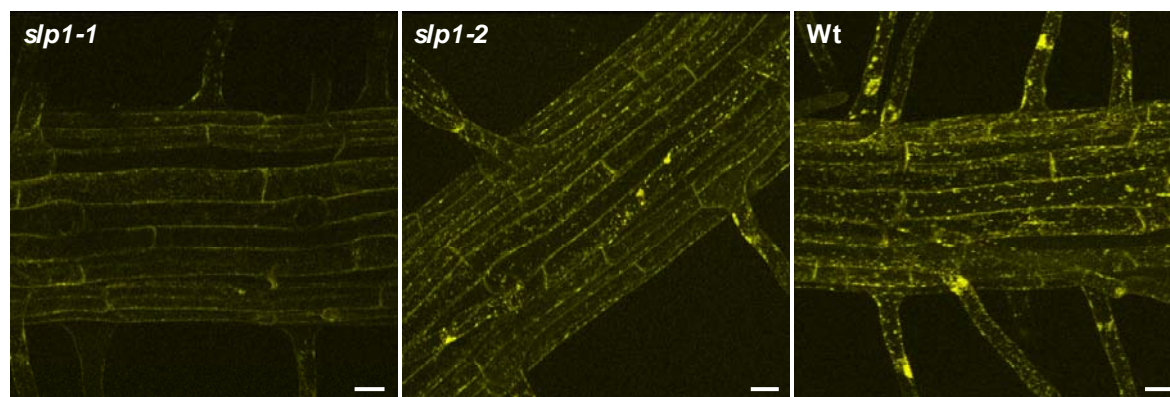


Figure 5-17. TMRE fluorescence in *slp1-1* and wild type (Wt) roots. The images show three-dimensional reconstructions of confocal scans through the entire root in a particular area. The confocal settings were identical in all three images. Scale bar = 20 μ m.

The overall TMRE fluorescence of each image was quantified and the result is presented in Figure 5-18. Part (A) shows a quantification from a single experiment in which three to four independent seedling roots were imaged at three different places along the length of the roots. The quantification shows that TMRE fluorescence intensity in *slp1-1* mutant roots is significantly decreased compared to *slp1-2* and wild type TMRE fluorescence. Part (B) shows a graph with data combined from two independent datasets, averaging a total of six seedlings from each genotype. TMRE fluorescence is still significantly reduced by approximately 20% in *slp1-1* roots compared to *slp1-2*, but the reduction was not significant compared to wild type roots.

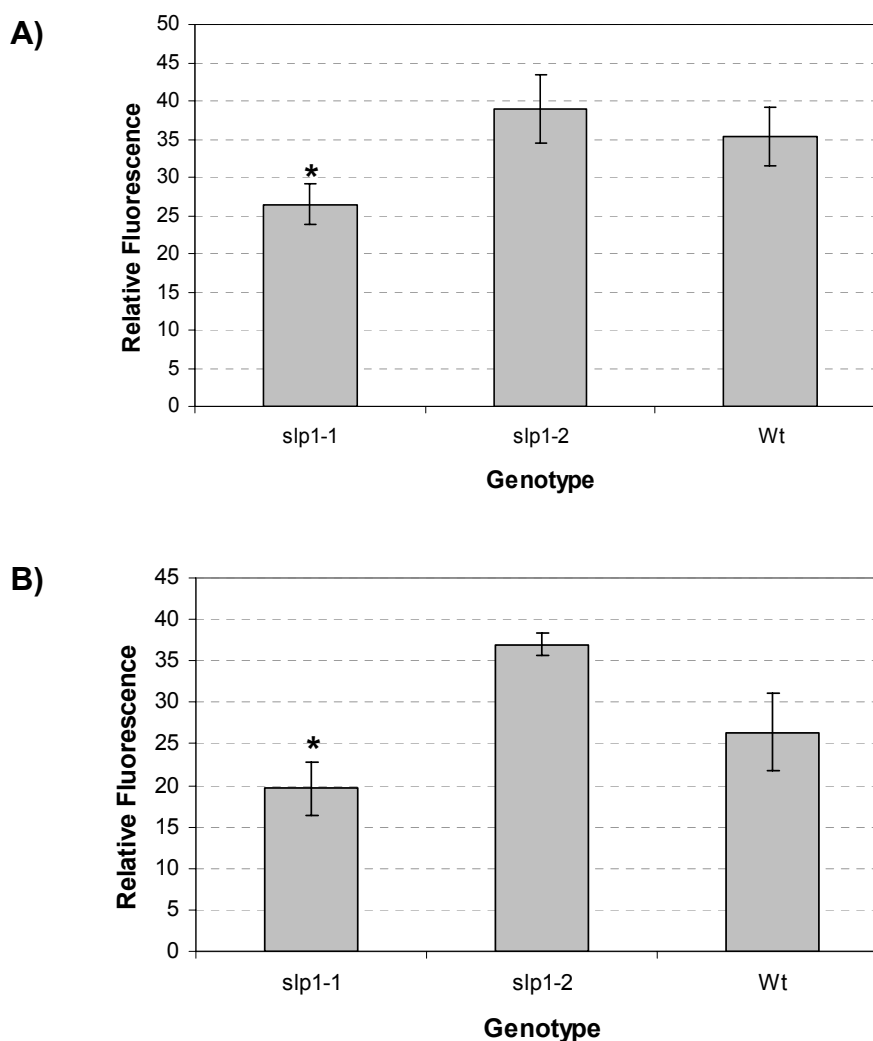


Figure 5-18. Quantification of TMRE fluorescence from three-dimensional reconstructed images obtained from *slp1* mutant roots and wild type plants. Background fluorescence was subtracted from each image.

A) A dataset obtained from a single experiment shows significantly decreased fluorescence in *slp1-1* roots compared to both *slp1-2* and wild type roots (paired t-test, $n=12$, $p<0.05$).

B) A dataset showing the average of two independent experiments each consisting of at least three separate seedlings. The reduction in TMRE fluorescence in *slp1-1* roots is still significant (paired t-test, $p<0.05$) compared to *slp1-2* roots, but not to wild type.

Quantification of TMRE fluorescence as presented here can only give a very crude qualitative estimate of the mitochondrial membrane potential, and thus the functional state of mitochondria. Despite the fact that the reduction in TMRE fluorescence in *slp1-1* plants was not statistically significant to wild type plants when two datasets were averaged, the trend indicating reduced mitochondrial membrane potential was still visible. Overall the

TMRE staining of whole seedlings was repeated three times for *slp1-1*, and four times for *slp1-2*. Because of different confocal settings and TMRE concentrations used initially, quantitative comparisons with other datasets was not possible. However, the trend of reduced TMRE fluorescence in *slp1-1* seedlings was reproducible throughout.

5.3.2 Oxygen consumption rates

Mitochondria have several important metabolic roles in plant cells that make them crucial for aerobic energy production, photosynthesis, anabolic (e.g. the provision of carbon skeletons for nitrogen assimilation) and catabolic (fatty acid oxidation) reactions. During the photoperiod, mitochondrial ATP production provides energy for sucrose synthesis in the cytosol, but mitochondria also participate in photorespiration and antioxidant metabolism to minimise the formation of reactive oxygen species (ROS) and to sustain optimal photosynthesis rates (Ferne *et al.*, 2004). During the dark period and in heterotrophic tissues such as roots, mitochondria provide the main energy source in the form of ATP produced by oxidative phosphorylation in the electron transport chain (ETC) of the inner membrane.

The whole process of aerobic respiration actually consists of three interdependent processes: cytosolic glycolysis, the TCA (tricarboxylic acid) cycle and oxidative phosphorylation inside mitochondria. Glucose is oxidised to pyruvate during glycolysis that is then transported into mitochondria. During the reactions catalysed by pyruvate dehydrogenase and the TCA cycle, reducing equivalents such as NADH and FADH₂ are produced whose electrons feed into the mitochondrial ETC under simultaneous substrate oxidation to provide energy in the form of ATP (Ferne *et al.*, 2004).

The plant mitochondrial ETC differs from the ETC of animals and fungi in the context of enzyme composition. In contrast to animals, plant mitochondria contain five additional enzyme complexes. Two additional NAD(P)H dehydrogenases localised in the outer leaflet of the inner membrane (= NDex), two additional NAD(P)H dehydrogenases in the inner leaflet (= NDin), and the alternative oxidase (= AOX) facing the matrix side. Figure 5-19 gives an overview over the composition and organisation of the plant mitochondrial ETC. All plant-specific enzymes are shown in blue, whereas proteins in common with animal mitochondria are shown in grey. As in animals, the plant ETC also contains complex I (NADH dehydrogenase/NADH-Q-reductase), complex II (succinate dehydrogenase/succinate-Q-reductase), complex III (ubiquinol-cytochrome bc1 reductase) and complex IV (cytochrome-c oxidase), as well as the inner membrane ATP synthase (sometimes

referred to as complex V). Protons are pumped from the matrix side into the intermembrane space by complexes I, III and IV to generate a gradient across the inner membrane. This gradient generates an electrical potential (see above) that is utilised for transport processes. The energy stored in this proton gradient is also used to synthesise ATP on the matrix side by the ATP synthase (= phosphorylating respiratory pathway). The plant specific enzymes NDex, NDin and AOX, as well as complex II do not contribute to the build-up of the proton gradient and are thus non-phosphorylating (alternative respiratory pathway) (Affourtit *et al.*, 2001). This plant-specific architecture of the ETC provides additional means by which electrons can flow and oxygen is consumed (by AOX), without the simultaneous translocation of protons. As such, they allow respiration to continue even in the presence of a high membrane potential and are thus thought to ensure continuous electron flow when the ETC is overreduced. AOX lies in competition with complex III for the flow of electrons from the reduced ubiquinone pool. However, its contribution under non-stress conditions to overall oxygen consumption rates is low. It is active when the Q-pool is overreduced and the membrane potential high (Borecky & Vercesi, 2005). Additionally to this alternative respiratory pathway that lowers the membrane potential and ensures adequate electron flow, plants and animals also possess uncoupling proteins (UCPs) that act as protonophores in the inner membrane upon specific signals. These proteins dissipate the proton gradient by causing a controlled leak in the inner membrane that is used to generate heat in small mammals (Nicholls, 1979). The ubiquitously expressed Arabidopsis UCP AtUCP1 was demonstrated to be important to ensure continuous photorespiration rates under light conditions in leaves (Sweetlove *et al.*, 2006).

An unavoidable byproduct of this aerobic metabolism is the formation of reactive oxygen species by the mitochondrial ETC in the form of superoxide anions (O_2^-). Superoxide is formed when the electron flow is inadequate and the build-up of membrane potential high. The majority of superoxide is formed at complexes I and III, when oxygen interacts with NADH and ubiquinone (Moller, 2001). The effects and impact of ROS formation on metabolism are discussed in the following section 5.3.3.

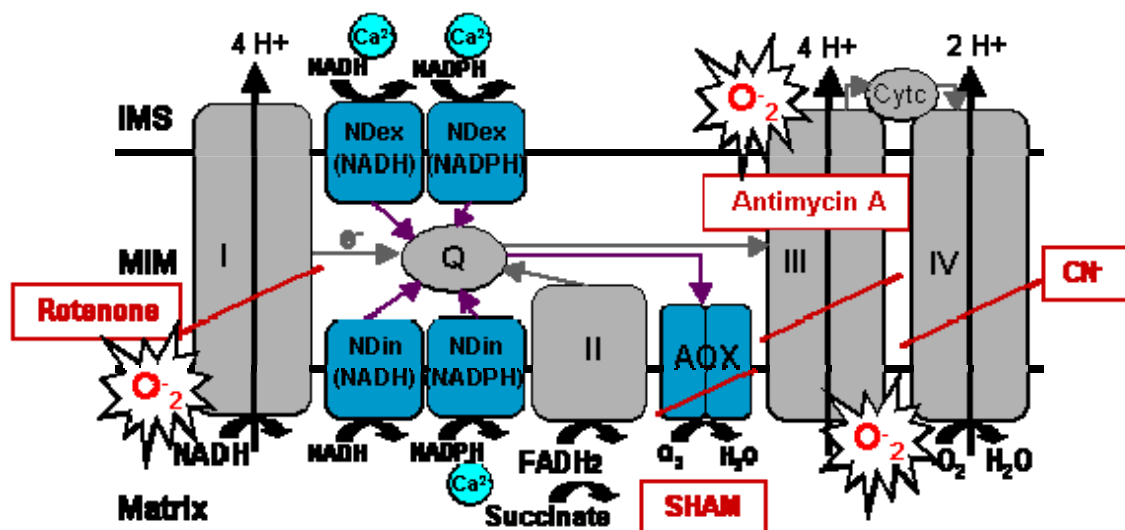


Figure 5-19. Schematic presentation of mitochondrial electron transport chain (ETC). Plant-specific enzymes are shown in blue. Protons are pumped by complexes I, III and IV as indicated. The inner membrane ATP synthase is not included. The normal electron flow is indicated by grey arrows. Dissipation of the proton gradient either happens via ATP synthesis and cytochrome oxidation, or via alternative routes involving either NDex, NDin, and/or the alternative oxidase (AOX). Additionally, the uncoupling proteins (UCPs) can contribute to this task (not included here). Complexes I-VI are numbered as indicated and shown in grey. Complex I (NADH dehydrogenase/NADH-Q-reductase), Complex II (succinate dehydrogenase/succinate-Q-reductase), complex III (ubiquinol-cytochrome bc1 reductase), complex IV (cytochrome c oxidase). The alternative electron flow routes are shown by purple arrows. Chemical inhibitors of the various reactions are shown in red. The formation of ROS as superoxide anions at complexes I and III is indicated by the star shapes. The Ca^{2+} dependence of the plant-specific NAD(P)H dehydrogenases is indicated. Abbreviations are MIM (mitochondrial inner membrane), IMS (intermembrane space), NDex (external NAD(P)H dehydrogenases), NDin (internal NAD(P)H dehydrogenases), Q (ubiquinone), CytC (cytochrome C), SHAM (salicyl hydroxamic acid), AOX (alternative oxidase). This figure is redrawn after a scheme by IM Møller (Møller, 2001).

The oxygen consumption rates of isolated plant and animal mitochondria can be measured with an oxygen electrode by stimulation of respiration with externally added substrates. Commonly, isolated mitochondria can be stimulated with TCA cycle intermediates (organic acids) such as pyruvate, malate or succinate. In contrast to animal mitochondria, isolated plant mitochondria are also capable of oxidising externally added NADH by the rotenone-insensitive NDex enzyme complex. Organic acids and other molecules can pass the outer mitochondrial membrane through pores formed by beta-barrel type proteins called porins. These allow access for small molecules to the intermembrane space up to a molecular weight of 10 kDa (Zalman *et al.*, 1980), (Moore & Proudlove, 1983). Gases such as oxygen and CO_2 can pass freely through the inner membrane, whereas it is impermeable for larger molecules as well as ions. Substrates such as TCA-cycle intermediates and pyruvate are transported into the mitochondrial matrix via dicarboxylate carriers in exchange for inorganic phosphate (P_i). Additionally, a tricarboxylate transporter takes up citrate via exchange for a dicarboxylic acid such as malate, and pyruvate enters

via the pyruvate transporter. NAD(P)H is shuttled indirectly via electron transfer by the malate/oxaloacetate shuttle system which is not functional in isolated organelles. ADP is transported into mitochondria in exchange for ATP by a translocase, and P_i can enter the matrix through a proton/ P_i symporter (Douce, 1985). As mentioned above, succinate oxidation at complex II is not coupled to the translocation of protons and thus does not contribute to the formation of the proton gradient. Theoretically, plant mitochondria are capable of oxidising succinate and NAD(P)H through the AOX and thereby circumventing the build-up of the proton gradient.

Because of the proposed submitochondrial localisation of AtSlps to the inner membrane, the effect of the *slp1-1* T-DNA insertion on mitochondrial oxygen consumption rates was investigated.

A commonly used type of oxygen electrode is the Clark-type. It consists of a working electrode made of platinum (= cathode) and an Ag/AgCl reference electrode (= anode). The two poles are connected by an electrolyte solution. An oxygen-permeable Teflon membrane is placed over the electrodes and the electrolyte solution. Located above the membrane is a chamber filled with assay medium and isolated mitochondria. A voltage is applied on the Pt electrode that causes reduction of dissolved oxygen and the flow of 4 electrons/reduced O_2 molecule. The resulting current is directly proportional to the partial oxygen pressure in the surrounding assay medium. Oxygen consumption by mitochondria is followed with a chart recorder whose full deflection represents the total oxygen content of the assay medium. In the presence of excess phosphate and endogenous or externally added ADP, oxidative phosphorylation takes place inside isolated mitochondria, and the loss of molecular oxygen from the medium is followed over time. Various substrates can be added via injection with a Hamilton syringe while the mitochondria solution is stirred.

To measure oxygen consumption of isolated *slp1-1* and wild type mitochondria, crude organelle pellets containing mitochondria were prepared by differential centrifugation. These resuspensions contained primarily also chloroplasts and peroxisomes and were green in colour. To avoid interference by oxygen evolution from chloroplasts, the measurements were taken in the darkness by covering up the electrode chamber. For each round of measurement, 200 μ L of the mitochondrial resuspension (containing approximately 1 mg total protein) were added to the chamber and the oxygen consumption of one substrate at a time was measured. Table 5-3 contains all substrates and their concentrations used in these experiments. Oxygen consumption rates were calculated based on changes followed by the chart recorder in nmoles O_2 consumed/minute/mg of protein present. The injection

protocol was always such that one substrate was injected, followed by the addition of ADP. This was repeated if no good respiration rates could be measured. Following ADP, SHAM was added to block AOX, followed by DNP (2,4-dinitrophenol), an ionophoric uncoupling agent, and finally NaCN to block oxygen consumption by complex IV. In some cases, oligomycin was added afterwards to block proton-translocation (and therefore dissipation of the proton gradient) by the ATP synthase.

Substrate/Inhibitor	Concentration [mM]
Succinate	10
NADH	1
Malate/pyruvate	10
ADP	0.1
SHAM	0.1
DNP	1 μ M
Oligomycin	1 μ g/ml
NaCN	1

Table 5-3. Respiration substrates and inhibitors used in oxygen consumption measurements. The final concentration in the assay medium is given in mM unless otherwise stated.

Altogether five separate measurements with *slp1-1* and wild type mitochondria were carried out. The measured oxygen consumption rates varied greatly between those individual measurements for all substrates tested. Three measurements for each genotype were averaged and the results are presented in Figure 5-20. Consistently it was found that NADH gave the highest oxidation rates (20-50 nmoles/min/mg protein), followed by succinate (20-40 nmoles/min/mg). Oxidation of malate and pyruvate at the given concentrations was very slow (<10 nmoles/min/mg) and in some cases almost impossible to quantify accurately. However, between those measurements it was noticed that mitochondria from *slp1-1* consistently oxidised succinate and NADH at higher rates than wild type mitochondria. Despite the large standard error values in Figure 5-20, this trend can be seen between *slp1-1* and wild type oxygen consumption.

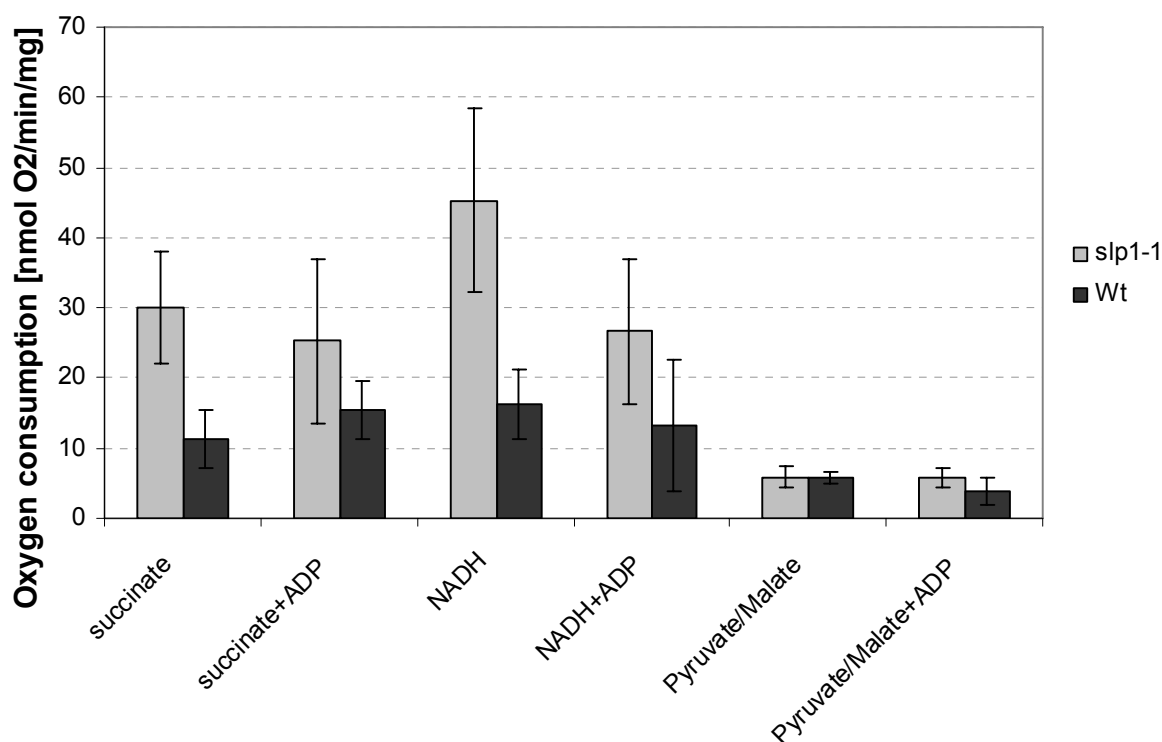


Figure 5-20. Oxygen consumption rates of *slp1-1* and wild type isolated mitochondrial pellets. Three independent measurements were averaged. Only the oxidation of the initially added substrate, and the change in oxygen consumption after addition of ADP (= state 3 respiration) are shown.

These calculated oxygen consumption values were well below what can be found elsewhere in the literature for *Arabidopsis* mitochondria. Sweetlove *et al.* (Sweetlove *et al.*, 2002) reported oxygen consumption values of approximately 160 nmoles/min/mg for succinate and NADH, and 60 for malate/pyruvate without added ADP. However, the measured mitochondria were isolated from an actively dividing suspension cell culture. In the experiments presented here, mitochondria were isolated from fully expanded leaf tissue grown under short day light. The cells from which the mitochondria originated here were clearly not dividing any more and thus metabolically less active. Additionally, because the mitochondrial preparation used here was very impure, the actual content of mitochondria-derived protein was much lower than quantified from the Amidoblack assay. Therefore, the normalisation of respiration values to the protein content is inaccurate in terms of absolute values. It is most likely an underestimate of the real oxygen consumption contributed by actual mitochondria. Additionally, these lower values could indicate that mitochondria were damaged or not fully active any more.

Curiously, additions of ADP to substrate-oxidising mitochondria hardly resulted in the expected stimulation of oxygen consumption. The addition of ADP was expected to

increase oxygen consumption and electron flow because of the dissipation of the proton gradient by the ATP synthase. However, this increase can only happen if the mitochondria are tightly coupled, i.e. if the inner and the outer membrane are both intact. Figure 5-21 presents quantifications of the relative changes in oxygen consumption of a particular substrate upon addition of ADP, DNP or sodium cyanide (NaCN). When wild type mitochondria were oxidising succinate, ADP addition increased oxygen consumption moderately, but significantly from the basal rate (on average by 50%). This is also known as state 3 respiration. Once all ADP has been consumed, the respiration rate is expected to slow down again, which would correspond to state 4 respiration. The ratio of these two states can be used to estimate the intactness (i.e. coupling efficiency) and thus quality of the mitochondria used (Chance & Williams, 1955). Compared to the wild type, *slp1-1* mitochondria did not show any increased oxygen consumption upon ADP addition, the respiration rate even decreased slightly. The uncoupling agent DNP was added after SHAM that blocks oxygen consumption by the AOX. SHAM was supplied as a 300x concentrated stock solution dissolved in ethanol. The final concentration in the chamber was 100 μ M with an ethanol concentration of 0.6 %. Because of this rather high ethanol content, a sharp increase in oxygen consumption was observed (not shown), that probably arose from damaged mitochondria by organic solvent. Most likely, the added ethanol dissolved at least the outer membrane and therefore dissipated the proton gradient. In this scenario, oxygen consumption resumes uncontrolled from the demand of the ATP synthase and therefore increases. It is also possible that the ethanol present in the medium even damaged the inner membrane or inactivated the respiration enzymes. Therefore, what was observed upon subsequent addition of DNP probably did not reflect actual uncoupling effects by this ionophore. During succinate oxidation, DNP addition after SHAM decreased respiration of wild type mitochondria, but had hardly any effect on *slp1-1* mitochondria in state 3 respiration. Following DNP, NaCN was added to stop oxygen consumption by complex IV. This resulted in an almost complete halt of respiration, indicating that oxygen was previously still taken up by what were probably at least partly damaged mitochondria.

Compared to succinate oxidation, NADH-driven oxygen consumption was clearly decreased by ADP addition in *slp1-1* mitochondria, and also slightly in wild type mitochondria. This observation was partly unexpected. Under non-stress situations, ADP addition to NADH-oxidising mitochondria would be expected to stimulate oxygen consumption rates. However, externally added NADH can only be oxidised by the NDex complex in isolated, intact plant mitochondria. This oxidation is not directly coupled to the

generation of the proton gradient. Protons can only be pumped and ATP generated if the electrons from NADH oxidation are further passed to ubiquinol, and from there to complexes III and IV. If AOX diverts this flow however, oxygen is consumed without proton pumping and is therefore uncoupled from ATP generation. The observation made here would either indicate that AOX diverted the electron flow, or that the isolated mitochondria were partly damaged as described above. DNP addition following SHAM injection did not change respiration rates significantly, and NaCN almost completely abolished them. In mitochondria oxidising malate/pyruvate, ADP addition did not cause a significant change, whereas DNP following SHAM this time actually caused an increase in respiration rates in both mutant and wild type mitochondria. The addition of cyanide ions afterwards almost completely abolished this respiration.

These data can be interpreted in different ways. Generally there was a clear trend towards overall higher respiration rates from *slp1-1* mitochondria compared to the wild type. Even if the calculated values were not correct in terms of absolute oxygen consumption by actual mitochondria, the relative difference in respiration rate compared to wild type would nevertheless remain. The relative responses after ADP stimulation observed with *slp1-1* mitochondria were more stable than those from wild type (note the smaller standard errors in the relative responses in Figure 5-21). Combined with the observed lower membrane potential and the lack of state 3 respiration, these results could indicate that the integrity of the inner membrane of *slp1-1* mitochondria was impaired. This would give rise to partly uncoupled mitochondria. It is assumed that Slp1 participates in higher molecular weight protein complexes (see chapter 4) and also provides microdomains or platforms for the regulation of such complexes in the inner membrane. Thus, a lack of Slp1 could lead to a leakiness of this membrane that also embeds the proteins of the ETC.

Alternatively to this explanation, the decrease in membrane potential of *slp1-1* mitochondria could also point towards an upregulation of the alternative respiratory pathway involving AOX. This could be the result of an upregulation or activation on the protein level of the alternative components (including NDex, NDin and AOX), or an inhibition of the ordinary respiratory complexes. Additionally, lack of Slp1 could influence the activity of the UCPs that would in turn lead to a partly dissipated proton gradient.

These respiratory measurements were all conducted with independently isolated mitochondria from the same batch of plants. A second round of experiments to confirm these results is still in preparation. These experiments will also include measurements with the *slp1-2* allele.

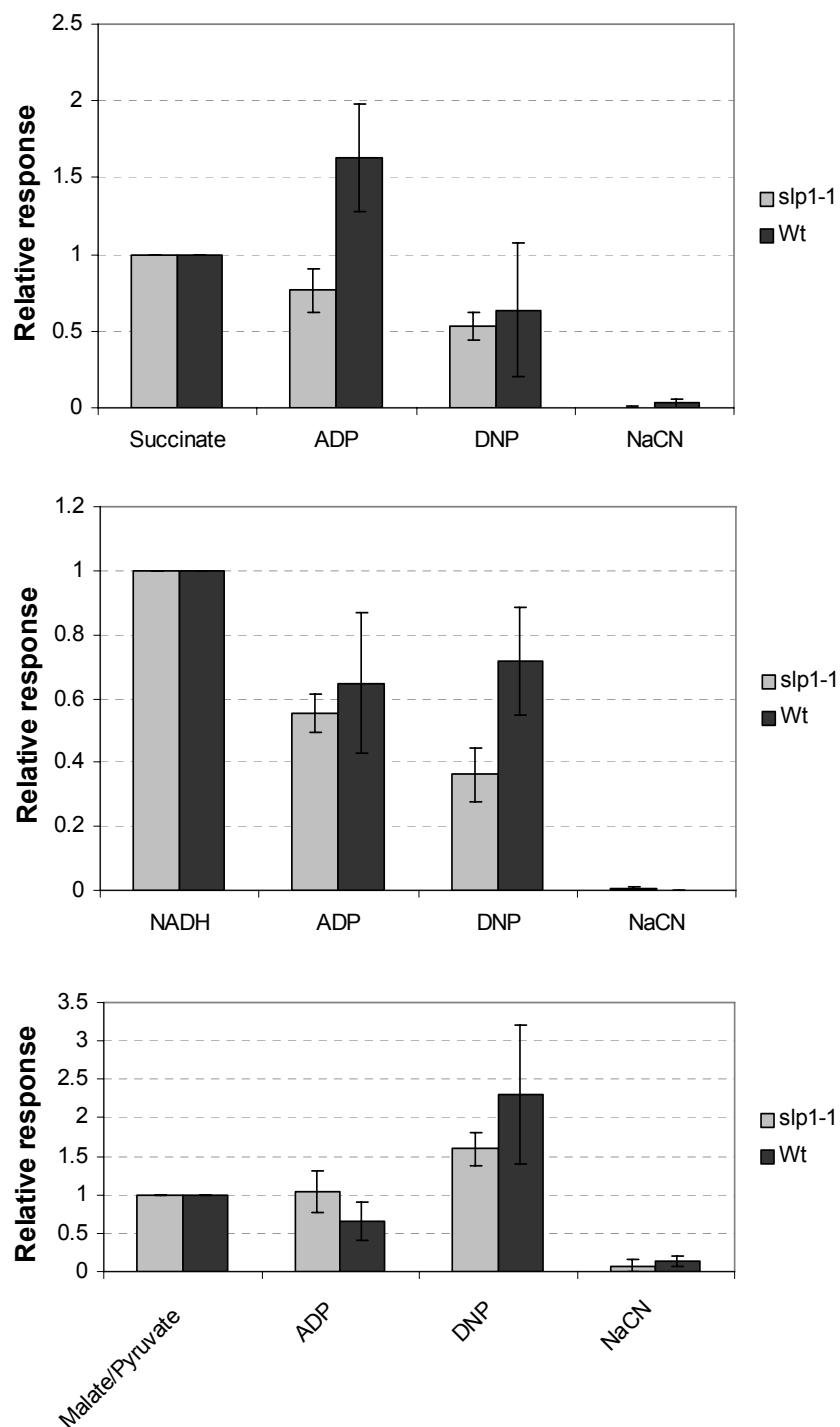


Figure 5-21. Relative responses of oxygen consumption rates upon addition of ADP, DNP and CN^- ($n=3$). All values were normalised to the oxygen consumption rates of the initially added substrate. ADP addition was expected to stimulate oxygen uptake if the mitochondria are tightly coupled because of dissipation of the proton gradient. DNP acts as an uncoupling agent that was expected to increase respiration rates. The addition of NaCN almost completely blocked respiration through complex IV. It should be noted that DNP was added after the addition of SHAM dissolved in ethanol which probably caused damage to the outer, and even the inner membrane.

5.3.3 Reactive oxygen species

An unavoidable consequence of aerobic metabolism is the formation of reactive oxygen species (ROS) and reactive nitrogen species (RNS). ROS generally increase locally under stress conditions and can cause damage, but they can also serve as signalling molecules. In plants, the major ROS production sites are chloroplasts and peroxisomes during the photoperiod, and mitochondria during darkness and in heterotrophic tissues such as roots (Moller *et al.*, 2007; Dutilleul *et al.*, 2003). Additionally, ROS are formed by the plasma membrane bound external NADPH oxidase during pathogen attack and in N₂-fixing root nodules (Moller, 2001). In chloroplasts, the major production sites are the two photosystems in the electron transport chain. Chloroplastic ROS include singlet oxygen (¹O₂) produced at photosystem II (PSII) and superoxide (O₂⁻) at photosystem I (PSI). Peroxisomes produce ROS during photorespiration, mainly in the form of superoxide and H₂O₂. The plasma membrane NADPH oxidase, as well as the mitochondrial ETC mainly cause superoxide accumulation. In the mitochondrial ETC, superoxide is produced by the transfer of a single electron to molecular oxygen at complexes I and III (see Figure 5-19) (Moller, 2001). The effects of ROS accumulation depend on the production sites and the nature of the ROS produced. For example, H₂O₂ is relatively stable and able to cross membranes through aquaporins. Thus, it can cause damage at a different location from its production site. By contrast, singlet oxygen and superoxide are only able to travel very short distances (nm to μm) and are chemically more reactive. Superoxide can be converted by superoxide dismutase (SOD) to hydrogen peroxide, which in turn can react with free transition metal ions to the extremely reactive hydroxyl radical (OH[•]) in the Fenton reaction. Superoxide anions can also react with the Fe-S clusters of proteins and damage these. Hydroxyl radicals react with all classes of biomolecules, causing widespread irreversible damage. Generally, all ROS formed are capable of oxidising surrounding biomolecules such as proteins, lipids, carbohydrates and DNA. Lipid oxidation by singlet oxygen occurs particularly on conjugated double bonds of polyunsaturated fatty acids. Singlet oxygen can also oxidise certain amino acids in proteins such as tryptophan, histidine, tyrosine, methionine and cysteine. Sulfur-containing amino acids can generally be oxidised or nitrosylated by all ROS and RNS in a reversible manner, an event that can be important for cellular signalling. DNA molecules can be oxidised at the bases of nucleotides, in particular guanine bases, causing mutations and genetic damage.

The nitric oxide radical (NO^\cdot) is formed by nitrate reductase and at the mitochondrial electron transport chain (Moller *et al.*, 2007). It can react with superoxide to the more reactive peroxynitrite (ONOO^-), which can damage DNA and amino acids irreversibly.

All cells have endogenous antioxidant systems to scavenge ROS and limit damage. These are localised near the ROS production sites inside organelles (mitochondria, chloroplasts, peroxisomes), but also in the cytosol. Examples include non-enzymatic systems such as ascorbate/glutathione, and carotenoids in chloroplasts, but also enzymatic detoxifying systems including SODs, catalase and peroxidases (Duttilleul *et al.*, 2003). In mitochondria, MnSOD is the active enzymatic mechanism for the detoxification of superoxide. Additionally, ascorbate peroxidase, thioredoxin-dependent reductase, glutaredoxin and PRXII F provide other important detoxifying enzymatic mechanisms (Finkemeier *et al.*, 2005). Additional antioxidant properties are also provided by the reversible oxidation of free thiol groups and methionine in proteins ((Moller *et al.*, 2007). Relief of electron overload of the mitochondrial ETC is mediated by the activation of AOX, the plant-specific NAD(P)H dehydrogenases, and by the action of UCPs (see above).

If these ROS limiting systems are overwhelmed under stress, excessive amounts of ROS can accumulate and damage molecules as described. The effects of excessive ROS-induced damage in mitochondria include swelling of the matrix, a decrease in membrane potential, formation of the mitochondrial transition pore (MTP- holes in the inner membrane) and eventually rupture of the organelle (Logan, 2008b). Damaged organelles and protein aggregates can subsequently be removed by autophagy for degradation and recycling, and they can be replaced by subsequent mitochondrial fission if necessary. If cells are overwhelmed by oxidative damage, a type of programmed cell death takes place that resemble events during the HR response.

With the background of the observed effects of *slp1-1* on mitochondrial respiration, the formation and accumulation of ROS was investigated in *slp1* mutants and wild type seedlings. ROS can be detected by several approaches. Commonly, the H_2O_2 -triggered polymerisation of diaminobenzidine (DAB) in the presence of peroxidase is used as a ROS indicator *in vivo* and *in situ* (ThordalChristensen *et al.*, 1997). The amount of H_2O_2 is the limiting factor for the polymerisation of DAB, given that peroxidase is present. High light also stimulates DAB polymerisation because of excessive photosynthesis-driven H_2O_2 formation. In addition to DAB staining, several dyes (fluorescein derivatives) become fluorescent upon uptake by living cells and reaction with ROS (see below).

Leaves from fully-grown *slp1-1*, *slp1-3* (Figure 5-22 (A)) and *slp1-2* and wild type plants (Figure 5-22 (B)) were excised and their petioles dipped into DAB solution over several hours in dim light. Chlorophyll was subsequently cleared from leaves with ethanol to fully visualise polymerised DAB. DAB was taken up through the transpiration stream and mainly accumulated in and around vascular tissue as seen in Figure 5-22. This happened regardless of the genotype, because H_2O_2 is involved in the lignification of vascular tissue. Additionally, the cut sites on the petioles always become heavily stained because of H_2O_2 evolution during the wounding response. Around the veins, DAB polymer was mainly spread evenly throughout the tissue. In some leaves, intense DAB-stained spots were visible (as seen in top panel of Figure 5-22 (A)). However, no principal differences in DAB intensity or distribution could be clearly recognised between mutant and wild type leaves. This approach of ROS detection is rather crude and might not pick up ROS differences in unstressed plants. The dynamic range for detection of H_2O_2 by DAB staining lies between 1-10 μM H_2O_2 . Smaller amounts of H_2O_2 -related ROS are not detected by this method. In this respect, an obvious lack of differences between wild type and *slp1* mutants might not be surprising (ThordalChristensen *et al.*, 1997; Torres *et al.*, 2002; Dutilleul *et al.*, 2003).

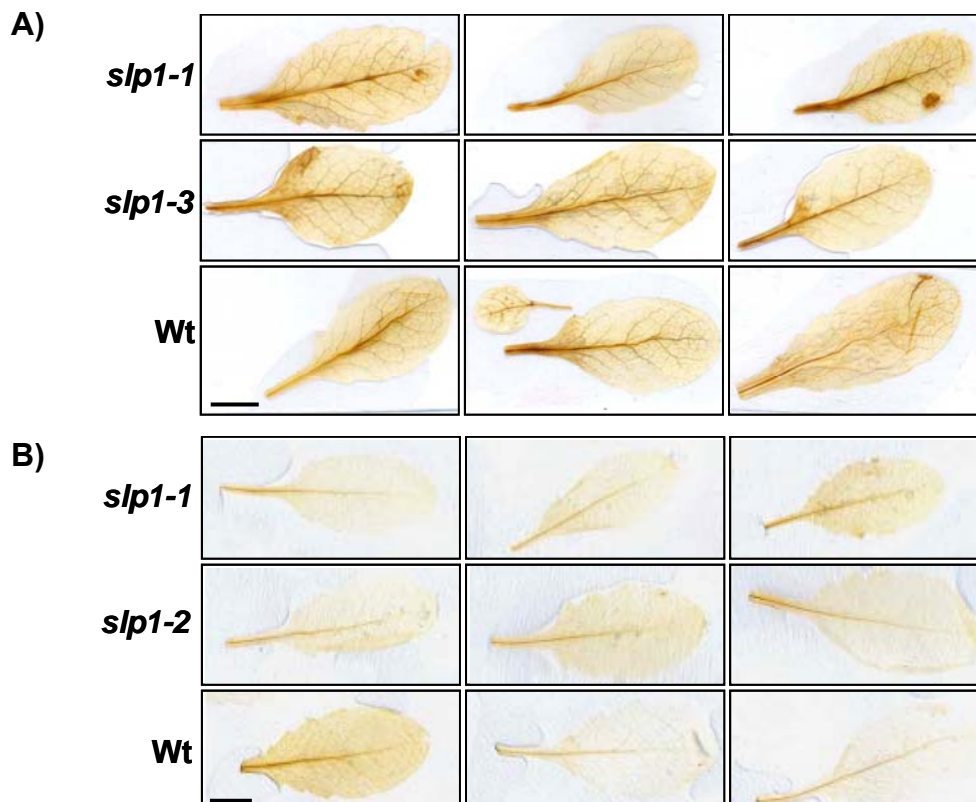


Figure 5-22. DAB-stained leaves from *slp1-1*, *slp1-3*, *slp1-2* and wild type plants. A) Leaves from a first batch of plants grown under long day light conditions stained with DAB. B) Leaves stained with DAB including *slp1-2* from an independent plant batch grown under the same conditions. Scale bars = 1cm.

ROS accumulation was also quantified from seedlings incubated with 2',7'-dichlorodihydrofluorescein diacetate (H₂DCFDA). This dye is non-fluorescent until it is taken up by cells and two acetate groups are removed by intracellular esterases. The resulting charged form of the dye is thus sequestered within the cells, by contrast with the original dye molecule. Following oxidation inside cells, the dye also becomes highly fluorescent and can be excited at 492 nm (Molecular Probes, "Reactive Oxygen Species (ROS) Detection Reagents"). This ROS probe has been previously used to detect and quantify ROS from plant cells (Desikan *et al.*, 2006; Ahn *et al.*, 2006). As with TMRE staining, FDA fluorescence was imaged from roots of *slp1-1*, *slp1-2* and wild type seedlings by reconstructing three-dimensional confocal scans and quantifying the relative fluorescence amounts. Seedlings were always incubated for identical periods before imaging on the confocal microscope to avoid accumulative effects of dye uptake. Only roots were imaged, because chloroplasts of shoot tissue gave excessive FDA fluorescence that was difficult to localise and to quantify. Figure 5-23 shows confocal images of three-dimensional reconstructions from FDA-stained roots. The fluorescence of each reconstructed stack was quantified and the result is presented in Figure 5-24. Three separate seedlings per genotype were imaged, and three to four areas per root were chosen for scanning. On average, mutant roots had 30-40 % reduced FDA fluorescence compared to wild type roots. This result was significantly different from the average wild type fluorescence and indicates decreased ROS accumulation in roots of *slp1* mutant plants. Currently, this finding can only be interpreted as a trend rather than a final result because the experiment was so far not independently confirmed at least a second time.

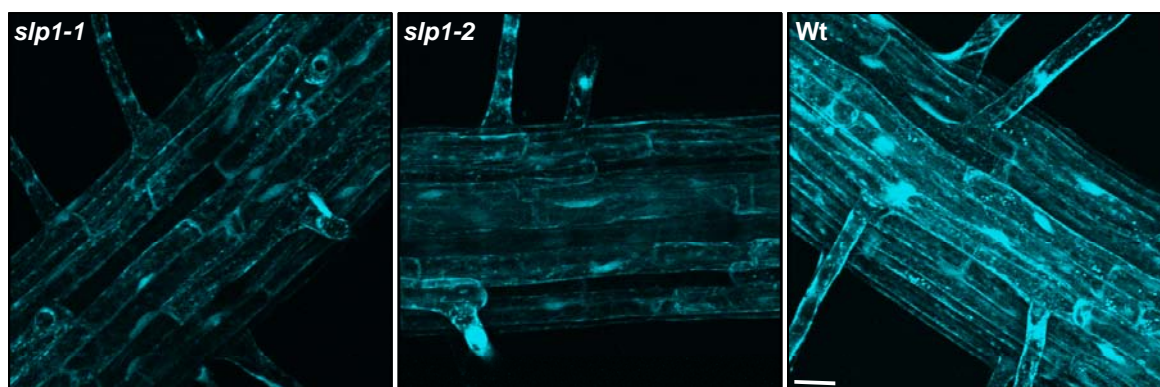


Figure 5-23. Three-dimensional reconstructions of confocal images of H₂DCFDA-stained seedling roots. Whole seedlings from *slp1-1*, *slp1-2* and wild type plants (5 days old) were stained with 2 μ M H₂DCFDA. Roots were scanned completely horizontally through the plane and images reconstructed. Scale bar = 20 μ m.

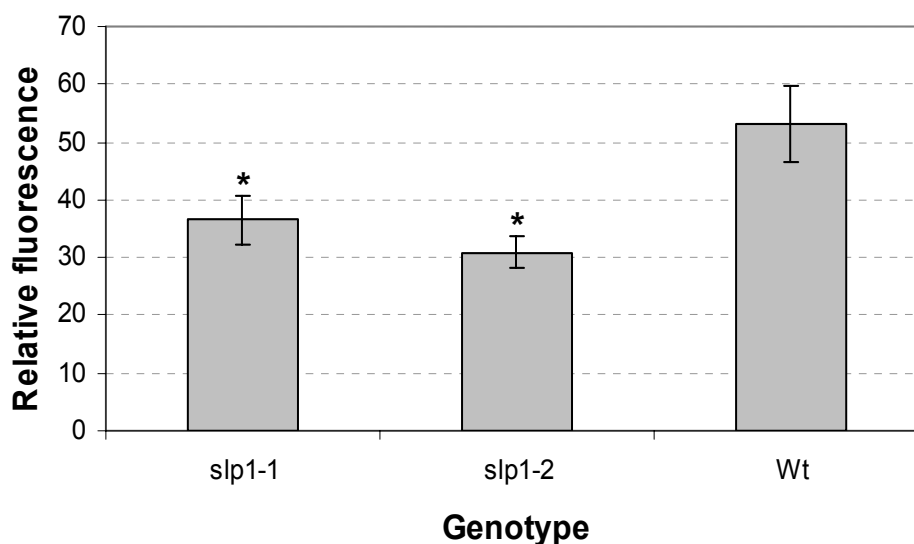


Figure 5-24. Quantified H₂DCFDA fluorescence. The relative fluorescence was quantified from at least three separate seedlings per genotype. In each seedling, three to four areas were scanned and quantified (n=13 (*slp1-1*), n=12 (wild type), n=9 (*slp1-2*)). Significant differences to the wild type value are indicated by asterisks. Error bars indicate standard error values.

According to these findings, no difference in ROS production and accumulation exist in mature leaves when DAB was utilised as a ROS probe. By contrast, *slp1* mutants seem to accumulate or produce less ROS in roots of five-day old seedlings when ROS were quantified by FDA fluorescence. This could indicate that Slp1 might have different functions in roots than in shoots. Alternatively, this difference could also simply reflect the difference in age and metabolic activity of the investigated tissues and plants. Mature, fully-grown leaves are metabolically differently active than roots of young seedlings. Leaf tissue is primarily occupied with photosynthesis and photorespiration, whereas root tissue of young seedlings is still actively growing and heterotrophic in nature. Mitochondrial ROS production is only secondary in terms of overall oxidative load in leaf cells during the photoperiod. Under this condition, the majority of ROS are produced by chloroplasts and peroxisomes during photosynthesis and photorespiration (Moller *et al.*, 2007). Nevertheless, mitochondria contribute to the maintenance of these processes via ATP production for sucrose synthesis and oxidative decarboxylation of glycine, respectively. Mitochondrial ROS production in shoots is also recognised to have important implications in stress responses (Dutilleul *et al.*, 2003). By contrast, in the darkness in leaves, and in heterotrophic tissues such as roots, mitochondria are the main site of ROS production. Thus, taking these metabolic differences into account, the observed local ROS difference could reflect both the nature and the age of the tissue investigated. Additionally, the fluorescence assay is more sensitive than DAB staining. For a better comparison, seedlings of the same age as used for the FDA stain should be stained with DAB. After a longer

DAB incubation time and especially under stress conditions (eg after irradiation with UV-B light), differences in DAB accumulation would be expected.

5.4 Dexamethasone-inducible RNAi knockdown lines

Because no homozygous T-DNA insertion lines could be isolated in the *AtSlp2* gene, additional transgenic plants were created that express a dexamethasone-inducible RNAi construct. Stable *Arabidopsis* lines expressing one of the two *AtSlp* RNAi constructs were selected.

5.4.1 Construct design

The fragments triggering gene silencing based on RNA hairpin formation were ordered from the AGRİKOLA consortium (Hilson *et al.*, 2004) as Gateway-based entry clones. The inserts from these clones were then recombined into the Gateway-based binary vector pOpOff2(Hyg) (Wielopolska *et al.*, 2005). This vector contains the bidirectional promoter pOp6 that drives transcription of the RNA hairpin as well a GUS reporter gene that allows for the control of dexamethasone induction. This promoter responds to the LhGR transcription factor upon activation with dexamethasone. LhGR is transcribed constitutively by the 35S promoter. Figure 5-19 gives an overview over the pOpOff T-DNA structure. The final constructs for both *AtSlp1* and *AtSlp2* RNAi were verified by restriction digestions and DNA sequencing, before being used for floral-dipping of Col-0 plants.

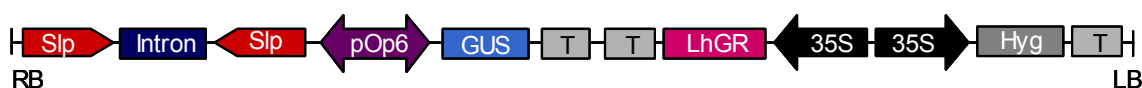


Figure 5-25. Schematic presentation of the pOpOff2(Hyg) T-DNA. The two *Slp* RNAi fragments (*Slp*) forming a hairpin are shown in red flanking the hairpin intron. The pOp6 promoter drives expression of both the *Slp* RNA hairpin and a GUS reporter gene (shown in light blue). The LhGR transcription factor (shown in pink) is driven by a 35S promoter. A second 35S promoter drives expression of the hygromycin resistance gene (Hyg). Abbreviations are: T (terminator), RB (T-DNA right border), LB (T-DNA left border). This figure is redrawn after Wielopolska *et al.*

5.4.2 Time course of RNAi knockdown effect

The effectiveness of RNAi-mediated knockdown of *AtSlp* genes was assessed on the protein level. Heterozygous seedlings of each line were grown hydroponically for 10 days, before dexamethasone-induction was followed in a time course over 48 hours. Figure 5-26 (A) shows Western blots from protein extracts obtained from RNAi lines for *Slp1* and *Slp2* probed with anti-*Slp1*. A clear reduction in protein level can be seen in the *Slp1* RNAi line

starting at 24 hours after initial dexamethasone addition. This reduction was even more pronounced after 48 hours, reducing the protein level to 50 % of the control level. The RNAi line for the *Slp2* gene did not cause reduction of *Slp1* protein. Thus, no crossreaction occurred in the *Slp2* line that might silence *AtSlp1*. The protein levels of these time courses were quantified based on the densities of the bands on the Western blots normalised to the Rubisco loading level seen on the Ponceau S stains. These quantifications are presented in the bar charts in Figure 5-26 (A). In the *Slp2* RNAi plants, the *Slp1* protein was not knocked down as seen on the Western blot, but even slightly increased in the three hour samples compared to the control taken at time zero. However, since this was only a single experiment, the observed upregulation may not necessarily be a reproducible event. Part (B) of Figure 5-26 shows Western blots from the same lines (homozygous) grown on soil and sprayed regularly with dexamethasone for several weeks. The knockdown level in the *Slp1* RNAi line can be clearly seen in the blot on the left side (“+” indicates dexamethasone treatment) compared to the control (“-“ indicates control treatment). As seen before, dexamethasone induction in the *Slp2* RNAi line did not have any obvious knockdown effect on *Slp1*, confirming the specificity of the RNAi construct.

Plants of homozygous induced RNAi lines of both genes were often smaller than wild type or control sprayed plants grown in parallel on soil. Growth parameters such as leaf surface area, flowering time and osmolarity were measured, but did not give reproducible results (not shown). The rather large variety amongst replicates probably reflects the variability of dexamethasone induction in these plants. Additionally, dexamethasone-induced wild type plants were sometimes also smaller or flowered earlier than control treated wild types. However, a reduction in the size of *Slp1* RNAi plants was frequently observed and taken as a real phenotype associated with the knockdown of this gene.

The homozygous single knockout *slp1-1* was floral-dipped with agrobacteria carrying the *Slp2* RNAi knockdown construct. The idea was to create plants that were homozygous for *slp1-1*, and carried at least one heterozygous insertion of the *Slp2* RNAi construct. The functional analysis of these plants is currently still under investigation. At this stage, it is not known whether a plant heterozygous for the *Slp2* RNAi will result in any obvious growth phenotype different from *slp1-1* alone.

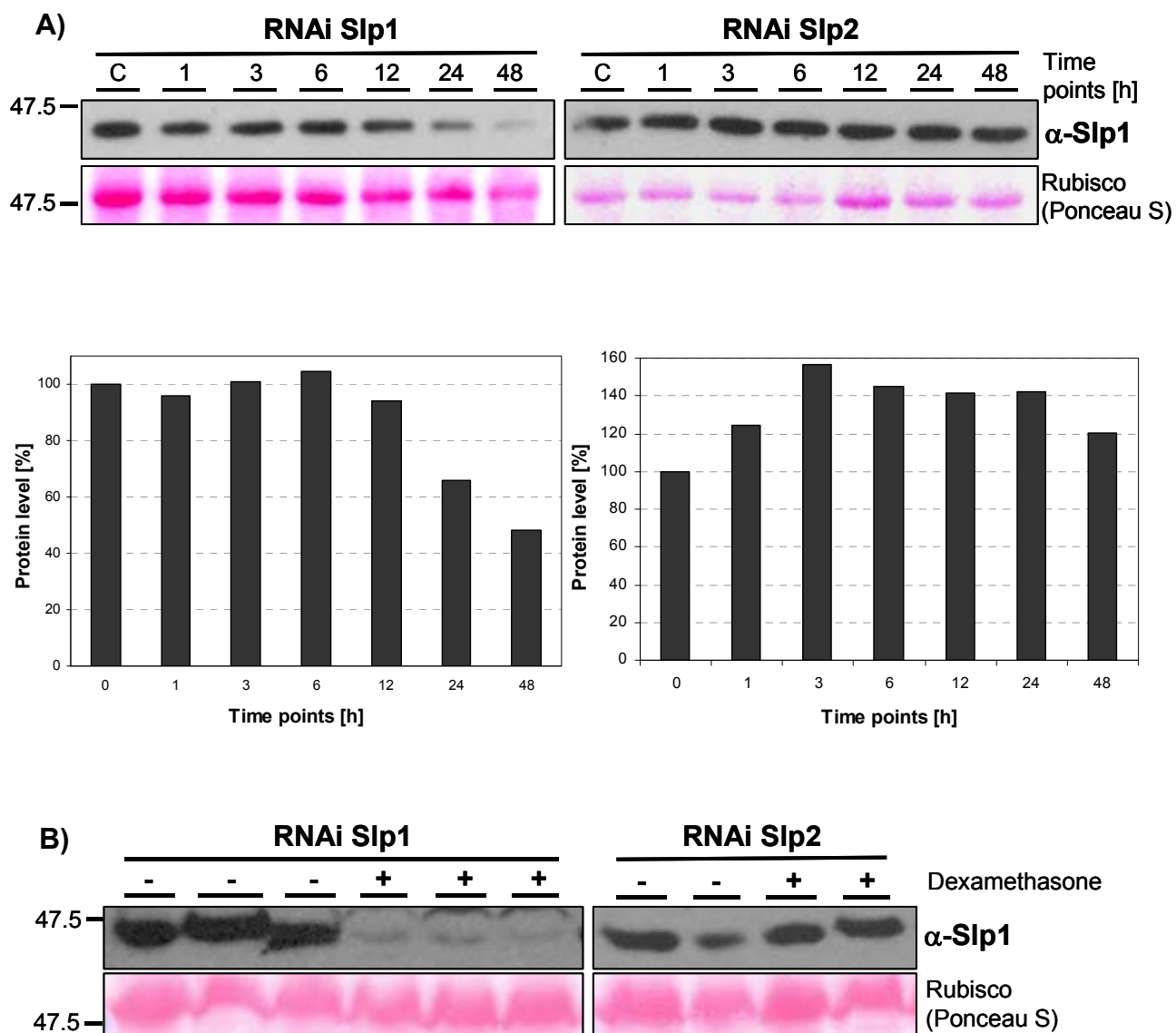


Figure 5-26. Western blot of time course showing RNAi-mediated knockdown of Slp1.

A) Western blots probed with anti-Slp1 of Slp1 and Slp2 RNAi lines. Samples were taken in a time course over 48 hours as indicated. The control sample ("C") was taken at time zero. The Rubisco band from the Ponceau S stain is included for loading reference underneath. Numbers on the left side indicate molecular weight markers in kDa. The bar charts underneath indicate the quantitated signal from the intensity of the protein bands on the Western blot normalised to the Rubisco intensity.

B) Western blot showing Slp1 knockdown level in dexamethasone-treated plants grown on soil. The left panel shows plants expressing Slp1 RNAi and the right panel Slp2 RNAi. "-" and "+" indicate the absence or presence of dexamethasone induction, respectively. Labelling is as above.

5.5 Overexpression of putative dominant-negative Slp fragments (DN Slps)

To gain further insight about the physiological function of Arabidopsis Slp proteins, additional transgenic plants were created. These plants overexpress truncated versions (so called dominant-negative (DN) proteins of both AtSlps, rather than full-length proteins. The rationale behind this approach was to overexpress proteins that lack an important part of the structure, but still contain domains that are functional to a certain extent. In this case, DN(AtSlps) were expressed that lack the hydrophobic domain putatively important for membrane binding (Figure 5-27). Thus, it was anticipated that these DN proteins might act as soluble competitors with the endogenous full-length Slp proteins. They would accomplish this by either titrating out putative interacting proteins, or by forming complexes with the endogenous Slp proteins, preventing other proteins from interaction. Thereby, the function of the full length Slps was expected to be inhibited, or partly taken over by the DN proteins.

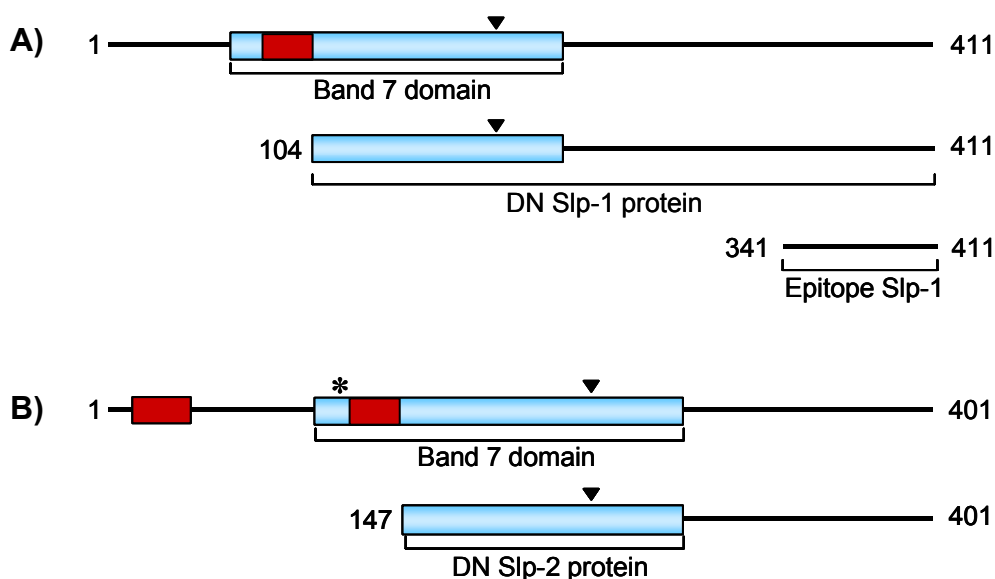


Figure 5-27. Construct design of DN Slps.

A) The DN protein of Slp1 (amino acids 104-411) includes the complete C-terminus and is truncated after the hydrophobic domain shown as a red box. The black triangle indicates the conserved cysteine implicated for S-acylation. The position of the Slp1 epitope is indicated underneath.

B) The DN protein of Slp2 (amino acids 147-401) was designed in the same way as a truncation after the second hydrophobic domain. The asterisk indicates the AtSlp2 unique cysteine residue.

5.5.1 Design of constructs

The expression of these DN proteins was designed as inducible constructs using the pTA7002 vector (Aoyama & Chua, 1997). Their expression can be triggered by the external application of dexamethasone to plants. The same approach has been applied previously to produce cytosolic soluble competitors of tobacco and Arabidopsis plasma membrane syntaxins (Geelen *et al.*, 2002). Figure 5-28 gives an overview over the DN T-DNA. Both DN Slp proteins were designed with an N-terminal myc tag to monitor protein expression because it was not clear at the time of cloning whether anti-Slp1 would result in protein-specific antiserum. The expression of the DN Slps is driven by the dexamethasone-activated GVG transcription factor that binds to the 6xUASg promoter and activates transcription. GVG itself is expressed under the constitutive 35S promoter. Dexamethasone is a glucocorticoid that supposedly has no effect on plant growth and development on its own.



Figure 5-28. Schematic presentation of DN(Slp) encoding T-DNA. The DN fragment is indicated by the red box. Both DN protein constructs were designed with an N-terminal myc tag as indicated. DN Slps were cloned into pTA7002 by using XhoI and SpeI restriction sites. Abbreviations are: RB (right border), 35S (CMV 35S promoter), GVG (dexamethasone-responsive transcription factor consisting of the GAL4 DNA binding domain, the VP16 transactivating domain and the GR receptor domain), E9 (pea rubisco terminator), Nos (Nos promoter), Hyg (hygromycin phosphotransferase gene), Nos (Nos terminator), 6xUASg (6x GAL4 UAS), 35S TATA (TATA region of 35S promoter), 3A (pea rubisco 3A terminator), LB (left border).

Both DN(Slp) constructs were used for stable transformation of Arabidopsis Col-0 plants. Several independent transgenic lines were obtained based on the hygromycin resistance gene, and three homozygous lines were chosen for further analysis.

Originally, these constructs were designed with the idea in mind that AtSlps were plasma membrane localised proteins. As such, DN Slps were expected to act as cytosolic competitors of plasma membrane-localised Slp proteins. The discovery of Slp mitochondria localisation was made after DN plants were created and analysed for phenotypes.

5.5.2 Dexamethasone induction properties

Transgenic plants were tested for the level and kinetics of dexamethasone-mediated protein induction. Dexamethasone induction of expression can be carried out with plants grown on soil by spraying, and on MS agar plates and liquid medium by supplementing the medium with dexamethasone. A series of plants were grown in liquid culture for 10 days. Dexamethasone was added directly to the medium to 10 μM , and plant samples taken out in a time course over 48 hours. In parallel, plants were grown under the same conditions and dexamethasone was added in a concentration gradient and incubated over 12 hours. Plants were then harvested and their proteins were extracted. Figure 5-29 shows Western blots of these protein extracts obtained from the time course and dexamethasone concentration gradient probed with anti-myc.

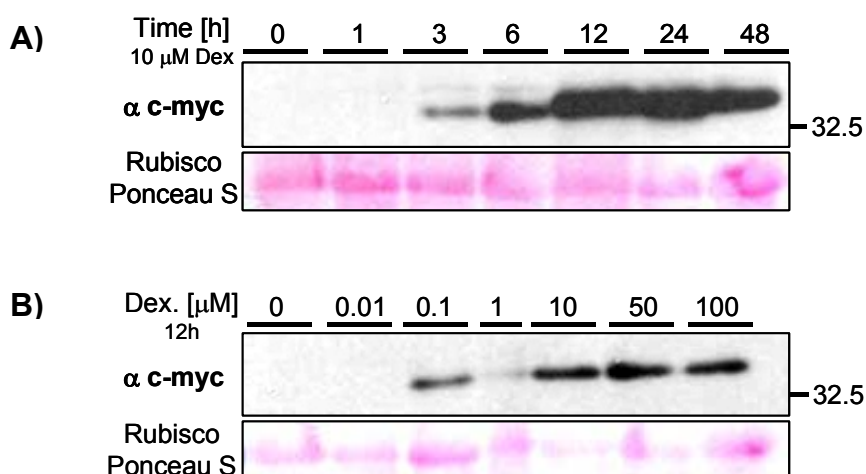


Figure 5-29. Dexamethasone induction kinetics of a DN(Slp1) transgenic line.

A) Time course of dexamethasone induction over 48 hours. Recombinant myc-tagged DN protein starts to accumulate 3 hours after the initial induction and then builds up in the following time points. The maximum induction level is already reached after 12 hours. The Rubisco loading control is shown underneath.

B) Dexamethasone concentration gradient after 12 hours incubation time. DN(Slp1) protein accumulates already when dexamethasone (Dex.) is applied at 0.1 μM concentration and can be seen when dexamethasone is applied up to 100 μM . The number on the right side indicates the molecular weight marker in kDa.

DN(Slp1) protein started to accumulate at the expected molecular weight (35 kDa for DN(Slp1)) already three hours after the initial dexamethasone application (Figure 5-29 (A)). The protein level then built up over time and was still present after 48 hours. Dexamethasone-triggered protein induction was possible over a range of concentrations applied over 12 hours (Figure 5-29 (B)). DN(Slp1) protein was visible when as little as

0.1 μ M dexamethasone were applied, but it accumulated at higher levels when 10-100 μ M were used. As a standard concentration for protein induction on plates or in liquid medium, 10 μ M were chosen for all future experiments.

5.5.3 Solubility of DN Slps

As mentioned, DN Slp proteins were designed as entirely soluble proteins. These truncated Slp versions lack the entire Slp N-termini encoding the mitochondrial (or other) targeting sequences. Additionally, DN Slp proteins lack the putative membrane-penetrating hydrophobic domains and can thus only be bound to membranes by other means.

5.5.3.1 Assessment of DN protein solubility

To check for the protein solubility of DN Slps, plant protein extracts of control and dexamethasone-treated plants grown on MS agar plates were separated into soluble and microsomal fractions. Figure 5-30 shows Western blots probed with anti-myc of extracts from wild type, DN(Slp1) and DN(Slp2) plants. The antibody did not recognise any specific bands from wild type plants either in the control or in the dexamethasone-treated samples, as it was expected. DN(Slp1) protein was clearly detectable in extracts from induced plants, but not in the control-treated seedlings. The DN protein was in fact present in the soluble fraction as anticipated, but it was also visible in the microsomal pellet. The ratio of soluble to microsomal DN(Slp1) was approximately 2:1. In DN(Slp2) plants, dexamethasone treatment caused expression of the myc-tagged DN protein mainly in the soluble fraction at the correct expected molecular weight of 29 kDa. A small proportion of DN protein was also associated with the membrane pellet, although to a lesser extent than the DN(Slp1) protein. No DN(Slp2) protein was detected in the control-treated samples (Figure 5-30 lower panel left side). This experiment illustrates the specificity of DN protein induction, and it also addresses the question of DN protein solubility. Unexpectedly, both DN Slp proteins were still at least partially associated with membrane fractions, despite lacking targeting information and hydrophobic amino acid stretches that could serve as membrane anchors.

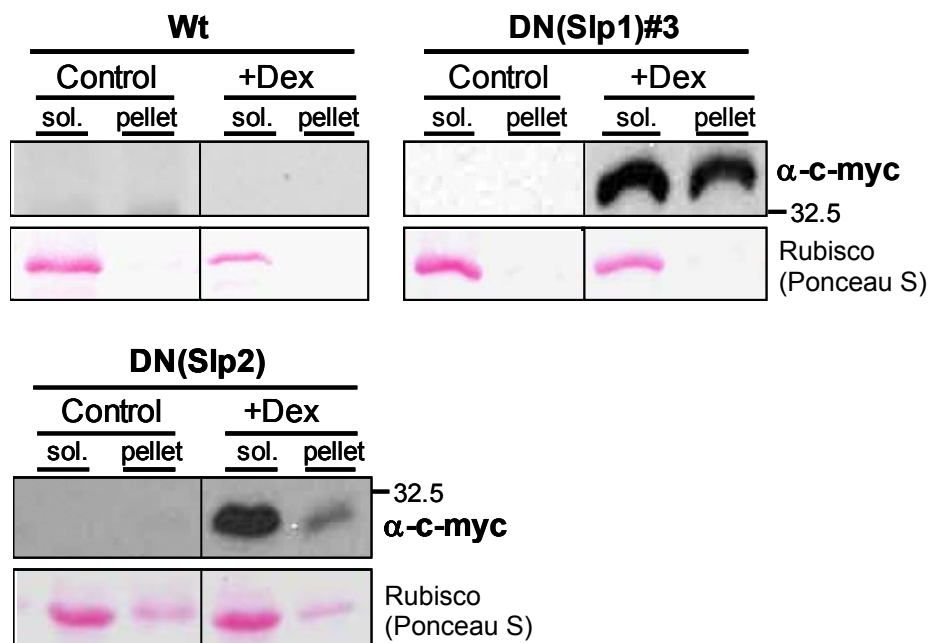


Figure 5-30. Assessment of DN Slp protein solubility. Wild type, DN(Slp1) (line #3) and DN(Slp2) seedlings were grown on control and dexamethasone-supplemented MS agar plates (+Dex). Soluble proteins (sol.) were separated from microsomal proteins (pellet) by ultracentrifugation. Shown are Western blots probed with anti-myc. The numbers on the right side of each blot refers to the position of the molecular weight marker in kDa. Ponceau S-stained Rubisco bands are included for reference of protein loading levels.

5.5.3.2 Putative S-acylation of DN Slps

The unexpected membrane association of DN Slp proteins raised the question by which alternative means these proteins might be bound to membranes. Since no hydrophobic domain is present, DN Slps could be membrane-bound by a post-translational modification. As discussed in chapter 4, S-acylation of endogenous Slp1 presents a likely form of such a modification. The proposed modified cysteine residue is also present in the DN proteins (indicated in Figure 5-27 by black triangles) and could be responsible for S-acylation-mediated membrane attachment.

To test this hypothesis, DN Slp and wild type seedlings were grown in the presence of dexamethasone and BPA on MS agar plates. The rationale behind this approach was to test whether DN proteins would be entirely soluble in the presence of BPA and dexamethasone to inhibit S-acylation. BPA in the growth medium severely affected seedling growth in roots and shoots (see photographs in Figure 5-31). Seedling roots on BPA medium were short and frequently developed adventive root tissue. Leaf tissue was pale with visibly

smaller leaves and grew very slowly. BPA is known to have inhibitory effects on root hair development, mimicking the *tip* root hair mutant (Hemsley *et al.*, 2005). The addition of dexamethasone to the medium in combination with BPA did not affect further the growth of DN or wild type seedlings than seen with BPA alone. Dexamethasone alone curiously caused an enhanced main root growth in wild type and DN(Slp2) seedlings. In DN(Slp2) seedlings, roots additionally showed more bending and had more adventive root tissue than on plain MS medium. DN(Slp1) seedlings grown with dexamethasone had fewer lateral roots than on the control plates. Wild type seedlings grown on dexamethasone medium had more lateral roots than on the control, and they also generated larger rosettes.

Seedlings grown under these four conditions were harvested from plates and their proteins were extracted. Soluble proteins were subsequently separated from microsomal fractions by ultracentrifugation. The extracts were separated on SDS-PAGE gels and Western blots prepared, probed with anti-myc and anti-Slp1 serum. Figure 5-32 shows the effect of BPA and dexamethasone on the solubility of the DN(Slp1) protein. With dexamethasone alone, the DN protein was present both in the soluble and microsomal fraction, as seen in Figure 5-30. In the presence of BPA alone, only an unspecific band was visible on the anti myc-probed Western blot, but no DN protein. Upon addition of dexamethasone and BPA, the DN protein was mainly soluble, with a smaller proportion than seen before still associated with membranes. However, these last two samples also had lower amounts of protein loaded than the previous samples (see Ponceau S stain), and could therefore mislead the impression of increased DN solubility. Despite the visible effect of BPA on seedling growth, the palmitoylation inhibitor did not cause complete solubility of DN(Slp1), as it was anticipated. A small proportion of the endogenous Slp1 protein was found in the soluble fraction in the presence of dexamethasone, BPA and both combined (red arrowhead Figure 5-32). However, no enhanced solubility upon BPA addition was observed with this protein, similar to the result presented in chapter 4 (section 4.4.3). In the dexamethasone-treated sample, the Slp1 antibody also recognised the overexpressed DN(Slp1) protein, as it was expected because the antibody epitope is included in the DN fragment. The overall Slp1 protein level in the dexamethasone-treated sample appeared however weaker than in the BPA sample, when the loading levels between those samples are compared. Overexpression of the DN(Slp2) protein did not have effects on Slp1 protein solubility either (not shown).

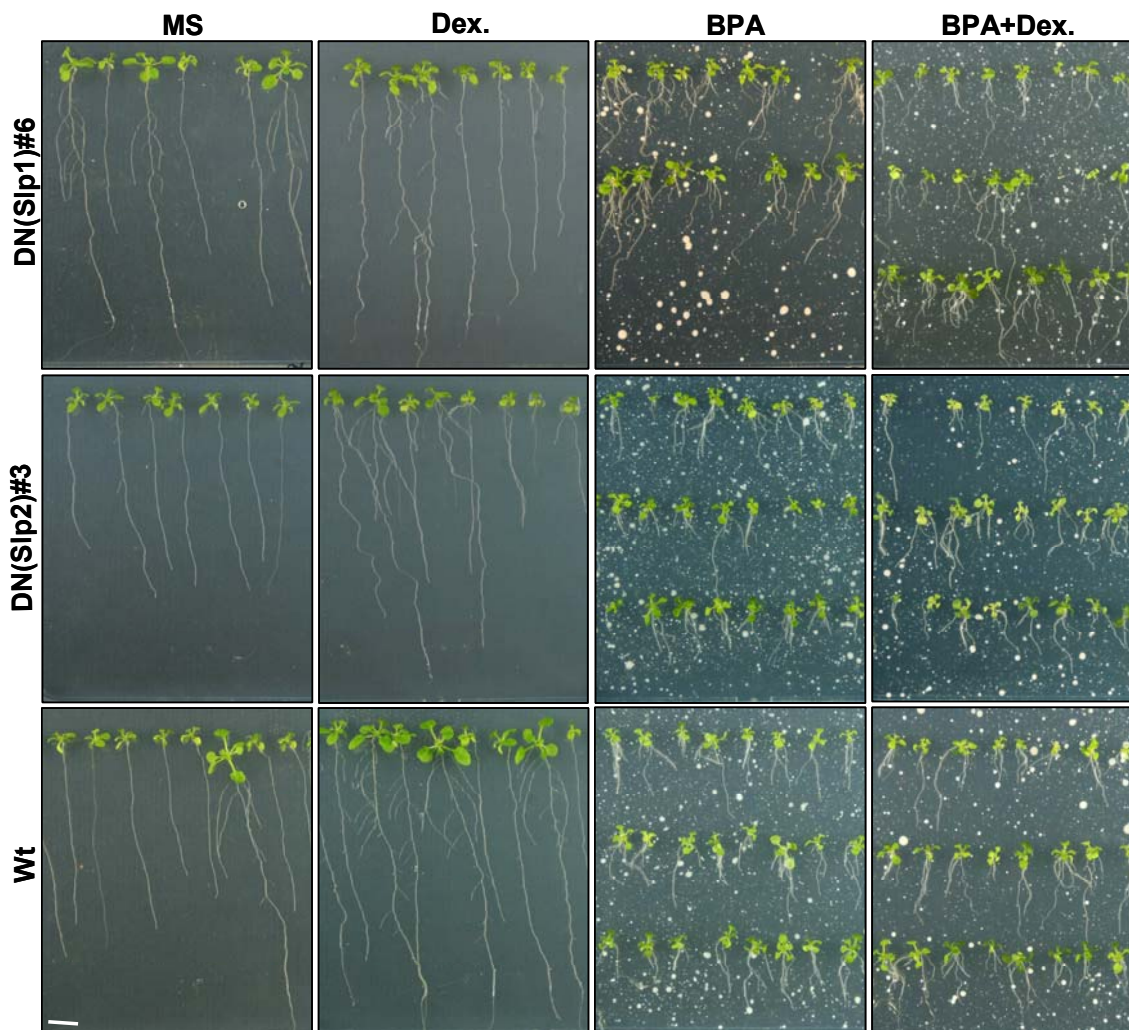


Figure 5-31. DN Slp seedlings grown on MS agar plates with dexamethasone and BPA. The left panel shows images from control (plain MS) plates, followed by MS supplemented with $10\mu\text{M}$ dexamethasone (Dex.), 1 mM BPA or dexamethasone and BPA (BPA+Dex.). Scale bar = 1cm. BPA is highly insoluble in aqueous solutions and therefore precipitated on MS agar plates as white clusters.

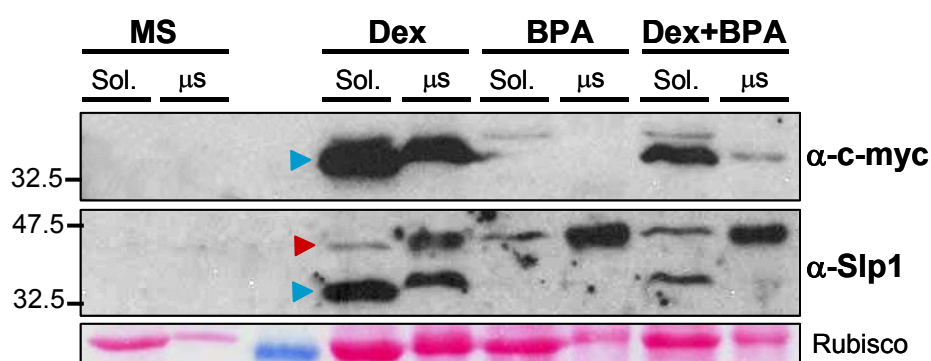


Figure 5-32. Effect of BPA on DN(Slp1) protein solubility. Seedlings were grown on plates as shown in Figure 5-31 as indicated. A Western blot of protein extracts separated into soluble (Sol.) and microsomal (μs) fractions is shown. The upper blot was probed with anti-myc, and the same blot below with anti-Slp1. The DN protein is marked by a blue arrowhead, and the endogenous Slp1 protein by a red arrowhead. The Rubisco bands are shown as Ponceau S stains at the bottom for reference of protein loading levels. The samples from plain MS plates are loaded with too little protein in comparison to the other samples. Therefore, not even the endogenous Slp1 protein can be seen, as it would be expected with anti-Slp1. Numbers on the left side indicate molecular weight markers in kDa.

In summary, these results indicate that the DN(Slp1) protein is probably membrane-attached by other means than palmitoylation of the conserved cysteine residue. S-acylation is not completely excluded by this result, since a much smaller proportion of the protein was membrane-attached in the presence of BPA. S-acylation seems not, however, the only mode of membrane binding of this truncated Slp1 protein.

5.6 Associated DN growth phenotypes

When grown on plates or in liquid culture in the presence of dexamethasone, DN(Slp) expressing plants did not show obvious growth phenotypes apart from the ones described in the previous section (Figure 5-31). However, these plants displayed a severe morphological phenotype when grown on soil and sprayed with a solution containing 30 μ M dexamethasone.

5.6.1 Growth phenotypes and reduction of leaf surface area

Plants that were continuously sprayed with dexamethasone solution from germination onwards had several growth defects (Figure 5-33). Approximately at the six-leaf stage, expanding rosette leaves started to curl up and produced dwarfed rosettes with a helical wheel growth phenotype (bottom images in Figure 5-33). Leaves were severely affected in their expansion and as a result, were smaller than those from wild types or control treated plants. Figure 5-34 shows a bar chart with quantified leaf surface areas from DN(Slp1), DN(Slp2) and wild type plants that were control treated, or induced with dexamethasone. DN-Slp induced plants had significantly reduced leaf surface areas compared to their controls, or treated wild type plants. Examples of affected leaves are shown in Figure 5-36 (right image) where DN(Slp1)-expressing leaves are shown next to wild type leaves from identically treated plants. Both DN Slp proteins caused virtually identical growth phenotypes. At a more mature stage, rosette leaves from both genotypes started to become chlorotic and displayed lesions with patches of dead tissue. Leaf senescence started earlier than in control treated plants or wild types, and in the most severe cases dwarfed plants even died prematurely. Cauline leaves of flowering plants were also curled in appearance, but did not become chlorotic and displayed the same severe lesions as seen in rosette leaves. Leaf necrosis also occurred when dexamethasone was applied to plants at a later growth stage, once they passed the flower transition. In this case, mature rosette leaves started to become uneven and displayed lesions of dead tissue spreading out from the

middle of the leaves (Figure 5-35). Once leaves became chlorotic, they did not recover, even when dexamethasone application was stopped completely.

DN expressing plants flowered and produced seeds that germinated, but the overexpressed DN proteins caused deformations of flowers and siliques. Frequently, flowers were smaller and the buds rounder in appearance than those from control plants (Figure 5-36). Siliques were shorter, and also thicker in shape, containing less seeds. In some cases, a lack of apical dominance was recognisable. Figure 5-36 shows images of whole flowering plants from the control and the dexamethasone treatments. The dexamethasone-sprayed plant had more than one main shoot growing simultaneously out of the basal rosette. The shoots were frequently also dwarfed in their overall length compared to control plants. All of these described growth defects were observed in plants grown on soil in growth chambers, both under long day and short day light conditions.

In summary, the most severe phenotypes were observed in leaves. Rosette leaves were always more affected than cauline leaves, with necrotic patches on the surface. Frequently, rosettes grew into a curled, helical shape and had severely reduced leaf expansion. This observation could point towards defective cell elongation or cell division, processes regulated by phytohormones such as auxin and cytokinins.

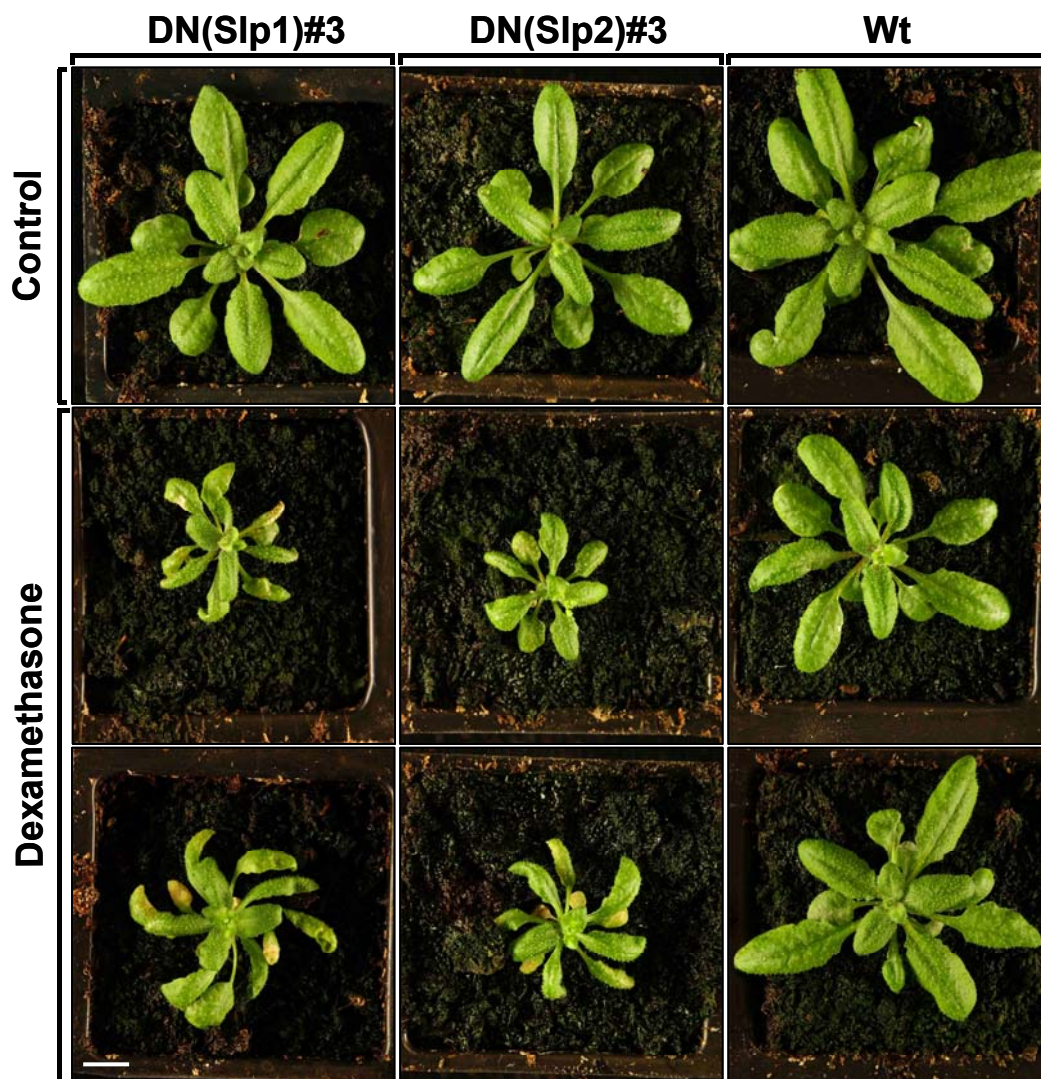


Figure 5-33. Phenotypes of DN Slp plants grown on soil. DN lines of Slp1 and Slp2 were grown in parallel with wild type plants and treated as indicated. The control treatment consisted of spraying plants with water and solvent. Protein-inducing treatment was applied by spraying the same solution as the control, but with added dexamethasone as indicated. Scale bar = 1cm.

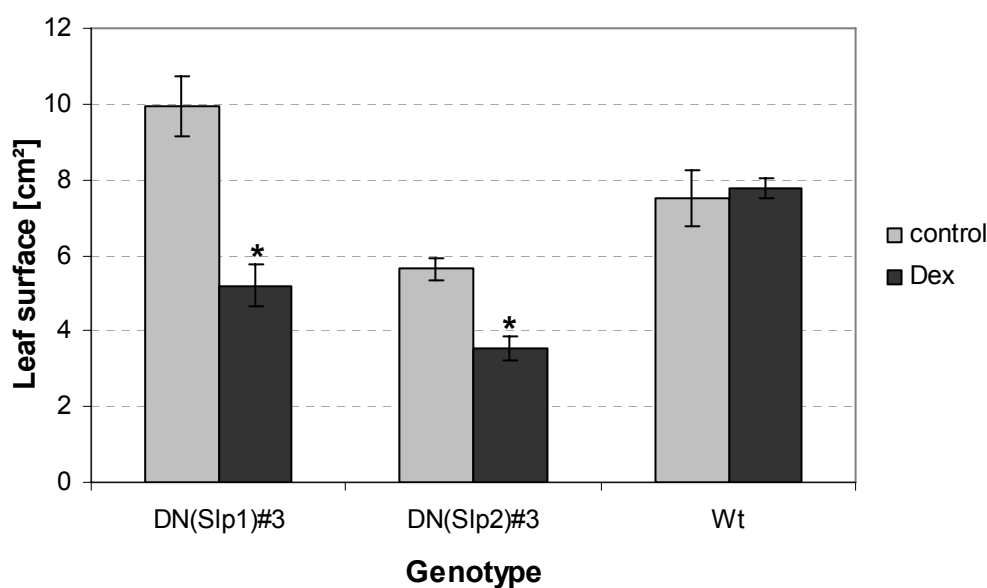


Figure 5-34. Quantification of leaf surface area from soil-grown DN and wild type plants. Significant differences between control and dexamethasone (Dex) treatment are indicated by asterisks (t-tests, $p < 0.001$, $n=12$).

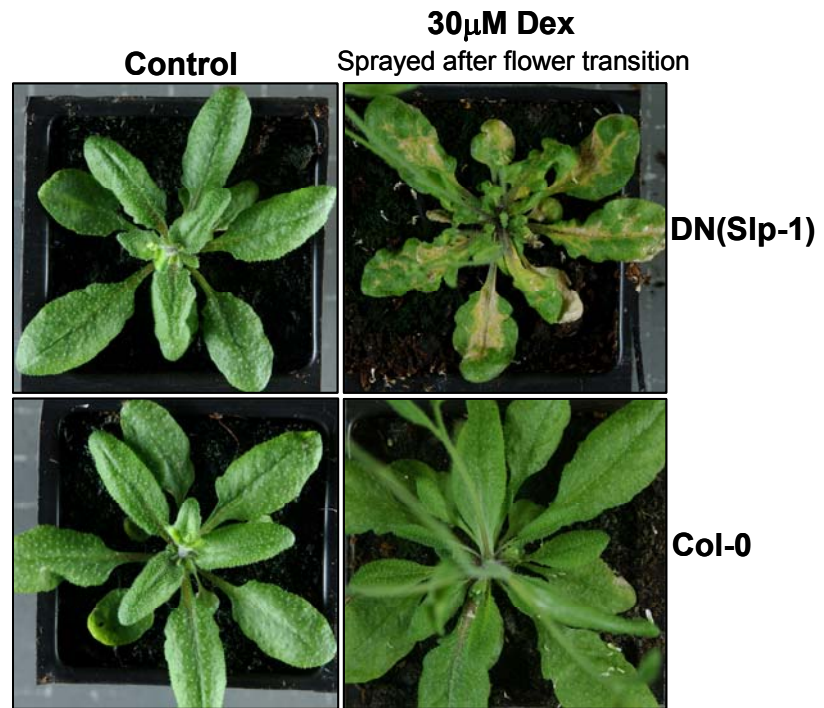


Figure 5-35. Growth phenotype of plants grown on soil and induced after the flower transition. Dexamethasone was applied once plants started to bolt. Shown is a transgenic line expressing DN(Slp1), and wild type plants treated with control and dexamethasone solutions (Dex). Scale bar = 1 cm.

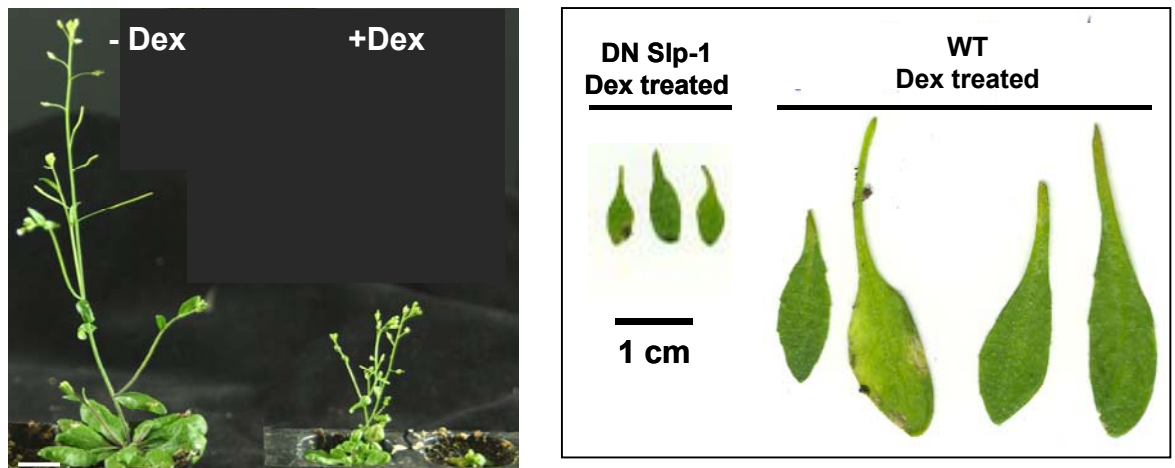


Figure 5-36. Growth phenotype of whole flowering plants and leaves. The left image shows a side view of a control DN(Slp1) plant (-Dex) and a dexamethasone-induced plant (+Dex) of the same line. Scale bar= 1cm. Right side: Images of single leaves from a dexamethasone-treated DN(Slp1) plant and a wild type plant treated in parallel.

5.6.2 Leaf osmolarity

Osmolarity levels of induced and visibly affected rosette leaves were measured directly from leaf sap of short day grown plants. Figure 5-37 shows a summary of these measurements. DN(Slp1)-expressing leaves had significantly elevated osmolarity levels compared to their control-treated counterparts and wild type plants. On average, dexamethasone-induced plants contained 400 mOsM osmolites, whereas control-treated or wild type plants contained approximately 320 mOsM. No significant difference was detected between dexamethasone-sprayed and control-sprayed wild type plants.

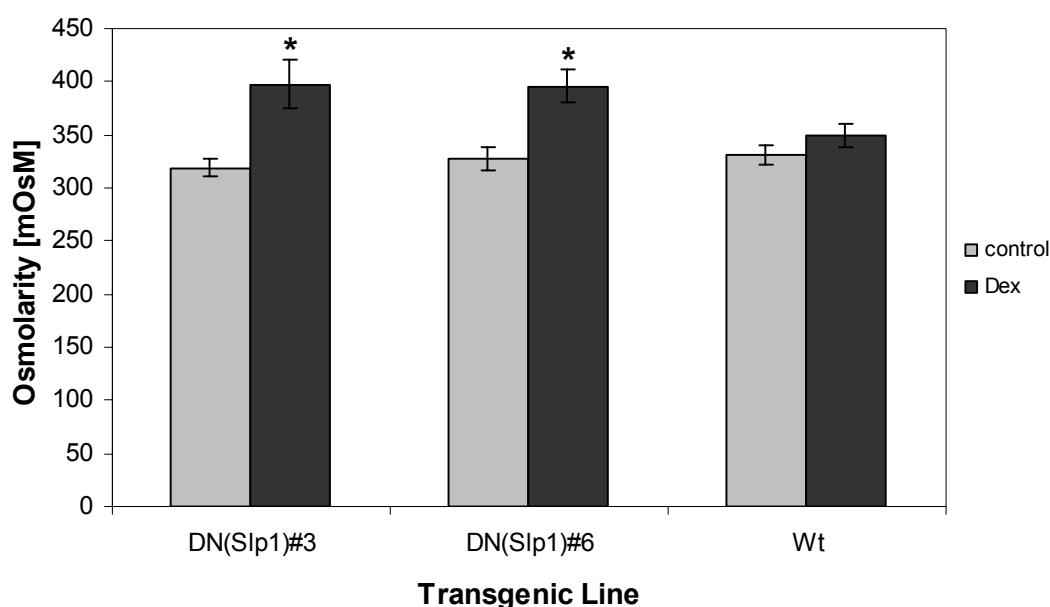


Figure 5-37. Osmolarity levels of dexamethasone-induced and control DN and wild type plants. Induced DN(Slp1) plants from two independent lines (nos. 3 and 6) had significantly elevated leaf osmolarity ($p < 0.05$, t-test; $n=3$). No difference was detected between control-sprayed and dexamethasone-sprayed wild type plants.

5.6.3 Flowering time

The effect of DN Slp expression on the onset of flower transition was tested by counting the number of vegetative leaves upon bolting. A plant was regarded as flowering when the shoot apex was located about one centimetre above the soil. Figure 5-38 shows a bar chart with the number of rosette leaves plotted per line. Two independent lines expressing DN(Slp1) were counted, and one line expressing DN(Slp2), as well as wild type. All dexamethasone-treated plants showed a tendency towards flowering at an earlier developmental stage than control treated plants. However, this phenomenon was observed

regardless of the genotype, and thus depended on the treatment itself. No statistically significant difference could be detected in each line between control and dexamethasone treatment, or between induced DN and wild type plants. Thus, despite the severe reduction of leaf expansion and shoot growth, the actual timing of flowering was unaffected.

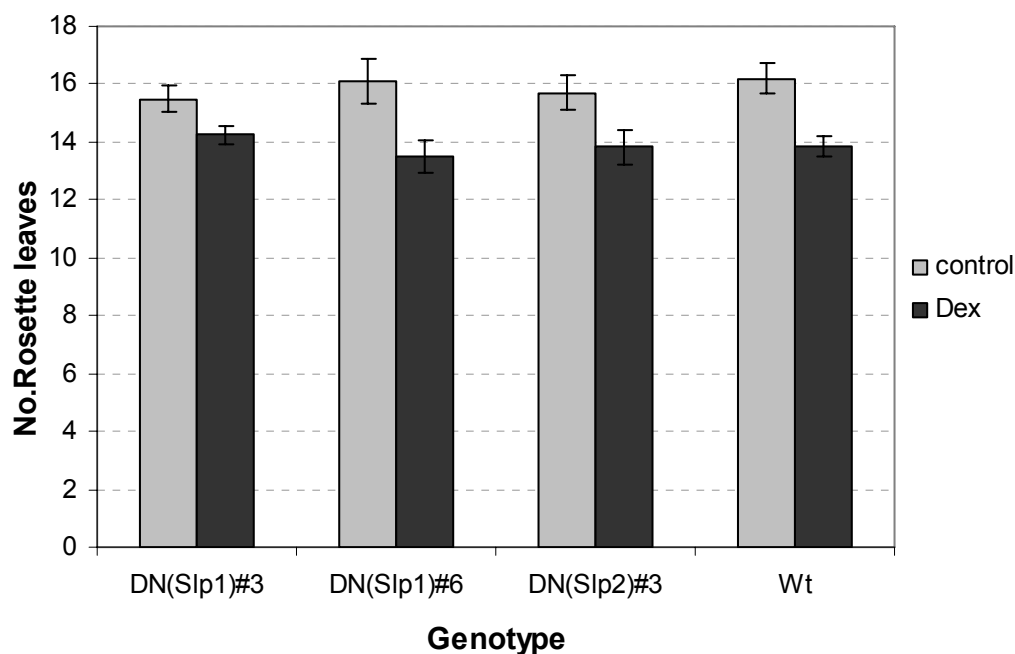


Figure 5-38. Effect of DN expression on the onset of flower transition in long day light. The number of vegetative leaves upon bolting was counted and plotted for each line. No statistically significant difference was found between control and dexamethasone (Dex) treatment in each line and between lines (t-test, $n=12$). Dexamethasone-treated plants all tended to flower at a slightly earlier stage, but this occurred regardless of the genotype.

5.6.4 Guard cell phenotypes

Chlorotic rosette leaves that started to become necrotic and curled up were further inspected under the light microscope. No obvious differences were observed in terms of leaf structure or cell density. Surprisingly however, guard cells from induced DN Slp plants were found to contain visibly enlarged chloroplasts compared to control-treated plants, or wild types. Guard cells are highly specialised cells arranged in pairs around stomatal pores. Their opening and closure governs the extent of leaf transpiration and gas exchange between the atmosphere and the leaf internal space. Guard cell chloroplasts from dexamethasone-induced DN plants were enlarged (at least double in size) and had less chlorophyll autofluorescence than chloroplasts from control-treated or wild type plants.

Figure 5-39 shows bright field images of affected guard cells from epidermal strips prepared from DN(Slp1) expressing plants and wild type controls. Typically, between 4-5 enlarged chloroplasts were found per guard cell that sometimes took up most of the cell volume. Control-treated and wild type plants usually had higher chloroplast numbers, and these were smaller and had brighter chlorophyll fluorescence. Figure 5-40 shows three-dimensional reconstructed confocal images of chlorophyll autofluorescence (shown as red fluorescence). Leaf tissue was counterstained with propidium iodide to visualise cell walls and nuclei (seen as yellow fluorescence). It was always found that affected guard cells did not contain any ordinary-looking chloroplasts, only enlarged ones. Additionally, enlarged guard cell chloroplasts were only identified from mature guard cells, but not from developing stomata. Closer inspection of the enlarged chloroplasts revealed that the changes probably originated in thylakoid ultrastructure. From the confocal image in Figure 5-40 (B) it can be seen that affected chloroplasts appeared hollow in structure, with reduced chlorophyll autofluorescence. To check whether chloroplasts from other cell types were also affected, plastids from underlying mesophyll cells were also scanned with the confocal microscope. These cells were found to contain ordinary-looking chloroplasts with autofluorescence levels similar to those observed in cells from control-treated plants or wild types (Figure 5-40 lower panel). Thus, the observed chloroplast phenotypes are assumed to be specific for guard cells. Interestingly, the majority of developing guard cells had propidium iodide-stained nuclei, indicating that these cells were not viable. This effect was restricted to younger stomata, but absent from mature ones. This might indicate that DN overexpression interferes with guard cell development from an early stage on, resulting in cell death.

Chloroplast enlargement was in some instances observed in only one cell of a particular guard cell pair. In this case, one cell contained ordinary fluorescent and sized chloroplasts, and the other guard cell contained enlarged and less fluorescent plastids. Thus, DN Slp protein-triggered chloroplast changes happened autonomously in each cell of a pair. However, more mature guard cell pairs always contained swollen chloroplasts simultaneously. Apparently, chloroplast enlargement was first triggered in one cell, and happened subsequently in the opposite-lying guard cell of one pair. Not all stomata of a chlorotic leaf had enlarged chloroplasts. Normally, ordinary-looking stomata were scattered between fields of stomata with large chloroplasts. No quantitative estimate was made to calculate the proportion of affected guard cells from a particular area.

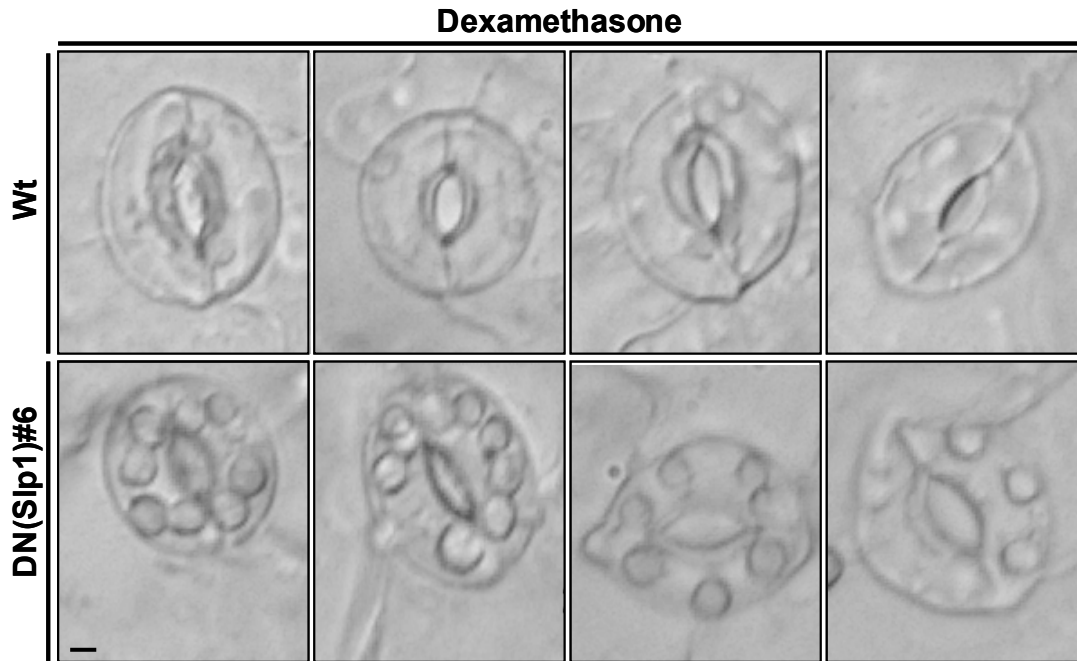


Figure 5-39. Enlarged guard cell chloroplasts. Brightfield view of dexamethasone-treated DN(Slp1) and wild type leaf epidermal strips showing guard cells. Enlarged chloroplasts can be seen from DN(Slp1) induced plants, but not from wild types treated under the same conditions on soil. Scale bar =5 μ m.

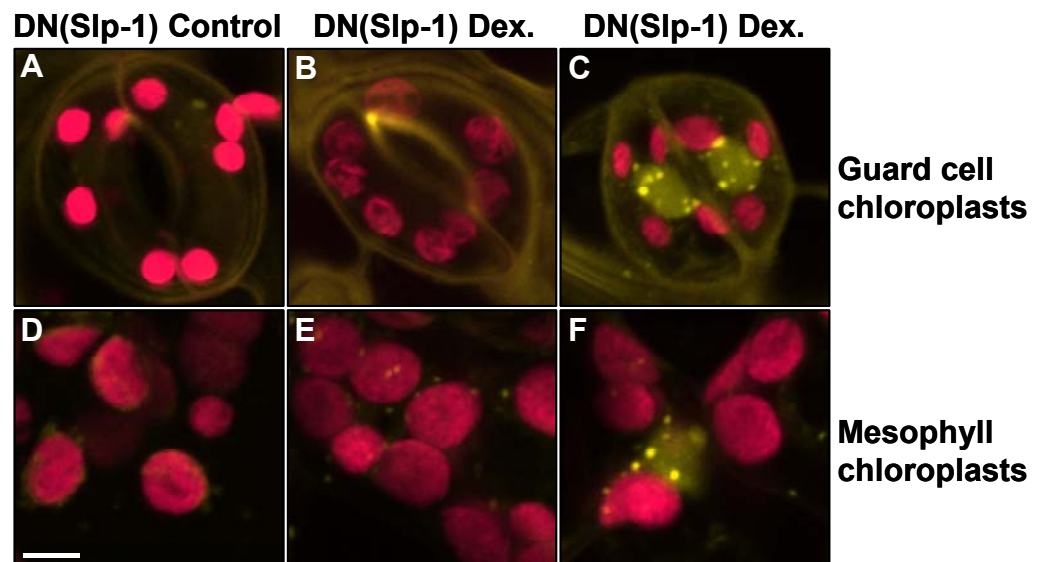


Figure 5-40. Confocal images of guard cell chloroplast autofluorescence (red) counterstained with propidium iodide (yellow). Three-dimensional images were reconstructed from scanned stacks. Shown are images from control-treated DN(Slp1) plants (A, D) and dexamethasone-sprayed identical plants (B, C, E, F). The upper panel shows guard cells (A-C), and the lower panel shows sections from mesophyll cell chloroplasts (D-F). Image B shows a mature pair of guard cells and image C a developing pair. Chloroplast ultrastructure is only perturbed in mature guard cells. Mesophyll cell chloroplasts are unaffected by DN(Slp1) expression. Scale bar =5 μ m. Yellow punctae are propidium-iodide stained nuclei.

To determine whether the expressed DN(Slp1) protein had any effects on the development of stomata in rosette leaves, the densities of guard cells per mm² area were determined. Random areas from leaves of the same developmental stage were chosen, and all stomata in a fixed area were counted on the confocal microscope. Stomatal densities from DN(Slp1) and wild type plants were determined. Figure 5-41 shows the result of a count comparing stomatal densities from mature (A) and growing (B) rosette leaves. Dexamethasone-induction of DN protein expression caused a slight decrease in stomatal density particularly in young leaves, compared to the control treatment of the same line. However, this difference was not statistically significant. In wild type plants, dexamethasone-treatment caused a slight increase in stomatal density, which in this case was more pronounced in mature leaves. As before, no significant difference between control and dexamethasone-treatment was found in wild type plants, or between dexamethasone-sprayed DN and wild type plants. Based on this result, it is concluded that the expression of the DN Slp1 protein does not affect the development of stomata per se. This is in agreement with the observed late onset of chloroplast enlargement only in mature cells. It is concluded that the DN protein has specific effects on the function of mature guard cell chloroplasts and guard cells, but this effect is specific to a late developmental stage of stomata.

To test the functionality of guard cells with enlarged chloroplasts, stomatal apertures were measured. Epidermal strips from dexamethasone-induced DN and wild type plants were prepared, attached to microscope cover slips and placed into a perfusion chamber for light microscopy. Stomata were allowed to open first by perfusing the chamber with depolarisation buffer. Stomatal closure was achieved by either adding ABA or Ca²⁺ to the perfusion medium. It was observed that stomata with enlarged chloroplasts responded to these stimuli, but the responses were less pronounced than in ordinary stomata. It was concluded that the change in chloroplast ultrastructure did not render these guard cells completely non-functional. These stomata were nevertheless affected in their ability to respond to externally applied stimuli. These experiments were only carried out twice for each genotype (DN(Slp1) and wild type), and therefore no reliable quantitative results could be obtained (data not shown).

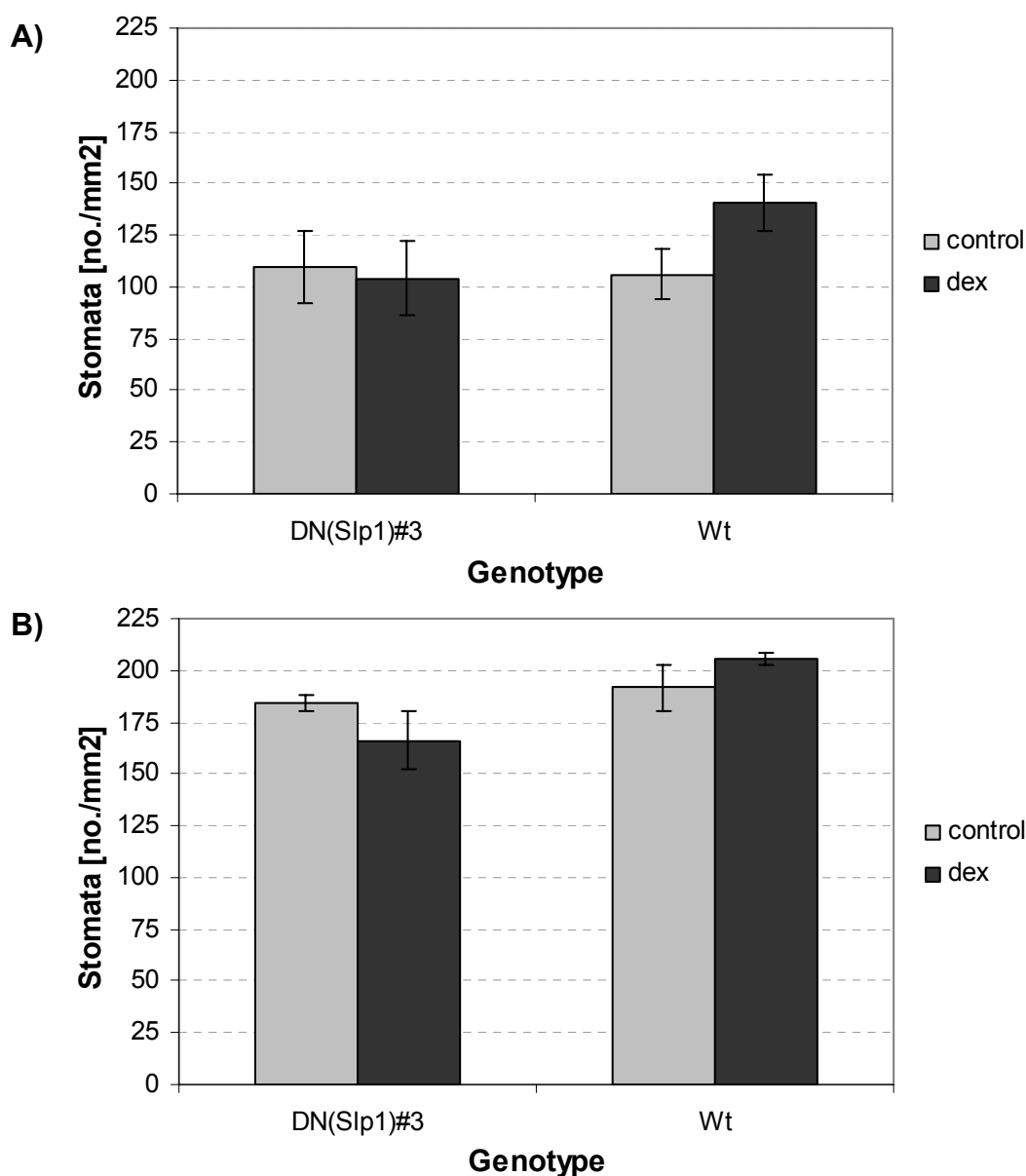


Figure 5-41. Guard cell density of DN and wild type plants grown in long day light. The number of stomata in a defined area was counted and the stomatal density calculated as the number of stomata per mm². A) shows the stomatal density in older leaves, B) the stomatal density in younger leaves. Three plants per line and treatment were chosen. Of each plant, one older and one younger leaf from the same relative position in the rosette were picked for counting. Per leaf, 12 areas were counted, each spanning 230x230 μm^2 . No statistically significant difference was found between the lines and treatments (as determined by paired t-tests).

5.6.5 Water content and whole plant transpiration

To further investigate whether overexpression of the DN proteins affected stomatal function, the water contents of treated DN and wild type plants were analysed as the difference in weight between fresh and dried tissue. The water content was calculated as

the percentage of initial fresh weight of leaves. Figure 5-42 (A) shows the water contents of plants grown in short day light for 53 days that were sprayed with dexamethasone or control solution when the rosettes were already grown to a more mature stage (but before flowering). Leaves were harvested that already displayed chlorosis and onset of necrotic patches. Dexamethasone treatment caused a slight increase in water content from 85% initial fresh weight in control plants to 90 % in both DN-expressing and dexamethasone-sprayed wild type plants. In both genotypes, this increase was statistically significant from the control treatment of each line. The DN-expressing plants also had slightly elevated water contents when compared to dexamethasone-sprayed wild type plants (90 % compared to 87 % respectively). A second set of plants grown under long day light (23 days old) was analysed for water content as well (Figure 5-42 (B)). This time, DN(Slp2)-expressing plants were included for analysis. Plants had been treated with control or dexamethasone-containing solution for several weeks and were visibly chlorotic in appearance. In this dataset, no significant difference between control and dexamethasone treatment was detected, neither in the DN nor in the wild type plants. Dexamethasone-treated DN(Slp2) plants had slightly elevated water contents (92 % compared to 91 %), but not to a significantly different extent. When these two datasets are compared, it appears that control-treated plants from Figure 5-42 (A) have actually decreased water contents compared to dexamethasone-treated plants, rather than the other way round. This finding is surprising, considering that the same amounts of dexamethasone solvent (0.15% ethanol) and detergent (0.01 % Tween-20) were present in the control spray than in the dexamethasone spray solution. Based on the results shown in this figure, it also cannot be excluded that the application of dexamethasone itself had pleiotropic effects, since the water content in wild type treated plants was also elevated compared to its control treatment. Based on the only small but significant difference in water content between dexamethasone-treated DN(Slp1) and wild type plants, DN overexpression only marginally affected guard cell function and their ability to control plant water loss. From this result it appears that under short day light, water loss and therefore stomatal opening might have been slightly impaired in these plants. Rather curiously, this did not seem to apply under long day light conditions. However, it must also be considered that these long-day grown plants were younger and not at the same developmental stage than those measured from short day light.

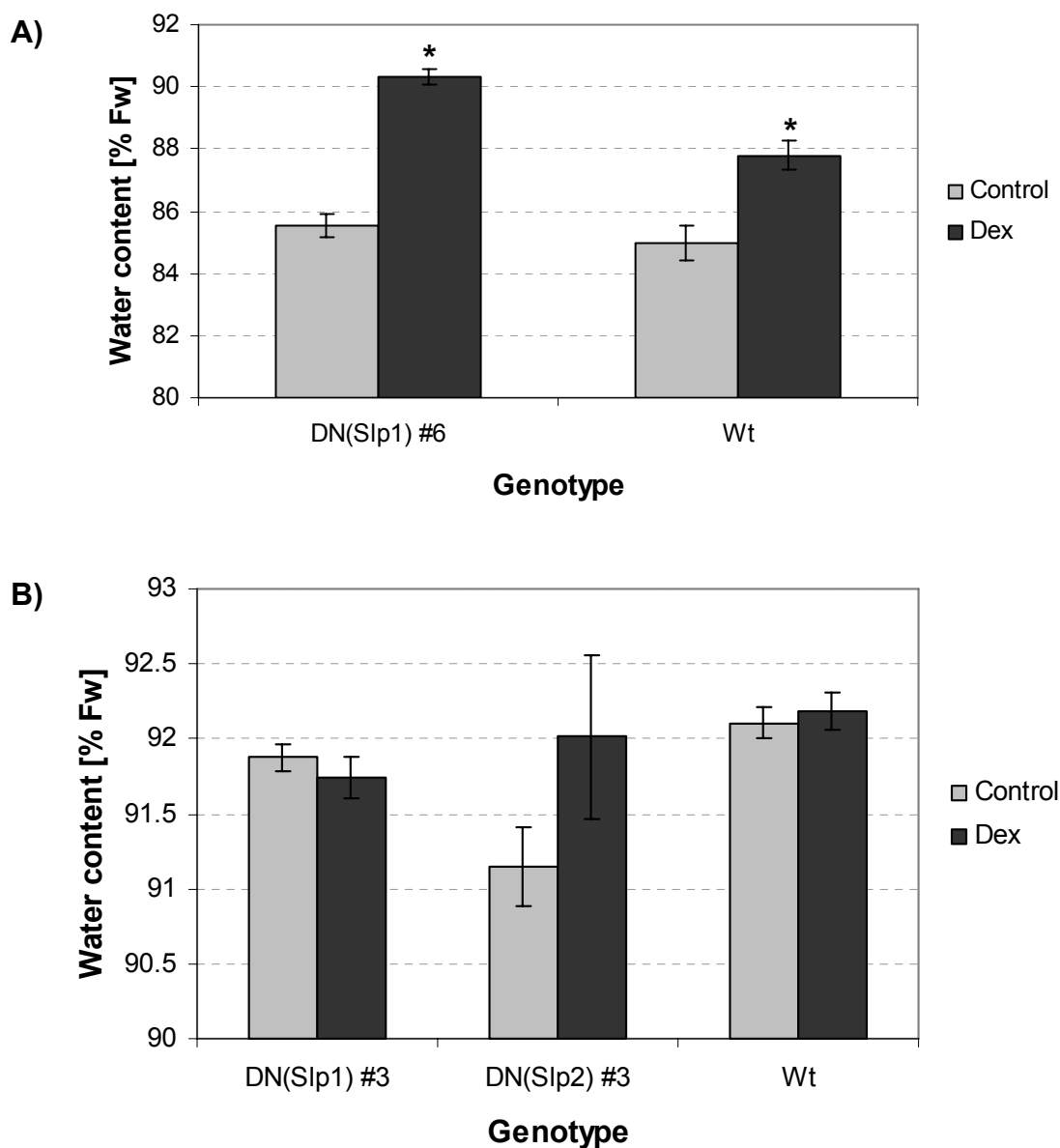


Figure 5-42. Leaf water content from DN Slp and wild type plants. Leaves from treated plants were harvested and their fresh weight was determined. The water content (as % initial fresh weight) was calculated based on the dry weight.

A) Water content from plants grown in short day light and sprayed once rosettes were mature. Both DN(Slp1) and wild type plants treated with dexamethasone had significantly higher water contents than control-treated plants. The water content of induced DN(Slp1) leaves was also significantly higher than from identically treated wild type leaves (t-test, n=9).

B) Water content from plants grown in long day light. The differences in water content are smaller than those from short-day grown plants and statistically not significant (t-test, n=6).

To determine further whether there would be differences in transpiration rates and water loss between dexamethasone-and control-treated plants, water loss was recorded over time from excised shoots. Short-day grown plants (42 days old) were harvested by cutting the rosette just above the soil, the cuts were sealed, and the plants were placed on a small tray. The weight of each plant was recorded every 15 minutes during the first hour after harvesting, and then every 30 minutes until eight hours after cutting. Figure 5-43 (A)-(C) shows water loss monitored over time from three independent DN(Slp1) lines that were either control-treated or sprayed with dexamethasone. In all three lines, dexamethasone-induced plants always lost water faster than control plants. Usually, water loss after eight hours in dexamethasone-treated plants was approximately 10% above the water loss from control plants. No comparably good datasets were obtained from wild type plants grown under the same conditions treated with dexamethasone.

The finding that dexamethasone-induced plants lost actually more water than their corresponding controls was surprising. The water contents measured previously from leaves obtained from plants of similar age and also grown under short day light (Figure 5-42 (A)) do not correspond to this finding. It would have been expected that dexamethasone-treated plants would actually retain water better than their controls.

However, it was also found that the size of the shoots and leaves influenced the rates of water loss in this experimental setup. In subsequent experiments it was indeed established that smaller shoots like the ones from the dwarfed DN-expressing plants lost water faster than larger treated plants. Because there was a difference in size between the control and the induced plants, these results might be influenced by this factor as well.

This type of experiment can only provide an estimate for the ability of stomata to regulate water loss from leaves, but it does not provide data about actual transpiration rates. These are influenced by several factors, amongst them the ability of plants to take up and transport water from the roots to the shoot.

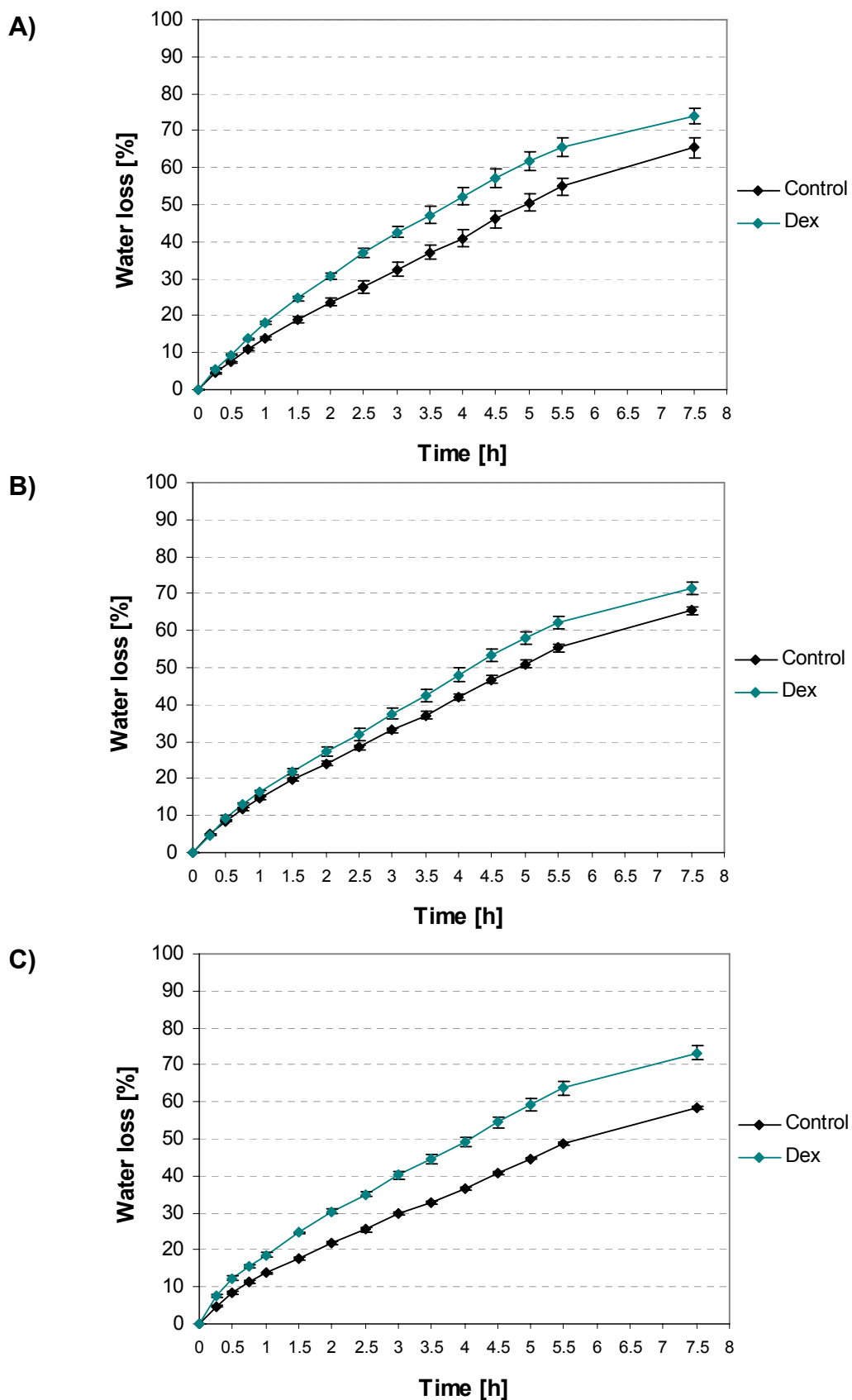


Figure 5-43. Water loss rates from whole excised DN(Slp1)-expressing shoots (48 days old grown under short day light). The cuts underneath the rosette were sealed with Vaseline. Water loss was measured over 8 hours by following weight loss. Water content was calculated as described before in % fresh weight. **A)** Water loss of DN(Slp1) line no. 1, **B)** water loss from DN(Slp1) line no.3, and **C)** water loss from DN(Slp1) line no. 6. (n=3 per treatment and genotype).

Whole plant transpiration rates of dexamethasone-induced and control-treated plants were measured in a customised environmentally-controlled chamber with set humidity, light and temperature conditions. Transpiration was followed over a time course of several days as water loss measured by putting sealed plant pots on balances inside the chamber. The humidity conditions were always kept constant either low (40% relative humidity, RH) or high (80% relative humidity) for periods of six hours at one time. Light conditions were set to the same levels and times as the ones that plants were grown previously under in the growth room (short day or long day light regimes). Alternatively, plants were measured under the described humidity conditions, but kept under constant light inside the chamber. The setup permitted two plants to be monitored simultaneously on two separate balances in the same chamber. One control-treated and one dexamethasone-induced plant were always measured in parallel. The weight of each plant was recorded every two minutes. Transpiration rates were calculated as the difference in weight between each time step normalised to the whole leaf surface area. Figure 5-44 (A) shows a typical result of a run under constant light with a control and a dexamethasone-treated DN(Slp1) plant grown under short day light until a mature stage. DN protein expression caused plants to have increased transpiration rates compared to the control treatment. This phenomenon was more pronounced in low RH conditions when transpiration rates were high. From Figure 5-44 (A) it can be seen that dexamethasone-induced plants lost approximately $0.01\text{mg}/\text{min}/\text{cm}^2$ more water than the corresponding control plants under low RH conditions. This observation was made consistently with independent transgenic lines. Figure 5-44 (B) shows an experiment with wild type plants that were treated with control spray or dexamethasone. In this case, no such difference could be observed, and the dexamethasone treated plants had even slightly lower transpiration rates towards the beginning of the experiment. In addition to the constant overall higher water loss through the transpiration stream, dexamethasone-induced plants also displayed altered kinetic behaviour of transpiration rates. This can be seen in Figure 5-44 (A) in the red curve (indicated by black arrowheads) upon transition from high to low RH. The decay of water uptake/loss followed by a relaxation phase in which stomata closed, happened actually faster than in the control curve. This phenomenon was only observed at this particular time point corresponding to 4am, when stomata started to open under their circadian rhythm. When the RH was forced down to 40% at this time point, stomatal closure seemed to be altered in the DN-expressing plants compared to the control plants. When the same treatment was repeated 12 hours later at 4pm (indicated by grey arrowheads), the closing behaviour of dexamethasone-treated DN plants resembled that of the control-treated plants.

This result in combination with the findings from the water loss measurements with excised shoots imply that dexamethasone-mediated induction of the DN(Slp1) protein affects stomatal function, both morphologically by changing chloroplast ultrastructure, and functionally by probably affecting the ability of stomata to close. Thus, the altered stomatal behaviour is probably a direct consequence of the changes in chloroplast morphology.

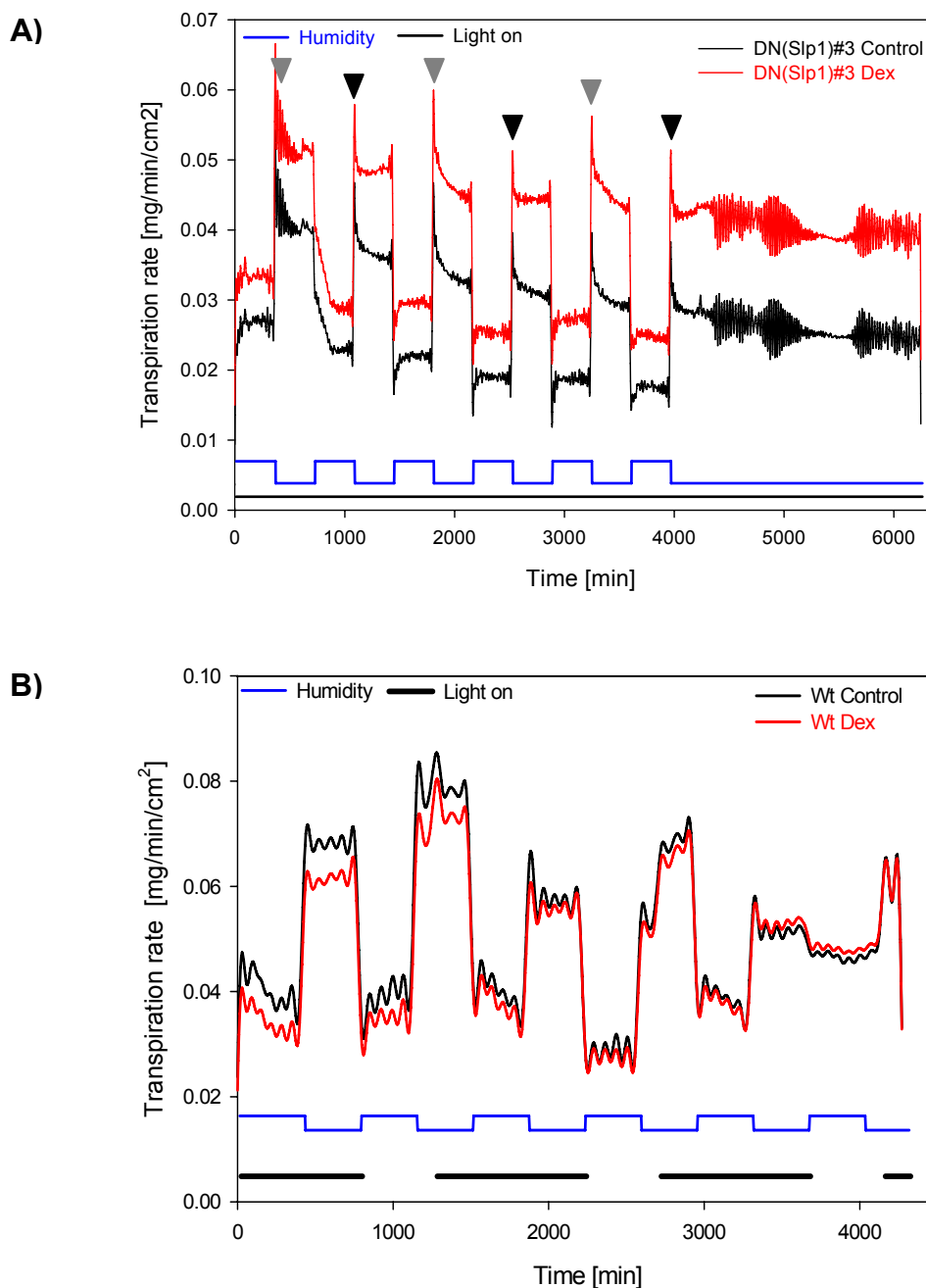


Figure 5-44. Transpiration rate measurements of DN control and induced plants.

A) Transpiration rates of DN(Slp1)#3 plants grown in short day light and treated with control solution (black line) or dexamethasone solution (red line). Transpiration rate was calculated as water loss in $\text{mg}/\text{min}/\text{cm}^2$ leaf surface area. The blue line indicates the level of relative humidity (RH) that was set either high as 80% RH (elevated level), or low at 40% RH (bottom line). The black line indicates that the light was on continuously throughout the measurement period. The temperature was kept stable at 21 °C continuously.

B) Transpiration rates measured from control-treated (black line) and dexamethasone-treated (red line) wild type plants. In this experiment the humidity changes (indicated by the blue diagram as described in (A)) were set in combination with a long day light regime (black thick line). Labelling is as above.

5.6.6 Reactive oxygen species

Because DN-expressing plants grown on soil had necrotic patches of dying tissue, the levels of ROS in these plants were investigated. Excessive ROS accumulation under stress situations can lead to cell death in the most extreme cases. Mitochondrial ROS production has been implicated in stress signalling and the triggering of programmed cell death in plants (Logan, 2006b; Logan, 2008a). One example of this type of cell death is represented by the hypersensitive response (HR) triggered in response to incompatible pathogen-host interactions. The HR is a form of programmed cell death that evolves around infection sites in an attempt to limit pathogen spread (Mittler *et al.*, 1997), (Lam *et al.*, 1999b).

The necrotic patches observed on DN Slp induced plants resembled HR-induced cell death in appearance. To investigate whether the observed cell death could be triggered by ROS or involved ROS-signalling, leaves of sprayed plants were stained with DAB as described before. Figure 5-45 shows images of DAB-stained leaves from DN(Slp1) and wild type plants that were treated with control solution or dexamethasone. DN(Slp1)-expressing plants showed indeed increased DAB accumulation compared with their control and treated wild type leaves. DAB stain was particularly intense around the leaf veins and spread into the surrounding tissue. This effect was absolutely specific for DN plants and supports the idea that DN-mediated cell death in leaves involves the formation of excessive amounts of ROS. It is likely that these ROS are produced in mitochondria rather than chloroplasts or peroxisomes in this particular situation. This would imply mitochondrial-mediated stress signalling resulting in apoptosis-like cell death, similar to HR responses.

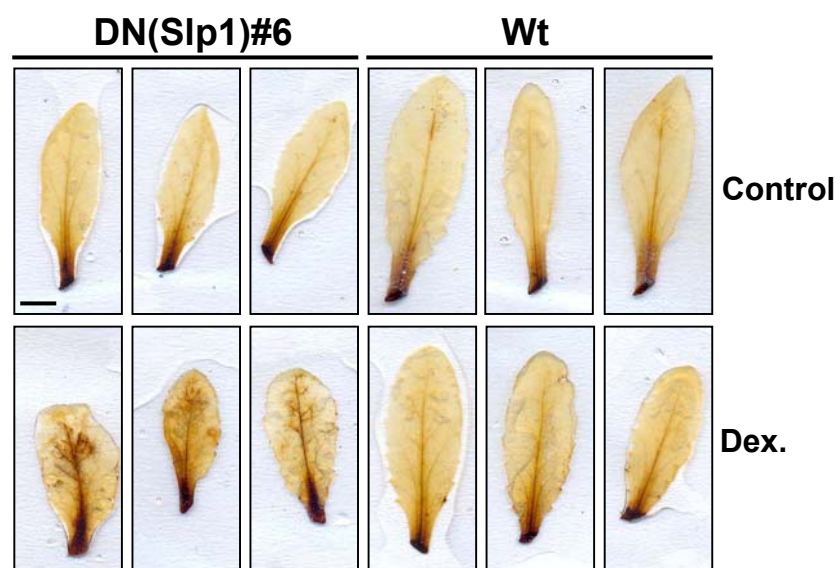


Figure 5-45. DAB-stained leaves from control and dexamethasone-treated DN(Slp1) and wild type plants. Leaves from the same relative position in the rosette were excised and stained with DAB as described before. Dexamethasone treatment caused increased stain in DN(Slp1) leaves, but not in wild type leaves. Scale bar = 1cm.

ROS levels were further investigated by quantifying H₂DCFDA fluorescence in seedling roots. DN Slp and wild type seedlings were grown hydroponically in medium supplemented with dexamethasone or control solvent. Roots were scanned in three dimensions on the confocal microscope and images reconstructed. Figure 5-46 shows examples of root stacks stained with the ROS probe. As seen in Figure 5-23, H₂DCFDA stained not only mitochondria, but also other areas around the nuclei, which could be ER. No difference in terms of fluorescence intensity was recognisable by visual inspection of the images. However, it was found that DN(Slp1)-induced seedlings had more clearly defined spots of bright fluorescence that could represent mitochondria (marked by a red arrowhead) compared to the control treatment or wild type roots. Fluorescence intensities were quantified and are presented in Figure 5-47. No statistically significant difference was found between control and dexamethasone treatments, and between wild type and DN-expressing seedlings. Uninduced DN Slp plants had overall slightly higher fluorescence than wild type seedlings. Dexamethasone treatment in wild type and DN(Slp2) seedlings caused slightly lower average fluorescence than the corresponding control treatments.

In summary, reactive oxygen species are clearly increased in leaves from soil-grown and dexamethasone-treated plants as judged by DAB staining. This strongly indicates an HR-like form of cell death triggered by high levels of ROS accumulation in leaves. By contrast, young seedlings that do not show obvious phenotypes when grown on plates or in liquid culture, do not have increased ROS levels. Thus, ROS levels correlate with leaf chlorosis and necrotic onset, leading to the observed growth phenotype of dexamethasone-induced DN Slp plants. The exact reason why this DN protein can cause such a severe phenotype is currently unknown.

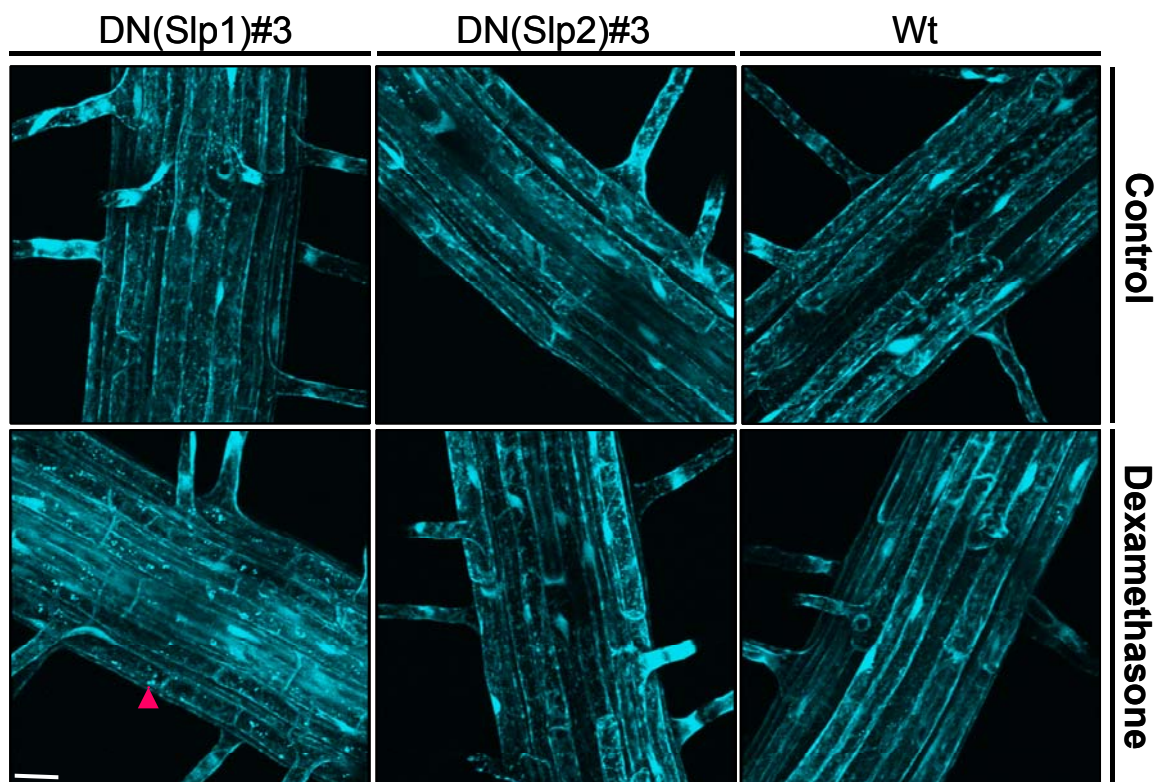


Figure 5-46. H₂DCFDA stained roots from DN Slp and wild type seedlings (grown for 5 days in hydroponic culture). The upper panel shows images from control treatments and the lower panel from dexamethasone-treated plants. The red arrowhead indicates what could be stained mitochondria. Scale bar = 20 μ m.

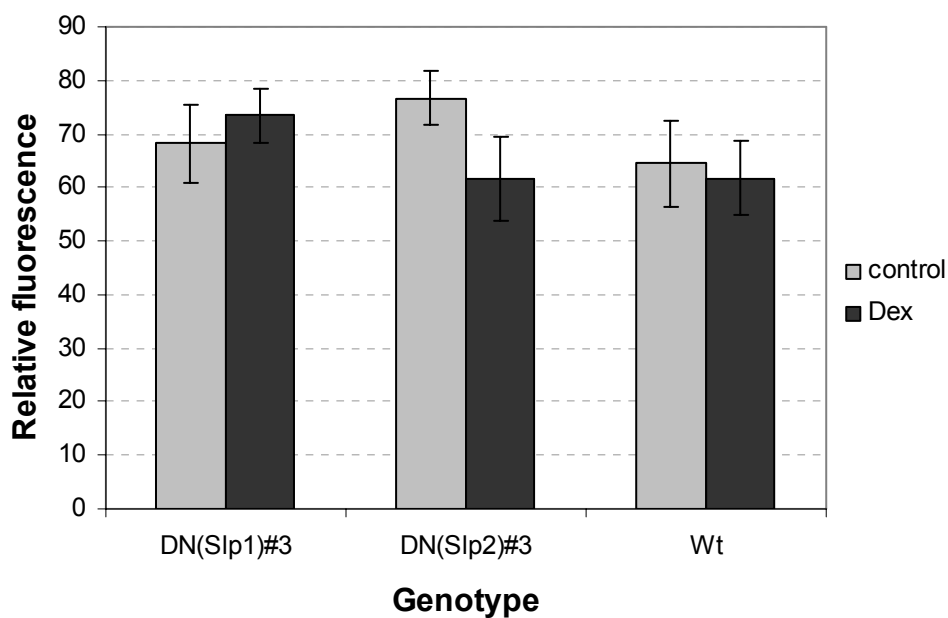


Figure 5-47. Quantified H₂DCFDA fluorescence. Relative fluorescence from the images collected in Figure 5-46. No significant difference could be detected between the treatments of one particular line or between the genotypes (t-test, n=12, p>0.05).

To investigate further the nature of necrotic patches on dexamethasone-treated DN-Slp leaves, Trypan Blue staining was applied. This stain is based on the ability of living cells to exclude this dye (= dye exclusion assay). Dead cells have damaged membranes through which Trypan Blue can be taken up and accumulates. Thus, only dead tissue can be stained. Trypan Blue staining is commonly used to detect dead tissue triggered by HR responses after pathogen attack (Vogel & Somerville, 2000). Figure 5-48 shows a series of images of Trypan Blue stained DN-Slp and wild type plants grown on soil and treated with control or dexamethasone solution. A clear difference in the Trypan Blue stained pattern can be seen between control and dexamethasone-treated plants expressing the DN protein. Leaves from control-treated plants and wild type leaves show mainly stain at the side of the cut (petiole) and occasionally in random spots spread over the leaf area. By contrast, dexamethasone-treated DN(Slp1) and DN(Slp2) plants showed more defined intensely stained spots (marked by red arrowheads) that were not visible in dexamethasone-treated wild type leaves or control treatments. These spots were clearly specific and further indicate HR-like cell death. This is supported by the notion that these spots resembled the pattern observed in the DAB stain (Figure 5-45). Thus, DN-Slp protein triggered cell death is linked to the accumulation of ROS at defined areas in the leaf (spreading around the veins) and causes cell death that resembles HR-like apoptosis. This causes a phenotype of chlorotic leaves and necrotic patches on the leaf surface and malfunctioning guard cells.

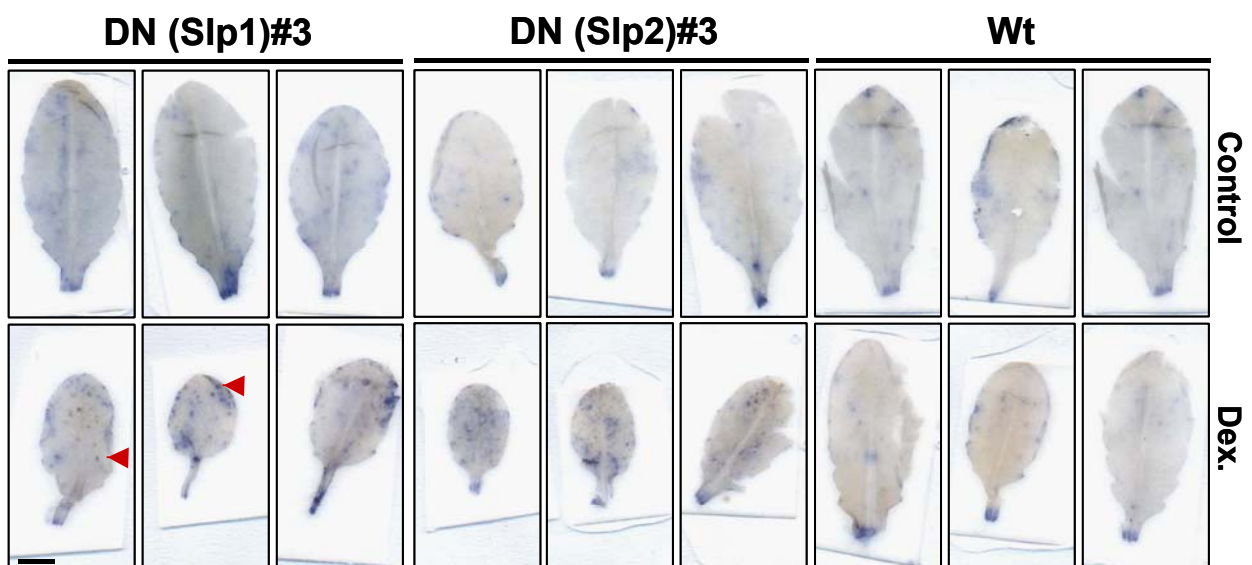


Figure 5-48. Trypan Blue-stained DN and wild type leaves from soil-grown treated plants. Leaves from dexamethasone-treated plants with visible leaf phenotypes and control leaves from the same relative position in the rosette were harvested and stained with Trypan Blue (dye exclusion assay). Dexamethasone-treatment of DN Slp plants causes Trypan Blue accumulation in distinct spots (indicated by red arrowheads) corresponding to dead tissue. These are not visible in identically treated wild type leaves. Scale bar = 1cm.

5.6.7 Mitochondrial membrane potential

To assess the function of mitochondria in DN-induced seedlings, TMRE stain was applied as described before in Figure 5-17. Seedlings were grown for three days in hydroponic culture in the presence of dexamethasone or control treatment. TMRE-stained roots were scanned on the confocal microscope and three-dimensional images were reconstructed. Figure 5-49 shows examples of TMRE-stained DN(Slp1) and wild type roots. Mitochondrial TMRE stain in these roots was overall more intense than previously observed with knockout mutants. This phenomenon is probably related to the younger age of the seedlings imaged here (three days compared to five days in Figure 5-17). Particularly root hairs accumulated high levels of TMRE in mitochondria. No obvious qualitative differences could be seen from these images between DN-expressing and wild type roots. TMRE fluorescence was quantified as described before and the result is presented in Figure 5-50. As expected from the confocal images, no statistically significant difference was calculated between DN(Slp1) control and dexamethasone-treated seedlings, or between DN(Slp1) and wild type seedlings. In the case of the DN-expressing plants, dexamethasone treatment caused a slight increase in TMRE fluorescence (from 70 to 80 arbitrary units), whereas there was a small decrease in dexamethasone-treated wild type seedlings compared to their control (from 80 to 70). This result is not surprising, because seedlings at that stage grown in hydroponic culture do not display any morphological phenotype in the presence of dexamethasone. As with ROS levels, these plants are not affected in their mitochondrial function. The DN phenotype linked to increased ROS levels is therefore tissue-, age- and growth condition-specific. Differences in TMRE fluorescence would be expected in affected DN-expressing leaves from soil-grown plants, since these leaves have been shown to accumulate ROS.

It should be also noted that this experiment was not repeated under identical conditions and therefore this result has to be independently confirmed before any final conclusions can be made. Oxygen consumption rates from DN-expressing leaves from plants grown on soil were attempted once, but gave no quantifiable results. Currently, this question is still under investigation. However, it would be expected that DN-expressing plants are affected in mitochondrial function and probably also mitochondrial morphology, especially with respect to the changed chloroplast morphology.

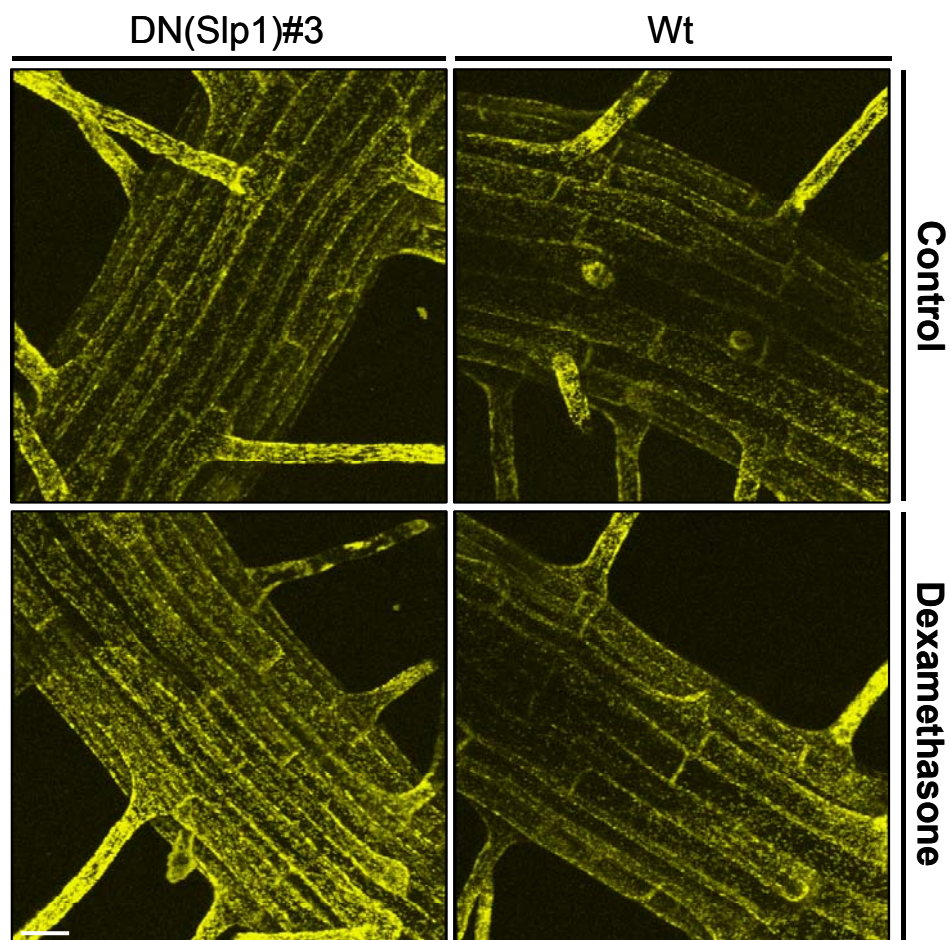


Figure 5-49. TMRE-stained seedling roots of DN(Slp1) and wild type plants. Seedlings grown for three days in liquid medium (fully submerged) were stained with 50 nM TMRE and imaged on the confocal microscope. Three-dimensional reconstructions of scanned roots are shown in this figure. Scale bar = 20 μ m.

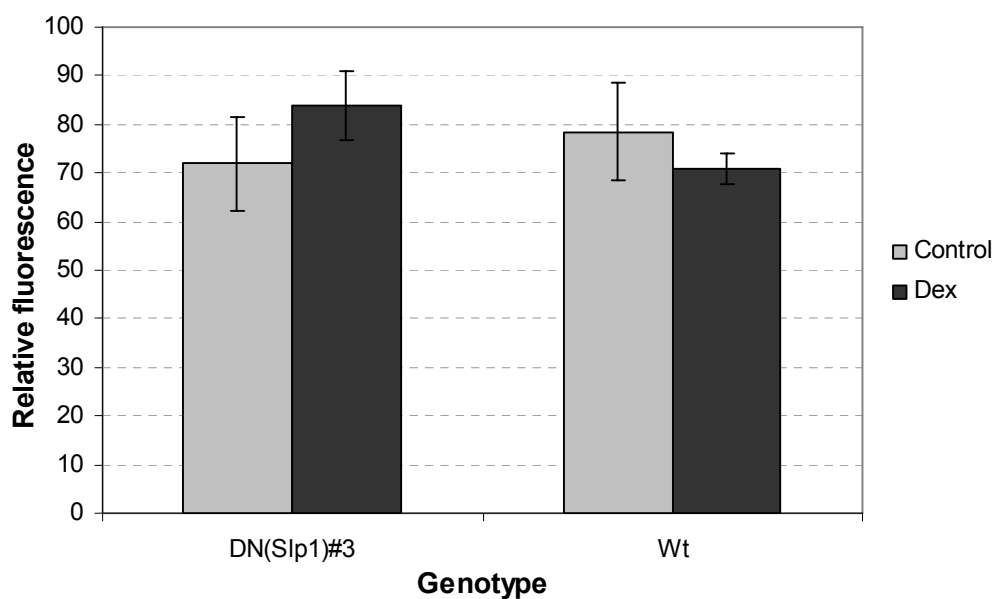


Figure 5-50. Quantified TMRE fluorescence from DN(Slp1) and wild type seedlings. No statistically significant difference could be observed between the two treatments and genotypes (t-tests, n=9).

5.7 Cross of DN(Slp1) and *slp1-1* knockout line

To further investigate the causes of the observed phenotypes in DN-Slp expressing plants, crosses were prepared between *slp1-1* mutants and homozygous DN(Slp1) plants. The rationale behind this approach was to see whether the DN phenotype would change if no endogenous Slp1 protein would be present. This way, one could test whether the proposed DN protein acts indeed on the endogenous Slp1 protein as a soluble competitor. The first generation of seeds from these crosses (heterozygous for both *slp1-1* and DN(Slp1)) were harvested, sown out on soil and sprayed with control or dexamethasone solution. Figure 5-51 shows a series of images from these plants at a mature stage (45 days old). Surprisingly, even in the heterozygous *slp1-1* and DN backgrounds the phenotypes of DN(Slp1) expression persisted and were even stronger than in homozygous DN(Slp1) lines. Dexamethasone-sprayed plants were extremely dwarfed, and cell death on leaves was even more pronounced than in DN(Slp1) plants, with entire leaves dying (top panel Figure 5-51). Despite this massive cell death, the crossed treated plants still produced flowers, although these were also dwarfed in their appearance. By comparison, control treated crosses or dexamethasone-treated *slp1-1* and wild type plants did not show such severe phenotypes (second and third row).

The observation of an enhanced cell death phenotype in heterozygous crosses of the knockout mutant and the DN(Slp1)-expressing plants was entirely unexpected. In a homozygous *slp1-1* background, the DN protein should theoretically have no effect related to the endogenous function of the Slp1 protein. However, these plants were heterozygous for the *slp1-1* insertion. Thus, protein levels of Slp1 were either as those in wild type plants, or they might have been reduced due to the knockout of one gene copy. This was not checked in these plants by Western blotting using Slp1-antibody. If a reduction in Slp1 protein levels was indeed the case, the DN effect should have been less pronounced, since less Slp1 protein would have been present. Since this was not the case, this result would indicate that the overexpression of the DN(Slp1) protein must have other pleiotropic effects that could be unrelated to the endogenous Slp1 function. In this case, it remains open why a heterozygous cross with the knockout mutant resulted in enhanced leaf cell death, unless the DN protein resulted in additional functions.

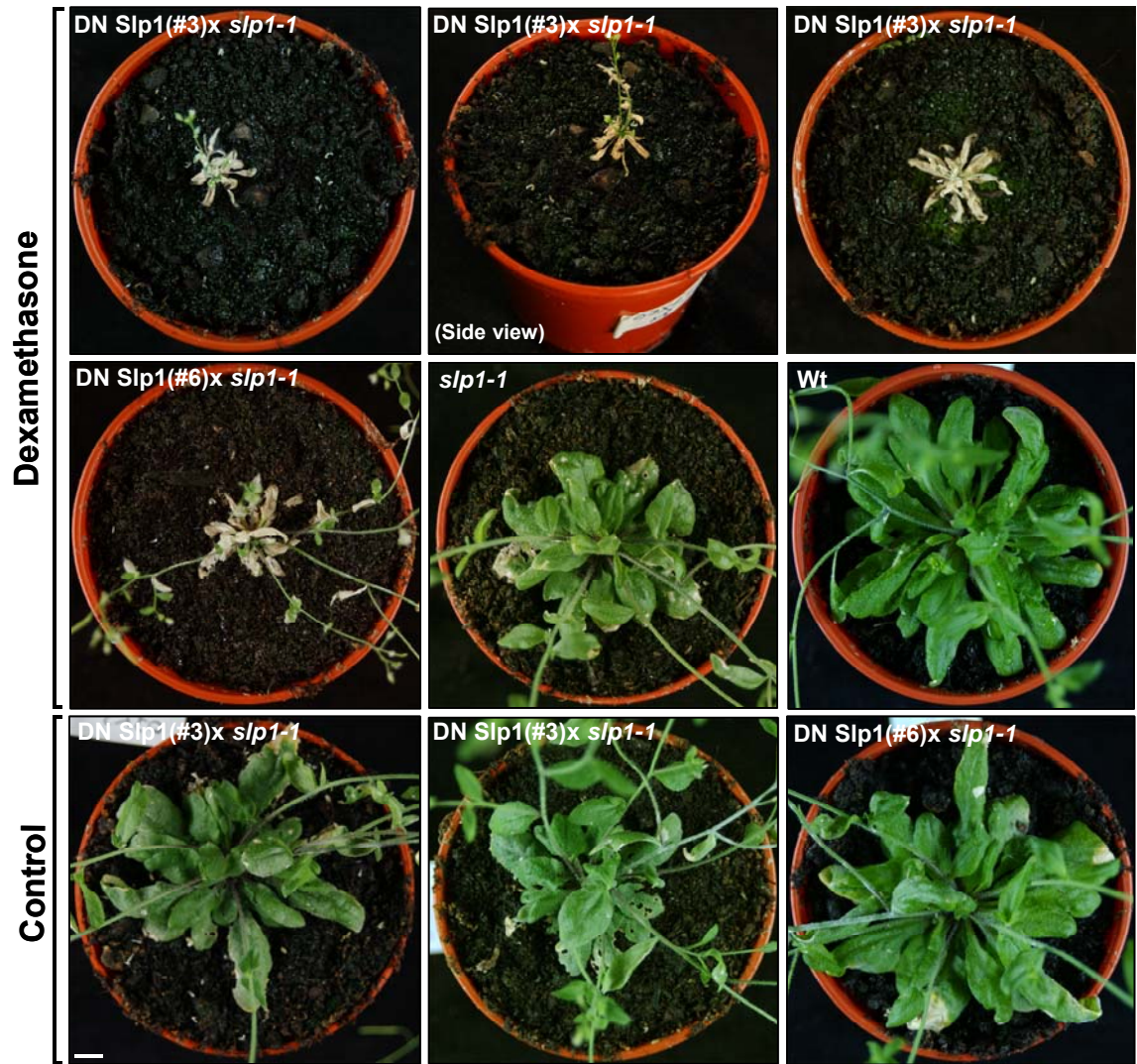


Figure 5-51. Phenotypes of crossed heterozygous DN(Slp1)x *slp1-1* lines. The first generation of seeds obtained after crossing was sown on soil. One batch of plants (lower panel) was treated with control solution, and the other batch (two top panels) were sprayed with dexamethasone. As additional controls, *slp1-1* and wild type plants were treated in parallel as indicated. The most severe phenotypes are shown in the top row (DN Slp1(#3)x *slp1-1*) of two independent crosses. Scale bar =1 cm. All images are taken from above the plants apart from the second image in the first row (indicated as side view).

5.8 Discussion

5.8.1 General *slp1* mutant phenotypes

Generally, the two knockout mutant alleles *slp1-1* and *slp1-2* share several growth-related phenotypes, but they also differ in some. Amongst the shared features are reduced seed germination, reduced root growth, reduced seed production, increased sensitivity to salinity stress and decreased levels of ROS in seedling roots compared to wild type plants. Additionally, both *slp1* alleles do not differ in the onset of flowering from wild type plants and in the rates of photosynthesis and transpiration. The two alleles differ however in shoot growth and morphology when grown on soil. Whereas *slp1-1* plants showed decreased leaf surface areas and altered leaf morphology, *slp1-2* plants resembled wild type plants in both aspects. Additionally, the reduction in mitochondrial membrane potential was only observed in *slp1-1* plants, but not in *slp1-2* plants. Indeed, *slp1-2* plants showed increased TMRE fluorescence compared to both *slp1-1* and wild type seedlings.

One explanation for the observed similarities, but also differences could be the T-DNA insertion sites. It remains to be confirmed by Southern blotting that both mutant alleles only carry a single T-DNA insertion site in their genome. The possibility remains currently that a second T-DNA insertion somewhere else in the genome might cause certain secondary phenotypes unrelated to the gene's function. Additionally, the RT-PCR in Figure 5-4 shows that small amounts of RNA are still produced upstream of the *slp1-1* insertion site. It is currently not known whether similar RNA levels are also found upstream of *slp1-2*. The *slp1-1* allele has an exon insertion, whereas the *slp1-2* allele has an insertion site inside an intron. This difference could cause accumulation and maybe even translation of RNA in one allele, but not in the other allele. Since both insertion sites lie at the 3' end of the gene, it is impossible to test for upstream protein production. No N-terminal antibody that would enable to test for the presence of the N-terminal part of the protein was available, although an effort was made to obtain specific antibodies of this kind (see chapter 3). If the observed RNA in *slp1-1* is indeed stable and even translated into a truncated Slp1 protein, this mutation would cause the expression of a true dominant-negative acting protein. This protein would probably still be imported into mitochondria since the targeting sequence is present. Thus, this T-DNA insertion could act as a recessive mutation and could cause different phenotypes from the other T-DNA insertion mutants.

Another interesting notion concerns the presence of mRNA and protein in the *slp1-3* mutant allele. This mutant has a homozygous T-DNA insertion in the AtSlp1 gene's 5'UTR which does not affect transcription (Figure 5-4). This would imply that the 5'UTR has actually no important regulatory effects on this gene's expression levels, at least not under normal growth conditions. Similarly, the *slp1-4* T-DNA insertion inside the promoter region did not cause any observable changes in Slp1 RNA or protein, and the plants were phenotypically like wild types.

All observed phenotypes with the single *slp1* knockout mutants are rather subtle and do not put severe restrictions on plant growth or fertility. The exception is the reduced or delayed growth of the *slp1-1* allele that even results in changed leaf morphology. Currently it is not known whether this reduced growth is a result of restricted cell elongation or cell division. Both scenarios could be imagined with respect to effects on mitochondrial function. Mitochondria undergo significant morphological changes before cell division takes place (Logan, 2006a), and it could well be that the single mutant could have defects in these processes. A simple cell count should yield answers to this question.

It is expected at this stage that these phenotypes are relatively mild because of a certain redundancy level between both AtSlp genes. A double knockout mutant would be expected to have more severe phenotypes, or it could putatively even be embryo or pollen lethal. Currently, the cross between *slp1-1* and the RNAi line knocking down transcription levels of Slp2 is hoped to give answers to this question. If no stronger phenotype will be observed in the proposed *slp1-1x* RNAi(Slp2) plants, the possibility of redundancy amongst other band-7 family members would be likely. In this case, mitochondrial prohibitins might take over Slp functions and partly replace these. On the amino acid sequence level, these proteins differ remarkably from Slps (chapter 3), but if the presence of the band-7 domain is required for their function, gene family redundancy could be possible.

The reason that no homozygous *slp2* mutant allele could be isolated was probably related to technical difficulties rather than lethality of such a mutant. Meanwhile, homozygous T-DNA mutants in this gene are available from the NASC. Additionally, the AGRİKOLA consortium published images of constitutively silenced Slp2 RNAi lines. Not all published lines show the same phenotype (based on the website), but a tendency towards an overall growth reduction is recognisable and was also observed with some of the dexamethasone-inducible RNAi lines here. Generally it was observed that this gene is expressed at lower levels throughout the plant (chapter 3). In addition, the overexpression of Slp2-YFP resulted in a growth phenotype consisting of reduced shoot growth with leaf necrosis

(chapter 4). Generally it is assumed that any phenotypes associated with this gene are more severe than *Slp1* phenotypes. Thus, the double *Slp* mutant is expected to have severely affected growth parameters.

The observed phenotypes of the single *slp1* mutants partly correlate with what has been observed with the dexamethasone-inducible RNAi lines of this gene. Generally, growth reduction was also observed in these plants, but it was not as consistent as in the T-DNA insertion mutant. This is probably related to differing levels of dexamethasone-mediated RNAi induction. Even when plants were sprayed almost continuously with dexamethasone when grown on soil, the achieved knockdown level of AtSlp1 was probably not as high as in the T-DNA insertion mutants. Additionally, the RNAi fragment might also have off-target secondary effects on unrelated genes.

Since AtSlps are expressed throughout the plant in all developmental stages, the variety of the observed associated growth phenotypes in *slp1* alleles is not surprising. Certain growth phenotypes such as delayed seed germination, reduced seed production and reduced root growth correspond well with the observed expression patterns as seen with the promoter GUS stains (Figures 3-33 to 3-37). With respect to the high expression levels in pollen, reduced pollen germination rates would be expected in the *slp1* single mutant, and potentially also in a double mutant. In this case, pollen might be functionally affected leading to embryo lethality and sterility.

With respect to the changed leaf morphology of *slp1-1* plants, the expression pattern of this gene offers rather little explanations. According to the GUS stains, the AtSlp1 promoter is mainly active in vascular tissue and stipules, but not spread over entire leaves when plants are grown on soil. If this gene is indeed expressed in leaf primordia and meristems, effects on the plant's ability to expand leaves could be expected. This is not immediately obvious from the promoter GUS stains, but can be deduced from data on the eFP browser (Figure 3-22).

5.8.2 *slp1* mitochondrial phenotypes

The reduction in mitochondrial membrane potential as determined qualitatively by TMRE fluorescence was only observed in the *slp1-1* mutant. The *slp1-2* mutant by contrast had even increased TMRE fluorescence compared to *slp1-1* and wild type seedlings of the same age. This difference was consistently observed over five independent experiments. This raises again the question about the specificity of either mutant allele. Assuming that both alleles have only single T-DNA insertions, this difference in the mitochondrial membrane potential would indicate additional features in one allele.

A change in mitochondrial membrane potential in roots agrees with the relatively high expression levels of Slp1 observed in this tissue (see Western blot Figure 3-41). However, it is currently not known whether *slp1-1* shoot tissue would also have reduced TMRE fluorescence. Additionally, mitochondria have different functions in roots than in leaves. Thus, it would not be surprising if the observed decrease in TMRE accumulation in *slp1-1* roots could also be tissue specific. Secondly, the decrease in TMRE fluorescence could also be linked to the age of the imaged plants. AtSlps are expressed at higher levels in seedlings, particularly from hydroponic cultures than in plants grown on soil. Therefore, effects on mitochondrial membrane potential and also mitochondrial function would be expected to correlate with the expression level of AtSlps and the activity of the plants' metabolism. Less or no effect on mitochondrial membrane potential could be expected in mature leaves from soil-grown plants. It would be very interesting to test how the mitochondrial membrane potential of pollen grains from *slp1* mutants would be affected. Since AtSlps are highly expressed in this tissue type, even larger differences in mitochondrial function would be expected.

TMRE dye does not purely accumulate in mitochondria. As mentioned in section 5.3.1, this dye is initially taken up by cells through the plasma membrane and accumulates subsequently in organelles such as mitochondria according to their membrane potential. Thus, the observed and quantified fluorescence reflects both the seedlings' membrane potential across the plasma membrane and the mitochondria combined. Additionally, the dye probably also accumulates in other organelles such as the ER. The main stain observed in seedling roots was probably localised to mitochondria, since their membrane potential has a higher negative value than that of the plasma membrane or of other organelles. TMRE is expected to accumulate eventually in the matrix and partly in the inner membrane because of the molecule's charge and solubility. A red shift in the TMRE absorption and emission spectrum can be observed upon organellar accumulation (Scaduto

& Grotyohann, 1999). A certain level of background fluorescence was however also noticed in the apoplast, and around other unidentified structures in roots.

Where TMRE was used to determine the membrane potential of animal cells, the dye was always allowed to be taken up to equilibrium before imaging. In this experiment, the incubation time with TMRE was kept relatively short (five minutes) to avoid artefacts associated with excessive labelling in non-mitochondrial membranes. The seedlings were then placed into fresh medium twice to remove excess unbound dye. Under these conditions, TMRE was sequestered rapidly into the mitochondria of the root tissues and dye accumulation could be assumed to have reached equilibrium.

In the original studies on the use of TMRE as a dye to quantify membrane potentials, it was reported that no significant self-quenching would occur upon dye accumulation (Ehrenberg *et al.*, 1988; Farkas *et al.*, 1989). However, fluorescence quenching in the mitochondrial matrix and inhibition of respiration were reported by Scaduto *et al.* (Scaduto & Grotyohann, 1999). In another report, depolarisation of the mitochondrial membrane potential by the addition of an ionophore caused an increase in TMRE fluorescence, because fluorescence was quenched inside mitochondria. When the dye was released into the cytosol, increased fluorescence was measured (Coelho *et al.*, 2002).

Despite these reports about inhibitory effects on respiration, TMRE is commonly used to assess mitochondrial membrane potential and function. TMRE has been used to determine changes in the mitochondrial membrane potential of protoplasts from tobacco cells transfected with prohibitin-silencing RNAi constructs (Ahn *et al.*, 2006). It was also used to monitor changes in the mitochondrial membrane potential in HeLa cells silenced for HsSlp2 (Hajek *et al.*, 2007). In both cases, TMRE fluorescence was significantly reduced compared to controls, an indication of a reduction in membrane potential. Decreased TMRE fluorescence in root mitochondria of *slp1-1* mutants could theoretically also reflect a decrease in the plasma membrane potential. TMRE has to be taken up initially by cells through the plasma membrane, therefore the dyes ultimate accumulation in mitochondria is also dependent on the whole cell's membrane potential. This possibility still has to be taken into account. It appears however unlikely, given the mitochondrial localisation of Slp proteins in roots.

A second possibility how *slp1-1* could account for decreased TMRE fluorescence could be related to the protein's function as a regulator of an ion channel or pump in the

mitochondrial inner membrane. This conserved feature of animal stomatins might also be a function of stomatin-like proteins of type 2.

Oxygen consumption rates

Mitochondrial pellets isolated from *slp1-1* plants had higher oxygen consumption rates than identically extracted pellets from wild type plants. To obtain as much material as possible, short day grown shoot tissue was utilised for these extractions. It has been previously demonstrated in this study that leaves of mature plants express Slp1 at reasonable levels, since this protein is normally easily detectable from this tissue on Western blots.

The calculated absolute values of oxygen consumption varied greatly between individual measurements using the same substrates. Partly these differences were probably down to the rather crude way of manual quantification used here, or to partially damaged organelles. Centrifugation steps were kept to a minimum in the isolation protocol to avoid organelle rupture.

Additionally, the values of oxygen consumption from wild type mitochondria were also far lower than those reported elsewhere for Arabidopsis mitochondria (Sweetlove *et al.*, 2002; Millar *et al.*, 2001). As already discussed, these differences are probably due to the tissue type used here, the age of the plants, and the impurity of the mitochondrial pellets. Only 25 grams of fresh shoot material was used here to extract mitochondrial pellets with an average protein content of 1-1.5 mg/ml. To improve mitochondrial yields, the preparation should be scaled up by at least a factor of two. Alternatively, oxygen consumption rates from leaf tissue should be compared to rates from young seedlings. Mitochondria from actively growing seedlings would be expected to have higher respiration rates than from mature leaves. Alternatively, it would be interesting to compare leaf oxygen consumption with that from root mitochondria. In roots, mitochondrial-produced ATP provides the main source of energy. Therefore, it is expected that oxygen consumption rates would also be higher than in leaves. Since AtSlps are highly expressed in pollen, oxygen consumption from flower tissue would be another interesting parameter to measure. The reduction in seed production is supposedly linked to reduced fertility or amount of viable pollen grains in *slp1* mutants. Pollen viability has so far not been tested, for example by viability staining. Reduced metabolic activity and viability of pollen mitochondria could be one expected outcome. Mitochondrial activity in stamen is very high, and frequently mutations that affect mitochondrial function are male sterile or

impaired in pollen production (Moller *et al.*, 2007). Based on this evidence, it could be expected that the *slp1/slp2* double mutant plant might be sterile based on dramatically reduced pollen viability.

It has been reported that crude organellar pellets obtained by differential centrifugation such as the ones used here only have a mitochondrial protein content of approximately 30%. The majority of proteins (60 %) are derived from chloroplasts, and another 10% are peroxisomal (Heazlewood *et al.*, 2004). Thus, the values calculated here are underestimates of the oxygen consumption contributed by mitochondria in the pellet, since oxygen consumption rates were normalised to the total protein content. If corrected for the actual mitochondrial content, these values are still smaller than the ones reported for mitochondria from Arabidopsis cell suspension cultures (approximately 100 nmol/min/mg for succinate and 120 nmol/min/mg for NADH with *slp1-1* mitochondria compared to 160 nmol/min/mg for mitochondria from wild type cell suspension cultures as reported by Sweetlove (Sweetlove *et al.*, 2002).

Oxidation of externally added NADH to isolated *slp1-1* mitochondria resulted in the highest oxygen consumption rates measured here (45 nmol/min/mg). In other reports, succinate was oxidised at approximately similar rates to NADH (Sweetlove *et al.*, 2002). NADH can be readily oxidised by isolated plant mitochondria by the external NADH dehydrogenase facing the IMS. If the isolated mitochondria are intact, this enzyme presents the only way of NADH oxidation, since this substrate is unable to cross the inner membrane without the necessary cytosolic factors of the shuttle systems. Thus, NADH does not rely on carrier systems to be oxidised before electrons can enter the ETC. With no added ADP, NADH oxidation is also expected to be fast because its oxidation is initially uncoupled from the translocation of protons and the dissipation of the proton gradient by the ATP synthase. If electrons are passed through ubiquinone to the AOX, no protons at all would be pumped simultaneously, and thus NADH oxidation would be entirely uncoupled from ATP synthesis. It is more likely however, that at least a part of the electron flow caused by NADH oxidation was passed to complexes III and IV and therefore resulted in the build up of the proton gradient.

Peroxisomes from leaf tissue probably contribute to the overall measured oxygen consumption. The photorespiratory C2 oxidative photosynthetic carbon cycle should be interrupted in isolated organelle extracts, but peroxisomes could still consume oxygen by the action of glycolate oxidase under the simultaneous evolution of hydrogen peroxide. Since oxygen consumption was brought to a near complete halt by the addition of cyanide

ions, it is assumed that the majority of oxygen was consumed by mitochondria in the crude organelle pellets. Finally, oxygen consumption by Rubisco in chloroplasts during photorespiration could present another pathway by which the results presented here could be obscured. Since all measurements were however carried out in very dim light, this possibility was kept at a minimum.

The addition of cyanide ions was made after the addition of substrates, ADP and SHAM to the organelle pellets. Under all conditions, cyanide stopped oxygen consumption almost completely. Since SHAM was added before cyanide, no residual AOX-mediated oxygen consumption was measured. However, as mentioned in section 5.3.2, the addition of SHAM was accompanied by an ethanol concentration of 0.6% that might have damaged mitochondrial membranes. Under these conditions, partial oxygen consumption by enzymes of the mitochondrial ETC must still have been carried out. Cyanide addition must have blocked these then completely.

In this study, no ATP was added externally to succinate-oxidising mitochondria. However, this is commonly done to fully activate succinate dehydrogenase (Sweetlove *et al.*, 2002). Additionally, the study by Sweetlove *et al.* applied five times more ADP to isolated mitochondria than in this study (0.5mM compared to 0.1mM here). The lower values observed here could also be explained by the different experimental setup.

The lack of respiratory stimulation by the addition of external ADP was observed with *slp1-1* mitochondria with all substrates tested. Wild type mitochondria responded to ADP addition with increased oxygen consumption when succinate was present, but not with NADH or pyruvate/malate. The lack of respiratory stimulation in *slp1-1* under succinate oxidation would indicate partial uncoupling of mitochondria. However, wild type mitochondria should have also responded to ADP addition when NADH was present. This lack of response could indicate that also wild type mitochondria were at least partially uncoupled through a damage of the outer membrane, or that mitochondria were already saturated with ADP and therefore did not respond to further additions. The integrity of the inner membrane should have been assessed by determination of the respiratory control index (the ratio of state 3 over state 4 respiration). This was technically difficult in these experiments, because a clear response upon ADP addition was lacking with *slp1-1*, and also wild type mitochondria. A ratio of 1 would indicate that mitochondria were uncoupled, whereas a ratio of 3 would be expected with a substrate such as malate (Moore & Proudlove, 1983). Mitochondrial intactness can also be determined by the latency of oxidation of externally added cytochrome c with ascorbate as an electron donor.

Alternatively, proton leakage could also be directly measured as a function of the membrane potential as described by Sweetlove et al. (Sweetlove *et al.*, 2006).

The increased oxygen consumption rates in *slp1-1* organelle pellets could have several reasons. Since the mitochondrial membrane potential is supposedly lower in *slp1-1* plants, proton leakage across the inner membrane might be one way of increasing, and therefore uncoupling respiration rates. In this case, the lack of Slp1 has supposedly similar effects as uncoupling ionophores (such as DNP) or UCPs. Slp1 is expected to participate in protein complexes in the inner membrane. By putatively binding to specific lipids, Slp1 might provide unique microdomains necessary for the intactness of the inner membrane. Thus, AtSlps might contribute to the inner membrane integrity as proteins that help to ensure coupling efficiency. However, they are not expected to act analogous to the UCPs by providing a pore in the inner membrane on their own. Rather, Slps could regulate the activity of proteins acting as pores or facilitating transport across the inner membrane.

Another explanation for increased respiration rates would be the upregulation of the alternative respiratory pathways. In this case too, oxygen consumption would be uncoupled from the formation of the proton gradient driving ATP synthesis. To determine whether AOX-mediated oxygen consumption differs from wild type levels, rotenone- and cyanide – resistant respiration should be measured in the absence and presence of SHAM. Upregulation of the alternative pathway has been reported for the tobacco CMSII mutant that has impaired complex I activity. In this case, H₂O₂ levels in leaves were decreased and the expression of antioxidant enzymes accordingly modified (Dutilleul *et al.*, 2003).

The HsSlp2 protein was reported to affect the stability of respiratory complexes directly in HeLa cells (Da Cruz *et al.*, 2008). In this case, effects on the activities of proteases by HsSlp2 were suggested as the reason for this phenomenon. Based on the close homology between this protein and AtSlps, a similar situation might also occur in plants. In this case, upregulation of the alternative pathways could be interpreted as a compensatory response to a lack in general ETC activity.

Since photosynthesis efficiency and transpiration rates were unaffected in *slp1-1* mutant plants (as determined under a set photon flux density of 500 $\mu\text{mol}/\text{m}^2/\text{s}$), it is assumed that the loss of Slp1 and therefore increased oxygen consumption from isolated leaf mitochondria did not affect the functionality of other organelles dramatically. It is currently not known whether photorespiration (i.e. chloroplast and peroxisome function) is affected in this mutant. Since all these organelles closely interact in leaves, effects on other

metabolic pathways (e.g. sucrose synthesis) would be expected. An interesting feature would be to measure ATP levels in *slp1-1* plants, since a proton leak would be expected to affect the amount of ATP produced by the ATP synthase. This would also hold true with respect to a putative upregulation of the alternative respiration pathway. Therefore, insufficient ATP synthesis would be expected to affect overall growth rates, particularly in organs with high ATP demands such as stamen and guard cells.

Based on these assumptions, the delayed growth observed in *slp1-1* plants is probably a result of malfunctioning mitochondrial respiratory control. It is currently not known whether *slp1-2* plants show the same respiration phenotype than *slp1-1* plants. Since plants with this allele do not grow slower to the same extent on soil, a lack in a respiratory phenotype might not be surprising. However, other shared phenotypes such as seed production, root growth and seed germination could also be affected by malfunctioning control of mitochondrial respiration. The results about increased oxygen consumption rates presented here have been obtained from just one identical batch of plants. A second independent set of measurements will be carried out to confirm these observations from plants of the same age.

Mitochondrial ROS levels

ROS levels as measured by DAB intensity did not differ in rosette leaves of mature plants between *slp1-1*, *slp1-2* and wild type plants. As outlined in section 5.3.3, this might not be a surprising finding with respect to the overall relatively low expression levels of Slps in this tissue at this developmental stage. Effects on ROS production and accumulation by loss of Slp1 would be expected in young seedlings or metabolically active tissue such as meristems or stamens. In contrast to leaves, ROS levels as quantified by H₂DCFDA fluorescence were found to be lower in young seedling roots of mutant plants compared to wild type plants. This finding would imply that mitochondrial function and ROS production might be more impaired in growing root tissue than in mature plants. Since it is not known whether oxygen consumption is affected in root tissue of seedlings, only speculations can be made about effects of *slp1* knockouts on root respiration and metabolism.

As outlined in section 5.3.3., the methods applied here to detect ROS vary greatly in their sensitivity. It would be interesting to compare ROS detected by DAB accumulation in seedlings with those found in leaves. Alternative methods to detect and quantify ROS accumulation exist, for example based on enzymatic assays or chromatographic techniques

(Hideg, 2004). These have not been made use of in this study. As an alternative approach to DAB staining of leaves, H₂DCFDA fluorescence was also attempted to be quantified from green tissue. However, imaging of leaf epidermal cells proved difficult because of high background fluorescence levels. There was a clear difference in fluorescence intensity between roots and leaves. This is probably down to ROS production by chloroplasts and peroxisomes in the light. By comparison, ROS are mainly produced by mitochondria in roots, and therefore this tissue was chosen for imaging. From the images presented in Figure 5-23 and 5-46 it can be seen that H₂DCFDA fluorescence was localised to several organelles. The size and distribution of some of them would imply stained mitochondria, but also nuclear regions were frequently intensely fluorescent, as well as cytoplasmic strands. A certain level of background fluorescence was also present in the cell walls.

With respect to the observed increased oxygen consumption rates in leaves and under the assumption that similar rates would also be observed in roots, the identified lower ROS levels are unexpected. In fact, uncontrolled electron flow through complex I and III as proposed in *slp1-1* leaves would be expected to result in increased ROS production under normal operation of the antioxidant systems. ROS in the form of superoxide anions are formed by the transfer of an electron to molecular oxygen in situations where the ETC is overreduced (Moller, 2001). The exception would be a scenario in which oxygen consumption by the AOX would be increased in *slp1-1* plants, and therefore ROS production at complexes I and III indeed reduced. As with the oxygen consumption measurements, ROS accumulation in *slp1* mutants has to be confirmed independently.

As described, mitochondrial respiration and ATP synthesis have a different significance for metabolism in root tissue than in shoots. This is related to the heterotrophic nature of roots that rely primarily on mitochondrial ATP synthesis. Mitochondria-produced ROS in leaves are nevertheless implicated to have important functions in stress situations and stress-mediated signalling, despite being secondary in terms of the overall ROS load (Moller, 2001). Stress-triggered programmed cell death is implied to be a result of mitochondrial signalling that involves the excess accumulation of ROS. If cellular antioxidant systems are overwhelmed and ROS-triggered damage of biomolecules becomes irreversible, cells might either sacrifice whole organelles or undergo a form of programmed cell death that resembles the HR (Moller, 2001; Moller *et al.*, 2007; Logan, 2008a). The function of Slps in influencing either the intactness of the inner membrane, or the activity of the alternative respiration pathways would imply that *slp1* mutants could possibly be defective in stress-mediated signalling. Therefore, the functionality of *slp1* plants under stress conditions should be investigated, for instance in response to pathogen attack with *Pseudomonas*

synringae, or under abiotic stress. Differences in the HR response would be expected and could be assayed by Trypan Blue staining. Different levels of DAB accumulation would also be expected between stressed mutants and wild type plants. *slp1* mutants have already been shown to respond differently to high salinity, a finding that would support this hypothesis. Slp proteins could also be indirectly involved in the process of replacing damaged mitochondria or affecting cell division. With respect to the known protein interaction between HsSlp2 and mitofusin-2, a role for AtSlps in controlling the ability of mitochondria to fuse or divide would be a reasonable assumption. In this scenario, AtSlp proteins could be indirectly important for the maintenance of mitochondrial function and health. This task is probably more pronounced under stress and in metabolically highly active tissues such as stamen, where ROS production is high.

In summary, the observed mutant phenotypes lead to the conclusion that AtSlps have important basic functions to support mitochondrial metabolism and health that influence the plant's ability to grow and propagate. Under stress conditions, Slps are expected to contribute to the maintenance of mitochondrial function and putatively also to the cell's ability to replace damaged organelles. With respect to cell division, Slps could have basic effects on the redistribution of mitochondria. In principal, Slps are expected to have the same basic functions in mitochondria from roots and shoots. However, the tissue-specific metabolic activity determines specific requirements of Slp levels. In situations when plants are stressed, Slp function is expected to affect the mitochondria's ability to limit and repair damage.

5.8.3 DN-Slp growth phenotypes

The expression of dominant-negative Slp truncations caused several growth-related phenotypes in plants grown on soil. Leaves were severely affected in their ability to expand. As a result, they curled up and showed a helical growth phenotype. In addition, leaves became prematurely senescent and displayed chlorosis, and flowers differed in shape. Interestingly, these growth phenotypes could only be observed when plants were grown in air on soil, but not when they were kept under high humidity on agar plates or in hydroponic culture. This observation was made independently of the DN expression level as confirmed by Western blotting. Thus, these phenotypes were conditional for these particular growth conditions. Putatively, the difference in transpiration and concentrations of CO₂ and O₂ played a role in the development of these phenotypes. When grown under sealed conditions, seedlings are expected not to transpire since the humidity levels are

saturated. Thus, transport processes as well as photosynthesis rates must be affected under these conditions.

It was anticipated that DN-Slp phenotypes would be observed related to the endogenous function of AtSlps. However, since it became clear that AtSlps are actually localised to mitochondria, effects on Slp function by DN proteins are questionable. Most importantly, DN-Slps were designed as soluble competitors that would interfere with proteins facing the cytosol. Since AtSlps are clearly not localised to the mitochondrial outer membrane facing the cytosol, such effects are not easily credible. Both DN-Slps lack the mitochondrial targeting sequence and should not be imported into mitochondria on their own, even in the presence of the N-terminal myc tag. The result from Figure 5-30 demonstrates localisation of DN-Slps to the cytosol, but also to membranes that could be derived from organelles such as mitochondria. The cytosolic part of DN-Slp proteins could however still interact with the endogenous proteins on their import pathway to mitochondria. Currently this would provide one explanation of any specific effect by DN Slps on native Slp function. If Slps indeed oligomerise via their C-terminus, DN versions might bind to the full length proteins and hinder their mitochondrial import via prevention of unfolding. In this scenario, no or reduced amounts of Slp protein should reach mitochondria and would result in a loss-of-function plant. However, since the *slp1* knockout plants do not have the same phenotypes, this scenario seems unlikely. Theoretically, membrane binding of DN-Slp proteins could also be mediated by other unrelated proteins that the DN versions could bind to. Another possibility would be that DN-Slps unspecifically bind to other band-7 family members localised throughout the cell. The DN proteins still have a partially intact band-7 domain and might therefore interfere with band-7 family proteins at locations where only one specific member would normally act.

The remaining part of DN-Slps bound to membranes could indeed originate from mitochondria. One scenario might be that the DN versions bind to endogenous Slps and are imported as partly unfolded complexes. This way, DN proteins would localise inside mitochondria where they could have specific effects on Slp function. This possibility could be tested by checking for the presence of myc-tagged DN protein in isolated mitochondria of dexamethasone-induced DN plants. Currently it is not known whether this is the case.

The treatment of DN-expressing seedlings with the palmitoylation inhibitor BPA did not result in complete protein solubility as it was anticipated. This could either be related to incomplete palmitoylation inhibition by externally added BPA, or by the fact that the DN proteins' ability to bind to membranes is mediated by other means than palmitoylation.

From the Western blot in Figure 5-32, the DN protein appears to be more, but not completely soluble upon BPA addition. Since no palmitoylated marker protein was used to assess the level of palmitoylation inhibition, it is currently not possible to relate the increased DN solubility with certainty just to a lack of palmitoylation. This result only indicates that the DN protein could partly be membrane-anchored via S-acylation of the conserved cysteine residue. All seedlings grown on MS agar plates supplemented with BPA showed severe growth reductions, particularly affecting roots. From the photographs in Figure 5-31 no obvious difference between DN seedlings grown on BPA, or on BPA and dexamethasone could be seen. Thus, the increased solubility of the DN protein did not result in further growth reduction of seedlings. Because Slp proteins are putatively important for root growth, such a finding would have been expected if the DN proteins were S-acylated and had specific effects on Slp proteins. It could therefore be assumed that the soluble fraction of DN-Slps probably causes the growth phenotypes observed on soil.

The assumption remains that at least a part of the observed phenotypes in dexamethasone-treated plants is probably caused by unspecific side effects of cytosolic DN-Slp protein. Dexamethasone treatment on its own also affected some properties measured in wild type plants compared to their control treatments. For example, dexamethasone-treated wild type plants also flowered slightly earlier than control-treated plants. Dexamethasone treatment also affected stomatal density in older leaves of long day grown plants, and decreased the water content of short day grown plants. Most of these observations were not statistically significant, but they nevertheless demonstrate that dexamethasone-treatment per se has certain effects on plant physiology. When applied to MS agar plated, plants grown in the presence of dexamethasone consistently appeared larger than their controls. Dexamethasone is a steroid-derivative and could as such have multiple effects on plant metabolism. Sterols in general were reported to have metabolic effects that are unrelated to transcriptional modification in animals (Losel *et al.*, 2003). The original publication of this vector system did not state any observations like the ones made here about dexamethasone treatment. To better control for the effects of dexamethasone in this vector system, transgenic plants were created that contain the empty pTA7002 T-DNA. This way, any phenotypic effects contributed by the expression of the GVG transcription factor can be controlled. With heterozygous pTA7002 plants, no obvious growth phenotypes have been so far observed, at least not any that would resemble phenotypes of DN-Slp plants. No images of these plants treated with dexamethasone were included in this thesis because transformants were not available at the time when images of the DN-expressing plants were taken.

Since both DN(Slp1) and DN(Slp2) plants have virtually the same phenotype, the question of specificity amongst these two truncated proteins arises. Generally, DN(Slp2) overexpression caused phenotypes that were slightly more severe than those observed with DN(Slp1) plants. This correlates with the assumption that AtSlp2 is naturally lower expressed, and that its overexpression with YFP under the constitutive promoter caused a growth phenotype resembling the DN(Slp2) phenotype in some respects (lesions for example). Assuming that both AtSlps interact and act in a complex, the expression of either DN version would be expected to affect the function of both proteins. It also has to be kept in mind that both DN-Slp proteins are highly similar around the band-7 domain, and differ only in the C-terminal end. Thus, the identical features could interfere with other similar band-7 family proteins and cause the same effects.

5.8.4 DN-Slp effects on guard cells

The expression of the DN proteins is expected to affect every plant tissue in which the 35S promoter driving the GVG expression is active. Leaves of DN-Slp expressing plants had specific phenotypes affecting guard cells. In independent lines it was consistently found that guard cell chloroplasts were enlarged and had less chlorophyll autofluorescence than those from control-treated plants. It is assumed that the organelle enlargement is caused by changes in their thylakoid ultrastructure. Mitochondria are also expected to have altered ultrastructures in these cells. Chloroplast enlargement was only observed when treated leaves started to become chlorotic, and it specifically affected mature guard cells. This phenotype rendered guard cells less functional and probably lead to the observed increase in water loss and whole plant transpiration compared to control plants. It is assumed that guard cells with enlarged chloroplasts were impaired in stomatal closure, but this needs to be confirmed independently by direct aperture measurements. In addition to guard cells, DN expression could also affect transpiration through growth defects in other tissues. For example, water uptake by roots could be altered, as well as water transport through defects in xylem structure.

This specific effect on guard cell functionality was probably a secondary effect of DN-Slp protein expression. It is currently not assumed that endogenous Slp proteins affect transpiration and guard cell function per se (Figure 5-16). In relation to this, AtSlp transcripts were identified in guard cells (chapter 3 section 3.5.1.2), and the AtSlp1 promoter was actively driving GUS expression in hydroponically-grown seedlings (Figure 5-33), but not in leaves from soil-grown plants. Since guard cells have specific metabolic demands and higher numbers of mitochondria than mesophyll cells for example (Taiz &

Zeiger, 2002), (Zeiger *et al.*, 2002), the observed changes in behaviour probably underlie general DN effects on organelle metabolism. If DN proteins indeed disturb the function of endogenous Slps inside mitochondria and change mitochondrial metabolism, guard cell-specific effects would not be surprising. The guard cell phenotype is unlikely to be the primary cause of the observed leaf necrosis and senescence. Currently it is assumed that the reverse is the case; once leaves become chlorotic, altered guard cells can be observed. It is also unlikely that the increased transpiration rates of DN plants are the direct cause of the ongoing cell death. Rather, the increased water loss by leaves could enhance cell death.

The observed leaf cell death involves the excessive accumulation of ROS, pointing towards a form of stress-signalling mediated pathway that involves mitochondrial ROS production. Clusters of dead tissue patches as visualised by Trypan Blue staining indicate hot spots of ROS-mediated cell death. It is currently not clear whether more ROS are produced overall because of a malfunctioning mitochondrial ETC and then not sufficiently scavenged. ROS probably also accumulate from malfunctioning chloroplasts, or a combination of both organelles.

The swelling or enlargement of chloroplasts has been linked to stress responses before. For example, repeatedly drought-stressed cotton plants developed swollen chloroplasts with enlarged starch granules (Ackerson & Hebert, 1981). Effects on chloroplast morphology were also reported in response to other abiotic stresses, including salinity (Izawa & Good, 1966; Abdelkader *et al.*, 2007), cold acclimation (Stefanowska *et al.*, 2002), and heat (Holzinger *et al.*, 2007). Arabidopsis mutants of the gamma subunit of the plastid ATPase were seedling lethal and had swollen thylakoids under illumination with increased proton concentrations in the lumen (Dal Bosco *et al.*, 2004). The maize mutant *lls1* encodes a chloroplast protein and was reported to have swollen and distorted chloroplasts. This mutant also developed light-induced lesions (Gray *et al.*, 2002). Overexpression of the proapoptotic mammalian Bax protein in Arabidopsis under the control of the dexamethasone-inducible promoter caused plant cell death through the destruction of organelles (Yoshinaga *et al.*, 2005). Bax is known to associate with the mitochondrial outer membrane where it is targeted to by its C-terminus. It has several effects on mitochondria-mediated apoptotic signalling such as the release of cytochrome c (Lam *et al.*, 1999a). The observed phenotypes upon Bax expression were actually remarkably similar to the phenotypes described for DN-Slp expressing plants. Bax-expressing leaves developed leaky chloroplasts with loose lamellae and misshaped, rounded mitochondria. Mitochondria also stopped movements and aggregated. Leaves of dexamethasone-treated seedlings became chlorotic only when plants were kept under light. All of these

observations were made in mesophyll cells from seedlings grown on MS medium. The authors did not comment on changes of organelles in guard cells. The overall high similarity of phenotypes between Bax-expressing and DN-Slp expressing plants indicates a common underlying reason for the observed cell death that involves the accumulation of ROS and the interruption of organellar function. The exact reason for organellar damage by DN-Slp expression is unknown. It is proposed in the case of DN-Slp-mediated cell death that guard cells are particularly vulnerable to these changes because of their metabolic demands and are therefore the earliest indicators of organellar damage. To confirm these assumptions, organellar ultrastructures should be imaged by electron microscopy. Additionally, mitochondrial marker dyes or mitochondrial-targeted GFP could serve as markers to assess the size and distribution of these organelles in DN-expressing leaves and guard cells. Mitochondrial activity as judged by TMRE or MitoTracker DeepRed could be compared to the overall mitochondrial mass determined by staining with MitoTracker Green, a dye that accumulates in mitochondria regardless of their membrane potential.

5.8.5 Effects of DN expression on ROS production

The expression of DN-Slps in leaves caused leaf necrosis and cell death after prolonged dexamethasone treatment. This phenotype was leaf specific, and mainly associated with rosette leaves. According to the levels of DAB polymerisation in DN-expressing plants, the observed changes involve the production and/or accumulation of ROS in these organs in the light. So far it has not been determined whether the same changes also occur when plants are kept in darkness. Should these changes be light-specific, the assumption is likely that excessive ROS are formed in malfunctioning chloroplasts and putatively also peroxisomes during photosynthesis and photorespiration. It is currently not known how the DN protein could directly affect the functioning of the chloroplast and also mitochondrial ETCs implicated in ROS generation. Putatively it can also not be excluded that the antioxidant systems of these organelles could also be malfunctioning and thus further support ROS accumulation. The DAB stained pattern on leaves indicates ROS accumulation in tissue around the central veins that appears in distinct punctae. This is also the place where leaf necrosis started when plants were sprayed after the flower transition (Figure 5-35). Trypan Blue staining also detected distinct punctuate patches of dead cells spread all over the leaves of dexamethasone-induced DN plants. These observations strongly support the idea of locally-triggered ROS mediated cell death that is probably linked to organellar damage in a HR-like fashion. HR responses are triggered by attack of

incompatible pathogens and involve localised forms of programmed cell death to limit pathogen spread (Mittler *et al.*, 1997).

ROS accumulation and cell death were observed to be leaf-specific in soil-grown plants. Accordingly, no enhanced ROS accumulation was observed in seedling roots. With respect to the higher Slp expression levels in roots and the importance of root-produced mitochondrial ROS, this is a surprising finding. This result correlates however with the absence of any obvious growth phenotype under these conditions in dexamethasone-treated seedlings. In accordance with the lack of increased ROS and a growth phenotype in seedling roots, the mitochondrial (and other) membrane potentials were also unchanged. TMRE fluorescence intensities were not significantly different in dexamethasone-treated seedlings from their controls. In contrast to the absence of ROS-related phenotypes in seedlings, it would be expected that oxygen consumption rates of mitochondria isolated from DN-expressing leaves from soil would be impaired. The higher leaf ROS levels and the probably swollen organelle structures would support this assumption.

The question remains open how the DN protein can have such profound effects on organelle function and whether any of these effects are related to the endogenous Slp function. Currently it is not known whether the DN protein is targeted to mitochondria at all. At least a good proportion of overexpressed DN is clearly cytosolic, and it can only be speculated whether the protein could affect Slp function by interfering with mitochondrial import. Ideally, a protein-protein interaction between full length Slp and DN-Slps should be demonstrated at least *in vitro*. The observed DN effects could also relate to a prevention of Slp oligomerisation by DN-Slps in mitochondria. This way, Slp-provided microdomains or protein complexes might not assemble correctly and therefore directly affect the function of other inner membrane proteins.

Another question relates to the severity of the dominant-negative phenotype versus the relatively mild phenotypes of *slp1* single mutants. One explanation might be given by the fact that either DN-Slp can target both endogenously expressed Slps simultaneously. It will be interesting to compare the DN phenotype with the expected *slp1-1/RNAi(Slp2)* phenotype.

In summary, this chapter provided evidence for Slp functions in the plant at various developmental stages. All phenotypes observed correlate at least partly with the observed expression patterns of these genes as described in chapter 3 (such as during seed imbibition, seedling growth under certain types of stresses and pollen development). A

picture emerges in which Slps putatively provide and support the necessary conditions under which mitochondria operate upon increased demands on metabolism. Slp proteins are implicated to have important functions upon damage of mitochondrial function by increased stress or in the presence of cytotoxic stress reagents (UV-B irradiation, cycloheximide treatment) and when mitochondria need to regenerate.

6 General Discussion

6.1 Summary of main results

The Arabidopsis band-7 family consists of 18 members that belong to the prohibitins (8 proteins), the stomatins (2 proteins), the flotillins (3 proteins) and erlins (1 protein), and proteins upregulated in the hypersensitive response (4 HIR proteins). Within this family in Arabidopsis, stomatin-like proteins are most closely related to the HIR proteins, despite different subcellular localisations and structural diversities. Within the band-7 family from plants and other species, the Arabidopsis proteins are highly homologous to stomatin proteins of type 2 from human, mammals and certain fungi. This homology is also reflected on the sequence level despite the large evolutionary gap between humans and plants. The proposed structure of AtSlp proteins (based on secondary structure predictions) is also remarkably conserved to other stomatin-type proteins. These proteins are generally not membrane spanning. The AtSlp genes arose by a gene duplication event that could have taken place in an ancestor of dicotyledon plants. Arabidopsis Slps are mainly expressed at high levels in young seedlings and in specific organs of mature plants with high metabolic demands. These include the shoot apex, imbibed seeds and developing pollen. On the transcript level, AtSlps are highly upregulated upon cytotoxic stress treatments. Presumably, these treatments could affect mitochondrial function by disturbing the protein composition of the electron transport chain.

Arabidopsis stomatin-like proteins possess mitochondrial targeting sequences as amphipathic alpha helices. These are presumably cleaved off following mitochondrial import, although no corresponding cleavage products are detectable on Western blots of protein extracts. Mitochondrial localisation of AtSlp1 was confirmed biochemically and *in vivo* in a variety of cell types, amongst them guard cells. Overexpression of AtSlp2 as a fluorescent fusion protein under the constitutive 35S promoter resulted in an early senescent phenotype and dwarfed plants. *In vitro* crosslinking studies of Slp1 indicate that this protein exists as a homodimer, or in a complex with other proteins, putatively Slp2. Slp1 was confirmed to be a peripheral, but firmly attached membrane protein. Putatively, this protein could be post-translationally modified by S-acylation of a single conserved cysteine residue *in vivo*. The physiological significance of this modification could be related to Slp localisation to lipid microdomains in the inner mitochondrial membrane. AtSlp proteins could play an active role in the formation of such domains in mitochondria.

Two isolated T-DNA insertion lines resulted in loss-of function mutants. These two alleles gave overlapping, but also diverse growth phenotypes. The *slp1-1* allele gave a phenotype of delayed shoot growth in plants grown on soil. Leaves from these plants also had elevated osmolarity levels and reduced water contents. Plants from both knockout alleles had delayed seed germination rates, reduced growth of seedling main roots, they produced less seeds than wild type plants, they were more sensitive to salt treatment and produced less reactive oxygen species in seedling roots compared to wild type plants. On the mitochondrial level, *slp1-1* allele plants had a reduced mitochondrial membrane potential in seedling roots, whereas *slp1-2* allele plants had an elevated mitochondrial membrane potential. Isolated leaf mitochondria from plants carrying the *slp1-1* allele had higher oxygen consumption rates than wild type mitochondria, and these could not be stimulated by the addition of ADP. These findings indicate that lack of the Slp1 protein at the inner mitochondrial membrane could lead to proton leakage and therefore affect inner membrane integrity. Additionally, the alternative respiration pathway involving oxygen consumption by the alternative oxidase could be altered in *slp1-1* plants.

Overexpression under the dexamethasone-inducible promoter of Slp protein fragments designed as dominant-negative proteins resulted in the development of a severe growth phenotype in soil-grown plants. Dexamethasone-induced plants had curled leaves, a reduced stature and early leaf senescence with patches of dead tissue. Leaf cell death was accompanied by the accumulation of ROS and thus resembled HR-like programmed cell death. Elevated ROS levels were absent from roots of young seedlings. Young seedling roots were also not affected in their mitochondrial membrane potential. Leaves of DN-Slp overexpressing plants had elevated osmolarity levels and a guard cell phenotype with enlarged chloroplasts. These changes in organelle structure and the overall growth phenotype resembled phenotypes of plants overexpressing mammalian Bax protein (Yoshinaga *et al.*, 2005). Guard cells of these plants were impaired in their function, affecting transpiration rates and the shoot water content.

6.2 General functions of AtSlp proteins

AtSlps are ubiquitously expressed in most organs during plant development. High protein expression is specifically associated with certain organs and developmental stages. Generally, AtSlps localised to mitochondria are assumed to affect plant growth through effects on mitochondrial metabolism required for growth. This assumption correlates at least partly with the observed tissue-specific high expression levels in developing flowers,

during seed imbibition and in seedling growth. On a cellular level, pollen development and guard cells in particular have high metabolic demands and accordingly express high levels of AtSlps. The overall respiration activity is dependent on the tissue type and the developmental stage (Taiz & Zeiger, 2002; Moller, 2001).

Some of the phenotypes associated with *slp1* knockout alleles also agree with a proposed function related to increased metabolic demands. Accordingly, both *slp1* alleles have a delayed seed germination phenotype, decreased root growth and fertility and are more sensitive to salt treatment than wild type plants. For example, mitochondria are known to undergo morphological and metabolic changes during seed imbibition in relation with their biogenesis (Logan *et al.*, 2001). So far, only single knockout insertion lines of one Slp gene were available. It is regarded as likely that an *slp1/slp2* double knockout mutant would not be viable because of male gamete sterility. AtSlp function in relation to mitochondrial function is probably specifically required in pollen development. Therefore, pollen from a double mutant plant might be infertile.

Additionally to these basic metabolic changes during plant development, AtSlps are putatively also important for metabolic changes in response to certain, but not all stress situations. These are commonly known to put increased demands on the mitochondrial electron transport chain, leading to the increased production of reactive oxygen species. Amongst several stresses tested, a clear correlation was observed in both *slp1* alleles in response to salt stress. Other stresses that were found to upregulate Slp transcript levels did not specifically affect *slp1* plant phenotypes. For example, irradiation with UV-B light did not result in different growth phenotypes between knockout and wild type plants (results not shown). Interestingly, both *slp1* alleles had reduced levels of overall ROS in seedling roots. However, ROS production in mutant and wild type plants was not assessed during stress situations or in illuminated leaf tissue.

Stomatin-type proteins are commonly involved in the formation and/or anchorage of lipid microdomains. This feature was so far only demonstrated for plasma membrane-localised stomatins. This property appears generally specific for stomatins and flotillins, but remains to be demonstrated for prohibitins. Scaffolding of microdomains and anchorage to the cytoskeleton and membrane-embedded proteins has been suggested in independent studies to be the main function of stomatins (Salzer & Prohaska, 2001b; Umlauf *et al.*, 2004). So far, the question remains open whether this concept can be adapted for the function of stomatin-like proteins inside mitochondria. Lipid microdomains have not been described from mitochondria or chloroplasts yet. However, there is no obvious reason why inner-

organellar membranes would be an exception from this concept. In particular, the mitochondrial inner membrane is generally highly organised. Large protein complexes accumulate at specific sites of energy production to facilitate substrate-channeling between enzymes for efficient metabolism (Ferne *et al.*, 2004). Mitochondrial microdomains could differ in their lipid and protein composition from plasma membrane rafts (as described by insolubility in Triton-X100 at low temperatures). Evidence from work presented here only shows that a small fraction of the total AtSlp1 pool is insoluble in Triton-X100. Possibly these microdomains are not enriched in sterols, but they might constitute other lipid types and contribute to the enrichment of certain proteins at specific sites. In this way, AtSlp proteins might regulate the formation and stability of inner membrane embedded protein complexes. Analogous to the function of HsSlp2, this could also involve the regulation of a membrane-bound protease of the AAA type. Thus, a part of AtSlp function is probably to provide specialised scaffolds at the inner membrane. Putatively, specific lipids are recruited through the band-7 domain that aid the integrity of the inner membrane. This way, AtSlps contribute to the coupling efficiency of mitochondria.

Human Slp2 is the only studied member of the subgroup of Slp proteins of type 2 (or “paraslipins”)(Green & Young, 2008). Functional similarities between AtSlps and this protein are expected based on the close homology. HsSlp2 interacts with human prohibitins in the inner membrane and regulates the activity of a protease. Additionally, HsSlp2 is implicated to function in mitochondrial fusion via interaction with an outer membrane GTPase (Hajek *et al.*, 2007). Interestingly, HsSlp2 is also overexpressed in the early stages of certain human cancers. This appears to be correlated to the cell cycle stage, which in turns affects the distribution and function of animal cell mitochondria. These are known to undergo massive fusion events prior to cell division, followed by redistribution and mitochondrial fission. In plants, mitochondria are generally organised differently from animal cells, but nevertheless undergo similar events after cell division in protoplasts (Logan, 2006b; Logan *et al.*, 2003). Additionally, plant mitochondria are proposed to be divided into subgroups that have specific functions to meet metabolic demands and to maintain DNA replication and repair. Based on the proposed functional homology between AtSlps and HsSlp2, a similar role for the plant proteins would be expected in mitochondrial fusion, redistribution and maintenance of metabolism that accompanies cell division. Analogous to animal cells, a GTPase would be expected to interact with one of the Slp proteins in Arabidopsis. Mammalian mitofusins do not have direct homologues in Arabidopsis mitochondria. A similar GTPase (Fzo) however exists in the chloroplast outer membrane (Gao *et al.*, 2006). The fusion machinery of plant mitochondria is largely unknown (Logan, 2003; Logan *et al.*, 2003).

In summary, the functions of AtSlps are putatively governed by the state of the cell cycle affecting mitochondrial morphology and metabolic functions. They are highly expressed in specialised cells that undergo metabolic changes and cell division, such as guard cells and developing pollen. Figure 6-1 shown underneath represents a proposed model summarising the functions of AtSlps in the mitochondrial inner membrane according to homologies with human Slp2.

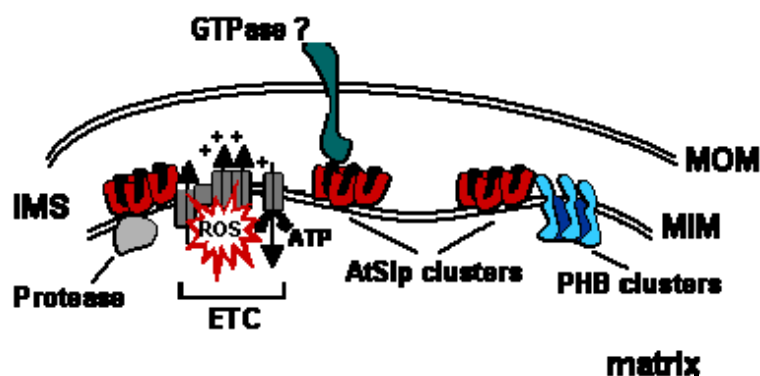


Figure 6-1. Proposed model for AtSlp function in the mitochondrial inner membrane. AtSlp1 (red) and AtSlp2 (black) assemble into hetero-oligomers that face the intermembrane space (IMS). They are anchored to the mitochondrial inner membrane (MIM) by their hydrophobic N-terminus and putatively S-acylation. The hetero-oligomers form clusters that recruit specific lipids and protein complexes. Amongst these are parts of the electron transport chain (ETC) and prohibitin clusters (shown in blue). Analogous to the function of HsSlp2, AtSlp clusters might stimulate the activity of a membrane-bound protease (shown in grey) that affects stability of inner membrane proteins. A GTPase located in the outer membrane (MOM) might also interact with AtSlp clusters which has a putative impact on mitochondrial fusion and morphology during the cell cycle.

Arabidopsis Slp1 and Slp2 are proposed to be at least partially redundant and to exist as a heterooligomeric complex in the inner membrane. Analogous to the situation in human cells, prohibitins might also be a part of an Slp containing protein complex. It is interesting to note that stomatin-like proteins of type 2 and prohibitins share the same subcellular localisation of all band-7 proteins in plants and mammals. Prohibitin-related phenotypes in Arabidopsis (Van Aken *et al.*, 2007) resemble partly those described for AtSlps in this study. Putatively, Slps and prohibitins complement each other functionally and might be partially redundant. This suggestion only partly agrees with the published tissue expression pattern of Arabidopsis prohibitins of type I. For example, AtSlp promoters were not active in root apices as PHBs are. However, AtSlps and PHBs probably contribute to leaf expansion and tissue growth in general. Thus, functional complementation of AtSlps and AtPHBs might be restricted to certain tissues and developmental stages.

Arabidopsis Slps are suggested to interact and to form a higher protein complex in the inner membrane. This might occur similar to the assembly of mammalian PHB1 and PHB2 into a large complex built out of smaller heterooligomeric units. The reported molecular weight of HsSlp2 protein complexes in mitochondria (1.8 MDa (Reifschneider *et al.*, 2006)) is similar to those of mammalian prohibitin complexes (1.2 MDa (Tatsuta *et al.*, 2005)). The concept of heterooligomerisation of AtSlp1 and AtSlp2 proteins is also supported by their identical tissue expression pattern. The appearance of an FA crosslinked AtSlp1 complex that could be a heterodimer consisting of AtSlp1 and AtSlp2 also supports this hypothesis. In its crosslinked form, the smallest AtSlp1 band on a Western blot is as large as a homo- or heterodimer. AtSlp2 is generally expressed at lower levels than AtSlp1 and could have a regulatory or otherwise limiting role on Slp1 assembly and function.

Another interesting notion is related to the existence of two stomatin-like proteins in Arabidopsis, compared to only one closely homologous protein in humans. This would either suggest specialised stomatin functions in plants and certain fungi compared to mammals, or partial redundancy of stomatins and prohibitins in mitochondria from animal cells. Certain organisms such as the yeast *S.cerevisiae* even lack stomatins completely. This would further suggest that stomatins and prohibitins could be partially redundant. Related to this, it is noteworthy to point out the existence of seven prohibitin genes in Arabidopsis, compared to only two in mammals and yeast. Based on these facts, band-7 family protein function is maybe generally more diverse and specialised in plants than in animals.

Of the three proteins with a stomatin domain in Arabidopsis, only the two Slps are structurally and functionally closely homologous. The third one (the HIR protein At3g01290) is a putative plasma membrane localised protein upregulated during the HR. The presence of the stomatin signature domain (that is largely similar to the band-7 domain) would still suggest a similar mechanism of action between these three proteins. Even if they are not functioning at the same location, the overall mechanism of action could be conserved and be related to the regulation of a protein complex containing an ion channel or transporter protein. Possibly, HIR proteins at the plasma membrane could function in a similar way to Slps at the mitochondrial inner membrane.

6.3 General functions of band-7 family proteins

Proteins with a band-7 domain are distributed at localisations throughout animal cells and have diverse functions (Browman *et al.*, 2007). The only common underlying theme

between these proteins is the presence of the band-7 domain. Only few members have additional domains, such as the flotillins that possess a unique domain. Stomatins have been shown to regulate the gating of diverse ion channels and transporters by direct protein interaction, mainly at the plasma membrane of a variety of cells. Certain stomatin-like proteins such as HsSlp2 might even be dually localised in specific cell types and provide scaffolds for the assembly and regulation of protein complexes. Additionally, they directly regulate the activity of certain membrane-bound mitochondrial proteases. Prohibitins are also localised to mitochondria where they assemble into large heterooligomeric complexes, and putatively also to other compartments. Their role as described in animal cells is largely similar to the stomatin-like proteins (Schleicher *et al.*, 2008). In plants, mitochondrial prohibitins of type I contribute to cell division and elongation and affect cellular senescence via ROS production (Van Aken *et al.*, 2007; Ahn *et al.*, 2006; Chen *et al.*, 2005). Flotillins provide a specialised subset of microdomains that are involved in a novel mode of endocytosis and act as membrane-bound scaffolds. Bacterial HflC/K proteins also modulate the activity of membrane-bound proteases. HIR proteins appear to be plant-specific band-7 family proteins. Their exact function is not known, but they are involved in the hypersensitive response, a form of programmed cell death in plants. The results of several proteomics studies placed them at the plasma membrane. How do SPFH domain proteins achieve such a variety of functions, and is there a common underlying mechanism? In other words, are different SPFH domain proteins responsible for the same tasks at different subcellular localisations?

Early on after the discovery of the SPFH domain (or band-7 domain) it was suggested that the common underlying mechanism of all members lies in the regulation of a membrane-bound protease (Tavernarakis *et al.*, 1999). This has so far been proven for prohibitins and stomatin-like proteins. When the PID protein family was identified in plants, the authors suggested this common mechanism to be the regulation of ion channels (Nadimpalli *et al.*, 2000). So far, both of these mechanisms have only been partly verified for a subset of band-7 family proteins.

A common mechanism of action between band-7 family proteins is now regarded the ability of the band-7 domain to bind certain lipids such as sterols. This way, band-7 family proteins actively contribute to the assembly of lipid microdomains and protein complexes in a variety of membranes. Thus, they can be described as “organisers” of organelles and subcellular compartments (Browman *et al.*, 2007). This apparently happens in a variety of subcellular compartments by different, specialised SPFH domain proteins. Closely related to this issue is the question about redundancy between band-7 family proteins. At least

some of them share the same subcellular compartment, as it is the case for prohibitins and stomatin-like proteins in mammalian and in plant cells. Very recent evidence suggests that both mitochondrial prohibitins and stomatin-like proteins from mammalian cells interact with membrane-bound GTPases. These proteins are implicated to mediate mitochondrial fusion events that are important during various stages of the cell cycle. Human Slp2 interacts with mitofusin-2, a GTPase of the outer mitochondrial membrane, whereas prohibitin interacts with OPA1, a GTPase of the inner membrane. At least in this case it appears that these two types of band-7 family proteins affect the same pathway by the same molecular mechanism, thereby complementing each other. Neither of these GTPases has direct homologues in plant mitochondria. However, mitochondria in plants are fundamentally differently organised from animal mitochondria, namely as discrete organelles rather than as a tubular network. Plant mitochondria also undergo constant fusion and fission, but unlike animal mitochondria, they do not exist as a continuing network (Logan, 2006a). Based on the relatively mild phenotypes observed after knockdown of HsSlp2 in mammalian cells, it was suggested that prohibitins could possibly partially take over Slp2 functions (Hajek *et al.*, 2007; Da Cruz *et al.*, 2008). However, the fundamental structure of prohibitin and Slp2 complexes in the mitochondrial inner membrane is rather different and would argue against a high level of redundancy. In Arabidopsis, the relatively subtle phenotypes observed with the single *slp1* knockout mutant would also argue for partial redundancy on the level of both Slp proteins. It remains currently open whether an *slp* double mutant would have more severe phenotypes, or whether prohibitins could take over general functions lost by an *slp* double knockout. The level of redundancy seems even more acute in the case of Arabidopsis that possesses altogether seven prohibitin genes and two stomatin-like genes. Evidence so far suggests that all of these are localised to the mitochondrial inner membrane. Additionally, prohibitin and stomatin knockouts appear to have similar phenotypes ((Van Aken *et al.*, 2007) and this study) and prohibitins are also expressed in cells with high metabolic demands (Coates *et al.*, 2001).

On a general level, partial redundancy between band-7 family proteins that are localised to the same subcellular compartment seems likely. All band-7 domain proteins are so far much better studied and understood from animals than from plants. Since these proteins form a very ancient family that evolved by convergent evolution, their overall protein structure and function could be remarkably conserved, at least within the core band-7 domain. Putatively, all band-7 domain proteins are additionally regulated by post-translational modifications such as phosphorylation and acylation. Throughout organisms,

these proteins commonly act in pairs and form hetero- and homooligomeric building blocks, or they form complexes with other band-7 family proteins.

6.4 Outlook and suggestions for further experiments

Many issues concerning the function of Slp proteins in Arabidopsis remain currently open. One of the most intriguing questions concerns the specificity of the two isolated knockout alleles. Whereas *slp1-1* shows a clear growth phenotype, *slp1-2* plants grow almost like wild type plants. On the mitochondrial level, *slp1-1* roots take up less TMRE, whereas *slp1-2* seedlings do the opposite. Thus, either *slp1* knockout allele supposedly affects the voltage across the inner membrane. To clarify that these effects are clearly related to the knockout of the AtSlp1 gene, a Southern blot should be performed. This way, a single T-DNA insertion site could be confirmed in both alleles.

Knockout of Slp1 appears to affect the production of ROS in seedling roots or otherwise actively growing tissue. If Slps influence general mitochondrial function, it would be expected that this might be even more pronounced in situations of stress. Thus, knockout plants could be challenged with plant pathogens, and their ROS levels assessed. Additionally, the extent of the HR following this challenge could be followed by Trypan blue staining and compared with wild type responses. Human Slp2 is highly upregulated upon the application of mitochondrial stress such as after treatment with chloramphenicol (Da Cruz *et al.*, 2008). This reagent blocks mitochondrial protein synthesis and disturbs the composition of the mitochondrial electron transport chain. It is predicted that this treatment would also upregulate AtSlps, similar to effects seen after irradiation with UV-B light and treatment with cycloheximide.

To completely exclude dual targeting of Slp proteins to mitochondria and other localisations such as the plasma membrane, the putative targeting sequence confined to the first 50 amino acids of Slp1 could be fused to GFP directly. The resulting subcellular localisation of this fusion could then be investigated by co-localisation with a mitochondrial marker. Additionally, the effect on mitochondrial targeting of N-terminally truncated Slp-GFP fusion proteins could be tested.

To confirm a role of Slp1 in basic oxygen consumption of isolated mitochondria, these measurements should be repeated with an independent batch of identically grown plants. Additionally, the effects of SHAM on oxygen consumption via blockage of AOX should be further investigated. In particular, the role of the alternative respiration should be

elucidated, and the basic level of proton leakage. This way, it could be confirmed that loss of Slp1 affects the integrity and level of coupling of the inner membrane.

AtSlp proteins putatively have important functions in specialised cell types with specific metabolic demands. Thus, Slp function in these cells should be specifically investigated. For example, the viability of *slp1* pollen grains (by a viability stain with FDA or the assessment of pollen germination rates) would be one way, since the AtSlp1 promoter is highly active in this cell type. With regard to the reduced production of seeds, it would be expected that mutant pollen have reduced viability. In addition to pollen, Slp function in stipules and guard cells could be closer inspected. As judged by basic transpiration rate measurements using the IRGA chamber, no effect could be seen in the *slp1* mutants compared to wild type plants. However, these quantifications were only calculated at one set level of photon flux density. Currently it is not known whether differences in stomatal behaviour would be visible under other circumstances (e.g. under lower or higher light, or with lower or higher levels of CO₂). The concentration of CO₂ could have effects on mitochondrial function in illuminated leaves via activation of the photorespiratory pathway. In guard cells, chloroplasts putatively function differently from mesophyll cells, which probably also affects mitochondrial function. The level of redundancy between the two AtSlps should be further assessed with transgenic plants that are homozygous for the *slp1-1* T-DNA insertion, and at least heterozygous for an RNAi construct silencing AtSlp2.

Currently it is also not known whether the *slp1* single insertions affect the morphology or fusion of mitochondria. It is therefore suggested to make use of mitochondrial marker dyes to clarify this issue *in vivo*. Similar to the TMRE staining results, effects on mitochondrial mass (by staining with MitoTracker Green that accumulates in mitochondria regardless of their membrane potential) and membrane potential should be compared as it was done for silenced tobacco prohibitins (Ahn *et al.*, 2006). Mitochondrial dynamics might also be altered in the *slp1* mutant plants. Thus, movements of mitochondria should be followed by using marker dyes or transient expression of mitochondrial-targeted GFP in the mutant plants. Since plant mitochondria are known to move along actin filaments, the effects of pharmacological agents such as cytochalasin D (disrupting the actin cytoskeleton) should be investigated and compared to wild type mitochondrial behaviour. Additionally, transmission electron microscopy should be applied to study effects of *slp1* knockout on mitochondrial ultrastructure.

The final confirmation of the specificity of the observed phenotypes in *slp1* mutant plants should be confirmed by complementing these plants with constructs overexpressing Slp1

protein ideally under its own promoter. Alternatively, it would be interesting to check whether these single knockout phenotypes could also be complemented by overexpression of the Slp2 protein. Additionally, the effects of overexpressing prohibitins or the human Slp2 protein would be interesting to study. This way, the proposed functional homology between the human protein and the Arabidopsis Slps could be confirmed. With respect to redundancy amongst Slps or Slps and prohibitins, it would be interesting to study the effects of a *slp1/prohibitin* double or even *slp1/slp2/prohibitin* triple mutant plant.

Considering the effects of dominant-negative Slp overexpression on plant development, it remains to be clarified whether the membrane-associated fraction of overexpressed protein could be associated with mitochondria. This could be achieved by tagging the existing DN proteins at their C-terminus with a fluorophore, or by testing for their presence in purified mitochondria fractions from dexamethasone-treated DN plants.

Another interesting option would be to overexpress Arabidopsis Slps in mammalian cells. AtSlps could also complement some of the phenotypes observed after knockdown of HsSlp2. This has partly already been achieved by Dr. Christian Wunder working in a collaborating laboratory at the NIH (Maryland, USA), who overexpressed native AtSlps tagged with a fluorophore at their C-termini. These fusion proteins were observed to be localised to mitochondria. However, rather than being evenly distributed throughout the organelles, the Arabidopsis fusion proteins were observed in patches on mitochondria that could stem from cristae junctions. Ultimately another goal is to assess the effects of overexpressed identical DN AtSlp constructs on the growth and cell division of mammalian cell cultures.

Additionally, a set of new transgenic plants in the *slp1* single or double knockout (and wild type) background should be created. These plants would be useful to help elucidating the role of certain conserved residues for Slp function, based on homology to other stomatin-type proteins. Specifically, the single conserved cysteine in Slp1 should be mutated to alanine. Putatively this residue becomes S-acylated and might aid membrane attachment and protein complex assembly at specific sites. Related to the mutation of this cysteine, neighbouring hydrophobic residues could also be mutated, because these are putatively involved in lowering the pKa required for cysteine protonation. Next, the conserved proline residue that is responsible for cholesterol binding in podocin and Mec-2 could be another candidate residue for a point mutation in AtSlps. Mutation of this residue would be expected to affect microdomain formation and association and might result in similarly catastrophic phenotypes as those observed in *C.elegans* (where animals were paralysed).

The putatively phosphorylated serine residue of the human stomatin protein is also present in both AtSlps and would be another prime candidate residue for point mutation. Plant band-7 family proteins also contain other conserved residues such as the alanine (see Figure 3-4), and a glycine that is conserved between various stomatins from different species (Figure 3-5). The effects of point mutations in these residues could also help to elucidate physiological functions of these proteins *in vivo*, especially with regard to mitochondria.

To investigate novel functions or to confirm functional homology between plant and animal Slps, protein interaction partners should be identified. In this case, the use of protein interaction screens based on the yeast split-ubiquitin system where full-length membrane proteins are expressed is of little use with respect to the mitochondrial localisation of these proteins. Similar to the approaches that were used in human cell lines, protein interaction partners should rather be identified by crosslinking of isolated mitochondria followed by immunoprecipitation. This could be carried out with wild type plants, or alternatively with tagged Slp versions that are ideally expressed under their native promoters. Similar protein interaction partners to those found in animals would be expected in Arabidopsis, amongst them prohibitins, and some kind of membrane-bound protease or GTPase.

Appendix 1

The first part of this appendix includes a set of tables of all protein sequences used for the phylogenetic analysis in chapter 3. The first two tables contain information about the animal proteins analysed. The next table contains the band-7 family proteins from yeast, and the last two tables contain the plant band-7 proteins.

The second part of this appendix shows two tables that include the results from the BLAST searches using the Plant Genome Duplication database mentioned in chapter 3 (section 3.5.3.1). The first of the two tables contains the results obtained when AtSlp1 was used as the query, and the second one contains results obtained with AtSlp2 as the query.

UniProt ID	Species	Name	Abbreviation	Gene ID	Length (aa)	PROSITE	Position	Domain #1	Position
P27105	<i>Homo sapiens</i>	Stomatin	HsStomatin	2040	288	PS01270	167-195	Band7	53-228
Q9NP85	<i>Homo sapiens</i>	Podocin	HsPodocin	7827	383	PS01270	238-266	Band7	124-299
Q9UBI4	<i>Homo sapiens</i>	Stomatin-like protein-1	HsSlp-1/STORP	9399	398			Band7	78-241
Q9UJZ1	<i>Homo sapiens</i>	Stomatin-like protein-2	HsSlp-2	30968	356			Band7	37-211
Q8TAV4	<i>Homo sapiens</i>	Stomatin-like protein-3	HsSlp-3	161003	291	PS01270	164-192	Band7	50-225
P35232	<i>Homo sapiens</i>	Prohibitin	HsPHB	5245	272			Band7	26-218
Q99623	<i>Homo sapiens</i>	Prohibitin-2	HsPHB-2	11331	299			Band7	39-232
O75955	<i>Homo sapiens</i>	Flotillin-1	HsFlotillin-1	10211	427			Band7	1-185
Q14254	<i>Homo sapiens</i>	Flotillin-2	HsFlotillin-2	N/A	379			Band7	1-139
O75477	<i>Homo sapiens</i>	Erlin-1	HsErlin-1	10613	346			Band7	22-211
O94905	<i>Homo sapiens</i>	Erlin-2	HsErlin-2	11160	339			Band7	24-211
P54116	<i>Mus musculus</i>	Stomatin	MmStomatin	13830	284	PS01270	167-195	Band7	53-228
Q8C166	<i>Mus musculus</i>	Stomatin-like protein-1	MmSlp-1	69106	399			Band7	78-285
Q99JB2	<i>Mus musculus</i>	Stomatin-like protein-2	MmSlp-2	66592	353			Band7	37-211
Q6PE84	<i>Mus musculus</i>	Stomatin-like protein-3	MmSlp-3	229277	287	PS01270	160-188	Band7	46-221
P67778	<i>Mus musculus</i>	Prohibitin	MmPHB	18673	272			Band7	26-218
O35129	<i>Mus musculus</i>	Prohibitin-2	MmPHB-2	12034	299			Band7	39-232
Q27433	<i>Caenorhabditis elegans</i>	Mec-2	CeMec-2	180826	481	PS01270	254-282	Band7	140-315
Q19200	<i>Caenorhabditis elegans</i>	Stomatin-1	CeSto-1	181017	330	PS01270	176-204	Band7	63-237
Q19958	<i>Caenorhabditis elegans</i>	Stomatin-2	CeSto-2	180802	314	PS01270	206-234	Band7	92-267
Q20657	<i>Caenorhabditis elegans</i>	Stomatin-3	CeSto-3	191966	267	PS01270	152-180	Band7	38-213
Q22165	<i>Caenorhabditis elegans</i>	Stomatin-4	CeSto-4	181350	281	PS01270	163-191	Band7	49-224
Q21190	<i>Caenorhabditis elegans</i>	UNC-1	CeUNC-1	180458	285	PS01270	168-196	Band7	54-229
Q17372	<i>Caenorhabditis elegans</i>	UNC-24	CeUNC-24	177594	415			Band7	87-278
P0ABC3	<i>Escherichia coli</i>	HflC	EcHflC	948697	334			Band7	19-244
P0ABC7	<i>Escherichia coli</i>	HflK	EcHflK	948698	419			Band7	96-270

Animal and bacterial band-7 family proteins (part I).

UniProt ID	Domain #2	Position	Domain #3	Position	Subcellular Localisation
P27105	Stomatin	59-81, 108-129, 143-160, 163-186, 187-205, 206-227, 231-254			PM, endosomes
Q9NP85	Stomatin	130-152, 179-200, 214-231, 234-257, 258-276, 277-298, 302-325			PM
Q9UBI4	Stomatin	84-106, 131-152, 166-183, 186-209	SCP2	287-398	Membrane
Q9UJZ1	Stomatin	43-65, 91-112, 126-143, 146-169, 170-188, 189-210			Mitochondrion
Q8TAV4	Stomatin	56-78, 105-126, 140-157, 160-183, 184-202, 203-224, 228-251			Membrane
P35232	Prohibitin	70-86, 88-107, 111-129, 134-150, 157-176, 182-205, 205-221			Mitochondrion
Q99623	Prohibitin	84-100, 102-121, 125-143, 148-164, 171-190, 196-219, 219-235			Mitochondrion
O75955	Flotillin	190-363			PM
Q14254	Flotillin	144-317			PM
O75477					ER
O94905					ER
P54116	Stomatin	59-81, 108-129, 143-160, 163-186, 187-205, 206-227, 231-254			PM
Q8CI66	Stomatin	84-106, 131-152, 166-183, 186-209	SCP2	288-399	Membrane
Q99JB2	Stomatin	43-65, 91-112, 126-143, 146-169, 170-188, 189-210			Membrane
Q6PE84	Stomatin	52-74, 101-122, 136-153, 156-179, 180-198, 199-220, 224-247			PM
P67778	Prohibitin	70-86, 88-107, 111-129, 134-150, 157-176, 182-205, 205-221			Mitochondrion, cytoplasm, nucleus
O35129	Prohibitin	84-100, 102-121, 125-143, 148-164, 171-190, 196-219, 219-235			Mitochondrion, cytoplasm, nucleus
Q27433	Stomatin	146-168, 195-216, 230-247, 250-273, 274-292, 293-314, 318-341			Membrane
Q19200	Stomatin	69-91, 117-138, 152-169, 172-195, 196-214, 215-236, 240-263			Membrane
Q19958	Stomatin	98-120, 147-168, 182-199, 202-225, 226-244, 245-266, 270-293			Membrane
Q20657	Stomatin	44-66, 93-114, 128-145, 148-171, 172-190, 191-212, 216-239			Membrane
Q22165	Stomatin	55-77, 104-125, 139-156, 159-182, 183-201, 202-223, 227-250			Membrane
Q21190	Stomatin	60-82, 109-130, 144-161, 164-187, 188-206, 207-228, 232-255			Membrane
Q17372	Stomatin	93-115, 140-161, 175-192, 221-239	SCP2	307-412	Membrane
P0ABC3	HflC	1-327			Membrane
P0ABC7	Stomatin	102-124, 149-170, 184-201	HflK	97-356	Membrane

Animal and bacterial band-7 family proteins (part II).

UniProt ID	Species	Name	Abbreviation	Gene ID	Length (aa)	Domain #1	Position
P40961	<i>Saccharomyces cerevisiae</i>	PHB-1	ScPHB-1	953033	287	Band7	28-220
P50085	<i>Saccharomyces cerevisiae</i>	PHB-2	ScPHB-2	853146	310	Band7	57-249
Q9P7H3	<i>Schizosaccharomyces pombe</i>	PHB-1	SpPHB-1	2542354	282	Band7	25-217
O94550	<i>Schizosaccharomyces pombe</i>	PHB-2	SpPHB-2	2538888	279	Band7	35-227
O60121	<i>Schizosaccharomyces pombe</i>	N/A	O60121	2539877	354	Band7	52-226
Q59X52	<i>Candida albicans</i>	Slp-2	Q59X52	3644246	263	Band7	100-263
Q59XK2	<i>Candida albicans</i>	Slp-2	Q59XK2	3644091	263	Band7	100-263
Q5A411	<i>Candida albicans</i>	Slp-99	Q5A411	3641891	350	Band7	75-248
Q59SS4	<i>Candida albicans</i>	PHB-1	Q59SS4	3645641	283	Band7	26-218
Q5AEB1	<i>Candida albicans</i>	PHB-12	Q5AEB1	3638297	321	Band7	64-256
Q5AND0	<i>Candida albicans</i>	PHB-2	Q5AND0	3635238	303	Band7	55-247
A3LYB1	<i>Pichia stipitis</i>	Slp-3	A3LYB1	4840269	340	Band7	68-241
A3LTY5	<i>Pichia stipitis</i>	Stomatin family protein	A3LTY5	4838935	367	Band7	76-251

UniProt ID	Domain #2	Position	Subcellular Localisation
P40961	Prohibitin	72-88, 90-109, 113-131, 136-152, 159-178, 184-207, 208-223	Mitochondrion
P50085	Prohibitin	101-117, 119-138, 142-160, 165-181, 188-207, 213-236, 237-252	Mitochondrion
Q9P7H3	Prohibitin	69-85, 87-106, 110-128, 133-149, 156-175, 181-204, 205-220	Mitochondrion
O94550	Prohibitin	79-95, 97-116, 120-138, 143-159, 166-185, 191-214, 215-230	Mitochondrion
O60121	Stomatin	58-80, 106-127, 141-158, 161-184, 185-203, 204-225	Mitochondrion
Q59X52	Stomatin	106-128, 154-175, 234-252	N/A
Q59XK2	Stomatin	106-128, 154-175, 234-252	N/A
Q5A411	Stomatin	128-149, 163-180, 183-206, 207-225, 226-247	N/A
Q59SS4	Prohibitin	70-86, 88-107, 111-129, 134-150, 157-176, 182-205, 206-221	N/A
Q5AEB1	Prohibitin	108-124, 126-145, 149-167, 172-188, 195-214, 220-243, 244-259	N/A
Q5AND0	Prohibitin	99-115, 117-136, 140-158, 163-179, 186-205, 211-234, 235-250	N/A
A3LYB1	Stomatin	121-142, 156-173, 176-199, 200-218, 219-240	N/A
A3LTY5	Stomatin	130-151, 165-182, 210-228, 229-250	N/A

Yeast band-7 family proteins.

UniProt ID	Species	Name	Abbreviation	Gene ID	Gene (AGI)	Length (aa)	Domain #1	Position
Q93VP9	<i>Arabidopsis thaliana</i>	Stomatin-like protein-1	AtSlp1	828868	At4g27585	411	Band7	62-236
Q9LVW0	<i>Arabidopsis thaliana</i>	Stomatin-like protein-2	AtSlp2	835497	At5g54100	401	Band7	105-279
Q9SRH6	<i>Arabidopsis thaliana</i>	HIR	At3g01290	821309	At3g01290	285	Band7	6-182
Q9FHM7	<i>Arabidopsis thaliana</i>	Band7/HIR?	At5g51570	835231	At5g51570	292	Band7	12-195
Q9FM19	<i>Arabidopsis thaliana</i>	HIR	At5g62740	836395	At5g62740	286	Band7	6-182
Q9CAR7	<i>Arabidopsis thaliana</i>	HIR-like	At1g69840	843320	At1g69840	286	Band7	6-182
Q9ZQ87	<i>Arabidopsis thaliana</i>	ER protein (Erlin-like)	At2g03510	814880	At2g03510	356	Band7	46-235
Q501E6	<i>Arabidopsis thaliana</i>	Flotillin/nodulin-like	At5g25250	832596	At5g25250	470	Band7-related	N/A
Q4V3D6	<i>Arabidopsis thaliana</i>	Flotillin/nodulin-like	At5g25260	832597	At5g25260	463	Band7-related	N/A
Q9LV90	<i>Arabidopsis thaliana</i>	Flotillin/nodulin-like	At5g64870	836610	At5g64870	479	Band7-related	N/A
O49460	<i>Arabidopsis thaliana</i>	PHB1	At4g28510	828969	At4g28510	288	Band7	35-227
Q9ZNT7	<i>Arabidopsis thaliana</i>	PHB2	At1g03860.1	839228	At1g03860.1	286	Band7	35-227
Q3EDJ1	<i>Arabidopsis thaliana</i>	PHB2	At1g03860.2	839228	At1g03860.2	221	Band7	2-162
O04331	<i>Arabidopsis thaliana</i>	PHB3	At5g40770	834077	At5g40770	277	Band7	31-223
Q9LK25	<i>Arabidopsis thaliana</i>	PHB4	At3g27280	822347	At3g27280	279	Band7	31-223
Q9LY99	<i>Arabidopsis thaliana</i>	PHB5	At5g14300	831210	At5g14300	249	Band7	23-189
Q9SIL6	<i>Arabidopsis thaliana</i>	PHB6	At2g20530	816575	At2g20530	286	Band7	33-225
Q9FFH5	<i>Arabidopsis thaliana</i>	PHB7	At5g44140	834437	At5g44140	278	Band7	35-227
A7P6L9	<i>Vitis vinifera</i>	Band7 protein	A7P6L9	N/A	N/A	420	Band7	68-242
A9T1F8	<i>Physcomitrella patens</i>	pred. protein (fragment)	A9T1F8	5935671	N/A	292	Band7	10-184
Q7EZD2	<i>Oryza sativa subsp. japonica</i>	Band7 protein	Q7EZD2	4344707	Os08g0158500	377	Band7	56-230
A2YRF1	<i>Oryza sativa subsp. indica</i>	Band7 protein	A2YRF1	N/A	N/A	377	Band7	56-230
A3BPU1	<i>Oryza sativa subsp. japonica</i>	Band7 protein	A3BPU1	N/A	N/A	405	Band7	84-258
Q9M585	<i>Zea mays</i>	Stomatin-like protein	Q9M585	541819	N/A	394	Band7	57-231
A8JI52	<i>Chlamydomonas reinhardtii</i>	pred.protein (fragment)	A8JI52	5729177	N/A	372	Band7	98-272

Plant band-7 family proteins (part I).

UniProt ID	Domain #2	Position	Subcellular Localisation
Q93VP9	Stomatin	116-137, 151-168, 171-194, 195-213, 214-235	mitochondrion, plastid
Q9LVW0	Stomatin	159-180, 194-211, 214-237, 238-256, 257-278	mitochondrion, plastid
Q9SRH6	Stomatin	60-81, 117-140, 160-181	membrane, PM
Q9FHM7			chloroplast?
Q9FM19			PM
Q9CAR7			PM
Q9ZQ87			ER
Q501E6	Flotillin-related	N/A	unknown
Q4V3D6	Flotillin-related	N/A	unknown
Q9LV90	Flotillin-related	N/A	unknown
O49460	Prohibitin	79-95, 97-116, 120-138, 143-159, 166-185, 191-214, 215-230	mitochondrion, complex1
Q9ZNT7	Prohibitin	79-95, 97-116, 120-138, 143-159, 166-185, 191-214, 215-230	mitochondrion, plastid, complex1
Q3EDJ1	Prohibitin	14-30, 32-51, 55-73, 78-94, 101-120, 126-149, 150-165	membrane
O04331	Prohibitin	75-91, 93-112, 116-134, 139-155, 162-181, 187-210, 211-226	mitochondrion, complex1
Q9LK25	Prohibitin	75-91, 93-112, 116-134, 139-155, 162-181, 187-210, 211-226	mitochondrion, cell wall?
Q9LY99	Prohibitin	67-83, 85-104	mitochondrion
Q9SIL6	Prohibitin	77-93, 95-114, 118-136, 141-157, 164-183, 189-212, 213-228	mitochondrion
Q9FFH5	Prohibitin	79-95, 97-116, 120-138, 143-159, 166-185, 191-214, 215-230	membrane/mitochondrion
A7P6L9	Stomatin	74-96, 122-143, 157-174, 177-200, 201-219, 220-241	membrane
A9T1F8	Stomatin	16-38, 64-85, 99-116, 119-142, 143-161, 162-183	membrane
Q7EZD2	Stomatin	62-84, 110-131, 145-162, 165-188, 189-207, 208-229	membrane
A2YRF1	Stomatin	62-84, 110-131, 145-162, 165-188, 189-207, 208-229	membrane
A3BPU1	Stomatin	90-112, 138-159, 173-190, 193-216, 217-235, 236-257	membrane
Q9M585	Stomatin	63-85, 111-132, 146-163, 166-189, 190-208, 209-230	membrane
A8JI52	Stomatin	104-126, 152-173, 187-204, 207-230, 231-249, 250-271	membrane

Plant band-7 family proteins (part II).

Results of the BLAST searches in the PGDD

Most relevant hits when AtSlp1 (At4g27585) was used as the query:

Locus	Score (bits)	e-value	Species
At4g27585.1	734	0	<i>A.thaliana</i>
Cp0003g0176	503	e-142	<i>C.papaya</i>
At5g54100.1	487	e-137	<i>A.thaliana</i>
Vv9g0145	469	e-132	<i>V.vinifera</i>
Pt12g0366	443	e-124	<i>P.trichocarpa</i>
Os08g0158500	374	e-103	<i>O.sativa</i>
Sb07g003970.1	365	e-100	<i>S.bicolor</i>
Pt3918g0001	360	6.00E-99	<i>P.trichocarpa</i>
Ak110776	191	4.00E-48	<i>O.sativa</i>
Pt21041g0002	182	2.00E-45	<i>P.trichocarpa</i>
Pt15g0018	160	5.00E-39	<i>P.trichocarpa</i>
Pt12g0363	130	7.00E-30	<i>P.trichocarpa</i>
Pt12g0362	127	4.00E-29	<i>P.trichocarpa</i>
Pt7830g0001	125	2.00E-28	<i>P.trichocarpa</i>
Pt12g0360	122	2.00E-27	<i>P.trichocarpa</i>
Os08g0255632	103	1.00E-21	<i>O.sativa</i>
Vv4g1066	68	4.00E-11	<i>V.vinifera</i>
At3g01290.1	64	6.00E-10	<i>A.thaliana</i>
At5g51570.1	60	1.00E-08	<i>A.thaliana</i>
Os10g0464000	59	2.00E-08	<i>O.sativa</i>
Vv1g0950	57	8.00E-08	<i>V.vinifera</i>
Pt12g1208	57	1.00E-07	<i>P.trichocarpa</i>
Sb02g022890.1	56	2.00E-07	<i>S.bicolor</i>
Os06g0136000	55	5.00E-07	<i>O.sativa</i>
Cp0017g0204	53	1.00E-06	<i>C.papaya</i>
Vv16rg0104	53	1.00E-06	<i>V.vinifera</i>
Os05g0591900	53	2.00E-06	<i>O.sativa</i>
Os08g0398400	53	2.00E-06	<i>O.sativa</i>
Sb10g002420.1	53	2.00E-06	<i>S.bicolor</i>
At5g62740.1	53	2.00E-06	<i>A.thaliana</i>
Vv17g0620	52	2.00E-06	<i>V.vinifera</i>
Sb07g019760.1	52	3.00E-06	<i>S.bicolor</i>
Pt15g1032	52	3.00E-06	<i>P.trichocarpa</i>
Pt17g0283	51	5.00E-06	<i>P.trichocarpa</i>
Os09g0361200	51	7.00E-06	<i>O.sativa</i>
Pt17g0282	51	7.00E-06	<i>P.trichocarpa</i>

Most relevant hits when AtSlp2 (At5g54100) was used as the query:

Locus	Score (bits)	e-value	Species
At5g54100.1	729	0	<i>A.thaliana</i>
At4g27585.1	498	e-141	<i>A.thaliana</i>
Cp0003g0176	474	e-133	<i>C.papaya</i>
Vv9g0145	460	e-129	<i>V.vinifera</i>
Pt12g0366	433	e-121	<i>P.trichocarpa</i>
Os08g0158500	381	e-105	<i>O.sativa</i>
Sb07g003970.1	378	e-104	<i>S.bicolor</i>
Pt3918g0001	362	1.00E-99	<i>P.trichocarpa</i>
Ak110776	218	2.00E-56	<i>O.sativa</i>
Pt21041g0002	183	6.00E-46	<i>P.trichocarpa</i>
Pt15g0018	147	7.00E-35	<i>P.trichocarpa</i>
Pt12g0363	142	2.00E-33	<i>P.trichocarpa</i>
Pt12g0362	117	8.00E-26	<i>P.trichocarpa</i>
Pt7830g0001	115	3.00E-25	<i>P.trichocarpa</i>
Pt12g0360	112	2.00E-24	<i>P.trichocarpa</i>
Os08g0255632	93	1.00E-18	<i>O.sativa</i>
At3g01290.1	74	6.00E-13	<i>A.thaliana</i>
At5g51570.1	66	2.00E-10	<i>A.thaliana</i>
Pt12g1208	66	2.00E-10	<i>P.trichocarpa</i>
Vv4g1066	65	4.00E-10	<i>V.vinifera</i>
At5g62740.1	65	5.00E-10	<i>A.thaliana</i>
Vv1g0950	64	6.00E-10	<i>V.vinifera</i>
Os06g0136000	64	1.00E-09	<i>O.sativa</i>
Sb02g022890.1	63	1.00E-09	<i>S.bicolor</i>
Cp0017g0204	62	2.00E-09	<i>C.papaya</i>
Vv17g0620	62	3.00E-09	<i>V.vinifera</i>
Os08g0398400	62	4.00E-09	<i>O.sativa</i>
Pt17g0283	61	5.00E-09	<i>P.trichocarpa</i>
Vv16g0104	61	5.00E-09	<i>V.vinifera</i>
Pt15g1032	61	6.00E-09	<i>P.trichocarpa</i>
Cp0003g0279	61	6.00E-09	<i>C.papaya</i>
Sb10g002420.1	61	6.00E-09	<i>S.bicolor</i>
Pt17g0282	59	3.00E-08	<i>P.trichocarpa</i>
Os05g0591900	58	5.00E-08	<i>O.sativa</i>
Sb07g019760.1	58	6.00E-08	<i>S.bicolor</i>
Pt12g0629	58	6.00E-08	<i>P.trichocarpa</i>
Os10g0464000	57	8.00E-08	<i>O.sativa</i>
Sb09g030530.1	56	2.00E-07	<i>S.bicolor</i>
Os09g0361200	55	4.00E-07	<i>O.sativa</i>
Cp0005g0273	54	7.00E-07	<i>C.papaya</i>
Pt3297g0001	51	6.00E-06	<i>P.trichocarpa</i>
At1g69840.1	51	6.00E-06	<i>A.thaliana</i>

Appendix 2

Table with primer sequences. Numbers correspond to the individual primers used as indicated in Materials and Methods. The table continues on the next page.

	Primer No.	Construct/Use	Primer name	Sequence
Results Chapter 3	1	Slp2	Forward	ATGAATCAGCTCGCGCTTTCAAG
	2	Slp2	Reverse	CTACTCCAGAAGTTTCCCTGAAAC
	3	pUC18-Slp2	Forward_PstI	TTTCTGCAGATGAATCAGCTCG
	4	pUC18-Slp2	Reverse_EcoRI	TTTGAATTCCTACTCCAGAAGTTTC
	5	pUC18-Slp2	M_for	CTCAAGCTTTAGGAATG
	6	pUC18-Slp2	R1-EcoRI_rev	GATTACGAATTCCTAC
	7	pUC18-Slp2	F2-PstI_for	GCTTGCATGCCTGCAGATGAATCAGCTCGCGC
	8	pQE80L-Slp1 epitope	Sol-stom-27585_for	GCTCAAGCTTTAGCATGCTACAAAAGCCTTGTC
	9	pQE80L-Slp1 epitope	Sol-stom-27585_rev	CTAGAAAGCTGGCTGCAGCCTGCG
	10	pQE80L-Slp2 epitope	Sol-stom-54100_for	GGGGGATCCAATCAGCTCGCGCTTTC
	11	pQE80L-Slp2 epitope	Sol-stom-54100_rev	GGGAAGCTTATCACTGCTGGGAGATGAG
	12	pGEX4T-1::Slp2 epitope	Sol54100-pGEX_for	CGCGGATCCAATCAGCTCGCGCTTTCAAGATC
	13	pGEX4T-1::Slp2 epitope	Sol54100-pGEX_rev	CCGCTCGAGATCACTGCTGGGAGATGAGAAG
	14	AtSlp1 probe	N-RT_for	AGCTAGAGCACAAAGCAACTGC
	15	AtSlp1 probe	N-RT_rev2	GGGAATAAAGGTGAATAAGAACAACAAG
	16	AtSlp2 probe	A-RT_for2	CAACGATGAATCAGCTCGCG
	17	AtSlp2 probe	A_LP	CGCTCAATCACACAAGCTTTC
	18	pDRIVE-AtSlp1 promoter	P.27585_for	TAGAGGTAGATGTGATGTTTTACTAC
	19	pDRIVE-AtSlp1 promoter	P.27585_rev	CTTCGTGGGAGAATCAGAAAAATG
	20	pDRIVE-AtSlp2 promoter	P.54100_for	CGGCTACGGTAGTTTTGGTTTG
	21	pDRIVE-AtSlp2 promoter	P.54100_rev	CGTTGAAAGCTGTGTAACCTAACTC
	22	pCAMBIA1301-P(AtSlp1)	P27585I-PstI_for	AAAAGCTGCAGTAGAGGTAGATGTGATGTTTTACTAC
	23	pCAMBIA1301-P(AtSlp1)	P27585-NcoI_rev	CATGCCATGGCTTCGTGGGAGAATCAGAAA AATG
	24	pCAMBIA1301-P(AtSlp2)	P54100s-PstI_for	AAAAGCTGCAGCGGTACGGTAGTTTTGGTTTG
	25	pCAMBIA1301-P(AtSlp2)	P54100-NcoI_rev	CATGCCATGGCGTTGAAAGCTGTGTAACCT AACTC
	26	RT-PCR Slp1	N-RT_rev	CTACTGCGGATCCTTGTTGC
	27	RT-PCR Slp2	ACK-RT_for	GAGAACGTCAAGCCATATC
	28	RT-PCR Slp2	ACK-RT_rev	ctCCAGAAGTTTCCCTGAAAC
	29	RT-PCR ubiquitin control	UBQ10_for	GATCTTTGCCGAAAACAATTGGAG
	30	RT-PCR ubiquitin control	UBQ10_rev	CGACTTGTATTAGAAAAGAAAGATAAC
Results Chapter 4	31	pTEY-Slp1-YFP	4g27585-NcoI_for	CATGCCATGGGAATGAACCACCTCGTTCGT AAAAGC
	32	pTEY-Slp1-YFP	4g27585-NcoI_rev	CATGCCATGGCCTGCGGATCCTTGTTGCGG
	33	pTEY-Slp2-YFP	5g54100-NcoI_for	CATGCCATGGGAATGAATCAGCTCGCGCTTTC
	34	pTEY-Slp2-YFP	5g54100-NcoI_rev	CATGCCATGGCCTCCAGAAGTTTCCCTGAAAC
	35	pTEY-YFP-Slp1	4g27585-EcoRI_for	TTGGAATTCATGAACCACCTCGTTCGTA AAA GCTCCG
	36	pTEY-YFP-Slp1	Stomatin1_rev_EcoRI	GGAATTCCTACTGCGGATCCTTGTTGCG
	37	pTEY-YFP-Slp2	5g54100-EcoRI_for	TTGGAATTCATGAATCAGCTCGCGCTTTC
	38	pTEY-YFP-Slp2	5g54100-EcoRI_rev	TTGGAATTCCTACTCCAGAAGTTTCCCTG
	39	pGEM-gen. Slp1	Genomic-sto1_for	AACTCAAACCTATGCACACTTACCTTTATATATAG
	40	pGEM-gen. Slp1	Genomic-sto1_rev	GGGAATAAAGGTGAATAAGAACAACAAGG
	41	pGEM-gen. Slp2	Genomic-sto2_for	GCGTTTTACTTCTGCGTCTGCG
	42	pGEM-gen. Slp2	Genomic-sto2_rev	AAAGATAACAAGAGCCAACACTTAGAAG
	43	pGEM-gen. Slp2-KpnI	Gen-sto2-NheI_for	CAATCCTGCTAGCATGATCGCTCAAG
	44	pGEM-gen. Slp2-KpnI	Gen-sto2-PstI_rev	GTGACCTGCAGGCGGCC
	45	pGEM-gen. Slp2-KpnI	Gen-sto2-KpnI_for2	AAACTTCTGGAGGGTACCTAGAATCCTC
	46	pGEM-gen. Slp2-KpnI	Gen-sto2-KpnI_rev2	AGGATTCTAGGTACCCTCCAGAAGTTTC
	47	pGEM-gen. Slp2-GFP6	GFP6-KpnI_for	CGGGGTACCATGGTAGATCTGACTAG
	48	pGEM-gen. Slp2-GFP6	GFP6-KpnI_rev	CGGGGTACCTTTGTATAGTTCATCCATG

Primer No.	Construct/Use	Primer name	Sequence
49	Genotyping of <i>slp1-1</i>	210_D11-_LP	AGCTAGAGCACAAGCAACTGC
50	Genotyping of <i>slp1-1</i>	210_D11_RP	AACCGAACCGAATAATAACGG
51	Genotyping of <i>slp1-2</i>	65_C05-LP	GGCAATCCCATATCAACATTG
52	Genotyping of <i>slp1-2</i>	65_C05-RP	TTCTCACCCATGTCTTCCAAC
53	Genotyping of <i>slp1-3</i>	J-LP	TTATATTGGCTCCGATTGGTG
54	Genotyping of <i>slp1-3</i>	J-RP	TCTCAACGCCATAAGAAGCTAAC
55	Genotyping of <i>slp1-4</i>	114_D09-LP	TCAAAAATTCCTTGCAAATGG
56	Genotyping of <i>slp1-4</i>	114_D09-RP	CAAGAGGAAAATGGATTGGTG
57	SAIL T-DNA insertion	LB3	TAGCATCTGAATTTTCATAACCAATCTCG ATACAC
58	SALK T-DNA insertion	Lba1	TGGTTCACGTAGTGGGCCATCG
59	SM insertion primer	Spm32	TACGAATAAGAGCGTCCATTTTAGAGTGA
60	SALK_090074	A_LP	CGCTCAATCACACAAGCTTTTC
61	SALK_090074	A_RP	CCATTTTCCCAAGGAGGAAAC
62	SM_3_810	C_LP	TGATTCATCGTTGAAAGCTGTGTAACTAA
63	SM_3_810	C_RP	ATGTCGCGAATTTTATGCATGTATGTTA
64	SALK_017306	K_LP	GAGGAAATCCAGAGAAAAACCTC
65	SALK_017306	K_RP	GTGGGCTGCGTTTGTATATTG
66	RT-PCR <i>slp1-1</i>	N-RT_for	AGCTAGAGCACAAGCAACTGC
67	RT-PCR <i>slp1-1</i>	N-RT_rev	CTACTGCGGATCCTTGTTGC
68	RT-PCR <i>slp1-3</i>	J-RT_for	GAAGATGAACCACCTCGTTC
69	RT-PCR <i>slp1-3</i>	J-RT_rev	CCATCGATGTGGATACTAACG
70	DN(<i>Slp1</i>)	27585-dn_for	CTCAAGGAAGAAGCTATCCCCG
71	DN(<i>Slp1</i>)	27585-dn_rev	CTACTGCGGATCCTTGTTGC
72	DN(<i>Slp2</i>)	54100-dn_for	CTAAAGGAAGAAGCGATTCTATTGG
73	DN(<i>Slp2</i>)	54100-dn_rev	CTACTCCAGAAGTTTCCCTGAAAC
74	pTA-myc-DN(<i>Slp1</i>)	27-dom-neg_for	CCGCTCGAGATGGAGCAGAAATTGATCAGCGA GGAAGACTTGCTCAAGGAAGAAGC
75	pTA-myc-DN(<i>Slp1</i>)	27-dom-neg_rev	GGGGGGGCCCAATTTTGGGGGACTAGTCTA CTGCGGATCC
76	pTA-myc-DN(<i>Slp2</i>)	54-dom-neg_for	CCGCTCGAGATGGAGCAGAAATTGATCAG CGAGGAAGACTTGCTAAAGGAAGAAGC
77	pTA-myc-DN(<i>Slp2</i>)	54-dom-neg_rev	CCCCGGGGGCCCAATTTTGGGGGACT AGTCTACTCCAGAAGTTTC

List of References

- Abdelkader, A. F., Aronsson, H., Solymosi, K., Boddi, B., & Sundqvist, C. (2007). High salt stress induces swollen prothylakoids in dark-grown wheat and alters both prolamellar body transformation and reformation after irradiation. *Journal of Experimental Botany* **58**, 2553-2564.
- AbouElela, S. & Nazar, R. N. (1997). Role of the 5.8S rRNA in ribosome translocation. *Nucleic Acids Research* **25**, 1788-1794.
- Ackerson, R. C. & Hebert, R. R. (1981). Osmoregulation in Cotton in Response to Water-Stress .1. Alterations in Photosynthesis, Leaf Conductance, Translocation, and Ultrastructure. *Plant Physiology* **67**, 484-488.
- Affourtit, C., Krab, K., & Moore, A. L. (2001). Control of plant mitochondrial respiration. *Biochimica et Biophysica Acta-Bioenergetics* **1504**, 58-69.
- Ahn, C. S., Lee, J. H., Hwang, A. R., Kim, W. T., & Pai, H. S. (2006). Prohibitin is involved in mitochondrial biogenesis in plants. *Plant Journal* **46**, 658-667.
- Akiyama, T., Takagi, S., Sankawa, U., Inari, S., & Saito, H. (1980). Saponin-Cholesterol Interaction in the Multibilayers of Egg-Yolk Lecithin As Studied by Deuterium Nuclear Magnetic-Resonance - Digitonin and Its Analogs. *Biochemistry* **19**, 1904-1911.
- Akiyama, Y., Kihara, A., Mori, H., Ogura, T., & Ito, K. (1998). Roles of the periplasmic domain of Escherichia coli FtsH (HflB) in protein interactions and activity modulation. *Journal of Biological Chemistry* **273**, 22326-22333.
- Alexandersson, E., Saalbach, G., Larsson, C., & Kjellbom, P. (2004). Arabidopsis plasma membrane proteomics identifies components of transport, signal transduction and membrane trafficking. *Plant and Cell Physiology* **45**, 1543-1556.
- Anderson, R. G. W. (1998). The caveolae membrane system. *Annual Review of Biochemistry* **67**, 199-225.
- Aoyama, T. & Chua, N. H. (1997). A glucocorticoid-mediated transcriptional induction system in transgenic plants. *Plant Journal* **11**, 605-612.
- Bacher, S., Achatz, G., Schmitz, M. L., & Lamers, M. C. (2002). Prohibitin and prohibitone are contained in high-molecular weight complexes and interact with alpha-actinin and annexin A2. *Biochimie* **84**, 1207-1220.

Balague, C., Lin, B. Q., Alcon, C., Flottes, G., Malmstrom, S., Kohler, C., Neuhaus, G., Pelletier, G., Gaymard, F., & Roby, D. (2003). HLM1, an essential signaling component in the hypersensitive response, is a member of the cyclic nucleotide-gated channel ion channel family. *Plant Cell* **15**, 365-379.

Bao, X. Z., Franks, R. G., Levin, J. Z., & Liu, Z. C. (2004). Repression of AGAMOUS by BELLRINGER in floral and inflorescence meristems. *Plant Cell* **16**, 1478-1489.

Bargmann, C. I. (1998). Neurobiology of the *Caenorhabditis elegans* genome. *Science* **282**, 2028-2033.

Barnes, T. M., Jin, Y., Horvitz, H. R., Ruvkun, G., & Hekimi, S. (1996). The *Caenorhabditis elegans* behavioral gene *unc-24* encodes a novel bipartite protein similar to both erythrocyte band 7.2 (stomatins) and nonspecific lipid transfer protein. *Journal of Neurochemistry* **67**, 46-57.

Bauer, M. & Pelkmans, L. (2006). A new paradigm for membrane-organizing and -shaping scaffolds. *Febs Letters* **580**, 5559-5564.

Baumann, C. A., Ribon, V., Kanzaki, M., Thurmond, D. C., Mora, S., Shigematsu, S., Bickel, P. E., Pessin, J. E., & Saltiel, A. R. (2000). CAP defines a second signalling pathway required for insulin-stimulated glucose transport. *Nature* **407**, 202-207.

Becker, T., Voegtle, F. N., Stojanovski, D., & Meisinger, C. (2008). Sorting and assembly of mitochondrial outer membrane proteins. *Biochimica et Biophysica Acta-Bioenergetics* **1777**, 557-563.

Bennion, B. J. & Daggett, V. (2003). The molecular basis for the chemical denaturation of proteins by urea. *Proceedings of the National Academy of Sciences of the United States of America* **100**, 5142-5147.

Berthiaume, L., Deichaite, I., Peseckis, S., & Resh, M. D. (1994). Regulation of Enzymatic-Activity by Active-Site Fatty Acylation - A New Role for Long-Chain Fatty-Acid Acylation of Proteins. *Journal of Biological Chemistry* **269**, 6498-6505.

Bickel, P. E., Scherer, P. E., Schnitzer, J. E., Oh, P., Lisanti, M. P., & Lodish, H. F. (1997). Flotillin and epidermal surface antigen define a new family of caveolae-associated integral membrane proteins. *Journal of Biological Chemistry* **272**, 13793-13802.

Birnbaum, K., Shasha, D. E., Wang, J. Y., Jung, J. W., Lambert, G. M., Galbraith, D. W., & Benfey, P. N. (2003). A gene expression map of the *Arabidopsis* root. *Science* **302**, 1956-1960.

Blazquez, M. A. & Weigel, D. (2000). Integration of floral inductive signals in *Arabidopsis*. *Nature* **404**, 889-892.

- Bolender, N., Sickmann, A., Wagner, R., Meisinger, C., & Pfanner, N. (2008). Multiple pathways for sorting mitochondrial precursor proteins. *Embo Reports* **9**, 42-49.
- Borecky, J. & Vercesi, A. E. (2005). Plant uncoupling mitochondrial protein and alternative oxidase: Energy metabolism and stress. *Bioscience Reports* **25**, 271-286.
- Borner, G. H. H., Sherrier, D. J., Weimar, T., Michaelson, L. V., Hawkins, N. D., MacAskill, A., Napier, J. A., Beale, M. H., Lilley, K. S., & Dupree, P. (2005). Analysis of detergent-resistant membranes in Arabidopsis. Evidence for plasma membrane lipid rafts. *Plant Physiology* **137**, 104-116.
- Bowie, J. U. (2004). Membrane proteins: A new method enters the fold. *Proceedings of the National Academy of Sciences of the United States of America* **101**, 3995-3996.
- Boyer, C. S., Neve, E. P. A., Moore, G. A., & Moldeus, P. (1994). Effect of Mitochondrial Protein-Concentration on the Efficiency of Outer-Membrane Removal by the Cholesterol-Selective Detergent Digitonin. *Biochimica et Biophysica Acta-Biomembranes* **1190**, 304-308.
- Browman, D. T., Hoegg, M. B., & Robbins, S. M. (2007). The SPFH domain-containing proteins: more than lipid raft markers. *Trends in Cell Biology* **17**, 394-402.
- Browman, D. T., Resek, M. E., Zajchowski, L. D., & Robbins, S. M. (2006). Erlin-1 and erlin-2 are novel members of the prohibitin family of proteins that define lipid-raft-like domains of the ER. *Journal of Cell Science* **119**, 3149-3160.
- Brown, D. A. & London, E. (2000). Structure and function of sphingolipid- and cholesterol-rich membrane rafts. *Journal of Biological Chemistry* **275**, 17221-17224.
- Bruce, B. D. (2000). Chloroplast transit peptides: structure, function and evolution. *Trends in Cell Biology* **10**, 440-447.
- Brugiere, S., Kowalski, S., Ferro, M., Seigneurin-Berny, D., Miras, S., Salvi, D., Ravel, S., d'Herin, P., Garin, J., Bourguignon, J., Joyard, J., & Rolland, N. (2004). The hydrophobic proteome of mitochondrial membranes from Arabidopsis cell suspensions. *Phytochemistry* **65**, 1693-1707.
- Cao, W. F., Zhang, L. Y., Liu, M. B., Tang, P. Z., Liu, Z. H., & Sun, B. C. (2007). Prognostic significance of stomatin-like protein 2 overexpression in laryngeal squamous cell carcinoma: clinical, histologic, and immunohistochemistry analyses with tissue microarray. *Human Pathology* **38**, 747-752.
- Carter, C., Pan, S. Q., Jan, Z. H., Avila, E. L., Girke, T., & Raikhel, N. V. (2004). The vegetative vacuole proteome of Arabidopsis thaliana reveals predicted and unexpected proteins. *Plant Cell* **16**, 3285-3303.

Chan, C. S., Guo, L., & Shih, M. C. (2001). Promoter analysis of the nuclear gene encoding the chloroplast glyceraldehyde-3-phosphate dehydrogenase B subunit of *Arabidopsis thaliana*. *Plant Molecular Biology* **46**, 131-141.

Chance, B. & Williams, G. R. (1955). Simple and Rapid Assay of Oxidative Phosphorylation. *Nature* **175**, 1120-1121.

Chauvin, S., Poulain, F. E., Ozon, S., & Sobel, A. (2008). Palmitoylation of stathmin family proteins domain A controls Golgi versus mitochondrial subcellular targeting. *Biology of the Cell* **100**, 577-589.

Chelur, D. S., Ernstrom, G. G., Goodman, M. B., Yao, C. A., Chen, L., O'Hagan, R., & Chalfie, M. (2002). The mechanosensory protein MEC-6 is a subunit of the *C. elegans* touch-cell degenerin channel. *Nature* **420**, 669-673.

Chen, B. J., Liu, Q., Ge, Q., Xie, J., & Wang, Z. W. (2007a). UNC-1 regulates gap junctions important to locomotion in *C. elegans*. *Current Biology* **17**, 1334-1339.

Chen, F., Yuan, Y. X., Li, Q., & He, Z. H. (2007b). Proteomic analysis of rice plasma membrane reveals proteins involved in early defense response to bacterial blight. *Proteomics* **7**, 1529-1539.

Chen, J. C., Jiang, C. Z., & Reid, M. S. (2005). Silencing a prohibitin alters plant development and senescence. *Plant Journal* **44**, 16-24.

Chen, W. Q., Provart, N. J., Glazebrook, J., Katagiri, F., Chang, H. S., Eulgem, T., Mauch, F., Luan, S., Zou, G. Z., Whitham, S. A., Budworth, P. R., Tao, Y., Xie, Z. Y., Chen, X., Lam, S., Kreps, J. A., Harper, J. F., Si-Ammour, A., Mauch-Mani, B., Heinlein, M., Kobayashi, K., Hohn, T., Dangl, J. L., Wang, X., & Zhu, T. (2002). Expression profile matrix of *Arabidopsis* transcription factor genes suggests their putative functions in response to environmental stresses. *Plant Cell* **14**, 559-574.

Chevallet, M., Lescuyer, P., Diemer, H., van Dorsselaer, A., Leize-Wagner, E., & Rabilloud, T. (2006). Alterations of the mitochondrial proteome caused by the absence of mitochondrial DNA: A proteomic view. *Electrophoresis* **27**, 1574-1583.

Christians, M. J. & Larsen, P. B. (2007). Mutational loss of the prohibitin AtPHB3 results in an extreme constitutive ethylene response phenotype coupled with partial loss of ethylene-inducible gene expression in *Arabidopsis* seedlings. *Journal of Experimental Botany* **58**, 2237-2248.

Claros, M. G. & Vincens, P. (1996). Computational method to predict mitochondrially imported proteins and their targeting sequences. *European Journal of Biochemistry* **241**, 779-786.

Clough, S. J., Fengler, K. A., Yu, I. C., Lippok, B., Smith, R. K., & Bent, A. F. (2000). The Arabidopsis dnd1 "defense, no death" gene encodes a mutated cyclic nucleotide-gated ion channel. *Proceedings of the National Academy of Sciences of the United States of America* **97**, 9323-9328.

Coates, P. J., Jamieson, D. J., Smart, K., Prescott, A. R., & Hall, P. A. (1997). The prohibitin family of mitochondrial proteins regulate replicative lifespan. *Current Biology* **7**, 607-610.

Coates, P. J., Nenutil, R., McGregor, A., Picksley, S. M., Crouch, D. H., Hall, P. A., & Wright, E. G. (2001). Mammalian prohibitin proteins respond to mitochondrial stress and decrease during cellular senescence. *Experimental Cell Research* **265**, 262-273.

Coelho, S. M., Taylor, A. R., Ryan, K. P., Sousa-Pinto, I., Brown, M. T., & Brownlee, C. (2002). Spatiotemporal patterning of reactive oxygen production and Ca²⁺ wave propagation in fucus rhizoid cells. *Plant Cell* **14**, 2369-2381.

Corvi, M. M., Soltys, C. L. M., & Berthiaume, L. G. (2001). Regulation of mitochondrial carbamoyl-phosphate synthetase 1 activity by active site fatty acylation. *Journal of Biological Chemistry* **276**, 45704-45712.

Da Cruz, S., Parone, P. A., Gonzalo, P., Bienvenut, W. V., Tondera, D., Jourdain, A., Quadroni, M., & Martinou, J. C. (2008). SLP-2 interacts with prohibitins in the mitochondrial inner membrane and contributes to their stability. *Biochimica et Biophysica Acta-Molecular Cell Research* **1783**, 904-911.

Da Cruz, S., Xenarios, I., Langridge, J., Vilbois, F., Parone, P. A., & Martinou, J. C. (2003). Proteomic analysis of the mouse liver mitochondrial inner membrane. *Journal of Biological Chemistry* **278**, 41566-41571.

Dal Bosco, C., Lezhneva, L., Biehl, A., Leister, D., Strotmann, H., Wanner, G., & Meurer, J. (2004). Inactivation of the chloroplast ATP synthase gamma subunit results in high non-photochemical fluorescence quenching and altered nuclear gene expression in Arabidopsis thaliana. *Journal of Biological Chemistry* **279**, 1060-1069.

del Pozo, O. & Lam, E. (2003). Expression of the baculovirus p35 protein in tobacco affects cell death progression and compromises N gene-mediated disease resistance response to tobacco mosaic virus. *Molecular Plant-Microbe Interactions* **16**, 485-494.

Dermine, J. F., Duclos, S., Garin, J., St Louis, F., Rea, S., Parton, R. G., & Desjardins, M. (2001). Flotillin-1-enriched lipid raft domains accumulate on maturing phagosomes. *Journal of Biological Chemistry* **276**, 18507-18512.

Desikan, R., Last, K., Harrett-Williams, R., Tagliavia, C., Harter, K., Hooley, R., Hancock, J. T., & Neill, S. J. (2006). Ethylene-induced stomatal closure in Arabidopsis occurs via AtrbohF-mediated hydrogen peroxide synthesis. *Plant Journal* **47**, 907-916.

- Dietrich, L. E. P. & Ungermann, C. (2004). On the mechanism of protein palmitoylation. *Embo Reports* **5**, 1053-1057.
- Douce, R. (1985). *Mitochondria in higher plants. Structure, function and biogenesis*. Academic Press, Orlando.
- Dowling, P., Meleady, P., Dowd, A., Henry, M., Glynn, S., & Clynes, M. (2007). Proteomic analysis of isolated membrane fractions from superinvasive cancer cells. *Biochimica et Biophysica Acta-Proteins and Proteomics* **1774**, 93-101.
- Dunkley, T. P. J., Hester, S., Shadforth, I. P., Runions, J., Weimar, T., Hanton, S. L., Griffin, J. L., Bessant, C., Brandizzi, F., Hawes, C., Watson, R. B., Dupree, P., & Lilley, K. S. (2006). Mapping the Arabidopsis organelle proteome. *Proceedings of the National Academy of Sciences of the United States of America* **103**, 6518-6523.
- Dutilleul, C., Garmier, M., Noctor, G., Mathieu, C., Chetrit, P., Foyer, C. H., & de Paepe, R. (2003). Leaf mitochondria modulate whole cell redox homeostasis, set antioxidant capacity, and determine stress resistance through altered signaling and diurnal regulation. *Plant Cell* **15**, 1212-1226.
- Ehrenberg, B., Montana, V., Wei, M. D., Wuskell, J. P., & Loew, L. M. (1988). Membrane-Potential Can be Determined in Individual Cells from the Nernstian Distribution of Cationic Dyes. *Biophysical Journal* **53**, 785-794.
- Eisenberg, D., Weiss, R. M., & Terwilliger, T. C. (1984). The Hydrophobic Moment Detects Periodicity in Protein Hydrophobicity. *Proceedings of the National Academy of Sciences of the United States of America-Biological Sciences* **81**, 140-144.
- Emanuelsson, O., Nielsen, H., Brunak, S., & von Heijne, G. (2000). Predicting subcellular localization of proteins based on their N-terminal amino acid sequence. *Journal of Molecular Biology* **300**, 1005-1016.
- Emini, E. A., Hughes, J. V., Perlow, D. S., & Boger, J. (1985). Induction of Hepatitis-A Virus-Neutralizing Antibody by A Virus-Specific Synthetic Peptide. *Journal of Virology* **55**, 836-839.
- Farkas, D. L., Wei, M. D., Febroriello, P., Carson, J. H., & Loew, L. M. (1989). Simultaneous Imaging of Cell and Mitochondrial-Membrane Potentials. *Biophysical Journal* **56**, 1053-1069.
- Fernie, A. R., Carrari, F., & Sweetlove, L. J. (2004). Respiratory metabolism: glycolysis, the TCA cycle and mitochondrial electron transport. *Current Opinion in Plant Biology* **7**, 254-261.
- Finkemeier, I., Goodman, M., Lamkemeyer, P., Kandlbinder, A., Sweetlove, L. J., & Dietz, K. J. (2005). The mitochondrial type II peroxiredoxin F is essential for redox

homeostasis and root growth of *Arabidopsis thaliana* under stress. *Journal of Biological Chemistry* **280**, 12168-12180.

Fricke, B., Argent, A. C., Chetty, M. C., Pizzey, A. R., Turner, E. J., Ho, M. M., Lolascon, A., von During, M., & Stewart, G. W. (2003a). The "stomatin" gene and protein in overhydrated hereditary stomatocytosis. *Blood* **102**, 2268-2277.

Fricke, B., Argent, A. C., Chetty, M. C., Pizzey, A. R., Turner, E. J., Ho, M. M., Lolascon, A., von During, M., & Stewart, G. W. (2003b). The "stomatin" gene and protein in overhydrated hereditary stomatocytosis. *Blood* **102**, 2268-2277.

Fricke, B., Lints, R., Stewart, G., Drummond, H., Dodt, G., Driscoll, M., & von During, M. (2000). Epithelial Na⁺ channels and stomatin are expressed in rat trigeminal mechanosensory neurons. *Cell and Tissue Research* **299**, 327-334.

Fricke, B., Parsons, S. F., Knopfle, G., During, M., & Stewart, G. W. (2005). Stomatin is mis-trafficked in the erythrocytes of overhydrated hereditary stomatocytosis, and is absent from normal primitive yolk sac-derived erythrocytes. *British Journal of Haematology* **131**, 265-277.

Friso, G., Giacomelli, L., Ytterberg, A. J., Peltier, J. B., Rudella, A., Sun, Q., & van Wijk, K. J. (2004). In-depth analysis of the thylakoid membrane proteome of *Arabidopsis thaliana* chloroplasts: New proteins, new functions, and a plastid proteome database. *Plant Cell* **16**, 478-499.

Fujiki, Y., Hubbard, A. L., Fowler, S., & Lazarow, P. B. (1982). Isolation of Intracellular Membranes by Means of Sodium-Carbonate Treatment - Application to Endoplasmic-Reticulum. *Journal of Cell Biology* **93**, 97-102.

Fujiwara, M., Umemura, K., Kawasaki, T., & Shimamoto, K. (2006). Proteomics of Rac GTPase signaling reveals its predominant role in elicitor-induced defense response of cultured rice cells. *Plant Physiology* **140**, 734-745.

Gao, H., Sage, T. L., & Steryoung, K. W. (2006). FZL, an FZO-like protein in plants, is a determinant of thylakoid and chloroplast morphology. *Proceedings of the National Academy of Sciences of the United States of America* **103**, 6759-6764.

Gardner, K. & Bennett, V. (1987). Modulation of spectrin-actin assembly by erythrocyte adducin. *Nature* **328**, 359-362.

Garin, J., Diez, R., Kieffer, S., Dermine, J. F., Duclos, S., Gagnon, E., Sadoul, R., Rondeau, C., & Desjardins, M. (2001). The phagosome proteome: Insight into phagosome functions. *Journal of Cell Biology* **152**, 165-180.

- Garnier, J., Osguthorpe, D. J., & Robson, B. (1978). Analysis of Accuracy and Implications of Simple Methods for Predicting Secondary Structure of Globular Proteins. *Journal of Molecular Biology* **120**, 97-120.
- Gasteiger, E., Hoogland, C., Gattiker, A., Duvot, S., Wilkins, M. R., Appel, R. D., & Bairoch, A. Protein Identification and Analysis Tools on the ExPASy Server. Walker, John M. 571-607. 2005. Humana Press. The Proteomics Protocols Handbook. 2005.
Ref Type: Serial (Book, Monograph)
- Geelen, D., Leyman, B., Batoko, H., Di Sansabastiano, G. P., Moore, I., & Blatt, M. R. (2002). The abscisic acid-related SNARE homolog NtSyr1 contributes to secretion and growth: Evidence from competition with its cytosolic domain. *Plant Cell* **14**, 387-406.
- Geldner, N., Friml, J., Stierhof, Y. D., Jurgens, G., & Palme, K. (2001). Auxin transport inhibitors block PIN1 cycling and vesicle trafficking. *Nature* **413**, 425-428.
- Gerke, V. & Moss, S. E. (2002). Annexins: From structure to function. *Physiological Reviews* **82**, 331-371.
- Glebov, O. O., Bright, N. A., & Nichols, B. J. (2006). Flotillin-1 defines a clathrin-independent endocytic pathway in mammalian cells. *Nature Cell Biology* **8**, 46-U16.
- Glick, B. S., Brandt, A., Cunningham, K., Muller, S., Hallberg, R. L., & Schatz, G. (1992). Cytochromes-C1 and Cytochromes-B2 Are Sorted to the Intermembrane Space of Yeast Mitochondria by A Stop-Transfer Mechanism. *Cell* **69**, 809-822.
- Glick, B. S., Wachter, C., Reid, G. A., & Schatz, G. (1993). Import of Cytochrome-B(2) to the Mitochondrial Intermembrane Space - the Tightly Folded Heme-Binding Domain Makes Import Dependent Upon Matrix Atp. *Protein Science* **2**, 1901-1917.
- Goda, H., Sasaki, E., & Akiyama, K. The AtGenExpress hormone and chemical treatment data set: experimental design, data evaluation, model data analysis and data access. *Plant Journal* **55**[3], 526-542. 2008.
Ref Type: Journal (Full)
- Goepfert, S. & Poirier, Y. (2007). beta-oxidation in fatty acid degradation and beyond. *Current Opinion in Plant Biology* **10**, 245-251.
- Goodman, M. B., Ernstrom, G. G., Chelur, D. S., O'Hagan, R., Yao, C. A., & Chalfie, M. (2002). MEC-2 regulates C-elegans DEG/ENaC channels needed for mechanosensation. *Nature* **415**, 1039-1042.
- Gray, J., Janick-Buckner, D., Buckner, B., Close, P. S., & Johal, G. S. (2002). Light-dependent death of maize lls1 cells is mediated by mature chloroplasts. *Plant Physiology* **130**, 1894-1907.

- Green, J. B., Fricke, B., Chetty, M. C., von During, M., Preston, G. F., & Stewart, G. W. (2004). Eukaryotic and prokaryotic stomatins: the proteolytic link. *Blood Cells Molecules and Diseases* **32**, 411-422.
- Green, J. B. & Young, J. P. W. (2008). Slipins: ancient origin, duplication and diversification of the stomatin protein family. *Bmc Evolutionary Biology* **8**.
- Gu, G. Q., Caldwell, G. A., & Chalfie, M. (1996). Genetic interactions affecting touch sensitivity in *Caenorhabditis elegans*. *Proceedings of the National Academy of Sciences of the United States of America* **93**, 6577-6582.
- Guo, Q. C., Shen, J. N., Jin, S., Wang, J., Huang, G., Zhang, L. J., Yin, J. Q., Zou, C. Y., & Li, M. T. (2007). Comparative proteomic analysis of human osteosarcoma and SV40-immortalized normal osteoblastic cell lines. *Acta Pharmacologica Sinica* **28**, 850-858.
- Hajek, P., Chomyn, A., & Attardi, G. (2007). Identification of a novel mitochondrial complex containing mitofusin 2 and stomatin-like protein 2. *Journal of Biological Chemistry* **282**, 5670-5681.
- Hakozaki, H., Endo, M., Masuko, H., Park, J. I., Ito, H., Uchida, M., Kamada, M., Takahashi, H., Higashitani, A., & Watanabe, M. (2004). Cloning and expression pattern of a novel microspore-specific gene encoding hypersensitive-induced response protein (LjHIR1) from the model legume, *Lotus japonicus*. *Genes & Genetic Systems* **79**, 307-310.
- Hayashi, T., McMahon, H., Yamasaki, S., Binz, T., Hata, Y., Sudhof, T. C., & Niemann, H. (1994). Synaptic Vesicle Membrane-Fusion Complex - Action of Clostridial Neurotoxins on Assembly. *Embo Journal* **13**, 5051-5061.
- Hayes, M. J., Rescher, U., Gerke, V., & Moss, S. E. (2004). Annexin-actin interactions. *Traffic* **5**, 571-576.
- Hazarika, P., Dham, N., Patel, P., Cho, M., Weidner, D., Goldsmith, L., & Duvic, M. (1999). Flotillin 2 is distinct from epidermal surface antigen (ESA) and is associated with filopodia formation. *Journal of Cellular Biochemistry* **75**, 147-159.
- Heazlewood, J. L. & Millar, A. H. (2005). AMPDB: the Arabidopsis Mitochondrial Protein Database. *Nucleic Acids Research* **33**, D605-D610.
- Heazlewood, J. L., Tonti-Filippini, J. S., Gout, A. M., Day, D. A., Whelan, J., & Millar, A. H. (2004). Experimental analysis of the Arabidopsis mitochondrial proteome highlights signaling and regulatory components, provides assessment of targeting prediction programs, and indicates plant-specific mitochondrial proteins. *Plant Cell* **16**, 241-256.
- Heazlewood, J. L., Verboom, R. E., Tonti-Filippini, J., Small, I., & Millar, A. H. (2007). SUBA: The Arabidopsis subcellular database. *Nucleic Acids Research* **35**, D213-D218.

Hemsley, P. A. & Grierson, C. S. (2008). Multiple roles for protein palmitoylation in plants. *Trends in Plant Science* **13**, 295-302.

Hemsley, P. A., Kemp, A. C., & Grierson, C. S. (2005). The TIP GROWTH DEFECTIVE1 S-acyl transferase regulates plant cell growth in Arabidopsis. *Plant Cell* **17**, 2554-2563.

Hemsley, P. A., Taylor, L., & Grierson, C. S. Assaying protein palmitoylation in plants. *Plant Methods* 4[2]. 2008.
Ref Type: Journal (Full)

Hideg, E. Detection of Free Radicals and Reactive Oxygen Species. [274], 249-260. 2004. *Methods in Molecular Biology (Photosynthesis Research Protocols)*.
Ref Type: Serial (Book, Monograph)

Hiebl dirschmied, C. M., Adolf, G. R., & Prohaska, R. (1991a). Isolation and Partial Characterization of the Human Erythrocyte Band-7 Integral Membrane-Protein. *Biochimica et Biophysica Acta* **1065**, 195-202.

Hiebl dirschmied, C. M., Entler, B., Glotzmann, C., Maurerfoggy, I., Stratowa, C., & Prohaska, R. (1991b). Cloning and Nucleotide-Sequence of Cdna-Encoding Human Erythrocyte Band-7 Integral Membrane-Protein. *Biochimica et Biophysica Acta* **1090**, 123-124.

Higo, K., Ugawa, Y., Iwamoto, M., & Korenaga, T. (1999). Plant cis-acting regulatory DNA elements (PLACE) database: 1999. *Nucleic Acids Research* **27**, 297-300.

Higuchi, R., Krummel, B., & Saiki, R. K. (1988). A General-Method of Invitro Preparation and Specific Mutagenesis of Dna Fragments - Study of Protein and Dna Interactions. *Nucleic Acids Research* **16**, 7351-7367.

Hilson, P., Allemeersch, J., Altmann, T., Aubourg, S., Avon, A., Beynon, J., Bhalerao, R. P., Bitton, F., Caboche, M., Cannoot, B., Chardakov, V., Cognet-Holliger, C., Colot, V., Crowe, M., Darimont, C., Durinck, S., Eickhoff, H., de Longevialle, A. F., Farmer, E. E., Grant, M., Kuiper, M. T. R., Lehrach, H., Leon, C., Leyva, A., Lundeberg, J., Lurin, C., Moreau, Y., Nietfeld, W., Paz-Ares, J., Reymond, P., Rouze, P., Sandberg, G., Segura, M. D., Serizet, C., Tabrett, A., Tacconnat, L., Thareau, V., Van Hummelen, P., Vercruyssen, S., Vuylsteke, M., Weingartner, M., Weisbeek, P. J., Wirta, V., Wittink, F. R. A., Zabeau, M., & Small, I. (2004). Versatile gene-specific sequence tags for Arabidopsis functional genomics: Transcript profiling and reverse genetics applications. *Genome Research* **14**, 2176-2189.

Ho, S. N., Hunt, H. D., Horton, R. M., Pullen, J. K., & Pease, L. R. (1989). Site-Directed Mutagenesis by Overlap Extension Using the Polymerase Chain-Reaction. *Gene* **77**, 51-59.

Holdsworth, M. J., Bentsink, L., & Soppe, W. J. J. (2008). Molecular networks regulating Arabidopsis seed maturation, after-ripening, dormancy and germination. *New Phytologist* **179**, 33-54.

Holzinger, A., Buchner, O., Lutz, C., & Hanson, M. R. (2007). Temperature-sensitive formation of chloroplast protrusions and stromules in mesophyll cells of *Arabidopsis thaliana*. *Protoplasma* **230**, 23-30.

Honys, D. & Twell, D. (2004). Transcriptome analysis of haploid male gametophyte development in *Arabidopsis*. *Genome Biology* **5**.

Hoppel, C. & Cooper, C. (1968). Action of Digitonin on Rat Liver Mitochondria - Effects on Enzyme Content. *Biochemical Journal* **107**, 367-&.

Horton, B. & Nakai, K. Better prediction of protein cellular localization sites with the k nearest neighbors classifier. *Proc Int Conf Intell Syst Mol Biol.* 5, 147-152. 1997.
Ref Type: Journal (Full)

Huang, M. X., Gu, G. Q., Ferguson, E. L., & Chalfie, M. (1995). A Stomatin-Like Protein Necessary for Mechanosensation in *C. Elegans*. *Nature* **378**, 292-295.

Huber, T. B., Kottgen, M., Schilling, B., Walz, G., & Benzing, T. (2001). Interaction with podocin facilitates nephrin signaling. *Journal of Biological Chemistry* **276**, 41543-41546.

Huber, T. B., Schermer, B., Muller, R. U., Hohne, M., Bartram, M., Calixto, A., Hagmann, H., Reinhardt, C., Koos, F., Kunzelmann, K., Shirokova, E., Krautwurst, D., Harteneck, C., Simons, M., Pavenstadt, H., Kerjaschki, D., Thiele, C., Walz, G., Chalfie, M., & Benzing, T. (2006b). Podocin and MEC-2 bind cholesterol to regulate the activity of associated ion channels. *Proceedings of the National Academy of Sciences of the United States of America* **103**, 17079-17086.

Huber, T. B., Schermer, B., Muller, R. U., Hohne, M., Bartram, M., Calixto, A., Hagmann, H., Reinhardt, C., Koos, F., Kunzelmann, K., Shirokova, E., Krautwurst, D., Harteneck, C., Simons, M., Pavenstadt, H., Kerjaschki, D., Thiele, C., Walz, G., Chalfie, M., & Benzing, T. (2006a). Podocin and MEC-2 bind cholesterol to regulate the activity of associated ion channels. *Proceedings of the National Academy of Sciences of the United States of America* **103**, 17079-17086.

Huber, T. B., Simons, M., Hartleben, B., Sernetz, L., Schmidts, M., Gundlach, E., Saleem, M. A., Walz, G., & Benzing, T. (2003). Molecular basis of the functional podocin-nephrin complex: mutations in the NPHS2 gene disrupt nephrin targeting to lipid raft microdomains. *Human Molecular Genetics* **12**, 3397-3405.

Huttly, A. K. & Phillips, A. L. (1995). Gibberellin-Regulated Plant Genes. *Physiologia Plantarum* **95**, 310-317.

- Ikeda, M., Kihara, A., & Igarashi, Y. (2004). Sphingosine-1-phosphate lyase SPL is an endoplasmic reticulum-resident, integral membrane protein with the pyridoxal 5'-phosphate binding domain exposed to the cytosol. *Biochemical and Biophysical Research Communications* **325**, 338-343.
- Ikonen, E., Fiedler, K., Parton, R. G., & Simons, K. (1995). Prohibitin, An Antiproliferative Protein, Is Localized to Mitochondria. *Febs Letters* **358**, 273-277.
- Inaba, T. & Schnell, D. J. (2008). Protein trafficking to plastids: one theme, many variations. *Biochemical Journal* **413**, 15-28.
- Innes, D. S., Sinard, J. H., Gilligan, D. M., Snyder, L. M., Gallagher, P. G., & Morrow, J. S. (1999). Exclusion of the stomatin, alpha-adducin and beta-adducin loci in a large kindred with dehydrated hereditary stomatocytosis. *American Journal of Hematology* **60**, 72-74.
- Izawa, S. & Good, N. E. (1966). Effect of Salts and Electron Transport on Conformation of Isolated Chloroplasts .2. Electron Microscopy. *Plant Physiology* **41**, 544-&.
- Jameson, B. A. & Wolf, H. (1988). The Antigenic Index - A Novel Algorithm for Predicting Antigenic Determinants. *Computer Applications in the Biosciences* **4**, 181-186.
- Jefferson, R. A. (1989). The Gus Reporter Gene System. *Nature* **342**, 837-838.
- Johnson, L. V., Walsh, M. L., Bockus, B. J., & Chen, L. B. (1981). Monitoring of Relative Mitochondrial-Membrane Potential in Living Cells by Fluorescence Microscopy. *Journal of Cell Biology* **88**, 526-535.
- Jupe, E. R., Liu, X. T., Kiehlbauch, J. L., Mcclung, J. K., & Dellorco, R. T. (1996). The 3' untranslated region of prohibitin and cellular immortalization. *Experimental Cell Research* **224**, 128-135.
- Kadurin, I., Golubovic, A., Leisle, L., Schindelin, H., & Grunder, S. (2008a). Differential effects of N-glycans on surface expression suggest structural differences between the acid-sensing ion channel (ASIC) 1a and ASIC1b. *Biochemical Journal* **412**, 469-475.
- Kadurin, I., Huber, S., & Grunder, S. A single conserved proline residue determines the membrane topology of stomatin. *Biochemical Journal* Epub ahead of print. 2008b.
Ref Type: Journal (Full)
- Kagaya, Y., Ohmiya, K., & Hattori, T. (1999). RAV1, a novel DNA-binding protein, binds to bipartite recognition sequence through two distinct DNA-binding domains uniquely found in higher plants. *Nucleic Acids Research* **27**, 470-478.

- Kammann, M., Laufs, J., Schell, J., & Gronenborn, B. (1989). Rapid Insertional Mutagenesis of Dna by Polymerase Chain-Reaction (Pcr). *Nucleic Acids Research* **17**, 5404.
- Kawaguchi, A. & Bloch, K. (1976). Inhibition of Glutamate-Dehydrogenase and Malate Dehydrogenases by Palmitoyl Coenzyme-A. *Journal of Biological Chemistry* **251**, 1406-1412.
- Kiernan, J. A. (2000). Formaldehyde, formalin, paraformaldehyde and glutaraldehyde: What they are and what they do. *Microscopy Today* **00**, 8-12.
- Kihara, A., Akiyama, Y., & Ito, K. (1996). A protease complex in the Escherichia coli plasma membrane: HflKC (HflA) forms a complex with FtsH (HflB), regulating its proteolytic activity against SecY. *Embo Journal* **15**, 6122-6131.
- Kihara, A., Akiyama, Y., & Ito, K. (1997). Host regulation of lysogenic decision in bacteriophage lambda: Transmembrane modulation of FtsH (HflB), the cII degrading protease, by HflKC (HflA). *Proceedings of the National Academy of Sciences of the United States of America* **94**, 5544-5549.
- Kihara, A., Akiyama, Y., & Ito, K. (2001). Revisiting the lysogenization control of bacteriophage lambda - Identification and characterization of a new host component, HflD. *Journal of Biological Chemistry* **276**, 13695-13700.
- Kihara, A. & Ito, K. (1998). Translocation, folding, and stability of the HflKC complex with signal anchor topogenic sequences. *Journal of Biological Chemistry* **273**, 29770-29775.
- Kilian, J., Whitehead, D., Horak, J., Wanke, D., Weinl, S., Batistic, O., D'Angelo, C., Bornberg-Bauer, E., Kudla, J., & Harter, K. (2007). The AtGenExpress global stress expression data set: protocols, evaluation and model data analysis of UV-B light, drought and cold stress responses. *Plant Journal* **50**, 347-363.
- Kirchhof, M. G., Chan, L. A., Lemke, C. A., Vardhana, S., Darlington, P. J., Marquez, M. E., Taylor, R., Rizkalla, K., Blanca, I., Dustin, M. L., & Madrenas, J. (2008). Modulation of T cell activation by stomatin-like protein 2. *Journal of Immunology* **181**, 1927-1936.
- Kokubo, H., Helms, J. B., Ohno-Iwashita, Y., Shimada, Y., Horikoshi, Y., & Yamaguchi, H. (2003). Ultrastructural localization of flotillin-1 to cholesterol-rich membrane microdomains, rafts, in rat brain tissue. *Brain Research* **965**, 83-90.
- Kolodziejczak, M., Kolaczowska, A., Szczesny, B., Urantowka, A., Knorpp, C., Kieleczawa, J., & Janska, H. (2002). A higher plant mitochondrial homologue of the yeast m-AAA protease - Molecular cloning, localization, and putative function. *Journal of Biological Chemistry* **277**, 43792-43798.

- Kominek, L. A. (1975). Cycloheximide Production by *Streptomyces-Griseus* - Control Mechanisms of Cycloheximide Biosynthesis. *Antimicrobial Agents and Chemotherapy* **7**, 856-860.
- Kostiuk, M. A., Corvi, M. M., Keller, B. O., Plummer, G., Prescher, J. A., Hangauer, M. J., Bertozzi, C. R., Rajaiah, G., Falck, J. R., & Berthiaume, L. G. (2008). Identification of palmitoylated mitochondrial proteins using a bio-orthogonal azido-palmitate analogue. *Faseb Journal* **22**, 721-732.
- Kruft, V., Eubel, H., Jansch, L., Werhahn, W., & Braun, H. P. (2001). Proteomic approach to identify novel mitochondrial proteins in Arabidopsis. *Plant Physiology* **127**, 1694-1710.
- Kuwahara, Y., Ohno, A., Morii, T., Yokoyama, H., Matsui, I., Tochio, H., Shirakawa, M., & Hiroaki, H. (2008). The solution structure of the C-terminal domain of NfeD reveals a novel membrane-anchored OB-fold. *Protein Science* **17**, 1915-1924.
- Laemmli, U. K. (1970). Cleavage of Structural Proteins During Assembly of Head of Bacteriophage-T4. *Nature* **227**, 680-&.
- Lam, E., del Pozo, O., & Pontier, D. (1999a). BAXing in the hypersensitive response. *Trends in Plant Science* **4**, 419-421.
- Lam, E., Pontier, D., & del Pozo, O. (1999b). Die and let live - programmed cell death in plants. *Current Opinion in Plant Biology* **2**, 502-507.
- Lamb, R. S., Hill, T. A., Tan, Q. K. G., & Irish, V. F. (2002). Regulation of APETALA3 floral homeotic gene expression by meristem identity genes. *Development* **129**, 2079-2086.
- Lande, W. M., Thiemann, P. V. W., & Mentzer, W. C. (1982). Missing Band-7 Membrane-Protein in 2 Patients with High Na, Low K-Erythrocytes. *Journal of Clinical Investigation* **70**, 1273-1280.
- Lang, D. M., Lommel, S., Jung, M., Ankerhold, R., Petrusch, B., Laessing, U., Wiechers, M. F., Plattner, H., & Stuermer, C. A. O. (1998). Identification of reggie-1 and reggie-2 as plasmamembrane- associated proteins which cocluster with activated GPI-anchored cell adhesion molecules in non-caveolar micropatches in neurons. *Journal of Neurobiology* **37**, 502-523.
- Langer, T., Kaser, M., Klanner, C., & Leonhard, K. (2001). AAA proteases of mitochondria: quality control of membrane proteins and regulatory functions during mitochondrial biogenesis. *Biochemical Society Transactions* **29**, 431-436.
- Langhorst, M. F., Reuter, A., Jaeger, F. A., Wippich, F. M., Luxenhofer, G., Plattner, H., & Stuermer, C. A. O. (2008). Trafficking of the microdomain scaffolding protein reggie-1/flotillin-2. *European Journal of Cell Biology* **87**, 211-226.

Larsson, C., Sommarin M., & Widell S. Isolation of highly purified plant plasma membranes and separation of inside-out and right-side-out vesicles. *Methods in Enzymology* **228**, 451-469. 1994.
Ref Type: Journal (Full)

Larsson, C., Widell, S., & Kjellbom, P. (1987). Preparation of High-Purity Plasma-Membranes. *Methods in Enzymology* **148**, 558-568.

Lawand, S., Dorne, A. J., Long, D., Coupland, G., Mache, R., & Carol, P. (2002). Arabidopsis a bout de soufflé, which is homologous with mammalian carnitine acyl carrier, is required for postembryonic growth in the light. *Plant Cell* **14**, 2161-2173.

Leimer, U., Franke, W. W., & Leube, R. E. (1996). Synthesis of the mammalian synaptic vesicle protein synaptophysin in insect cells: A model for vesicle biogenesis. *Experimental Cell Research* **224**, 88-95.

Leuenberger, D., Bally, N. A., Schatz, G., & Koehler, C. M. (1999). Different import pathways through the mitochondrial intermembrane space for inner membrane proteins. *Embo Journal* **18**, 4816-4822.

Li, C. H., Tzeng, S. L., Cheng, Y. W., & Kang, J. J. (2005). Chloramphenicol-induced mitochondrial stress increases p21 expression and prevents cell apoptosis through a p21-dependent pathway. *Journal of Biological Chemistry* **280**, 26193-26199.

Li, X., Matsuoka, Y., & Bennett, V. (1998). Adducin preferentially recruits spectrin to the fast growing ends of actin filaments in a complex requiring the MARCKS-related domain and a newly defined oligomerization domain. *Journal of Biological Chemistry* **273**, 19329-19338.

Linder, M. E. & Deschenes, R. J. (2003). New insights into the mechanisms of protein palmitoylation. *Biochemistry* **42**, 4311-4320.

Ling, M. M. & Robinson, B. H. (1997b). Approaches to DNA mutagenesis: An overview. *Analytical Biochemistry* **254**, 157-178.

Ling, M. M. & Robinson, B. H. (1997a). Approaches to DNA mutagenesis: An overview. *Analytical Biochemistry* **254**, 157-178.

Liu, J., DeYoung, S. M., Zhang, M., Dold, L. H., & Saltiel, A. R. (2005). The Stomatin/Prohibitin/Flotillin/HflK/C Domain of Flotillin-1 Contains Distinct Sequences That Direct Plasma Membrane Localization and Protein Interactions in 3T3-L1 Adipocytes. *Journal of Biological Chemistry* **280**, 16125-16134.

Livaja, M., Palmieri, M. C., von Rad, U., & Durner, J. (2008). The effect of the bacterial effector protein harpin on transcriptional profile and mitochondrial proteins of Arabidopsis thaliana. *Journal of Proteomics* **71**, 148-159.

Lock, S. P., Smith, R. S., & Hardisty, R. M. (1961). Stomatocytosis: a hereditary red cell anomaly associated with haemolytic anaemia. *British Journal of Haematology* **7**, 303-307.

Logan, D. C. (2003). Mitochondrial dynamics. *New Phytologist* **160**, 463-478.

Logan, D. C. (2006a). Plant mitochondrial dynamics. *Biochimica et Biophysica Acta-Molecular Cell Research* **1763**, 430-441.

Logan, D. C. (2006b). The mitochondrial compartment. *Journal of Experimental Botany* **57**, 1225-1243.

Logan, D. C. (2008a). Having a swell time - mitochondrial morphology and plant cell death programmes. *Journal of Microscopy-Oxford* **231**, 215-224.

Logan, D. C. (2008b). Having a swell time - mitochondrial morphology and plant cell death programmes. *Journal of Microscopy-Oxford* **231**, 215-224.

Logan, D. C. & Leaver, C. J. (2000). Mitochondria-targeted GFP highlights the heterogeneity of mitochondrial shape, size and movement within living plant cells. *Journal of Experimental Botany* **51**, 865-871.

Logan, D. C., Millar, A. H., Sweetlove, L. J., Hill, S. A., & Leaver, C. J. (2001). Mitochondrial biogenesis during germination in maize embryos. *Plant Physiology* **125**, 662-672.

Logan, D. C., Scott, I., & Tobin, A. K. (2003). The genetic control of plant mitochondrial morphology and dynamics. *Plant Journal* **36**, 500-509.

los Reyes, B. G., Morsy, M., Gibbons, J., Varma, T. S. N., Antoine, W., McGrath, J. M., Halgren, R., & Redus, M. (2003). A snapshot of the low temperature stress transcriptome of developing rice seedlings (*Oryza sativa* L.) via ESTs from subtracted cDNA library. *Theoretical and Applied Genetics* **107**, 1071-1082.

Losel, R. M., Falkenstein, E., Feuring, M., Schultz, A., Tillmann, H. C., Rossol-Haseroth, K., & Wehling, M. (2003). Nongenomic steroid action: Controversies, questions, and answers. *Physiological Reviews* **83**, 965-1016.

Lu, S. X. & Hrabak, E. M. (2002). An Arabidopsis calcium-dependent protein kinase is associated with the endoplasmic reticulum. *Plant Physiology* **128**, 1008-1021.

Lucero, H. A. & Robbins, P. W. (2004). Lipid rafts-protein association and the regulation of protein activity. *Archives of Biochemistry and Biophysics* **426**, 208-224.

Mackenzie, S. A. (2005). Plant organellar protein targeting: a traffic plan still under construction. *Trends in Cell Biology* **15**, 548-554.

- Magee, A. I., Koyama, A. H., Malfer, C., Wen, D., & Schlesinger, M. J. (1984). Release of Fatty-Acids from Virus Glycoproteins by Hydroxylamine. *Biochimica et Biophysica Acta* **798**, 156-166.
- Mairhofer, M., Steiner, M., Mosgoeller, W., Prohaska, R., & Salzer, U. (2002). Stomatin is a major lipid-raft component of platelet alpha granules. *Blood* **100**, 897-904.
- Malisan, F. & Testi, R. (2003). Mitochondrial lipids as apoptosis regulators. *Current Medicinal Chemistry* **10**, 1573-1580.
- Malorni, W., Garofalo, T., Tinari, A., Manganelli, V., Misasi, R., & Sorice, M. (2008). *Analyzing lipid raft dynamics during cell apoptosis*, pp. 125-140.
- Mannsfeldt, A. G., Carroll, P., Stucky, C. L., & Lewin, G. R. (1999). Stomatin, a MEC-5 like protein, is expressed by mammalian sensory neurons. *Molecular and Cellular Neuroscience* **13**, 391-404.
- Marmagne, A., Rouet, M. A., Ferro, M., Rolland, N., Alcon, C., Joyard, J., Garin, J., Barbier-Brygoo, H., & Ephritikhine, G. (2004). Identification of new intrinsic proteins in Arabidopsis plasma membrane proteome. *Molecular & Cellular Proteomics* **3**, 675-691.
- Martin, T., Sharma, R., Sippel, C., Waegemann, K., Soll, J., & Vothknecht, U. C. (2006). A protein kinase family in Arabidopsis phosphorylates chloroplast precursor proteins. *Journal of Biological Chemistry* **281**, 40216-40223.
- Martinez-Abundis, E., Garcia, N., Correa, F., Franco, M., & Zazueta, C. (2007). Changes in specific lipids regulate BAX-induced mitochondrial permeability transition. *Febs Journal* **274**, 6500-6510.
- Masterson, C. & Wood, C. (2000). Mitochondrial beta-oxidation of fatty acids in higher plants. *Physiologia Plantarum* **109**, 217-224.
- Mastrogiacomo, A., Kohan, S. A., Whitelegge, J. P., & Gundersen, C. B. (1998). Intrinsic membrane association of Drosophila cysteine string proteins. *Febs Letters* **436**, 85-91.
- Matsuoka, Y., Li, X., & Bennett, V. (1998). Adducin is an in vivo substrate for protein kinase C: phosphorylation in the MARCKS-related domain inhibits activity in promoting spectrin-actin complexes and occurs in many cells, including dendritic spines of neurons. *Journal of Cell Biology* **142**, 485-497.
- Mcclung, J. K., Jupe, E. R., Liu, X. T., & Dellorco, R. T. (1995). Prohibitin - Potential Role in Senescence, Development, and Tumor Suppression. *Experimental Gerontology* **30**, 99-124.

- Merkwirth, C., Dargazanli, S., Tatsuta, T., Geimer, S., Lower, B., Wunderlich, F. T., Kleist-Retzow, J. C., Waisman, A., Westermann, B., & Langer, T. (2008). Prohibitins control cell proliferation and apoptosis by regulating OPA1-dependent cristae morphogenesis in mitochondria. *Genes & Development* **22**, 476-488.
- Millar, A. H., Sweetlove, L. J., Giege, P., & Leaver, C. J. (2001). Analysis of the Arabidopsis mitochondrial proteome. *Plant Physiology* **127**, 1711-1727.
- Mitra, S. K., Gantt, J. A., Ruby, J. F., Clouse, S. D., & Goshe, M. B. (2007). Membrane proteomic analysis of Arabidopsis thaliana using alternative solubilization techniques. *Journal of Proteome Research* **6**, 1933-1950.
- Mittler, R., del Pozo, O., Meisel, L., & Lam, E. (1997). Pathogen-induced programmed cell death in plants, a possible defense mechanism. *Developmental Genetics* **21**, 279-289.
- Miyamoto, K., Koshihara, S., Inoue, M., Kigawa, T., & Yokoyama, S. Solution structure of the band 7 domain of the mouse flotillin 2 protein.. STRUCTURE BY NMR OF 1-123. PDB data bank . 2004. RIKEN structural genomics initiative (RSGI).
Ref Type: Generic
- Moller, I. M. (2001). Plant mitochondria and oxidative stress: Electron transport, NADPH turnover, and metabolism of reactive oxygen species. *Annual Review of Plant Physiology and Plant Molecular Biology* **52**, 561-591.
- Moller, I. M., Jensen, P. E., & Hansson, A. (2007). Oxidative modifications to cellular components in plants. *Annual Review of Plant Biology* **58**, 459-481.
- Mongrand, S., Morel, J., Laroche, J., Claverol, S., Carde, J. P., Hartmann, M. A., Bonneau, M., Simon-Plas, F., Lessire, R., & Bessoule, J. J. (2004). Lipid rafts in higher plant cells - Purification and characterization of triton X-100-insoluble microdomains from tobacco plasma membrane. *Journal of Biological Chemistry* **279**, 36277-36286.
- Montel-Hagen, A., Kinet, S., Manel, N., Mongellaz, C., Prohaska, R., Battini, J. L., Delaunay, J., Sitbon, M., & Taylor, N. (2008). Erythrocyte glut1 triggers dehydroascorbic acid uptake in mammals unable to synthesize vitamin C. *Cell* **132**, 1039-1048.
- Moore, A. L. & Proudlove, M. O. (1983). Mitochondria and sub-mitochondrial particles. In *Isolation of membranes and organelles from plant cells*, eds. Hall, J. L. & Moore, A. L., pp. 153-184. Academic Press, London.
- Moore, K. H., Dandurand, D. M., & Kiechle, F. L. (1992). Fasting Induced Alterations in Mitochondrial Palmitoyl-Coa Metabolism May Inhibit Adipocyte Pyruvate-Dehydrogenase Activity. *International Journal of Biochemistry* **24**, 809-814.
- Moore, R. B. & Shriver, S. K. (1997). Protein 7.2b of human erythrocyte membranes binds to calpromotin. *Biochemical and Biophysical Research Communications* **232**, 294-297.

- Morel, F., Lauquin, G., Lunardi, J., Duszyński, J., & Vignais, P. V. (1974). Appraisal of Functional Significance of Inhibitory Effect of Long-Chain Acyl-Coas on Mitochondrial Transports. *Febs Letters* **39**, 133-138.
- Morrow, I. C., Rea, S., Martin, S., Prior, I. A., Prohaska, R., Hancock, J. F., James, D. E., & Parton, R. G. (2002). Flotillin-1/Reggie-2 traffics to surface raft domains via a novel Golgi-independent pathway - Identification of a novel membrane targeting domain and a role for palmitoylation. *Journal of Biological Chemistry* **277**, 48834-48841.
- Morton, D. J., Hoppel, C., & Cooper, C. (1968). Action of Digitonin on Rat Liver Mitochondria - Electron Microscopy. *Biochemical Journal* **107**, 377-&.
- Mur, L. A. J., Kenton, P., Lloyd, A. J., Ougham, H., & Prats, E. (2008). The hypersensitive response; the centenary is upon us but how much do we know? *Journal of Experimental Botany* **59**, 501-520.
- Nadimpalli, R., Yalpani, N., Johal, G. S., & Simmons, C. R. (2000). Prohibitins, stomatins, and plant disease response genes compose a protein superfamily that controls cell proliferation, ion channel regulation, and death. *Journal of Biological Chemistry* **275**, 29579-29586.
- Nair, R. & Rost, B. (2005). Mimicking cellular sorting improves prediction of subcellular localization. *Journal of Molecular Biology* **348**, 85-100.
- Nakabayashi, K., Okamoto, M., Koshiha, T., Kamiya, Y., & Nambara, E. (2005). Genome-wide profiling of stored mRNA in Arabidopsis thaliana seed germination: epigenetic and genetic regulation of transcription in seed. *Plant Journal* **41**, 697-709.
- Nakai, K. & Kanehisa, M. (1991). Expert System for Predicting Protein Localization Sites in Gram-Negative Bacteria. *Proteins-Structure Function and Genetics* **11**, 95-110.
- Neumann-Giesen, C., Falkenbach, B., Beicht, P., Claasen, S., Luers, G., Stuermer, C. A. O., Herzog, V., & Tikkanen, R. (2004). Membrane and raft association of reggie-1/flotillin-2: role of myristoylation, palmitoylation and oligomerization and induction of filopodia by overexpression. *Biochemical Journal* **378**, 509-518.
- Newman, H. A. I., Gordesky, S. E., Hoppel, C., & Cooper, C. (1968). Action of Digitonin on Rat Liver Mitochondria - Phospholipid Content. *Biochemical Journal* **107**, 381-&.
- Nicholls, D. G. (1979). Brown Adipose-Tissue Mitochondria. *Biochimica et Biophysica Acta* **549**, 1-29.
- Nijtmans, L. G. J., de Jong, L., Sanz, M. A., Coates, P. J., Berden, J. A., Back, J. W., Muijsers, A. O., van der Spek, H., & Grivell, L. A. (2000). Prohibitins act as a membrane-bound chaperone for the stabilization of mitochondrial proteins. *Embo Journal* **19**, 2444-2451.

- Nijtmans, L. G. J., Sanz, M. A., Grivell, L. A., & Coates, P. J. (2002). The mitochondrial PHB complex: roles in mitochondrial respiratory complex assembly, ageing and degenerative disease. *Cellular and Molecular Life Sciences* **59**, 143-155.
- Noble, J. A., Innis, M. A., Koonin, E. V., Rudd, K. E., Banuett, F., & Herskowitz, I. (1993). The Escherichia-Coli Hfla Locus Encodes A Putative Gtp-Binding Protein and 2 Membrane-Proteins, One of Which Contains A Protease-Like Domain. *Proceedings of the National Academy of Sciences of the United States of America* **90**, 10866-10870.
- Nunnari, J., Fox, T. D., & Walter, P. (1993). A Mitochondrial Protease with 2 Catalytic Subunits of Nonoverlapping Specificities. *Science* **262**, 1997-2004.
- O'Connor, T. R., Dyreson, C., & Wyrick, J. J. (2005). Athena: a resource for rapid visualization and systematic analysis of Arabidopsis promoter sequences. *Bioinformatics* **21**, 4411-4413.
- Obrdlik, P., El Bakkoury, M., Hamacher, T., Cappellaro, C., Vilarino, C., Fleischer, C., Ellerbrok, H., Kamuzinzi, R., Ledent, V., Blaudez, D., Sanders, D., Revuelta, J. L., Boles, E., Andre, B., & Frommer, W. B. (2004). K⁺ channel interactions detected by a genetic system optimized for systematic studies of membrane protein interactions. *Proceedings of the National Academy of Sciences of the United States of America* **101**, 12242-12247.
- Owczarek, C. M., Treutlein, H. R., Portbury, K. J., Gulluyan, L. M., Kola, I., & Hertzog, P. J. (2001). A novel member of the STOMATIN/EPB72/mec-2 family, stomatin-like 2 (STOML2), is ubiquitously expressed and localizes to HSA chromosome 9p13.1. *Cytogenetics and Cell Genetics* **92**, 196-203.
- Page, R. D. M. (1996). TreeView: An application to display phylogenetic trees on personal computers. *Computer Applications in the Biosciences* **12**, 357-358.
- Palaniswamy, S. K., James, S., Sun, H., Lamb, R. S., Davuluri, R. V., & Grotewold, E. (2006). AGRIS and AtRegNet. A platform to link cis-regulatory elements and transcription factors into regulatory networks. *Plant Physiology* **140**, 818-829.
- Palmgren, M. G., Sommarin, M., Serrano, R., & Larsson, C. (1991). Identification of An Autoinhibitory Domain in the C-Terminal Region of the Plant Plasma-Membrane H⁺-Atpase. *Journal of Biological Chemistry* **266**, 20470-20475.
- Parry, D. A. D. (1982). Coiled-Coils in Alpha-Helix-Containing Proteins - Analysis of the Residue Types Within the Heptad Repeat and the Use of These Data in the Prediction of Coiled-Coils in Other Proteins. *Bioscience Reports* **2**, 1017-1024.
- Pearce, M. M. P., Wang, Y., Kelley, G. G., & Wojcikiewicz, R. J. H. (2007). SPFH2 mediates the endoplasmic reticulum-associated degradation of inositol 1,4,5-trisphosphate receptors and other substrates in mammalian cells. *Journal of Biological Chemistry* **282**, 20104-20115.

Pellegrini, L. L., Oconnor, V., Lottspeich, F., & Betz, H. (1995). Clostridial Neurotoxins Compromise the Stability of A Low-Energy Snare Complex Mediating Nsf Activation of Synaptic Vesicle Fusion. *Embo Journal* **14**, 4705-4713.

Peltier, J. B., Ytterberg, A. J., Sun, Q., & van Wijk, K. J. (2004). New functions of the thylakoid membrane proteome of *Arabidopsis thaliana* revealed by a simple, fast, and versatile fractionation strategy. *Journal of Biological Chemistry* **279**, 49367-49383.

Persson, B. & Argos, P. (1994). Prediction of Transmembrane Segments in Proteins Utilizing Multiple Sequence Alignments. *Journal of Molecular Biology* **237**, 182-192.

Pfanner, N. (2008). Import and assembly of mitochondrial proteins. *Biochimica et Biophysica Acta-Bioenergetics* **1777**, S3.

Phillips, A. L., Ward, D. A., Uknes, S., Appleford, N. E. J., Lange, T., Huttly, A. K., Gaskin, P., Graebe, J. E., & Hedden, P. (1995). Isolation and Expression of 3 Gibberellin 20-Oxidase Cdna Clones from *Arabidopsis*. *Plant Physiology* **108**, 1049-1057.

Price, M. P., Thompson, R. J., Eshcol, J. O., Wemmie, J. A., & Benson, C. J. (2004). Stomatin modulates gating of acid-sensing ion channels. *Journal of Biological Chemistry* **279**, 53886-53891.

Rajaram, S., Sedensky, M. M., & Morgan, P. G. (1998). *unc-1*: A stomatin homologue controls sensitivity to volatile anesthetics in *Caenorhabditis elegans*. *Proceedings of the National Academy of Sciences of the United States of America* **95**, 8761-8766.

Rajaram, S., Spangler, T. L., Sedensky, M. M., & Morgan, P. G. (1999). A stomatin and a degenerin interact to control anesthetic sensitivity in *Caenorhabditis elegans*. *Genetics* **153**, 1673-1682.

Rehling, P., Pfanner, N., & Meisinger, C. (2003). Insertion of hydrophobic membrane proteins into the inner mitochondrial membrane - A guided tour. *Journal of Molecular Biology* **326**, 639-657.

Reifschneider, N. H., Goto, S., Nakamoto, H., Takahashi, R., Sugawa, M., Dencher, N. A., & Krause, F. (2006). Defining the mitochondrial proteomes from five rat organs in a physiologically significant context using 2D blue-native/SDS-PAGE. *Journal of Proteome Research* **5**, 1117-1132.

Resh, M. D. (2006). Use of analogs and inhibitors to study the functional significance of protein palmitoylation. *Methods* **40**, 191-197.

Riechmann, J. L. & Meyerowitz, E. M. (1998). The AP2/EREBP family of plant transcription factors. *Biological Chemistry* **379**, 633-646.

Rivera-Milla, E., Stuermer, C. A. O., & Malaga-Trillo, E. (2006). Ancient origin of reggie (flotillin), reggie-like, and other lipid-raft proteins: convergent evolution of the SPFH domain. *Cellular and Molecular Life Sciences* **63**, 343-357.

Roselli, S., Gribouval, O., Boute, N., Sich, M., Benessy, F., Attie, T., Gubler, M. C., & Antignac, C. (2002). Podocin localizes in the kidney to the slit diaphragm area. *American Journal of Pathology* **160**, 131-139.

Rostoks, N., Schmierer, D., Kudrna, D., & Kleinhofs, A. (2003). Barley putative hypersensitive induced reaction genes: genetic mapping, sequence analyses and differential expression in disease lesion mimic mutants. *Theoretical and Applied Genetics* **107**, 1094-1101.

Rubin, D. & Ismail-Beigi, F. (2003). Distribution of Glut1 in detergent-resistant membranes (DRMs) and non-DRM domains: effect of treatment with azide. *American Journal of Physiology-Cell Physiology* **285**, C377-C383.

Saikawa, N., Akiyama, Y., & Ito, K. (2004). FtsH exists as an exceptionally large complex containing HflKC in the plasma membrane of Escherichia coli. *Journal of Structural Biology* **146**, 123-129.

Salaun, C., James, D. J., & Chamberlain, L. H. (2004). Lipid rafts and the regulation of exocytosis. *Traffic* **5**, 255-264.

Salzer, U., Ahorn, H., & Prohaska, R. (1993). Identification of the Phosphorylation Site on Human Erythrocyte Band-7 Integral Membrane-Protein - Implications for A Monotopic Protein-Structure. *Biochimica et Biophysica Acta* **1151**, 149-152.

Salzer, U., Hinterdorfer, P., Hunger, U., Borcken, C., & Prohaska, R. (2002). Ca⁺⁺-dependent vesicle release from erythrocytes involves stomatin-specific lipid rafts, synexin (annexin VII), and sorcin. *Blood* **99**, 2569-2577.

Salzer, U. & Prohaska, R. (2001b). Stomatin, flotillin-1, and flotillin-2 are major integral proteins of erythrocyte lipid rafts. *Blood* **97**, 1141-1143.

Salzer, U. & Prohaska, R. (2001a). Stomatin, flotillin-1, and flotillin-2 are major integral proteins of erythrocyte lipid rafts. *Blood* **97**, 1141-1143.

Scaduto, R. C. & Grotyohann, L. W. (1999). Measurement of mitochondrial membrane potential using fluorescent rhodamine derivatives. *Biophysical Journal* **76**, 469-477.

Scales, S. J., Yoo, B. Y., & Scheller, R. H. (2001). The ionic layer is required for efficient dissociation of the SNARE complex by alpha-SNAP and NSF. *Proceedings of the National Academy of Sciences of the United States of America* **98**, 14262-14267.

- Schaaf, G., Honsbein, A., Meda, A. R., Kirchner, S., Wipf, D., & von Wiren, N. (2006). AtIREG2 encodes a tonoplast transport protein involved in iron-dependent nickel detoxification in *Arabidopsis thaliana* roots. *Journal of Biological Chemistry* **281**, 25532-25540.
- Scheible, W. R., Fry, B., Kochevenko, A., Schindelasch, D., Zimmerli, L., Somerville, S., Loria, R., & Somerville, C. R. (2003). An *Arabidopsis* mutant resistant to thaxtomin A, a cellulose synthesis inhibitor from *Streptomyces* species. *Plant Cell* **15**, 1781-1794.
- Schlegel, W., Unfried, I., & Prohaska, R. (1996). Cloning and analysis of a cDNA encoding the BALB/c murine erythrocyte band 7 integral membrane protein. *Gene* **178**, 115-118.
- Schleicher, M., Shepherd, B. R., Suarez, Y., Fernandez-Hernando, C., Yu, J., Pan, Y., Acevedo, L. M., Shadel, G. S., & Sessa, W. C. (2008). Prohibitin-1 maintains the angiogenic capacity of endothelial cells by regulating mitochondrial function and senescence. *Journal of Cell Biology* **180**, 101-112.
- Schmid, M., Davison, T. S., Henz, S. R., Pape, U. J., Demar, M., Vingron, M., Scholkopf, B., Weigel, D., & Lohmann, J. U. (2005). A gene expression map of *Arabidopsis thaliana* development. *Nature Genetics* **37**, 501-506.
- Schnurr, J., Shockey, J., & Browse, J. (2004). The acyl-CoA synthetase encoded by LACS2 is essential for normal cuticle development in *Arabidopsis*. *Plant Cell* **16**, 629-642.
- Schnurr, J. A., Shockey, J. M., de Boer, G. J., & Browse, J. A. (2002). Fatty acid export from the chloroplast. Molecular characterization of a major plastidial acyl-coenzyme A synthetase from *Arabidopsis*. *Plant Physiology* **129**, 1700-1709.
- Schulte, T., Paschke, K. A., Laessing, U., Lottspeich, F., & Stuermer, C. A. O. (1997). Reggie-1 and reggie-2, two cell surface proteins expressed by retinal ganglion cells during axon regeneration. *Development* **124**, 577-587.
- Sedensky, M. M. & Meneely, P. M. (1987). Genetic-Analysis of Halothane Sensitivity in *Caenorhabditis- Elegans*. *Science* **236**, 952-954.
- Sedensky, M. M., Siefker, J. M., Koh, J. Y., Miller, D. M., & Morgan, P. G. (2004). A stomatin and a degenerin interact in lipid rafts of the nervous system of *Caenorhabditis elegans*. *American Journal of Physiology-Cell Physiology* **287**, C468-C474.
- Sedensky, M. M., Siefker, J. M., & Morgan, P. G. (2001b). Model organisms: New insights into ion channel and transporter function. Stomatin homologues interact in *Caenorhabditis elegans*. *American Journal of Physiology-Cell Physiology* **280**, C1340-C1348.

- Sedensky, M. M., Siefker, J. M., & Morgan, P. G. (2001a). Model organisms: New insights into ion channel and transporter function. Stomatin homologues interact in *Caenorhabditis elegans*. *American Journal of Physiology-Cell Physiology* **280**, C1340-C1348.
- Seidel, G. & Prohaska, R. (1998). Molecular cloning of hSLP-1, a novel human brain-specific member of the band 7 MEC-2 family similar to *Caenorhabditis elegans* UNC-24. *Gene* **225**, 23-29.
- Sessions, A., Burke, E., Presting, G., Aux, G., McElver, J., Patton, D., Dietrich, B., Ho, P., Bacwaden, J., Ko, C., Clarke, J. D., Cotton, D., Bullis, D., Snell, J., Miguel, T., Hutchison, D., Kimmerly, B., Mitzel, T., Katagiri, F., Glazebrook, J., Law, M., & Goff, S. A. (2002). A high-throughput Arabidopsis reverse genetics system. *Plant Cell* **14**, 2985-2994.
- Shotland, Y., Koby, S., Teff, D., Mansur, N., Oren, D. A., Tatematsu, K., Tomoyasu, T., Kessel, M., Bukau, B., Ogura, T., & Oppenheim, A. B. (1997). Proteolysis of the phage lambda CII regulatory protein by FtsH (HflB) of *Escherichia coli*. *Molecular Microbiology* **24**, 1303-1310.
- Sinard J.H., S. G. W. A. A. C. M. J. S. (1994). Stomatin binding to adducin: a novel link between transmembrane ion transport and the cytoskeleton. *Molecular Biology of the Cell* **5**, 421a.
- Sinha, R. P. & Hader, D. P. (2002). UV-induced DNA damage and repair: a review. *Photochemical & Photobiological Sciences* **1**, 225-236.
- Small, I., Peeters, N., Legeai, F., & Lurin, C. (2004). Predotar: A tool for rapidly screening proteomes for N-terminal targeting sequences. *Proteomics* **4**, 1581-1590.
- Snedden, W. A. & Fromm, H. (1997). Characterization of the plant homologue of prohibitin, a gene associated with antiproliferative activity in mammalian cells. *Plant Molecular Biology* **33**, 753-756.
- Snyder, J. R., Hall, A., Ni-Komatsu, L., Khersonsky, S. M., Chang, Y. T., & Orlow, S. J. (2005). Dissection of melanogenesis with small molecules identifies prohibitin as a regulator. *Chemistry & Biology* **12**, 477-484.
- Snyers, L. & Content, J. (1994). Induction of Metallothionein and Stomatin by Interleukin-6 and Glucocorticoids in A Human Amniotic Cell-Line. *European Journal of Biochemistry* **223**, 411-418.
- Snyers, L., ThinesSempoux, D., & Prohaska, R. (1997). Colocalization of stomatin (band 7.2b) and actin microfilaments in UAC epithelial cells. *European Journal of Cell Biology* **73**, 281-285.

- Snyers, L., Umlauf, E., & Prohaska, R. (1998). Oligomeric nature of the integral membrane protein stomatin. *Journal of Biological Chemistry* **273**, 17221-17226.
- Snyers, L., Umlauf, E., & Prohaska, R. (1999a). Association of stomatin with lipid-protein complexes in the plasma membrane and the endocytic compartment. *European Journal of Cell Biology* **78**, 802-812.
- Snyers, L., Umlauf, E., & Prohaska, R. (1999b). Cysteine 29 is the major palmitoylation site on stomatin. *Febs Letters* **449**, 101-104.
- Solis, G. P., Hoegg, M., Munderloh, C., Schrock, Y., Malaga-Trillo, E., Rivera-Milla, E., & Stuerivier, C. A. O. (2007). Reggie/flotillin proteins are organized into stable tetramers in membrane microdomains. *Biochemical Journal* **403**, 313-322.
- Soll, J. & Schleiff, E. (2004). Protein import into chloroplasts. *Nature Reviews Molecular Cell Biology* **5**, 198-208.
- Steck, T. L. (1974). The organization of proteins in the human red blood cell membrane. A review. [Review] [163 refs]. *Journal of Cell Biology* **62**, 1-19.
- Stefanowska, M., Kuras, M., & Kacperska, A. (2002). Low temperature-induced modifications in cell ultrastructure and localization of phenolics in winter oilseed rape (*Brassica napus* L. var. *oleifera* L.) leaves. *Annals of Botany* **90**, 637-645.
- Steglich, G., Neupert, W., & Langer, T. (1999). Prohibitins regulate membrane protein degradation by the m-AAA protease in mitochondria. *Molecular and Cellular Biology* **19**, 3435-3442.
- Stewart, G. W., Argent, A. C., & Dash, B. C. J. (1993). Stomatin - A Putative Cation-Transport Regulator in the Red-Cell Membrane. *Biochimica et Biophysica Acta* **1225**, 15-25.
- Stewart, G. W., Hepworthjones, B. E., Keen, J. N., Dash, B. C. J., Argent, A. C., & Casimir, C. M. (1992). Isolation of Cdna Coding for An Ubiquitous Membrane-Protein Deficient in High Na⁺, Low K⁺ Stomatocytic Erythrocytes. *Blood* **79**, 1593-1601.
- Stucki, J. W., Lehmann, L. H., & Siegel, E. (1989). Acylation of Proteins by Myristic Acid in Isolated-Mitochondria. *Journal of Biological Chemistry* **264**, 6376-6380.
- Suh, M. C., Samuels, A. L., Jetter, R., Kunst, L., Pollard, M., Ohlrogge, J., & Beisson, F. (2005). Cuticular lipid composition, surface structure, and gene expression in Arabidopsis stem epidermis. *Plant Physiology* **139**, 1649-1665.
- Swanson, R., Clark, T., & Preuss, D. Expression profiling of *Arabidopsis* stigma tissue identifies stigma-specific genes. *Sexual Plant Reproduction* **18**[4], 163-171. 2005.

Ref Type: Journal (Full)

Swarup, R., Parry, G., Graham, N., Allen, T., & Bennett, M. (2002). Auxin cross-talk: integration of signalling pathways to control plant development. *Plant Molecular Biology* **49**, 411-426.

Sweetlove, L. J., Heazlewood, J. L., Herald, V., Holtzapffel, R., Day, D. A., Leaver, C. J., & Millar, A. H. (2002). The impact of oxidative stress on Arabidopsis mitochondria. *Plant Journal* **32**, 891-904.

Sweetlove, L. J., Lytovchenko, A., Morgan, M., Nunes-Nesi, A., Taylor, N. L., Baxter, C. J., Eickmeier, I., & Fernie, A. R. (2006). Mitochondrial uncoupling protein is required for efficient photosynthesis. *Proceedings of the National Academy of Sciences of the United States of America* **103**, 19587-19592.

Taiz, L. & Zeiger, E. (2002). Respiration and lipid metabolism. In *Plant Physiology* pp. 223-258. Sinauer Associates, Sunderland, Massachusetts.

Takahashi, A., Kawasaki, T., Wong, H. L., Suharsono, U., Hirano, H., & Shimamoto, K. (2003). Hyperphosphorylation of a mitochondrial protein, prohibitin, is induced by calyculin A in a rice lesion-mimic mutant *cdr1*. *Plant Physiology* **132**, 1861-1869.

Tang, H. B., Bowers, J. E., Wang, X. Y., Ming, R., Alam, M., & Paterson, A. H. (2008). Perspective - Synteny and collinearity in plant genomes. *Science* **320**, 486-488.

Tatsuta, T., Model, K., & Langer, T. (2005). Formation of membrane-bound ring complexes by prohibitins in mitochondria. *Molecular Biology of the Cell* **16**, 248-259.

Tavernarakis, N. & Driscoll, M. (1997). Molecular modeling of mechanotransduction in the nematode *Caenorhabditis elegans*. *Annual Review of Physiology* **59**, 659-689.

Tavernarakis, N., Driscoll, M., & Kyrpides, N. C. (1999). The SPFH domain: implicated in regulating targeted protein turnover in stomatins and other membrane-associated proteins. *Trends in Biochemical Sciences* **24**, 425-427.

Tavernarakis, N., Shreffler, W., Wang, S. L., & Driscoll, M. (1997). *unc-8*, a DEG/ENaC family member, encodes a subunit of a candidate mechanically gated channel that modulates *C. elegans* locomotion. *Neuron* **18**, 107-119.

Terashima, M., Kim, K. M., Adachi, T., Nielsen, P. J., Reth, M., Kohler, G., & Lamers, M. C. (1994). The Igm Antigen Receptor of B-Lymphocytes Is Associated with Prohibitin and A Prohibitin-Related Protein. *Embo Journal* **13**, 3782-3792.

Thomas, D. R., Wood, C., & Masterson, C. (1988). Long-Chain Acyl Coa Synthetase, Carnitine and Beta-Oxidation in the Pea-Seed Mitochondrion. *Planta* **173**, 263-266.

- Thompson, J. D., Higgins, D. G., & Gibson, T. J. (1994). Clustal-W - Improving the Sensitivity of Progressive Multiple Sequence Alignment Through Sequence Weighting, Position-Specific Gap Penalties and Weight Matrix Choice. *Nucleic Acids Research* **22**, 4673-4680.
- ThordalChristensen, H., Zhang, Z. G., Wei, Y. D., & Collinge, D. B. (1997). Subcellular localization of H₂O₂ in plants. H₂O₂ accumulation in papillae and hypersensitive response during the barley-powdery mildew interaction. *Plant Journal* **11**, 1187-1194.
- Thornalley, P. J. & Vasak, M. (1985). Possible Role for Metallothionein in Protection Against Radiation-Induced Oxidative Stress - Kinetics and Mechanism of Its Reaction with Superoxide and Hydroxyl Radicals. *Biochimica et Biophysica Acta* **827**, 36-44.
- Torres, M. A., Dangl, J. L., & Jones, J. D. G. (2002). Arabidopsis gp91(phox) homologues AtrbohD and AtrbohF are required for accumulation of reactive oxygen intermediates in the plant defense response. *Proceedings of the National Academy of Sciences of the United States of America* **99**, 517-522.
- Towler, D. A., Gordon, J. I., Adams, S. P., & Glaser, L. (1988). The Biology and Enzymology of Eukaryotic Protein Acylation. *Annual Review of Biochemistry* **57**, 69-99.
- Ulmasov, T., Hagen, G., & Guilfoyle, T. J. (1999). Dimerization and DNA binding of auxin response factors. *Plant Journal* **19**, 309-319.
- Ulmasov, T., Murfett, J., Hagen, G., & Guilfoyle, T. J. (1997). Aux/IAA proteins repress expression of reporter genes containing natural and highly active synthetic auxin response elements. *Plant Cell* **9**, 1963-1971.
- Umlauf, E., Csaszar, E., Moertelmaier, M., Schuetz, G. J., Parton, R. G., & Prohaska, R. (2004). Association of stomatin with lipid bodies. *Journal of Biological Chemistry* **279**, 23699-23709.
- Umlauf, E., Mairhofer, M., & Prohaska, R. (2006). Characterization of the stomatin domain involved in homo-oligomerization and lipid raft association. *Journal of Biological Chemistry* **281**, 23349-23356.
- Van Aken, O., Pecenkova, T., van de Cotte, B., De Rycke, R., Eeckhout, D., Fromm, H., De Jaeger, G., Witters, E., Beemster, G. T. S., Inze, D., & Van Breusegem, F. (2007). Mitochondrial type-I prohibitins of Arabidopsis thaliana are required for supporting proficient meristem development. *Plant Journal* **52**, 850-864.
- Vanloon, A. P. G. M., Brandli, A. W., Pesoldhurt, B., Blank, D., & Schatz, G. (1987). Transport of Proteins to the Mitochondrial Intermembrane Space - the Matrix-Targeting and the Sorting Domains in the Cytochrome C1 Presequence. *Embo Journal* **6**, 2433-2439.

- Vogel, J. & Somerville, S. (2000). Isolation and characterization of powdery mildew-resistant *Arabidopsis* mutants. *Proceedings of the National Academy of Sciences of the United States of America* **97**, 1897-1902.
- Volonte, D., Galbiati, F., Li, S. W., Nishiyama, K., Okamoto, T., & Lisanti, M. P. (1999). Flotillins/cavatellins are differentially expressed in cells and tissues and form a hetero-oligomeric complex with caveolins in vivo - Characterization and epitope-mapping of a novel flotillin-1 monoclonal antibody probe. *Journal of Biological Chemistry* **274**, 12702-12709.
- Wang, S., Nath, N., Adlam, M., & Chellappan, S. (1999a). Prohibitin, a potential tumor suppressor, interacts with RB and regulates E2F function. *Oncogene* **18**, 3501-3510.
- Wang, S., Nath, N., Adlam, M., & Chellappan, S. (1999b). Prohibitin, a potential tumor suppressor, interacts with RB and regulates E2F function. *Oncogene* **18**, 3501-3510.
- Wang, Y. J. & Morrow, J. S. (2000). Identification and characterization of human SLP-2, a novel homologue of stomatin (Band 7.2b) present in erythrocytes and other tissues. *Journal of Biological Chemistry* **275**, 8062-8071.
- Wang, Y. Q., Yun, B. W., Kwon, E., Hong, J. K., Yoon, J., & Loake, G. J. (2006). S-nitrosylation: an emerging redox-based post-translational modification in plants. *Journal of Experimental Botany* **57**, 1777-1784.
- Webb, Y., Hermida-Matsumoto, L., & Resh, M. D. (2000). Inhibition of protein palmitoylation, raft localization, and T cell signaling by 2-bromopalmitate and polyunsaturated fatty acids. *Journal of Biological Chemistry* **275**, 261-270.
- Wen, T. J., Hochholdinger, F., Sauer, M., Bruce, W., & Schnable, P. S. (2005). The roothairless1 gene of maize encodes a homolog of sec3, which is involved in polar exocytosis. *Plant Physiology* **138**, 1637-1643.
- Wetzel, C., Hu, J., Riethmacher, D., Benckendorff, A., Harder, L., Eilers, A., Moshourab, R., Kozlenkov, A., Labuz, D., Caspani, O., Erdmann, B., Machelska, H., Heppenstall, P. A., & Lewin, G. R. (2007). A stomatin-domain protein essential for touch sensation in the mouse. *Nature* **445**, 206-209.
- Wielopolska, A., Townley, H., Moore, I., Waterhouse, P., & Helliwell, C. (2005). A high-throughput inducible RNAi vector for plants. *Plant Biotechnology Journal* **3**, 583-590.
- Wienkoop, S. & Saalbach, G. (2003). Proteome analysis. Novel proteins identified at the peribacteroid membrane from *Lotus japonicus* root nodules. *Plant Physiology* **131**, 1080-1090.
- Wilkinson, D. K., Turner, E. J., Parkin, E. T., Garner, A. E., Penny, J. H., Crawford, M., Stewart, G. W., & Hooper, N. M. (2008). Membrane raft actin deficiency and altered

- Ca²⁺-induced vesiculation in stomatin-deficient overhydrated hereditary stomatocytosis. *Biochimica et Biophysica Acta-Biomembranes* **1778**, 125-132.
- Winter, A., Kamarainen, O., & Hofmann, A. (2007a). Molecular modeling of prohibitin domains. *Proteins-Structure Function and Bioinformatics* **68**, 353-362.
- Winter, D., Vinegar, B., Nahal, H., Ammar, R., Wilson, G. V., & Provart, N. J. An "electronic fluorescent pictograph" browser for exploring and analyzing large-scale biological data sets. *PLoS ONE* **2**[1], e718. 2007b.
Ref Type: Journal (Full)
- Wood, C., Masterson, C., & Thomas, D. R. (1992). The role of carnithine in plant cell metabolism. In *Plant Organelles*, ed. Tobin, A. K., pp. 229-263. Cambridge University Press.
- Wu, S. J., Ding, L., & Zhu, J. K. (1996). SOS1, a genetic locus essential for salt tolerance and potassium acquisition. *Plant Cell* **8**, 617-627.
- Yalovsky, S., Rodriguez-Concepcion, M., & Gruissem, W. (1999). Lipid modifications of proteins - slipping in and out of membranes. *Trends in Plant Science* **4**, 439-445.
- Yamauchi, Y., Ogawa, M., Kuwahara, A., Hanada, A., Kamiya, Y., & Yamaguchi, S. (2004). Activation of Gibberellin biosynthesis and response pathways by low temperature during imbibition of *Arabidopsis thaliana* seeds. *Plant Cell* **16**, 367-378.
- Yang, J. Y., Gibson, B., Snider, J., Jenkins, C. M., Han, X. L., & Gross, R. W. (2005). Submicromolar concentrations of palmitoyl-CoA specifically thioesterify cysteine 244 in glyceraldehyde-3-phosphate dehydrogenase inhibiting enzyme activity: A novel mechanism potentially underlying fatty acid induced insulin resistance. *Biochemistry* **44**, 11903-11912.
- Yang, Y., Costa, A., Leonhardt, N., Siegel, R. S., & Schroeder, R. I. Isolation of a strong *Arabidopsis* guard cell promoter and its potential as a research tool. *Plant Methods* **4**[6]. 2008.
Ref Type: Journal (Full)
- Yao, N., Eisfelder, B. J., Marvin, J., & Greenberg, J. T. (2004). The mitochondrion - an organelle commonly involved in programmed cell death in *Arabidopsis thaliana*. *Plant Journal* **40**, 596-610.
- Yokoyama, H., Fujii, S., & Matsui, I. (2008a). Crystal structure of a core domain of stomatin from *Pyrococcus horikoshii* illustrates a novel trimeric and coiled-coil fold. *Journal of Molecular Biology* **376**, 868-878.

- Yokoyama, H., Fujii, S., & Matsui, I. (2008b). Crystal structure of a core domain of stomatin from *Pyrococcus horikoshii* illustrates a novel trimeric and coiled-coil fold. *Journal of Molecular Biology* **376**, 868-878.
- Yokoyama, H., Matsui, E., Akiba, T., Harata, K., & Matsui, I. (2006). Molecular structure of a novel membrane protease specific for a stomatin homolog from the hyperthermophilic archaeon *Pyrococcus horikoshii*. *Journal of Molecular Biology* **358**, 1152-1164.
- Yokoyama, H. & Matsui, I. (2005). A novel thermostable membrane protease forming an operon with a stomatin homolog from the hyperthermophilic archaeobacterium *Pyrococcus horikoshii*. *Journal of Biological Chemistry* **280**, 6588-6594.
- Yoshinaga, K., Arimura, S., Hirata, A., Niwa, Y., Yun, D. J., Tsutsumi, N., Uchimiya, H., & Kawai-Yamada, M. (2005). Mammalian Bax initiates plant cell death through organelle destruction. *Plant Cell Reports* **24**, 408-417.
- You, Z. R., Gao, X. F., Ho, M. M., & Borthakur, D. (1998). A stomatin-like protein encoded by the sip gene of *Rhizobium etli* is required for nodulation competitiveness on the common bean. *Microbiology-Sgm* **144**, 2619-2627.
- Yu, X. M., Yu, X. D., Qu, Z. P., Huang, X. J., Guo, J., Han, Q. M., Zhao, J., Huang, L. L., & Kang, Z. S. (2008). Cloning of a putative hypersensitive induced reaction gene from wheat infected by stripe rust fungus. *Gene* **407**, 193-198.
- Zalman, L. S., Nikaido, H., & Kagawa, Y. (1980). Mitochondrial Outer-Membrane Contains A Protein Producing Nonspecific Diffusion Channels. *Journal of Biological Chemistry* **255**, 1771-1774.
- Zeiger, E., Talbott, L. D., Frechilla, S., Srivastava, A., & Zhu, J. X. (2002). The guard cell chloroplast: a perspective for the twenty-first century. *New Phytologist* **153**, 415-424.
- Zhang, J. Z., Abbud, W., Prohaska, R., & Ismail-Beigi, F. (2001). Overexpression of stomatin depresses GLUT-1 glucose transporter activity. *American Journal of Physiology-Cell Physiology* **280**, C1277-C1283.
- Zhang, L. Y., Ding, F., Cao, W. F., Liu, Z. M., Liu, W., Yu, Z. C., Wu, Y., Li, W. D., Li, Y. D., & Liu, Z. H. (2006). Stomatin-like protein 2 is overexpressed in cancer and involved in regulating cell growth and cell adhesion in human esophageal squamous cell carcinoma. *Clinical Cancer Research* **12**, 1639-1646.
- Zhang, S. F., Arnadottir, J., Keller, C., Caldwell, G. A., Yao, C. A., & Chalfie, M. (2004). MEC-2 is recruited to the putative mechanosensory complex in *C. elegans* touch receptor neurons through its stomatin-like domain. *Current Biology* **14**, 1888-1896.
- Zhu, Y. W., Paszty, C., Turetsky, T., Tsai, S., Kuypers, F. A., Lee, G., Cooper, P., Gallagher, P. G., Stevens, M. E., Rubin, E., Mohandas, N., & Mentzer, W. C. (1999).

Stomatocytosis is absent in "stomatin"-deficient murine red blood cells. *Blood* **93**, 2404-2410.